UNIVERSITÀ
degli STUDI
di CATANIA

Department of Biomedical and Biotechnological Sciences

Ph.D. in Biotechnology

Curriculum in Pharmaceutical Biotechnology

XXXVI Cycle

_____

CINZIA CIMINO

Overcoming biological barriers through the use of drug delivery systems

_____

Ph.D. Thesis

Tutor: *Prof. Agostino Marrazzo*

Co-tutor: *Prof.ssa Claudia Carbone*

Coordinator: *Prof. Vito De Pinto*

_____

ACADEMIC YEARS 2020/2023

INDEX

SINTESI

Oggigiorno, il focus della ricerca farmaceutica è centrato sul superamento dei limiti delle forme farmaceutiche convenzionali, tramite l'utilizzo dei sistemi di rilascio (drug delivery systems, DDS), con la finalità di migliorare la biodistribuzione dei principi attivi. Tra i vantaggi di queste piattaforme tecnologiche, è importante ricordare, ad esempio, la capacità di incapsulare farmaci idrofili, generalmente soggetti a rapida degradazione dopo la somministrazione. A tal proposito, è stata sviluppata una piattaforma microemulsiva trifasica (W/O/W) per la potenziale veicolazione di molecole idrofile o vaccini tramite la via mucosale nasale, rivalutata recentemente per i suoi vantaggi in termini di compliance e risposta immunitaria. Tra gli altri vantaggi dei sistemi di rilascio, se opportunamente progettati, è la capacità di superare le barriere biologiche e di veicolare il principio attivo al sito target con una maggiore efficienza, che risulta molto importante, ad esempio, nelle terapie delle malattie neurodegenerative. L'inalazione di oli essenziali è nota da secoli (detta aromaterapia), e, sulla base di ciò, dopo aver approfondito l'utilizzo terapeutico di tali composti naturali, è stata progettata la loro veicolazione all'interno di sistemi di rilascio, in particolare tramite carrier lipidici nanostrutturati (NLC), per la potenziale somministrazione intranasale nel trattamento coadiuvante nelle patologie neurodegenerative; tale via di somministrazione, detta anche nose-to-brain, permette un diretto raggiungimento del sistema nervoso centrale, bypassando la barriera emato-encefalica. Un'altra importante barriera fisiologica è presente a livello oculare e, tramite barriere fisiche e meccanismi di protezione, diminuisce drasticamente la biodisponibilità dei principi attivi instillati topicamente. Per tale ragione, il trattamento di patologie dell'occhio interno, come l'aggressivo melanoma uveale, risultano ad oggi difficoltose. In tale contesto, la veicolazione dei principi attivi tramite sistemi di rilascio risulta vantaggioso nell'evitare la rapida eliminazione del principio attivo tramite la lacrimazione e l'ammiccamento, e nel veicolare il farmaco al sito target, posto nel segmento posteriore dell'occhio. Il targeting di questo tumore oculare è stato proposto tramite due piattaforme: un sistema di particelle lipidiche solide (SLN) caricate con sorafenib, e sistemi di carrier lipidici nanostrutturati (NLC) in cui è stato incapsulato il farmaco di nuova sintesi MRJF22. Dopo un approfondimento bibliografico sulle potenzialità delle tecniche di fluorescenza a livello oculare, sia nella diagnostica che nella biodistribuzione, tali conoscenze sono state applicate tramite studi *in vivo* al fine di verificare il potenziale utilizzo delle piattaforme sviluppate nel trattamento del melanoma uveale.

_____

ABSTRACT

Nowadays, the focus of the pharmaceutical research is addressed to the overcoming of the limits of the conventional dosage forms, through the use of drug delivery systems (DDS), aiming to improve the biodistribution of the encapsulated active drugs. Among the advantages of these platforms, it is worth to be mentioned the ability to encapsulate hydrophilic drugs, which generally are quickly degraded after administration. Basing on this, a triphasic microemulsion water-in-oil-in-water (W/O/W) was developed for the potential delivery of hydrophilic molecules or vaccines through the nasal mucosal route, which was recently reconsidered because of its properties of high patient compliance and immune response. Among the advantages of the drug delivery systems, if opportunely designed, there is also the capability to overcome the biological barriers and to deliver the drug to the target site with higher efficiency, which is an important feature in the treatment of neurodegenerative diseases, for instance. Inhalation of essential oils is known from centuries (defined aromatherapy), and, for this reason, after deepening the therapeutical applications of these natural compounds, it was developed their vehiculation into DDS, and nanostructured lipid carriers (NLC) in particular, for the potential intranasal administration in the adjuvant treatment of the neurodegenerative pathologies; this administration route, also called nose-to-brain, allows a direct achieving of the central nervous system, bypassing the blood brain barrier. Another important physiological limit is at ocular level, and, through physical barriers and protection mechanisms, it reduces drastically the bioavailability of the topically instilled drugs. For this reason, the treatment of the pathologies of the inner eye, as the aggressive uveal melanoma, is still difficult. In this framework, the delivery of the active molecule through DDS is advantageous since it avoids the quick elimination trough lacrimation and blinking and allows the delivery to the target site in the posterior segment of the eye. The targeting of this ocular tumor was investigated through two platforms: a solid lipid nanoparticles (NLC) platform loaded with sorafenib, and nanostructured lipid carriers (NLC) platforms in which the new synthetized MRJF22 was encapsulated. After a detailed bibliographic study on the potentiality of the fluorescence techniques in the ocular field, both in diagnostics and biodistribution, this knowledge was applied through *in vivo* studies aimed to the assessment of the potential use of the developed carriers in the treatment of uveal melanoma.

_____

KEYWORDS AND ABBREVIATIONS

DDS	Drug Delivery Systems
SLN	Solid Lipid Nanoparticles
NLC	Nanostructured Lipid Carriers
ME	Microemulsion
W/O	water-in-oil
O/W	oil-in-water
W/O/W	water-in-oil-in-water
O/W/O	oil-in-water-in-oil
HLB	Hydrophilic Lipophilic Balance
PIT	Phase Inversion Temperature
PEG	Polyethylene Glycol
PCS	Photon Correlation Spectroscopy
DLS	Dynamic Light Scattering
Z-ave	Mean particle (or droplet) size
PDI	Polydispersity index
ZP	Zeta Potential
ELS	Electrophoresis Light Scattering
BBB	Blood Brain Barrier
FDA	Food and Drug Administration
RH	Relative Humidity
TEM	Transmission Electron Microscopy
DSC	Differential Scanning Calorimetry
FT-IR	Fourier Transform Infrared spectroscopy
XRD	X-ray diffraction
EE%	Encapsulation Efficiency
DLC%	Drug Loading Capacity
CNS	Central Nervous System
BBB	Blood Brain Barrier
N2B	nose-to-brain
PD	Parkinson's disease
AD	Alzheimer's Disease
EOs	Essential Oils
BAB	Blood-aqueous barrier
BRB	Blood-retinal barrier
UM	Uveal melanoma
VEGF-A	Vascular endothelial growth factor A
MAPK	Mitogen-activated protein kinase
SRF	Sorafenib
HDAC	Histone deacetylase
HDACi	Histone deacetylase inhibitors
VPA	Valproic acid
HP	Haperidol
HP-mII	Haloperidol metabolite II
CAMs	Complementary and Alternative Medicines
DDAB	Didodecyldimethylammonium bromide
DOTAP	1,2-dioleoyl-3-trimethylammonium-propane
CAM	Chorioallantoic membrane
TBS	Trypan Blue Staining

_____

AFFILIATIONS

Laboratory of Drug Delivery Technology, Department of Drug and Health Sciences, University of Catania – Viale Andrea Doria, 6 – 95125 Catania, Italy

Department of Pharmacy, Pharmaceutical technology and Physical Chemistry, Faculty of Pharmacy and Food Sciences, University of Barcelona – Campus Diagonal, Av. De Joan XXIII, 27-31 – 08028 Barcelona, Spain

NANOMED, Research Centre for Nanomedicine and Pharmaceutical Nanotechnology, Department of Drug and Health Sciences, University of Catania – Viale Andrea Doria, 6 – 95125 Catania, Italy

_____

_____

1   INTRODUCTION

1.1   Limits in conventional dosage forms

Nowadays, the interest of researchers in the pharmaceutical field is mainly focused on the overcoming of the drawback of the conventional pharmaceutical forms, which could be related to the drug itself and to the formulation limits related to each specific route of administration[1].

The nature of the drug itself – hydrophilicity/lipophilicity, molecular weight, degradation after administration (depending on the route), etc. – influences the development of the delivery platform. Moreover, conventional pharmaceutical forms are often not able to maintain an adequate drug level as long as required for the therapeutic activity.

The difficulty to maintain drug level in the therapeutic window is usually related to its incapability to successful cross the biological barriers, to reach the target site, or to its fast metabolism or inactivation due to enzymatic reactions, etc. Currently, various strategies are used to guarantee the maintaining of the therapeutical dose from conventional dosage forms, such as repeated drug doses during the day or administration of higher amounts of drug; the drawbacks of these approaches are the increase of toxicity related to dose fluctuation and the appearance of greater adverse effects, which lead to low patient compliance[2].

Furthermore, depending on the administration site, the presence of physiological barriers could decrease even more the amount of drug that is efficiently able to reach the target site. Clinical barriers, such as individual variability, diseases conditions, as well could influence the effectiveness of the treatment, especially for enteral routes where the gastrointestinal transit time or the fed state could have a remarkable impact[1].

A summary of the most important advantages and limits of the main administration routes is reported in Table 1.

_____

Table 1. Most important advantages and disadvantages of the main administration routes.

	Route of administration	Advantages	Disadvantages
Parenteral routes	**Intravenous**[3]	▪ Rapid onset of activity. ▪ Almost complete bioavailability. ▪ Avoid first-pass hepatic metabolism. ▪ Administration in not-collaborative patients.	▪ Painful. ▪ Infection risk. ▪ Need of specialized professionals. ▪ Fast circulation dose.
	Intramuscular[4]	▪ Absence of fast circulation dose. ▪ High absorption and bioavailability. ▪ Useful for a great variety of drugs.	▪ Pain at the site of injection. ▪ Anxiety and pain of the patient. ▪ Dose should be adjusted considering muscle mass. ▪ Need of specialized professionals.
	Subcutaneous[5,6]	▪ Useful for bigger molecules. ▪ Could be self-administered. ▪ Shorter infusion time and less adverse effect compared to intravenous. ▪ Slow and sustained absorption and diffusion.	▪ Absorption influenced by fatty tissue. ▪ Irritation and pain. ▪ Frequently change the site of administration.
Enteral routes	**Oral**[7]	▪ Convenient administration. ▪ High compliance. ▪ Not invasiveness. ▪ Cost effectiveness. ▪ Patient preference. ▪ Direct targeting for gastrointestinal pathologies.	▪ Degradation of drug. ▪ High variation of absorption and bioavailability. ▪ Inactivation of drugs by acid pH of stomach. ▪ First-pass hepatic metabolism. ▪ Absorption influenced by ingestion of food. ▪ Some drugs could cause irritation.
	Sublingual and buccal[8]	▪ Convenient administration. ▪ Avoid first-pass hepatic metabolism. ▪ Low infection risk. ▪ Rapid absorption into circulation. ▪ Rapid onset of activity.	▪ Palatability. ▪ Difficulty to not swallow. ▪ Rapid dissolution if there is a lot of salivation. ▪ Risk of accidental aspiration.
	Rectal[9]	▪ Safe and convenient. ▪ High amount of dosage administrable. ▪ Avoid first-pass hepatic metabolism. ▪ Useful in emergencies. ▪ Less drug degradation compared to oral route.	▪ Not suitable for some hydrophilic compounds. ▪ Some drugs could cause irritation. ▪ High variation of absorption. ▪ Poor patient compliance.
Topical-systemic routes	**Inhalational**[10]	▪ Large absorption area. ▪ Avoid first-pass hepatic metabolism. ▪ Direct targeting for respiratory pathologies. ▪ Higher effectiveness requiring lower doses. ▪ Lower systemics levels and adverse effects.	▪ Size discrimination in absorption. ▪ Mucus causing rapid clearance. ▪ Incorrect self-administration procedure. ▪ Necessity of appropriated device. ▪ More expensive production.
	Transdermal[11]	▪ Avoid first-pass hepatic metabolism. ▪ Reduced systemic absorption. ▪ High compliance.	▪ Skin permeation related to drug characteristics (required low molecular weight, high lipophilicity, etc).

	Route of administration	Advantages	Disadvantages
Local routes	Intranasal[12]	▪ High permeability compared to gastrointestinal mucosa. ▪ Rapid absorption. ▪ Avoid first-pass hepatic metabolism. ▪ Safe and convenient. ▪ High compliance.	▪ Ciliary movement and mucus, causing rapid clearance. ▪ Metabolization through enzymes and drug loss. ▪ Low bioavailability. ▪ Damage of nasal mucosa.
	Ophthalmic[13]	▪ High compliance. ▪ Not invasive. ▪ Easiness of administration.	▪ Very low bioavailability. ▪ Difficulty to reach the posterior chamber with therapeutic doses.
	Skin topical[14]	▪ High compliance. ▪ Not invasive. ▪ Easiness of administration.	▪ Skin diffusion related to drug characteristics (small size, lipophilic or amphiphilic, etc).
	Vaginal[15]	▪ Prolonged release. ▪ Avoid first-pass hepatic metabolism. ▪ Reduced systemic absorption. ▪ Decrease side effect. ▪ Direct targeting for vaginal pathologies.	▪ Mainly for local treatments. ▪ Barrier of cultural beliefs. ▪ Low compliance in sexually active women. ▪ Local irritation. ▪ Variation of absorption.

In the following paragraphs, firstly it will be presented a general description of the carriers developed in the framework of this PhD project, as well as the characterization techniques used. Subsequently, the three main targets – nasal mucosal delivery, nose to brain administration and topical ophthalmic instillation – will be discussed in detail, focusing on the barriers involved and on the advantages of the use of these nanosystems to successfully deliver hydrophilic and lipophilic molecules with target action.

1.2 Lipid-based Drug Delivery Systems

Aiming to improve drug bioavailability, overcoming its limits and bypassing the physiological barriers to reach the target site, different types of drug delivery systems (DDS) were developed. Among them, lipid-based drug delivery systems are being extensively investigated by the researchers, because of their great advantages, especially for being biocompatible and biodegradable[16]. Moreover, other advantages include their high encapsulation efficiency, the capability to provide a controlled drug release, the possibility to encapsulate lipophilic or hydrophilic molecules, their versatility[17].

Lipid-based drug delivery systems could be classified as reported in Figure 1[17].

_____
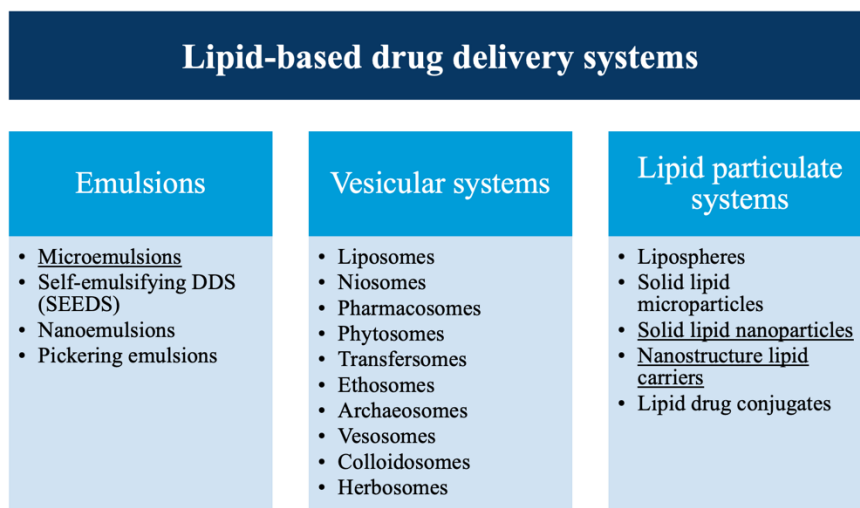
Figure 1. Classification of lipid-based drug delivery systems. The ones investigated in this PhD project are underlined.

The DDS of interest for this thesis are: microemulsions, solid lipid nanoparticles (SLN) and NLC, that will be discussed in terms of their general features.

It will follow a synthetic description of the rationale behind the main characterization studies performed in the framework of this project.

1.2.1 Microemulsions

An emulsion can be defined as a dispersion of two immiscible liquids stabilized by the presence of surfactants[18]. Considering the droplet size, emulsions are classified as macroemulsions (>400 nm), nanoemulsions (200-400 nm) and microemulsions (< 200 nm)[19], while, depending on the external phase, biphasic emulsions are divided in water-in-oil (W/O) and oil-in-water (O/W)[20] (Figure 2). For their composition, the system is regulated by a fine equilibrium between two opposed forces, surface energy and entropy: increasing the number of droplets causes an increased entropy, and also causes an increased surface energy[20]. For this reason, slight changes in the composition could affect the balance of the system and thus its characteristics. As mentioned above, the role of the surfactant is to lower the interfacial tension and decrease the free energy of the system[21], thus it influences the structure of each drop, their curvature and rigidity[22,23]. Therefore, the mixture of surfactants have to be carefully selected, basing on Griffin's hydrophilic lipophilic balance (HLB)[24], which is 2-7 for hydrophilic emulsifiers and 6-16 for lipophilic emulsifiers[25], and also on Bancroft rule, which states "a hydrophile colloid will tend to make water the dispersing phase while a hydrophobic colloid will tend to make water the dispersed phase"[26].

_____

Due to their structure, microemulsions are able to deliver hydrophilic or lipophilic drugs, or also both at the same time, overcoming drug solubility issues and thus making these systems versatile in their application. Moreover, the presence of high amounts of emulsifiers and the high contact area with the administration site guarantee a high interaction with the tissues thus enhancing the absorption of the loaded drugs[22]; on the other hand, it could also be a disadvantage, since surfactants could be toxic over certain concentrations[27]. Additional advantages are the ability of the inner phase to act as a reservoir, producing a prolonged absorption[18], the easiness of the preparation method, which allows scalability, and the biocompatibility, that is related to the materials used.

Considering the challenging delivery of hydrophilic molecules, W/O microemulsions represent a successful strategy to overcome solubility problems, even if some disadvantages, such as lipid oxidation, could limit their therapeutical application[28].
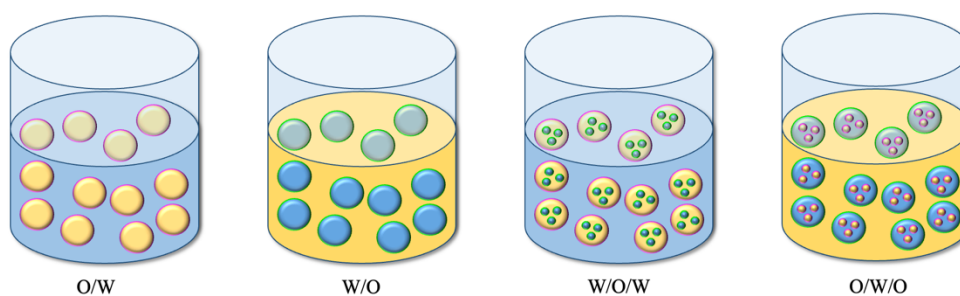
Figure 2. Schematic representation of emulsion types. In yellow is represented the oily phase, and in blue the aqueous phase. The surfactants are represented in green (HLB 2-7) and in pink (HLB 6-16).

More innovative systems as the multiple or double emulsions were developed, performing a further inversion of the double emulsion into an external phase. There are two types of multiple emulsions, water-in-oil-in-water (W/O/W) and oil-in-water-in-oil (O/W/O), where the inner and the outer phase could also be different[29] (Figure 2). A critical step in the development of a multiple emulsion is the choice of the surfactants, since appropriate lipophilic and hydrophilic emulsifiers are needed[30]. Multiple W/O/W emulsions, in particular, result to be promising since they are able to overcome the degradation risk of the W/O external oil; moreover, they can deliver hydrophilic molecules in the inner water phase, and eventually also a lipophilic drug in the oily middle phase[30].

Administering heat or stirring energy to overcome the interfacial tension of the raw materials (which is lowered by the presence of surfactants), microemulsions could form with a low-cost and low-energy preparation method[27].

Instability phenomena affecting the microemulsions are:

_____

- Coalescence: occurs when droplets merge together and affects mainly the inner water phase[30].

- Sedimentation: it is the separation of aqueous and oily phases; following the Stokes law, an increase in the amount of the inner phase causes an increased viscosity, which stabilizes the system[31].

- Creaming: is the irreversible breaking of the interface between the phases; it could be avoided through the increase of the density and the decrease of the droplet size[31].

- Flocculation: occurs when electrostatic repulsive forces are overpowered by Van der Waals interactions[32], thus causing the merging of droplets; it could be promoted by an excessive amount of surfactant.

- Ostwald ripening: consists in the merging of small droplets into the bigger ones, which, in final extreme conditions, could lead to a phase inversion[33].

1.2.2 Solid lipid nanoparticles and Nanostructured lipid carriers

Solid lipid nanoparticles (SLN) were known as lipospheres[34] and were firstly defined by Müller and Lucks in a patent about thirty years ago[35]. SLN are characterized by the presence of a core constituted of solid lipids at room temperature, surrounded by surfactants in order to emulsify the colloidal dispersion in the aqueous external phase. The production of SLN needs the addition of energy to the system, since they are not able to form spontaneously; for this reason, they could be subjected to instability phenomena, and certain strategies are required to prevent the aggregation processes, such as electrostatic stabilization[36–38].

Considering the different possibility for drug localization into the lipid core, three structures can be identified (Figure 3). The homogeneous matrix model (type I) occurs when the drug is homogeneously dissolved into the lipid matrix and could be obtained both with high-pressure homogenization and hot homogenization. When using the hot homogenization method, a drug-enriched shell model structure (type II) could be obtained, in case that the lipid core precipitates sooner, and the drug locates in an outer shell; type II SLN provide an immediate release of the drug. Finally, drug-enriched core model (type III) is obtained when the concentration of the drug in the lipid is almost reaching the saturation, so it precipitates forming an inner drug-rich shell, surrounded by the lipid which is able to provide a slow and prolonged release of the encapsulated drug[39].

Depending on the materials used, these nanoparticles could be highly biocompatible and versatile. Other advantages are the improvement of drug absorption and the targeted delivery; on the counterpart, the rigid structure of the SLN could decrease drug loading and promote drug expulsion during the storage[34].

_____
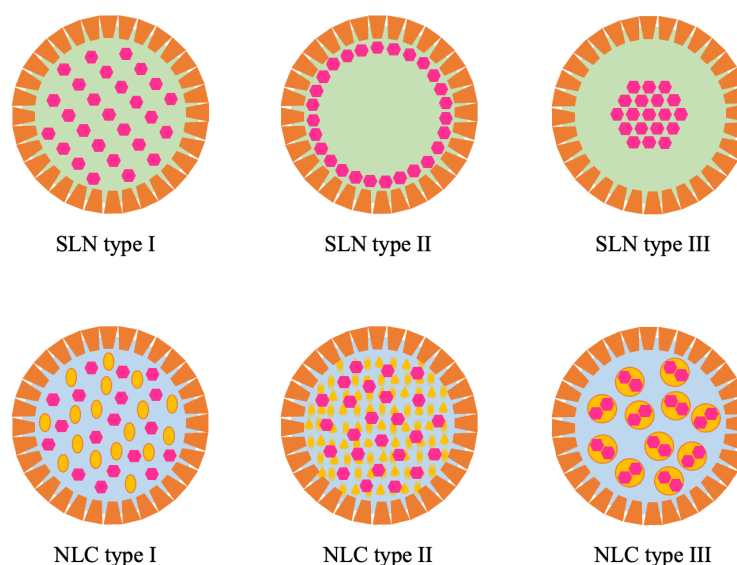
Figure 3. Schematic representation of SLN and NLC structures. In orange is represented the surfactants corona, in yellow the liquid lipid, in pink the drug.

Nanostructured lipid carriers (NLC) were proposed to overcome these limitations of SLN, by introducing in the core structure a liquid lipid at room temperature, thus forming more imperfect structures which are able to incorporate higher amounts of drug. Moreover, this composition of the core guarantees a certain rearrangement of the particle matrix thus reducing drug loss during storage, with the consequent improvement of their physical stability[39].

Depending on the selection of the lipids, different NLC structures could be obtained (Figure 3). Mixing different chain length lipids or mono-, di- and triglycerides, an imperfect crystal structure (type I) is obtained, which is associated with the higher drug encapsulation among NLC. The use of medium chain length lipids and solid lipids promotes the formation of amorphous cores (type II), but, since the solid lipid does not crystallize, it reduces the occurrence of drug expulsion during storage, compared to SLN. Finally, multiple type cores (type III) could be obtained by mixing a solid lipid with oils or medium/long chain triacylglycerols, with the oil being used at amount lower than its solubility in the solid lipid, in order to create oil nano-compartments inside the core.

Both SLN and NLC have particle size between 40 nm and 1000 nm[40], even if it was demonstrated that, using the same amount and type of surfactants, the same amount of total lipids and the same preparation method, SLN could present a mean particle diameter greater that NLC (297 nm vs. 210 nm)[41]. Among the various production methods suitable to obtain SLN and NLC, the phase inversion temperature (PIT) method has the great advantage of being eco-sustainable. Briefly, the lipidizc and aqueous phases are separately heated over

___

their transition temperature (until about 90°C); then, the aqueous phase is added dropwise to the lipidic phase under constant stirring, and finally the system is left to cool until room temperature obtaining the phase inversion[42]. This method has aroused great interest among researchers for being an organic solvent-free and low energy technique, thus potentially decreasing the ecological impact in the event of an industrial scale-up[43]; at the same time, the produced nanoparticles maintain optimal features in terms of size and homogeneity[44]. Among the instability phenomena affecting SLN and NLC, nanoparticles have a certain tendence to fuse, especially if they are very small, thus inducing the loss of the encapsulated drug. Different strategies have been proposed to overcome thus drawback, such as the addition of a PEG coating or charged coating[43], that will be discussed afterwards.

1.2.3 DDS characterization

1.2.3.1 Particle size and polydispersity index

One of the main features that should be assessed for lipid-based nanosystems is mean particle (or droplet) size, defined as Z-Ave. This parameter is crucial in determining the fate of the nanosystem after the administration. First of all, it determines if the carrier is able to be absorbed, depending on the specific features of the administration route. For instance, in pulmonary drug delivery the particle size has the significant role of determining which pulmonary region can be reached[45], and it is also restrictive in drug delivery to the brain through the Blood Brain Barrier (BBB) or to the deeper skin layers through transdermal delivery[46,47]. A wider size range could be accepted for ocular administration, with an optimal 50-150 nm size to achieve the inner eye[48], while for nasal administration, a wider range is able to provide epithelial adsorption, from 65 to 300 nm[49]; in general, smaller particles result to be better tolerated[50].

Furthermore, after being absorbed, nanoparticles should arrive to the target site and interact with the cells, which are also crucial steps in determining the success of the developed carriers. In fact, usually nanoparticles cellular uptake occurs by endocytosis: it was found an optimal size of 50 nm even if it strongly depends on the type of cells considered and on eventual surface modifications[51,52].

Finally, particle size was defined as "critical quality attributes (CQAs)" FDA's "Guidance for Industry" referring to liposomes[53].

Particle size is usually measured by Photon Correlation Spectroscopy (PCS), also named Dynamic Light Scattering (DLS). It is based on the measurement of the intensity of the scattered angle that a light ray undergoes after passing through a particles' dispersion. The scattering is measured in function of time, since, depending on the Brownian motions, small

___

particles move faster while big particles move slower, thus differently affecting the intensity of the scattering[54].

The same instrument also allows the measurement of the polydispersity index (PDI), a parameter which describes the size distribution thus providing information about the homogeneity of the samples. Its values could range from 0.0 (which means that the sample is a perfect mono-dispersion) to 1.0 (for highly multi-dispersed samples). For lipid nanoparticles, the carrier could be considered acceptably homogeneous if PDI value is above 0.3[50].

1.2.3.2 Zeta Potential

Zeta Potential (ZP) gives a quantification of the superficial charge of the nanoparticles and is measured by electrophoresis light scattering (ELS). Through the application of an electric field in the sample, nanoparticles move towards the electrodes with opposite charge, and their charge will determine the rapidity[55]. Thus, this instrument is able to measure the difference between the electric potential on the nanoparticles surface and the one of the solution where they are dispersed[56], giving information about particles' superficial charge. ZP measurement is fundamental because it allows to predict the stability of the sample. In fact, aggregation could be a consequence of particles interaction[57], and, for this reason, markedly positive or negative charge (> ±30 mV) provides electrostatic repulsions that could prevent the occurrence of aggregation, coagulation and flocculation[58]. This analysis gives general information about stability, that needs to be properly assessed through specific methods (as furtherly discussed).

Furthermore, ZP influences cellular uptake, since membranes glycosaminoglycans are negatively charged; for this reason, cationic nanoparticles could strongly interact through electrostatic attraction, thus being highly internalized into cells. Tumoral cells show even more negatively charged surface for their ability to translocate negative components on their membranes. On the other hand, negatively charged nanoparticles could be non-specifically internalized or could interact with the cationic domains present on the cell membranes. Considering the different cell target, ZP should be appropriately optimized in order to favor cellular uptake[55].

Since cellular surface is usually negatively charged, ZP could actually influence nanoparticle absorption depending on the administration route. Skin drug delivery, for example, requires cationic nanoparticles due to the presence of phosphatidyl choline[55], as well as nasal mucosal or ocular delivery due to the presence of the negatively charged mucin on the mucosae[59,60]. Brain targeting also involves electrostatic interactions with negative residues in order to penetrate using the adsorptive mediated endocytosis[61].

_____

Actually, in the design of a drug carrier, it is also mandatory to take into account the cytocompatibility of the carrier. In fact, in literature it has been extensively reported that cationic additives could be more cytotoxic, thus compromising the effective therapeutic use of cationic particles[62]. As reported by Wei[63], cationic liposomes caused cell depolarization followed by a charge-dependent necrosis. As they reach the bloodstream, cationic nanoparticles could cause hemolysis by interaction with blood components[64]; moreover, cationic particles are susceptible to macrophages clearance which reduces their availability and increases liver accumulation[65].

1.2.3.3 pH

pH describes the concentration of H^+ ions in a solution and it is finely balanced in the human body, with specific tolerated ranges for each organ, in order to maintain the integrity of the tissues and the functionality of the enzymes[66]. The presence of buffers in the body allows to guarantee this balance, and values of pH outside of the physiological range are usually symptoms of pathologic states. The so-called "physiological pH" is referred to the blood pH, which goes from 7.36 to 7.42[67], which is similar to the interstitial fluids' pH range (7.35-7.45)[66]; a slight change in blood pH of 0.2 could determine death for acidosis or alkalosis[68]. pH of saliva is about 6.7, helping to protect from various diseases and inflammation, and to avoid teeth damage[69]. Gastrointestinal pH values differ depending on the region, since it has a role in the digestive process. An empty stomach has about a 1-1.5 pH, and this value is neutralized by the bile during digestion; if this equilibrium is altered, inefficient digestion, microbial infections or ulcers could occur[66,67]. Lungs have a neutral pH which could change in presence of pathologic conditions such as cystic fibrosis or infections[70]. Acidic pH values are physiological in skin (4-6.5) and vagina (4), having the role of protecting from environmental pathogens[67]. Similar pH values are physiological for nasal mucosa (4.5–6.5): even if a wide range of values is tolerated[71], pH should not be lower than 3 or higher them 10 to avoid irritations[72]. Eye physiological pH is the one of tears (7.11 ± 1.5), and liquid preparations for ophthalmic instillation are required – from European Pharmacopoeia and FDA – to have pH between 6.8 and 7.4[73]; in fact, pH should be finely balanced to avoid ocular chemical damage, which could occur with values of pH<4 or pH>10[74]. Taking into accounts the administration route, pH value of the formulation has to be evaluated, in order to fall within the tolerated range for the intended organ.

_____

_____

1.2.3.4   Osmolality

Osmolality is the parameter which quantify the milliosmoles of solutes per liter or per kilogram, and is proportional to the osmotic pressure[75]. This parameter has a great importance since determines the cell volume and could affect cells growth and metabolic activity[76,77]. In fact, hyperosmotic conditions suggested to cause DNA damage in B cells, promoting apoptosis[78], and to reduce energy and promote lactate accumulation in muscles[79]. On hepatic cells, it was reported protein breakdown in hypoosmotic situations and proteolysis in hyperosmotic ones[80]. Aiming to not unbalance the osmotic pressure of the cells after the administration of the drug delivery system, osmolality value should be properly optimized to guarantee the safety of the formulation. In particular, the eye is able to tolerate osmolality values from 200 to 500 mOsm/Kg, even if the optimal range is the tears' one, between 280 and 300 mOsm/Kg[81]. Also for nasal administration, osmolality is an important parameter to be optimized, since isotonic formulations are able to inhibit ciliary activity[72], while hypotonic samples (300-700 mOsm/Kg) can increase permeation through nasal mucosa[82].

1.2.3.5   Stability

Colloidal suspensions of nanoparticles could be subjected to various kind of instability phenomena, which compromise their long-term use. Among them, sedimentation occurs when nanoparticles move to the bottom of their storage container, and it depends on particle size, viscosity and density, following Stokes' law[83]. Flocculation, which describes the tendency of the nanoparticle to agglomerate, determines the sedimentation rate, which is slow for deflocculated suspensions and rapid for flocculate ones. Usually, sediments are easily redispersed by simple agitation, but, if the particles are very tightly agglomerated, the resuspension is difficult, and it is defined as caking. Agglomeration is another important instability phenomenon which reflects the tendency of the nanoparticles to minimize the thermodynamic energy by merging thus reducing the surface energy[83]. Analyzing the long-term stability of colloidal suspensions represents an important prerequisite to assure the maintaining of their characteristic features over time.

The stability of the formulations can be analyzed following the ICH guidelines Q1A (R2), that describes the stability testing required from EMA (European Medicines Agency) for the new drug substances and products. Three storage conditions are identified:

- long-term: minimum 12 months at 25±2°C with 60±5% RH;
- intermediate: minimum 6 months at 30±2°C with 65±5% RH;
- accelerated: minimum 6 months at 40±2°C with 75±5% RH.

_____

_____

Testing frequency is also described for each situation – it is usually every 3 or 6 months, depending on the intended storage time– as well as the criteria for the evaluation. At each timepoint, nanoparticles characterization should be performed in order to verify the occurrence of instability phenomena. For this aim, PCS analysis of particle size is suitable to highlight the occurrence of agglomeration[84]. This kind of analysis could be performed by storing the samples in constant climate chambers, with the proper setting according to the desired type of temperature and humidity conditions. Moreover, optical analyzers are available in commerce and allow to visualize the instability phenomena by scanning the entire cuvette with a pulsed near-infrared light, thus being able to highlight the occurrence of particles migration or aggregation[85].

1.2.3.6 *Transmission electron microscopy*

Morphology and structural organization of the nanoparticles – which also influence their functions[86] – could be assessed through different microscopy techniques, and, among them, also Transmission electron microscopy (TEM) could be used. Images of the nanoparticles are obtained through an electron beam passing through the sample; the part of the beam that is not scattered or absorbed, is transmitted and creates the image of the particle[86]. In order to be analyzed through this technique, the sample should be very thin.

Cryo-TEM, which was successively developed, allows to visualize also the inner structure of the nanoparticles, providing detailed information about the core and thus allowing to classify the nanoparticles' type (as previously explained for SLN and NLC classifications)[84,85].

Furthermore, these techniques allow a direct measurement of particles diameters, corroborating the data obtainable from PCS studies[85].

1.2.3.7 *Differential scanning calorimetry*

Differential scanning calorimetry (DSC) is a technique used to characterize the structural changes in materials under thermal stress. Progressively adding heat, the instrument registers the heat of the sample compared to the heat of the system, basing on the principle that a difference in heat occurs during phase transitions[87]. In that way, it is possible to obtain a thermogram relating the energy of the sample in function of time or temperature. In lipid-based nanoparticles, DSC analysis provides information about the behaviors of raw materials after nanoparticles formation, through the assessment of polymorphic state and crystallinity[88], allowing also the differentiation between SLN and NLC through the analysis of eventual temperature shifts at the melting points[89]. Crystallinity, in particular, is also helpful to understand the organization of the nanoparticles, and thus predicting the

_____

encapsulation efficiency and release of the loaded active compound, which is related to the presence of imperfections in the core[88]. Moreover, the success of the encapsulation could be verified, since the comparison of the thermograms of blank and loaded samples is able to show if the drug is solubilized inside the core or if it is crystallized[89,90]. Furthermore, it is important because the properties of lipid materials could be affected by temperature changes: obtaining information about the temperatures of the melting and crystallization transitions could be useful to assess the suitability of some preparation methods which need heating steps[88].

1.2.3.8 Fourier transform infrared spectroscopy

Fourier transform infrared (FTIR) spectroscopy allows to measure the vibrations and rotations of molecular binding. The intensity of the IR radiation passing through the sample at different wavelengths is measured and reported in a spectrum, which correlate the absorbance or transmittance of the radiation at the respective wavenumber. Considering that certain molecular groups have specifics absorption/transmission wavelength, it is possible to obtain information about molecular binding changes[91]. For nanocarriers, this information could highlight – for instance – the behavior of the raw materials in the organization of the nanoparticles[44] and the eventual formation of new binding during the preparation process.

1.2.3.9 X-ray diffraction

X-ray diffraction (XRD) allows to analyze the organization of the molecules, thus providing information about their physical state or polymorphic form[92]. Moreover, it permits the measurement of the crystallinity of the sample, which is related to polymorphism, thus allowing to predict the occurrence of transitional changes during storage[93]. Usually, considering lipid-based DDS, the crystallinity is related to the liquid oil structure[94]. Moreover, it is possible to obtain information about the long-range and short-range lipid conformation, which is informative of the organization of the components in the nanoparticles[95].

1.2.3.10 Raman

Raman is a technique able to give information about the conformation and arrangement of the components into the nanoparticles, basing on the analysis of the electromagnetic spectrum. In particular, a laser beam passing through produces molecular vibrations, which constitute the "molecular footprint" and, considering the wave number of the peaks, provide information about the functional groups presents[86,93]. This analysis allows to understand the structure of the external layer of the nanoparticles[85].

_____

1.2.3.11 Encapsulation efficiency and drug loading capacity

The quantification of the effective amount of drug that could be encapsulated into the nanoparticles is a relevant parameter to measure, in order to make proper assumption about the maximum amount of molecule that the system could actually host, the release of the drug from the carrier and eventual *in vitro* and *in vivo* subsequent evaluation of the drug behavior. This parameter is strictly related to the nature of the drug and its compatibility with the lipid matrix of the nanoparticles[96]. Since a direct quantification is usually difficult to perform, indirect method can be used measuring the unencapsulated drug and subtracting from the total amount of drug weighted in the preparation step. The separation of the unencapsulated drug from the nanoparticles could be performed by tangential flow filtration, dialysis or ultracentrifugation, depending on the specific characteristic of the colloidal suspension.

The encapsulation efficiency (EE%) is thus defined as the ratio between the amount of the encapsulated drug (indirectly measured) and the amount of weighted drug, expressed as percentage value[84]. The EE% of drugs into SLN is usually lower than those into NLC, due to the presence of a more ordered structure, as previously discusses, with values usually in the range from 57-67%[97], as reported in literature. NLC EE% results to be usually higher because of the presence of imperfections in the nanoparticles' structure, which allows the accommodation of higher amount of drug, with literature data raging from 57-67%[98,99] up to 98.5%[100]. Considering lipid-based nanoparticles, drug loading capacity (DLC%) could also be calculated, as the measure of the amount of entrapped drug related to the weight of the lipid material and expressed as a percentage[84].

1.2.3.12 Drug release

Drug release from the nanoparticle is a relevant feature which provides information about the carrier behavior, thus defining its efficacy[101]. One of the most common methods is the dialysis bag technique, which could be regular and reverse. The regular method consists in placing the sample into the dialysis tube, which is immersed into the release medium; at selected timepoints, the amount of drug in the external medium is measured. In this method, the stirring results to be a crucial parameter to be properly set; moreover, also the surface of the dialysis bag and the volume of the sample inside are relevant in determining the release rate, and sometimes sink condition could not be guaranteed[102]. The reverse dialysis method consists in putting the release medium inside the tube and immerging it into the sample; the withdrawals could be performed by removing the whole tube and replacing it, or by opening it to take a certain volume of release medium. Considering the surface of the membrane, these dialysis methods seem to be more appropriated for intravenous

_____

administration. Another technique for *in vitro* release studies[103], especially used for topical and transdermal applications, involves the use of Franz diffusion cells, which were developed in 1975 and could be employed also for the assessment of *ex-vivo* permeation through skin[104]. They are composed by a donor, where is located the formulation, and a receptor, where there is the release medium, which are separated by a barrier; both synthetic membranes (cellulose acetate or regenerated cellulose) and human/animal skin could be employed[104]. The system could be subjected to stirring and/or heating. The withdrawals are taken from the sampling at specific timepoints and the amount of drug in the release medium is quantified properly[104].

For all the aforementioned techniques, some key parameters need to be adequately modulated. First of all, the release medium should be selected considering the solubility and the stability of the drug and also maintaining the sink condition for an accurate analysis[101]. Furthermore, the membrane molecular weight cut-off should be chosen basing on the drug[84]. Finally, the stirring rate in the external medium should be selected in order to properly homogenize system. The release of the drug from nanosystems is related to several factors, such as the drug entrapment efficiency and the carrier structure. It is also important, during the preformulative phase, to verify the solubility of the drug into the matrix[105]. The choice of the materials was demonstrated to be crucial[106,107], especially liquid lipid percentage and surfactant concentration[108]. Considering SLN and NLC in particular, a high solubility of the drug into the lipid matrix corresponds to a higher amount of encapsulated drug, which may result in higher amount of drug released[105]. Moreover, their crystallinity (thus the presence of imperfections) and their polymorphism could influence drug release, since ordered structures promote lower encapsulated drug and higher drug loss during storage[105,107].

The localization of the drug into the nanoparticle determines the rapidity of the release from the nanosystem[106], since usually drug is released from nanoparticles through two mechanisms: erosion and disruption of the matrix, or diffusion through the matrix[109]. Generally, both SLN and NLC show a biphasic release pattern, constituted by an initial burst effect, followed by a prolonged release. The initial burst effect could be related to the presence of drug on nanoparticles' surface, that in NLC is attributable to the presence of liquid lipid at the outermost part of the nanoparticles[110]; this burst phase is also affected by the solubility of the drug into the external aqueous medium, and could be modulated by varying the temperature or the surfactant concentrations during the preparation (raising these values results in reduced burst effect)[111].

_____

The presence of surface modification could also affect drug release, as reported for PEG which reduces the surface tension of the lipid nanoparticle, thus usually increasing the release rate[112,113]. Furthermore, also the particle size influences the release, since smaller particles possess higher surface area which result in faster release[108].

The size-release correlation was also demonstrated for emulsions[114], which could provide both a biphasic release with an initial burst affect[115] and a zero-order slow and prolonged release[116], basing on the type of emulsion (W/O, O/W, or multiple) and on the materials involved – mainly surfactants[115].

1.3 Nasal mucosal delivery

1.3.1 Anatomy of the nose and nasal administration

The inner nose is composed by the septum that separates the two nostrils, in which is possible to identify the turbinates. The nasal cavity is composed by three parts (Figure 4), which are reported from the outer to the inner: vestibular region, respiratory region and olfactory region. The vestibular region is responsible of the blockage towards external agents such as pathogens and particles; in the respiratory region there are blood vessels and the trigeminal sensory nerve; in the olfactory region there are branch of the trigeminal nerve, and the olfactory sensory neurons which are in direct contact with the brain[117]. Epithelial cells, connected through tight junctions, could be classified into: columnar cells with microvilli (70%); ciliated cells responsible of mucociliary clearance (20-50%); goblet cells producing mucus (5-15%). The mucus is mainly composed of water (95%), but also of mucin (2-3%) and salts (1-2%)[118], with a pH of 5.5-6.5 and a negative charge attributable to the presence of sialic and sulfonic acids[119]. The role of the mucus is to create a defense from undesired external agents, antimicrobial, humidifying and filtering activity[120]. The mucus has the ability to interact with particles through Van der Waals, electrostatic and hydrophobic interactions[120], and to block particles with size higher than 1 μm[121]. Moreover, mucociliary clearance mechanism is able to move the daily 1.5-2 L of mucus with a speed of about 6 mm/min, thus further reducing the contact time of a nasal administered drug[120]. Mucus production and mucociliary clearance could be altered in the presence of pathologic conditions as rhinitis, sinusitis, asthma, or allergies[122,123]. Another nasal defense mechanism is performed by immune cells which are highly present in sub-epithelial tissue and belong to the nasal associated lymphoid tissue (NALT). B cells, T cells, macrophages, dendritic cells and antigen presenting cells are the most present[124], and, in case of necessity, other immunocompetent cells, such as natural killer cells, could provide support[125].

_____
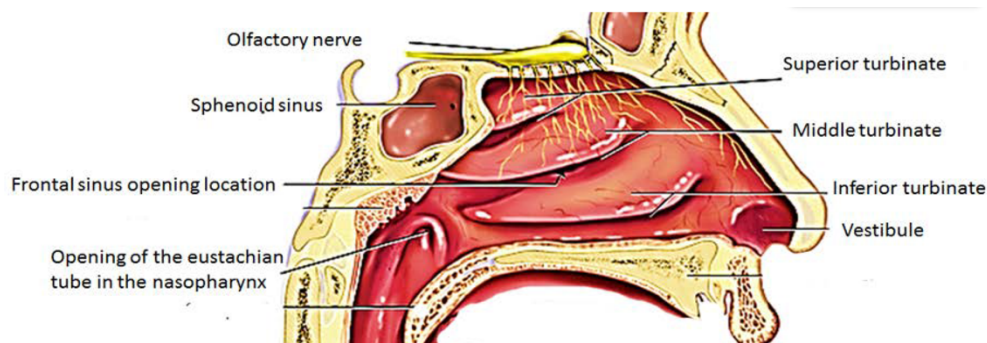
***Figure 4**. Structure of the nose[126].*

Drugs nasally administered could be absorbed through four different routes: transcellular (low-weight lipophilic molecules), paracellular (small hydrophilic molecules of < 100-200 Da), receptor mediated, and carrier mediated[127,128].

Limits of this administration route are primarily related to the nature of the active molecule (hydrophilicity-lipophilicity, molecular weight[128]) and to the several defense mechanisms already mentioned. Moreover, even if nasal mucosa is quite porous and has a large absorption surface[129], considering the small area of the nasal cavity (~7 cm^3 young-adult men and almost 6 cm^3 for young-adult-women[130], only an amount of 25-200 μL could actually be administered, because higher amounts could increase side effects related to the systemic diffusion[131]. On the other hands, this route results advantageous for being needle-free, not-invasive and highly patient compliance[132].

1.3.2 Vaccine delivery and DDS

For its physiological immune role, nasal mucosal has been consistently investigated for the administration of vaccines because it is able to induce mucosal and systemic immune responses[128]. Moreover, nasal mucosal administration could avoid systemic routes limits, such as invasiveness, risk of infection, need of specialized personnel, but also oral administration drawbacks, like enzymatic and gastric degradation[124]. Nowadays, some nasal vaccines are already used in clinic, but there are still some limitations to be overcome. In particular, the inefficient bioavailability of the vaccine due to the mucociliary clearance, as well as the low permeation into the nasal epithelium[132]. For this purpose, different delivery platforms have been developed, showing promising results. First of all, nanoparticles with adequate features are able to improve retention time thus limiting the clearance elimination; moreover, due to their longer interaction in the reactive site, they were reported to enhance immune response[133], and, modulating carrier properties, could selectively target M cells or reach the lymph nodes[124]. Clearly, the encapsulation into DDS protects the active compound and could allow multi-vaccine administration.

Among the lipid-based nanoparticles which were developed for vaccine delivery, also some can be found in literature. Nanoemulsions were used to load hepatitis B antigen, showing promising results in various mice models by inducing an immune response comparable to the one induced by intramuscular vaccination[134]. Moreover, a developed soybean O/W nanoemulsion demonstrated to be absorbed through transcellular pathway, without needing to open the tight junctions or to require M cells[135]. It is important to mention the versatility of emulsions for vaccine delivery, since, by opportunely changing their composition (both qualitative and/or quantitative) it is possible to activate specific immune responses[136].

1.4 Brain delivery

1.4.1 Central Nervous System barriers

The treatment of central pathologies has always been challenging due to the intrinsic difficulty to achieve the Central Nervous System (CNS) for the presence of several physiological barriers. Among all, the most important barrier is the Blood Brain Barrier (BBB), which prevents the diffusion of molecules in the brain and maintains the homeostasis[137], blocking more that 98% of the therapeutic molecules[138]. It is composed of microvascular endothelial cells continuous to the cerebral capillaries, which presents three peculiar characteristics (Figure 5): the fenestrations are not present; there are tight junctions which prevent the unregulated passage of polar compounds from the blood; the absence of pinocytosis and the presence of specific active transporters able to deliver essential substances while blocking potentially damaging molecules[139]. Moreover, there are efflux transporters and metabolic enzymes belonging to the CYP 450 family[137]. All these obstacles prevent the achieving of the brain for the majority of the drugs[140]. In the occurrence of some physiological or pathological situations, the BBB could be altered thus decreasing its filtering ability[141]. The available treatments are invasive and costly or are considered effective despite being associated with side effects that decrease patient compliance[120].
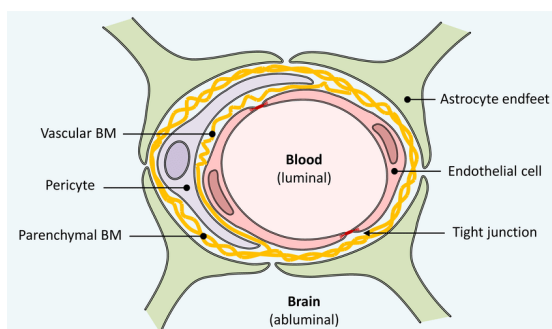
Figure 5. Structure of the BBB[142].

1.4.2 Nose-to-brain administration and DDS

A successful strategy to achieve the brain is represented by the nose-to-brain (N2B) administration, which provides a direct access to the CNS while avoiding the BBB filter. This results in a higher bioavailability of the drug, avoiding gastrointestinal or systemic metabolism, and in reduced side effects[143].

Anatomy of the nose was already described in the previous section. The vestibular region, as already mentioned, acts as a filter for the external substances, thanks to the presence of nasal mucus and mucociliary clearance mechanism. Once overcame this first part, an intranasally administered drug could follow two direct pathways in its way to the brain: the olfactory one and the trigeminal one. The olfactory pathway involves the interaction with the olfactory receptors, while the trigeminal pathway involves the branches that arrive to the respiratory mucosa and olfactory mucosa. In both the pathways the formulation could be transported intraneuronally through the axons or extraneuronally thanks to diffusion and channel flow[144,145]. A N2B administered formulation could also reach the brain through the systemic indirect pathway, since the respiratory region is extensively irrorated with blood vessels, thus small lipophilic drugs can diffuse in the blood stream, even if they will face the limitations of the BBB and produce side effects.

On the counterpart, N2B administration presents the limits related to the physiological structure of the nose, as previously discussed. Furthermore, the efficacy of N2B route is strictly related to the device and to patient's administration, intended as angle of administration and respiration[143]. Finally, cytocompatibility of the administered formulations should be extensively analyzed since central pathologies usually require multiple or chronic treatments, thus long-term toxicity should not occur[143].

1.4.3 Drug Delivery Systems for N2B administration

In order to overcome N2B limitations, different nanocarriers have been proposed and due to their high biocompatibility, lipid-based nanosystems were the extensively studied. Among their advantages, they could protect the drug from degradation and transporters, and produce reduced cytotoxicity; moreover, depending on their features, they are able to prolong the residence time, permeation into the nasal mucosa, and more targeted delivery reducing side effects[120].

In order to provide a successful drug delivery from DDS using N2B route, the nanoparticles should be developed with specific characteristics. One of the most important features is particle size, which also affects other parameters such as encapsulation efficiency, drug release and physical stability; moreover, it determines the biodistribution of the

nanoparticles, defining the deposition in the anterior part of the nasal cavity or in the olfactory zone[146], also depending on retention time and targeting ability[147]. Zeta potential should be also properly optimized, since mucin has anionic residues, thus positively charged nanoparticles guarantee prolonged mucosal retention time. On the counterpart, cationic nanoparticles were reported to cause cytotoxicity by disruption of the BBB, effect that was not reported for neutral and anionic nanoparticles[148].

Numerous examples of the use of lipid-based nanoparticles for the treatment of CNS disorders can be found in literature. SLN were used to encapsulate a conjugate prodrug (based on geraniol and ursodeoxycholic acid) for Parkinson's disease (PD); the intranasal administration of the SLN formulation in rats provided higher cerebrospinal fluid (CSF) levels, compared to the prodrug suspension, and also guaranteed a longer retainment in the brain compared to oral administered geraniol[149]. SLN loaded with efavirenz were intranasally administered in rats and compared with the market-available oral capsules: the nanoparticles demonstrated to be able to increase 150 times the brain targeting and 70 times the absorption potential compared to the marketed formulations[150]. High brain targeting was also reported for NLC loaded with ketoconazole, after intranasal administration in an infection mouse model[151], as well as demonstrated for NLC loaded with pioglitazone as a repurposed treatment for Alzheimer's Disease (AD)[152]. Sumatriptan-loaded NLC were investigated for the treatment of migraine headache and, also in this study, it emerged that intranasal administration route was able to provide a 4-fold higher drug level in the brain, compared to intravenous administration[153].

1.4.4 Essential oils in the treatment of neurodegenerative diseases

Essential Oils (EOs) have been known for their therapeutics properties since the Egyptians[154], but in the last decades scientists found a rediscovered interest for their potential application as adjuvant treatment in several pathologies. About one century ago, in 1928, Rene-Maurice Gattefossé invented the term "Aromatherapie" to indicate the therapeutical practice of the inhalation of EOs, and several countries, such as France, UK, USA and Australia, include aromatherapy as complementary medicine in association with conventional treatments[155]. More recently, the effect of EOs on the central nervous system was demonstrated[156] and numerous are the pathologies for which they are effective.

Inhibition of acetylcholinesterase activity is one of the most important parameters analyzed in the diagnosis of Alzheimer's disease (AD), and several EO have been studied[157]. Just to mention some EO studied for AD, *Artemisia annua* L. and *Glycyrrhiza glabra* L.[158], as well as *Allium tuncelianum*[159], *Citrus sinensis* [L.] Osbeck[160], *Lavandula viridis* L'Her[161], *Mentha spicata* L.[162], *Origanum rotundifolium* Boiss.[163], *Panax ginseng*[164],

Salvia officinalis[165] demonstrated to inhibit acetylcholinesterase activity *in vitro*. Moreover, *in vivo* studies demonstrated that *Boswellia serrata* improves learning and memory[166], *Citrus limon* prevents from synaptic loss and memory impairment[167], as well as *Ocimum basilicum* which also reduces hippocampal degeneration[168]; cognitive functions were ameliorated also by inhaled *Rosmarinus officinalis*[169] and a combined treatment with *Origanum vulgare* and *Thymus vulgaris* showed *in vivo* success for the treatment of AD[170]. Considering Parkinson's disease (PD), the target of the pharmacological studies is to delay the neurodegeneration since, in the advanced stages, there are no drugs which are efficient[157]. For this reason, EOs were studies because of their neuroprotective activity, which was demonstrated *in vitro* for *Cinnamomum verum* and *Cinnamomum cassia*[171], and also *in vivo* for *Eplingiella fruticosa*[172] and *Rosa damascena* Mill.[173]; moreover, the ability to reduce α-synuclein gene expression was reported *in vivo* for *Pulicaria undulata*[174] and *Acorus tatarinowii* Schott (Shi Chang Pu)[175].

The potential use of EOs in dementia was also demonstrated[176]. A clinical trial was carried on administering *Lavandula angustifolia* Mill. and *Melissa officinalis* L. in patient with severe dementia and demonstrating sedation in case of agitation and consolidation of memory[177]; moreover, limonene from limon EO was found to improve memory in dementia models[178].

In addition, anxious individuals have benefited from the inhalation of essential oils, potentiating the effects of current anxiolytic treatments[155]. *Lavandula angustifolia*, in particular, demonstrated to provide effects similar to diazepam[179], also reducing aggressivity and improving social interactions *in vivo*[180]. Clinical trials on the anxiolytic activity of *Lavandula angustifolia* were also carried on students experiencing anxiety during the Premenstrual Syndrome (PMS)[181], as well as in perioperative patients with local anesthesia surgeries[182] and in colonoscopy patients treated with *Osmanthus fragrans* oil and grapefruit oil[183]. *Rosa damascena* EO was useful in the first hours of labor[184], while *Lavandula angustifolia* was used in post-partum women, in which reduced also depression[185].

Despite all the beneficial effects of EOs, their use in therapy is limited by their volatility and their instability to degradation. For this reason, their encapsulation into DDS represents a successful strategy to improve their pharmacokinetic profile thus increasing their bioavailability[155].

_____

1.5 Ocular delivery

1.5.1 Anatomy of the eye

Despite seeming easily accessible, drug administration in the eye has the great limit of low bioavailability, especially related to traditional pharmaceutical dosage forms, due to the presence of several barriers and protection mechanisms[186].

The eye is composed by three structures (Figure 6), identified by the nature of the tissue: the inner layer is the retina, composed by nervous tissue (converging in the optic nerve); retina is covered by a vascular tissue, called uvea, which includes iris, ciliary body and choroid); the outer part is the sclera, which has fibrous nature. The ocular structures divide the eye into three regions: the anterior part, which is located between the cornea and the iris; the vitreous chamber, between iris and lens; the posterior segment, from the lens to the retina. To maintain ocular structures, two fluids are present: the aqueous humor, in the anterior and posterior chambers, and the vitreous humor, located in the vitreous chamber.

The movement of particles from the blood to the eye is regulated by two barriers: the blood-aqueous barrier (BAB), protecting the anterior region, and the blood-retinal barrier (BRB), which protect the retina similarly to BBB. Immune activity is provided by the BRB, and also by the presence of immunomodulatory factors in aqueous humor and parenchymal cells[187]. Because of the aforementioned barriers, systemic treatments of ocular diseases are strictly limited, with a 2% of the administered dose achieving the vitreous[188].

First protection from external agents is provided by the presence of the tears, which are produced by the lacrimal glands and are constituted of 7.0 pH water[189] with electrolytes, lipids and proteins (among them, also mucin is present as well as lysozyme)[186]. About 0.5-2.2 µl are produced every minute, and, together with blinking reflex and tears drainage (which cause the elimination of about 75% of administered drug, together with systemically absorbed drug), it limits the residence time of topically administered drugs to 1-2 min[190,191]. Furthermore, the cornea, for its characteristic structure of epithelium-stroma-epithelium expressing mucin, is able to filter the non-polar molecules basing on their oil-water partition coefficient, blocking the 90% of the hydrophilic drugs; on the other hand, lipophilic drugs are blocked only for a 10%. Drugs could permeate the cornea preferentially through transcellular pathway basing on their pKa[186]; the paracellular pathways is preferred by small hydrophilic molecules while intracellular route could be used by lipophilic drugs. For all these reasons, only a 3-5% of the topical administered drug is actually able to achieve the inner ocular tissues[192].

_____
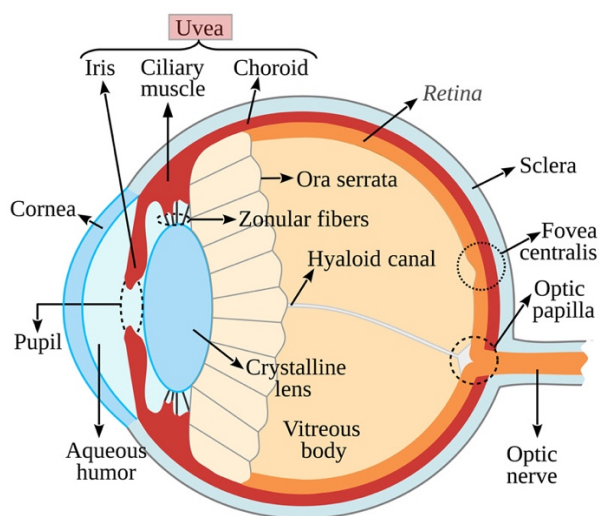
Figure 6. Structure of the eye (https://eyepatient.net/Home/articledetail/uvea-322, last accessed on the 1st September 2023).

1.5.2 Posterior chamber treatments and DDS

The achievement of the posterior segment of the eye is a great challenge for all the aforementioned limits provided by ocular barriers. Topical and systemic administrations were already described, and both provide a low amount of bioavailable drug in the posterior chamber; on the other hand, transscleral and intravitreal injections are the most effective routes for the therapeutic treatment of posterior region pathologies, but these routes require highly qualified personnel and strongly reduce patient compliance[193].

To overcome these limitations, DDS were proposed for the achievement of the inner eye through topical administration, guaranteeing several advantages, such as prolonged ocular residence time, enhanced permeation, protecting from inactivation, prolonged and controlled release of the drug from the carrier, increased patient compliance[186].

As already mentioned, lipid-based nanosystems resulted to be more biocompatible, due to the nature of the raw materials used, and to better interact with ocular structures acting as a depot[194]. In the development of DDS for the ocular site, particle size is one of the most important parameters to be optimized. In fact, ocular permeation could occur only for particles $\leq$ 200 nm[195]; very small particles ($\leq$ 20 nm), on the other side, are easily eliminated. Also zeta potential should be evaluated since mucin residues are negatively charged; as a consequence, cationic nanoparticles provide a better interaction, improving residence time on ocular surface[195].

A great number of literature studies have been published for the treatment of posterior chamber pathologies (Uveitis, Glaucoma, Retinitis Pigmentosa, Diabetic Retinopathy, Age-Related Macular Degeneration, etc.), and some of them also verified the effective achievement of the target through *in vivo* experiments[196]. Myriocin, a natural molecule possessing immunosuppressive properties, was encapsulated into NLC (with a 68% EE%) and administered in mice and rabbits, showing the ability to reach the retina with the 57% of the administered dose[197]. SLN delivering tobramycin, for the treatment of ocular infections, were tested on rabbit eyes comparing with the commercial eye drops, demonstrating a better achievement of the posterior chamber for the encapsulated drug[198]. Biodistribution studies on mice eyes were performed on NLC loaded with Nile red, showing the achievement of the retina through fluorescence analysis[199]. SLN surface modification with chitosan[200,201], clearly demonstrated an enhanced retention time because of their improved mucoadhesive properties. Liposomes are already on clinical trials for ophthalmic administration, and this raises the hope also for SLN and NLC[195].

1.5.3 Sorafenib and (±)-MRJF22 in the treatment of uveal melanoma

Uveal melanoma (UM) is the most incident intraocular tumor in adult age, with 6.3 annual incidence among white people, especially in their 60s[202]. Moreover, UM is one of the most aggressive tumors for its great capability to metastasize (in 50% of the cases within the first year), mainly in liver (89%), but also in lungs (29%), bone (17%), Skin and subcutaneous tissues (12%) and lymph nosed (11%)[203]. For this reason, the mortality rate is 80% in one year and 92% in two years from the appearance of metastasis[204].

UM occurs mainly in choroid (90% of the cases) but could also appear in ciliary body (7%) and iris (3%)[205], being circumscribed in 90% of the cases. Iris UM is usually circumscribed and easy to be early diagnosed due to its location[206], thus representing a mortality rate 5-10-folds lower than the other UM[207]. Ciliary body UM has a polymorphic shape, and it is thus more difficult to be identified because it is often hidden by the iris[208] thus it is diagnosed when it becomes bigger or involves choroid or iris. Finally, choroidal melanoma needs to be diagnosed through specific tests, causing difficult detection when it is small[209]. Predisposing factors seem to be light-colored iris [210], ocular/oculodermal melanocytosis[211], iris nevus, mutation of BAP1 (nuclear protein 1 associated with BRCA1 tumor suppressor gene). The early symptom is blurred vision, but it could be diagnosed by ultrasound in asymptomatic patients; the recent improvement in the instruments allows early diagnoses in the first stages, extending life expectancy. For these reasons, first-line treatments actually available – surgery, radiation and enucleation[212] – are aimed to be replaced by pharmacological and less invasive therapies.

The inhibition of the angiogenesis in UM patients could represent a potential strategy for UM treatment, since VEGFRs (vascular endothelial growth factor receptors) was found in higher concentrations in aqueous humor of UM patients, especially in metastatic ones[213]. Another target could also be MAPK (mitogen-activated protein kinase) pathway, which was found to be constitutively active in UM, and involved in cell proliferation[214]. Basing on these premises, the use of sorafenib (SRF) in UM therapy seemed interesting, for its multi-kinase inhibition ability, acting both on VEGFR and on Raf kinases of the MAPK pathway[214]. For these reasons, a phase I clinical trial was carried on in association with carboplatin and paclitaxel, giving encouraging results for the partial responses obtained for 27% of the patients (as performed by Flaherty in 2006 and reported by Bhatia[214]). Subsequently, a phase II trial using the same drug combination on 32 patients for 24 months showed a stabilization of the tumor in 31.2% of the patients[215]. The presence of several side effects, as diarrhea, weight loss, alopecia, etc., limits its therapeutical use, but the encapsulation into nanoparticles represents a strategy to overcome these limitations and enhance SRF activity[216–218].

Histone deacetylase (HDAC) could be another target for the treatment of cancers, since it is involved in cell growth through the regulation of gene expression; for this reason, HDAC inhibitors (HDACi), such as valproic acid (VPA), have been proposed as anticancer drugs[204]. Cell proliferation is also regulated by sigma (σ) receptors, which are overexpressed in various tumors. In particular, σ_1 receptor, involved in apoptotic process increasing the secretion of VEGF and enhancing cell motility[219], while σ_2 receptor is involved in autophagy and apoptosis[220]. Ligands for σ receptors, as haloperidol (HP) and haloperidol metabolite II (HP-mII), are potentially efficient in the treatment of UM. Basing on these considerations, a new prodrug ($\pm$)-MRJF22 was synthetized combining the HDACi activity of VPA and the σ binding of HP-mII, giving promising results in *in vitro* studies as antitumoral drug for UM treatment[219]. In detail, this prodrug and its enantiomers demonstrated the ability to reduce cells proliferation, as well as cell motility and tube formation, with a higher activity when stimulated by VEGF-A, compared to basal conditions. Among them, (*S*)-(−)-MRJF22 presented a higher binding activity that resulted in higher antiangiogenic activity compared to ($\pm$)-MRJF22 and (*R*)-(+)-MRJF22. Its loading into nanoparticles could be advantageous for both protecting the drug and achieving the target site.

1.6 Aim of the PhD project

The aim of the present PhD project was the development of nanotechnological carriers, loaded with natural or synthetical drugs, able to overcome different biological barriers, thus allowing a better achievement of the target sites. The three-years project was developed by pursuing two main sub-goals: CNS achievement through intranasal administration, and inner eye targeting through topical instillation; nasal administration was also investigated as local route for vaccines.

1.6.1 CNS targeting and nasal administration

CSN targeting, as discussed, represents a great challenge for researchers and the treatments of neurodegenerative disorders are still complicated mainly for the side effects related to drug administration. In the lasts years, there was a growing interest for complementary and alternative medicines (CAMs) as adjuvants for several pathologies. Essential oils (EOs) were deeply investigated in literature[155] since they possess a thousand-years tradition of ritual and therapeutic use; in particular, their antioxidative, anti-inflammatory, antimicrobial, wound-healing, and anxiolytic properties were extensively demonstrated by literature studies, confirming their potential use in medicine. Aromatherapy, which is the inhalation of EOs, is used since centuries, and clinical studies confirmed its success as complementary approach for Alzheimer's disease (AD) treatment[221,222]. To reduce EOs' instability, providing a targeted and controlled release and improving their effectiveness, their encapsulation into nanocarriers could be exploited. Lipid-based nanocarriers, in particular, were demonstrated to constitute a successful strategy for the loading of EOs, as demonstrated by literature description of different approaches exploited for EOs delivery, such as micro- and nanoemulsions, liposomes, SLN and NLC[155].

During the first part of the PhD project, rosemary, lavender and mint EOs were chosen to be encapsulated into NLC intended for the nose-to-brain administration as coadjuvants in the treatment of neurodegenerative pathologies[93]. *Rosmarinus officinalis* L. was selected for its ability to improve memory in school students[223], *Lavandula × intermedia* "Sumian" was chose for its activity in Alzheimer's dementia, anxiety and depression[224], and finally *Mentha piperita* was considered for its acetylcholinesterase (AChE) and butyrylcholinesterase (BuChE) inhibition which increase memorization[162]. The features of the EO-loaded samples were compared to NLC with Tegosoft CT oil (as EO-free control) and to NLC with Neem oil (as negative toxic control). Particle size, homogeneity, zeta potential, pH and osmolarity were measured. Their stability was measured using Turbiscan® technology, while their morphology was assessed through TEM; moreover, the

nanoparticles' structure was investigated through X-ray analysis, while their safety was assessed on murine (NIH-3T3) and human (HFF1) fibroblast cell lines. Also, EOs EE% was determined and their release from NLC was assessed using Franz cells. Finally, the platform was optimized adding a cationic lipid didodecyldimethylammonium bromide (DDAB) and the mucoadhesive features were analyzed, aiming to predict the achievement of the CSN through the nose-to-brain route.

Nasal administration route was subsequently investigated as promising route for the administration of vaccines, since the nasal mucosa has favorable properties in terms of immune response and patient compliance[225,226]. Since vaccines and hydrophilic molecules are difficult to be administered because of their chemical nature (low permeability, absorption and distribution, occurrence of enzymatic degradation, etc.[227]), their encapsulation into DDS could improve their effectiveness. Among the various carriers, W/O microemulsions represent a valid strategy for the presence of an aqueous core which could successfully load hydrophilic drugs, improving their bioavailability[228]. Herein, W/O microemulsions are prone to instability phenomena due to the presence of the lipid external phase[28], triphasic W/O/W microemulsions were developed. Thus, a triphasic W/O/W microemulsion was designed and optimized, aiming to encapsulate hydrophilic drugs or vaccines into the inner aqueous core, to be administered on the nasal mucosa (manuscript submitted). In the preformulative phase, different materials were screened and the optimal quali-quantitative composition of the biphasic W/O microemulsion was defined and subsequently also modified through the addition of the cationic DDAB. The W/O microemulsions were inverted in aqueous medium with a proper amount of surfactant, obtaining the respective triphasic neutral and cationic W/O/W microemulsions. The samples were characterized (droplet size, PDI, ZP, pH, osmolality) and accelerated stability studies were performed following ICH guidelines Q1A (R2). *In vitro* assessment of mucoadhesion was performed by turbidimetric assay and ZP measurement at different timepoints, as well as cytocompatibility on human fibroblast (HFF1) and human airway epithelial (Calu-3) cell lines. Fluorescein was loaded as hydrophilic model-drug and its release form the carriers was assessed.

1.6.2 Achievement of the inner eye

Another great challenge is the achievement of the inner eye, which is necessary for the treatment of pathologies such as UM. This tumor in particular results to be one of the most common melanomas in adults and one of the most aggressive for its ability to metastasize[229,230]. Sorafenib was proposed as therapy for some carcinomas, and as well for UM, since it inhibits Raf kinases, responsible of cell growth in cancers[214], and VEGF

receptors[216,231]. Considering the difficulties in achieving the inner eye, a SLN platform was developed[81]. Two different solid lipids were considered, and the obtained optimal formulation was investigated in terms of particle size, homogeneity, pH and osmolality. Turbiscan® apparatus was used to assess SLN stability, and the samples cytocompatibility was tested on Statens Seruminstitut Rabbit Cornea (SIRC) cells using different treatment protocols. The surface of the nanoparticles was optimized using cationic DDAB or (1,2-dioleoyl-3-trimethylammonium-propane) DOTAP and the mucoadhesive properties of the samples were assessed. Finally, sorafenib EE% into the optimal SLN was measured and its release behavior was assessed.

A new synthetized prodrug, (±)-MRJF22, was developed for the treatment of UM, demonstrating to reduce cells proliferation through its σ activity (antagonism for σ_1 and agonism for σ_2) and histone deacetylase inhibition (HDACi)[219]. Aiming to protect the prodrug from degradation and to perform a targeted delivery into the inner eye, the prodrug and its enantiomers were encapsulated into a NLC platform[232]. A preformulative study on the prodrugs was performed by DSC to verify the thermic behavior of the molecules and the suitability of the hot-temperature preparation method. After the ordinary characterization of the nanoparticles (size, PDI, ZP, pH, osmolality) and the assessment of the prodrugs EE%, accelerated stability studies were performed in constant climate chamber, using the parameters defined by ICH guidelines Q1A (R2). Particles organization was deepened using DSC and FT-IR analyses, and the release of the prodrug was assessed using Franz diffusion cells. Mucoadhesive properties were investigated using turbidimetric method and mucin particle method. Finally, *in vitro* compatibility was verified on 92-1 UM cells, and the cell proliferation after administration of loaded NLC and free prodrugs was studied.

From the previous study, (*S*)-(–)-MRJF22 loaded-NLC was selected for the potential adjuvant treatment of UM, and nanoparticles' surface was modified adding PEG or the cationic DDAB, aiming to perform a targeted delivery of the prodrug to the inner eye (manuscript not published). The three NLC samples were ordinarily characterized (size, homogeneity, ZP, pH and osmolality) and their physico-chemical stability was analyzed using Turbiscan®. Moreover, particles morphology was investigated through TEM and their mucoadhesive capability was measured using the mucin particle method. (*S*)-(–)-MRJF22 EE% was determined, and its release was assessed using Franz diffusion cells compared to free prodrug solution. The cytocompatibility of the samples was assessed on human corneal epithelium (HCE-2) and human UM 92-1 cell lines, and their tolerability was confirmed by HET-CAM and HET-CAM TBS *in vitro* tests on 10-day embryonated

eggs and by *in vivo* Draize test on New Zealand albino rabbits. Furthermore, antiangiogenic capability was measured through a modified chorioallantoic membrane (CAM) test on 3-days fertilized eggs, while preventive anti-inflammatory activity was assessed *in vivo* in rabbits. Finally, the *in vivo* biodistribution of the nanoparticles was performed using fluorescent probe loaded-NLC topically instilled in rabbits' eyes, since it was extensively reported the importance of these studies in the assessment of the targeting ability of the carrier[233].

2 RESULTS AND DISCUSSION

2.1 CNS targeting and nasal administration

In the framework of the first goal of this project, the CNS addressed for the treatment of neurodegenerative disorders through the development of NLC loaded with EOs. *Rosmarinus officinalis* L., *Lavandula × intermedia* "Sumian" and *Mentha piperita*, as well as Tegosoft CT and Neem oil, were encapsulated into nanoparticles obtaining L-NLC, R-NLC, M-NLC, CT-NLC and N-NLC, respectively; the EO-loaded samples demonstrated to have small (size < 200 nm) and homogeneous (PDI < 0.3) particles[234], while CT-NLC and N-NLC both showed higher particles diameters and lower homogeneity. All the samples showed physiological pH and osmolarity values. The EE% of the EO into the nanoparticles was found to be 76% for L-NLC, 67% for M-NLC and 64% for R-NLC; less than 20% of Neem oil was encapsulated, while Tegosoft CT EE% was 100%. The negative ZP values, reported for all the formulations, suggested a potential long-term stability[235], which was verified by Turbiscan® stability studies operated at room temperature (25°C) for 30 days, with the highest stability reported for L-NLC (not significant particle migration with backscattering ΔBS < 20%). Turbiscan Stability Index (TSI) values provided the following stability scale: L-NLC = R-NLC ≥ N-NLC ≥ M-NLC >> CT-NLC. X-ray analysis showed higher crystallinity, thus a more ordered structure[94], for L-NLC (68%) and R-NLC (40%), compared to M-NLC (30%), N-NLC (15%) and CT-NLC (10%), providing a scale analogue to the stability one, thus suggesting a relation between structure and stability. This hypothesis was confirmed by TEM morphology studies, which showed the formation of different structures, with L-NLC and R-NLC composed by many oil droplets thus a more imperfect structure[236], while CT-NLC and N-NLC were characterized by a central oily core, demonstrating that the order of the structure could affect particles' stability. Cytocompatibility studies on human (HFF1) and murine (NIH-3T3) fibroblast cell lines were assessed treating the cells for 24h with different concentrations of the samples; it was demonstrated a high viability for L-NLC, R-NLC and CT-NLC[44], while M-NLC and N-NLC were safe only at higher dilutions. EOs release from L-NLC and R-NLC was performed by Franz diffusion cells, showed a similar slow and sustained release for both the formulations, with ~20% released in 8h, ~50% after 24h and ~80% at 48h, thus confirming the importance of the carrier in providing a controlled release[237]. Finally, aiming to increase the residence time on the nasal mucosa, a cationic coating with DDAB was added, since mucin sialic residues are negatively charged. The obtained

L-NLC+, R-NLC+ and CT-NLC+ were analyzed to assess samples' mucoadhesive properties, and the following mucoadhesion scale was obtained: L-NLC+ > R-NLC+ > CT-NLC+, demonstrating a potential prolonged permanence in the nose, increasing the therapeutic response[238].

Nasal route was also exploited for the mucosal administration of hydrophilic drugs, through the design of a multiple emulsion platform. The preformulative studies allowed the selection of the more suitable materials and the determination of the quantitative composition: the optimal biphasic W/O microemulsion obtained, namely ME2-A, was composed of Labrafil® at 12.8% w/w, Kolliphor® at 6.8% w/w, IPM at 70.4% w/w and water at 10.0% w/w. The preparation method was optimized analyzing different stirring times[239,240], and selecting 30 min as optimal time to obtain the lowest droplets' size and the highest homogeneity. The optimal triphasic W/O/W microemulsion (ME3-A) was obtained screening both the amount of Tween® 80 and the dilutions of the biphasic W/O microemulsion: 4% w/w of surfactant and 1:3 dilution were selected. ME3-A showed droplet size lower than 172.5 nm, a good homogeneity (PDI 0.3) and a slight negative ZP (-8 mV).

The optimal formulation was modified adding 0.15% w/w of DDAB to the primary microemulsion, then obtaining the W/O/W triphasic ME3+A, whose size and homogeneity resulted similar to ME3-A, with a markedly positive ZP (19 mV). Both the samples had physiological pH and osmolality values. The characterization results demonstrated features adequate for the nasal administration route. Stability studies were performed in constant climate chamber, set at accelerated conditions[241], demonstrating a good stability of both ME3-A and ME3+A for 6 months; in detail, the neutral formulation showed a slight variation in droplet size (remaining in the <200 nm range), while the higher stability of the cationic sample was related to its more marked ZP values which promote particles' repulsion[242]. Mucoadhesion studies demonstrated that both the samples were able to interact with the mucin of the nasal mucosa, with a greater extent for the cationic ME3+A because of the electrostatic interactions occurring with the negative residues of the mucin glycoproteins, suggesting a prolonged permanence on nasal mucosa for both the microemulsions. As a hydrophilic-model drug, fluorescein was encapsulated into the inner water phase of the microemulsions (with a slight increase in particle sizes and homogeneities[243], and almost-unaltered ZP values), and its release was assessed using dialysis bag method. Fluorescein solution was used as a reference, showing a complete release after 6h; conversely, the neural microemulsion was able to provide a sustained release over 24h (50% released at 2h, and 100% at 24h), while the cationic sample provided

_____

a slow and prolonged release (50% at 6h and 60% at 24h). The cytocompatibility studies performed on human airway epithelial (Calu-3) and human fibroblast (HFF1) cells lines demonstrated a higher biocompatibility for ME3-A compared to ME3+A, probably related to the presence of the cationic DDAB, as already reported in literature[44]. It is worth to be mentioned that usually a nasal residence is short, thus the tested treatment times are actually beyond the actual permanence of the formulations on the cells.

2.2 Achievement of the inner eye

The achievement of the inner eye for the treatment of UM was performed firstly encapsulating sorafenib into SLN. The preformulative study allowed the selection of the proper solid lipid, among Suppocire and Softisan, considered at different concentrations (5, 7, 8, 9% w/v). Lower amounts of solid lipids (5 and 7% w/v) produced heterogeneous particles characterized by multiple peaks of size distribution. Samples named B8 (with 8% w/v Suppocire), B9 (with 9% w/v Suppocire), and A9 (containing 9% w/v Softisan) resulted adequate for ophthalmic administration[244], in terms of particle size (B8 and B9 < 200nm, A9 < 100 nm), homogeneity (PDI < 0.3), physiological pH and osmolality values. Turbiscan® equipment was used to assess the physical stability of the samples, stored at room temperature (25±2°C) for 1 month, showing the following stability scale: A8 ≥ B9 >> B8. These results, also confirmed by PCS analysis performed every week, could be explained by the different chemical structure of the solid lipids and their different melting temperatures. Cytocompatibility studies were performed testing A8, B8 and B9 on SIRC cells, using a Short Time Repeated Exposure (S.T.R.E.) method in wash and no-wash conditions, with mimic the ophthalmic application[245]. The higher tolerability was demonstrated by A8 and B9 formulations in the extreme no-wash protocol, even if A8 viability was higher in the wash protocol. Thus, SLN A8 was optimized through the addition of a cationic coating, using DDAB or DOTAP (A8-DB or A8-DP, respectively), obtaining ZP values of about +20 mV. Mucoadhesive properties of the samples (A8, A8-DB and A8-DP) were tested *in vitro* through the mucin particle method, demonstrating the following mucoadhesion trend A8-DB > A8-DP > A8. The slightest interaction of negative A8 with mucin was expected, as well as the high mucoadhesion of cationic A8-DB and A8-DP; the difference among DDAB and DOTAP in providing interactions with mucin could be attributable to the different saturation of the residues basing on temperature[246]. The selected A8-DB was loaded with different amounts of sorafenib (0.8% or 1.0% w/v), showing similar EE% values (~75%). Release profile was assessed using

_____

Franz diffusion cells and compared to sorafenib suspension (which showed a 50% released after 2h and ~90% after 6h): both the samples demonstrated to provide a slow and prolonged release, with ~25% of sorafenib released after 72h, demonstrating the advantage of the encapsulation in guaranteeing a longer release over time.

The same UM target was addressed encapsulating the new-synthetized prodrug (±)-MRJF22 and its (R)- and (S)-enantiomers into NLC, obtaining (M)-NLC, (S)-NLC and (R)-NLC, respectively. The suitability of the PIT preparation method was verified through DSC preformulative study on the three molecules (that showed fusion temperatures of 80°C, 84°C and 82°C, respectively), and further confirmed by UV-vis analysis of the molecules before and after the heating phase of the PIT technique. The prepared loaded NLC samples were ordinarily characterized by PCS, having size of about 140-150 nm, PDI < 0.25 and neutral ZP of ~4-6 mV, while pH and osmolality were physiological. Encapsulation efficiency was found to be higher for (M)-NLC (87%) compared to (R)-NLC and (S)-NLC (68% and 57%, respectively). Accelerated stability studies were performed following the ICH guidelines Q1A (R2) and storing the samples at 40±2°C and 75±5% RH for 6 months, demonstrating no occurrence of instability phenomena. Nanoparticles organization was investigated through DSC[88] and FT-IR[94] studies, which demonstrated the successful encapsulation of the prodrugs into the nanoparticles. Franz diffusion cells were employed to assess the release of the prodrug from the nanoparticles, demonstrating a slow and prolonged release for all the samples (at each timepoint from T0 to 24h, (R)-NLC > (S)-NLC > (M)-NLC), compared to the prodrug solutions (all prodrug released within the firsts few hours). The lower release of (±)-MRJF22 compared to the enantiomers-loaded formulations could be explained by the higher encapsulation efficiency showed by (M)-NLC, since literature findings demonstrated that higher EE% could result in lower release[247]. Mucoadhesive studies were performed using turbidimetric assay and mucin particle method, demonstrating no differences in the interaction with mucin. Cytocompatibility studies were performed on 92-1 UM cell line demonstrated good tolerability up to 5 µM concentration of prodrug loaded into the NLCs., which was previously reported to be the optimal efficient concentration[219]. Furthermore, cell proliferation was assessed performing crystal violet assay and demonstrated an enhancement of antiproliferative activity of the prodrugs after encapsulation into the carrier. In particular, 0.3 µM concentration of (S)-NLC and 0.8 µM concentration of (R)-NLC were able to provide significant inhibition of cell proliferation. Considering the more favourable features of (S)-NLC (in terms of characterization and release) and its higher antiproliferative efficiency, this enantiomer was selected for further studies.

Aiming to increase the retention time on the ocular surface, the same NLC platform was subsequently modified adding PEG or the cationic DDAB (namely P-NLC and D-NLC, respectively), obtaining homogeneous particles, with sizes adequate for the ophthalmic administration. pH and osmolality were into the physiological range. Great physical stability was reported for all the samples stored in Turbiscan® technology at room temperature (25.0±1.0°C), physiological temperature (36.5±1.0°C) and extreme temperature (50.0± 1.0°C). Morphology of the samples was assessed through TEM, demonstrating spherical shape for all the NLCs, without significant difference in the surface after the addition of the coating layer[95,248]. *In vitro* cytocompatibility of NLC, P-NLC and D-NLC was assessed on human corneal epithelium cells (HCE-2) and uveal melanoma (UM 92-1) cells, showing a certain toxicity of D-NLC sample related to the presence of the cationic DDAB coating[249]. NLC and P-NLC demonstrated to be safe (viability > 80%) at concentration lower than 1 μM and 3 μM respectively, with a dose-dependent trend. Mucoadhesion of NLC and P-NLC assessed through mucin particle method demonstrated slight interaction of both samples with mucin residues, suggesting adequate features to avoid loss with the tears flow while not remaining adhered on the ocular surface. Furthermore, (*S*)-(–)-MRJF22 was encapsulated into the two carriers, producing (*S*)-NLC and (*S*)-P-NLC, without significant variation in the characterization compared to the blank samples. EE% was found to be 57.7% and 52.9 % respectively. Both NLCs showed a similar slow and prolonged release, with 28.20% and 19.78% of prodrug released after 24h, compared to the free prodrug which was completely released after 3h. Interestingly, the treatment on HCE-2 with both the loaded samples demonstrated an improved tolerability compared to the (*S*)-(–)-MRJF22 solution, suggesting that the encapsulation could prevent undesired toxicity on the ocular surface. *In vitro* tolerance was also verified through HET-CAM and HET-CAM TBS tests on embryonated eggs confirming the higher safety of the loaded samples compared to the prodrug solution, which caused all the three analyzed events (vasoconstriction, hemorrhage, and coagulation). *In vivo* Draize test on New Zealand albino rabbits confirmed the HCE-2 viability results, demonstrating – once again – the higher tolerability of the samples compared to the (*S*)-(–)-MRJF22 solution. The antiangiogenic activity of the prodrug was verified *in vivo* on fertilized eggs treated with (*S*)-NLC, (*S*)-P-NLC and (*S*)-(–)-MRJF22 solution for 48h. It emerged a similar behavior for all the tested samples, demonstrating that drug encapsulation into the NLCs did not limit the prodrug effectiveness while reducing its potential side effects. Furthermore, the capability to prevent the inflammation was assessed *in vivo* on New Zealand albino rabbits: it resulted that, at the final timepoint, all the samples

provided a similar anti-inflammatory activity, but with different trends. The prodrug solution activity was slower at the beginning, probably because the anti-inflammatory activity was counterbalanced (for a certain extent) by the irritant effect of the prodrug solution. Conversely, the two NLC systems were able to significantly reduce the inflammation from the very firsts timepoints, being safe and providing a prolonged and sustained activity probably attributable also to their longer permanence time on the ocular surface. Finally, in order to investigate the biodistribution of the nanoparticles, the two samples were loaded with the fluorescent probe FITC (obtaining F-NLC and F-P-NLC), maintaining analogue technological features of the original carriers and being able to retain the probe inside the particles, as confirmed by *in vitro* release studies. Thus, the fluorescent samples were topically administered on New Zealand albino rabbits' eyes, which were sacrificed, and the eyes collected. The fluoresce microscopy analysis of the eyes' sections showed the capability of the nanocarriers to successfully reach the retina[48] and the quantification of the fluorescence showed a higher intensity for F-NLC compared to F-P-NLC, both in the whole eye and in the retina; on the other hand, fluorescence of FITC solution gave low intensity values, confirming the importance of the carrier to successfully achieve the inner eye.

_____

3 CONCLUSIONS

The goal of this PhD project of overcoming biological barriers through the use of drug delivery systems was achieved in different fields.

CNS targeting was accomplished through the development of a NLC carrier loaded with *Lavandula* and *Rosmarinus* essential oils. The adequate technological features, as well as the mucoadhesive properties and the cell tolerability, demonstrated the suitability of the produced nanosystems for the nose-to-brain administration of the essential oils, as a potential strategy to reduce the irritation while maintaining the beneficial effects of these natural compounds in the adjuvant treatment of neurodegenerative disorders. An interest was also directed to the nasal route for the potential administration of vaccines, designing a triphasic W/O/W microemulsion able to encapsulate hydrophilic molecules in the inner aqueous core. The preformulative screening allowed the selection of the most adequate quali-quantitative composition of the microemulsion, which demonstrated to be suitable for the nasal mucosal absorption of the hydrophilic loaded drug, as promising strategy for vaccine delivery.

Inner eye achievement for targeted treatment of uveal melanoma was investigated firstly loading sorafenib into a SLN, which was properly designed in terms of quali-quantitative composition. For the interesting tolerability of the carrier, and also for the interesting mucoadhesive properties, the developed SLN could be a promising platform for the treatment of this aggressive cancer. Moreover, the antitumoral activity of (*S*)-(−)-MRJF22 in the treatment of uveal melanoma was exploited encapsulating the prodrug into NLC nanoparticles, aiming to ameliorate the inner-eye targeting while reducing eventual drug loss or side effects occurrence. The platform resulted to be adequate and safe for the intended ophthalmic administration; furthermore, the enhancement of the antiproliferative activity of the prodrug after the encapsulation into NLC was the input to further verify the relevance of the carrier in the treatment of uveal melanoma. More exhaustive studies were performed to characterize this NLC system by *in vitro* and *in vivo* tests, obtaining remarkable results. The developed carrier was able to maintain the therapeutical activity of the encapsulated prodrug, while reducing the corneal toxicity, which is a side effect of the (*S*)-(−)-MRJF22 prodrug. Moreover, the targeting ability of the produced nanoparticles was verified through *in vivo* biodistribution studies, which demonstrated a successful achievement of the inner eye. These results suggest a potential therapeutical use of the produced (*S*)-(−)-MRJF22 loaded NLC in the add-on treatment of uveal melanoma.

_____

References

1. Lotfipour F, Shahi S, Farjami A, Salatin S, Mahmoudian M, Dizaj SM. Safety and Toxicity Issues of Therapeutically Used Nanoparticles from the Oral Route. Husain K, ed. *BioMed Res Int*. 2021;2021:1-14. doi:10.1155/2021/9322282

2. Adepu S, Ramakrishna S. Controlled Drug Delivery Systems: Current Status and Future Directions. *Molecules*. 2021;26(19):5905. doi:10.3390/molecules26195905

3. McDonald T, Zepeda M, Tomlinson M, Bee W, Ivens I. Subcutaneous administration of biotherapeutics: Current experience in animal models. *Curr Opin Mol Ther*. 2010;12:461-470.

4. Ayinde O, Hayward RS, Ross JDC. The effect of intramuscular injection technique on injection associated pain; a systematic review and meta-analysis. Peña Fernández MÁ, ed. *PLOS ONE*. 2021;16(5):e0250883. doi:10.1371/journal.pone.0250883

5. Jonaitis L, Marković S, Farkas K, et al. Intravenous versus subcutaneous delivery of biotherapeutics in IBD: an expert's and patient's perspective. *BMC Proc*. 2021;15(S17):25. doi:10.1186/s12919-021-00230-7

6. Kim H, Park H, Lee SJ. Effective method for drug injection into subcutaneous tissue. *Sci Rep*. 2017;7(1):9613. doi:10.1038/s41598-017-10110-w

7. Alqahtani MS, Kazi M, Alsenaidy MA, Ahmad MZ. Advances in Oral Drug Delivery. *Front Pharmacol*. 2021;12:618411. doi:10.3389/fphar.2021.618411

8. Hua S. Advances in Nanoparticulate Drug Delivery Approaches for Sublingual and Buccal Administration. *Front Pharmacol*. 2019;10:1328. doi:10.3389/fphar.2019.01328

9. Rathi R, Sanshita, Kumar A, et al. Advancements in Rectal Drug Delivery Systems: Clinical Trials, and Patents Perspective. *Pharmaceutics*. 2022;14(10):2210. doi:10.3390/pharmaceutics14102210

10. Rau JL. The Inhalation of Drugs: Advantages and Problems. *Respir Care*. 2005;50(3):367.

11. Murthy. Transdermal drug delivery: approaches and significance. *Res Rep Transdermal Drug Deliv*. Published online May 2012:1. doi:10.2147/RRTD.S31738

12. Tai J, Han M, Lee D, Park IH, Lee SH, Kim TH. Different Methods and Formulations of Drugs and Vaccines for Nasal Administration. *Pharmaceutics*. 2022;14(5):1073. doi:10.3390/pharmaceutics14051073

13. Patel A. Ocular drug delivery systems: An overview. *World J Pharmacol*. 2013;2(2):47. doi:10.5497/wjp.v2.i2.47

14. Raina N, Rani R, Thakur VK, Gupta M. New Insights in Topical Drug Delivery for Skin Disorders: From a Nanotechnological Perspective. *ACS Omega*. 2023;8(22):19145-19167. doi:10.1021/acsomega.2c08016

15. Srikrishna S, Cardozo L. The vagina as a route for drug delivery: a review. *Int Urogynecology J*. 2013;24(4):537-543. doi:10.1007/s00192-012-2009-3

16. Xu L, Wang X, Liu Y, Yang G, Falconer RJ, Zhao CX. Lipid Nanoparticles for Drug Delivery. *Adv NanoBiomed Res*. 2022;2(2):2100109. doi:10.1002/anbr.202100109

17. Shrestha H, Bala R, Arora S. Lipid-Based Drug Delivery Systems. *J Pharm*. 2014;2014:1-10. doi:10.1155/2014/801820

18. Suhail N, Alzahrani AK, Basha WJ, et al. Microemulsions: Unique Properties, Pharmacological Applications, and Targeted Drug Delivery. *Front Nanotechnol*. 2021;3:754889. doi:10.3389/fnano.2021.754889

19. Dhaval M, Vaghela P, Patel K, et al. Lipid-based emulsion drug delivery systems — a comprehensive review. *Drug Deliv Transl Res*. 2022;12(7):1616-1639. doi:10.1007/s13346-021-01071-9

20. Karunaratne DN, Pamunuwa G, Ranatunga U. Introductory Chapter: Microemulsions. In: Karunaratne DN, Pamunuwa G, Ranatunga U, eds. *Properties and Uses of Microemulsions*. InTech; 2017. doi:10.5772/intechopen.68823

21. Sharma AK, Garg T, Goyal AK, Rath G. Role of microemuslions in advanced drug delivery. *Artif Cells Nanomedicine Biotechnol*. Published online February 25, 2015:1-9. doi:10.3109/21691401.2015.1012261

22. Egito EST, Amaral-Machado L, Alencar EN, Oliveira AG. Microemulsion systems: from the design and architecture to the building of a new delivery system for multiple-route drug delivery. *Drug Deliv Transl Res*. 2021;11(5):2108-2133. doi:10.1007/s13346-020-00872-8

23. Leung R, Shah DO. Solubilization and phase equilibria of water-in-oil microemulsions. *J Colloid Interface Sci*. 1987;120(2):320-329. doi:10.1016/0021-9797(87)90360-2

24. Griffin WC. Classification of Surface-Active Agents by "HLB." *J Cosmet Sci*. 1949;1:311-326.

25. Saffarionpour S, Diosady LL. Multiple Emulsions for Enhanced Delivery of Vitamins and Iron Micronutrients and Their Application for Food Fortification. *Food Bioprocess Technol*. 2021;14(4):587-625. doi:10.1007/s11947-021-02586-2

26. Bancroft WD. The Theory of Emulsification, V. *J Phys Chem*. 1913;17(6):501-519. doi:10.1021/j150141a002

27. Callender SP, Mathews JA, Kobernyk K, Wettig SD. Microemulsion utility in pharmaceuticals: Implications for multi-drug delivery. *Int J Pharm*. 2017;526(1-2):425-442. doi:10.1016/j.ijpharm.2017.05.005

28. Pan Y, Xu Y, Zhu L, et al. Stability and rheological properties of water-in-oil (W/O) emulsions prepared with a soyasaponin-PGPR system. *Future Foods*. 2021;4:100096. doi:10.1016/j.fufo.2021.100096

29. Yaqoob Khan A, Talegaonkar S, Iqbal Z, Jalees Ahmed F, Krishan Khar R. Multiple Emulsions: An Overview. *Curr Drug Deliv*. 2006;3(4):429-443. doi:10.2174/156720106778559056

30. Kumar A, Kaur R, Kumar V, Kumar S, Gehlot R, Aggarwal P. New insights into water-in-oil-in-water (W/O/W) double emulsions: Properties, fabrication, instability mechanism, and food applications. *Trends Food Sci Technol*. 2022;128:22-37. doi:10.1016/j.tifs.2022.07.016

31. Ilyasoglu Buyukkestelli H, El SN. Development and characterization of double emulsion to encapsulate iron. *J Food Eng*. 2019;263:446-453. doi:10.1016/j.jfoodeng.2019.07.026

32. Akhtar M, Murray BS, Afeisume EI, Khew SH. Encapsulation of flavonoid in multiple emulsion using spinning disc reactor technology. *Food Hydrocoll*. 2014;34:62-67. doi:10.1016/j.foodhyd.2012.12.025

33. Lamba H, Sathish K, Sabikhi L. Double Emulsions: Emerging Delivery System for Plant Bioactives. *Food Bioprocess Technol*. 2015;8(4):709-728. doi:10.1007/s11947-014-1468-6

34. Paliwal R, Paliwal SR, Kenwat R, Kurmi BD, Sahu MK. Solid lipid nanoparticles: a review on recent perspectives and patents. *Expert Opin Ther Pat*. 2020;30(3):179-194. doi:10.1080/13543776.2020.1720649

References

___

35. Mueller Rainer DR, Lucks JS. *Arzneistofftraeger Aus Festen Lipidteilchen-Feste Lipidnanosphaeren (SLN).*; 1991.

36. Scioli Montoto S, Muraca G, Ruiz ME. Solid Lipid Nanoparticles for Drug Delivery: Pharmacological and Biopharmaceutical Aspects. *Front Mol Biosci*. 2020;7:587997. doi:10.3389/fmolb.2020.587997

37. Keck CM, Kovačević A, Müller RH, Savić S, Vuleta G, Milić J. Formulation of solid lipid nanoparticles (SLN): The value of different alkyl polyglucoside surfactants. *Int J Pharm*. 2014;474(1-2):33-41. doi:10.1016/j.ijpharm.2014.08.008

38. Kovačević AB, Müller RH, Savić SD, Vuleta GM, Keck CM. Solid lipid nanoparticles (SLN) stabilized with polyhydroxy surfactants: Preparation, characterization and physical stability investigation. *Colloids Surf Physicochem Eng Asp*. 2014;444:15-25. doi:10.1016/j.colsurfa.2013.12.023

39. Viegas C, Patrício AB, Prata JM, Nadhman A, Chintamaneni PK, Fonte P. Solid Lipid Nanoparticles vs. Nanostructured Lipid Carriers: A Comparative Review. *Pharmaceutics*. 2023;15(6):1593. doi:10.3390/pharmaceutics15061593

40. Souto EB, Baldim I, Oliveira WP, et al. SLN and NLC for topical, dermal, and transdermal drug delivery. *Expert Opin Drug Deliv*. 2020;17(3):357-377. doi:10.1080/17425247.2020.1727883

41. Fang JY, Fang CL, Liu CH, Su YH. Lipid nanoparticles as vehicles for topical psoralen delivery: Solid lipid nanoparticles (SLN) versus nanostructured lipid carriers (NLC). *Eur J Pharm Biopharm*. 2008;70(2):633-640. doi:10.1016/j.ejpb.2008.05.008

42. Pandey S, Shaikh F, Gupta A, Tripathi P, Yadav JS. A Recent Update: Solid Lipid Nanoparticles for Effective Drug Delivery. *Adv Pharm Bull*. Published online May 16, 2021:1. doi:10.34172/apb.2022.007

43. Akbari J, Saeedi M, Ahmadi F, et al. Solid lipid nanoparticles and nanostructured lipid carriers: a review of the methods of manufacture and routes of administration. *Pharm Dev Technol*. 2022;27(5):525-544. doi:10.1080/10837450.2022.2084554

44. Carbone C, Martins-Gomes C, Caddeo C, et al. Mediterranean essential oils as precious matrix components and active ingredients of lipid nanoparticles. *Int J Pharm*. 2018;548(1):217-226. doi:10.1016/j.ijpharm.2018.06.064

45. Labiris NR, Dolovich MB. Pulmonary drug delivery. Part I: Physiological factors affecting therapeutic effectiveness of aerosolized medications: Physiological factors affecting the effectiveness of inhaled drugs. *Br J Clin Pharmacol*. 2003;56(6):588-599. doi:10.1046/j.1365-2125.2003.01892.x

46. Verma D. Particle size of liposomes influences dermal delivery of substances into skin. *Int J Pharm*. 2003;258(1-2):141-151. doi:10.1016/S0378-5173(03)00183-2

47. Hua S. Lipid-based nano-delivery systems for skin delivery of drugs and bioactives. *Front Pharmacol*. 2015;6. doi:10.3389/fphar.2015.00219

48. Puglia C, Santonocito D, Romeo G, et al. Lipid Nanoparticles Traverse Non-Corneal Path to Reach the Posterior Eye Segment: In Vivo Evidence. *Molecules*. 2021;26(15):4673. doi:10.3390/molecules26154673

49. Albarki MA, Donovan MD. Bigger or Smaller? Size and Loading Effects on Nanoparticle Uptake Efficiency in the Nasal Mucosa. *AAPS PharmSciTech*. 2020;21(8):294. doi:10.1208/s12249-020-01837-3

50. Danaei M, Dehghankhold M, Ataei S, et al. Impact of Particle Size and Polydispersity Index on the Clinical Applications of Lipidic Nanocarrier Systems. *Pharmaceutics*. 2018;10(2):57. doi:10.3390/pharmaceutics10020057

51. Kettler K, Veltman K, Van De Meent D, Van Wezel A, Hendriks AJ. Cellular uptake of nanoparticles as determined by particle properties, experimental conditions, and cell type: Cellular uptake of nanoparticles. *Environ Toxicol Chem*. 2014;33(3):481-492. doi:10.1002/etc.2470

52. Mosquera J, García I, Liz-Marzán LM. Cellular Uptake of Nanoparticles versus Small Molecules: A Matter of Size. *Acc Chem Res*. 2018;51(9):2305-2313. doi:10.1021/acs.accounts.8b00292

53. *FDA—Liposome Drug Products; Chemistry, Manufacturing, and Controls; Human Pharmacokinetics and Bioavailability; Labeling Documentation.* U.S. Department of Health and Human Services Food and Drug Administration Center for Drug Evaluation and Research (CDER); 2018. https://www.fda.gov/regulatory-information/search-fda-guidance-documents/liposome-drug-products-chemistry-manufacturing-and-controls-human-pharmacokinetics-and

54. Pecora R. Dynamic Light Scattering Measurement of Nanometer Particles in Liquids. *J Nanoparticle Res*. 2000;2(2):123-131. doi:10.1023/A:1010067107182

55. Honary S, Zahir F. Effect of Zeta Potential on the Properties of Nano-Drug Delivery Systems - A Review (Part 1). *Trop J Pharm Res*. 2013;12(2):255-264. doi:10.4314/tjpr.v12i2.19

56. Berbel Manaia E, Paiva Abuçafy M, Chiari-Andréo BG, Lallo Silva B, Oshiro-Júnior JA, Chiavacci L. Physicochemical characterization of drug nanocarriers. *Int J Nanomedicine*. 2017;Volume 12:4991-5011. doi:10.2147/IJN.S133832

57. Brar SK, Verma M. Measurement of nanoparticles by light-scattering techniques. *TrAC Trends Anal Chem*. 2011;30(1):4-17. doi:10.1016/j.trac.2010.08.008

58. Lin PC, Lin S, Wang PC, Sridhar R. Techniques for physicochemical characterization of nanomaterials. *Biotechnol Adv*. 2014;32(4):711-726. doi:10.1016/j.biotechadv.2013.11.006

59. Chen ZG, Wang ZN, Yan Y, et al. Upregulation of cell-surface mucin MUC15 in human nasal epithelial cells upon influenza A virus infection. *BMC Infect Dis*. 2019;19(1):622. doi:10.1186/s12879-019-4213-y

60. Shirai K, Saika S. Ocular surface mucins and local inflammation—studies in genetically modified mouse lines. *BMC Ophthalmol*. 2015;15(S1):154. doi:10.1186/s12886-015-0137-5

61. Juillerat-Jeanneret L. The targeted delivery of cancer drugs across the blood–brain barrier: chemical modifications of drugs or drug-nanoparticles? *Drug Discov Today*. 2008;13(23-24):1099-1106. doi:10.1016/j.drudis.2008.09.005

62. Lv H, Zhang S, Wang B, Cui S, Yan J. Toxicity of cationic lipids and cationic polymers in gene delivery. *J Controlled Release*. 2006;114(1):100-109. doi:10.1016/j.jconrel.2006.04.014

63. Wei X, Shao B, He Z, et al. Cationic nanocarriers induce cell necrosis through impairment of Na+/K+-ATPase and cause subsequent inflammatory response. *Cell Res*. 2015;25(2):237-253. doi:10.1038/cr.2015.9

64. Di J, Gao X, Du Y, Zhang H, Gao J, Zheng A. Size, shape, charge and "stealthy" surface: Carrier properties affect the drug circulation time in vivo. *Asian J Pharm Sci*. 2021;16(4):444-458. doi:10.1016/j.ajps.2020.07.005

65. Maher R, Moreno-Borrallo A, Jindal D, Mai BT, Ruiz-Hernandez E, Harkin A. Intranasal Polymeric and Lipid-Based Nanocarriers for CNS Drug Delivery. *Pharmaceutics*. 2023;15(3):746. doi:10.3390/pharmaceutics15030746

66. Proksch E. pH in nature, humans and skin. *J Dermatol*. 2018;45(9):1044-1052. doi:10.1111/1346-8138.14489

67. Abdella S, Abid F, Youssef SH, et al. pH and its applications in targeted drug delivery. *Drug Discov Today*. 2023;28(1):103414. doi:10.1016/j.drudis.2022.103414

___

68. Aoi W, Marunaka Y. Importance of pH Homeostasis in Metabolic Health and Diseases: Crucial Role of Membrane Proton Transport. *BioMed Res Int*. 2014;2014:1-8. doi:10.1155/2014/598986

69. Baliga S, Muglikar S, Kale R. Salivary pH: A diagnostic biomarker. *J Indian Soc Periodontol*. 2013;17(4):461. doi:10.4103/0972-124X.118317

70. Pezzulo AA, Tang XX, Hoegger MJ, et al. Reduced airway surface pH impairs bacterial killing in the porcine cystic fibrosis lung. *Nature*. 2012;487(7405):109-113. doi:10.1038/nature11130

71. Pires PC, Rodrigues M, Alves G, Santos AO. Strategies to Improve Drug Strength in Nasal Preparations for Brain Delivery of Low Aqueous Solubility Drugs. *Pharmaceutics*. 2022;14(3):588. doi:10.3390/pharmaceutics14030588

72. Javia A, Kore G, Misra A. Polymers in Nasal Drug Delivery: An Overview. In: *Applications of Polymers in Drug Delivery*. Elsevier; 2021:305-332. doi:10.1016/B978-0-12-819659-5.00011-2

73. Pignatello R. Optimization and Validation of a New Method for the Production of Lipid Nanoparticles for Ophthalmic Application. *Int J Med Nano Res*. 2014;1(1). doi:10.23937/2378-3664/1410006

74. Lim LT, Ah-Kee EY, Collins CE. Common eye drops and their implications for pH measurements in the management of chemical eye injuries. *Int J Ophthalmol*. 2014;7(6):1067-1068. doi:10.3980/j.issn.2222-3959.2014.06.29

75. Rasouli M. Basic concepts and practical equations on osmolality: Biochemical approach. *Clin Biochem*. 2016;49(12):936-941. doi:10.1016/j.clinbiochem.2016.06.001

76. Berneis K, Ninnis R, Häussinger D, Keller U. Effects of hyper- and hypoosmolality on whole body protein and glucose kinetics in humans. *Am J Physiol-Endocrinol Metab*. 1999;276(1):E188-E195. doi:10.1152/ajpendo.1999.276.1.E188

77. Alhuthali S, Kotidis P, Kontoravdi C. Osmolality Effects on CHO Cell Growth, Cell Volume, Antibody Productivity and Glycosylation. *Int J Mol Sci*. 2021;22(7):3290. doi:10.3390/ijms22073290

78. Cvetkovic L, Perisic S, Titze J, Jäck HM, Schuh W. The Impact of Hyperosmolality on Activation and Differentiation of B Lymphoid Cells. *Front Immunol*. 2019;10:828. doi:10.3389/fimmu.2019.00828

79. Antolic A, Harrison R, Farlinger C, et al. Effect of extracellular osmolality on cell volume and resting metabolism in mammalian skeletal muscle. *Am J Physiol-Regul Integr Comp Physiol*. 2007;292(5):R1994-R2000. doi:10.1152/ajpregu.00653.2006

80. Häussinger D, Hallbrucker C, Vom Dahl S, et al. Cell volume is a major determinant of proteolysis control in liver. *FEBS Lett*. 1991;283(1):70-72. doi:10.1016/0014-5793(91)80556-I

81. Bonaccorso A, Pepe V, Zappulla C, et al. Sorafenib Repurposing for Ophthalmic Delivery by Lipid Nanoparticles: A Preliminary Study. *Pharmaceutics*. 2021;13(11):1956. doi:10.3390/pharmaceutics13111956

82. Marx D, Williams G, Birkhoff M. Intranasal Drug Administration — An Attractive Delivery Route for Some Drugs. In: Vallisuta O, Olimat S, eds. *Drug Discovery and Development - From Molecules to Medicine*. InTech; 2015. doi:10.5772/59468

83. Wu L, Zhang J, Watanabe W. Physical and chemical stability of drug nanoparticles. *Adv Drug Deliv Rev*. 2011;63(6):456-469. doi:10.1016/j.addr.2011.02.001

84. Fan Y, Marioli M, Zhang K. Analytical characterization of liposomes and other lipid nanoparticles for drug delivery. *J Pharm Biomed Anal*. 2021;192:113642. doi:10.1016/j.jpba.2020.113642

85. Carbone C, Caddeo C, Grimaudo MA, Manno DE, Serra A, Musumeci T. Ferulic Acid-NLC with Lavandula Essential Oil: A Possible Strategy for Wound-Healing? *Nanomaterials*. 2020;10(5):898. doi:10.3390/nano10050898

86. McClements J, McClements DJ. Standardization of Nanoparticle Characterization: Methods for Testing Properties, Stability, and Functionality of Edible Nanoparticles. *Crit Rev Food Sci Nutr*. 2016;56(8):1334-1362. doi:10.1080/10408398.2014.970267

87. Bunjes H, Unruh T. Characterization of lipid nanoparticles by differential scanning calorimetry, X-ray and neutron scattering☆. *Adv Drug Deliv Rev*. 2007;59(6):379-402. doi:10.1016/j.addr.2007.04.013

88. Carbone C, Campisi A, Musumeci T, Raciti G, Bonfanti R, Puglisi G. FA-loaded lipid drug delivery systems: Preparation, characterization and biological studies. *Eur J Pharm Sci*. 2014;52:12-20. doi:10.1016/j.ejps.2013.10.003

89. Carbone C, Fuochi V, Zielińska A, et al. Dual-drugs delivery in solid lipid nanoparticles for the treatment of Candida albicans mycosis. *Colloids Surf B Biointerfaces*. 2020;186:110705. doi:10.1016/j.colsurfb.2019.110705

90. Carbone C, Martins-Gomes C, Pepe V, et al. Repurposing itraconazole to the benefit of skin cancer treatment: A combined azole-DDAB nanoencapsulation strategy. *Colloids Surf B Biointerfaces*. 2018;167:337-344. doi:10.1016/j.colsurfb.2018.04.031

91. Faghihzadeh F, Anaya NM, Schifman LA, Oyanedel-Craver V. Fourier transform infrared spectroscopy to assess molecular-level changes in microorganisms exposed to nanoparticles. *Nanotechnol Environ Eng*. 2016;1(1):1. doi:10.1007/s41204-016-0001-8

92. Hartel RW. Advances in Food Crystallization. *Annu Rev Food Sci Technol*. 2013;4(1):277-292. doi:10.1146/annurev-food-030212-182530

93. Bonaccorso A, Cimino C, Manno DE, et al. Essential Oil-Loaded NLC for Potential Intranasal Administration. *Pharmaceutics*. 2021;13(8):1166. doi:10.3390/pharmaceutics13081166

94. Teeranachaideekul V, Morakul B, Boonme P, Pornputtapitak W, Junyaprasert V. Effect of Lipid and Oil Compositions on Physicochemical Properties and Photoprotection of Octyl Methoxycinnamate-loaded Nanostructured Lipid Carriers (NLC). *J Oleo Sci*. 2020;69(12):1627-1639. doi:10.5650/jos.ess20093

95. Carbone C, Campisi A, Manno D, et al. The critical role of didodecyldimethylammonium bromide on physico-chemical, technological and biological properties of NLC. *Colloids Surf B Biointerfaces*. 2014;121:1-10. doi:10.1016/j.colsurfb.2014.05.024

96. Saez V, Souza IDL, Mansur CRE. Lipid nanoparticles (SLN & NLC) for delivery of vitamin E: a comprehensive review. *Int J Cosmet Sci*. 2018;40(2):103-116. doi:10.1111/ics.12452

97. Cirri M, Mennini N, Maestrelli F, Mura P, Ghelardini C, Di Cesare Mannelli L. Development and in vivo evaluation of an innovative "Hydrochlorothiazide-in Cyclodextrins-in Solid Lipid Nanoparticles" formulation with sustained release and enhanced oral bioavailability for potential hypertension treatment in pediatrics. *Int J Pharm*. 2017;521(1-2):73-83. doi:10.1016/j.ijpharm.2017.02.022

98. Yong-Zhong Du YZD, Fu-Qiang Hu FQH, Xiao-Ying Ying XYY, et al. Preparation and characterization of modified lipid nanoparticles for doxorubicin controlled release. *Pharmazie*. 2008;(12):878-882. doi:10.1691/ph.2008.8162

References

_____

99. Patel D. Nanostructured Lipid Carriers (NLC)-Based Gel for Topical Delivery of Aceclofenac: Preparation, Characterization and In Vivo Evaluation. *Sci Pharm*. 2012;80(3):749-764. doi:10.3797/scipharm.1202-12

100. Pezeshki A, Ghanbarzadeh B, Mohammadi M, Fathollahi I, Hamishehkar H. Encapsulation of Vitamin A Palmitate in Nanostructured Lipid Carrier (NLC)-Effect of Surfactant Concentration on the Formulation Properties. *Adv Pharm Bull EISSN 2251-7308*. Published online 2014. doi:10.5681/APB.2014.083

101. D'Souza S. A Review of In Vitro Drug Release Test Methods for Nano-Sized Dosage Forms. *Adv Pharm*. 2014;2014:1-12. doi:10.1155/2014/304757

102. Kim Y, Park EJ, Kim TW, Na DH. Recent Progress in Drug Release Testing Methods of Biopolymeric Particulate System. *Pharmaceutics*. 2021;13(8):1313. doi:10.3390/pharmaceutics13081313

103. Salamanca C, Barrera-Ocampo A, Lasso J, Camacho N, Yarce C. Franz Diffusion Cell Approach for Pre-Formulation Characterisation of Ketoprofen Semi-Solid Dosage Forms. *Pharmaceutics*. 2018;10(3):148. doi:10.3390/pharmaceutics10030148

104. Kumar M, Sharma A, Mahmood S, Thakur A, Mirza MA, Bhatia A. Franz diffusion cell and its implication in skin permeation studies. *J Dispers Sci Technol*. Published online March 29, 2023:1-14. doi:10.1080/01932691.2023.2188923

105. Attama AA, Umeyor CE. The use of solid lipid nanoparticles for sustained drug release. *Ther Deliv*. 2015;6(6):669-684. doi:10.4155/tde.15.23

106. Gordillo-Galeano A, Ponce A, Mora-Huertas CE. In vitro release behavior of SLN, NLC, and NE: An explanation based on the particle structure and carried molecule location. *J Drug Deliv Sci Technol*. 2022;76:103768. doi:10.1016/j.jddst.2022.103768

107. Zoubari G, Staufenbiel S, Volz P, Alexiev U, Bodmeier R. Effect of drug solubility and lipid carrier on drug release from lipid nanoparticles for dermal delivery. *Eur J Pharm Biopharm*. 2017;110:39-46. doi:10.1016/j.ejpb.2016.10.021

108. Khosa A, Reddi S, Saha RN. Nanostructured lipid carriers for site-specific drug delivery. *Biomed Pharmacother*. 2018;103:598-613. doi:10.1016/j.biopha.2018.04.055

109. Ghasemiyeh P, Mohammadi-Samani S. Solid lipid nanoparticles and nanostructured lipid carriers as novel drug delivery systems: applications, advantages and disadvantages. *Res Pharm Sci*. 2018;13(4):288. doi:10.4103/1735-5362.235156

110. Khan S, Baboota S, Ali J, Khan S, Narang R, Narang J. Nanostructured lipid carriers: An emerging platform for improving oral bioavailability of lipophilic drugs. *Int J Pharm Investig*. 2015;5(4):182. doi:10.4103/2230-973X.167661

111. Ganesan P, Narayanasamy D. Lipid nanoparticles: Different preparation techniques, characterization, hurdles, and strategies for the production of solid lipid nanoparticles and nanostructured lipid carriers for oral drug delivery. *Sustain Chem Pharm*. 2017;6:37-56. doi:10.1016/j.scp.2017.07.002

112. Seo Y, Lim H, Park H, et al. Recent Progress of Lipid Nanoparticles-Based Lipophilic Drug Delivery: Focus on Surface Modifications. *Pharmaceutics*. 2023;15(3):772. doi:10.3390/pharmaceutics15030772

113. Liu X, Zhang Z, Jiang Y, et al. Novel PEG-grafted nanostructured lipid carrier for systematic delivery of a poorly soluble anti-leukemia agent Tamibarotene: characterization and evaluation. *Drug Deliv*. 2015;22(2):223-229. doi:10.3109/10717544.2014.885614

114. Momoh MA, Franklin KC, Agbo CP, et al. Microemulsion-based approach for oral delivery of insulin: formulation design and characterization. *Heliyon*. 2020;6(3):e03650. doi:10.1016/j.heliyon.2020.e03650

115. Kamath H, A S. Microemulsion Based Formulation as Drug Delivery System for Gliclazide. *Indian J Pharm Educ Res*. 2017;51(4s):s571-s579. doi:10.5530/ijper.51.4s.85

116. Subongkot T, Ngawhirunpat T. Development of a novel microemulsion for oral absorption enhancement of all-trans retinoic acid. *Int J Nanomedicine*. 2017;Volume 12:5585-5599. doi:10.2147/IJN.S142503

117. Formica ML, Real DA, Picchio ML, Catlin E, Donnelly RF, Paredes AJ. On a highway to the brain: A review on nose-to-brain drug delivery using nanoparticles. *Appl Mater Today*. 2022;29:101631. doi:10.1016/j.apmt.2022.101631

118. Pires A, Fortuna A, Alves G, Falcão A. Intranasal Drug Delivery: How, Why and What for? *J Pharm Pharm Sci*. 2009;12(3):288. doi:10.18433/J3NC79

119. Deruyver L, Rigaut C, Gomez-Perez A, Lambert P, Haut B, Goole J. In vitro Evaluation of Paliperidone Palmitate Loaded Cubosomes Effective for Nasal-to-Brain Delivery. *Int J Nanomedicine*. 2023;Volume 18:1085-1106. doi:10.2147/IJN.S397650

120. Lee D, Minko T. Nanotherapeutics for Nose-to-Brain Drug Delivery: An Approach to Bypass the Blood Brain Barrier. *Pharmaceutics*. 2021;13(12):2049. doi:10.3390/pharmaceutics13122049

121. Cone RA. Barrier properties of mucus. *Adv Drug Deliv Rev*. 2009;61(2):75-85. doi:10.1016/j.addr.2008.09.008

122. Williams OW, Sharafkhaneh A, Kim V, Dickey BF, Evans CM. Airway Mucus: From Production to Secretion. *Am J Respir Cell Mol Biol*. 2006;34(5):527-536. doi:10.1165/rcmb.2005-0436SF

123. Bustamante-Marin XM, Ostrowski LE. Cilia and Mucociliary Clearance. *Cold Spring Harb Perspect Biol*. 2017;9(4):a028241. doi:10.1101/cshperspect.a028241

124. Marasini N, Skwarczynski M, Toth I. Intranasal delivery of nanoparticle-based vaccines. *Ther Deliv*. 2017;8(3):151-167. doi:10.4155/tde-2016-0068

125. Beule AG. Physiology and pathophysiology of respiratory mucosa of the nose and the paranasal sinuses. *GMS Curr Top Otorhinolaryngol - Head Neck Surg 9Doc07 ISSN 1865-1011*. Published online 2010. doi:10.3205/CTO000071

126. Aderibigbe B, Naki T. Design and Efficacy of Nanogels Formulations for Intranasal Administration. *Molecules*. 2018;23(6):1241. doi:10.3390/molecules23061241

127. Fortuna A, Alves G, Serralheiro A, Sousa J, Falcão A. Intranasal delivery of systemic-acting drugs: Small-molecules and biomacromolecules. *Eur J Pharm Biopharm*. 2014;88(1):8-27. doi:10.1016/j.ejpb.2014.03.004

128. Thwala LN, Préat V, Csaba NS. Emerging delivery platforms for mucosal administration of biopharmaceuticals: a critical update on nasal, pulmonary and oral routes. *Expert Opin Drug Deliv*. 2017;14(1):23-36. doi:10.1080/17425247.2016.1206074

129. Maggio ET. Intravail™: highly effective intranasal delivery of peptide and protein drugs. *Expert Opin Drug Deliv*. 2006;3(4):529-539. doi:10.1517/17425247.3.4.529

130. Emirzeoglu M, Şahin B, Çelebi M, Uzun A, Bilgic S, Tontus O. Estimation of nasal cavity and conchae volumes by stereological method. *Folia Morphol*. 2012;71:105-108.

131. Pandey V, Gadeval A, Asati S, et al. Formulation strategies for nose-to- brain delivery of therapeutic molecules. In: ; 2020:291-332.

_____

132. Lobaina Mato Y. Nasal route for vaccine and drug delivery: Features and current opportunities. *Int J Pharm*. 2019;572:118813. doi:10.1016/j.ijpharm.2019.118813

133. Zaman M, Chandrudu S, Giddam AK, et al. Group A Streptococcal vaccine candidate: contribution of epitope to size, antigen presenting cell interaction and immunogenicity. *Nanomed*. 2014;9(17):2613-2624. doi:10.2217/nnm.14.190

134. Makidon PE, Bielinska AU, Nigavekar SS, et al. Pre-Clinical Evaluation of a Novel Nanoemulsion-Based Hepatitis B Mucosal Vaccine. Zimmer J, ed. *PLoS ONE*. 2008;3(8):e2954. doi:10.1371/journal.pone.0002954

135. Makidon PE, Belyakov IM, Blanco LP, et al. Nanoemulsion mucosal adjuvant uniquely activates cytokine production by nasal ciliated epithelium and induces dendritic cell trafficking: Immunity to infection. *Eur J Immunol*. 2012;42(8):2073-2086. doi:10.1002/eji.201142346

136. Wong PT, Leroueil PR, Smith DM, et al. Formulation, High Throughput In Vitro Screening and In Vivo Functional Characterization of Nanoemulsion-Based Intranasal Vaccine Adjuvants. Renukaradhya GJ, ed. *PLOS ONE*. 2015;10(5):e0126120. doi:10.1371/journal.pone.0126120

137. Kadry H, Noorani B, Cucullo L. A blood–brain barrier overview on structure, function, impairment, and biomarkers of integrity. *Fluids Barriers CNS*. 2020;17(1):69. doi:10.1186/s12987-020-00230-3

138. Blasi P, Giovagnoli S, Schoubben A, Ricci M, Rossi C. Solid lipid nanoparticles for targeted brain drug delivery☆. *Adv Drug Deliv Rev*. 2007;59(6):454-477. doi:10.1016/j.addr.2007.04.011

139. Ballabh P, Braun A, Nedergaard M. The blood–brain barrier: an overview. *Neurobiol Dis*. 2004;16(1):1-13. doi:10.1016/j.nbd.2003.12.016

140. Pardridge WM. The blood-brain barrier: Bottleneck in brain drug development. *NeuroRX*. 2005;2(1):3-14. doi:10.1602/neurorx.2.1.3

141. Daneman R, Prat A. The Blood–Brain Barrier. *Cold Spring Harb Perspect Biol*. 2015;7(1):a020412. doi:10.1101/cshperspect.a020412

142. Neumaier F, Zlatopolskiy BD, Neumaier B. Drug Penetration into the Central Nervous System: Pharmacokinetic Concepts and In Vitro Model Systems. *Pharmaceutics*. 2021;13(10):1542. doi:10.3390/pharmaceutics13101542

143. Jeong SH, Jang JH, Lee YB. Drug delivery to the brain via the nasal route of administration: exploration of key targets and major consideration factors. *J Pharm Investig*. 2023;53(1):119-152. doi:10.1007/s40005-022-00589-5

144. Costa CP, Moreira JN, Sousa Lobo JM, Silva AC. Intranasal delivery of nanostructured lipid carriers, solid lipid nanoparticles and nanoemulsions: A current overview of in vivo studies. *Acta Pharm Sin B*. 2021;11(4):925-940. doi:10.1016/j.apsb.2021.02.012

145. Cunha S, Forbes B, Sousa Lobo JM, Silva AC. Improving Drug Delivery for Alzheimer's Disease Through Nose-to-Brain Delivery Using Nanoemulsions, Nanostructured Lipid Carriers (NLC) and in situ Hydrogels. *Int J Nanomedicine*. 2021;Volume 16:4373-4390. doi:10.2147/IJN.S305851

146. Boyuklieva R, Pilicheva B. Micro- and Nanosized Carriers for Nose-to-Brain Drug Delivery in Neurodegenerative Disorders. *Biomedicines*. 2022;10(7):1706. doi:10.3390/biomedicines10071706

147. Pires PC, Santos AO. Nanosystems in nose-to-brain drug delivery: A review of non-clinical brain targeting studies. *J Controlled Release*. 2018;270:89-100. doi:10.1016/j.jconrel.2017.11.047

148. Lockman PR, Koziara JM, Mumper RJ, Allen DD. Nanoparticle Surface Charges Alter Blood–Brain Barrier Integrity and Permeability. *J Drug Target*. 2004;12(9-10):635-641. doi:10.1080/10611860400015936

149. De Oliveira Junior ER, Truzzi E, Ferraro L, et al. Nasal administration of nanoencapsulated geraniol/ursodeoxycholic acid conjugate: Towards a new approach for the management of Parkinson's disease. *J Controlled Release*. 2020;321:540-552. doi:10.1016/j.jconrel.2020.02.033

150. Gupta S, Kesarla R, Chotai N, Misra A, Omri A. Systematic Approach for the Formulation and Optimization of Solid Lipid Nanoparticles of Efavirenz by High Pressure Homogenization Using Design of Experiments for Brain Targeting and Enhanced Bioavailability. *BioMed Res Int*. 2017;2017:1-18. doi:10.1155/2017/5984014

151. Du W, Li H, Tian B, et al. Development of nose-to-brain delivery of ketoconazole by nanostructured lipid carriers against cryptococcal meningoencephalitis in mice. *Colloids Surf B Biointerfaces*. 2019;183:110446. doi:10.1016/j.colsurfb.2019.110446

152. Jojo GM, Kuppusamy G, De A, Karri VVSNR. Formulation and optimization of intranasal nanolipid carriers of pioglitazone for the repurposing in Alzheimer's disease using Box-Behnken design. *Drug Dev Ind Pharm*. 2019;45(7):1061-1072. doi:10.1080/03639045.2019.1593439

153. Masjedi M, Azadi A, Heidari R, Mohammadi-Samani S. Nose-to-brain delivery of sumatriptan-loaded nanostructured lipid carriers: preparation, optimization, characterization and pharmacokinetic evaluation. *J Pharm Pharmacol*. 2020;72(10):1341-1351. doi:10.1111/jphp.13316

154. Gurib-Fakim A. Medicinal plants: Traditions of yesterday and drugs of tomorrow. *Mol Aspects Med*. 2006;27(1):1-93. doi:10.1016/j.mam.2005.07.008

155. Cimino C, Maurel OM, Musumeci T, et al. Essential Oils: Pharmaceutical Applications and Encapsulation Strategies into Lipid-Based Delivery Systems. *Pharmaceutics*. 2021;13(3):327. doi:10.3390/pharmaceutics13030327

156. Gnatta JR, Kurebayashi LFS, Turrini RNT, Silva MJPD. Aromatherapy and nursing: historical and theoretical conception. *Rev Esc Enferm USP*. 2016;50(1):127-133. doi:10.1590/S0080-623420160000100017

157. Abd Rashed A, Abd Rahman AZ, Rathi DNG. Essential Oils as a Potential Neuroprotective Remedy for Age-Related Neurodegenerative Diseases: A Review. *Molecules*. 2021;26(4):1107. doi:10.3390/molecules26041107

158. Kaufmann D, Dogra AK, Wink M. Myrtenal inhibits acetylcholinesterase, a known Alzheimer target. *J Pharm Pharmacol*. 2011;63(10):1368-1371. doi:10.1111/j.2042-7158.2011.01344.x

159. Karakaya S, Eksi G, Koca M, et al. Chemical and morphological characterization of Allium tuncelianum (Amaryllidaceae) and its antioxidant and anticholinesterase potentials. *An Jardín Botánico Madr*. 2019;76(2):085. doi:10.3989/ajbm.2523

160. Ademosun AO, Oboh G, Olupona AJ, Oyeleye SI, Adewuni TM, Nwanna EE. Comparative Study of Chemical Composition, *In Vitro* Inhibition of Cholinergic and Monoaminergic Enzymes, and Antioxidant Potentials of Essential Oil from Peels and Seeds of Sweet Orange (C *itrus Sinensis* [L.] Osbeck) Fruits: Volatile Oil, Anticholinergic, Anti-Monoaminergic. *J Food Biochem*. 2016;40(1):53-60. doi:10.1111/jfbc.12187

161. Costa P, Grosso C, Gonçalves S, et al. Supercritical fluid extraction and hydrodistillation for the recovery of bioactive compounds from Lavandula viridis L'Hér. *Food Chem*. 2012;135(1):112-121. doi:10.1016/j.foodchem.2012.04.108

References

162. Ali-Shtayeh MS, Jamous RM, Abu-Zaitoun SY, Khasati AI, Kalbouneh SR. Biological Properties and Bioactive Components of *Mentha spicata* L. Essential Oil: Focus on Potential Benefits in the Treatment of Obesity, Alzheimer's Disease, Dermatophytosis, and Drug-Resistant Infections. *Evid Based Complement Alternat Med*. 2019;2019:1-11. doi:10.1155/2019/3834265

163. Özbek H, Güvenalp Z, Özek T, et al. Chemical Composition, Antioxidant and Anticholinesterase Activities of the Essential oil of Origanum rotundifolium Boiss. from Turkey. *Rec Nat Prod*. 2017;11(5):485-490. doi:10.25135/rnp.62.16.05.040

164. Kawamoto H, Takeshita F, Murata K. Inhibitory Effects of Essential Oil Extracts From Panax Plants Against β-Secretase, Cholinesterase, and Amyloid Aggregation. *Nat Prod Commun*. 2019;14(10):1934578X1988154. doi:10.1177/1934578X19881549

165. El Euch SK, Hassine DB, Cazaux S, Bouzouita N, Bouajila J. Salvia officinalis essential oil: Chemical analysis and evaluation of anti-enzymatic and antioxidant bioactivities. *South Afr J Bot*. 2019;120:253-260. doi:10.1016/j.sajb.2018.07.010

166. Zhang Z, Chen W, Luan J, Chen D, Liu L, Feng X. Ameliorative effects of olibanum essential oil on learning and memory in Aβ1-42-induced Alzheimer's disease mouse model. *Trop J Pharm Res*. 2020;19(8):1643-1651. doi:10.4314/tjpr.v19i8.12

167. Liu B, Kou J, Li F, et al. Lemon essential oil ameliorates age-associated cognitive dysfunction via modulating hippocampal synaptic density and inhibiting acetylcholinesterase. *Aging*. 2020;12(9):8622-8639. doi:10.18632/aging.103179

168. Ayuob NN, El Wahab MGA, Ali SS, Abdel-Tawab HS. Ocimum basilicum improve chronic stress-induced neurodegenerative changes in mice hippocampus. *Metab Brain Dis*. 2018;33(3):795-804. doi:10.1007/s11011-017-0173-3

169. Satou T, Hanashima Y, Mizutani I, Koike K. The effect of inhalation of essential oil from *Rosmarinus officinalis* on scopolamine-induced Alzheimer's type dementia model mice. *Flavour Fragr J*. 2018;33(3):230-234. doi:10.1002/ffj.3435

170. Medhat D, El-mezayen HA, El-Naggar ME, et al. Evaluation of urinary 8-hydroxy-2-deoxyguanosine level in experimental Alzheimer's disease: Impact of carvacrol nanoparticles. *Mol Biol Rep*. 2019;46(4):4517-4527. doi:10.1007/s11033-019-04907-3

171. Ramazani E, YazdFazeli M, Emami SA, et al. Protective effects of Cinnamomum verum, Cinnamomum cassia and cinnamaldehyde against 6-OHDA-induced apoptosis in PC12 cells. *Mol Biol Rep*. 2020;47(4):2437-2445. doi:10.1007/s11033-020-05284-y

172. Beserra-Filho JIA, De Macêdo AM, Leão AHFF, et al. Eplingiella fruticosa leaf essential oil complexed with β-cyclodextrin produces a superior neuroprotective and behavioral profile in a mice model of Parkinson's disease. *Food Chem Toxicol*. 2019;124:17-29. doi:10.1016/j.fct.2018.11.056

173. Nikolova G, Karamalakova Y, Gadjeva V. Reducing oxidative toxicity of L-dopa in combination with two different antioxidants: an essential oil isolated from Rosa Damascena Mill., and vitamin C. *Toxicol Rep*. 2019;6:267-271. doi:10.1016/j.toxrep.2019.03.006

174. Issa MY, Ezzat MI, Sayed RH, Elbaz EM, Omar FA, Mohsen E. Neuroprotective effects of Pulicaria undulata essential oil in rotenone model of parkinson's disease in rats: Insights into its anti-inflammatory and anti-oxidant effects. *South Afr J Bot*. 2020;132:289-298. doi:10.1016/j.sajb.2020.04.032

175. Ning B, Deng M, Zhang Q, Wang N, Fang Y. β-Asarone Inhibits IRE1/XBP1 Endoplasmic Reticulum Stress Pathway in 6-OHDA-Induced Parkinsonian Rats. *Neurochem Res*. 2016;41(8):2097-2101. doi:10.1007/s11064-016-1922-0

176. Ayaz M, Sadiq A, Junaid M, Ullah F, Subhan F, Ahmed J. Neuroprotective and Anti-Aging Potentials of Essential Oils from Aromatic and Medicinal Plants. *Front Aging Neurosci*. 2017;9:168. doi:10.3389/fnagi.2017.00168

177. Elliott M, Abuhamdah S, Howes MJ, et al. The essential oils from Melissa officinalis L. and Lavandula angustifolia Mill. as potential treatment for agitation in people with severe dementia. *Int J Essent Oil Ther*. 2007;1:143-152.

178. Zhou W, Yoshioka M, Yokogoshi H. Sub-Chronic Effects of s-Limonene on Brain Neurotransmitter Levels and Behavior of Rats. *J Nutr Sci Vitaminol (Tokyo)*. 2009;55(4):367-373. doi:10.3177/jnsv.55.367

179. Bradley BF, Starkey NJ, Brown SL, Lea RW. Anxiolytic effects of Lavandula angustifolia odour on the Mongolian gerbil elevated plus maze. *J Ethnopharmacol*. 2007;111(3):517-525. doi:10.1016/j.jep.2006.12.021

180. Linck VDM, Da Silva AL, Figueiró M, et al. Inhaled linalool-induced sedation in mice. *Phytomedicine*. 2009;16(4):303-307. doi:10.1016/j.phymed.2008.08.001

181. Uzunçakmak T, Ayaz Alkaya S. Effect of aromatherapy on coping with premenstrual syndrome: A randomized controlled trial. *Complement Ther Med*. 2018;36:63-67. doi:10.1016/j.ctim.2017.11.022

182. Karan NB. Influence of lavender oil inhalation on vital signs and anxiety: A randomized clinical trial. *Physiol Behav*. 2019;211:112676. doi:10.1016/j.physbeh.2019.112676

183. Hozumi H, Hasegawa S, Tsunenari T, et al. Aromatherapies using Osmanthus fragrans oil and grapefruit oil are effective complementary treatments for anxious patients undergoing colonoscopy: A randomized controlled study. *Complement Ther Med*. 2017;34:165-169. doi:10.1016/j.ctim.2017.08.012

184. Hamdamian S, Nazarpour S, Simbar M, Hajian S, Mojab F, Talebi A. Effects of aromatherapy with Rosa damascena on nulliparous women's pain and anxiety of labor during first stage of labor. *J Integr Med*. 2018;16(2):120-125. doi:10.1016/j.joim.2018.02.005

185. Conrad P, Adams C. The effects of clinical aromatherapy for anxiety and depression in the high risk postpartum woman – A pilot study. *Complement Ther Clin Pract*. 2012;18(3):164-168. doi:10.1016/j.ctcp.2012.05.002

186. Sánchez-López E, Espina M, Doktorovova S, Souto EB, García ML. Lipid nanoparticles (SLN, NLC): Overcoming the anatomical and physiological barriers of the eye – Part I – Barriers and determining factors in ocular delivery. *Eur J Pharm Biopharm*. 2017;110:70-75. doi:10.1016/j.ejpb.2016.10.009

187. Nissen MH, Röpke C. Innate and Adaptive Immunity of the Eye. In: Fischbarg J, ed. *Advances in Organ Biology*. Vol 10. Elsevier; 2005:291-305. doi:10.1016/S1569-2590(05)10011-1

188. Delplace V, Payne S, Shoichet M. Delivery strategies for treatment of age-related ocular diseases: From a biological understanding to biomaterial solutions. *J Controlled Release*. 2015;219:652-668. doi:10.1016/j.jconrel.2015.09.065

189. Abelson MB, Udell IJ, Weston JH. Normal Human Tear pH by Direct Measurement. *Arch Ophthalmol*. 1981;99(2):301-301. doi:10.1001/archopht.1981.03930010303017

190. Ameeduzzafar, Ali J, Fazil M, Qumbar M, Khan N, Ali A. Colloidal drug delivery system: amplify the ocular delivery. *Drug Deliv*. 2016;23(3):700-716. doi:10.3109/10717544.2014.923065

191. Natarajan JV, Chattopadhyay S, Ang M, et al. Sustained Release of an Anti-Glaucoma Drug: Demonstration of Efficacy of a Liposomal Formulation in the Rabbit Eye. Villoslada P, ed. *PLoS ONE*. 2011;6(9):e24513. doi:10.1371/journal.pone.0024513

192. Hughes P, Olejnik O, Changlin J, Wilson C. Topical and systemic drug delivery to the posterior segments. *Adv Drug Deliv Rev*. 2005;57(14):2010-2032. doi:10.1016/j.addr.2005.09.004

193. Thrimawithana TR, Young S, Bunt CR, Green C, Alany RG. Drug delivery to the posterior segment of the eye. *Drug Discov Today*. 2011;16(5-6):270-277. doi:10.1016/j.drudis.2010.12.004

194. Urtti A. Challenges and obstacles of ocular pharmacokinetics and drug delivery. *Adv Drug Deliv Rev*. 2006;58(11):1131-1135. doi:10.1016/j.addr.2006.07.027

195. Bonilla L, Espina M, Severino P, et al. Lipid Nanoparticles for the Posterior Eye Segment. *Pharmaceutics*. 2021;14(1):90. doi:10.3390/pharmaceutics14010090

196. De Oliveira IF, Barbosa EJ, Peters MCC, et al. Cutting-edge advances in therapy for the posterior segment of the eye: Solid lipid nanoparticles and nanostructured lipid carriers. *Int J Pharm*. 2020;589:119831. doi:10.1016/j.ijpharm.2020.119831

197. Platania CBM, Dei Cas M, Cianciolo S, et al. Novel ophthalmic formulation of myriocin: implications in retinitis pigmentosa. *Drug Deliv*. 2019;26(1):237-243. doi:10.1080/10717544.2019.1574936

198. Chetoni P, Burgalassi S, Monti D, et al. Solid lipid nanoparticles as promising tool for intraocular tobramycin delivery: Pharmacokinetic studies on rabbits. *Eur J Pharm Biopharm*. 2016;109:214-223. doi:10.1016/j.ejpb.2016.10.006

199. Araújo J, Nikolic S, Egea MA, Souto EB, Garcia ML. Nanostructured lipid carriers for triamcinolone acetonide delivery to the posterior segment of the eye. *Colloids Surf B Biointerfaces*. 2011;88(1):150-157. doi:10.1016/j.colsurfb.2011.06.025

200. Balguri SP, Adelli GR, Majumdar S. Topical ophthalmic lipid nanoparticle formulations (SLN, NLC) of indomethacin for delivery to the posterior segment ocular tissues. *Eur J Pharm Biopharm*. 2016;109:224-235. doi:10.1016/j.ejpb.2016.10.015

201. Selvaraj K, Kuppusamy G, Krishnamurthy J, Mahalingam R, Singh SK, Gulati M. Repositioning of Itraconazole for the Management of Ocular Neovascularization Through Surface-Modified Nanostructured Lipid Carriers. *ASSAY Drug Dev Technol*. 2019;17(4):178-190. doi:10.1089/adt.2018.898

202. Andreoli MT, Mieler WF, Leiderman YI. Epidemiological trends in uveal melanoma. *Br J Ophthalmol*. 2015;99(11):1550-1553. doi:10.1136/bjophthalmol-2015-306810

203. Kaliki S, Shields CL. Uveal melanoma: relatively rare but deadly cancer. *Eye*. 2017;31(2):241-257. doi:10.1038/eye.2016.275

204. Moschos MM, Dettoraki M, Androudi S, et al. The Role of Histone Deacetylase Inhibitors in Uveal Melanoma: Current Evidence. *Anticancer Res*. 2018;38(7):3817-3824. doi:10.21873/anticanres.12665

205. Spagnolo F, Caltabiano G, Queirolo P. Uveal melanoma. *Cancer Treat Rev*. 2012;38(5):549-553. doi:10.1016/j.ctrv.2012.01.002

206. Shields CL. Metastasis of Uveal Melanoma Millimeter-by-Millimeter in 8033 Consecutive Eyes. *Arch Ophthalmol*. 2009;127(8):989. doi:10.1001/archophthalmol.2009.208

207. Kaliki S, Shields CL, Mashayekhi A, Ganesh A, Furuta M, Shields JA. Influence of Age on Prognosis of Young Patients with Uveal Melanoma: A Matched Retrospective Cohort Study. *Eur J Ophthalmol*. 2013;23(2):208-216. doi:10.5301/ejo.5000200

208. Damato EM, Damato BE. Detection and Time to Treatment of Uveal Melanoma in the United Kingdom: An Evaluation of 2384 Patients. *Ophthalmology*. 2012;119(8):1582-1589. doi:10.1016/j.ophtha.2012.01.048

209. Shields CL, Kaliki S, Rojanaporn D, Ferenczy SR, Shields JA. Enhanced Depth Imaging Optical Coherence Tomography of Small Choroidal Melanoma: Comparison With Choroidal Nevus. *Arch Ophthalmol*. 2012;130(7):850. doi:10.1001/archophthalmol.2012.1135

210. Schmidt-Pokrzywniak A, Jöckel KH, Bornfeld N, Sauerwein W, Stang A. Positive Interaction Between Light Iris Color and Ultraviolet Radiation in Relation to the Risk of Uveal Melanoma. *Ophthalmology*. 2009;116(2):340-348. doi:10.1016/j.ophtha.2008.09.040

211. Shields CL, Kaliki S, Livesey M, et al. Association of Ocular and Oculodermal Melanocytosis With the Rate of Uveal Melanoma Metastasis: Analysis of 7872 Consecutive Eyes. *JAMA Ophthalmol*. 2013;131(8):993. doi:10.1001/jamaophthalmol.2013.129

212. Rahmi A, Mammar H, Thariat J, et al. Proton beam therapy for presumed and confirmed iris melanomas: a review of 36 cases. *Graefes Arch Clin Exp Ophthalmol*. 2014;252(9):1515-1521. doi:10.1007/s00417-014-2735-y

213. Croce, Ferrini, Pfeffer, Gangemi. Targeted Therapy of Uveal Melanoma: Recent Failures and New Perspectives. *Cancers*. 2019;11(6):846. doi:10.3390/cancers11060846

214. Bhatia S, Moon J, Margolin KA, et al. Phase II Trial of Sorafenib in Combination with Carboplatin and Paclitaxel in Patients with Metastatic Uveal Melanoma: SWOG S0512. Stemmer SM, ed. *PLoS ONE*. 2012;7(11):e48787. doi:10.1371/journal.pone.0048787

215. Mouriaux F, Servois V, Parienti JJ, et al. Sorafenib in metastatic uveal melanoma: efficacy, toxicity and health-related quality of life in a multicentre phase II study. *Br J Cancer*. 2016;115(1):20-24. doi:10.1038/bjc.2016.119

216. Bondì ML, Botto C, Amore E, et al. Lipid nanocarriers containing sorafenib inhibit colonies formation in human hepatocarcinoma cells. *Int J Pharm*. 2015;493(1-2):75-85. doi:10.1016/j.ijpharm.2015.07.055

217. Mangana J, Levesque MP, Karpova MB, Dummer R. Sorafenib in melanoma. *Expert Opin Investig Drugs*. 2012;21(4):557-568. doi:10.1517/13543784.2012.665872

218. Santonocito M, Zappulla C, Viola S, et al. Assessment of a New Nanostructured Microemulsion System for Ocular Delivery of Sorafenib to Posterior Segment of the Eye. *Int J Mol Sci*. 2021;22(9):4404. doi:10.3390/ijms22094404

219. Barbaraci C, Giurdanella G, Leotta CG, et al. Haloperidol Metabolite II Valproate Ester (*S*)-(−)-MRJF22: Preliminary Studies as a Potential Multifunctional Agent Against Uveal Melanoma. *J Med Chem*. 2021;64(18):13622-13632. doi:10.1021/acs.jmedchem.1c00995

220. Xie XY, Li YY, Ma WH, et al. Synthesis, binding, and functional properties of tetrahydroisoquinolino-2-alkyl phenones as selective σ2R/TMEM97 ligands. *Eur J Med Chem*. 2021;209:112906. doi:10.1016/j.ejmech.2020.112906

References

_____

221. Scuteri D, Morrone LA, Rombolà L, et al. Aromatherapy and Aromatic Plants for the Treatment of Behavioural and Psychological Symptoms of Dementia in Patients with Alzheimer's Disease: Clinical Evidence and Possible Mechanisms. *Evid Based Complement Alternat Med*. 2017;2017:1-8. doi:10.1155/2017/9416305

222. Jimbo D, Kimura Y, Taniguchi M, Inoue M, Urakami K. Effect of aromatherapy on patients with Alzheimer's disease. *Psychogeriatrics*. 2009;9(4):173-179. doi:10.1111/j.1479-8301.2009.00299.x

223. Filiptsova OV, Gazzavi-Rogozina LV, Timoshyna IA, Naboka OI, Dyomina YeV, Ochkur AV. The effect of the essential oils of lavender and rosemary on the human short-term memory. *Alex J Med*. 2018;54(1):41-44. doi:10.1016/j.ajme.2017.05.004

224. Hritcu L, Cioanca O, Hancianu M. Effects of lavender oil inhalation on improving scopolamine-induced spatial memory impairment in laboratory rats. *Phytomedicine*. 2012;19(6):529-534. doi:10.1016/j.phymed.2012.02.002

225. Agu RU. Challenges in nasal drug absorption: how far have we come? *Ther Deliv*. 2016;7(7):495-510. doi:10.4155/tde-2016-0022

226. Sastre J, Mosges R. Local and systemic safety of intranasal corticosteroids. *J Investig Allergol Clin Immunol*. 2012;22(1):1-12.

227. Mirchandani Y, Patravale VB, S. B. Solid lipid nanoparticles for hydrophilic drugs. *J Controlled Release*. 2021;335:457-464. doi:10.1016/j.jconrel.2021.05.032

228. Singh Y, Meher JG, Raval K, et al. Nanoemulsion: Concepts, development and applications in drug delivery. *J Controlled Release*. 2017;252:28-49. doi:10.1016/j.jconrel.2017.03.008

229. Buzzacco DM. Long-Term Survivors with Metastatic Uveal Melanoma. *Open Ophthalmol J*. 2012;6(1):49-53. doi:10.2174/1874364101206010049

230. Assessment of Metastatic Disease Status at Death in 435 Patients With Large Choroidal Melanoma in the Collaborative Ocular Melanoma Study (COMS). *Arch Ophthalmol*. 2001;119:670-676.

231. Benizri S, Ferey L, Alies B, et al. Nucleoside-Lipid-Based Nanocarriers for Sorafenib Delivery. *Nanoscale Res Lett*. 2018;13(1):17. doi:10.1186/s11671-017-2420-2

232. Cimino C, Leotta CG, Marrazzo A, et al. Nanostructured lipid carrier for the ophthalmic delivery of haloperidol metabolite II valproate ester (±)-MRJF22: A potential strategy in the treatment of uveal melanoma. *J Drug Deliv Sci Technol*. Published online August 2023:104811. doi:10.1016/j.jddst.2023.104811

233. Zingale E, Romeo A, Rizzo S, et al. Fluorescent Nanosystems for Drug Tracking and Theranostics: Recent Applications in the Ocular Field. *Pharmaceutics*. 2022;14(5):955. doi:10.3390/pharmaceutics14050955

234. Bonaccorso A, Pellitteri R, Ruozi B, et al. Curcumin Loaded Polymeric vs. Lipid Nanoparticles: Antioxidant Effect on Normal and Hypoxic Olfactory Ensheathing Cells. *Nanomaterials*. 2021;11(1):159. doi:10.3390/nano11010159

235. Musumeci T, Bonaccorso A, Carbone C, Russo G, Pappalardo F, Puglisi G. Design and optimization of PEGylated nanoparticles intended for Berberine Chloride delivery. *J Drug Deliv Sci Technol*. 2019;52:521-530. doi:10.1016/j.jddst.2019.05.012

236. Reeta RM, John M, Newton A. Fabrication and Characterisation of Lavender Oil and Plant Phospholipid Based Sumatriptan Succinate Hybrid Nano Lipid Carriers. *Pharm Biomed Res*. Published online June 28, 2020. doi:10.18502/pbr.v6i1.3430

237. Vieira R, Severino P, Nalone LA, et al. Sucupira Oil-Loaded Nanostructured Lipid Carriers (NLC): Lipid Screening, Factorial Design, Release Profile, and Cytotoxicity. *Molecules*. 2020;25(3):685. doi:10.3390/molecules25030685

238. Rehman S, Nabi B, Zafar A, Baboota S, Ali J. Intranasal delivery of mucoadhesive nanocarriers: a viable option for Parkinson's disease treatment? *Expert Opin Drug Deliv*. 2019;16(12):1355-1366. doi:10.1080/17425247.2019.1684895

239. Akram S, Anton N, Omran Z, Vandamme T. Water-in-Oil Nano-Emulsions Prepared by Spontaneous Emulsification: New Insights on the Formulation Process. *Pharmaceutics*. 2021;13(7):1030. doi:10.3390/pharmaceutics13071030

240. Major-Godlewska M. The influence of stirring time and frequency of impeller rotation on evaluation of drops dimensions and rheological properties of the multiple emulsion. *Chem Pap*. 2020;74(9):3135-3143. doi:10.1007/s11696-020-01146-w

241. Agrawal M, Saraf S, Pradhan M, et al. Design and optimization of curcumin loaded nano lipid carrier system using Box-Behnken design. *Biomed Pharmacother*. 2021;141:111919. doi:10.1016/j.biopha.2021.111919

242. Da Costa S, Basri M, Shamsudin N, Basri H. Stability of Positively Charged Nanoemulsion Formulation Containing Steroidal Drug for Effective Transdermal Application. *J Chem*. 2014;2014:1-8. doi:10.1155/2014/748680

243. Sakeena MHF, Elrashid SM, Munavvar AS, Azmin MN. Effects of Oil and Drug Concentrations on Droplets Size of Palm Oil Esters (POEs) Nanoemulsion. *J Oleo Sci*. 2011;60(4):155-158. doi:10.5650/jos.60.155

244. Puglia C, Offerta A, Carbone C, Bonina F, Pignatello R, Puglisi G. Lipid Nanocarriers (LNC) and their Applications in Ocular Drug Delivery. *Curr Med Chem*. 2015;22(13):1589-1602. doi:10.2174/0929867322666150209152259

245. Takahashi Y, Hayashi K, Abo T, Koike M, Sakaguchi H, Nishiyama N. The Short Time Exposure (STE) test for predicting eye irritation potential: Intra-laboratory reproducibility and correspondence to globally harmonized system (GHS) and EU eye irritation classification for 109 chemicals. *Toxicol In Vitro*. 2011;25(7):1425-1434. doi:10.1016/j.tiv.2011.04.012

246. Kubackova J, Holas O, Zbytovska J, et al. Oligonucleotide Delivery across the Caco-2 Monolayer: The Design and Evaluation of Self-Emulsifying Drug Delivery Systems (SEDDS). *Pharmaceutics*. 2021;13(4):459. doi:10.3390/pharmaceutics13040459

247. Sharif Makhmal Zadeh B, Niro H, Rahim F, Esfahani G. Ocular Delivery System for Propranolol Hydrochloride Based on Nanostructured Lipid Carrier. *Sci Pharm*. 2018;86(2):16. doi:10.3390/scipharm86020016

248. Karmakar G, Nahak P, Guha P, Roy B, Nath RK, Panda AK. Role of PEG 2000 in the surface modification and physicochemical characteristics of pyrazinamide loaded nanostructured lipid carriers. *J Chem Sci*. 2018;130(4):42. doi:10.1007/s12039-018-1448-x

249. Razavi MS, Ebrahimnejad P, Fatahi Y, D'Emanuele A, Dinarvand R. Recent Developments of Nanostructures for the Ocular Delivery of Natural Compounds. *Front Chem*. 2022;10:850757. doi:10.3389/fchem.2022.850757

4 ESSENTIAL OILS: PHARMACEUTICAL APPLICATIONS AND ENCAPSULATION STRATEGIES INTO LIPID-BASED DELIVERY SYSTEMS

Cinzia Cimino[1], Oriana Maurel[2], Teresa Musumeci[1], Angela Bonaccorso[1], Filippo Drago[2], Eliana Maria Barbosa Souto[3,4], Rosario Pignatello[1] and Claudia Carbone[1,*]

[1] Laboratory of Drug Delivery Technology, Department of Drug and Health Sciences, University of Catania, Viale A. Doria 6, 95125 Catania, Italy.

[2] Department of Biomedical and Biotechnological Sciences, University of Catania, 95125 Catania, Italy.

[3] Department of Pharmaceutical Technology, Faculty of Pharmacy, University of Coimbra, 3000-548 Coimbra, Portugal

[4] CEB – Centre of Biological Engineering, University of Minho, Campus de Gualtar, 4710-057 Braga, Portugal

[*] Corresponding author

Abstract: Essential oils are being studied for more than 60 years, but a growing interest has emerged in the recent decades due to a desire for a rediscovery of natural remedies. Essential oils are known for millennia and, already in prehistoric times, they were used for medicinal and ritual purposes due to their therapeutic properties. Using a variety of methods refined over the centuries, essential oils are extracted from plant raw materials: the choice of the extraction method is decisive, since it determines the type, quantity, and stereochemical structure of the essential oil molecules. To these components belong all properties that make essential oils so interesting for pharmaceutical uses; the most investigated ones are antioxidant, anti-inflammatory, antimicrobial, wound-healing, and anxiolytic activities. However, the main limitations to their use are their hydrophobicity, instability, high volatility, and risk of toxicity. A successful strategy to overcome these

limitations is the encapsulation within delivery systems, which enable the increase of essential oils bioavailability and improve their chemical stability, while reducing their volatility and toxicity. Among all the suitable platforms, our review focused on the lipid-based ones, in particular micro- and nanoemulsions, liposomes, solid lipid nanoparticles, and nanostructured lipid carriers.

Keywords: extraction method; anti-inflammatory; antioxidant; antimicrobial; wound healing; anxiolytic; nanoemulsions; microemulsions; liposomes; SLN; NLC.

4.1 History of Essential Oils

Essential oils (EOs) have been known for millennia: during the Neolithic Age (before 4000 B.C.) they were extracted from plants by simple squeezing and this was the turning point that gave rise to the sedentary lifestyle. This led to the construction of the first sacred monuments where EOs were used in rituals. Besides clay cuneiform writing pieces (2600 B.C.) discovered in Mesopotamia, one of the oldest discoveries that proves the use of EOs for medical purposes is an Egyptian papyrus dated 2551–2528 B.C. [1]. Moreover, the Egyptians used aromatic oils for beauty treatments and spiritual rituals, including the ceremony of mummification; the use of EOs has allowed a good preservation of some mummies. Generally, the Egyptians used to extract oils by infusion of the plant in a fatty substance and consequent boiling, in this way, the aroma evaporated and fixed itself in the fat [1]. Based on some evidences, they were aware of an oil extraction procedure by distillation, even if this was not commonly used. "Shennong's Herbal" is the oldest medical book, dating back to 2700 B.C. and belonging to the Chinese tradition: it contains the usage guidelines for 365 plants. China is still the world's leading producer of EOs. The use of EOs has been a fundamental part of Indian medical practice for five thousand years. Ayurveda is a traditional book that describes the use, both medical and religious, of over 700 different types of plants, and it is still the basis of the Indian healthcare [1]. The discovery of the stimulating and calming properties of some EOs belongs to the Greek culture; in the temples of Asclepius and Aphrodite, marble tablets with engraved recipes of some medicinal aromas have been found [2]. Hippocrates, considered the father of modern medicine, documented the medicinal importance of over 300 plants [3]. He strongly believed in the medical benefits of fumigation with aromatic oils in the treatment of the plague; he was also convinced that the topical use of aromatic preparations could produce systemic effects. Romans, under the influence of Greeks, used EOs for bathing and

massages. Among the findings belonging to Romans, there is an interesting treatise on herbal medicine dating back to the first century A.D., De Materia Medica, in which Pedanius Dioscorides reported more than 600 remedies [1]; in the following centuries the effectiveness of most of them was confirmed. Not less than 12 different types of EOs are mentioned in the Holy Bible, both in Old and New Testament [3]. During the Middle Ages, the Catholic Church banned the use of EOs for medical treatment: those who used them were burned at the stake, because they were associated to witchcraft. Despite the persecutions, the monks secretly kept the tradition [1]. A writing found in the island of Cyprus and dating back to the Ottoman Empire (1571–1878) describes 231 plants and 494 prescriptions of herbs, which were used by Orthodox monks in their hospitals [4]. In the 10th century, the Persian alchemist Avicenna gave a great contribution to science and medicine, discovering the distillation method: the first EO extracted was from rose [1]. During the 13th century, there was a great expansion of the practice of oil distillation, extracting a great variety of aromas. In the 17th century, the use of natural extracts was abandoned due to the discovery of chemical substances. The interest in EOs was rekindled in 1928 thanks to Rene-Maurice Gattefossé, who coined the term "Aromatheraphie" and discovered the healing properties of lavender EO. In 1990, the book "L'Aromatherapie Exactement" was published, in which Daniel Pénoël and Pierre Franchomme reported the medical properties of more than 270 EOs, and this was the starting point for many studies.

4.2 Principal Extraction Methods for Essential Oils

According to the definition given by the International Organization for Standardization (ISO), the term EO is related to a "product obtained from vegetable raw material, either by distillation with water or steam, or from the epicarp of citrus fruits by a mechanical process or by dry distillation." In order to extract EOs from vegetable raw material, different methods can be exploited, which can be classified in two categories: the classical (or conventional) methods and the innovative (or advanced) ones [5]. The choice of the extraction method is decisive, since it determines the type, quantity, and stereochemical structure of the essential oil molecules [6]. It is important to underline that the oil composition is strictly influenced by the variety of the plant, the place where it has grown (climate and environment, any stress suffered), the type of nutrition and fertilizers used [7]. Below a brief description of the main methods is provided. Conventional methods (Figure 1) are not very advantageous due to the thermolability of EOs (high temperatures used) and the low quality of the extract (production of chemical artefacts, due to long extraction time).

Among these methods *Hydrodistillation* can be considered a simple and old technique (it was used by Avicenna in 10th century). The parts of the plants (particularly flowers and petals) are directly boiled inside the water; this alembic is connected with a condenser (which holds the essential oil) and a decanter (that collects the evaporated water) [8]. Another technique used for EOs extraction is *Entrainment by water steam*. The principle is the same as hydrodistillation, but the plant is not in contact with water. There are several variants of this method, such as vapor-hydrodistillation, steam distillation, hydro- diffusion [9]. *Organic solvent extraction* is the third common method. The parts of the plant are put inside an organic solvent and macerated; the solvent is removed under pressure, in order to concentrate the extract. EOs extraction can also be performed by *cold pressing*. This is a traditional method used to extract EOs from citrus fruit zest. Oil sacs or oil glands break during extraction, releasing the volatile oil, which is mechanically recovered by centrifugation [10].

Conventional methods
- Hydrodistillation
- Entrainment by water steam
- Organic solvent extraction
- Cold pressing

Innovative methods
- Supercritical fluid extraction
- Subcritical extraction liquids
- Ultrasound assisted extraction
- Microwave assisted extraction
- Instant controlled pressure drop
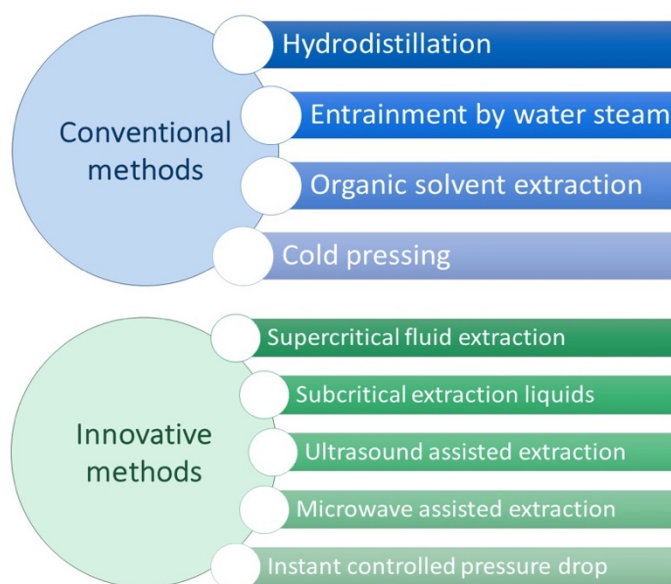
Figure 1. Schematic summary of conventional and innovative extraction methods.

Innovative methods (Figure 1), compared to the classical ones, have numerous advantages, due to the reduction in the use of solvents and in the extraction time. *Supercritical fluid extraction* is one of the most common innovative methods. The solvent used is generally CO_2, which is compressed and heated to reach the supercritical state; passing through the parts of the plant, supercritical CO_2 is loaded by volatile components and extracts; in the end, the depression phase allows the separation of the oil [11]. *Subcritical extraction liquids* can be exploited using water and CO_2 at the subcritical state, thus using lower temperatures. In *ultrasound-assisted extraction*, the vegetable is immersed in water or other solvent: the

ultrasound action favors the release of EOs from the plant, owing to mechanical vibration of the cellular walls and membranes [12]. *Microwave-assisted extraction* is one of the most potent and promising extraction methods. There are many variants: solvent free microwaves extraction (SFME); microwave hydrodiffusion and gravity (MHG); microwave steam distillation (MSD); microwave steam diffusion (MSDf). Farhat and co-worked studied the use of MSDf to extract *Lavandula* EO [13]. Comparing with other extraction methods of Lavandula EOs proposed by Périno-Issartier and co-workers, it was proved that MSDf is more efficient in terms of extraction time, and the quality of the extract is superior [14]. *Instant controlled pressure drop* (DIC) method is composed of four steps: first, the plants have to be placed under the vacuum, the steam bath is applied at determined pressure and temperature, then the void is instantly detained and the sample is taken back to the atmospheric pressure.

In Table 1 the advantages and drawbacks of the different EOs extraction methods described are reported.

Table 1. Advantages and drawbacks of different essential oils (EOs) extraction methods.

	Methods	Advantages	Drawbacks
Conventional Methods	Hydrodistillation	• EOs and water are easily separated by decantation.	• Long extraction time; • Chemical alteration due to the prolonged boiling; • Loss of some polar compounds in the evaporated water [15].
	Entrainment by water steam	• Less artefacts are generated; • The extraction time is reduced [9].	• Several hours of heating; • Degradation of thermos labile compounds; • Odor deterioration.
	Organic solvent extraction	• Alterations and chemical artefacts are avoided.	• The organic solvent can leave residues in the oil produced, compromising the safety of the product (not usable for pharmaceutics) [16].
	Cold pressing	• Native properties (in terms of beneficial compounds) are preserved [17–22]; • Low costs; • No plant safety problems.	• Nutraceutical content is lower compared with the oil obtained by solvent extraction; • Pungent odors, due to the breakdown products of glucosinolates [19,23].
Innovative Methods	Supercritical fluid extraction	• Higher quality of extracts, with better activities [24]; • Relatively low temperatures [25]; • Chemical inertness [25].	• High costs (equipment and maintenance); • Necessity of high CO_2 purity [26]; • Affinity of the supercritical CO_2 to low-polar and non-polar compounds [26].
	Subcritical extraction liquids	• The extraction time is reduced; • No loss of volatile and thermolabile compounds; • Low costs [27].	• Less presence of monoterpene compounds that in hydrodistillated oil [28]; • High amount of extractant requires [28].

	Methods	Advantages	Drawbacks
Innovative Methods	Ultrasound-assisted extraction	• High efficiency [29]; • Low temperature [29]; • Reduced solvent consumption [30]; • Less energy input [30].	• Potential formation of free radicals during sonolysis of the solvent, with consequent degradation of labile compound by oxidation.
	Microwave-assisted extraction	• Reduction of extraction time; • Environmentally friendly [31]; • Reduction of solvents; • Fast and efficient extraction; • Better sensory properties.	• Use of high temperatures with formation of undesirable compounds; • Frequent use of toxic organic solvents [26].
	Instant controlled pressure drop	• Reduction of extraction time; • Decrease of energy and water consumption [32].	• No significant disadvantages: it is currently considered the most efficient method of extracting essential oils [33].

4.3 Essential Oils Main Applications and Limits in the Pharmaceutical Field

EOs are liquid mixtures of volatile components produced by aromatic plant secondary metabolism. The main components are monoterpenes and sesquiterpenes and, to a lesser extent, aromatic and aliphatic compounds, therefore, the complex mixtures of compounds usually include terpenoids, alcohols, ethers, esters, ketones, and aldehydes in variable concentrations, and can be obtained by over 60 families of plants [34]. Concentration variability leads to significant heterogeneity in the products used in different studies and makes a comparison among results difficult [35]. Generally, EOs contain about 20–60 components up to more than 100 single substances, at quite different concentrations. Usually, two or three are the major components at high concentrations (20–70%) compared to other components present in trace amounts [6]. EOs show characteristic physical properties (e.g., color and solubility in water) that can represent some criteria for the classification and qualification to different groups [36]. The use of EOs is limited due to the following drawbacks: hydrophobicity (and, consequently, insolubility in water); instability (caused by hydrolysis and oxidation); high volatility [37,38]. Therefore, nowadays the researchers' efforts are focused on the possibility to use innovative formulation for the EO encapsulation. However, the therapeutic application of EOs as pure compounds was studied, mainly for external applications (mouthwashes or inhalation), since it is generally safe, except for some skin reactions and UV sensitivity (the exposure to sunlight could cause irritation or darkening of the skin). It is important to not exceed in the amount of the administered dose of EO and to avoid their application on broken skin, which would induce the occurrence of significant systemic absorption and, therefore, serious side effects. The administration of EOs by inhalation is the most rapid way (followed by the topic one). The use of strong oils (for direct inhalation or for diffusing) is

not recommended because they may cause eye irritation. EOs oral administration is rare, even if it is considered safe, and the EOs are generally diluted in olive oil or milk.

4.3.1 Anti-Inflammatory and Antioxidant Activities

Inflammation is an essential biological mechanism, which provides a response to harmful stimuli coming from the outside. The inflammation can be acute, when the stimulus produces a limited response over time, and therefore ends within a few days. It may also be chronic, if the external insult persists over time, the person is particularly sensitive or suffers from autoimmune pathologies. Acute inflammation is characterized by five symptoms: *calor* (increase in local vascularization with elevation of the temperature), *tumor* (formation of an exudate, which causes oedema), *rubor* (active hyperaemia causing redness), *dolor* (the inflammatory components of exudate cause stimulation of sensorial nerves and compression), and *functio laesa* (impairment of the functionality of the inflamed tissue). Chronic inflammation is mainly caused by the migration, into tissues, of mononuclear blood cells, such as monocytes and lymphocytes. The most effective therapy is the etiological one, acting on the cause of the inflammation, for example by administering an antibiotic if the cause is an infection. If this is not enough, or if the cause is not clear, traditional anti-inflammatory drugs are also used. They belong to two categories: non-steroidal anti-inflammatory drugs (NSAIDs) and corticosteroids. Especially when treating chronic inflammation, prolonged intake of these drugs could produce significant adverse effects, such as ulcers and gastritis for NSAIDs, or the risk of over-infection using glucocorticoids. For this reason, there is now a growing interest in the use of natural compounds as adjuvants for these therapies, especially chronic ones. The importance of natural medicines in the treatment of many inflammatory diseases has always been well-known. The "water of the Queen of Hungary", an infusion of rosemary EO, dates back to the 16th century, as Queen Isabell used it to cure rheumatism; it was at the court of Louis XIV that this preparation spread in the form of medicine [39]. Many other historical evidences, linked to traditional medicine, indicate the use of rosemary EO to treat inflammatory conditions of different nature, like rheumatoid arthritis, asthma, bronchitis, etc., [39–41]. One of the most commonly used *in vivo* model to analyze the anti-inflammatory power of EOs is the carrageenan-induced pleurisy experiment: a group of mice is pre-treated with the EO, while the others are monitored as positive and negative control; each mouse is treated with the inflammatory agent, which in this situation is carrageenan, and, at defined intervals, the paw oedema is measured. Using the above mentioned model, Ogunwande et al. analyzed *Bougainvillea glabra* EO to assess its effectiveness as an anti-inflammatory agent [42]. The groups of mice were treated with

different concentrations of the EO and then compared with the standard group (treated with diclofenac) and the control group (administered with saline solution). Anti-inflammatory activity of the EO was demonstrated, and it was related to its ability of inhibiting both histamine- and prostaglandins-mediated responses. Besides carrageenan, it is also possible to use dextran as an inflammatory agent, as operated by Rodrigues and co-workers who exploited both experiments to analyze *Ocimum basilicum* EO [43]. In the same work, also histamine and arachidonic acid were used as a model to analyze their inflammatory pathways. All doses administered, even lower ones, showed excellent anti-inflammatory properties in all the performed experiments. Also, *Cinnamomum osmophloeum* Kanehira leaf EO demonstrated anti-inflammatory activity, due to the presence of the two main components, cinnamaldehyde and linalool. In another study, some mice were pre-treated with one of the two compounds and then all were injected with endotoxin to activate the inflammatory pathway [44]. The results obtained from these analyses were consistent and extremely detailed: in mesenteric lymph nodes and spleen, pre-treated mice have developed fewer inflammation mediators than the non-treated ones, including interleukin (IL)-1β, tumor necrosis factor (TNF)-α, IL-18, interferon (IFN)-γ, nitrate/nitrite, etc. Furthermore, the expression of different genes, proteins, receptors, and enzymes, induced by endotoxin, was suppressed. *Artemisia argyi* EO was widely used in China for the treatment of chronic bronchitis, due to the anti-inflammatory activity of his components, as asserted by Chen et al. [45]. Among many others, they proved that the dose-dependent anti-inflammatory activity of *Artemisia argyi* EO is linked to the inhibition of two important events: the release of pro-inflammatory mediators, such as TNF-α, IL-6, IFN-β, NO, PGE2, etc., and the phosphorylation of JAK2 and STAT1/3. The suppression of JAK/STATs pathway also demonstrated the antioxidant property of this EO against reactive oxygen species (ROS). Upon this point, besides the anti-inflammatory properties of EOs, experienced for centuries, in a more contemporary age, the researchers' interest has also focused on the antioxidant properties. Oxidation occurs when the balance between free radicals and antioxidants is shifted toward the oxidizing species. Free radicals could induce a plethora of biological events, affecting various cell's components, like DNA or proteins, thus inducing several consequential pathologies, such as cancers, neurodegenerative diseases and chronic inflammation disorders. Certainly, environmental, dietary or lifestyle conditions could result in an increased amount of radical species produced by the organism and, therefore, in a condition of oxidative stress. It is well-known that through diet it is possible to compensate the inadequacy of endogenous antioxidants by consuming foods rich in vitamin A, C, and E, resveratrol, lycopene, and so on. The benefits of antioxidant

supplementation are still subject of debate and further investigation, as an attempt is nowadays focused to quantify the extent of this improvement. Many EOs have antioxidant properties, and the use of EOs as natural antioxidants is a field of growing interest because some synthetic antioxidants such as butylated hydroxyanisole (BHA) and butylated hydroxytoluene (BHT) are now suspected to be potentially harmful to human health. Addition of EOs to edible products, either by direct mixing or in active packaging and edible coatings, may therefore represent a valid alternative to prevent autoxidation and to prolong shelf life. The evaluation of the antioxidant performance of EOs still represents a crucial issue, because many commonly used "tests" are inappropriate and give contradictory results that may mislead future research. The chemistry explaining EO antioxidant activity is discussed along with an analysis of the potential in food protection. Literature methods to assess EOs antioxidant performance are critically reviewed. Currently, antioxidants have become essential in nutrition because of their ability to protect the body against oxidative cell damage that can produce dangerous diseases. EOs are one of the major sources of different bioactive molecules that directly act on the body. Literature studies describe a variety of approaches to demonstrate the antioxidant power of EOs. Among the most common essays we can identify the DPPH (1,1-diphenyl-2-picrylhydrazyl radical) method: this radical is characterized by an absorption band at 515 nm, which changes after the administration of an antioxidant; the radical scavenger activity of a compound is often quantified as IC_{50}, which is the amount of antioxidant necessary to halve the absorbance of the DPPH. This method was used by Silva and co-workers, who analyzed lavender EO, extracted from *Lavandula augustifolia* [46]. As an antioxidant, lavender EO showed good IC_{50} values, indicating that antioxidant activity is dose dependent, with a peak of activity associated with concentration of 150, 120, and 100 mg/mL. Da Silva also investigated the anti-inflammatory activity of lavender EO performing the carrageenan assay on mice, comparing it to saline solution as negative control and dexamethasone as positive control. The leukocytes diminishing effect was qualitatively similar to that produced by dexamethasone, which, however, proved to be more effective. The author suggested an involvement of a G protein-coupled receptor and/or phospholipase C/inositol phosphate messenger. Another species of lavender EO, *Lavandula x intermedia* "Sumian", was studied by Carbone and co-workers [47] together with *Rosmarinus officinalis* L. and *Origanum vulgare* subsp. *hirtum* EO, to assess their antioxidant and anti-inflammatory activities. The 2,2-diphenyl-1-picrylhydrazyl (DPPH) analysis indicated that only *Origanum* possesses a remarkable antioxidant activity, with a value of 216 μg/mL of Trolox equivalents. This is certainly attributable to the presence of

large amounts of phenolic compounds, which, on the other hand, are scarcely present in *Lavandula* and *Rosmarinus*. The same study also demonstrated the anti-inflammatory activity of the three EOs, in the following order: *Lavandula* > *Rosmarinus* ≥ *Origanum* [47]. Another widely used reagent is the 2,2-azino-bis-3-ethylbenzothiazoline-6-sulfonic acid (ABTS) cationic radical, whose protocol of use also consists in measuring the variation of the specific absorbance. It was used by Elaguel et al., in conjunction with the DPPH method and phosphomolybdenum assay, for demonstrating the antioxidant activity of *Lawsonia inermis* EO, thus suggesting the EO possible application as adjuvant in anticancer therapies [48]. DPPH and ABTS assays were also used to confirm the antioxidant property of the EO extracted from blossoms of *Citrus aurantium* L. var. *amara* Engl (CAVAO), which has also shown an even more marked anti-inflammatory activity, that could be exploited for the development of functional foods to be used in patients with inflammatory diseases [49]. Another assay worth mentioning is the ferric-reducing ability of plasma (FRAP), which measures the ability to cause ferric reduction. Together with other assays, it was useful to analyze the main active components of *Anethum graveolens* seed EO, which were demonstrated to be carvone, limonene, and camphor, thus showing that carvone is an excellent antioxidant due to the presence of unsaturated hydroxyl group [50]. Furthermore, the antioxidant activity of *Mentha spicata* was confirmed by performing FRAP and ABTS assays, suggesting a possible use of this EO in the pharmaceutical field [51].

4.3.2 Antimicrobial Activity and Wound Healing

The treatment of microbial infections has always been one of the highest and most ambitious goals in the pharmacological field. The ability of microorganisms to continuously develop new drug resistance mechanisms makes this an ever-evolving field. In fact, the resistance toward antibiotics is one of the main impediments to perform an appropriate treatment for certain infections. Despite the availability of many classes of antibiotics, and therefore a large number of molecules, today this problem is increasingly relevant and alternative therapies, such as EOs, are being investigated to overcome it. Even Hippocrates, more than two thousand years ago, affirmed that the fumigation of EOs was useful to protect from the plague [3]. This was proved in the Middle Ages when some gangs of robbers, due to the assumption of tinctures containing EOs, were able to steal from the houses of the plague victims without being infected. For this reason, EOs have been extensively studied and have been considered as a valid alternative therapy against bacterial infections. The antibacterial activity of EOs depends on the presence of certain components, especially mono- and sesquiterpenes, which are known as efficient

antimicrobial agents [52]. Moreover, the highest antibacterial activity belongs to phenolic groups, followed by cinnamic aldehydes. Other groups are also important, including alcohols, aldehydes, ketones, ethers, and hydrocarbons [53]; specifically, antimicrobial activity against Gram-positive bacteria is related to the amount of long-chain alcohols and aldehydes, as stated by Shojaee-Aliabadi [52], while antimicrobial activity of alcohols is directly proportional to their molecular weight [52,54]. Many EOs have been studied to determine their effectiveness as antibacterial, and the most commonly used assays are the diameter of the inhibition zone (DIZ) evaluation, by measuring the halo diameter, and the determination of the minimum inhibitory concentration (MIC) and/or minimum bactericidal concentration (MBC), through the microdilution method. The research conducted by Hammer et al. [55] demonstrated the antimicrobial activity of a large number of plant oils and extracts, derived from 37 genera, which were investigated against different kinds of microorganisms, such as *Acinetobacter baumanii*, *Aeromonas veronii biogroup sobria*, *Candida albicans*, *Enterococcus faecalis*, *Escherichia coli*, *Klebsiella pneumoniae*, or *Pseudomonas aeruginosa*. As a result, tested EOs and plant extracts have demonstrated *in vitro* antibacterial and antifungal activity against a wide range of organisms, comprising Gram-positive and Gram-negative bacteria and a yeast [55]. Particularly relevant were the results obtained by *Cymbopogon citratus*, *Origanum vulgare*, and *Pimenta racemosa* EOs. *Aniba rosaeodora*, *Coriandrum sativum*, *Cymbopogon martinii*, *Melaleuca alternifolia*, *Melaleuca quinquenervia*, *Mentha piperita*, *Mentha spicata*, *Salvia officinalis*, and *Origanum majorana* results were also noteworthy. The lowest MIC value (0.008% v/v) was measured by *Vetiveria zizanioides* against *S. aureus*, while *Thymus vulgaris* showed a great activity against *C. albicans* and *E. coli*, with a MIC value of 0.03% v/v. Moreover, the study carried out by Nikolić, Jovanović et al. [56] confirmed a significant antimicrobial activity of five EOs *Mentha piperita*, *Mentha pulegium*, *Lavandula angustifolia*, *Satureja montana*, and *Salvia lavandulifolia*. Seven bacterial species— namely *Streptococcus mutans*, *Streptococcus sanguis*, *Streptococcus salivarius*, *Streptococcus pyogenes*, *Pseudomonas aeruginosa*, *Lactobacillus acidophilus*, and *Enterecoccus faecalis*—as well as fifty-eight clinical oral *Candida* spp. were subjected to the treatment with these EOs, confirming their potentiality as antibacterial agent [56]. The antimicrobial potential of the tested EOs increased in the order: *L. angustifolia < M. pulegium < S. lavandulifolia < M. pipe*rita *< S. montana. P. aeruginosa* [57]. As extensively reported by Bilia et al. [58], *Artemisia annua* has showed great antimicrobial activity against Gram-positive and Gram-negative bacteria, and also fungi. The review deeply describes the interesting studies on different Gram-positive bacterial strains, with the lowest MIC values reported for

_____

Staphylococcus aureus, *Enterococcus hirae*, *Enterococcus faecalis*, *Bacillus cereus*, *Bacillus subtilis*, *Bacillus thuringiensis*, and *Bacillus* spp. (all raging from 0.00781 mg/mL of B. subtilis to 0.053 mg/mL of B. cereus). Gram-negative lowest MIC values were 0.013 mg/mL of *Escherichia coli*, 0.026 mg/mL of UPEC (*Escherichia coli* Uropathogenic), and 0.025 mg/mL of *P. aeruginosa*. Furthermore, the most susceptible fungi were described to be *Candida albicans* and *Saccharomyces cerevisiae*, with a 2 mg/mL MIC value. The interesting antimicrobial property of *Artemisia annua* is strictly related to all its components as a whole. In fact, the same research group further analyzed the antimicrobial activity of its main components (artemisia ketone, 1,8-cineole and camphor), in comparison with the whole EO [59]. Disk diffusion method and broth microdilution assay were performed on the most common food pathogens, namely *Escherichia coli*, *Salmonella enteritidis*, *Salmonella typhi*, *Yersinia enterocolitica*, and *Listeria monocytogenes*. As expected, the components separately tested were not able to perform as well as the entire EO, even if the values of the diameters of inhibition zones and the obtained MBC values were remarkable, thus suggesting that the synergism and/or antagonism occurring between the components is necessary to achieve such a great antimicrobial activity. Zhang et al. analyzed the antimicrobial activity of *Melaleuca alternifolia* EO in different strains: *Escherichia coli*, *Staphylococcus aureus*, *Pseudomonas aeruginosa*, *Penicillium italicum* Wehmer, and *Penicillium digitatum* Sacc [60]. The EO showed a good antimicrobial activity toward all the tested strains, with a slightly more pronounced action toward Gram-positive bacteria, compared to Gram-negative bacteria and fungi. This is not surprising since it is known that the wall of Gram-positive bacteria simply consists of several layers of peptidoglycan, while the wall of Gram-negative bacteria has an additional hydrophilic outer wall; for this reason EOs components, which are mainly hydrophobic, find it difficult to penetrate inside the Gram-negative cells [61]. Thus, authors demonstrated that the presence of hydrophobic terpenes is critical for Gram-positive antibacterial action, as previously stated by Cox [62]. Moreover, terpenes' mechanism of action was verified in altering the permeability of the membrane by interacting with the lipid components, thus inducing cell death [62]. A similar mechanism of action was found for *Cinnamomum glanduliferum* EO [63], tested against some Gram-positive and Gram-negative bacterial strains, and also some fungi. Through the transmission electron microscopy (TEM) assay performed by Taha et al. on *E. coli*, there emerged an irreversible damage in the cell membrane. According to the evidence obtained from this study, another plausible mechanism of action involves the blockage of the production of some important enzymes, such as protease and amylase, leading to cell components coagulation [64–67]. These

_____

phenomena are also used by fungi, which are able to cause the destruction of the cell membrane even through the ability to inhibit the production of cellular energy and to create a pH gradient between the cell and the external medium. These phenomena, in this particular EO context, are caused by the great amount of eucalyptol, and also due to the significant presence of other terpenes (terpinen-4-ol and α-terpineol); these three major compounds, as the author suggested, were responsible for the antimicrobial activity of *Cinnamomum glanduliferum* EO. Insawang and co-workers compared five cultivars of *Lavandula stoechas*, in order to assess the differences in their antimicrobial behavior against some bacterial strains [68]. This study is a further confirmation that the presence of eucalyptol (and terpenes in general) is crucial for the antimicrobial activity of the EO. Thymol and carvacrol have been investigated for their antimicrobial properties by Pesavento and coworkers [69], who reported the antimicrobial activity of Origanum vulgare EO on opportunistic respiratory pathogens. In this work, 59 bacterial strains belonging to Staphylococcus aureus, Stenotrophomonas maltophilia, and Achromobacter xylosoxidans species were subjected to the treatment with *Origanum vulgare* EO [69]. All strains resulted to be highly susceptible, even in the treatment with low EO concentrations. In particular, a 48-h-long treatment with a 0.5% v/v concentration of the EO was able to completely inhibit (100%) the growth of *A. xylosoxidans*, *S. maltophilia* and multi-resistant *Staphylococcus aureus* (MRSA). Interestingly, the selected strains belonged to different bacterial species or genera, and it emerged that none of them muted becoming resistant: these findings suggested that the broad activity of *Origanum vulgare* EO could be achieved through the interaction with multiple cellular targets, thus minimizing the possible occurrence of mutant-resistant strains. These results encourage a possible use of *Origanum vulgare* EO in the treatment of multidrug-resistant cystic fibrosis (CF) pathogens, as suggested by the authors [69].

Thymus sipyleus was investigated to demonstrate its effectiveness in the treatment of rhinosinusitis, as already used in traditional medicine [70]. Eight bacterial strains – *Staphylococcus aureus*, methicillin-resistant *S. aureus* (MRSA), *S. epidermidis*, *S. pyogenes*, *S. pneumoniae*, *P. aeruginosa*, *M. catarrhalis*, and *H. influenzae* – were analyzed using three different methods. Comparing with ampicillin, clarithromycin, chloramphenicol, and amoxicillin/clavulanic acid (1:1) as positive controls, the agar diffusion method demonstrated that all bacterial strains were susceptible, with a maximum value for *S. aureus*; the only exception was *P. aeruginosa*, however this result is related to the higher resistance of Gram-negative bacteria compared to Gram-positive ones, as previously described [3,65,71–73]. The microdilution method has shown that the EO

showed an excellent antimicrobial activity on these species at all the tested concentrations, though the effectiveness was lower than one of the positive controls. The vapor diffusion method has also produced encouraging results, especially by demonstrating good action against MRSA strain. The antimicrobial activity of EOs can be exploited in the treatment of skin injury infections. In fact, the presence of the wound causes the reduction in the primary barrier effect, performed by the skin toward the external environment and, as the most dangerous consequence, an increased risk of exposure to microbial infections [65,74–76]. EOs have been recognized as a valid therapy in injured skin infections for their proven antimicrobial activity against multidrug-resistant skin pathogens; however, at certain concentrations, EOs could be cytotoxic, so the risk-benefit ratio for each one should be previously assessed [77]. Another feature supporting the topical use of EOs is their ability to promote wound healing. This potential was discovered by the French chemist Rene-Maurice Gattefossé about a century ago: an explosion in his laboratory caused a severe burn to his hand, but the immersion in lavender EO provided a quick healing, without infection or scar marks. Since that period, many studies aimed at deepening the biochemical basis of this phenomenon, in order to confirm a possible use of EOs for skin healing. Wound healing is composed by three phases: The first one is the inflammatory phase, which includes bleeding blockage, then vasodilation and immune system recruitment [78]; the second phase involves the proliferation of various cell lines, including fibroblast, leading to tissue granulation and angiogenesis [79–81]; finally, in the third phase new collagen fibers are generated and fibroblasts differentiate, bringing the two edges of the wound closer to each other [78–82]. Costa and co-workers demonstrated that the presence of carvacrol and thymol, the most widespread monoterpenes, is relevant in determining EO tissue repairing activity [75]. In fact, among their various biological activities, they can modulate all phases of tissue regeneration, especially the first one, because of their great anti-inflammatory action. Moreover, due to their remarkable anti-inflammatory action, sesquiterpenes are also able to promote tissue repair, eventually in synergy with monoterpenes [83]. Recently, Seyed Ahmadi et al. illustrated the biochemical mechanisms that permit wound healing through the topical administration of *Cinnamon verum* EO, using a mice model of wound infected by *Staphylococcus aureus* and *Pseudomonas aeruginosa* [84]. Besides the proven antimicrobial activity of the EO, also its antioxidant and anti-inflammatory activities were found relevant, because the shorter the inflammatory phase lasts, the faster the proliferative process that leads to wound healing begins. Furthermore, the three main biochemical mediators modulated by the EO were identified: IGF1, whose expression was enhanced, leading, among other implications, to an increase

of fibroblast cells and proliferation; VEGF and FGF-2, whose biosynthesis and expression were up-regulated, respectively, improving the angiogenesis, which is important in various stages of inflammation and cell proliferation. *Melaleuca alternifolia* was investigated by Edmondson and co-workers to assess its antimicrobial and wound-healing activity [85]. The volunteers, who had wounds infected with Methicillin-resistant *Staphylococcus aureus* (MRSA), were medicated for a few days with an EO solution: the antibacterial action of the EO toward this resistant bacterial strain was demonstrated. Moreover, the reduction in size of the wound was found significant according to the analytical method used, thus authors demonstrated that the EO is able to promote the wound healing. Wounds infected with MRSA were also subjected to the treatment with *Anethum graveolens* EO, obtaining many important results [86]. Antimicrobial activity was demonstrated by the significant reduction in bacterial growth. In addition, this EO proved to be able to influence various phases of wound healing. In the inflammatory phase, it increased the expression of p53 and caspase-3, which respectively promote apoptosis and stimulate the proliferation of stem cells to repair tissue [87]. Moreover, this EO up-regulated the expression of Bcl2, an anti-apoptotic agent, as well as VEGF and FGF2, which have important roles in angiogenesis and epithelial cells proliferation and differentiation [88–90]. Finally, it influenced the expression of Erα-promoting collagen biosynthesis. These results demonstrated the potential use of *Anethum graveolens* EO in the treatment of infected wounds, due to the healing properties related to the presence of its major compounds, α-phellandrene, p-cymene, and carvone. *Lavandula angustifolia* EO has also proven to have great beneficial effects on wounds. Mori and co-workers demonstrated that the topical application of this EO on wounded mice caused a faster closure of the lesion compared to the untreated and control groups, suggesting its potential use in the initial stages of tissue regeneration [91]. Moreover, the ELISA analysis showed a significant augmentation of TGF-β levels, which promotes wound contraction through increasing the number of fibroblasts, thus resulting in an intensified collagen production. Finally, it emerges that *Lavandula angustifolia* EO caused a quicker switch from collagen type III to collagen type I. All the cited studies therefore showed that EOs for topical use may constitute, in the close future, the alternative therapy for the treatment of chronic and infected wounds.

4.3.3 Anxiolytic Activity

Since past ages, it is well-known that natural substances are able to affect the psychic functions of an individual [92]. In literature an impressive number of information is reported about the plants employed to treat symptoms related to the most common psychiatric disorders [93,94]. Among these, it is noteworthy to mention the mandrake,

whose magical qualities were showed during the Middle ages, probably for its sedative-hypnotics effects or the hellebore, a drug known to treat paranoia, epilepsy [92,95], and also hysterical suffocation which today refers to "functional neurologic symptom disorder" [96]. In this context, it is remarkable to mention the important traditional drugs extracted from plants, able to affect the central nervous system (CNS). For instance, reserpine isolated from *Rauwolfia serpentina*, has revolutionized schizophrenia treatment [97], as well as morphine, derived from *Papaver somniferum*, which act to decrease the feeling of pain [98]. In the past few years, the competition between synthetic and natural drugs has led to the reevaluation of the plant world, with a significant increase in pharmaceutical plantation investments. In this recent scenario, EOs represent a new challenge by means of their pharmaceutical applications to improve physical, mental, and emotional well-being. The beneficial effects of EOs are achieved by administering (e.g., inhalation, ingestion or cutaneous application) these substances within therapeutic doses, but if these dosages are exceeded, the effects may be harmful to the human body [99]. Inhalation is most commonly used in the acute administration [100]. Remarkably, olfactory system is considered the primordial sensory system in animals: its role is the identification of mixed molecules, present in the environment, to capture new information. To date, the most supported mechanism about olfactory system was described by Linda Buck and Richard Axel. Accordingly, they showed that the detection of distinct odorants may be the result of the association of odorous ligands with specific receptors on olfactory sensory neurons [101]. In particular, through the inhalation, odorant molecules combine with olfactory receptors (ORs) located on the nasal olfactory epithelium, whence the transmission of signals start from olfactory tracts to the olfactory bulb which, in turn, has a link to the limbic system-mostly with amygdala, responsible for emotional regulation, and hippocampus, involved in memory processes [35]. Therefore, emotional effects of smells can include fear, anxiety, aversion, as well as pleasure or relaxation, through releasing neurotransmitters, such as endorphins, producing a sense of well-being [102]. For this reason, recent scientific reports suggested benefits in aromatherapy. Accordingly, it is not surprising that today a PubMed search with the keywords "essential oil" results in more than 22,700 publications. In this regard, it is noteworthy to mention Marguerite Maury, one of the first researchers demonstrating the potential effects of EO on the nervous system, mostly in the limbic system [99]. Nowadays aromatherapy is practiced in several countries, including UK, France, USA and Australia, as "*complementary therapy*" in association with the traditional medicine. The desire to re-evaluate some traditional forms of medicine as integrative remedy has recently been expressed by the World Health Organization (WHO) (World

Health Organization. WHO Traditional Medicine Strategy: 2014–2023, Geneva: WHO; 2014). Considering the effects of EOs at the CNS and according to a plethora of evidences [103,104], the use of EO as supplementary treatment can be a powerful coadjuvant in the care of patients with anxiety disorders [105]. Anxiety disorders, in its pathological meaning, represent one of the most common classes of psychiatric disorders, which impact negatively the quality of people's life [106]. According to the Diagnostic and Statistical Manual of Mental Health Disorders, anxiety disorders can be classified into several main types: generalized anxiety disorder (GAD), panic disorder, specific phobia (SP), agoraphobia, selective mutism, social anxiety disorder (SAD) or social phobia, separation anxiety disorder, as described by the American Psychiatric Association. Common comorbidities include mood substance and personality disorders [107]; moreover anxiety disorder affects women more easily than men [100]. Psychological, environmental, biological, and genetic factors represent the main causes of predisposition to anxiety disorders [108]. Currently the first and second line treatments for anxiety include *benzodiazepines* (BZD), *selective serotonin reuptake inhibitors* (SSRI), *serotonin norepinephrine reuptake inhibitors* (SNRI), *tricyclic antidepressant* (TCA), *monoamine oxidase inhibitor* (MAOI), up to the most recent atypical antidepressants. Furthermore, innovative compounds are being developed for glutamate, neuropeptide, and endocannabinoid systems [109]. Although many efforts have been made, unfortunately the most anxiolytic drugs, even if effective, can cause a series of side effects, as well as induction of a state of dependence and tolerability problems. Moreover, another obstacle in the development process of anxiety drugs includes lack of the full understanding of anxiety disorders related physiopathology [110]. For these reasons, it is essential to consider the additional effective treatments. The use of EOs would seem a promising way to reduce mild anxiety symptoms or at least to potentiate the effect of traditional anxiolytic approaches: accordingly, an innovative "pharmaco-ethology" approach attempting to find drugs with new mechanism of action is needed [111]. Most of the EOs have been proven to be anxiolytic in clinical trials as well as in animals through the most reliable behavioral models, such as open field (OF) test [112], elevated plus maze (EPM) test [113], social interaction (SI) test [114], light and dark box (LDB) test [115], marble-burying (MB) test [116], etc., and pharmacological approaches to induce anxiety in mice or rats [117]. Among all the studies reported, *Lavandula angustifolia* (the most used species of lavender) is widely studied also for its anxiolytic effects [118]. The exposure to lavender smell showed an anxiolytic profile similar to diazepam, mostly in female gerbils [119]. Investigation of the effects of inhaled linalool, a monoterpene commonly found in several aromatic plant,

as well as in *Lavandula angustifolia*, showed anxiolytic properties in mice, increased social interaction, and decreased aggressive behavior [120]. Results showed that the inhalation of *L. angustifolia* EO had an anxiolytic effect in rats with decrease of freezing, as well as a reduced expression of c-Fos in prefrontal cortex and amygdala [121]. Shaw et al. compared the effects of lavender oil with the chlordiazepoxide (CDP), as anxiolytic reference, suggesting that lavender oil has anxiolytic effects on rats during the open field test, but that a sedative effect can also occur at the highest doses [122]. Interestingly, there are also some clinical evidences, which confirm *in vivo* studies. Karan et al. (Germany), described that the anxiolytic effect of lavender oil inhalation was able to reduce peri-operative anxiety in patients undergoing surgical procedures under local anesthesia [123]. Kritsidima and co-workers, in a randomized controlled trial on patients, described how the lavender scent reduces state anxiety in dental patients [124]. A pilot study on the effects of lavender oil on anxiety and depression in the high risk postpartum woman showed a significant improvement of the Edinburgh Postnatal Depression Scale and Generalized Anxiety Disorder Scale after four consecutive weeks of lavender administration [125]. In another study on forty-five adult outpatients which met the DSM-5 criteria for major depression, anti-cholinergic side effects of imipramine, such as dry mouth and urinary retention, were observed less often when lavender was administered with that drug, suggesting an effective adjuvant therapy in combination with this latter [126]. A study including 40 students with Premenstrual Syndrome (PMS) problems and 37 students as control groups showed that lavender inhalation could be used to reduce symptoms of PMS, such as anxiety [127]. Several studies reported pharmacological properties of lavender EO to interact with neuropharmacological targets. Chioca et al. described that serotoninergic transmission, in particular 5-HT_{1A} receptors, could play an important role in the anxiolytic-like effect of lavender EO. Surprisingly in the same study lavender oil inhalation appeared to attenuate the serotoninergic syndrome induced by SNRI [128]. However, other findings suggested that the serotonergic transmission via $5\text{-HT}_{1A}R$ may not be involved in the anxiolytic effects induced by linalool odor: a potential role of GABAergic transmission was described, especially on GABA-A receptors, enhancing the inhibitory tone of the nervous system [129]. Other papers suggested a novel mechanism, compared with traditional anxiolytic drugs, in which linalool and linalyl acetate displayed inhibitory activity on Ca^{2+} influx mediated by voltage-dependent *calcium channels* (VGCCs) [104]. To date in Germany, the EO extract of *L. angustifolia* for oral administration has been developed, approved and it is a registered drug for the treatment of restlessness accompanying anxious mood. The SLO product (Silexan, W. Spitzner Arzneimittelfabrik GmbH, Ettlingen,

Germany) contains the two primary constituents of lavender oil—linalool and linalyl acetate—at concentrations of 36.8% and 34.2%, respectively [105,130,131]. This drug has significant anxiolytic and sleep-improving effects not associated with sedation [132] and also the absence of potential dependency [133]. Lavender, as well as a lot of EOs (Table 2), is "generally recognized as safe" (GRAS) as a food by the U.S. Food and Drug Administration. In general, lavender is well tolerated, but more information is needed, as well the safety on the excretion of some lavender components into breastmilk. Because different or also identical chemotypes can have very different chemical components, it is not surprising that linalool is not the only one having anxiolytic action (Table 2). According to the available clinical studies, *Citrus aurantium* EO on the treatment of anxiety, in patients with chronic myeloid leukemia (CML) [134], as well as in patients with acute coronary syn-drome (ACS) [135] showed a reduction of symptoms associated with anxiety. Also, *Citrus sinensis* and *Citrus bergamia* EO demonstrated positive effects against signs of mild anxiety [136]. In another studies the researchers assessed the effect of *Rosa damascene* EO, showing a reduction of anxiety and pain in the first stage of labor [137], as well as *Osmanthus fragrans* oil and grapefruit oil were effective complementary treatments for anxious patients undergoing colonoscopy [138]. Tankam and co-workers investigated the potential of *Piper guineense* EO in mice, demonstrating that its inhalation could induce a mild tranquilizing effect [139]. Other studies suggested that lemon oil possesses anxiolytic and antidepressant-like effects, probably through the suppression of DA activity related to enhanced 5-HTergic neurons [140]. Zhang et al. showed an anxiolytic effect on male mice after inhalation of *Cananga odorata* EO (ylang-ylang EO) [141]. Another study analyzed the potential anxiolytic properties of inhaled coriander volatile oil, extracted from *Coriandrum sativum*, on a rat model of Alzheimer's disease [142]. Forms of emotional memory associated to anxiety states were observed in a pilot study on postpartum women, demonstrating a reduction of anxiety levels using a rose/lavender oil blend for 15 min twice weekly during 4 weeks [125]. Even if our purpose is to discuss about aromatherapy, it is noteworthy to admit that all the anxiolytic-like effects in animal models have been obtained also through oral or IP administration [143–146]. Evidence suggests that aromatherapy might be used as a complementary treatment, however some papers seem to support the ineffectiveness of Eos. For instance, Fazlollahpour and co-workers described that inhalation of aromatherapy with 4% rose EO could not significantly alleviate anxiety in patients undergoing coronary artery bypass graft (CABG) surgery [147]. Another study trials conducted in 2007 did not demonstrate a statistically significant relationship between the use of EOs and anxiety reduction [148].

Table 2. EOs generally recognized as safe by Food and Drug Administration (FDA). Source:
https://www.ecfr.gov/cgi- bin/text-
idx?SID=69c1693f1fe5cddde23bdc34d0731b05&mc=true&node=pt21.6.582&rgn=div5#se21.6.582_120.
Accessed on 10 February 2021.

Common Name	Botanical Name of Plant Source
Alfalfa	*Medicago sativa* L.
Allspice	*Pimenta officinalis* Lindl.
Almond, bitter (free from prussic acid)	*Prunus amygdalus* Batsch, *Prunus armeniaca* L. or *Prunus persica* (L.) Batsch.
Ambrette (seed)	*Hibiscus moschatus* Moench.
Angelica root	*Angelica archangelica* L.
Angelica seed	Do.
Angelica stem	Do.
Angostura (cusparia bark)	*Galipea officinalis* Hancock.
Anise	*Pimpinella anisum* L.
Asafetida	*Ferula assa-foetida* L. and related spp. of Ferula.
Balm (lemon balm)	*Melissa officinalis* L.
Balsam of Peru	*Myroxylon pereirae* Klotzsch.
Basil	*Ocimum basilicum* L.
Bay leaves	*Laurus nobilis* L.
Bay (myrcia oil)	*Pimenta racemosa* (Mill.) J. W. Moore.
Bergamot (bergamot orange)	*Citrus aurantium* L. subsp. bergamia Wright et Arn.
Bitter almond (free from prussic acid)	*Prunus amygdalus* Batsch, *Prunus armeniaca* L., or *Prunus persica* (L.) Batsch.
Bois de rose	*Aniba rosaeodora* Ducke.
Cacao	*Theobroma cacao* L.
Camomile (chamomile) flowers, Hungarian	*Matricaria chamomilla* L.
Camomile (chamomile) flowers, Roman or English	*Anthemis nobilis* L.
Cananga	*Cananga odorata* Hook. f. and Thoms.
Capsicum	*Capsicum frutescens* L. and *Capsicum annuum* L.
Caraway	*Carum carvi* L.
Cardamom seed (cardamon)	*Elettaria cardamomum* Maton.
Carob bean	*Ceratonia siliqua* L.
Carrot	*Daucus carota* L.
Cascarilla bark	*Croton eluteria* Benn.
Cassia bark, Chinese	*Cinnamomum cassia* Blume.
Cassia bark, Padang or Batavia	*Cinnamomum burmanni* Blume.
Cassia bark, Saigon	*Cinnamomum loureirii* Nees.
Celery seed	*Apium graveolens* L.
Cherry, wild, bark	*Prunus serotina* Ehrh.
Chervil	*Anthriscus cerefolium* (L.) Hoffm.
Chicory	*Cichorium intybus* L.
Cinnamon bark, Ceylon	*Cinnamomum zeylanicum* Nees.
Cinnamon bark, Chinese	*Cinnamomum cassia* Blume.
Cinnamon bark, Saigon	*Cinnamomum loureirii* Nees.
Cinnamon leaf, Ceylon	*Cinnamomum zeylanicum* Nees.
Cinnamon leaf, Chinese	*Cinnamomum cassia* Blume.
Cinnamon leaf, Saigon	*Cinnamomum loureirii* Nees.
Citronella	*Cymbopogon nardus* Rendle.
Citrus peels	*Citrus* spp.
Clary (clary sage)	*Salvia sclarea* L.
Clove bud	*Eugenia caryophyllata* Thunb.
Clove leaf	Do.
Clove stem	Do.
Clover	*Trifolium* spp.
Coca (decocainized)	*Erythroxylum coca* Lam. and other spp. of Erythroxylum.
Coffee	*Coffea* spp.
Cola nut	*Cola acuminata* Schott and Endl., and other spp. of Cola.

Common Name	Botanical Name of Plant Source
Coriander	*Coriandrum sativum* L.
Corn silk	*Zea mays* L.
Cumin (cummin)	*Cuminum cyminum* L.
Curacao orange peel (orange, bitter peel)	*Citrus aurantium* L.
Cusparia bark	*Galipea officinalis* Hancock.
Dandelion	*Taraxacum officinale* Weber and *T. laevigatum* DC.
Dandelion root	Do.
Dill	*Anethum graveolens* L.
Dog grass (quackgrass, triticum)	*Agropyron repens* (L.) Beauv.
Elder flowers	*Sambucus canadensis* L. and S. nigra L.
Estragole (esdragol, esdragon, tarragon)	*Artemisia dracunculus* L.
Estragon (tarragon)	Do.
Fennel, sweet	*Foeniculum vulgare* Mill.
Fenugreek	*Trigonella foenum-graecum* L.
Galanga (galangal)	*Alpinia officinarum* Hance.
Garlic	*Allium sativum* L.
Geranium	*Pelargonium* spp.
Geranium, East Indian	*Cymbopogon martini* Stapf.
Geranium, rose	*Pelargonium graveolens* L'Her.
Ginger	*Zingiber officinale* Rosc.
Glycyrrhiza	*Glycyrrhiza glabra* L. and other spp. of Glycyrrhiza.
Glycyrrhizin, ammoniated	Do.
Grapefruit	*Citrus paradisi* Macf.
Guava	*Psidium* spp.
Hickory bark	*Carya* spp.
Horehound (hoarhound)	*Marrubium vulgare* L.
Hops	*Humulus lupulus* L.
Horsemint	*Monarda punctata* L.
Hyssop	*Hyssopus officinalis* L.
Immortelle	*Helichrysum augustifolium* DC.
Jasmine	*Jaminum officinale* L. and other spp. of Jasminum.
Juniper (berries)	*Juniperus communis* L.
Kola nut	*Cola acuminata* Schott and Endl., and other spp. of Cola.
Laurel berries	*Laurus nobilis* L.
Laurel leaves	*Laurus* spp.
Lavender	*Lavandula officinalis* Chaix.
Lavender, spike	*Lavandula latifolia* Vill.
Lavandin	Hybrids between *Lavandula officinalis* Chaix and *Lavandula latifolin* Vill.
Lemon	*Citrus limon* (L.) Burm. f.
Lemon balm (see balm).	
Lemon grass	*Cymbopogon citratus* DC. and *Cymbopogon flexuosus* Stapf.
Lemon peel	*Citrus limon* (L.) Burm. f.
Licorice	*Glycyrrhiza glabra* L. and other spp. of Glycyrrhiza.
Lime	*Citrus aurantifolia* Swingle.
Linden flowers	*Tilia* spp.
Locust bean	*Ceratonia siliqua* L.
Lupulin	*Humulus lupulus* L.
Mace	*Myristica fragrans* Houtt.
Malt (extract)	*Hordeum vulgare* L., or other grains.
Mandarin	*Citrus reticulata* Blanco.
Marjoram, sweet	*Majorana hortensis* Moench.
Mate 1	*Ilex paraguariensis* St. Hil.
Melissa (see balm).	
Menthol	*Mentha* spp.
Menthyl acetate	Do.
Molasses (extract)	*Saccharum officinarum* L.

Common Name	Botanical Name of Plant Source
Mustard	*Brassica* spp.
Naringin	*Citrus paradisi* Macf.
Neroli, bigarade	*Citrus aurantium* L.
Nutmeg	*Myristica fragrans* Houtt.
Onion	*Allium cepa* L.
Orange, bitter, flowers	*Citrus aurantium* L.
Orange, bitter, peel	Do.
Orange leaf	*Citrus sinensis* (L.) Osbeck.
Orange, sweet	Do.
Orange, sweet, flowers	Do.
Orange, sweet, peel	Do.
Origanum	*Origanum* spp.
Palmarosa	*Cymbopogon martini* Stapf.
Paprika	*Capsicum annuum* L.
Parsley	*Petroselinum crispum* (Mill.) Mansf.
Pepper, black	*Piper nigrum* L.
Pepper, white	*Piper nigrum* L.
Peppermint	*Mentha piperita* L.
Peruvian balsam	*Myroxylon pereirae* Klotzsch.
Petitgrain	*Citrus aurantium* L.
Petitgrain lemon	*Citrus limon* (L.) Burm. f.
Petitgrain mandarin or tangerine	*Citrus reticulata* Blanco.
Pimenta	*Pimenta officinalis* Lindl.
Pimenta leaf	*Primenta officinalis* Lindl.
Pipsissewa leaves	*Chimaphila umbellata* Nutt.
Pomegranate	*Punica granatum* L.
Prickly ash bark	*Xanthoxylum* (*or Zanthoxylum*) *Americanum* Mill. or *Xanthoxylum clava-herculis* L.
Rose absolute	*Rosa alba* L., *Rosa centifolia* L., *Rosa damascena* Mill., *Rosa gallica* L., and vars. of these spp.
Rose (otto of roses, attar of roses)	Do.
Rose buds	Do.
Rose flowers	Do.
Rose fruit (hips)	Do.
Rose geranium	*Pelargonium graveolens* L'Her.
Rose leaves	*Rosa* spp.
Rosemary	*Rosmarinus officinalis* L.
Rue	*Ruta graveolens* L.
Saffron	*Crocus sativus* L.
Sage	*Salvia officinalis* L.
Sage, Greek	*Salvia triloba* L.
Sage, Spanish	*Salvia lavandulaefolia* Vahl.
St. John's bread	*Ceratonia siliqua* L.
Savory, summer	*Satureia hortensis* L.
Savory, winter	*Satureia montana* L.
Schinus molle	*Schinus molle* L.
Sloe berries (blackthorn berries)	*Prunus spinosa* L.
Spearmint	*Mentha spicata* L.
Spike lavender	*Lavandula latifolia* Vill.
Tamarind	*Tamarindus indica* L.
Tangerine	*Citrus reticulata* Blanco.
Tannic acid	Nutgalls of *Quercus infectoria* Oliver and related spp. of Quercus. Also in many other plants.
Tarragon	*Artemisia dracunculus* L.
Tea	*Thea sinensis* L.
Thyme	*Thymus vulgaris* L. and *Thymus zygis* var. gracilis Boiss.
Thyme, white	Do.
Thyme, wild or creeping	*Thymus serpyllum* L.
Triticum (see dog grass).	

Common Name	Botanical Name of Plant Source
Tuberose	*Polianthes tuberosa* L.
Turmeric	*Curcuma longa* L.
Vanilla	*Vanilla planifolia* Andr. or *Vanilla tahitensis* J. W. Moore.
Violet flowers	*Viola odorata* L.
Violet leaves	Do.
Violet leaves absolute	Do.
Wild cherry bark	*Prunus serotina* Ehrh.
Ylang-ylang	*Cananga odorata* Hook. f. and Thoms.
Zedoary bark	*Curcuma zedoaria* Rosc.

4.4 EOs Encapsulation Strategies in Drug Delivery Systems

Despite many interesting applications, the EOs are fragile and unstable volatile compounds, subject to enzymatic reactions, phenomena that compromise their biological properties, causing a decrease of activity and an increase of toxicity (irritation, photosensitization, etc.,), which limit their traditional use. These limits could be improved exploiting the encapsulation of EOs in drug delivery systems (DDS) that provide a controlled drug release, increasing the bioavailability and efficiency of EO, thus providing an optimal pharmacokinetic profile [6]. Literature production on the encapsulation of EOs mostly deals with food, textile, and cosmetic industry [149], even if in the recent decade the interest in the pharmaceutical field has raised, as demonstrated by the increasing number of published papers concerning the delivery of EOs for pharmaceutical applications (Figure 2).
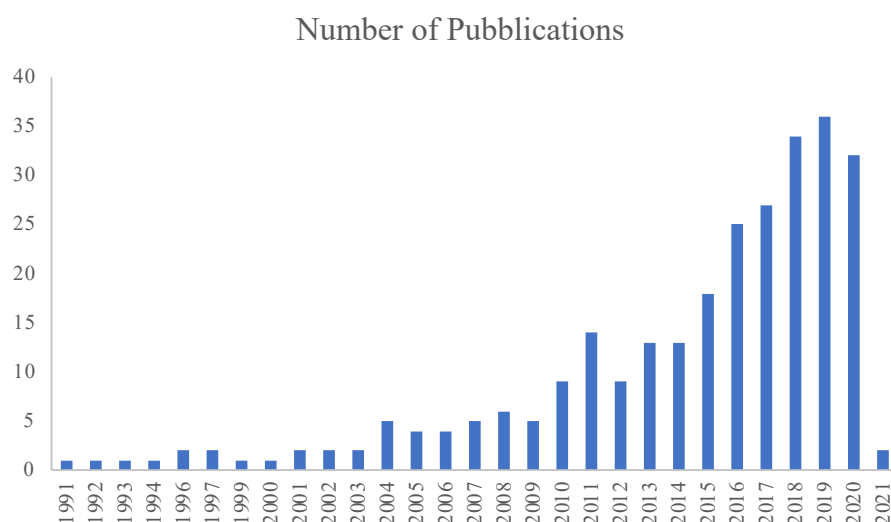

Figure 2. Number of published research articles searching the keywords "essential oils" and "delivery" and "pharmaceutical", source PubMed, last update 12 January 2021.

Many advantages can be listed when exploiting EOs encapsulation in DDS, such as: increased bioavailability (due to the ability of DDS to adhere to the mucous membrane); protection from hydrolysis and oxidation, thus increasing EO chemical stability; reduction of toxicity and volatility; the possibility of reaching target sites with therapeutic doses, thus increasing the patient's compliance. Different strategies related to the use of DDS have been explored for the potential encapsulation of EOs, including polymeric nanoparticles and inclusion complexes with cyclodextrins, which have been extensively reviewed [6,150]. Herein, we focus on vesicular and nanoparticulate lipid-based delivery formulations, such as micro- and nanoemulsion, liposomes, solid lipid nanoparticles (SLN), and nanostructured lipid carriers (NLC) (Figure 3).
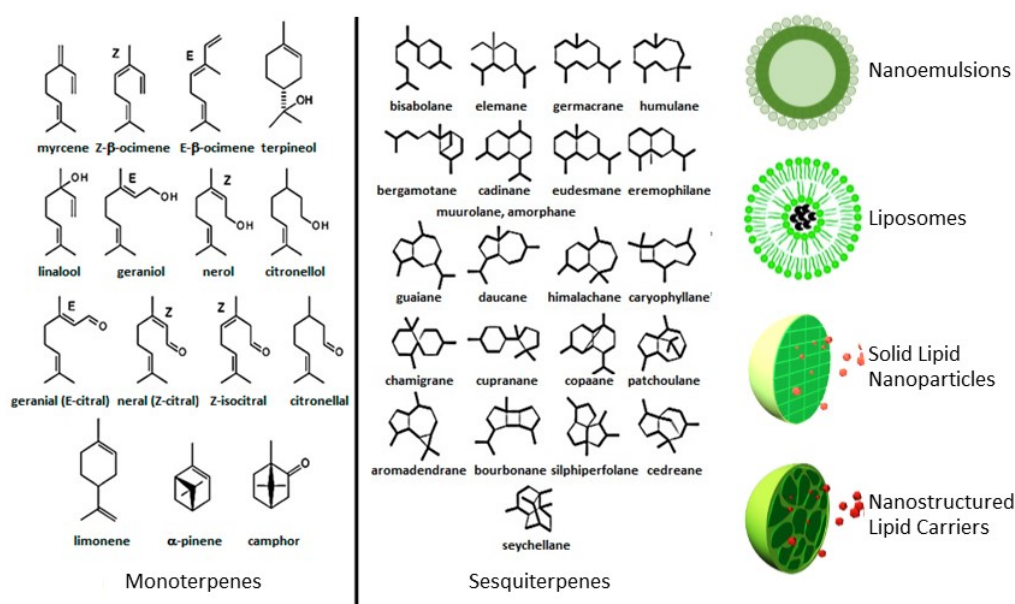

Figure 3. Main lipid-based delivery systems for EOs delivery. Adapted from [151].

4.4.1 Micro- and Nanoemulsions

Microemulsions (mean droplet size 100–400 nm [152]) and nanoemulsions (1 to 100 nm [153]) are isotropic dispersions of two non-miscible liquids (oil and water). The former is thermodynamically stable system in which the inner phase can figure as spheroid, cylinder-like, plane-like, or as a bicontinuous structure [154], whereas the latter is thermodynamically unstable, usually requiring a co-surfactant because its free energy is higher than the free energy of the separate oil and water [155].

A range of different EOs formulated both in micro- and nanoemulsions have demonstrated certain antimicrobial, antiviral, and antifungal activities [156] (Figure 4).
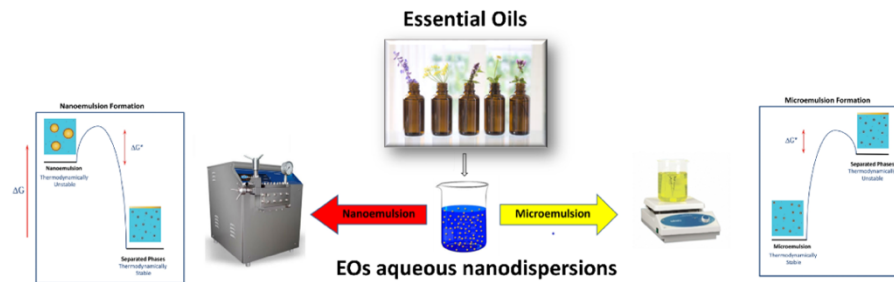
Figure 4. Nanoemulsions and microemulsions s for EOs delivery. Adapted from [157].

EOs have also demonstrated analgesic, anti-inflammatory, antioxidant, antibacterial, anti-fungal, sedative, and antidepressant effects, and through topical application, can effectively heal burns and insect bites [158], therefore they can be used in the treatment of skin wounds. This effect is related to their ability to damage the bacterial cell wall or cell membrane, thus increasing cell membrane permeability and solubilization, with the consequent release of membrane proteins, leading to bacteriostasis [159]. Despite the very promising medicinal activities, some factors limit the pharmaceutical application of EOs as antimicrobial agent in topical treatment, mainly because their directly exposure to the skin could potentially induce an allergic reaction. Moreover, EOs are highly instable and easily degrade when exposed to external factors (oxidation, evaporation, heat, and light) [6]. Furthermore, low aqueous solubility and high volatility limit their free use without a pharmaceutical vehicle. One of the ways to overcome these limits is the use of encapsulation strategies, into vesicular or particulate delivery systems. One strategy consists in the use of micro or nanoemulsions. These vesicular nanosystems have been demonstrated to increase the EOs bioavailability and diffusion—thanks to their small droplets size—and contribute to the antimicrobial and anti-biofilm activities—due to the wetting ability of surfactants [160], since the high surface tension of the droplets favors their fusion with the membranes of prokaryotes, viruses and eukaryotic cell of fungi, leading to the destruction of these organisms [161]. Interestingly, Donsì et al. demonstrated that the nanoencapsulation of terpenes extracted from *Melaleuca alternifolia* improved the antimicrobial activity compared to the unencapsulated mixture, but they also reported that the theoretical higher delivery efficiency of nanoemulsion loaded with terpenes, associated with its smaller mean droplet diameter, is likely counter-balanced by the partial degradation of some active compounds, and in particular, carvacrol [162]. Sugumar and co-workers studied the antimicrobial effect of *Eucalyptus* EO, both in pure form and encapsulated into nanoemulsions [163]. The antibacterial studies of nanoemulsion obtained by sonication against *Staphylococcus aureus* by time kill analysis showed complete loss of viability within 15 min of interaction, thus confirming a high interaction with the bacterial

membrane and therefore an increase in antimicrobial activity. The integrity of the bacterial membrane was analyzed in the range 0–60 min, showing an immediate loss of cytoplasmic contents of 83.32%. Interestingly, wound contraction activity studies showed better wound-healing activity in animals treated with nanoemulsion (100% wound healing on day 16), compared with the commercially available drug neomycin treated (94.2% healing rate) and control rats, probably due to the ability of the droplets to form a film on the skin after the evaporation of nanoemulsion water phase, and to the presence of cineole in the eucalyptus oil, a well-known penetration enhancer in transdermal DDS and topical application studies [164]. Alam and co-workers investigated the wound contraction activity of clove EO in nanoemulsion by *in vivo* studies on rats, in comparison to clove EO pure treatment and positive control treated with gentamycin [165]. The collected results demonstrated that the wound contraction and epithelialization time obtained with clove EO-loaded nanoemulsion and gentamycin were comparable, while EO-loaded nanoemulsion results to be more effective than the pure clove EO. The authors also investigated the wound contraction activity of nanoemulsions loaded with *Eucalyptus* EO [166]. Again, the effectiveness of the EO-nanoemulsion was statistically higher compared to the pure EO, reaching epithelization time results similar to those obtained in the treatment with gentamycin. All the results obtained by Alam and co-workers underline that EO encapsulation into nanoemulsion allows increasing the effectiveness in the wound-healing treatment. Recently, the potential application of *Lavandula angustifolia* EO and licorice extracted from *Glycyrrhiza glabra*, in a nanoemulsion delivery system was investigated [167]. In this work, Kazemi et al. demonstrated that this formulation strongly improved the wound-healing process at different stages (wound closure, epithelialization, and molecular processes). In particular, nanoemulsion loaded with *Lavandula angustifolia* EO and licorice extract was able to increase the expression of TGF-β1, type I and type III collagen genes, which are involved in the acceleration of the wound-healing process. The authors attributed this effect to the role of *Lavandula angustifolia* EO on the stimulation of TGF-β1, an important regulatory factor in reproduction fibroblasts which is involved in the formation of granular tissue as well as in the synthesis and accumulation of collagen fibers [167]. EOs-loaded nanoemulsions have also been studied for their potential anti-inflammatory activity by *in vitro* and *in vivo* (in zebrafish) assays [39,168]. In particular, Borges et al. focused on the anti-inflammatory activity of nanoemulsions loaded with *Rosmarinus officinalis* L. EO, exploiting two parameters: the cellular antioxidant activity (CAA) and the nitric oxide (NO·) production. Interestingly, authors found that the values obtained from the antioxidant activity studies of the pure EO were not significantly

different to the one of the respective nanoemulsion, even if the concentration of *Rosmarinus officinalis* L. EO in the nanoemulsion was three times lower compared to the pure EO. The obtained results were correlated to the lipophilicity of the nanoemulsion droplets, which facilitate the penetration into the cell membranes thus promoting the release of EO. Furthermore, Borges et al. demonstrated that *Rosmarinus officinalis* L. EO was able to induce a dose-dependent reduction of NO· production, whereas a dose-independent effect was observed for nanoemulsions whose activity was greater than pure EO [39]. Therefore, authors concluded that the produced nanoemulsions was able to enhance the anti-inflammatory effect of EO, further reducing the production of NO·. In particular, the potential pro- or anti-inflammatory effect of EO was investigated on human keratinocytes and fibroblasts, in order to evaluate their safe use for operators [168]. Herein, Rossi et al., as well as proving that EOs present a strong toxicity against larvae and pupae of the main malaria vectors *An. stephensi* and *An. gambiae*, in Asia and Africa, also demonstrated that the CBD-free hemp EOs did not induce an inflammatory condition. In particular, these compounds were able to revert the inflammation, reducing the release of the cytokine on skin cell lines, thus demonstrating that they could be safely used by operators [168].

4.4.2 Liposomes

Liposomes are vesicular self-assembled system characterized by one or more bilayers, constituted by phospholipids, surrounding an aqueous core. They were first studied as drug delivery systems in 1970, since they can be used as carriers for both lipophilic and hydrophilic molecules, due to the presence of the hydrophilic compartment and lipophilic bilayer [169] (Figure 5). The encapsulation of an active compound into liposomes allows both the protection from degradation and the increase of solubility.
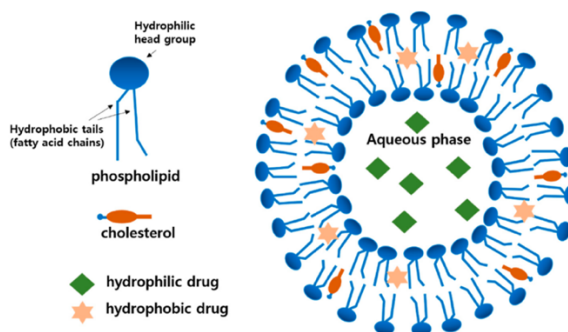

Figure 5. Liposome's structure characterized by a spherical vesicle with a phospholipid bilayer membrane used to deliver hydrophilic or hydrophobic drug. Adapted from [170].

Different studies demonstrated the potentiality of liposomes in the delivery of EOs. Valenti et al. reported that *Santolina insularis* EO showed a good *in vitro* antiherpetic activity

_____

against Herpes simplex virus type 1 (HSV-1) and that its stability was improved when loaded into liposomes [171]. The same research group also developed multilamellar vesicles (MLV) and small unilamellar vesicles (SUV) to improve the antiviral properties of *Artemisia arborescens* L. EO [172]. Interestingly, authors found that EO-loaded MLVs enhanced the antiviral activity against HSV-1, while no significant differences of the antiviral activity were observed between the free EO and SUV vesicles, which showed a poor activity as determined by both the reduction of viral cytopathic effect assay and plaque reduction assay. Therefore, they concluded that the incorporation of *A. arborescens* EO in multilamellar liposomes greatly improved its activity against intracellular HSV-1 [172]. Liolios and co-workers further investigated the influence of the liposomial encapsulation on the antimicrobial activity of *Origanum dictamnus* L. EO [173]. Carvacrol, thymol, p-cymene, and c-terpinene, identified as the major constituents of *Origanum dictamnus* L., were isolated and successfully encapsulated in phosphatidyl choline-based liposomes, in order to evaluate the potential improvement of their antioxidant and antimicrobial activities against four Gram-positive and four Gram-negative bacteria and three human pathogenic fungi, as well as the food-borne pathogen, *Listeria monocytogenes*. Interestingly, authors found that the encapsulation of monoterpenes leads to vesicles' stabilization, as demonstrated by the increase in the onset temperature. Furthermore, a significant increase of the antimicrobial activity was found after the encapsulation in liposomes [173]. Liposomal formulation loaded with *Zataria multiflora Boiss* EO, a well-known aromatic medicinal herb in Persian as "Avishan Shirazi" or "Azkand", were successfully produced in order to compare the antibacterial activity of free EO and EO-loaded liposomes against *E. coli* [174]. Authors found that MIC and MBC values of EO-loaded liposomes were 1.4% and 1.8%, respectively, thus demonstrating the increasing antibacterial activity of the EO when loaded into liposomes. This result was related to the ability of liposomal formulation to improve the cellular transport and to release the active components inside the cell, due to cells interaction (inter-membrane transfer, contact release, absorption, fusion, and phagocytosis), whose mechanism is related to the cell type (cell wall/membrane composition), as well as liposome membrane's physicochemical properties, as previously reported [175]. Sebaaly et al. investigated the encapsulation of clove EO in natural soybean phospholipid liposomal vesicles, prepared by using the ethanol injection method [176]. Authors demonstrated that liposomes were able to protect eugenol, the main component of clove EO, from the degradation induced by UV exposure, without any reduction of its DPPH scavenging activity. Interestingly, the same authors also investigated the possibility to prepare clove EO and eugenol-loaded liposomes using large scale procedures, such as

_____

membrane contactor [177,178]. The potential antibacterial activity against *E. coli* was demonstrated by Najafi et al. for liposomes prepared with lecithin/cholesterol and loaded with barije EO, extracted from *Ferula gummosa* [179]. An interesting application of EO-loaded liposomes was recently investigated by Palmas et al. [180]. Herein, liposomes prepared with *Citrus limon* var. *pompia* were prepared as potential mouthwash product for the treatment of oropharyngeal diseases. Citral-loaded liposomes were demonstrated to be biocompatible and able to protect cells from the damages caused by oxidative stress. The vesicles also demonstrated to promote the healing of wounded mucosa, favoring the closure of lesions induced in a keratinocytes cell monolayer, and to inhibit the proliferation of *Streptococcus mutans*, when loading 50 mg/mL of citral EO [180]. An interesting approach was recently developed basing on drug-in-cyclodextrin-in-liposomes (DCLs), which are constituted by one or more phospholipid bilayers and an aqueous internal cavity where a cyclodextrin/drug inclusion complex is loaded [181]. Herein, Hammoud et al. encapsulated different EO components (estragole, eucalyptol, isoeugenol, pulegone, terpineol, and thymol) into DCLs, prepared by the ethanol injection method using lipoid S100 and hydroxypropil-β-cyclodextrin, as a promising tool for extending EOs shelf life and activity. The physico-chemical and technological characterization of DCLs revealed their ability in significantly improving the loading ratio of estragole, pulegone, and thymol, and prolong the release of EO components compared to traditional liposomes [181,182]. Recently, Lin and co-workers developed an interesting strategy for the encapsulation of thyme EO into solid liposomes coated with ε-polylysine [183]. Solid liposomes are novel nanosystems, with higher stability and longer storage time compared with traditional aqueous liposomes [184].

4.4.3 Lipid Nanoparticles: SLN and NLC

SLN were proposed in the early 1990s as a tool to overcome the limits related to liposomes, exploiting the use of physiological lipids (e.g., blends of mono-, di- or triglycerides, fatty acids, waxes) [185], solid at room and/or body temperature, in mixture with surfactants and water. The solidity of the lipid attributes some advantages to the system, such as increased chemical protection, less leakage, and sustained release [186]. Other relevant advantages are the high targeting effect and low toxicity, which is related to the use of biodegradable and biocompatible lipid substances with a GRAS ("generally recognized as safe") status [187]. Different studies on EOs-loaded SLN report the enhanced anticancer activity of EOs [188]. Frankincense and myrrh oil obtained from the genera *Boswellia* and *Commiphora*, respectively, were loaded into SLN prepared with Compritol 888 ATO by high-pressure homogenization, and their anticancer activity after oral administration was evaluated *in*

vivo in H22-bearing Kunming mice [189]. The obtained results demonstrated the possibility to encapsulate EO into SLN having mean size smaller than 220 nm, with high encapsulation efficiency (>98%). Furthermore, a significantly higher *in vivo* antitumor efficacy was observed compared to EO suspension and EO-loaded into β-cyclodextrin, used to increase EO solubility, at the same dosage. Another interesting anticancer application was recently proposed by Rodenak-Kladniew and co-workers based on the delivery of linalool into SLN prepared with different solid lipids (myristyl myristate, cetyl esters and cetyl palmitate) prepared by sonication using Pluronic®F68 as surfactant [190]. The aim of this work was to exploit the potential anticancer activity of linalool (an acyclic monoterpene alcohol commonly found in EOs of different plants and herbs including lavender, basil, rosemary, citric fruits, green, and black tea) as a mono-drug agent or in combination with traditional drugs. Collected results demonstrated the possibility to obtain stable formulations with mean size around 100 nm, able to provide a controlled release of linalool EO. Interestingly, a cytotoxic activity was observed against human lung- and liver-derived tumor cells (A549 and HepG2, respectively), thus demonstrating that linalool-SLN represents a potential combined approach to enhance the activity of anticancer drugs [190]. Another application of EO-SLN was investigated by Zhao et al., who focused their research on the pulmonary delivery of *Yuxingcao* EO in SLN prepared with Compritol 888 ATO by high-shear homogenization, using polyvinyl alcohol as emulsifier agent, thus overcoming the rapid clearance of pulmonary absorption [191]. Authors demonstrated the feasibility of the encapsulation strategy to produce a *Yuxingcao* EO-SLN inhalation delivery able to improve the elimination half-life in the lungs, enhancing the active compound local bioavailability, thus potentially limiting the administration doses to one per day. Due to the antimicrobial activity of EOs, their encapsulation into SLN has also been investigated as a promising strategy to reduce the microbial resistance to antibiotics, one of the major problems in the treatment of different diseases, such as topical infections, and in wound healing. In order to improve the antibacterial and antifungal activity of clove oil (the EO obtained from *Eugenia caryophyllata*), Fazly et al. prepared SLN by high-shear homogenization and ultrasound method, using glyceryl monostearate, precirol, and stearic acid as lipid phase [192]. Clove encapsulation into SLN effectively improved its antimicrobial activity, reducing the MIC/MCC values from 2–20 folds, with higher effects against Gram-negative bacteria and fungi. This result was related to the ability of SLN to interact with microbial cell membrane and to the improvement of the EO stability and solubility [192]. Authors observed that clove-loaded SLN prepared with stearic acid showed better results compared to SLN prepared with the other selected lipids, and related

this result to its lower particles size which would increase passive cellular absorption enhancing antimicrobial activity, as reported by Nasseri et al. [193]. SLN can be also used as carrier for more than one antimicrobial drug: in order to enhance the antimicrobial activity of ofloxacin against *Pseudomonas aeruginosa* and *Staphylococcus aureus*, Rodenak-Kladniew prepared a SLN platform containing the aforementioned drug together with two antibacterial active components, chitosan and eugenol, considering various matches: ofloxacin, ofloxacin-SLN, ofloxacin-chitosan-SLN, ofloxacin-chitosan-eugenol SLN. Considering the *Pseudomonas aeruginosa* model, the obtained MIC values went from about 1.73 ± 0.40 μg/mL of free ofloxacin to 0.29 ± 0.07 μg/mL of ofloxacin-chitosan-eugenol SLN, thus causing a six-fold decrease of this parameter. Even better results emerged for *Staphylococcus aureus* model, with a 16-fold reduction of MIC values, from 0.31 ± 0.05 μg/mL of free ofloxacin to 0.02 ± 0.01 μg/mL of ofloxacin-chitosan-eugenol SLN. This excellent microbial toxicity is not associated with toxicity to human cells, as shown by the MTT assay. On the other hand, with concentrations 10–150-fold higher than the ones required for therapeutic action, eugenol alters glutathione levels leading to cell death [190]. The effect of physicochemical properties on the different activities of nanoparticulate systems was also investigated by Pereira et al., [194], who developed and optimized, using factorial design, linalool-SLN with long-term stability, demonstrating that the variation of surfactant concentration significantly influences mean particles size and homogeneity, since as the surfactant concentration increased, a reduction in particle size was observed. The design of experiment was exploited also by Zielinska et al. to develop citral-loaded SLN by hot high-pressure homogenization [195]. The 2^2 factorial design determined the optimal concentration of components: 1 wt% of citral, 4 wt% of lipid glycerol monostearate and 2.5 wt% of poloxamer 188, selected as surfactant to obtain homogeneous nanoparticles with mean size lower than 100 nm. In the same study, the anti-inflammatory activity of citral and geraniol, comparing pure EOs and EO-loaded SNL, was evaluated. The analysis of the inhibition of NO· production, measured on RAW 264.7 cells, showed a greater anti-inflammatory activity of citral compared to geraniol. The results of the cytotoxicity assay showed that cell viability in HaCaT cells was significantly reduced by citral, even if its effect was more evident in the treatment of A431 cells, thus demonstrating the skin anti-cancer potential of this monoterpene [195]. Saporito and co-workers recently developed lipid nanoparticles of first generation (SLN) and second generation (nanostructured lipid carriers, NLC) (Figure 6) for the delivery of eucalyptus or rosemary EOs as potential medical devices, to improve healing of skin wounds [196].
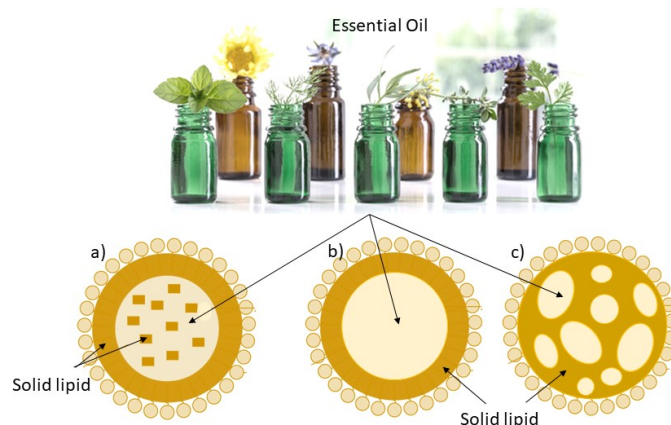
Figure 6. EOs delivery into solid lipid nanoparticles (SLN) (a) or nanostructured lipid carriers (NLC) of different types, depending on the formation of a single (b) or different nanocompartments of oil (c).

NLC represent a second generation of lipid nanoparticles, born in 1999 in order to overcome the limits related to SLN, such as limited drug-loading capacity and potential drug expulsion during storage. NLC are characterized by the presence of a liquid lipid, together with the solid lipid, which allows the formation of an imperfect or amorphous structure, able to guarantee higher drug loading values compared to SLN, thus avoiding drug loss during storage [185]. Cocoa butter was selected as solid lipid, while olive oil or sesame oil were used as liquid lipids in NLC formulations [196]. Interestingly, NLC showed higher bioadhesive properties compared to SLN, probably due to their flexible structure which would promote interactions with biologic substrate, thus promoting lesion closure. As reported in the *in vitro* cytotoxicity studies, the presence of olive oil increased the cell viability due to the high content of oleic acid, previously demonstrated to promote cell proliferation. Furthermore, *in vivo* studies on a rat burn model confirmed that NLC prepared with olive oil and loaded with Eucalyptus EO were able to promote the closure of the wound, providing good reepithelization and stratum corneum formation [196]. Cocoa butter and olive oil were also used as solid lipid and liquid lipid respectively to encapsulate cardamom EO, producing small NLC (<150 nm) with an encapsulation efficiency higher than 90%. Results obtained from *in vitro* release studies and DPPH scavenging activity assay demonstrated that the DDS structure is able to protect the EO—during the storage—and thus enhance its antioxidant property, also because of the presence of the two natural oils [197]. The suitability of the monoterpene carvacrol as a component of binary mixtures of NLC solid lipids was deeply analyzed by Galvao and co-workers [198]. The considered solid lipids were stearic acid, beeswax, and carnauba wax, which were analyzed both as pure components and in mixture with different ratio of carvacrol (10%, 25%, and 50% w/w). The obtained binary mixtures showed lower values of enthalpy and melting

temperatures, highlighting the relevance of this active ingredient in the formulation of NLC. Moreover, carvacrol demonstrated to increase the loading capacity and the encapsulation efficiency of carnauba wax and beeswax—through the extension of the interlayer—when compared with the pure waxes [198]. A comparison between beeswax or carnauba wax was also made in order to select the optimal solid lipid component in the formulation of clove oil-loaded NLC. It resulted that the presence of carnauba wax led to the formation of NLC with higher particles size and PDI values compared to the ones produced with beeswax; furthermore, even better values were obtained by also introducing the liquid lipid crodamol, with the production of NLC that were stable even after storage. Additionally, beeswax-crodamol nanoparticles showed a higher clove encapsulation efficiency (66 ± 1%–63 ± 0%) when compared with carnauba wax-crodamol ones (60 ± 2%–58 ± 0%): again, the presence of the liquid lipid is decisive. In both situations, the formulations showed no decrease in encapsulated clove percentages after 30 days storage, demonstrating the great suitability of these component in the formulation of NLC for clove delivery [199]. The wound-healing application of thymol-loaded NLC was recently investigated [200]. Herein, Pivetta and co-workers prepared NLC exploiting the hydrating, cicatrizing, and anti-inflammatory properties of two natural lipids, Illipe butter and Calendula oil, to encapsulate thymol EO, whose anti-inflammatory activity could improve the wound healing [200]. Thymol-NLC, with mean particles size < 150 nm, narrow size distribution (PDI < 0.3), negative zeta potential (−12.5 mV), and high encapsulation efficiency (90%), were prepared by hot emulsion followed by sonication. NLC were able to reduce the cytotoxicity of the EO on a non-tumorigenic immortalized human keratinocytes cell line (HaCatT). Thymol-NLC hydrogel obtained using Carbopol gel, selected for its high biological compatibility, were able to provide a fast EO release and to maintain the EO release over time. Interestingly, thymol-NLC hydrogel showed higher anti-inflammatory activity compared to the free EO, as confirmed by *in vitro* studies. The results of the *in vivo* antipsoriatic activity test performed using a model of imiquimod psoriasis-like inflammation, enabled to observe that the mice treated with thymol-NLC hydrogel showed a delay in the development of the inflammation and that the severity of the inflammation was reduced compared to the negative control group [200]. A combined approach to the treatment of wound healing was recently proposed by Carbone et al., who prepared ferulic acid-loaded NLC using *Lavandula* EO or isopropyl myristate (IPM) as the liquid oil component [201]. NLC with homogeneous particles lower than 150 nm were obtained by the phase inversion temperature (PIT) method; the presence of *Lavandula* EO, instead of the liquid synthetic oil, increased the long-term stability of the suspension,

probably due to the tendency of the particles to flocculate. Interestingly, the morphological study revealed that the choice of the liquid oil component affected the NLC structure, since *Lavandula*-NLC presented small spherically shaped particles with a type-II (amorphous) structure, while the presence of the synthetic oil induced the formation of a similar multiple-type-III NLC, with the presence of grape-like aggregates of very small oil nano-components outside the main nanoparticle [201]. The type-II structure of ferulic acid-NLC prepared with *Lavandula* EO also affected the cumulative amount of drug released, which was found to be lower compared to those of NLC prepared with the synthetic oil (46% and 62%, respectively). Interestingly, the type-II structure also improved the cytocompatibility on human fibroblasts and enhanced fibroblast migration promoting wound healing. Therefore, authors concluded that a potential combined protective effect of the antioxidant drug and *Lavandula* EO was achieved using NLC, in which the co-presence shows a synergistic effect in promoting cell migration. In order to reduce the volatilization and improve the bioavailability of linalool EO, NLC were prepared and optimized by high-pressure homogenization using glycerin monostearate as solid lipid and decanoyl/octanoyl-glycerides as liquid lipid [202]. The optimized formulation obtained using 2.5% w/w of each lipid in the surfactant mixture span80/tween80 (2.0 and 4.0% w/w, respectively) showed homogeneous spherical particles of about 50 nm able to provide a controlled EO release. *In vivo* pharmacokinetics studies confirmed that linalool-loaded NLC were able to significantly improve the EO absorption and bioavailability, as confirmed by the higher values of $t_{1/2}$, t_{max} and C_{max} obtained for the loaded EO compared to the free linalool solution [202]. Peppermint essential oil was analyzed in order to explore its wound-healing and antibacterial activity, when encapsulated into NLC. Although the encapsulation efficiency of EO into NLC has been found to be very high (93.2 ± 1.2%), *in vitro* studies on various bacterial cell lines have shown that its antimicrobial activity is comparable to the pure essential oil one; in particular, pure EO MIC values were in the range 5.16 ± 1.48–20.00 ± 0.00, while EO-loaded NLC MIC values were between 5.10 ± 1.49 and 20.00 ± 0.00. The importance of the incorporation of this EO into DDS has been highlighted, instead, by *in vivo* studies on infected wound models: the wound-healing rate was accelerated due to the ability of the EO-NLC to decrease the bacterial count, in addition to the intrinsic anti-inflammatory property of the EO, which was also improved by the NLC structure [203]. The antimicrobial activity of menthol-loaded NLC, with mean size of 115 nm and high EO encapsulation efficiency (98.73%), was investigated by Piran et al. [204]. In particular, menthol-loaded NLC showed higher antibacterial activity against fungi and Gram-positive bacteria compared to the EO emulsion: NLC were able to inhibit the growth of

Staphylococcus aureus, *Bacillus cereus*, *Escherichia coli*, and *C. albicans* at concentration of 125, 250, 500, and 78 μg/mL, respectively, while the corresponding MIC values for menthol emulsion were 1000, 2000, 2000, and 156 μg/mL. Piran et al., therefore concluded that menthol encapsulation in NLC allows decreasing the amount of the EO for preserving foodstuffs from microorganism growth and spoilage. The influence of the preparation method in determining the characteristics of EO-loaded NLC was investigated by Carbone et al., who investigated a lab-scale (phase inversion temperature method) and a scalable (high-pressure homogenization) production method [47]. Authors demonstrated that the greater energy used in the second method allowed obtaining smaller particles and more stable colloidal NLC, using *Rosmarinus officinalis* L., *Lavandula x intermedia* "Sumian" and *Origanum vulgare* subsp. *hirtum* as liquid lipid. Interestingly, results of in vitro biological cell viability test on murine macrophage cell line (RAW 264.7) showed that the nanoencapsulation of the EO enhanced its biocompatibility, being *Lavandula* and *Rosmarinus* NLC the most biocompatible formulations up to a concentration of 0.1% (v/v). Furthermore, the nanoencapsulation did not reduce the intrinsic anti-inflammatory activity of the EO, which was found to decrease in the order *Lavandula > Rosmarinus ≥ Origanum* [47]. Therefore, it was demonstrated that EO can be used as both active ingredients and oily components of NLC, thus enhancing the biocompatibility and reducing the cytotoxicity of the pure oils. The topical application of gel vehicles containing *Rosmarinus*-loaded NLC was also investigated, confirming the potentiality of the EO encapsulation strategy in the treatment of cutaneous alterations involving loss of skin hydration and elasticity [205]. *Lavandula* and *Rosmarinus* were shown to be anti-proliferative agents with the potential to be used as coadjuvants in combination with clotrimazole-loaded NLC in the treatment of topical candidiasis [206]. In this recent study, homogeneous small sized NLC (<100 nm) with long-term stability were successfully prepared using *Lavandula* and *Rosmarinus* as liquid lipid, and loaded with clotrimazole. Interestingly, EO encapsulation into NLC induced an increase in the antiproliferative activity of the selected oils on keratinocytes cell line originated from human skin (HaCaT) and human epidermoid carcinoma cell line (A431), thus suggesting a possible use of *Rosmarinus* and/or *Lavandula* loaded NLC as coadjuvants in non-cancerous proliferative skin diseases. The results of the *in vitro* test against *Candida albicans*, *Candida krusei*, and *Candida parapsilosis*, confirmed that clotrimazole-loaded NLC containing *Lavandula* or *Rosmarinus* were able to improve the antifungal drug activity, thus representing a promising strategy to enhance the effectiveness of traditional antimycotic drug against non-tumoral proliferative dermal diseases [206]. Topical delivery of drugs using DDS was further explored by Miranda and

co-workers, studying *Ridolfia segetum* (L.) Moris essential oil, which was encapsulated into homogeneous NLC with a mean size of 143 ± 5 nm. To increase biocompatibility and permeation, also EO-NLC hydrogel were prepared. Using dialysis membrane, it was analyzed the *in vitro* release of the EO from the nanoplatform, which resulted to be biphasic: at the beginning a low release was detected, which boosted at about 12 h. The *in vivo* permeation of both EO-NLC and EO-NLC hydrogel was studied using newborn pig epidermal membranes and it remarked that the hydrogel structure allowed a higher permeation than the simple NLC. The skin retention studies also supported the evidence that the hydrogel NLC formulation was able to provide a sustained release of the EO, acting as a reservoir [207]. As noted in many of the above papers, particles dimension and polydispersion index appear to be significant for the development of appropriate nanoplatform systems. Therefore, the preformulation study is often decisive. A full factorial design approach was developed by Vieira and co-workers, in order to select the optimal amount of surfactant and solid lipid (2^2 factorial design) to prepare Sucupira Oil-Loaded NLC. It was obtained that the particle size decreased with higher surfactant concentration, while increased with growing concentrations of solid lipid; moreover, polydispersity index and zeta potential both increased with higher surfactant or solid lipid concentrations [208]. The preformulation study was decisive also in the evaluation of the feasibility of spray-drying method in the production of redispersable lipid systems, considering both SLN and NLC loaded with *Syzygium aromaticum* EO. It was developed a quality by design study considering four variables, analyzed at two levels: two of them were related to formulation composition—the presence (1%) or absence (0%) of the liquid lipid oleic acid and the cationic surfactant CTAB—while the other two were referred to spray drying conditions—the inlet drying temperature (60 °C and 80 °C) and the drying aids ratio in relation to the total formulation weight (1:1 and 2:1). Throughout this analysis, it was highlighted a probable interaction between the lipid CTAB—which has positive charge—and the gum Arabic— which has negative charge—as revealed by the increase in particle size and the inversion of the zeta potential. After redispersion of the powders, dynamic light scattering measurements showed no significant changes in particle size and PDI, demonstrating that spray drying method is adequate for this aim [209].

4.5   Authors Opinion and Future Perspectives

To the best of our knowledge, there is no evidence about the effectiveness of EOs as primary treatment in pharmacological treatments. It is worth to remind that unlike many

plants, which are marketed as biochemical actives in humans, therefore classified as drugs, after proper scientific studies about effectiveness and safety, EOs are not subjected to the same studies about reproducible usefulness and safety. To date, in the U.S. Food and Drug Administration (FDA) classification, EOs are considered either cosmetics/food supplements or drugs, depending on their intended use, however their sales and uses are not regulated by FDA. Companies who manufacture or market EOs have a legal responsibility for ensuring their safety. Therefore, researchers and users should take into consideration the quality of the EOs based on the reputation of their sources. Nevertheless, the researchers' interest in EOs applications is increasing due to the possibility to exploit them.

The need of EO encapsulation represents a valid strategy to reach their pharmaceutical application, which is limited by their many drawbacks. Herein, we described different potential applications of EOs in the pharmaceutical field, and we presented the results obtained by different researchers in the development of lipid-based DDS for EOs encapsulation, such as micro and nanoemulsions, liposomes, SLN and NLC. According to literature data, all strategies demonstrated a good ability in improving EOs stability and effectiveness, increasing their bioavailability compared to the pure compound. Some interesting recent applications are related to the combined encapsulation of the EO with a conventional synthetic drug, in order to improve the effectiveness, the biocompatibility, and reducing the resistant mechanisms. As discussed above, the selection of the quali-quantitative composition of the formulation and of the preparation method represent key parameters for obtaining a final formulation with the most appropriate properties for the desired pharmaceutical application. A direct comparison of the different lipid-based delivery systems studied is not easily achievable due to the substantial differences existing among them in terms of structure and behavior. In particular, in the design of a proper system for the delivery of a specific EO, different variables should be taken into consideration, such as the production method (use of heat or organic solvents), the selection of biocompatible and biodegradable raw materials, and the desired nanocarrier properties (i.e., mean size, stability, encapsulation efficiency and release profile).

However, thinking in terms of a near-future prospective for potential EOs application among the various colloidal lipid-based carriers analyzed in this review, it is the opinion of the authors that NLC have a greater possibility of being employed as a nanomedicine in the combined delivery of EOs and conventional drugs. In fact, the possibility of using EOs as intrinsic components of the lipid matrix in combination with solid lipids and surfactants

approved by international commits for safety drugs and administration could represent the new frontier of EOs combined coadjuvant therapy in nanomedicine.

In our opinion, the efforts of researchers should be more focused on the development of patentable products by scalable production methods of interest for the pharmaceutical industry. In order to exploit EOs potential use as coadjuvant to traditional drugs and therapies, thanks to their many interesting biological activities, further investigations should be developed to describe their mechanisms of action and their eventual toxicological side effects. Therefore, more *in vivo* studies should be undertaken to provide reliable results of pharmaceutical interest, thus allowing the pharmaceutical application of newest EO-loaded delivery systems as anti-inflammatory, antimicrobial, antioxidant, antifungal coadjuvant approaches.

Author Contributions: C.C. (Cinzia Cimino), O.M.M., T.M. and A.B.: data curation, writing—review and editing. F.D. and E.M.B.S.: writing—review and editing. R.P. editing and funding acquisition. C.C. (Claudia Carbone): conceptualization, methodology, writing—original draft, writing—review and editing, supervision, funding acquisition. All authors have read and agreed to the published version of the manuscript.

Conflicts of Interest: The authors declare no conflict of interest.

References:

1. Gurib-Fakim, A. Medicinal plants: Traditions of yesterday and drugs of tomorrow. Mol. Asp. Med. 2006, 27, 1–93, doi:10.1016/j.mam.2005.07.008.
2. Valiakos, E.; Marselos, M.; Sakellaridis, N.; Constantinidis, T.; Skaltsa, H. Ethnopharmacological approach to the herbal medicines of the "antidotes" in Nikolaos Myrepsos' Dynameron. J. Ethnopharmacol. 2015, 163, 68–82.
3. MM, C. Plant products as antimicrobial agents. Clin. Microbiol. Rev. 1999, 12, 564–582.
4. A., L. The botanical material medica of the Iatrosophikon—A collection of prescriptions from a monastery in Cyprus. J. Ethnopharmacol. 2006, 104, 387–406.
5. El Asbahani, A.; Miladi, K.; Badri, W.; Sala, M.; Ait Addi, E.H.; Casabianca, H.; El Mousadik, A.; Hartmann, D.; Jilale, A.; Renaud, F.N.; et al. Essential oils: From extraction to encapsulation. Int. J. Pharm. 2015, 483, 220–243, doi:10.1016/j.ijpharm.2014.12.069.
6. Bilia, A.R.; Guccione, C.; Isacchi, B.; Righeschi, C.; Firenzuoli, F.; Bergonzi, M.C. Essential oils loaded in nanosystems: A developing strategy for a successful therapeutic approach. Evid. Based Complementary Altern. Med. 2014, 2014, 651593, doi:10.1155/2014/651593.

7. Bona, E.; Cantamessa, S.; Pavan, M.; Novello, G.; Massa, N.; Rocchetti, A.; Berta, G.; Gamalero, E. Sensitivity of Candida albicans to essential oils: Are they an alternative to antifungal agents? J. Appl. Microbiol. 2016, 121, 1530–1545, doi:10.1111/jam.13282.

8. Meyer-Warnod, B. Natural essential oils: Extraction processes and application to some major oils. Perfum. Flavorist 1984, 9, 93– 104.

9. Masango, P. Cleaner production of essential oils by steam distillation. J. Clean. Prod. 2005, 13, 833–839.

10. Ferhat, M.A.; Meklati, B.Y.; Chemat, F. Comparison of different isolation methods of essential oil from Citrus fruits: Cold pressing, hydrodistillation and microwave 'dry' distillation. Flavour Fragr. J. 2007, 22, 494–504.

11. Fornari, T.; Vicente, G.; Vazquez, E.; Garcia-Risco, M.R.; Reglero, G. Isolation of essential oil from different plants and herbs by supercritical fluid extraction. J. Chromatogr. A 2012, 1250, 34–48, doi:10.1016/j.chroma.2012.04.051.

12. Vinatoru, M. An overview of the ultrasonically assisted extraction of bioactive principles from herbs. Ultrason Sonochem 2001, 8, 303–313, doi:10.1016/s1350-4177(01)00071-2.

13. Farhat, A.; Ginies, C.; Romdhane, M.; Chemat, F. Eco-friendly and cleaner process for isolation of essential oil using microwave energy. Experimental and theoretical study. J. Chromatogr. A 2009, 1216, 5077–5085.

14. Périno-Issartier, S.; Giniesa, C.; Cravotto, G.; Chemata, F. A comparison of essential oils obtained from lavandin via different extraction processes: Ultrasound, microwave, turbohydrodistillation, steam and hydrodistillation. J. Chromatogr. A 2013, 1305, 41–47.

15. Bohra, P.M.V.; Pangarkar, V.G.; Taskar, A. Adsorptive recovery of water soluble essential oil components. J. Chem. Technol. Biotechnol. 1994, 60, 97–102.

16. Faborode, M.O.; Favier, J.F. Identification and significance of the oil-point in seed-oil expression. J. Agr Eng. Res. 1996, 65, 335–345, doi:10.1006/jaer.1996.0107.

17. Pekkarinen, S.; Hopia, A.; Heinonen, M. Effect of processing on the oxidative stability of low erucic acid turnip rapeseed (Brassica rapa) oil. Lipid/Fett 1998, 100, 69–74.

18. Koski, A.; Psomiadou, E.; Tsimidou, M.; Hopia, A.; Kefalas, P.; Wahala, K.; Heinonen, M. Oxidative stability and minor constituents of virgin olive oil and cold-pressed rapeseed oil. Eur Food Res. Technol. 2002, 214, 294–298, doi:10.1007/s00217-001-0479-5.

19. Baik, H.Y.; Juvik, J.; Jeffery, E.H.; Wallig, M.A.; Kushad, M.; Klein, B.P. Relating glucosinolate content and flavor of broccoli cultivars. J. Food Sci. 2003, 68, 1043–1050, doi:10.1111/j.1365-2621.2003.tb08285.x.

20. Matthaus, B.; Bruhl, L. Quality of cold-pressed edible rapeseed oil in Germany. Nahrung 2003, 47, 413–419, doi:10.1002/food.200390092.

21. Azadmard-Damirchi, S.; Habibi-Nodeh, F.; Hesari, J.; Nemati, M.; Achachlouei, B.F. Effect of pretreatment with microwaves on oxidative stability and nutraceuticals content of oil from rapeseed. Food Chem. 2010, 121, 1211–1215, doi:10.1016/j.foodchem.2010.02.006.

22. Da Porto, C.; Decorti, D.; Natolino, A. Microwave pretreatment of Moringa oleifera seed: Effect on oil obtained by pilot-scale supercritical carbon dioxide extraction and Soxhlet apparatus. J. Supercrit Fluid 2016, 107, 38–43, doi:10.1016/j.supflu.2015.08.006.

23. Blazevic, I.; Mastelic, J. Glucosinolate degradation products and other bound and free volatiles in the leaves and roots of radish (Raphanus sativus L.). Food Chem. 2009, 113, 96–102, doi:10.1016/j.foodchem.2008.07.029.

24. Capuzzo, A.; Maffei, M.E.; Occhipinti, A. Supercritical fluid extraction of plant flavors and fragrances. Molecules 2013, 18, 7194–7238, doi:10.3390/molecules18067194.

25. de Castro, M.D.L.; Jimenez-Carmona, M.M.; Fernandez-Perez, V. Towards more rational techniques for the isolation of valuable essential oils from plants. Trend Anal. Chem 1999, 18, 708–716.

26. Basile, A.; Jimenez-Carmona, M.M.; Clifford, A.A. Extraction of rosemary by superheated water. J. Agric. Food Chem. 1998, 46, 5205–5209, doi:10.1021/Jf980437e.

27. Herrero, M.; Cifuentes, A.; Ibanez, E. Sub- and supercritical fluid extraction of functional ingredients from different natural sources: Plants, food-by-products, algae and microalgae—A review. Food Chem. 2006, 98, 136–148, doi:10.1016/j.foodchem.2005.05.058.

28. Jimenez-Carmona, M.M.; Ubera, J.L.; Luque de Castro, M.D. Comparison of continuous subcritical water extraction and hydrodistillation of marjoram essential oil. J. Chromatogr. A 1999, 855, 625–632, doi:10.1016/s0021-9673(99)00703-7.

29. Romanik, G.; Gilgenast, E.; Przyjazny, A.; Kaminski, M. Techniques of preparing plant material for chromatographic separation and analysis. J. Biochem Bioph. Meth. 2007, 70, 253–261, doi:10.1016/j.jbbm.2006.09.012.

30. Olgac, E.; Gurkan, R. Coupling of ion pair ultrasound assisted-cloud point extraction to microvolume UV-Vis spectrophotometry for speciation analysis of ionic NO2-,NO3- and total NO2-/NO3- without and with reduction in the selected beverage and food matrices. Food Addit. Contam. Part Achem. Anal. Controlexpo. Risk Assess. 2020, 37, 1811–1830, doi:10.1080/19440049.2020.1811402.

31. Vian, M.A.; Fernandez, X.; Visinoni, F.; Chemat, F. Microwave hydrodiffusion and gravity, a new technique for extraction of essential oils. J. Chromatogr. A 2008, 1190, 14–17, doi:10.1016/j.chroma.2008.02.086.

32. Allaf, T.; Tomao, V.; Ruiz, K.; Chemat, F. Instant controlled pressure drop technology and ultrasound assisted extraction for sequential extraction of essential oil and antioxidants. Ultrason. Sonochem. 2013, 20, 239–246, doi:10.1016/j.ultsonch.2012.05.013.

33. Rashidi, S.; Eikani, M.H.; Ardjmand, M. Extraction of Hyssopus officinalis L. essential oil using instant controlled pressure drop process. J. Chromatogr. A 2018, 1579, 9–19, doi:10.1016/j.chroma.2018.10.020.

34. Raut, J.S.; Karuppayil, S.M. A status review on the medicinal properties of essential oils. Ind. Crop. Prod. 2014, 62, 250–264.

35. Malcolm, B.J.; Tallian, K. Essential oil of lavender in anxiety disorders: Ready for prime time? Ment. Health Clin. 2017, 7, 147–155, doi:10.9740/mhc.2017.07.147.

36. Soetjipto, H. Antibacterial Properties of Essential Oil in Some Indonesian Herbs. In Potential Essentials Oils; IntechOpen: London, UK, 2018; Volume 41.

37. Hosseini, S.F.; Zandi, M.; Rezaei, M.; Farahmandghavi, F. Two-step method for encapsulation of oregano essential oil in chitosan nanoparticles: Preparation, characterization and in vitro release study. Carbohydr. Polym. 2013, 95, 50–56, doi:10.1016/j.carbpol.2013.02.031.

38. Trinetta, V.; Morgan, M.T.; Coupland, J.N.; Yucel, U. Essential Oils Against Pathogen and Spoilage Microorganisms of Fruit Juices: Use of Versatile Antimicrobial Delivery Systems. J. Food Sci. 2017, 82, 471–476, doi:10.1111/1750-3841.13614.

39. Borges, R.S.; Keita, H.; Ortiz, B.L.S.; Dos Santos Sampaio, T.I.; Ferreira, I.M.; Lima, E.S.; de Jesus Amazonas da Silva, M.; Fernandes, C.P.; de Faria Mota Oliveira, A.E.M.; da Conceicao, E.C.; et al. Anti-inflammatory activity of nanoemulsions of essential oil from Rosmarinus officinalis L.: In vitro and in zebrafish studies. Inflammopharmacology 2018, 26, 1057–1080, doi:10.1007/s10787-017-0438-9.

40. Benatti, F.B.; Pedersen, B.K. Exercise as an anti-inflammatory therapy for rheumatic diseases-myokine regulation. Nat. Rev. Rheumatol. 2015, 11, 86–97, doi:10.1038/nrrheum.2014.193.

41. Brightling, C.E. Eosinophils, bronchitis and asthma: Pathogenesis of cough and airflow obstruction. Pulm. Pharm. 2011, 24, 324– 327, doi:10.1016/j.pupt.2010.11.001.

42. Ogunwande, I.A.; Avoseh, O.N.; Olasunkanmi, K.N.; Lawal, O.A.; Ascrizzi, R.; Flamini, G. Chemical composition, anti-nociceptive and anti-inflammatory activities of essential oil of Bougainvillea glabra. J. Ethnopharmacol. 2019, 232, 188–192, doi:10.1016/j.jep.2018.12.017.

43. Rodrigues, L.B.; Oliveira Brito Pereira Bezerra Martins, A.; Cesario, F.R.; Ferreira, E.C.F.; de Albuquerque, T.R.; Martins Fernandes, M.N.; Fernandes da Silva, B.A.; Quintans Junior, L.J.; da Costa, J.G.; Melo Coutinho, H.D.; et al. Anti-inflammatory and antiedematogenic activity of the Ocimum basilicum essential oil and its main compound estragole: In vivo mouse models. Chem. Biol. Interact. 2016, 257, 14–25, doi:10.1016/j.cbi.2016.07.026.

44. Lee, S.C.; Wang, S.Y.; Li, C.C.; Liu, C.T. Anti-inflammatory effect of cinnamaldehyde and linalool from the leaf essential oil of Cinnamomum osmophloeum Kanehira in endotoxin-induced mice. J. Food Drug Anal. 2018, 26, 211–220, doi:10.1016/j.jfda.2017.03.006.

45. Chen, L.L.; Zhang, H.J.; Chao, J.; Liu, J.F. Essential oil of Artemisia argyi suppresses inflammatory responses by inhibiting JAK/STATs activation. J. Ethnopharmacol. 2017, 204, 107–117, doi:10.1016/j.jep.2017.04.017.

46. Silva, G.L.; Luft, C.; Lunardelli, A.; Amaral, R.H.; Melo, D.A.; Donadio, M.V.; Nunes, F.B.; de Azambuja, M.S.; Santana, J.C.; Moraes, C.M.; et al. Antioxidant, analgesic and anti-inflammatory effects of lavender essential oil. Acad. Bras. Cienc. 2015, 87, 1397–1408, doi:10.1590/0001-3765201520150056.

47. Carbone, C.; Martins-Gomes, C.; Caddeo, C.; Silva, A.M.; Musumeci, T.; Pignatello, R.; Puglisi, G.; Souto, E.B. Mediterranean essential oils as precious matrix components and active ingredients of lipid nanoparticles. Int. J. Pharm. 2018, 548, 217–226, doi:10.1016/j.ijpharm.2018.06.064.

48. Elaguel, A.; Kallel, I.; Gargouri, B.; Ben Amor, I.; Hadrich, B.; Ben Messaoud, E.; Gdoura, R.; Lassoued, S.; Gargouri, A. Lawsonia inermis essential oil: Extraction optimization by RSM, antioxidant activity, lipid peroxydation and antiproliferative effects. Lipids Health Dis. 2019, 18, 196, doi:10.1186/s12944-019-1141-1.

49. Shen, C.Y.; Jiang, J.G.; Zhu, W.; Ou-Yang, Q. Anti-inflammatory Effect of Essential Oil from Citrus aurantium L. var. amara Engl. J. Agric. Food Chem. 2017, 65, 8586–8594, doi:10.1021/acs.jafc.7b02586.

50. Kaur, N.; Chahal, K.K.; Kumar, A.; Singh, R.; Bhardwaj, U. Antioxidant activity of Anethum graveolens L. essential oil constituents and their chemical analogues. J. Food Biochem. 2019, 43, doi:10.1111/jfbc.12782.

51. Bardaweel, S.K.; Bakchiche, B.; ALSalamat, H.A.; Rezzoug, M.; Gherib, A.; Flamini, G. Chemical composition, antioxidant, antimicrobial and Antiproliferative activities of essential oil of Mentha spicata L. (Lamiaceae) from Algerian Saharan atlas. BMC Complementary Altern. Med. 2018, 18, doi:10.1186/S12906-018-2274-X.

52. Shojaee-Aliabadi, S.; Hosseini, S.M.; Mirmoghtadaie, L. Antimicrobial Activity of Essential Oil. In Essential Oils in Food Processing: Chemistry, Safety and Applications; John Wiley & Sons, Ltd.: Chichester, UK, 2017; pp. 191–229.

53. Saad, N.Y.; Muller, C.D.; Lobstein, A. Major bioactivities and mechanism of action of essential oils and their components. Flavour Fragr. J. 2013, 28, 269–279, doi:10.1002/ffj.3165.

54. Delaquis, P.J.; Stanich, K.; Girard, B.; Mazza, G. Antimicrobial activity of individual and mixed fractions of dill, cilantro, coriander and eucalyptus essential oils. Int. J. Food Microbiol. 2002, 74, 101–109.

55. Hammer, K.A.; Carson, C.F.; Riley, T.V. Antimicrobial activity of essential oils and other plant extracts. J. Appl. Microbiol. 1999, 86, 985–990.

56. Nikolić, M.; Jovanović, K.K.; Marković, T.; Marković, D.; Gligorijević, N.; Radulović, S.; Soković, M. Chemical composition, antimicrobial, and cytotoxic properties of five Lamiaceae essential oils. Ind. Crop. Prod. 2014, 61, 225–232.

57. Guillén, M.D.; Cabo, N.; Burillo, J. Characterisation of the essential oils of some cultivated aromatic plants of industrial interest. J. Sci. Food Agric. 1996, 70, 359–363.

58. Bilia, A.R.; Santomauro, F.; Sacco, C.; Bergonzi, M.C.; Donato, R. Essential Oil of Artemisia annua L.: An Extraordinary Component with Numerous Antimicrobial Properties. Evid. Based Complementary Altern. Med. 2014, 2014, 159819, doi:10.1155/2014/159819.

59. Donato, R.S.F.; Bilia, A.R.; Flamini, G.; Sacco, C. Antibacterial activity of Tuscan Artemisia annua essential oil and its major components against some foodborne pathogens. LWT Food Sci. Technol. 2015, 64, 1251–1254.

60. Zhang, X.; Guo, Y.; Guo, L.; Jiang, H.; Ji, Q. In Vitro Evaluation of Antioxidant and Antimicrobial Activities of Melaleuca alternifolia Essential Oil. Biomedc Res. Int. 2018, 2018, 2396109, doi:10.1155/2018/2396109.

61. Kim, J.M.M.; Wei, C.I. Antibacterial activity of some essential oil components against five foodborne pathogens. J. Agric. Food Chem. 1995, 43, 2839–2845.

62. Cox, S.D.; Mann, C.M.; Markham, J.L.; Bell, H.C.; Gustafson, J.E.; Warmington, J.R.; Wyllie, S.G. The mode of antimicrobial action of the essential oil of Melaleuca alternifolia (tea tree oil). J. Appl. Microbiol. 2000, 88, 170–175, doi:10.1046/j.1365- 2672.2000.00943.x.

63. Taha, A.M.; Eldahshan, O.A. Chemical Characteristics, Antimicrobial, and Cytotoxic Activities of the Essential Oil of Egyptian Cinnamomum glanduliferum Bark. Chem. Biodivers. 2017, 14, doi:10.1002/cbdv.201600443.

64. Bakkali, F.; Averbeck, S.; Averbeck, D.; Idaomar, M. Biological effects of essential oils—A review. Food Chem. Toxicol. Int. J. Publ. Br. Ind. Biol. Res. Assoc. 2008, 46, 446–475, doi:10.1016/j.fct.2007.09.106.

65. Hammer, K.A.; Carson, C.F.; Dunstan, J.A.; Hale, J.; Lehmann, H.; Robinson, C.J.; Prescott, S.L.; Riley, T.V. Antimicrobial and anti-inflammatory activity of five Taxandria fragrans oils in vitro. Microbiol. Immunol. 2008, 52, 522–530, doi:10.1111/j.1348- 0421.2008.00070.x.

66. Burt, S. Essential oils: Their antibacterial properties and potential applications in foods—A review. Int. J. Food Microbiol. 2004, 94, 223–253, doi:10.1016/j.ijfoodmicro.2004.03.022.

67. Di Pasqua, R.; Betts, G.; Hoskins, N.; Edwards, M.; Ercolini, D.; Mauriello, G. Membrane toxicity of antimicrobial compounds from essential oils. J. Agric. Food Chem. 2007, 55, 4863–4870, doi:10.1021/jf0636465.

68. Insawang, S.; Pripdeevech, P.; Tanapichatsakul, C.; Khruengsai, S.; Monggoot, S.; Nakham, T.; Artrod, A.; D'Souza, P.E.; Panuwet, P. Essential Oil Compositions and Antibacterial and Antioxidant Activities of Five Lavandula stoechas Cultivars Grown in Thailand. Chem. Biodivers. 2019, 16, e1900371, doi:10.1002/cbdv.201900371.

69. Pesavento, G.; Maggini, V.; Maida, I.; Lo Nostro, A.; Calonico, C.; Sassoli, C.; Perrin, E.; Fondi, M.; Mengoni, A.; Chiellini, C.; et al. Essential Oil from Origanum vulgare Completely Inhibits the Growth of Multidrug-Resistant Cystic Fibrosis Pathogens. Nat. Prod. Commun. 2016, 11, 861–864.

70. Demirci, F.; Karaca, N.; Tekin, M.; Demirci, B. Anti-inflammatory and antibacterial evaluation of Thymus sipyleus Boiss. subsp. sipyleus var. sipyleus essential oil against rhinosinusitis pathogens. Microb. Pathog. 2018, 122, 117–121, doi:10.1016/j.micpath.2018.06.025.

71. van Vuuren, S.F.; Suliman, S.; Viljoen, A.M. The antimicrobial activity of four commercial essential oils in combination with conventional antimicrobials. Lett. Appl. Microbiol. 2009, 48, 440–446, doi:10.1111/j.1472-765X.2008.02548.x.

72. Dorman, H.J.; Deans, S.G. Antimicrobial agents from plants: Antibacterial activity of plant volatile oils. J. Appl. Microbiol. 2000, 88, 308–316, doi:10.1046/j.1365-2672.2000.00969.x.

73. Fabio, A.; Cermelli, C.; Fabio, G.; Nicoletti, P.; Quaglio, P. Screening of the antibacterial effects of a variety of essential oils on microorganisms responsible for respiratory infections. Phytother. Res. 2007, 21, 374–377, doi:10.1002/ptr.1968.

74. Fu, Y.; Zu, Y.; Chen, L.; Shi, X.; Wang, Z.; Sun, S.; Efferth, T. Antimicrobial activity of clove and rosemary essential oils alone and in combination. Phytother. Res. 2007, 21, 989–994, doi:10.1002/ptr.2179.

75. Costa, M.F.; Durco, A.O.; Rabelo, T.K.; Barreto, R.S.S.; Guimaraes, A.G. Effects of Carvacrol, Thymol and essential oils containing such monoterpenes on wound healing: A systematic review. J. Pharm. Pharm. 2019, 71, 141–155, doi:10.1111/jphp.13054.

76. Pattnaik, S.; Subramanyam, V.R.; Bapaji, M.; Kole, C.R. Antibacterial and antifungal activity of aromatic constituents of essential oils. Microbios 1997, 89, 39–46.

77. Kozics, K.; Buckova, M.; Puskarova, A.; Kalaszova, V.; Cabicarova, T.; Pangallo, D. The Effect of Ten Essential Oils on Several Cutaneous Drug-Resistant Microorganisms and Their Cyto/Genotoxic and Antioxidant Properties. Molecules 2019, 24, 4570, doi:10.3390/molecules24244570.

78. Martin, P.; Leibovich, S.J. Inflammatory cells during wound repair: The good, the bad and the ugly. Trends Cell Biol. 2005, 15, 599–607, doi:10.1016/j.tcb.2005.09.002.

79. Diegelmann, R.F.; Evans, M.C. Wound healing: An overview of acute, fibrotic and delayed healing. Front. Biosci. A J. Virtual Libr. 2004, 9, 283–289, doi:10.2741/1184.

80. Wilgus, T.A. Immune cells in the healing skin wound: Influential players at each stage of repair. Pharm. Res. 2008, 58, 112–116, doi:10.1016/j.phrs.2008.07.009.

81. Gurtner, G.C.; Werner, S.; Barrandon, Y.; Longaker, M.T. Wound repair and regeneration. Nature 2008, 453, 314–321, doi:10.1038/nature07039.

82. Wang, P.H.; Huang, B.S.; Horng, H.C.; Yeh, C.C.; Chen, Y.J. Wound healing. J. Chin. Med. Assoc. Jcma 2018, 81, 94–101, doi:10.1016/j.jcma.2017.11.002.

83. Fernandes, E.S.; Passos, G.F.; Medeiros, R.; da Cunha, F.M.; Ferreira, J.; Campos, M.M.; Pianowski, L.F.; Calixto, J.B. Anti-inflammatory effects of compounds alpha-humulene and (-)-trans-caryophyllene isolated from the essential oil of Cordia verbenacea. Eur. J. Pharm. 2007, 569, 228–236, doi:10.1016/j.ejphar.2007.04.059.

84. Seyed Ahmadi, S.G.; Farahpour, M.R.; Hamishehkar, H. Topical application of Cinnamon verum essential oil accelerates infected wound healing process by increasing tissue antioxidant capacity and keratin biosynthesis. Kaohsiung J. Med. Sci. 2019, 35, 686–694, doi:10.1002/kjm2.12120.

85. Edmondson, M.; Newall, N.; Carville, K.; Smith, J.; Riley, T.V.; Carson, C.F. Uncontrolled, open-label, pilot study of tea tree (Melaleuca alternifolia) oil solution in the decolonisation of methicillin-resistant Staphylococcus aureus positive wounds and its influence on wound healing. Int. Wound J. 2011, 8, 375–384, doi:10.1111/j.1742-481X.2011.00801.x.

86. Manzuoerh, R.; Farahpour, M.R.; Oryan, A.; Sonboli, A. Effectiveness of topical administration of Anethum graveolens essential oil on MRSA-infected wounds. Biomed. Pharm. 2019, 109, 1650–1658, doi:10.1016/j.biopha.2018.10.117.

87. Li, F.; Huang, Q.; Chen, J.; Peng, Y.; Roop, D.R.; Bedford, J.S.; Li, C.Y. Apoptotic cells activate the "phoenix rising" pathway to promote wound healing and tissue regeneration. Sci. Signal. 2010, 3, ra13, doi:10.1126/scisignal.2000634.

88. Kano, M.R.; Morishita, Y.; Iwata, C.; Iwasaka, S.; Watabe, T.; Ouchi, Y.; Miyazono, K.; Miyazawa, K. VEGF-A and FGF-2 synergistically promote neoangiogenesis through enhancement of endogenous PDGF-B-PDGFRbeta signaling. J. Cell Sci. 2005, 118, 3759–3768, doi:10.1242/jcs.02483.

89. Oryan, A.; Moshiri, A. A long term study on the role of exogenous human recombinant basic fibroblast growth factor on the superficial digital flexor tendon healing in rabbits. J. Musculoskelet. Neuronal Interact. 2011, 11, 185–195.

90. Berridge, M.J. Cell stress, inflammatory responses and cell death. Cell Signal. Biol. 2012, 11, 29.

91. Mori, H.M.; Kawanami, H.; Kawahata, H.; Aoki, M. Wound healing potential of lavender oil by acceleration of granulation and wound contraction through induction of TGF-beta in a rat model. BMC Complementary Altern. Med. 2016, 16, doi:10.1186/S12906-016-1128-7.

92. Laios, K.; Lytsikas-Sarlis, P.; Manes, K.; Kontaxaki, M.I.; Karamanou, M.; Androutsos, G. Drugs for mental illnesses in ancient greek medicine. Psychiatrike 2019, 30, 58–65, doi:10.22365/jpsych.2019.301.58.

93. Nwobodo, N.N.; Offiah, R.O. The use of medicinal plants in the treatment of mental disorders: An overview. Int. J. Phytopharm. 2017, 7, 18–22.

94. La Croce, E. Concept of insanity in classical Greece. Acta Psiquiatr. Psicol. Am. Lat. 1981, 27, 285–291.

95. Olivieri, M.F.; Marzari, F.; Kesel, A.J.; Bonalume, L.; Saettini, F. Pharmacology and psychiatry at the origins of Greek medicine: The myth of Melampus and the madness of the Proetides. J. Hist. Neurosci. 2017, 26, 193–215, doi:10.1080/0964704X.2016.1211901.

96. Tasca, C.; Rapetti, M.; Carta, M.G.; Fadda, B. Women and hysteria in the history of mental health. Clin. Pract. Epidemiol. Ment. Health 2012, 8, 110–119, doi:10.2174/1745017901208010110.

97. Martin, E.A.; Moore, J.N. Trial of reserpine in treatment of schizophrenia. Br. Med. J. 1957, 1, 8–14, doi:10.1136/bmj.1.5009.8.

98. Miller, L.G. Herbal medicinals: Selected clinical considerations focusing on known or potential drug-herb interactions. Arch. Intern. Med. 1998, 158, 2200–2211, doi:10.1001/archinte.158.20.2200.

99. Gnatta, J.R.; Kurebayashi, L.F.; Turrini, R.N.; Silva, M.J. Aromatherapy and nursing: Historical and theoretical conception. Rev. Esc. Enferm. USP 2016, 50, 130–136, doi:10.1590/S0080-623420160000100017.

100. Zhang, N.; Yao, L. Anxiolytic Effect of Essential Oils and Their Constituents: A Review. J. Agric. Food Chem. 2019, 67, 13790–13808, doi:10.1021/acs.jafc.9b00433.

101. Buck, L.; Axel, R. A Novel Multigene Family May Encode Odorant Receptors—A Molecular-Basis for Odor Recognition. Cell 1991, 65, 175–187, doi:10.1016/0092-8674(91)90418-X.

102. Ballanger, B.; Bath, K.G.; Mandairon, N. Odorants: A tool to provide non pharmacological intervention to reduce anxiety during normal and pathological aging. Neurobiol. Aging 2019, 82, 18–29, doi:10.1016/j.neurobiolaging.2019.06.007.

103. Ito, A.; Miyoshi, M.; Ueki, S.; Fukada, M.; Komaki, R.; Watanabe, T. "Green odor" inhalation by rats down-regulates stress- induced increases in Fos expression in stress-related forebrain regions. Neurosci. Res. 2009, 65, 166–174, doi:10.1016/j.neures.2009.06.012.

104. Schuwald, A.M.; Noldner, M.; Wilmes, T.; Klugbauer, N.; Leuner, K.; Muller, W.E. Lavender oil-potent anxiolytic properties via modulating voltage dependent calcium channels. PLoS ONE 2013, 8, e59998, doi:10.1371/journal.pone.0059998.

105. Kasper, S. An orally administered Lavandula oil preparation (Silexan) for anxiety disorder and related conditions: An evidence based review. Int. J. Psychiatry Clin. Pract. 2013, 17 (Suppl. 1), 15–22, doi:10.3109/13651501.2013.813555.

106. Craske, M.G.; Stein, M.B. Anxiety. Lancet 2016, 388, 3048–3059, doi:10.1016/S0140-6736(16)30381-6.

107. Ressler, K.J.; Mayberg, H.S. Targeting abnormal neural circuits in mood and anxiety disorders: From the laboratory to the clinic. Nat. Neurosci. 2007, 10, 1116–1124, doi:10.1038/nn1944.

108. Craske, M.G.; Stein, M.B.; Eley, T.C.; Milad, M.R.; Holmes, A.; Rapee, R.M.; Wittchen, H.U. Anxiety disorders. Nat. Rev. Dis. Primers 2017, 3, 17024, doi:10.1038/nrdp.2017.24.

109. Sartori, S.B.; Singewald, N. Novel pharmacological targets in drug development for the treatment of anxiety and anxiety-related disorders. Pharmacol. Ther. 2019, 204, 107402, doi:10.1016/j.pharmthera.2019.107402.

110. Murrough, J.W.; Yaqubi, S.; Sayed, S.; Charney, D.S. Emerging drugs for the treatment of anxiety. Expert Opin. Emerg. Drugs 2015, 20, 393–406, doi:10.1517/14728214.2015.1049996.

111. Saiyudthong, S.; Pongmayteegul, S.; Marsden, C.A.; Phansuwan-Pujito, P. Anxiety-like behaviour and c-fos expression in rats that inhaled vetiver essential oil. Nat. Prod. Res. 2015, 29, 2141–2144, doi:10.1080/14786419.2014.992342.

112. Ramboz, S.; Oosting, R.; Amara, D.A.; Kung, H.F.; Blier, P.; Mendelsohn, M.; Mann, J.J.; Brunner, D.; Hen, R. Serotonin receptor 1A knockout: An animal model of anxiety-related disorder. Proc. Natl. Acad. Sci. USA 1998, 95, 14476–14481, doi:10.1073/pnas.95.24.14476.

113. Faturi, C.B.; Leite, J.R.; Alves, P.B.; Canton, A.C.; Teixeira-Silva, F. Anxiolytic-like effect of sweet orange aroma in Wistar rats. Prog. Neuro-Psychopharmacol. Biol. Psychiatry 2010, 34, 605–609, doi:10.1016/j.pnpbp.2010.02.020.

114. Linck, V.M.; da Silva, A.L.; Figueiro, M.; Caramao, E.B.; Moreno, P.R.; Elisabetsky, E. Effects of inhaled Linalool in anxiety, social interaction and aggressive behavior in mice. Phytomedicine Int. J. Phytother. Phytopharm. 2010, 17, 679–683, doi:10.1016/j.phymed.2009.10.002.

115. Chen, S.W.; Min, L.; Li, W.J.; Kong, W.X.; Li, J.F.; Zhang, Y.J. The effects of angelica essential oil in three murine tests of anxiety. Pharmacol. Biochem. Behav. 2004, 79, 377–382, doi:10.1016/j.pbb.2004.08.017.

116. Pultrini Ade, M.; Galindo, L.A.; Costa, M. Effects of the essential oil from Citrus aurantium L. in experimental anxiety models in mice. Life Sci. 2006, 78, 1720–1725, doi:10.1016/j.lfs.2005.08.004.

117. Baretta, I.P.; Felizardo, R.A.; Bimbato, V.F.; dos Santos, M.G.; Kassuya, C.A.; Gasparotto Junior, A.; da Silva, C.R.; de Oliveira, S.M.; Ferreira, J.; Andreatini, R. Anxiolytic-like effects of acute and chronic treatment with Achillea millefolium L. extract. J. Ethnopharmacol. 2012, 140, 46–54, doi:10.1016/j.jep.2011.11.047.

118. Perry, R.; Terry, R.; Watson, L.K.; Ernst, E. Is lavender an anxiolytic drug? A systematic review of randomised clinical trials. Phytomedicine Int. J. Phytother. Phytopharm. 2012, 19, 825–835, doi:10.1016/j.phymed.2012.02.013.

119. Bradley, B.F.; Starkey, N.J.; Brown, S.L.; Lea, R.W. Anxiolytic effects of Lavandula angustifolia odour on the Mongolian gerbil elevated plus maze. J. Ethnopharmacol. 2007, 111, 517–525, doi:10.1016/j.jep.2006.12.021.

120. Linck, V.M.; da Silva, A.L.; Figueiro, M.; Piato, A.L.; Herrmann, A.P.; Dupont Birck, F.; Caramao, E.B.; Nunes, D.S.; Moreno, P.R.; Elisabetsky, E. Inhaled linalool-induced sedation in mice. Phytomedicine Int. J. Phytother. Phytopharm. 2009, 16, 303–307, doi:10.1016/j.phymed.2008.08.001.

121. Coelho, L.S.; Correa-Netto, N.F.; Masukawa, M.Y.; Lima, A.C.; Maluf, S.; Linardi, A.; Santos-Junior, J.G. Inhaled Lavandula angustifolia essential oil inhibits consolidation of contextual- but not tone-fear conditioning in rats. J. Ethnopharmacol. 2018, 215, 34–41, doi:10.1016/j.jep.2017.12.038.

122. Shaw, D.; Annett, J.M.; Doherty, B.; Leslie, J.C. Anxiolytic effects of lavender oil inhalation on open-field behaviour in rats. Phytomedicine Int. J. Phytother. Phytopharm. 2007, 14, 613–620, doi:10.1016/j.phymed.2007.03.007.

123. Karan, N.B. Influence of lavender oil inhalation on vital signs and anxiety: A randomized clinical trial. Physiol. Behav.2019,211, 112676, doi:10.1016/j.physbeh.2019.112676.

124. Kritsidima, M.; Newton, T.; Asimakopoulou, K. The effects of lavender scent on dental patient anxiety levels: A cluster randomised-controlled trial. Community Dent. Oral Epidemiol. 2010, 38, 83–87, doi:10.1111/j.1600-0528.2009.00511.x.

125. Conrad, P.; Adams, C. The effects of clinical aromatherapy for anxiety and depression in the high risk postpartum woman—A pilot study. Complementary Ther. Clin. Pract. 2012, 18, 164–168, doi:10.1016/j.ctcp.2012.05.002.

126. Akhondzadeh, S.; Kashani, L.; Fotouhi, A.; Jarvandi, S.; Mobaseri, M.; Moin, M.; Khani, M.; Jamshidi, A.H.; Baghalian, K.; Taghizadeh, M. Comparison of Lavandula angustifolia Mill. tincture and imipramine in the treatment of mild to moderate depression: A double-blind, randomized trial. Prog. Neuro-Psychopharmacol. Biol. Psychiatry 2003, 27, 123–127, doi:10.1016/s0278- 5846(02)00342-1.

127. Uzuncakmak, T.; Ayaz Alkaya, S. Effect of aromatherapy on coping with premenstrual syndrome: A randomized controlled trial. Complementary Ther. Med. 2018, 36, 63–67, doi:10.1016/j.ctim.2017.11.022.

128. Chioca, L.R.; Ferro, M.M.; Baretta, I.P.; Oliveira, S.M.; Silva, C.R.; Ferreira, J.; Losso, E.M.; Andreatini, R. Anxiolytic-like effect of lavender essential oil inhalation in mice: Participation of serotonergic but not GABAA/benzodiazepine neurotransmission. J. Ethnopharmacol. 2013, 147, 412–418, doi:10.1016/j.jep.2013.03.028.

129. Harada, H.; Kashiwadani, H.; Kanmura, Y.; Kuwaki, T. Linalool Odor-Induced Anxiolytic Effects in Mice. Front. Behav. Neurosci. 2018, 12, 241, doi:10.3389/fnbeh.2018.00241.

130. Kasper, S.; Gastpar, M.; Muller, W.E.; Volz, H.P.; Moller, H.J.; Schlafke, S.; Dienel, A. Lavender oil preparation Silexan is effective in generalized anxiety disorder—A randomized, double-blind comparison to placebo and paroxetine. Int. J. Neuropsychopharmacol. 2014, 17, 859–869, doi:10.1017/S1461145714000017.

131. Kasper, S.; Muller, W.E.; Volz, H.P.; Moller, H.J.; Koch, E.; Dienel, A. Silexan in anxiety disorders: Clinical data and pharmacological background. World J. Biol. Psychiatry Off. J. World Fed. Soc. Biol. Psychiatry 2018, 19, 412–420, doi:10.1080/15622975.2017.1331046.

132. Seifritz, E.; Schlafke, S.; Holsboer-Trachsler, E. Beneficial effects of Silexan on sleep are mediated by its anxiolytic effect. J. Psychiatr. Res. 2019, 115, 69–74, doi:10.1016/j.jpsychires.2019.04.013.

133. Gastpar, M.; Muller, W.E.; Volz, H.P.; Moller, H.J.; Schlafke, S.; Dienel, A.; Kasper, S. Silexan does not cause withdrawal symptoms even when abruptly discontinued. Int. J. Psychiatry Clin. Pract. 2017, 21, 177–180, doi:10.1080/13651501.2017.1301488.

134. Pimenta, F.C.; Alves, M.F.; Pimenta, M.B.; Melo, S.A.; de Almeida, A.A.; Leite, J.R.; Pordeus, L.C.; Diniz Mde, F.; de Almeida, R.N. Anxiolytic Effect of Citrus aurantium L. on Patients with Chronic Myeloid Leukemia. Phytother. Res. Ptr 2016, 30, 613–617, doi:10.1002/ptr.5566.

135. Moslemi, F.; Alijaniha, F.; Naseri, M.; Kazemnejad, A.; Charkhkar, M.; Heidari, M.R. Citrus aurantium Aroma for Anxiety in Patients with Acute Coronary Syndrome: A Double-Blind Placebo-Controlled Trial. J. Altern. Complementary Med. 2019, 25, 833– 839, doi:10.1089/acm.2019.0061.

136. Mannucci, C.; Calapai, F.; Cardia, L.; Inferrera, G.; D'Arena, G.; Di Pietro, M.; Navarra, M.; Gangemi, S.; Ventura Spagnolo, E.; Calapai, G. Clinical Pharmacology of Citrus aurantium and Citrus sinensis for the Treatment of Anxiety. Evid. Based Complementary Altern. Med. 2018, 2018, 3624094, doi:10.1155/2018/3624094.

137. Hamdamian, S.; Nazarpour, S.; Simbar, M.; Hajian, S.; Mojab, F.; Talebi, A. Effects of aromatherapy with Rosa damascena on nulliparous women's pain and anxiety of labor during first stage of labor. J. Integr. Med. 2018, 16, 120–125, doi:10.1016/j.joim.2018.02.005.

138. Hozumi, H.; Hasegawa, S.; Tsunenari, T.; Sanpei, N.; Arashina, Y.; Takahashi, K.; Konnno, A.; Chida, E.; Tomimatsu, S. Aromatherapies using Osmanthus fragrans oil and grapefruit oil are effective complementary treatments for anxious patients undergoing colonoscopy: A randomized controlled study. Complementary Ther. Med. 2017, 34, 165–169, doi:10.1016/j.ctim.2017.08.012.

139. Tankam,J .M.; Ito, M. Inhalation of the essential oil of Piper guineense from Cameroon shows sedative and anxiolytic-like effects in mice. Biol. Pharm. Bull. 2013, 36, 1608–1614, doi:10.1248/bpb.b13-00491.

140. Komiya, M.; Takeuchi, T.; Harada, E. Lemon oil vapor causes an anti-stress effect via modulating the 5-HT and DA activities in mice. Behav. Brain Res. 2006, 172, 240–249, doi:10.1016/j.bbr.2006.05.006.

141. Zhang, N.; Zhang, L.; Feng, L.; Yao, L. The anxiolytic effect of essential oil of Cananga odorata exposure on mice and determination of its major active constituents. Phytomedicine Int. J. Phytother. Phytopharm. 2016, 23, 1727–1734, doi:10.1016/j.phymed.2016.10.017.

142. Cioanca, O.; Hritcu, L.; Mihasan, M.; Trifan, A.; Hancianu, M. Inhalation of coriander volatile oil increased anxiolytic-antidepressant-like behaviors and decreased oxidative status in beta-amyloid (1-42) rat model of Alzheimer's disease. Physiol. Behav. 2014, 131, 68–74, doi:10.1016/j.physbeh.2014.04.021.

143. Rombola, L.; Scuteri, D.; Adornetto, A.; Straface, M.; Sakurada, T.; Sakurada, S.; Mizoguchi, H.; Corasaniti, M.T.; Bagetta, G.; Tonin, P.; et al. Anxiolytic-Like Effects of Bergamot Essential Oil Are Insensitive to Flumazenil in Rats. Evid. Based Complementary Altern. Med. 2019, 2019, 2156873, doi:10.1155/2019/2156873.

144. Majnooni, M.B.; Mohammadi-Farani, A.; Gholivand, M.B.; Nikbakht, M.R.; Bahrami, G.R. Chemical composition and anxiolytic evaluation of Achillea wilhelmsii C. Koch essential oil in rat. Res. Pharm. Sci. 2013, 8, 269–275.

145. Costa, C.A.; Cury, T.C.; Cassettari, B.O.; Takahira, R.K.; Florio, J.C.; Costa, M. Citrus aurantium L. essential oil exhibits anxiolytic-like activity mediated by 5-HT(1A)-receptors and reduces cholesterol after repeated oral treatment. BMC Complement. Altern. Med. 2013, 13, 42, doi:10.1186/1472-6882-13-42.

146. de Sousa, D.P.; de Almeida Soares Hocayen, P.; Andrade, L.N.; Andreatini, R. A Systematic Review of the Anxiolytic-Like Effects of Essential Oils in Animal Models. Molecules 2015, 20, 18620–18660, doi:10.3390/molecules201018620.

147. Fazlollahpour-Rokni, F.; Shorofi, S.A.; Mousavinasab, N.; Ghafari, R.; Esmaeili, R. The effect of inhalation aromatherapy with rose essential oil on the anxiety of patients undergoing coronary artery bypass graft surgery. Complementary Ther. Clin. Pract. 2019, 34, 201–207, doi:10.1016/j.ctcp.2018.11.014.

148. Stirling, L.; Raab, G.; Alder, E.M.; Robertson, F. Randomized trial of essential oils to reduce perioperative patient anxiety: Feasibility study. J. Adv. Nurs. 2007, 60, 494–501, doi:10.1111/j.1365-2648.2007.04461.x.

149. Bakry, A.M.; Abbas, S.; Ali, B.; Majeed, H.; Abouelwafa, M.Y.; Mousa, A.; Liang, L. Microencapsulation of Oils: A Comprehensive Review of Benefits, Techniques, and Applications. Compr. Rev. Food Sci. F 2016, 15, 143–182, doi:10.1111/1541- 4337.12179.

150. Werdin Gonzalez, J.O.; Jesser, E.N.; Yeguerman, C.A.; Ferrero, A.A.; Fernandez Band, B. Polymer nanoparticles containing essential oils: New options for mosquito control. Environ. Sci. Pollut. Res. Int. 2017, 24, 17006–17015, doi:10.1007/s11356-017- 9327-4.

151. Dhifi, W.; Bellili, S.; Jazi, S.; Bahloul, N.; Mnif, W. Essential Oils' Chemical Characterization and Investigation of Some Biological Activities: A Critical Review. Medicines 2016, 3, 25, doi:10.3390/medicines3040025.

152. Callender, S.P.; Mathews, J.A.; Kobernyk, K.; Wettig, S.D. Microemulsion utility in pharmaceuticals: Implications for multi- drug delivery. Int. J. Pharm. 2017, 526, 425–442, doi:10.1016/j.ijpharm.2017.05.005.

153. Pandey, P.; Gulati, N.; Makhija, M.; Purohit, D.; Dureja, H. Nanoemulsion: A Novel Drug Delivery Approach for Enhancement of Bioavailability. Recent Pat. Nanotechnol. 2020, 14, 276–293, doi:10.2174/1872210514666200604145755.

154. Ita, K. Chapter 6—Microemulsions. In Transdermal Drug Delivery; Ita, K., Ed.; Academic Press: New York, NY, USA, 2020; pp. 97–122, doi:10.1016/B978-0-12-822550-9.00006-5.

155. Patel, R.B.; Patel, M.R.; Thakore, S.D.; Patel, B.G. Chapter 17—Nanoemulsion as a Valuable Nanostructure Platform for Pharmaceutical Drug Delivery. In Nano- and Microscale Drug Delivery Systems; Grumezescu, A.M., Ed.; Elsevier: Amsterdam, The Netherlands, 2017; pp. 321–341; doi:10.1016/B978-0-323-52727-9.00017-0.

156. Franklyne, J.S.; Mukherjee, A.; Chandrasekaran, N. Essential oil micro- and nanoemulsions: Promising roles in antimicrobial therapy targeting human pathogens. Lett. Appl. Microbiol. 2016, 63, 322–334, doi:10.1111/lam.12631.

157. Pavoni, L.; Perinelli, D.R.; Bonacucina, G.; Cespi, M.; Palmieri, G.F. An Overview of Micro- and Nanoemulsions as Vehicles for Essential Oils: Formulation, Preparation and Stability. Nanomaterials 2020, 10, 135, doi:10.3390/nano10010135.

158. Cavanagh, H.M.; Wilkinson, J.M. Biological activities of lavender essential oil. Phytother. Res. 2002, 16, 301–308, doi:10.1002/ptr.1103.

159. Kohli, K.; Chopra, S.; Dhar, D.; Arora, S.; Khar, R.K. Self-emulsifying drug delivery systems: An approach to enhance oral bioavailability. Drug Discov. Today 2010, 15, 958–965, doi:10.1016/j.drudis.2010.08.007.

160. Donsi, F.; Ferrari, G. Essential oil nanoemulsions as antimicrobial agents in food. J. Biotechnol. 2016, 233, 106–120, doi:10.1016/j.jbiotec.2016.07.005.

161. Ferreira, J.P.; Alves, D.; Neves, O.; Silva, J.; Gibbs, P.A.; Teixeira, P.C. Effects of the components of two antimicrobial emulsions on food-borne pathogens. Food Control. 2010, 21, 227–230, doi:10.1016/j.foodcont.2009.05.018.

162. Donsi, F.; Annunziata, M.; Sessa, M.; Ferrari, G. Nanoencapsulation of essential oils to enhance their antimicrobial activity in foods. LWT Food Sci. Technol. 2011, 44, 1908–1914, doi:10.1016/j.lwt.2011.03.003.

163. Sugumar, S.; Ghosh, V.; Nirmala, M.J.; Mukherjee, A.; Chandrasekaran, N. Ultrasonic emulsification of eucalyptus oil nanoemulsion: Antibacterial activity against Staphylococcus aureus and wound healing activity in Wistar rats. Ultrason. Sonochem. 2014, 21, 1044–1049, doi:10.1016/j.ultsonch.2013.10.021.

164. Gannu, R.; Palem, C.R.; Yamsani, V.V.; Yamsani, S.K.; Yamsani, M.R. Enhanced bioavailability of lacidipine via microemulsion based transdermal gels: Formulation optimization, ex vivo and in vivo characterization. Int. J. Pharm. 2010, 388, 231–241, doi:10.1016/j.ijpharm.2009.12.050.

165. Alam, P.; Ansari, M.J.; Anwer, M.K.; Raish, M.; Kamal, Y.K.T.; Shakeel, F. Wound healing effects of nanoemulsion containing clove essential oil. Artif. Cell Nanomed B 2017, 45, 591–597, doi:10.3109/21691401.2016.1163716.

166. Alam, P.; Shakeel, F.; Anwer, M.K.; Foudah, A.I.; Alqarni, M.H. Wound Healing Study of Eucalyptus Essential Oil Containing Nanoemulsion in Rat Model. J. Oleo Sci. 2018, 67, 957–968, doi:10.5650/jos.ess18005.

167. Kazemi, M.; Mohammadifar, M.; Aghadavoud, E.; Vakili, Z.; Aarabi, M.H.; Talaei, S.A. Deep skin wound healing potential of lavender essential oil and licorice extract in a nanoemulsion form: Biochemical, histopathological and gene expression evidences. J. Tissue Viability 2020, 29, 116–124, doi:10.1016/j.jtv.2020.03.004.

168. Rossi, P.; Cappelli, A.; Marinelli, O.; Valzano, M.; Pavoni, L.; Bonacucina, G.; Petrelli, R.; Pompei, P.; Mazzara, E.; Ricci, I.; et al. Mosquitocidal and Anti-Inflammatory Properties of The Essential Oils Obtained from Monoecious, Male, and Female Inflorescences of Hemp (Cannabis sativa L.) and Their Encapsulation in Nanoemulsions. Molecules 2020, 25, doi:10.3390/molecules25153451.

169. Musthaba, S.M.; Baboota, S.; Ahmed, S.; Ahuja, A.; Ali, J. Status of novel drug delivery technology for phytotherapeutics. Expert Opin Drug Del 2009, 6, 625–637, doi:10.1517/17425240902980154.

170. Lee, M.K. Liposomes for Enhanced Bioavailability of Water-Insoluble Drugs: In Vivo Evidence and Recent Approaches. Pharmaceutics 2020, 12, doi:10.3390/pharmaceutics12030264.

171. Valenti, D.; De Logu, A.; Loy, G.; Sinico, C.; Bonsignore, L.; Cottiglia, F.; Garau, D.; Fadda, A.M. Liposome-incorporated santolina insularis essential oil: Preparation, characterization and in vitro antiviral activity. J. Liposome Res. 2001, 11, 73–90, doi:10.1081/LPR-100103171.

172. Sinico, C.; De Logu, A.; Lai, F.; Valenti, D.; Manconi, M.; Loy, G.; Bonsignore, L.; Fadda, A.M. Liposomal incorporation of Artemisia arborescens L. essential oil and in vitro antiviral activity. Eur. J. Pharm. Biopharm. Off. J. Arb. Fur Pharm. Verfahr. E.V 2005, 59, 161–168, doi:10.1016/j.ejpb.2004.06.005.

173. Liolios, C.C.; Gortzi, O.; Lalas, S.; Tsaknis, J.; Chinou, I. Liposomal incorporation of carvacrol and thymol isolated from the essential oil of Origanum dictamnus L. and in vitro antimicrobial activity. Food Chem. 2009, 112, 77–83, doi:10.1016/j.foodchem.2008.05.060.

174. Khosravi-Darani, K.; Khoosfi, M.E.; Hosseini, H. Encapsulation of Zataria multiflora Boiss. Essential Oil in Liposome: Antibacterial Activity against E-Coli O157:H7 in Broth Media and Minced Beef. J. Food Saf. 2016, 36, 515–523, doi:10.1111/jfs.12271.

175. Dorman, H.J.D.; Peltoketo, A.; Hiltunen, R.; Tikkanen, M.J. Characterisation of the antioxidant properties of de-odourised aqueous extracts from selected Lamiaceae herbs. Food Chem. 2003, 83, 255–262, doi:10.1016/S0308-8146(03)00088-8.

176. Sebaaly, C.; Jraij, A.; Fessi, H.; Charcosset, C.; Greige-Gerges, H. Preparation and characterization of clove essential oil-loaded liposomes. Food Chem. 2015, 178, 52–62, doi:10.1016/j.foodchem.2015.01.067.

177. Sebaaly, C.; Greige-Gerges, H.; Agusti, G.; Fessi, H.; Charcosset, C. Large-scale preparation of clove essential oil and eugenol- loaded liposomes using a membrane contactor and a pilot plant. J. Liposome Res. 2016, 26, 126–138, doi:10.3109/08982104.2015.1057849.

178. Sebaaly, C.; Charcosset, C.; Stainmesse, S.; Fessi, H.; Greige-Gerges, H. Clove essential oil-in-cyclodextrin-in-liposomes in the aqueous and lyophilized states: From laboratory to large scale using a membrane contactor. Carbohydr. Polym. 2016, 138, 75–85, doi:10.1016/j.carbpol.2015.11.053.

179. Najafi, M.N.; Arianmehr, A.; Sani, A.M. Preparation of Barije (Ferula gummosa) Essential Oil-Loaded Liposomes and Evaluation of Physical and Antibacterial Effect on Escherichia coli O157:H7. J. Food Prot. 2020, 83, 511–517, doi:10.4315/0362-028X.JFP-19- 285.

180. Palmas, L.; Aroffu, M.; Petretto, G.L.; Escribano-Ferrer, E.; Diez-Sales, O.; Usach, I.; Peris, J.E.; Marongiu, F.; Ghavam, M.; Fais, S.; et al. Entrapment of Citrus limon var. pompia Essential Oil or Pure Citral in Liposomes Tailored as Mouthwash for the Treatment of Oral Cavity Diseases. Pharmaceuticals 2020, 13, 216, doi:10.3390/ph13090216.

181. Hammoud, Z.; Gharib, R.; Fourmentin, S.; Elaissari, A.; Greige-Gerges, H. Drug-in-hydroxypropyl-beta-cyclodextrin-in-lipoid S100/cholesterol liposomes: Effect of the characteristics of essential oil components on their encapsulation and release. Int. J. Pharm. 2020, 579, doi:10.1016/j.ijpharm.2020.119151.

182. Hammoud, Z.; Gharib, R.; Fourmentin, S.; Elaissari, A.; Greige-Gerges, H. New findings on the incorporation of essential oil components into liposomes composed of lipoid S100 and cholesterol. Int. J. Pharm. 2019, 561, 161–170, doi:10.1016/j.ijpharm.2019.02.022.

183. Lin, L.; Zhu, Y.L.; Thangaraj, B.; Abdel-Samie, M.A.S.; Cui, H.Y. Improving the stability of thyme essential oil solid liposome by using beta-cyclodextrin as a cryoprotectant. Carbohydr. Polym. 2018, 188, 243–251, doi:10.1016/j.carbpol.2018.02.010.

184. Guan, P.P.; Lu, Y.; Qi, J.P.; Niu, M.M.; Lian, R.Y.; Wu, W. Solidification of liposomes by freeze-drying: The importance of incorporating gelatin as interior support on enhanced physical stability. Int. J. Pharm. 2015, 478, 655–664, doi:10.1016/j.ijpharm.2014.12.016.

185. Carbone, C.; Cupri, S.; Leonardi, A.; Puglisi, G.; Pignatello, R. Lipid-based nanocarriers for drug delivery and targeting: A patent survey of methods of production and characterization. Pharm. Pat. Anal. 2013, 2, 665–677, doi:10.4155/ppa.13.43.

186. Weiss, J.; Decker, E.A.; McClements, D.J.; Kristbergsson, K.; Helgason, T.; Awad, T. Solid lipid nanoparticles as delivery systems for bioactive food components. Food Biophys. 2008, 3, 146–154, doi:10.1007/s11483-008-9065-8.

187. Muller, R.H.; Shegokar, R.; Keck, C.M. 20 years of lipid nanoparticles (SLN and NLC): Present state of development and industrial applications. Curr. Drug Discov. Technol. 2011, 8, 207–227, doi:10.2174/157016311796799062.

188. Severino, P.; Andreani, T.; Chaud, M.V.; Benites, C.I.; Pinho, S.C.; Souto, E.B. Essential oils as active ingredients of lipid nanocarriers for chemotherapeutic use. Curr. Pharm. Biotechnol. 2015, 16, 365–370, doi:10.2174/1389201016666150206111253.

189. Shi, F.; Zhao, J.H.; Liu, Y.; Wang, Z.; Zhang, Y.T.; Feng, N.P. Preparation and characterization of solid lipid nanoparticles loaded with frankincense and myrrh oil. Int. J. Nanomed. 2012, 7, 2033–2043, doi:10.2147/IJN.S30085.

190. Rodenak-Kladniew, B.; Islan, G.A.; de Bravo, M.G.; Duran, N.; Castro, G.R. Design, characterization and in vitro evaluationof linalool-loaded solid lipid nanoparticles as potent tool in cancer therapy. Colloids Surf. B Biointerfaces 2017, 154, 123–132, doi:10.1016/j.colsurfb.2017.03.021.

191. Zhao, Y.; Chang, Y.X.; Hu, X.; Liu, C.Y.; Quan, L.H.; Liao, Y.H. Solid lipid nanoparticles for sustained pulmonary delivery of Yuxingcao essential oil: Preparation, characterization and in vivo evaluation. Int. J. Pharm. 2017, 516, 364–371, doi:10.1016/j.ijpharm.2016.11.046.

192. Fazly Bazzaz, B.S.; Khameneh, B.; Namazi, N.; Iranshahi, M.; Davoodi, D.; Golmohammadzadeh, S. Solid lipid nanoparticles carrying Eugenia caryophyllata essential oil: The novel nanoparticulate systems with broad-spectrum antimicrobial activity. Lett. Appl. Microbiol. 2018, 66, 506–513, doi:10.1111/lam.12886.

193. Nasseri, M.; Golmohammadzadeh, S.; Arouiee, H.; Jaafari, M.R.; Neamati, H. Antifungal activity of Zataria multiflora essential oil-loaded solid lipid nanoparticles in-vitro condition. Iran. J. Basic Med. Sci. 2016, 19, 1231–1237.

194. Pereira, I.; Zielinska, A.; Ferreira, N.R.; Silva, A.M.; Souto, E.B. Optimization of linalool-loaded solid lipid nanoparticles using experimental factorial design and long-term stability studies with a new centrifugal sedimentation method. Int. J. Pharm. 2018, 549, 261–270, doi:10.1016/j.ijpharm.2018.07.068.

195. Zielinska, A.; Martins-Gomes, C.; Ferreira, N.R.; Silva, A.M.; Nowak, I.; Souto, E.B. Anti-inflammatory and anti-canceractivity of citral: Optimization of citral-loaded solid lipid nanoparticles (SLN) using experimental factorial design and LUMiSizer(R). Int. J. Pharm. 2018, 553, 428–440, doi:10.1016/j.ijpharm.2018.10.065.

196. Saporito, F.; Sandri, G.; Bonferoni, M.C.; Rossi, S.; Boselli, C.; Icaro Cornaglia, A.; Mannucci, B.; Grisoli, P.; Vigani, B.; Ferrari, F. Essential oil-loaded lipid nanoparticles for wound healing. Int. J. Nanomed. 2018, 13, 175–186, doi:10.2147/IJN.S152529.

197. Nahr, F.K.; Ghanbarzadeh, B.; Kafil, H.S.; Hamishehkar, H.; Hoseini, M. The colloidal and release properties of cardamom oil encapsulated nanostructured lipid carrier. J. Disper Sci. Technol. 2019, doi:10.1080/01932691.2019.1658597.

198. Galvao, J.G.; Santos, R.L.; Lira, A.A.M.; Kaminski, R.; Sarmento, V.H.; Severino, P.; Dolabella, S.S.; Scher, R.; Souto, E.B.; Nunes, R.S. Stearic Acid, Beeswax and Carnauba Wax as Green Raw Materials for the Loading of Carvacrol into Nanostructured Lipid Carriers. Appl. Sci. 2020, 10, 6267, doi:10.3390/App10186267.

199. de Meneses, A.C.; Marques, E.B.P.; Leimann, F.V.; Goncalves, O.H.; Ineu, R.P.; de Araujo, P.H.H.; de Oliveira, D.; Sayer, C. Encapsulation of clove oil in nanostructured lipid carriers from natural waxes: Preparation, characterization and in vitro evaluation of the cholinesterase enzymes. Colloid Surf. A 2019, 583, doi:10.1016/j.colsurfa.2019.123879.

200. Pivetta, T.P.; Simoes, S.; Araujo, M.M.; Carvalho, T.; Arruda, C.; Marcato, P.D. Development of nanoparticles from natural lipids for topical delivery of thymol: Investigation of its anti-inflammatory properties. Colloids Surf. B Biointerfaces 2018, 164, 281–290, doi:10.1016/j.colsurfb.2018.01.053.

201. Carbone, C.; Campisi, A.; Musumeci, T.; Raciti, G.; Bonfanti, R.; Puglisi, G. FA-loaded lipid drug delivery systems: Preparation, characterization and biological studies. Eur. J. Pharm. Sci. Off. J. Eur. Fed. Pharm. Sci. 2014, 52, 12–20, doi:10.1016/j.ejps.2013.10.003.

202. Shi, F.; Zhao, Y.; Firempong, C.K.; Xu, X. Preparation, characterization and pharmacokinetic studies of linalool-loaded nanostructured lipid carriers. Pharm. Biol. 2016, 54, 2320–2328, doi:10.3109/13880209.2016.1155630.

203. Ghodrati, M.; Farahpour, M.R.; Hamishehkar, H. Encapsulation of Peppermint essential oil in nanostructured lipid carriers: In-vitro antibacterial activity and accelerative effect on infected wound healing. Colloid Surf. A 2019, 564, 161–169, doi:10.1016/j.colsurfa.2018.12.043.

204. Piran, P.; Kafil, H.S.; Ghanbarzadeh, S.; Safdari, R.; Hamishehkar, H. Formulation of Menthol-Loaded Nanostructured Lipid Carriers to Enhance Its Antimicrobial Activity for Food Preservation. Adv. Pharm. Bull. 2017, 7, 261–268, doi:10.15171/apb.2017.031.

205. Montenegro, L.; Pasquinucci, L.; Zappala, A.; Chiechio, S.; Turnaturi, R.; Parenti, C. Rosemary Essential Oil-Loaded Lipid Nanoparticles: In Vivo Topical Activity from Gel Vehicles. Pharmaceutics 2017, 9, 48, doi:10.3390/pharmaceutics9040048.

206. Carbone, C.; Teixeira, M.D.; Sousa, M.D.; Martins-Gomes, C.; Silva, A.M.; Souto, E.M.B.; Musumeci, T. Clotrimazole-Loaded Mediterranean Essential Oils NLC: A Synergic Treatment of Candida Skin Infections. Pharmaceutics 2019, 11, 231, doi:10.3390/pharmaceutics11050231.

207. Miranda, M.; Cruz, M.T.; Vitorino, C.; Cabral, C. Nanostructuring lipid carriers using Ridolfia segeturn (L.) Moris essential oil. Mat. Sci Eng. C Mater. 2019, 103, doi:10.1016/J.Msec.2019.109804.

208. Vieira, R.; Severino, P.; Nalone, L.A.; Souto, S.B.; Silva, A.M.; Lucarini, M.; Durazzo, A.; Santini, A.; Souto, E.B. Sucupira Oil- Loaded Nanostructured Lipid Carriers (NLC): Lipid Screening, Factorial Design, Release Profile, and Cytotoxicity. Molecules 2020, 25, 685, doi:10.3390/Molecules25030685.

209. Rosa, D.M.; Oliveira, W.P. Spray drying of lipid nanosystems (SLN and NLC) loaded with Syzygium aromaticum essential oil. In Proceedings of the Ids'2018: 21st International Drying Symposium, Valencia, Spain, 11–14 September 2018; pp. 895–902, doi:10.4995/ids2018.2018.7554.

5 ESSENTIAL OIL-LOADED NLC FOR POTENTIAL INTRANASAL ADMINISTRATION

Angela Bonaccorso[1,†], Cinzia Cimino[1,†], Daniela Erminia Manno[2], Barbara Tomasello[1], Antonio Serra[2], Teresa Musumeci[1], Giovanni Puglisi[1], Rosario Pignatello[1] and Claudia Carbone[1,*]

[1] Laboratory of Drug Delivery Technology, Department of Drug and Health Sciences, University of Catania, Viale A. Doria 6, 95124 Catania, Italy.

[2] Dipartimento di Matematica e Fisica, University of Salento, 73100 Lecce, Italy.

[*] Corresponding author

[†] These authors contributed equally to this work.

Abstract: Complementary and alternative medicines represent an interesting field of research on which worldwide academics are focusing many efforts. In particular, the possibility to exploit pharmaceutical technology strategies, such as the nanoencapsulation, for the delivery of essential oils is emerging as a promising strategy not only in Italy but also all over the world. The aim of this work was the development of nanostructured lipid carriers (NLC) for the delivery of essential oils (*Lavandula*, *Mentha*, and *Rosmarinus*) by intranasal administration, an interesting topic in which Italian contributions have recently increased. Essential oil-loaded NLC, projected as a possible add-on strategy in the treatment of neurodegenerative diseases, were characterized in comparison to control formulations prepared with Tegosoft CT and Neem oil. Homogeneous (polydispersity index, PDI < 0.2) nanoparticles with a small size (<200 nm) and good stability were obtained. Morphological and physical-chemical studies showed the formation of different structures depending on the nature of the liquid oil component. In particular, NLC prepared with *Lavandula* or *Rosmarinus* showed the formation of a more ordered structure with higher cytocompatibility on two cell lines, murine and human fibroblasts. Taken together,

our preliminary results show that optimized positively charged NLC containing *Lavandula* or *Rosmarinus* can be proposed as a potential add-on strategy in the treatment of neurodegenerative diseases through intranasal administration, due to the well-known beneficial effects of essential oils and the mucoadhesive properties of NLC.

Keywords: nanomedicine; nose-to-brain; *Lavandula*; *Mentha*; *Rosmarinus*; TEM; cell viability; mucoadhesion

5.1 Introduction

Essential oils (EOs) are important natural mixtures produced by aromatic plants during their secondary metabolism, characterized by the presence of monoterpenes and sesquiterpenes, with other important aliphatic compounds, including terpenoids, alcohols, ethers, esters, ketones, and aldehydes [1]. Their quali-quantitative composition is influenced by several factors, including the variety of the plant, growing place (in particular, environment, climate, and eventual stress suffered), nutrition and fertilizers used, and extraction method. Due to the many properties of pharmaceutical interest (antioxidant, anti-inflammatory, antimicrobial, wound-healing, and anxiolytic), an increasing interest in complementary and alternative medicines (CAMs) has spread during the last years, with several studies exploring the potential use of EOs as adjuvants in various diseases, in particular when encapsulated into vesicular or nanoparticulate delivery systems [1–16]. The advantages of EOs encapsulation are related to the possibility to overcome different drawbacks by enhancing their stability, providing a controlled release and thus increasing their bioavailability and effectiveness.

As recently described by Scuteri et al. [12], the use of EOs via inhalation (aromatherapy), such as *Lavandula officinalis* and *Melissa officinalis*, represents a complementary approach in the treatment of Alzheimer's disease (AD), since the treatment with antipsychotic drugs is limited by the short-term use (maximum 12 weeks). Even if the mechanisms of actions of EOs are still not clear, their ability to bind to the olfactory nerve system is responsible for the transmission of the signal to specific areas of the central nervous systems (hippocampus, limbic system, amygdala, and hypothalamus). The potential application of different EOs in AD treatment was also reported by Jimbo et al. [17], who developed a clinical trial on 28 elderly people affected by dementia, demonstrating the importance of aromatherapy in AD treatment. The success of the treatment, demonstrated by the resulting significant improvement in cognitive function, was based on the use of a combined therapy,

with two administrations per day for 28 days, of four different EOs. In the morning, 0.04 mL of *Citrus limon* (L.) and 0.08 mL of *Rosmarinus officinalis* were administered based on the idea that this mixture is able to activate the sympathetic nervous system, thus promoting concentration and memory. In the evening, aiming to induce relaxation through the activation of the parasympathetic nervous system, a mixture constituted of 0.04 mL of *Citrus sinensis* (L.) Osbeck and 0.04 mL *Lavandula angustifolia* was administered. Interestingly, Rinaldi et al. recently developed chitosan coated nanoemulsions for the intranasal delivery of *Thymus vulgaris* and *Syzygium aromaticum* EOs, in the treatment of brain infections (meningitis and encephalitis) caused by bacterial strains of clinical concern [18]. The good mucoadhesive properties of nanoemulsions would enhance EOs' nasal administration, thus allowing EOs' antibacterial activity, as demonstrated on different bacterial strains [18].

Based on these considerations, the aim of this work was the development of EO- loaded nanostructured lipid carriers (NLC) for intranasal administration as potential adjuvant in the treatment of neurodegenerative diseases. Polymeric and lipid nanoparticles, solid lipid nanoparticles (SLN), and second-generation NLC have been widely investigated for brain targeting [18–31]. Herein, NLC were selected for their ability to directly release active compounds to the brain endothelial cells, as recently demonstrated by Arduino et al. [32]. *Rosmarinus officinalis* L., *Lavandula × intermedia* "Sumian", and *Mentha piperita* were selected due to their potential beneficial effects reported in AD treatment. *Lavandula* [33] and *Rosmarinus* [34] showed promising results in behavioral tests, demonstrating their ability to provide benefits in the treatment of scopolamine-induced Alzheimer's-type dementia. *Lavandula* was able to reduce depression, anxiety, and memory impairment [33], while *Rosmarinus* increased imaged and number memory in a trial carried out on school students [35]. *Mentha* EO was also found to enhance memorization process, through its ability to inhibit both acetylcholinesterase (AChE) and butyrylcholinesterase (BuChE) in a dose-dependent manner, thus suggesting a potential use in the treatment of neurodegenerative disorders [36].

EO-loaded NLC were characterized from a physical-chemical and technological point of view in comparison to NLC prepared with Tegosoft CT oil, used as EO-free control formulation, and NLC loaded with Neem oil, used as negative control due to its documented toxic effects [37–39]. All NLC formulations were analyzed to determine their mean size, polydispersity, and zeta potential by photon correlation spectroscopy (PCS) analysis. NLC were also characterized in terms of osmolarity, pH measurements, entrapment efficiency (EE%) of the loaded EO, and stability over time exploiting

Turbiscan® AG Station. In order to highlight the potential influence of the liquid oil component on NLC structure and morphology, X-ray analysis, Raman spectrometry and transmission electron microscopy (TEM) were also performed. *In vitro* NLC cytocompatibility was assessed on two fibroblast cell lines, one murine (NIH-3T3) and one human (HFF1). Finally, mucoadhesive properties were evaluated on the selected NLC, optimized by the addition of a coating layer of the positively charged cationic lipid didodecyldimethylammonium bromide (DDAB).

5.2 Materials and Methods

5.2.1 Materials

Kolliphor RH40 was provided by BASF Italia S.p.a. (Cesano Modena, Italy). Oleoyl Macrogol-6 Glycerides (Labrafil) was gifted by Gattefossé Italia s.r.l. (Milano, Italy). Hydrogenated Coco-Glycerides (Softisan 100) was bought from IOI Oleo GmbH (Oleochemicals, IOI group). *Rosmarinus officinalis* L. and *Lavandula × intermedia* "Sumian" essential oils were provided by Exentiae s.r.l. (Catania, Italy). *Mentha piperita* was gifted by the Department of Agriculture, Food and Environment (Di3A), University of Catania. Triglyceride caprylic-capric (Tegosoft CT, Miglyol 812) was supplied by Farmalabor (Canosa di Puglia, Italy). Neem oil was supplied by La Saponaria (Vallefoglia, Italy). Dioctadecylammonium bromide (DDAB), mucin from porcine stomach type II, sodium chloride, potassium chloride, calcium chloride dehydrated, and polysorbate 80 were bought from Sigma (Milan, Italy).

5.2.2 Nanoparticles Preparation

NLC were produced by the phase inversion temperature (PIT) method, as previously described [40]. The lipid phase containing the surfactant mixture (6.0% w/v of Kolliphor RH40 and 7.5% w/v of Labrafil) and the lipid Softisan (10% w/v) and the aqueous phase were separately heated to 70 °C. Then, the EO was added to the lipid phase at 1:1 ratio with the solid lipid. Finally, the aqueous phase was added dropwise to the lipid phase and the mixture was rapidly cooled in an ice bath under stirring for 1 h, thus obtaining different NLC formulations: L-NLC, containing *Lavandula*; M-NLC, prepared with *Mentha*; R-NLC, using *Rosmarinus*. Tegosoft CT-loaded NLC (CT-NLC) were prepared as positive control, while Neem oil was used to obtain N-NLC, as negative control. The produced NLC were purified through ultracentrifuge (SL16R Centrifuge, Thermo Scientific, Rodano, Italy) at 13,000 rpm for 2 h at 1 °C, in order to remove the excess surfactants from the

colloidal suspensions. The obtained pellet was vortexed (Heidolph Reax 2000, VWR, Milan, Italy) for 60 s.

5.2.3 Photon Correlation Spectroscopy (PCS)

After 24 h from the preparation, samples were diluted 1:10 in deionized water and analyzed using a Zetasizer Nano S90 (Malvern Instruments, Malvern, UK), in order to measure the mean particle size (Zave), the polydispersity index (PDI), and the zeta potential (ZP). The obtained values were reported as the mean of at least three measurements ± standard deviation (SD).

5.2.4 Osmolarity and pH Measurement

The osmolarity of each formulation was detected using an osmometer (Osmomat 3000, Gonotec, Berlin, Germany) previously calibrated with ultra-purified water and physiological solution. Moreover, the pH value of each formulation was measured through a pH-meter (Mettler Toledo, Milano, Italy).

5.2.5 Entrapment Efficiency

In order to quantify the entrapment efficiency (EE%) of each EO, all formulations were centrifuged at 13,000 rpm, 4 °C for 2 h. The separated supernatants were diluted with an ethanol-water mixture (75:25) and analyzed using a UV-vis spectrophotometer (UH5300 UV-Visible Double-Beam Spectrophotometer, Hitachi Europe, Milan, Italy). The used wavelengths were 228 nm for *Rosmarinus* EO, 230 nm for *Mentha* and *Lavandula* EO, and 224 nm for Neem oil. The calibration curves used for the quantitative evaluation of each oil were linear, considering the following ranges: 2-0.06 mg/mL (R^2 = 0.9927) for *Rosmarinus* EO; 2-0.03 mg/mL (R^2 = 0.9960) for *Mentha* EO; 2-0.03 mg/mL (R^2 = 0.9865) for *Lavandula* EO; 2-0.06 mg/mL (R^2 = 0.9915) for Neem oil. Entrapment efficiency was determined using the following equation:

$$EE\% = \frac{(\text{total amount of oil used} - \text{amount of unencapsulated oil})}{\text{total amount of oil used}} \times 100$$

5.2.6 Stability Studies by Turbiscan® AG STATION

The optical analyzer Turbiscan® Ageing Station (TAGS, Formulaction, L'Union, France) was used to assess the formulations physical stability, as it has been demonstrated to be reliable in the analysis of aggregation and/or migration instability phenomena [40–45]. In our experiment, 20 mL of each sample was inserted into a cylindrical glass cell, stored at 25.0 ± 1.0 °C and analyzed for 30 days. For detailed explanation of the analyzer functioning, we remand to the literature [15]. The variation of backscattering profiles

(ΔBS) was used to compare the formulations, considering the Turbiscan® Stability Index (TSI), which numerically quantifies the formulation's stability.

5.2.7 X-ray Analysis

The assessment of X-ray diffraction of the samples was carried out with a MiniFlex Rigaku diffractometer, operating in step-scan mode and equipped with a Cu Kα source (wavelength λ = 0.154 nm) at 30 kV and 100 mA. The X-ray diffraction data were collected in the Bragg-Brentano geometry, from 5 to 35 deg, at a scanning speed of 0.02 deg/s. Crystallinity index values, related to the intensity of the peak obtained, were calculated following the equation below:

$$C = \frac{S_{tot} - S_a}{S_{tot}}$$

where S_{tot} is the total area under the graph and S_a is the area subtended to the only amorphous region.

5.2.8 Raman Spectrometry

As previously described [15,46], Raman spectroscopy analysis was carried out using a micro-Raman spectrometer (INVIA, Renishaw, Gloucestershire, UK), which includes a 514.5 nm air-cooled Argon ions laser source and an 1800 lines/mm grating monochromator/grid polychromator with RenCam CCD detection, with a resolution of 1 cm^{-1}. The laser source was focused on the suspension of NLC with 100× long working objectives (a long working distance) to a stop diameter of about 1 μm. The acquisition time of Raman spectra varied according to the intensity of the Raman signals and lasted until a satisfactory signal-to-noise ratio was reached. Data analysis was performed by using Renishaw Wire 2.0 software. The results are reported as the mean of the intensity of 100 accumulation spectra acquired from 5 different regions, with a spatial resolution of 5 microns in each sample.

5.2.9 Morphological Analysis by TEM

In order to analyze the morphology of the produced nanoformulations, transmission electron microscopy (TEM) analysis was performed. The samples were prepared placing 5 μL of each NLC on a 600-mesh carbon coated copper grid (TAAB Laboratories Equipment, Berks, UK), adding a drop of 2% w/v aqueous solution of gadolinium triacetate (Uranyl Acetate Alternative), for 2 min, and finally drying at room temperature after the removal of the exceeding solution. The analysis was carried out through a transmission electron microscope (model HITACHI) operating at 100 KV acceleration voltage.

5.2.10 In Vitro Release Study

Lavandula and *Rosmarinus* release from L-NLC and R-NLC, respectively, was evaluated by using Franz-type diffusion cells (LGA, Berkeley, CA, USA). Before being mounted in Franz-type diffusion cells, 0.75 cm^2 regenerated cellulose membranes (Spectra/Por CE; Mol. Weight Cut-off 3.5 kDa) were moistened by immersion in water for 1 h at room temperature. The receptor compartment was filled with 4.5 mL of simulated nasal electrolytic solution (SNES) (sodium chloride 0.745 g, potassium chloride 0.129 g, calcium chloride dehydrated 0.005 g, and distilled water q. s. 100 mL) containing 0.5% of polysorbate 80, to reach the sink conditions [47], thermostated at 37 °C, and constantly stirred at 600 rpm. Then, 500 μL of each sample was applied in the donor compartment. The experiments were run for 48 h. At scheduled time intervals (0, 1, 2, 3, 4, 5, 6, 7, 8, 9, 24, and 48 h), 200 μL of the receptor medium was withdrawn and replaced with an equal volume of medium equilibrated to 37 °C. Each sample was analyzed by the UV method described in Section 2.4 to determine the EO content.

5.2.11 Cytocompatibility Assay

The cytocompatibility was assessed on two fibroblast cell lines, the NIH-3T3 mouse embryonic and the HFF1 human cell lines. NIH 3T3 and HFF1 were cultured in Dulbecco's modified Eagle's Medium (DMEM, ATCC, Manassas, VA, USA) supplemented with 10% v/v fetal bovine serum and (50 IU/mL) penicillin/(50 μg/mL) streptomycin, in a controlled environment with a temperature of 37 °C, 5% CO_2 concentration, and 95% relative humidity [48]. The cells were seeded in a 96-well plate (1×10^4 cells/well) and incubated for 24 h to allow adherence. EO-NLC were diluted in DMEM in order to test different concentrations (100, 200, 400, and 500 μg/mL) and the cells were treated for 24 h. The two cell lines were also treated with DMEM medium alone, as negative control, and vehicle (Tris buffer) as positive control. The cell viability was evaluated by adding 200 μL of MTT (0.5 mg/mL) in culture medium to each well and incubated for 2 h. The optical density (OD) was measured with a microplate spectrophotometer reader (Synergy HT multi-mode microplate reader, BioTek, Milano, Italy) at λ 550 nm. The results are expressed as percentage of cell viability with respect to untreated control viable cells, whose value was equal to 100%.

5.2.12 Mucoadhesive Evaluation of NLC

Positively charged NLC (L-NLC+, R-NLC+, and CT-NLC+), respectively, prepared with *Lavandula*, *Rosmarinus*, or Tegosoft CT, were obtained as previously described [49], adding 0.15% w/w of the cationic lipid DDAB to the oily phase. An *in vitro* method based

on the evaluation of two parameters (zeta potential and turbidimetry) was used to assess the mucoadhesive properties of NLC. Briefly, mucin (0.1% w/v) was suspended in PBS (pH 5.8) and stirred overnight to allow its complete dispersion. The interaction between each positively charged NLC and mucin was determined by mixing equal volumes of mucin dispersion and NLC for 15 min at 25 °C. After 1 and 24 h of incubation at 37 °C, zeta potential and turbidimetric measurements were performed. In particular, turbidimetric measurements were evaluated comparing the absorbances at 650 nm by UV-Vis spectrophotometer of the native mucin and each dispersion.

5.2.13 Statistical Analysis

All data are reported as mean values ± SD. Differences, analyzed by two-sample hypothesis testing (t-test), using Origin Software (version 8.5.1), were considered statistically significant for $p < 0.05$. For cytocompatibility studies, statistical differences among treatments were assessed by one-way ANOVA followed by Bonferroni test.

5.3 Results and Discussions

5.3.1 Physicochemical and Technological Characterization

EO-loaded NLC for intranasal administration were produced by the PIT method, previously reported as a green technology that allows reducing the amount of surfactants and energy required [40]. All NLC were analyzed 24 h after their production in order to evaluate their mean size, polidispersity, zeta potential, osmolarity, pH, and the EE% of the EO. PCS results (Figure 1) show that NLC prepared with *Lavandula*, *Mentha*, or *Rosmarinus* showed the presence of small-sized nanoparticles of about 200 nm (Figure 1), therefore adequate for the intranasal route [25]. In particular, EO-loaded NLC were smaller compared to those prepared using Tegosoft CT or Neem oil, which also showed higher PDI values related to the presence of heterogeneous nanosuspensions. It is worth noting that *Lavandula*, *Mentha* or *Rosmarinus* favor the formation of nanoparticles with great homogeneity, as confirmed by the low PDI, a relevant parameter that strongly affects NLC feature and stability [50]. Indeed, PDI values were found to be lower than 0.3, therefore related to the presence of a single peak of size distribution, in agreement with previous data [4].
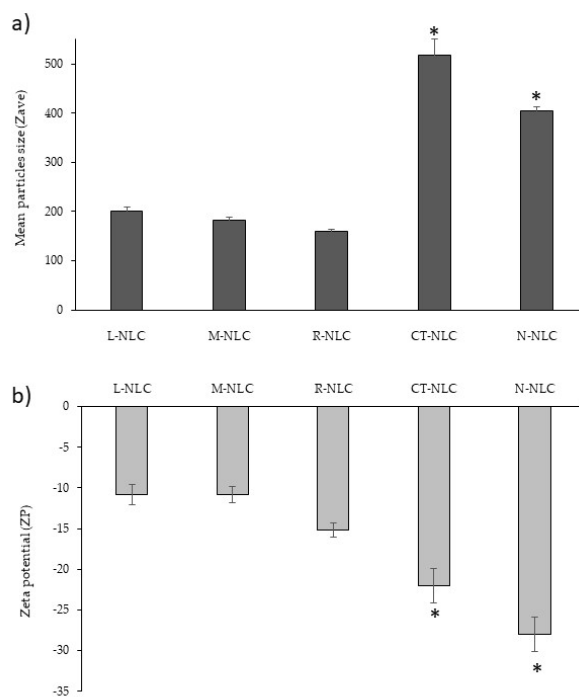
Figure 1. (a) Mean particle size (Zave, nm) and (b) Zeta Potential (ZP) ± standard deviation (SD) of the prepared *Lavandula* NLC (L-NLC), *Mentha* NLC (M-NLC), *Rosmarinus* NLC (R-NLC), Tegosoft CT NLC (CT-NLC) and Neem NLC (N-NLC). * Significance for $p < 0.05$, comparison between EO-loaded NLC (L-NLC, M-NLC, and R-NLC) and the control NLC (CT-NLC and N-NLC).

In order to ensure the formulation's safety on cell functioning, viability, and stability, without potential damages and alterations due to water movements through the membranes, it is important that NLC osmolarity and pH values are kept in the physiological range [51]. As reported in Table 1, osmolarity values of the produced NLC were in the range 291-299 mOsm/kg. In addition, pH measurements showed that pH values were in the physiological range for all nanosuspensions, with values between 7.09 and 7.28 for all formulations. It is interesting to highlight that *Lavandula*, *Mentha*, and *Rosmarinus* showed significantly higher EE% values compared to Neem oil (Table 1). As expected, a certain loss of EO was observed, due to the presence of micelles of surfactants, which do not participate in the formation of nanoparticles. For this reason, each system was further analyzed after the purification step.

Table 1. Values of pH, osmolarity, and entrapment efficiency (EE%) ± standard deviation (SD) of NLC prepared with *Lavandula* (L-NLC), *Mentha* (M-NLC), *Rosmarinus* (R-NLC), Tegosoft CT (CT- NLC), and Neem (N-NLC).

Sample	pH ± SD	Osmolarity (mOsm/kg ± SD)	EE% ± SD
L-NLC	7.13 ± 0.5	299.5 ± 0.1	76.47 ± 0.8
M-NLC	7.19 ± 0.6	293.1 ± 0.3	67.15 ± 0.3
R-NLC	7.20 ± 0.5	291.0 ± 0.5	64.09 ± 0.9
CT-NLC	7.28 ± 0.7	297.9 ± 0.2	100.00 ± 0.0
N-NLC	7.09 ± 0.4	291.5 ± 0.7	19.61 ± 0.8

These findings, in agreement with PCS results, would suggest a better organization of the raw materials at the interface when using the three EOs, as also suggested by the smaller particles obtained for L-NLC, M-NLC, and R-NLC.

As shown in Figure 1, all samples were negatively charged (≈ -20 mV), without significant differences related to the oil, even if the presence of Neem oil induced a slight increase in ZP value, confirming literature findings [52]. As reported in the literature [53], high ZP values would suggest a long-term physical stability of the colloidal suspension, due to nanoparticles' repulsions.

In order to deepen the NLC stability, a key parameter for nano-sized colloids [50], we exploited Turbiscan® technology, storing samples for 30 days at 25 °C. Interestingly, the instability kinetics obtained by TSI values, as reported in Table 2, showed that NLC prepared with the three EOs were more stable compared to CT-NLC, which showed a significant increase already after 3 weeks of storage. In particular, the following decreasing scale of stability can be described as follows: L-NLC = R-NLC ≥ N-NLC ≥ M-NLC >> CT-NLC. Therefore, NLC prepared with *Lavandula* and *Rosmarinus* showed a greater stability compared to other samples, probably due to the smaller mean size and the higher homogeneity of the nanoparticles in suspensions. Among all the prepared formulations, the use of the commercial oil CT reduced the colloidal suspension's stability, as confirmed by the backscattering variation reported in Figure 2a. Herein, significant instability phenomena related to both particle migration and aggregation occurred ($\Delta BS \geq 20\%$).

Table 2. Turbiscan Stability Index (TSI) of NLC analyzed for 30 days at 25 °C using Turbiscan® Aging Station. * Significance for $p < 0.05$.

Sample	Day of the Measurement				
	Day 1	Day 7	Day 14	Day 21	Day 28
CT-NLC	0.42	2.28	6.03	8.60*	11.16*
L-NLC	0.38	1.73	2.39	3.14	5.99
R-NLC	0.37	1.74	2.33	3.02	5.96
M-NLC	0.40	1.62	3.98	5.28	7.02*
N-NLC	0.40	1.61	3.86	5.15	6.52

The greater stability of L-NLC and N-NLC was confirmed by the absence of significant variation in BS profiles, as resulted by the low values registered, related to slight particle migration at the bottom of the cuvette (Figure 2b,c). R-NLC and M-NLC showed similar profiles to those reported for L-NLC and N-NLC, respectively (data not reported).
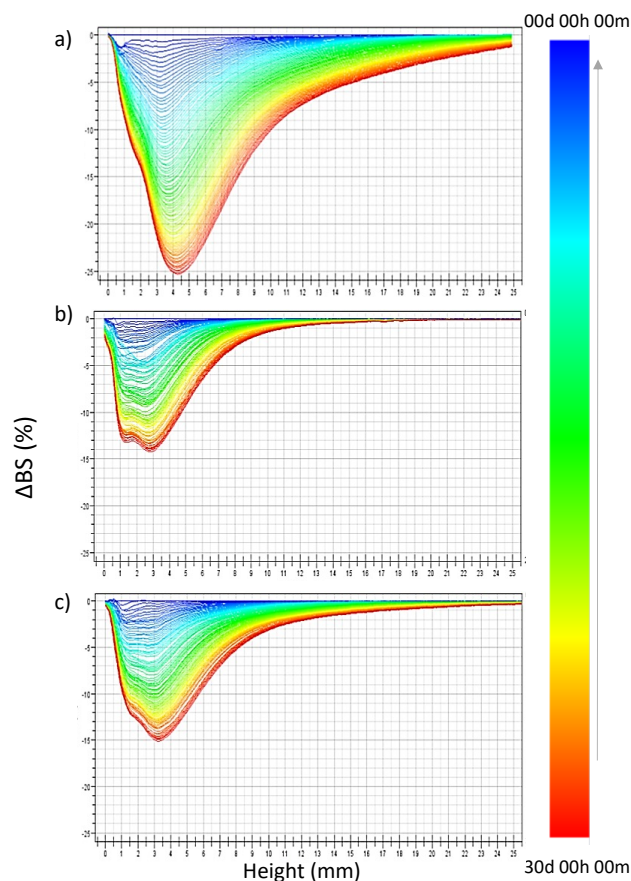
Figure 2. Backscattering profiles (ΔBS) of CT-NLC (a), L-NLC (b), and N-NLC (c) stored in Turbiscan® for 30 days at a temperature of 25.0 ± 1.0 °C. Data are presented as a function of time (0-30 days) of sample height (0 to 20 mm) (the direction of analysis time is indicated by the arrow).

The stability results are in agreement with PCS measurements of samples analyzed after 28 days of storage, showing that, at the 0.05 level of significance, the difference between the population mean size and PDI was significantly different for mean size only for CT-NLC, whose particles were found to be of about 500 nm (Figure S1). These data are in agreement with previous findings, with L-NLC showing a more stable long-term behavior thanks to the tendency of the nanoparticles to agglomerate, thus determining the formation of a flocculated suspension, whose nanoparticles can be easily dispersed by gentle shaking. In order to analyze the influence of the oily component on the NLC structure, X-ray diffraction, Raman spectroscopy, and Transmission Electron Microscopy (TEM) were performed. In particular, NLC were analyzed through Raman spectroscopy using a micro-Raman spectrometer, in order to obtain the so-called "molecular footprint" of the sample, which provides information about the sample's molecular composition and structure [54]. In particular, through molecular vibrations produced by a laser beam, a map of chemical and structural changes in molecules can be obtained, which describes conformation and arrangement in lipid chain after the addition of the oil [55]. Since a similar behavior was

observed for NLC produced using Neem oil or *Mentha* EO compared to NLC prepared using *Lavandula* or *Rosmarinus* EO, for a clearer representation of data, we report only L-NLC and N-NLC Raman spectra vs. CT-NLC (Figure 3). The Raman spectra of all the prepared NLC are reported in Figure S2. Although no shifts in the frequencies of the Raman transitions arise in a comparison of the different samples, the relative intensities in significant regions change conspicuously for L-NLC compared to controls, CT-NLC and N-NLC (Figure 3).
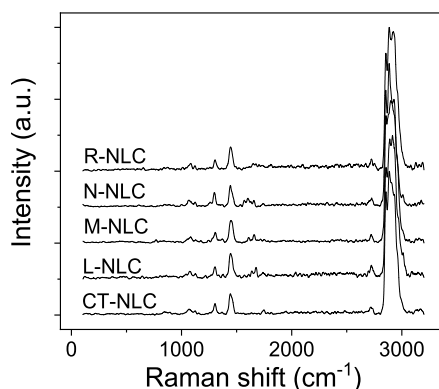
Figure 3. Raman spectra of L-NLC, CT-NLC, and N-NLC.

The most intense bands in the spectra of molecules including alkanes and lipids with alkyl groups are the CH stretching modes. The most common vibrational Raman active modes in the analyzed systems are summarized in Table 3. Both frequency differences and relative intensity changes for these vibrational modes have been used to monitor specific conformational changes in the hydrocarbon chains [56]. The 1100 cm^{-1} region in particular has been shown to be a superposition of the C–C stretching modes for segments of all-trans hydrocarbon conformations.

Table 3. Common vibrational modes.

Functional Group Mode	Approximate Wave Number (cm^{-1})
-CH$_3$, symmetric and antisymmetric stretch	2920–2960
-CH$_3$, symmetric and antisymmetric stretch	2850–2890
-PO$_2$, symmetric and antisymmetric stretch	1080–1200
-C-C-	1050–1150
-C-O-	1410
-C=O	1720
-COH	870–890
-OH	1080–1090
-CH$_2$-, deformation	1460–1470

An increase in intensity of the 1115 cm^{-1} band relative to the intensities of the 1050 cm^{-1} transitions (I1115/I1050) is indicative of a greater fluidity within the hydrocarbon chains; therefore, the increase in the 1115 cm^{-1} band originates from the increased intramolecular disorder in the systems. The Raman spectra of the NLC systems in the 2750-3050 cm^{-1}

spectral region, i.e., the C–H stretching vibration region, are well fitted as a sum of six Gaussian bands, as reported in the Table S1. It is well known that lipids interact with phospholipidic membrane. De Lange et al. [57] reported that Raman spectra of binary vesicles-cholesterol bilayers showed little variation associated with cholesterol, which allows spectral changes to be assigned to the lipid-chain vibrational signatures of the liquid-disordered (l-d), solid-ordered (s-o), and liquid-ordered (l-o) phases. Analyzing the C–H stretching, C=O stretching, and CH_2 bending modes, it is possible to monitor the structural order evolution of cholesterol in vesicle systems [58]. The region around 3000 cm^{-1} of the Raman spectrum consists of a large number of overlapping peaks, containing both fundamental CH-stretch vibrations and Fermi resonance bands. The CH_3 symmetric stretching modes appear in the 2870-2880 cm^{-1} spectral region, with a Fermi resonance (FR) component in the 2930-2940 cm^{-1} region. The peaks in the 2950-2970 cm^{-1} spectral region are the CH_3 out-of-plane and in-plane methyl antisymmetric stretches. The methylene vibrations at approximately 2850, 2880, 2900, and 2930 cm^{-1} are sensitive to conformational changes as well as intermolecular interactions of the alkyl chains of lipids. The $va(CH_2)$ antisymmetric stretch is coupled to rigid rotations–torsional vibrations, so that it broadens considerably with temperature, and increases continuously in frequency, from 2880 to 2900 cm^{-1}, as gauche conformers are introduced. The $vs(CH_2)$ symmetric stretch contains three components, centered at 2852, 2900, and 2928 cm^{-1}, because of extensive Fermi resonance interactions with overtones of the bending modes, and it is affected by intra- and inter-molecular interactions. The relative intensities of the peaks in this last spectral region change notably with changes in hydration state, packing, and conformational order [57,58]. In order to exploit this spectral sensitivity toward the lipid environment, several spectral parameters have been used in the literature that empirically describe the order of the lipid matrix. The peak height ratio I2890/I2850 has been used as a marker for chain packing and conformational disorder, where higher values indicate a higher ordering of the chains [59]. Table 4 resumes the Raman intensity ratios related to C–C stretching vibrational bands (I1115/I1050) and C–H stretching vibrational bands I2890/I2850 for all samples.

Table 4. Raman intensity ratios related to C–C stretching vibrational bands (I1115/I1050) and C–H stretching vibrational bands I2890/I2850.

Sample	I_{1115}/I_{1050}	I_{2890}/I_{2850}
CT-NLC	0.69	1.20
L-NLC	0.74	1.94
M-NLC	0.53	0.50
N-NLC	0.71	0.62
R-NLC	0.67	1.00

The Raman spectra of L-NLC, CT-NLC, and N-NLC systems in the C–H stretching vibration region are shown in Figure 4. The spectrum in the 2750-3050 cm^{-1} spectral region is well fitted as a sum of six Gaussian bands, as reported in the Supplementary Materials.
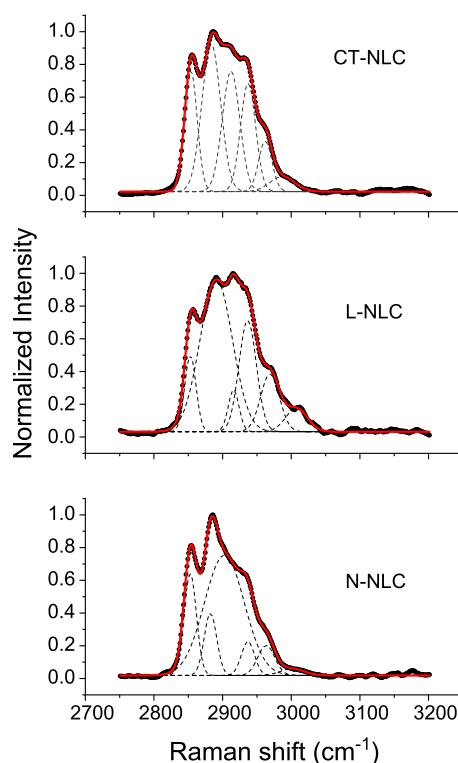

Figure 4. Raman spectra of NLC prepared with *Lavandula* (L-NLC), Tegosoft CT (CT-NLC), and Neem oil (N-NLC): region around 3000 cm^{-1}.

XRD measurements were performed for all NLC, showing a similar behavior between *Lavandula*, *Mentha* and *Rosmarinus* with respect to the controls CT-NLC and N-NLC. Figure 5 shows the XRD spectra recorded for L-NLC vs. control NLC samples. The presence of discrete peaks, more or less pronounced, emerging from a very large peak is evident in each spectrum. This indicates that the observed material is characterized by a semicrystalline structure. The discrete peaks (labeled 1-4) correspond to the interplanar spacings of 1.22, 0.46, 0.42, and 0.38 nm, respectively. These four peaks are clearly visible for L-NLC. M-NLC and R-NLC showed similar XRD spectra to that of L-NLC (Figure S3). Contrarily, CT-NLC and N-NLC showed a considerably reduced intensities of Peaks 2 and 3. The occurrence of such peaks indicates the presence of ordered solid lipids in the β and β' crystallographic modifications [60]. In addition, in Figure 4, it is evident that the relative intensity of the various peaks is different for each sample: the peaks are well pronounced in all EO-loaded NLC, as reported for L-NLC (Figure 5), but are very low in the controls CT-NLC and N-NLC.
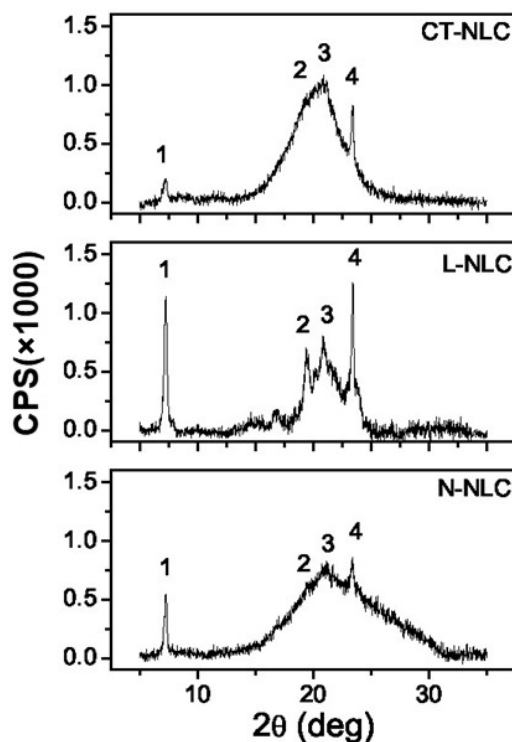
Figure 5. XRD spectra of representative samples L-NLC, CT-NLC, and N-NLC.

Through X-ray diffraction, it was possible to measure the NLC crystallinity index (C), an important parameter that allows predicting polymorphic transitional changes during storage [55]. Crystallinity was measured between 5 and 30 degrees, and the obtained results are reported in Table 5. Comparing the NLC produced with different EOs, it emerged that the use of *Lavandula* and *Rosmarinus* led to the formation of NLC with the highest values of crystallinity (68% and 40%, respectively), while NLC prepared using *Mentha* or Neem oil showed lower values (30% and 20%, respectively). It is possible that the high amount of linalool present in the complex mixture of *Lavandula* and *Rosmarinus* increases the NLC stability, as we previously reported [4]. Interestingly, the lowest crystallinity value (10%) was registered for CT-NLC, related to the presence of a less ordered structure. As reported in the literature, the crystallinity of the lipid matrix is affected by the structure of the liquid oil [61]. Therefore, the following scale based on the reduction of the crystallinity value can be described: L-NLC > R-NLC > M-NLC > N-NLC > CT-NLC. The lowest crystallinity found for caprylic/capric triglyceride is consistent with literature findings, in which the addition of a synthetic oil was demonstrated to strongly reduce the crystallinity of the lipid matrix [61,62]. It is interesting to highlight that the crystallinity scale presents the same order of the stability scale obtained by Turbiscan® analysis, with L-NLC and R-NLC as the most stable formulations compared to other NLC.

Table 5. Crystallinity (C%) of Tegosoft CT NLC (CT-NLC), Neem NLC (N-NLC), *Mentha* NLC (M- NLC), *Lavandula* NLC (L-NLC), and *Rosmarinus* NLC (R-NLC).

Sample	C (%)
CT-NLC	10%
N-NLC	15%
M-NLC	30%
L-NLC	68%
R-NLC	40%

In order to analyze the NLC morphology, TEM analysis was performed. Figure 6 reports TEM images of L-NLC, CT-NLC and N-NLC. In particular, CT-NLC (Figure 6a,b) showed a very irregular arrangement of nanoparticles, with a central oily core and a large shell. N-NLC (Figure 6c,d) and M-NLC (Figure S4) showed the presence of a faint central oily core surrounded by the solid lipid and surfactants layers, in agreement with previous studies [63,64]. On the other side, L-NLC (Figure 6f) and R-NLC (Figure S5) showed a structure characterized by the presence of many oily droplets dispersed in the solid lipid matrix, in agreement with previous findings [65]. It is possible that the ability of *Lavandula* and *Rosmarinus* to create imperfections in the NLC matrix also affects the nanoparticles' structure, improving their order and, consequently, stability during storage, probably due to their composition characterized by high amount of linalool [4,15,16].
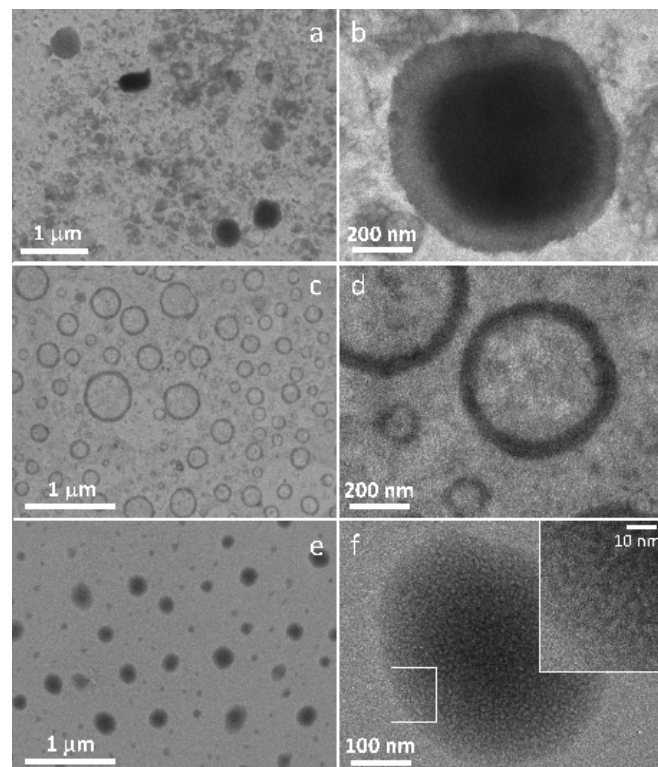
Figure 6. Transmission electron microscopy (TEM) images of: CT-NLC (a,b); N-NLC (c,d); L-NLC (e,f).

As reported in Figure 7, the release profiles of EOs from NLC was similar for *Lavandula* and *Rosmarinus*, with a sustained release over the first 8 h, with about 20% of EO released from NLC. After 24 and 48 h, the cumulative amount of EO reached about 50% and 80% of the loaded oil, respectively (Figure 7). Our results are in agreement with previous findings [66], confirming the advantages of EO encapsulation into NLC that would provide a sustained and prolonged release.
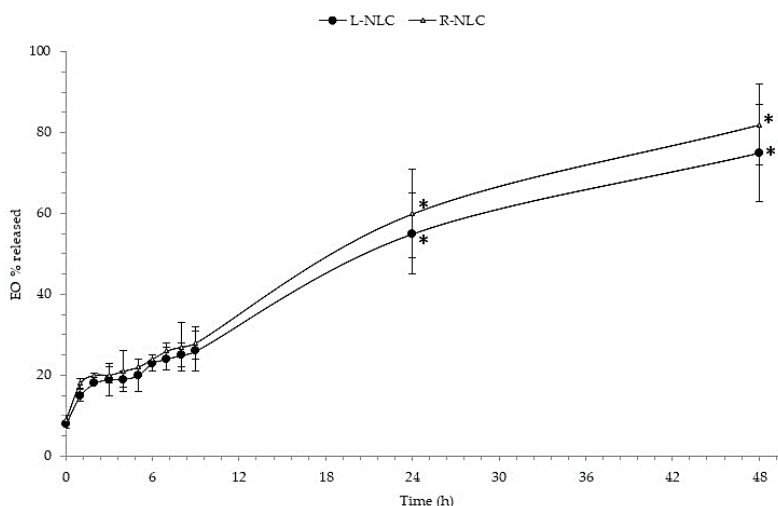

Figure 7. Percentage of *Lavandula* and *Rosmarinus* EOs released from L-NLC and R-NLC, respectively, at different time intervals up to 48 h. Each value is the mean of six independent experiments. * Significance for $p < 0.05$.

5.3.2 In Vitro Cytocompatibility

3-(4,5-dimethylthiazol-2-yl)-2,5-diphenyltetrazolium bromide (MTT) assay was performed in order to assess NLC cytocompatibility. Some NAD(P)H-dependent oxidoreductase enzymes are produced by living cells and are able to cause the conversion of yellow MTT salt into purple formazan. The intensity of the color is directly related to the cells' viability; quantification of formazan crystals is carried out through absorbance measurement. MTT assay was performed on human (HFF1) and murine (NIH-3T3) fibroblast cell lines, selected to test the biocompatibility and safety of NLC nanosuspensions, which is essential to ensure that the NLC do not affect the capability of normal cells to produce trophic growth factor, which support a variety of cellular processes of the above epithelial tissues [67]. All the prepared NLC were tested at different concentrations (100, 200, 400, and 500 μg/mL) and compared to controls. The results are reported in Figures 8 and 9.
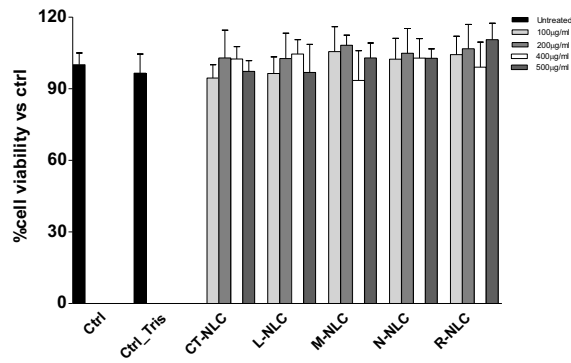
Figure 8. Murine fibroblasts NIH-3T3 viability after 24 h treatment with different concentrations of Tegosoft CT NLC (CT-NLC), *Lavandula* NLC (L-NLC), *Rosmarinus* NLC (R-NLC), *Mentha* NLC (M-NLC), and Neem NLC (N-NLC). All values are mean ± SD of three experiments in triplicate.
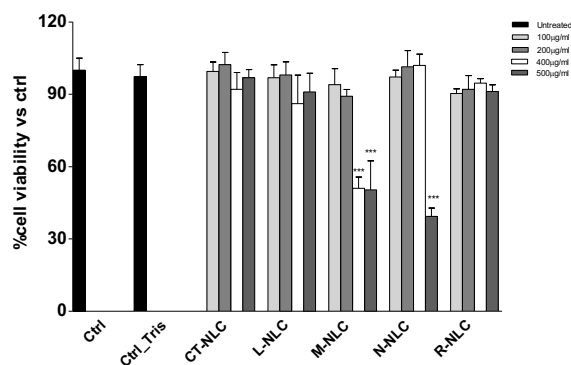

Figure 9. Human fibroblasts HFF1 viability after 24 h treatment with different concentrations of Tegosoft CT NLC (CT-NLC), *Lavandula* NLC (L-NLC), *Rosmarinus* NLC (R-NLC), *Mentha* NLC (M-NLC), and Neem NLC (N-NLC). All values are mean ± SD of three experiments in triplicate. *** $p < 0.001$ vs. control.

As expected, the control formulation prepared using Tegosoft CT (CT-NLC), did not affect cell viability of both murine and human fibroblasts, showing a cell viability higher than 90% at all tested concentrations. No cytotoxic effects were observed when murine fibroblasts were treated with N-NLC, while the highest concentration (500 µg/mL) significantly reduced human fibroblast viability by a hefty 60%. This result is supported by previous studies showing Neem cytotoxic effects on different cell lines (embryonic 3T3 fibroblasts, HeLa tumor cells, HaCat keratinocytes, and V79-4 pulmonary fibroblasts) when used at low concentration and in combination with oleic acid [63]. Furthermore, Neem oil was found to induce cell death in a time-dependent manner on HCT116 cells, whose effect was attributed to the cell cycle arrest and apoptosis due to Neem limonoids, even if the molecular mechanism of Neem limonoid-induced cell death has not been described [68]. Interestingly, L-NLC and R-NLC showed good biocompatibility on both murine and human cell lines, at all tested concentrations. This result is consistent with previous studies demonstrating that the EO encapsulation is able to improve the oil biocompatibility on Raw 264.7 cells (macrophage cell line) [4]. *Mentha* EO-loaded NLC

(M-NLC) showed a dose-dependent effect, since concentrations equal to 100 and 200 µg/mL resulted to be highly biocompatible, while a 50% reduction in fibroblasts viability was observed at 400 and 500 µg/mL. This result is consistent with earlier research, in which *Mentha* species EOs have been reported to exert cytotoxic effects that can be exploited to treat cancer, due to their ability to inhibit the cell proliferation of numerous tumor cells by acting on mitochondrial dysfunctions, apoptosis induction, and autophagy processes [69,70].

Based on the obtained results, *Lavandula* and *Rosmarinus* were selected as safe and promising EOs to be encapsulated into NLC for the potential treatment of Alzheimer's disease, thanks to the formation of small and homogeneous particles and a more ordered structure related to the formation of oily droplets into the lipid matrix. In order to exploit the intranasal delivery, we aimed at improving the mucoadhesive properties of the systems, with the addition of a coating layer of the cationic lipid DDAB, thus obtaining L-NLC+, R-NLC+, and CT-NLC+, respectively, prepared with *Lavandula*, *Rosmarinus*, and Tegosoft CT. DDAB at 150 µg/mL was selected as a safe concentration able to guarantee positive ZP value. As recently reported, DDAB is safe on human keratinocytes (HaCaT) and osteoblast-like (SAOS-2) cell lines, with cell viability being higher than 90% of control at 165 µg/mL and higher than 50% for twice this concentration (330 µg/mL) [71]. As expected, the addition of such a low amount of the positively charged coating layer did not induce significant modification in mean size, whose values were found to be 211.1 and 184.5 nm for L-NLC and R-NLC, respectively, without affecting PDI (<0.3). ZP was found to be highly positive, with values equal to +40.5 and +43.0 mV for L-NLC and R-NLC, respectively. In order to verify the mucoadhesive properties of L-NLC+ and R-NLC+, compared to the control CT-NLC+, the interaction with mucin was evaluated over a period of 24 h, by measuring the turbidity at 650 nm (ABS) and the change in the ZP values (Figure 10).
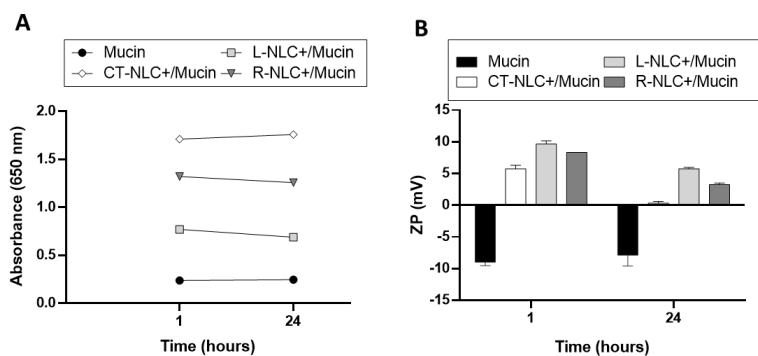

Figure 10. *In vitro* assessment of mucin interactions with CT-NLC+, R-NLC+, and L-NLC+ by turbidimetric assay at 650 nm (A) and Zeta potential (ZP) modifications (B).

Absorbance measurement was reported to give a rough estimation of particle-mucin interaction [72]. The mucoadhesive interaction between particles and mucin results in the adsorption of the mucin around the surface of the particles with a consequent slight aggregation that can be detected as an increase in UV absorbance [73]. For this reason, the turbidity value after mixing CT-NLC+, R-NLC+, and L-NLC+ with native mucin was determined after 1 h and followed up to 24 h. As shown in Figure 10A, the turbidity of all NLC+/mucin dispersions was higher than the turbidity of mucin dispersion itself at both the time points considered, thus suggesting the interaction between NLC+ and mucin [74]. Furthermore, high absorbance values of CT-NLC+, R-NLC+, and L-NLC+ dispersions before incubation with mucin (whose values were 2.015, 1.226, and 2.049, respectively) reflected particle motion [72], while reduced values after their incubation with mucin (Figure 10A) are related to possible particle immobilization due to adsorption of mucin on their surface [75]. As reported by D'Angelo et al., mucin's adsorption on particle surface is expected to reduce particle mobility, agglomeration, and to a certain extent precipitation might take place [76]. Our results suggest higher interactions for both nanosystems with EO compared to the CT-NLC+.

Particle-mucin interactions were further confirmed by ZP measurements. Important changes in ZP value are related to strong mucoadhesive properties. In our previous study, the interaction between mucin and PLGA-PEG nanoparticles (NPs) intended for intranasal administration was evaluated [77]. Herein, ZP of PLGA-PEG NPs remained almost unchanged in the presence of mucin, demonstrating that weak interactions occurred between PEGylated NPs and mucin [77].

In the present study, upon addition of CT-NLC+, R-NLC+, and L-NLC+ to mucin, the negative ZP of mucin (~-9 mV) was inverted to a positive value (Figure 10B), and consequently a significative variation in the ZP of CT-NLC+, R-NLC+, and L-NLC+ ($\sim+20$ mV) was observed after incubation with mucin owing to the mucin coating. According to turbidimetric results, the interaction was higher for NLC+ with EOs in the following order: L-NLC+ > R-NLC+ > CT-NLC+.

Mucins are highly glycosylated glycoproteins with a large peptide backbone and oligosaccharides as side chains. Their protein backbone is characterized by the presence of repeating sequences rich in serine, threonine, and proline residues. The net negative charge is due to the presence of deprotonated carboxylate groups (sialic acid) and ester sulfates at the terminus of some sugar units [78]. The mucoadhesive study was carried out at a specific pH value (pH 5.8) according to the intranasal administration route. The loss of electrostatic interaction of mucin at low pH led to a conformational change from a random coil to a rod-

like structure by exposing hydrophobic regions, which were folded and sequestered in the inner part at neutral pH. This is a favorable condition for the interactions between mucin and other entities [77,79]. The electrostatic interaction is the most expectable mucoadhesive mechanism. This may be due to the interactions between the negatively charged sialic groups of mucin and DDAB tertiary amino group present on the nanoparticles surface. Therefore, the reduction of ZP values observed for all NLC+ after 1 and 24 h of incubation with mucin could be attributed to the ionic interaction between the negatively charged mucin particles and NLC+. As a result, the interaction led to a decrease in NLC+ motion, which in turn could decrease their wash out by nasal mucociliary motion after administration, limiting the loss due to sneezing, thus allowing the sustained and prolonged release of the EO to directly reach the brain. These findings are very promising, because, although nasal drug delivery offers direct access of the therapeutics to the brain, it faces hindrances, such as the mucociliary clearance, that prevents drug retention at the mucosal surface with consequent loss of drug therapeutic effectiveness [80,81]. Mucoadhesive carriers could overcome this issue by prolonging the residence time of the drug in the nasal area, thereby increasing absorption and resulting in a remarkable therapeutic response [81].

5.4 Conclusions

Taken together, our results show that the use of *Lavandula* or *Rosmarinus* allowed the formation of smaller and more homogeneous nanoparticles, with a more ordered structure related to the formation of oily droplets into the lipid matrix compared to the other tested oils. The results of *in vitro* studies show that EO nanoencapsulation provides a sustained and prolonged release. Furthermore, *Lavandula* and *Rosmarinus* NLC were safe on both murine and human cell lines, at all tested concentrations. This preliminary study suggests that optimized positively charged NLC containing *Lavandula* or *Rosmarinus* can be proposed as a potential add-on strategy in the treatment of neurodegenerative diseases through intranasal administration, due to the well-known beneficial effects of essential oils and the mucoadhesive properties of the prepared NLC.

investigation, methodology, data curation, writing—original draft, writing—review and editing, and supervision. All authors have read and agreed to the published version of the manuscript.

Institutional Review Board Statement: Not applicable.

Informed Consent Statement: Not applicable.

Data Availability Statement: The data presented in this study are available on request from the corresponding author.

Conflicts of Interest: The authors declare no conflict of interest.

Supplementary Materials: The following are available online at www.mdpi.com/article/10.3390/pharmaceutics13081166/s1.
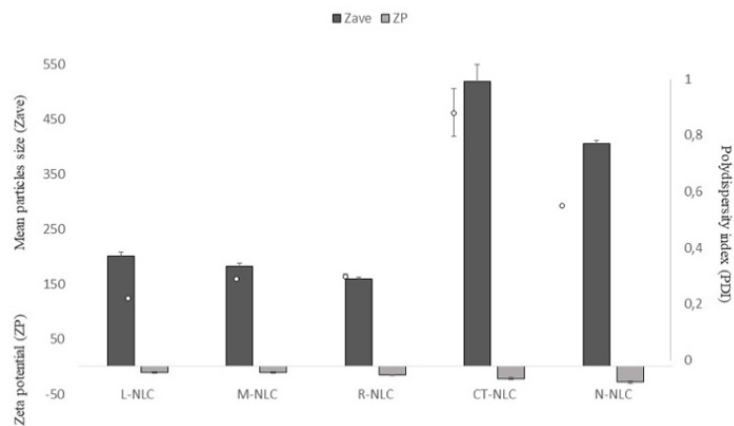
Figure S1. Mean particle size (Zave, nm), polydispersity index (PDI) and Zeta Potential (ZP) ± standard deviation (SD) of the prepared *Lavandula* NLC (L-NLC), *Mentha* NLC (M-NLC), *Rosmarinus* NLC (R-NLC), Tegosoft CT NLC (CT-NLC) and Neem NLC (N-NLC) analysed after 30 days of storage in Turbiscan.
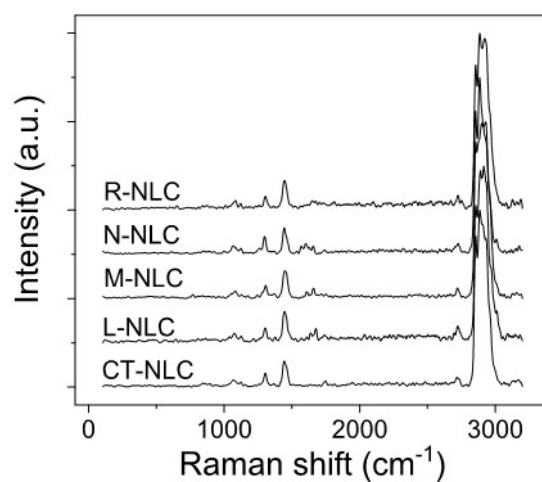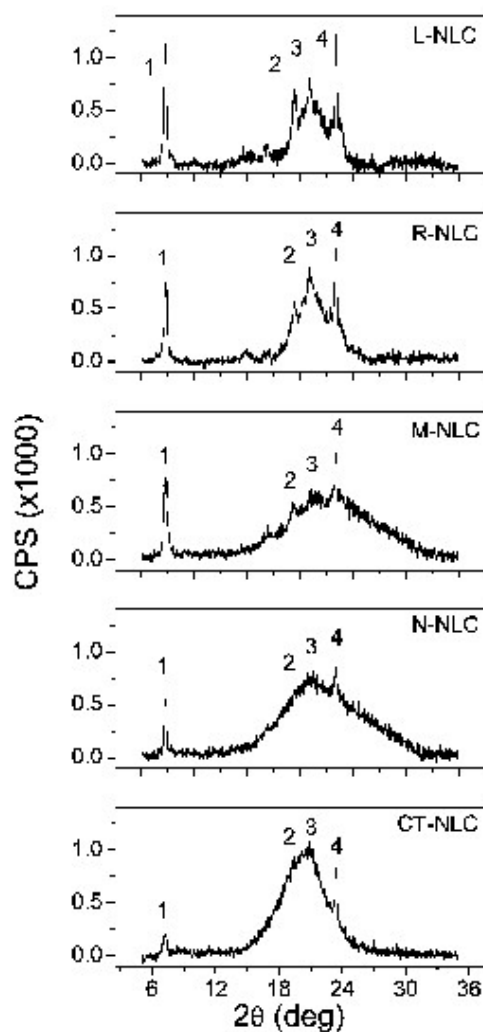
Figure S2. Raman spectra of all the prepared NLC.

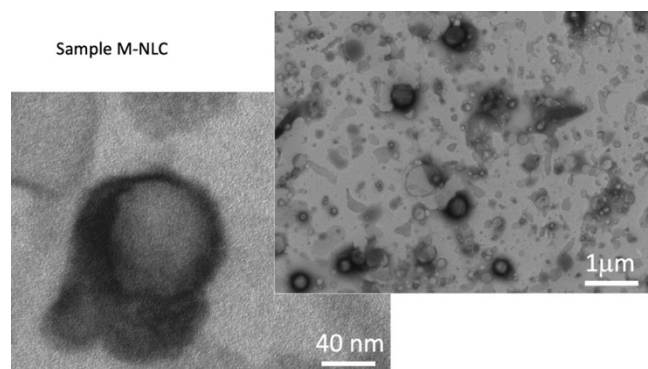**Figure S3**. XRD spectra of all the prepared NLC.

Figure S4. Transmission electron microscopy (TEM) images of NLC prepared using *Mentha* EO (M-NLC).
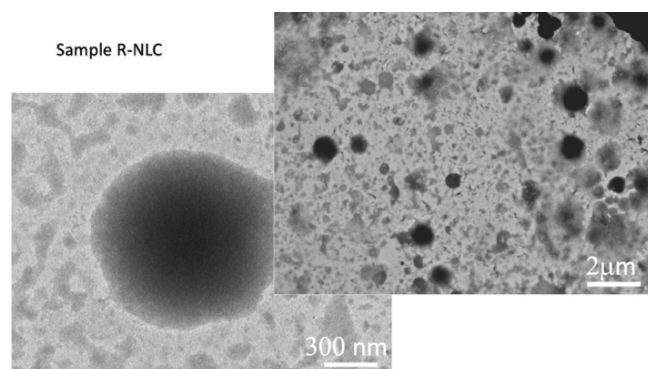

Figure S5. Transmission electron microscopy (TEM) images of NLC prepared using *Rosmarinus* EO (R-NLC).

Table S1. Raman parameters for the C-H stretching vibrational bands of NLC systems.

Sample	Peak position (cm^{-1})	FWHM (cm^{-1})	Strength (a.u.)
CT-NLC	2853	19	0.75
	2883	27	0.92
	2912	25	0.76
	2937	22	0.68
	2962	19	0.32
	2986	36	0.11
L-NLC	2853	16	0.49
	2890	47	0.95
	2916	16	0.29
	2936	25	0.71
	2969	27	0.38
	3007	32	0.17
M-NLC	2852	15	0.53
	2881	19	0.25
	2907	60	0.97
	2934	22	0.39
	2961	23	0.33
	2983	48	0.12
N-NLC	2853	18	0.64
	2882	18	0.40
	2902	58	0.76
	2936	19	0.22
	2963	24	0.20
	3001	34	0.06

Sample	Peak position (cm^{-1})	FWHM (cm^{-1})	Strength (a.u.)
R-NLC	2853	18	0.7
	2881	27	0.71
	2923	50	0.96
	2966	12	0.13
	2978	47	0.21
	3010	30	0.02

References:

1. Bilia, A.R.; Guccione, C.; Isacchi, B.; Righeschi, C.; Firenzuoli, F.; Bergonzi, M.C. Essential oils loaded in canosystems: A developing strategy for a successful therapeutic approach. Evid. Based Complement. Alternat. Med. 2014, 651593, doi:10.1155/2014/651593.

2. Bilia, A.R.; Santomauro, F.; Sacco, C.; Bergonzi, M.C.; Donato, R. Essential oil of Artemisia annua L.: An extraordinary component with numerous antimicrobial properties. Evid. Based Complement. Alternat. Med. 2014, 159819, doi:10.1155/2014/159819.

3. Cacciatore, F.A.; Dalmas, M.; Maders, C.; Isaia, H.A.; Brandelli, A.; Malheiros, P.D. Carvacrol encapsulation into nanostructures: Characterization and antimicrobial activity against foodborne pathogens adhered to stainless steel. Food Res. Int. 2020, 133, doi:10.1016/j.foodres.2020.109143.

4. Carbone, C.; Martins-Gomes, C.; Caddeo, C.; Silva, A.M.; Musumeci, T.; Pignatello, R.; Puglisi, G.; Souto, E.B. Mediterranean essential oils as precious matrix components and active ingredients of lipid nanoparticles. Int. J. Pharm. 2018, 548, 217–226, doi:10.1016/j.ijpharm.2018.06.064.

5. Celia, C.; Trapasso, E.; Locatelli, M.; Navarra, M.; Ventura, C.A.; Wolfram, J.; Carafa, M.; Morittu, V.M.; Britti, D.; Di Marzio, L.; et al. Anticancer activity of liposomal Bergamot essential oil (Beo) on human neuroblastoma cells. Col. Surf. B Biointerfaces 2013, 112, 548–553, doi:10.1016/j.colsurfb.2013.09.017.

6. Donato, R.S.; Santomauro, F.; Bilia, A.R.; Flamini, G.; Sacco, C. Antibacterial activity of Tuscan Artemisia annua essential oil and its major components against some foodborne pathogens. LWT Food Sci. Tech. 2015, 64, 1251–1254.

7. Donsi, F.; Annunziata, M.; Sessa, M.; Ferrari, G. Nanoencapsulation of essential oils to enhance their antimicrobial activity in foods. LWT Food Sci. Technol. 2011, 44, 1908–1914, doi:10.1016/j.lwt.2011.03.003.

8. Lai, F.; Wissing, S.A.; Muller, R.H.; Fadda, A.M. Artemisia arborescens L essential oil-loaded solid lipid nanoparticles for potential agricultural application: Preparation and characterization. AAPS PharmSciTech 2006, 7, E2, doi:10.1208/pt070102.

9. Mannucci, C.; Calapai, F.; Cardia, L.; Inferrera, G.; D'Arena, G.; Di Pietro, M.; Navarra, M.; Gangemi, S.; Ventura Spagnolo, E.; Calapai, G. Clinical pharmacology of Citrus aurantium and Citrus sinensis for the treatment of anxiety. Evid. Based Complement. Alternat. Med. 2018, 2018, 3624094, doi:10.1155/2018/3624094.

10. Montenegro, L.; Pasquinucci, L.; Zappala, A.; Chiechio, S.; Turnaturi, R.; Parenti, C. Rosemary essential oil-loaded lipid nanoparticles: In vivo topical activity from gel vehicles. Pharmaceutics 2017, 9, doi:10.3390/pharmaceutics9040048.

11. Saporito, F.; Sandri, G.; Bonferoni, M.C.; Rossi, S.; Boselli, C.; Icaro Cornaglia, A.; Mannucci, B.; Grisoli, P.; Vigani, B.; Ferrari, F. Essential oil-loaded lipid nanoparticles for wound healing. Int. J. Nanomed. 2018, 13, 175–186, doi:10.2147/IJN.S152529.

12. Scuteri, D.; Morrone, L.A.; Rombola, L.; Avato, P.R.; Bilia, A.R.; Corasaniti, M.T.; Sakurada, S.; Sakurada, T.; Bagetta, G. Aromatherapy and aromatic plants for the treatment of behavioural and psychological symptoms of dementia in patients with Alzheimer's disease: Clinical evidence and possible mechanisms. Evid. Based Complement. Alternat. Med. 2017, 2017, 9416305, doi:10.1155/2017/9416305.

13. Sinico, C.; De Logu, A.; Lai, F.; Valenti, D.; Manconi, M.; Loy, G.; Bonsignore, L.; Fadda, A.M. Liposomal incorporation of Artemisia arborescens L. essential oil and in vitro antiviral activity. Eur. J. Pharm. Biopharm. 2005, 59, 161–168, doi:10.1016/j.ejpb.2004.06.005.

14. Manconi, M.; Petretto, G.; D'Hallewin, G.; Escribano, E.; Milia, E.; Pinna, R.; Palmieri, A.; Firoznezhad, M.; Peris, J.E.; Usach, I.; et al. Thymus essential oil extraction, characterization and incorporation in phospholipid vesicles for the antioxidant/antibacterial treatment of oral cavity diseases. Coll. Surf. B Biointerfaces 2018, 171, 115–122, doi:10.1016/j.colsurfb.2018.07.021.

15. Carbone, C.; Caddeo, C.; Grimaudo, M.A.; Manno, D.E.; Serra, A.; Musumeci, T. Ferulic acid-NLC with Lavandula essential oil: A possible strategy for wound-healing? Nanomaterials 2020, 10, doi:10.3390/nano10050898.

16. Carbone, C.; Teixeira, M.D.C.; Sousa, M.D.C.; Martins-Gomes, C.; Silva, A.M.; Souto, E.M.B.; Musumeci, T. Clotrimazole-loaded Mediterranean essential oils NLC: A synergic treatment of Candida skin infections. Pharmaceutics 2019, 11, doi:10.3390/pharmaceutics11050231.

17. Jimbo, D.; Kimura, Y.; Taniguchi, M.; Inoue, M.; Urakami, K. Effect of aromatherapy on patients with Alzheimer's disease. Psychogeriatrics 2009, 9, 173–179, doi:10.1111/j.1479-8301.2009.00299.x.

18. Rinaldi, F.; Oliva, A.; Sabatino, M.; Imbriano, A.; Hanieh, P.N.; Garzoli, S.; Mastroianni, C.M.; De Angelis, M.; Miele, M.C.; Arnaut, M.; et al. Antimicrobial essential oil formulation: Chitosan coated nanoemulsions for nose to brain delivery. Pharmaceutics 2020, 12, doi:10.3390/pharmaceutics12070678.

19. Battaglia, L.; Panciani, P.P.; Muntoni, E.; Capucchio, M.T.; Biasibetti, E.; De Bonis, P.; Mioletti, S.; Fontanella, M.; Swaminathan, S. Lipid nanoparticles for intranasal administration: Application to nose-to-brain delivery. Expert Opin. Drug Deliv. 2018, 15, 369–378, doi:10.1080/17425247.2018.1429401.

20. Blasi, P.; Giovagnoli, S.; Schoubben, A.; Puglia, C.; Bonina, F.; Rossi, C.; Ricci, M. Lipid nanoparticles for brain targeting I. Formulation optimization. Int. J. Pharm. 2011, 419, 287–295, doi:10.1016/j.ijpharm.2011.07.035.

21. Blasi, P.; Giovagnoli, S.; Schoubben, A.; Ricci, M.; Rossi, C. Solid lipid nanoparticles for targeted brain drug delivery. Adv. Drug Deliv. Rev. 2007, 59, 454–477, doi:10.1016/j.addr.2007.04.011.

22. Blasi, P.; Schoubben, A.; Giovagnoli, S.; Rossi, C.; Ricci, M. Lipid nanoparticles for drug delivery to the brain: In vivo veritas. J. Biomed. Nanotechnol. 2009, 5, 344–350, doi:10.1166/jbn.2009.1043.

23. Blasi, P.; Schoubben, A.; Romano, G.V.; Giovagnoli, S.; Di Michele, A.; Ricci, M. Lipid nanoparticles for brain targeting II. Technological characterization. Coll. Surf. B Biointerfaces 2013, 110, 130–137, doi:10.1016/j.colsurfb.2013.04.021.

24. Blasi, P.; Schoubben, A.; Traina, G.; Manfroni, G.; Barberini, L.; Alberti, P.F.; Cirotto, C.; Ricci, M. Lipid nanoparticles for brain targeting III. Long-term stability and in vivo toxicity. Int. J. Pharm. 2013, 454, 316–323, doi:10.1016/j.ijpharm.2013.06.037.

25. Bonaccorso, A.; Pellitteri, R.; Ruozi, B.; Puglia, C.; Santonocito, D.; Pignatello, R.; Musumeci, T. Curcumin loaded polymeric vs. lipid nanoparticles: Antioxidant effect on normal and hypoxic olfactory ensheathing cells. Nanomaterials 2021, 11, doi:10.3390/nano11010159.

26. Cometa, S.; Bonifacio, M.A.; Trapani, G.; Di Gioia, S.; Dazzi, L.; De Giglio, E.; Trapani, A. In vitro investigations on dopamine loaded solid lipid nanoparticles. J. Pharm. Biomed. Anal. 2020, 185, 113257, doi:10.1016/j.jpba.2020.113257.

27. de Oliveira Junior, E.R.; Truzzi, E.; Ferraro, L.; Fogagnolo, M.; Pavan, B.; Beggiato, S.; Rustichelli, C.; Maretti, E.; Lima, E.M.; Leo, E.; et al. Nasal administration of nanoencapsulated geraniol/ursodeoxycholic acid conjugate: Towards a new approach for the management of Parkinson's disease. J. Control. Rel. 2020, 321, 540–552, doi:10.1016/j.jconrel.2020.02.033.

28. Rassu, G.; Soddu, E.; Posadino, A.M.; Pintus, G.; Sarmento, B.; Giunchedi, P.; Gavini, E. Nose-to-brain delivery of bace1 sirna loaded in solid lipid nanoparticles for Alzheimer's therapy. Coll. Surf. B Biointerfaces 2017, 152, 296–301, doi:10.1016/j.colsurfb.2017.01.031.

29. Gavini, E.; Rassu, G.; Ferraro, L.; Beggiato, S.; Alhalaweh, A.; Velaga, S.; Marchetti, N.; Bandiera, P.; Giunchedi, P.; Dalpiaz, A. influence of polymeric microcarriers on the in vivo intranasal uptake of an anti-migraine drug for brain targeting. Eur. J. Pharm. Biopharm. 2013, 83, 174–183, doi:10.1016/j.ejpb.2012.10.010.

30. Gavini, E.; Rassu, G.; Ferraro, L.; Generosi, A.; Rau, J.V.; Brunetti, A.; Giunchedi, P.; Dalpiaz, A. Influence of chitosan glutamate on the in vivo intranasal absorption of rokitamycin from microspheres. J. Pharm. Sci. 2011, 100, 1488–1502, doi:10.1002/jps.22382.

31. Rassu, G.; Porcu, E.P.; Fancello, S.; Obinu, A.; Senes, N.; Galleri, G.; Migheli, R.; Gavini, E.; Giunchedi, P. Intranasal delivery of genistein-loaded nanoparticles as a potential preventive system against neurodegenerative disorders. Pharmaceutics 2018, 11, doi:10.3390/pharmaceutics11010008.

32. Arduino, I.; Iacobazzi, R.M.; Riganti, C.; Lopedota, A.A.; Perrone, M.G.; Lopalco, A.; Cutrignelli, A.; Cantore, M.; Laquintana, V.; Franco, M.; et al. Induced expression of p-gp and bcrp transporters on brain endothelial cells using transferrin functionalized nanostructured lipid carriers: A first step of a potential strategy for the treatment of Alzheimer's disease. Int. J. Pharm. 2020, 591, 120011, doi:10.1016/j.ijpharm.2020.120011.

33. Hritcu, L.; Cioanca, O.; Hancianu, M. Effects of Lavender oil inhalation on improving scopolamine-induced spatial memory impairment in laboratory rats. Phytomedicine 2012, 19, 529–534, doi:10.1016/j.phymed.2012.02.002.

34. Satou, T.H.; Hanashima, Y.; Mizutani, I.; Koike, K. The effect of inhalation of essential oil from Rosmarinus Officinalis on scopolamine-induced Alzheimer's type dementia model in mice. Flavour Fragr. J. 2017, 33, 1–5.

35. Filiptsova, O.V.; Gazzavi-Rogozina, L.V.; Timoshyna, I.A.; Naboka, O.I.; Dyomina Ye, V.; Ochkur, A.V. The effect of the essential oils of Lavender and Rosemary on the human short-term memory. Alexandria J. Med. 2018, 54, 41–44.

36. Ali-Shtayeh, M.S.; Jamous, R.M.; Abu-Zaitoun, S.Y.; Khasati, A.I.; Kalbouneh, S.R. Biological properties and bioactive components of Mentha Spicata L. essential oil: Focus on potential benefits in the treatment of obesity, Alzheimer's disease, dermatophytosis, and drug-resistant infections. Evid. Based Complement. Alternat. Med. 2019, 2019, 3834265, doi:10.1155/2019/3834265.

37. Suresha, A.R.; Rajesh, P.; Anil Raj, K.S.; Torgal, R. A rare case of toxic optic neuropathy secondary to consumption of Neem oil. Indian J. Ophthalmol. 2014, 62, 337–339, doi:10.4103/0301-4738.121129.

38. Rahman, M.F.; Siddiqui, M.K.; Jamil, K. Sub-Chronic Effect of Neem based pesticide (Vepacide) on acetylcholinesterase and atpases in rat. J. Environ. Sci. Health B 1999, 34, 873–884, doi:10.1080/03601239909373232.

39. Lai, S.M.; Lim, K.W.; Cheng, H.K. Margosa oil poisoning as a cause of toxic encephalopathy. Singapore Med. J. 1990, 31, 463–465.

40. Carbone, C.; Campisi, A.; Musumeci, T.; Raciti, G.; Bonfanti, R.; Puglisi, G. Fa-loaded lipid drug delivery systems: Preparation, characterization and biological studies. Eur. J. Pharm. Sci. 2014, 52, 12–20, doi:10.1016/j.ejps.2013.10.003.

41. Caddeo, C.; Pucci, L.; Gabriele, M.; Carbone, C.; Fernandez-Busquets, X.; Valenti, D.; Pons, R.; Vassallo, A.; Fadda, A.M.; Manconi, M. Stability, biocompatibility and antioxidant activity of peg-modified liposomes containing resveratrol. Int. J. Pharm. 2018, 538, 40–47, doi:10.1016/j.ijpharm.2017.12.047.

42. Rezvani, M.; Manca, M.L.; Caddeo, C.; Escribano-Ferrer, E.; Carbone, C.; Peris, J.E.; Usach, I.; Diez-Sales, O.; Fadda, A.M.; Manconi, M. Co-loading of ascorbic acid and tocopherol in eudragit-nutriosomes to counteract intestinal oxidative stress. Pharmaceutics 2019, 11, doi:10.3390/pharmaceutics11010013.

43. Carbone, C.; Musumeci, T.; Lauro, M.R.; Puglisi, G. Eco-friendly aqueous core surface-modified nanocapsules. Coll. Surf. B Biointerfaces 2015, 125, 190–196, doi:10.1016/j.colsurfb.2014.11.038.

44. Santonocito, D.; Sarpietro, M.G.; Carbone, C.; Panico, A.; Campisi, A.; Siciliano, E.A.; Sposito, G.; Castelli, F.; Puglia, C. Curcumin containing pegylated solid lipid nanoparticles for systemic administration: A preliminary study. Molecules 2020, 25, doi:10.3390/molecules25132991.

45. Puglia, C.; Santonocito, D.; Ostacolo, C.; Maria Sommella, E.; Campiglia, P.; Carbone, C.; Drago, F.; Pignatello, R.; Bucolo, C. Ocular formulation based on palmitoylethanolamide-loaded nanostructured lipid carriers: Technological and pharmacological profile. Nanomaterials 2020, 10, doi:10.3390/nano10020287.

46. Carbone, C.; Manno, D.; Serra, A.; Musumeci, T.; Pepe, V.; Tisserand, C.; Puglisi, G. Innovative hybrid vs polymeric nanocapsules: The influence of the cationic lipid coating on the "4s". Coll. Surf. B Biointerfaces 2016, 141, 450–457, doi:10.1016/j.colsurfb.2016.02.002.

47. Castile, J.; Cheng, Y.H.; Simmons, B.; Perelman, M.; Smith, A.; Watts, P. Development of in Vitro Models to Demonstrate the Ability of Pecsys (R), an in Situ Nasal Gelling Technology, to Reduce Nasal Run-Off and Drip. Drug Dev. Ind. Pharm. 2013, 39, 816–824, doi:10.3109/03639045.2012.707210.

48. Tomasello, B.; Di Mauro, M.D.; Malfa, G.A.; Acquaviva, R.; Sinatra, F.; Spampinato, G.; Laudani, S.; Villaggio, G.; Bielak-Zmijewska, A.; Grabowska, W.; et al. Rapha Myr((R)), a blend of sulforaphane and myrosinase, exerts antitumor and anoikis-sensitizing effects on human astrocytoma cells modulating sirtuins and DNA methylation. Int. J. Mol. Sci. 2020, 21, doi:10.3390/ijms21155328.

49. Carbone, C.; Campisi, A.; Manno, D.; Serra, A.; Spatuzza, M.; Musumeci, T.; Bonfanti, R.; Puglisi, G. The critical role of didodecyldimethylammonium bromide on physico-chemical, technological and biological properties of NLC. Coll. Surf. B Biointerfaces 2014, 121, 1–10, doi:10.1016/j.colsurfb.2014.05.024.

50. Danaei, M.; Dehghankhold, M.; Ataei, S.; Hasanzadeh Davarani, F.; Javanmard, R.; Dokhani, A.; Khorasani, S.; Mozafari, M.R. Impact of particle size and polydispersity index on the clinical applications of lipidic nanocarrier systems. Pharmaceutics 2018, 10, doi:10.3390/pharmaceutics10020057.

51. Lang, F.; Busch, G.L.; Volkl, H. The diversity of volume regulatory mechanisms. Cell. Physiol. Biochem. 1998, 8, 1–45, doi:10.1159/000016269.

52. Patravale, V.B.; Date, A.A.; Kulkarni, R.M. Nanosuspensions: A promising drug delivery strategy. J. Pharm. Pharmacol. 2004, 56, 827–840, doi:10.1211/0022357023691.

53. Musumeci, T.; Bonaccorso, A.; Carbone, C.; Russo, G.; Pappalardo, F.; Puglisi, G. Design and optimization of pegylated nanoparticles intended for berberine chloride delivery. J. Drug Del. Sci. Tech. 2019, 52, 521–530, doi:10.1016/j.jddst.2019.05.012.

54. Esmonde-White, K.A.; Cuellar, M.; Uerpmann, C.; Lenain, B.; Lewis, I.R. Raman spectroscopy as a process analytical technology for pharmaceutical manufacturing and bioprocessing. Anal. Bioanal. Chem. 2017, 409, 637–649, doi:10.1007/s00216-016-9824-1.

55. Chauhan, I.; Yasir, M.; Verma, M.; Singh, A.P. Nanostructured lipid carriers: A groundbreaking approach for transdermal drug delivery. Ad. Pharm. Bull. 2020, 10, 150–165, doi:10.34172/apb.2020.021.

56. Spiker, R.C.; Levin, I.W. Effect of bilayer curvature on vibrational Raman spectroscopic behavior of phospholipid-water assemblies. Biochim. Biophys. Acta 1976, 455, 560–575, doi:10.1016/0005-2736(76)90325-4.

57. De Lange, M.J.L.; Bonn, M.; Muller, M. Direct Measurements of Phase Coexistence in Dppc/Cholesterol Vesicles Using Raman Spectroscopy. Chem. Phys. Lipids 2007, 146, 76–84.

58. Levin, Z.D.S.a.I.W. Vibrational spectroscopy of biomembranes. Annu. Rev. Anal. Chem. 2011, 4, 343–366, doi:10.1146/annurev- anchem-061010-114048.

59. George, W.H.; Wurpel, J.M.S.; Muller, M. Direct measurement of chain order in single phospholipid mono- and bilayers with multiplex cars. J. Phys. Chem. B 2004, 108, 3400–3403.

60. Sato, K.; Ueno, S.; Yano, J. Molecular interactions and kinetic properties of fats. Prog. Lipid Res. 1999, 38, 91–116, doi:10.1016/s0163-7827(98)00019-8.

61. Teeranachaideekul, V.; Morakul, B.; Boonme, P.; Pornputtapitak, W.; Junyaprasert, V. Effect of lipid and oil compositions on physicochemical properties and photoprotection of octyl methoxycinnamate-loaded nanostructured lipid carriers (NLC). J. Oleo. Sci. 2020, 69, 1627–1639, doi:10.5650/jos.ess20093.

62. Tetyczka, C.; Hodzic, A.; Kriechbaum, M.; Juraic, K.; Spirk, C.; Hartl, S.; Pritz, E.; Leitinger, G.; Roblegg, E. Comprehensive characterization of nanostructured lipid carriers using laboratory and synchrotron X-ray scattering and diffraction. Eur. J. Pharm. Biopharm. 2019, 139, 153–160, doi:10.1016/j.ejpb.2019.03.017.

63. Mostafa, D.A.; Bayoumi, F.S.; Taher, H.M.; Abdelmonem, B.H.; Eissa, T.F. Antimicrobial Potential of Mentha Spp. Essential Oils as Raw and Loaded Solid Lipid Nanoparticles against Dental Caries. Res. J. Pharm. Tech. 2020, 13, 4415–4422.

64. Pasquoto-Stigliani, T.; Campos, E.V.R.; Oliveira, J.L.; Silva, C.M.G.; Bilesky-Jose, N.; Guilger, M.; Troost, J.; Oliveira, H.C.; Stolf- Moreira, R.; Fraceto, L.F.; et al. Nanocapsules containing Neem (Azadirachta indica) oil: Development, characterization, and toxicity evaluation. Sci. Reports 2017, 7, doi:10.1038/S41598-017-06092-4.

65. Reeta, M.R.; Newton, A.M.J. Fabrication and characterisation of Lavender oil and plant phospholipid based sumatriptan succinate hybrid nano lipid carriers. Pharm. Biomed. Res. 2020, 6, 91–104, doi:10.18502/pbr.v6i1.3430.

66. Vieira, R.; Severino, P.; Nalone, L.A.; Souto, S.B.; Silva, A.M.; Lucarini, M.; Durazzo, A.; Santini, A.; Souto, E.B. Sucupira Oil-Loaded Nanostructured Lipid Carriers (NLC): Lipid Screening, Factorial Design, Release Profile, and Cytotoxicity. Molecules 2020, 25, doi:10.3390/Molecules25030685.

67. Yun, Y.R.; Won, J.E.; Jeon, E.; Lee, S.; Kang, W.; Jo, H.; Jang, J.H.; Shin, U.S.; Kim, H.W. Fibroblast growth factors: Biology, function, and application for tissue regeneration. J. Tissue Eng. 2010, 2010, 218142, doi:10.4061/2010/218142.

68. Srivastava, P.; Yadav, N.; Lella, R.; Schneider, A.; Jones, A.; Marlowe, T.; Lovett, G.; O'Loughlin, K.; Minderman, H.; Gogada, R.; et al. Neem Oil Limonoids Induces P53-Independent Apoptosis and Autophagy. Carcinogenesis 2012, 33, 2199–2207, doi:10.1093/carcin/bgs269.

69. Brahmi, F.; Hadj-Ahmed, S.; Zarrouk, A.; Bezine, M.; Nury, T.; Madani, K.; Chibane, M.; Vejux, A.; Andreoletti, P.; Boulekbache- Makhlouf, L.; et al. Evidence of biological activity of Mentha species extracts on apoptotic and autophagic targets on murine raw264.7 and human U937 monocytic cells. Pharm. Biol. 2017, 55, 286–293, doi:10.1080/13880209.2016.1235208.

70. Torres-Martinez, Y.; Arredondo-Espinoza, E.; Puente, C.; Gonzalez-Santiago, O.; Pineda-Aguilar, N.; Balderas-Renteria, I.; Lopez, I.; Ramirez-Cabrera, M.A. Synthesis of silver nanoparticles using a Mentha Spicata extract and evaluation of its anticancer and cytotoxic activity. PeerJ 2019, 7, e8142, doi:10.7717/peerj.8142.

71. Silva, A.M.; Martins-Gomes, C.; Coutinho, T.E.; Fangueiro, J.E.; Sanchez-Lopez, E.; Pashirova, T.N.; Andreani, T.; Souto, E.B. Soft cationic nanoparticles for drug delivery: Production and cytotoxicity of solid lipid nanoparticles (SLNs). Appl. Sci. 2019, 9, doi:10.3390/App9204438.

72. Makled, S.; Nafee, N.; Boraie, N. Nebulized Solid lipid nanoparticles for the potential treatment of pulmonary hypertension via targeted delivery of phosphodiesterase-5-inhibitor. Int. J. Pharm. 2017, 517, 312–321, doi:10.1016/j.ijpharm.2016.12.026.

73. Amore, E.; Ferraro, M.; Manca, M.L.; Gjomarkaj, M.; Giammona, G.; Pace, E.; Bondi, M.L. Mucoadhesive solid lipid microparticles for controlled release of a corticosteroid in the chronic obstructive pulmonary disease treatment. Nanomedicine 2017, 12, 2287–2302, doi:10.2217/nnm-2017-0072.

74. Rencber, S.; Karavana, S.Y.; Yilmaz, F.F.; Erac, B.; Nenni, M.; Ozbal, S.; Pekcetin, C.; Gurer-Orhan, H.; Hosgor-Limoncu, M.; Guneri, P.; et al. Development, characterization, and in vivo assessment of mucoadhesive nanoparticles

containing fluconazole for the local treatment of oral candidiasis. Int. J. Nanomed. 2016, 11, 2641–2653, doi:10.2147/IJN.S103762.

75. Sallam, M.A.; Helal, H.M.; Mortada, S.M. Rationally designed nanocarriers for intranasal therapy of allergic rhinitis: Influence of carrier type on in vivo nasal deposition. Int. J. Nanomed. 2016, 11, 2345–2357, doi:10.2147/IJN.S98547.

76. D'Angelo, I.; Casciaro, B.; Miro, A.; Quaglia, F.; Mangoni, M.L.; Ungaro, F. Overcoming barriers in Pseudomonas Aeruginosa lung infections: Engineered nanoparticles for local delivery of a cationic antimicrobial peptide. Coll. Surf. B Biointerfaces 2015, 135, 717–725, doi:10.1016/j.colsurfb.2015.08.027.

77. Bonaccorso, A.; Musumeci, T.; Carbone, C.; Vicari, L.; Lauro, M.R.; Puglisi, G. Revisiting the role of sucrose in PLGA-PEG nanocarrier for potential intranasal delivery. Pharm. Dev. Technol. 2018, 23, 265–274, doi:10.1080/10837450.2017.1287731.

78. Szilagyi, B.A.; Mammadova, A.; Gyarmati, B.; Szilagyi, A. Mucoadhesive interactions between synthetic polyaspartamides and porcine gastric mucin on the colloid size scale. Coll. Surf. B Biointerfaces 2020, 194, 111219, doi:10.1016/j.colsurfb.2020.111219.

79. das Neves, J.; Sverdlov Arzi, R.; Sosnik, A. Molecular and cellular cues governing nanomaterial-mucosae interactions: From nanomedicine to nanotoxicology. Chem. Soc. Rev. 2020, 49, 5058–5100, doi:10.1039/c8cs00948a.

80. Musumeci, T.; Bonaccorso, A.; Puglisi, G. Epilepsy disease and nose-to-brain delivery of polymeric nanoparticles: An overview. Pharmaceutics 2019, 11, doi:10.3390/pharmaceutics11030118.

81. Rehman, S.; Nabi, B.; Zafar, A.; Baboota, S.; Ali, J. Intranasal delivery of mucoadhesive nanocarriers: A viable option for Parkinson's disease treatment? Expert Opin. Drug Deliv. 2019, 16, 1355–1366, doi:10.1080/17425247.2019.1684895.

6 W/O/W MICROEMULSIONS FOR NASAL DELIVERY OF HYDROPHILIC COMPOUNDS: A PRELIMINARY STUDY

Cinzia Cimino[1,2,3], Angela Bonaccorso[2,3], Barbara Tomasello[4], Giovanni Anfuso Alberghina[2], Teresa Musumeci[2,3], Carmelo Puglia[2,3], Rosario Pignatello[2,3], Agostino Marrazzo[3,5], Claudia Carbone[2,3,*]

[1] PhD in Biotechnology, Department of Biomedical and Biotechnological Sciences, University of Catania, Via Santa Sofia 97, 95123 Catania, Italy;

[2] Laboratory of Drug Delivery Technology, Department of Drug and Health Sciences, University of Catania, Viale A. Doria 6, 95124 Catania, Italy;

[3] NANOMED, Research Centre for Nanomedicine and Pharmaceutical Nanotechnology, University of Catania, Viale A. Doria 6, 95124 Catania, Italy;

[4] Section of Biochemistry, Department of Drug and Health Sciences, University of Catania, Viale A. Doria 6, 95124 Catania, Italy;

[5] Medicinal Chemistry Laboratory, Department of Drug and Health Sciences, University of Catania, Viale A. Doria 6, 95124 Catania, Italy.

[*] Correspondence: claudia.carbone@unict.it

Abstract: The administration of hydrophilic therapeutics has always been a great challenge because of their low bioavailability after administration. For this purpose, W/O/W microemulsion resulted to be a potential successful strategy for the delivery of hydrophilic compounds, interesting for the nasal mucosal vaccine therapy. Herein, an optimized biphasic W/O microemulsion was designed, through a preliminary screening, and it was inverted in a triphasic W/O/W microemulsion, intended for the nasal administration. In order to enhance the mucosal retention, surface modification of the biphasic W/O microemulsion was performed adding DDAB, and then converting the system into a cationic triphasic W/O/W microemulsion. The developed samples were characterized in terms of droplet size, polydispersity, zeta potential, pH and osmolality. The physical long-term stability was analyzed storing samples at accelerated conditions (40±2°C and 75±5%

RH) for 6 months in a constant climate chamber, following ICH guidelines Q1A (R2). In order to verify the potential retention on the nasal mucosa, the two triphasic systems were analyzed in terms of mucoadhesive properties, measuring the *in vitro* interaction with mucin over time. Furthermore, fluorescein sodium salt was selected as a model hydrophilic drug to be encapsulated into the inner core of the two triphasic W/O/W microemulsions, and its release was analyzed compared to the free probe solution. The cytocompatibility of the two platforms was assessed on two cell lines, human fibroblasts HFF1 and Calu-3 cell lines, chosen as pre-clinical models for nasal and bronchial/tracheal airway epithelium.

Keywords: Drug delivery system; Emulsions; Mucosal vaccination; Nasal drug delivery; Physical stability; Preformulation; Self-emulsifying; Vaccine delivery.

6.1 Introduction

Currently, the need to obtain increased drug efficacy or reduced side effects led scientific community to develop innovative drug delivery systems for hydrophilic molecules, which are becoming more relevant in therapy. Many therapeutical compounds, such as vaccines, nucleic acids, proteins and some anti-cancer molecules, have a hydrophilic nature with poor permeability, low intracellular absorption, rapid enzymatic degradation and clearance, moderate distribution, low therapeutic index, and poor pharmacokinetic profile[1]. To overcome these limitations, the focus of researchers is aimed to the development of Drug Delivery Systems (DDS) which are effectively capable to vehiculate hydrophilic molecules, since these compounds have weak interactions with many drug carriers, resulting in a low encapsulation efficiency, unwanted loss and initial burst release[2]. Having an inner water core, W/O emulsions could be suitable for the encapsulation of hydrophilic molecules. They present the advantage of providing a higher solubilization compared to simple micellar dispersions, assuring greater kinetic stability. Furthermore, their small droplets size provides a pathway to drastically increase the drug dissolution rate and subsequently their systemic bioavailability[3]. Nevertheless, W/O emulsions could present critical issues because of their thermodynamic instability; they are prone to demulsification, eventually leading to bulk phase separation, sedimentation, coalescence and flocculation. Furthermore, other factors can result in physically instability for lipid oxidation, such as temperature, ionic strength, and oxygen content, which can severely restrict W/O emulsion development and application in therapeutics[4]. Otherwise, in order to enhance the delivery of drugs, multiple emulsions, such as water-oil-water (W/O/W) ones,

also called double or triphasic emulsions, have been developed. They consist of a primary water in oil (W/O) emulsion of water droplets dispersed in an oily phase (primary biphasic system), which is then dispersed in an external water phase, thus leading to the formation of the W/O/W double emulsion (secondary triphasic system). Due to their composition and structure, W/O/W emulsions ensure the absorption of hydrophilic compounds and can also be exploited for simultaneously transporting hydrophilic and lipophilic compounds in a single vehicle[5]. Considering droplets dimensions, emulsions could be divided into: macroemulsions (>400 nm), nanoemulsions (200-400 nm) and microemulsions (<200 nm)[6]. Herein, the terms nanoemulsions and microemulsions are used following these considerations[7].

Nowadays, the scientific community is focusing its interest on the potential use of the nasal route for drug delivery, which represents an interesting strategy to deliver drugs locally, systemically, and directly to the brain (crossing over the Blood Brain Barrier, BBB) and being in direct contact with the external environment. Compared to the oral and parenteral routes, nasal administration presents different benefits, including being needle free, potentially self-administrable and non-invasive, allowing a great uptake surface area, avoiding first pass rate metabolism[8], eliminating the gastrointestinal drawbacks and side effects and guaranteeing the possibility to obtain therapeutical drug levels with a faster onset of drug activity[9]. Moreover, intranasal route is preferred in children and elderly people since it enables a better patient compliance[10]. One of the drawbacks of the nasal administration route is the low bioavailability of hydrophilic and high molecular weight (HMW) peptide and protein drugs, which is normally less than 1%[11]. However, even if nasal administration seems to be potentially efficient, the use of free drug presents several limitations, related to its chemical-physical features, such as their weak mucosal membrane permeability, but also to physiological mechanism, because of the mucociliary clearance and enzymatic degradation[11–14]. Based on these considerations, the encapsulation into DDS could be a successful strategy. One of the most important applications of mucosal route is for vaccines' administration because it offers an immunoreactive site in the mucosal epithelium, while reducing anaphylactic shock risks due to the slow uptake and preventing antigen degradation in the stomach from gastric enzymes, compared with parenteral and oral administrations[15]. Vaccine can be absorbed into the blood circulation system by mucosal, relatively quickly. This is the most suitable route of immunization because it is rich in T-cells, B-cells and plasma cells and encourages both systemic and mucosal antigen-specific adaptive immune responses[15].

Basing on these considerations, different raw materials were screened to select the more adequate components to obtain the primary W/O biphasic microemulsion (ME2); subsequently, the produced ME2 was inverted in order to produce an optimized secondary triphasic W/O/W microemulsion (ME3). The optimized ME2 was also modified through the addition of didodecydimethylammonium bromide (DDAB), namely ME2+, and then inverted to obtain the cationic ME3+. Droplets size (Z-ave) and polydispersity (PDI), as well as zeta potential (ZP), were assessed using Photon Correlation Spectroscopy (PCS), and pH and osmolality were measured. In order to analyze the physical long-term stability, samples were stored at accelerated conditions (40±2°C and 75±5% RH) for 6 months in a constant climate chamber, following ICH guidelines Q1A (R2)[16]. ME3 and ME3+ were also investigated to evaluate their mucoadhesive properties. Different concentrations of both formulations and different treatment times were analyzed to assess *in vitro* biocompatibility on human fibroblast (HFF1) and human airway epithelial (Calu-3) cell lines, selected chosen as pre-clinical models for nasal and bronchial/tracheal airway epithelium. Fluorescein sodium salt was encapsulated as hydrophilic model drug into the inner aqueous core of the biphasic W/O microemulsions ME2 and ME+. The obtained fluorescein-loaded ME3 and ME3+ were characterized and dialysis bag studies were performed to evaluate the probe release.

6.2 Materials and Methods

6.2.1 Materials

Kolliphor® RH40 was provided by BASF Italia S.p.a. (Cesano Modena, Italy); Oleoyl Macrogol-6 Glycerides (Labrafil®) was a gift from Gattefossé Italia s.r.l. (Milano, Italy); Isopropyl myristate (IPM) and Triglyceride caprylic-capric (Tegosoft CT, Miglyol 812) were purchased from Farmalabor (Canosa di Puglia, Italy). Tween® 80 (Polysorbate 80), Span® 80 (Sorbitan monooleate), Didodecyldimethylammonium bromide (DDAB), Fluorescein sodium salt, Tris (hydroxymethyl)aminomethane buffer, Phosphate Buffered Saline pH 7.4 (PBS) were bought from Merck (Darmstadt, Germany). Mucin (mucin from porcine stomach type II), NaCl, NaHCO$_3$, CaCl$_2$·2H$_2$O and KCl were purchased from Merck. Regenerated cellulose membranes (Spectra/Por CE; Mol. Wet. Cutoff 3500) were supplied by Spectrum (Los Angeles, CA, USA). All materials for the biological assays were purchased from Merck. All solvents (LC grade) were from VWR International (Milan, Italy).

_____

6.2.2 Preformulative studies on biphasic ME2 and triphasic ME3 and preparation method

6.2.2.1 Materials screening for ME2 composition

Materials to be used to produce the primary W/O biphasic microemulsion (ME2) were screened, selecting Labrafil® or Span® 80 as surfactants, Kolliphor® or Tween® 80 as co-surfactants, and Tegosoft CT or IPM as liquid lipids. To determine the optimal quantitative composition of ME2, water phase was fixed at 10% w/V[17], the following equations were used to calculate the percentages of surfactants (1) and co-surfactants (2) and the amount of oil was selected up to 100%.

$$\%_{SURFACTANT} = HLB_{TOT} - HLB_{SURFACTANT} \qquad (1)$$

$$\%_{CO-SURFACTANT} = HLB_{TOT} - HLB_{CO-SURFACTANT} \qquad (2)$$

The raw materials were considered in different combinations, as reported in Supplementary Table 1, obtaining 8 samples, from ME2-A to ME2-H, each one composed by: 10.0% of water, 12.8% of surfactant, 6.8% of co-surfactant and 70.4% of oil.

6.2.2.2 ME2 preparation method

Primary W/O biphasic microemulsions (ME2-A to ME2-H) were prepared mixing the established amounts of surfactant and co-surfactant at 300 rpm, subsequently adding the oil at 500 rpm and finally dropping the internal water phase under constant stirring at 500 rpm.

6.2.2.3 Photon Correlation Spectroscopy (PCS) analysis of ME2

The produced primary W/O biphasic microemulsions (ME2) were analyzed through a Zetasizer Nano S90 (Malvern Instruments, Malvern, UK), using quartz cuvettes, in order to measure the mean droplets size (Z-ave) and polydispersity (PDI) of the inner water phase.

6.2.2.4 ME2-A stirring time optimization

The optimization of ME2-A preparation was performed analyzing different stirring times after the dropwise addition of the internal water phase (5, 30, 60, 90, 120, 150 min). The obtained samples ME2-A_5, ME2-A_30, ME2-A_60, ME2-A_90, ME2-A_120, ME2-A_150, were analyzed using Photon Correlation Spectroscopy described above (paragraph 2.2.3).

6.2.2.5 ME3-A composition screening

In order to obtain the secondary triphasic W/O/W microemulsion (ME3-A), Tween® 80 was added to ME2-A at different concentrations (0%, 1%, 2%, 3%, 4%, 5%, 6%, 7%, 8%,

_____

9%, 10% w/V) and ME2-A was inverted in TRIS external phase at different dilutions (1:3, 1:6, 1:9) under constant mixing at 500 rpm for 10 min. The obtained ME3-A samples were analyzed using Photon Correlation Spectroscopy as described below (paragraph 2.3.1).

6.2.2.6   ME3-A surface modification

The optimized ME3-A was modified with the cationic lipid DDAB, which was added at a concentration of 0.15% w/V into the inner biphasic microemulsion (obtaining ME2+A), before its inversion to triphasic microemulsion (obtaining ME3+A).

6.2.2.7   Fluorescein loading

Fluorescein, as a hydrophilic model drug, was loaded into the inner water phase of ME2-A and ME2+A at a concentration of 1 mg/mL, before their inversion to triphasic microemulsions, thus obtaining F-ME3-A and F-ME3+A, respectively.

6.2.3 Physico-chemical and technological characterization of triphasic ME3s

6.2.3.1   Photon Correlation Spectroscopy (PCS) analysis of ME3s

Zetasizer Nano S90 (Malvern Instruments, Malvern, UK) was also employed to analyze the secondary triphasic W/O/W microemulsion (ME3-A), using polystyrene cuvettes to measure Z-ave and PDI, and folding capillary cuvettes for measuring ZP. Three analyses of each sample were performed, and results are reported as mean ± SD.

6.2.3.2   Osmolality and pH measurements

Osmolality of the samples was analyzed using an osmometer (Osmomat 3000, Gonotec, Berlin, Germany) previously calibrated using ultra-purified water and physiological solution.

A pH-meter (Mettler Toledo, Milano, Italy) was used to measure samples pH, after calibration with pH 4.0, 7.0 and 10.0 solutions.

6.2.3.3   Accelerated stability studies

ICH guidelines Q1A (R2)[16] were followed to assess accelerated stability of blank ME3-A and ME3+A, through the incubation in constant climatic chamber (BINDER GmbH, KBF-S 115 E6, Tuttlingen, Germany) at accelerated conditions ($40\pm2°C$ temperature and $75\pm5\%$ RH) for 6 months. Z-ave and PDI were measured each month, for 6 months of storage.

_____

6.2.4 In vitro studies

6.2.4.1 Mucoadhesion studies

An *in vitro* method based on the evaluation of two parameters (turbidimetry and ZP) was used to assess the mucoadhesive properties of the secondary triphasic W/O/W microemulsions (ME3-A and ME3+A). Briefly, mucin (0.1% w/v) was suspended in simulated nasal fluid (SNF: 2.192g NaCl, 0.145g $CaCl_2$ and 0.745g KCl in 250 mL of double distilled water; pH 5) and stirred overnight to allow its complete dispersion. The interaction between each sample and mucin was determined by mixing equal volumes of mucin dispersion and sample suspension for 15 min at 25°C. After 0.5, 1, 2 and 3h of incubation at 37°C, turbidimetry and ZP were assessed. In particular, turbidimetric measurements were evaluated comparing the absorbances at 650 nm by UV-Vis spectrophotometer (UH5300 UV-Visible Double-Beam Spectrophotometer, Hitachi Europe, Milan, Italy) of the native mucin and each dispersion.

6.2.4.2 Probe release

In vitro release of fluorescein from F-ME3-A and F-ME3+A, compared with fluorescein solution, was evaluated using the dialysis bag method. After 24h of moistening in PBS medium, dialysis tubes (Spectra/Por® membranes, MWCO 3.5 kDa) were filled with 1 mL of each sample and incubated in 20 mL of PBS medium, maintained at 37°C under stirring at 300 rpm. At selected time-points (from T0 to 24h), 1 mL of medium was withdrawn and replaced with 1 mL of fresh medium to guarantee pseudo-sink conditions. Each sample was analyzed by UV-VIS spectrophotometer at 490 nm in order to quantify the amount of fluorescein released during time (calibration curve from 0.6 μg/mL to 15.0 μg/mL; R^2=0.9914).

6.2.4.3 Cell cultures and treatments

HFF1 cells (ATCC, SCRC-1041TM) were cultured in Dulbecco's modified Eagle's Medium (DMEM) supplemented with 10% v/v fetal bovine serum and (50 IU/mL) penicillin/(50 μg/mL) streptomycin. Calu-3 cells (Calu-3, HTB-55™) were grown in Minimum Essential Medium Eagle (MEM) supplemented with 10% fetal bovine serum (FBS), 1% sodium pyruvate, 1% MEM non-essential amino acid solution, 1% L-glutamine and 100 U/mL penicillin, and 100 μg/mL streptomycin (PAA Laboratories GmbH, Austria) antibiotic solution. After seeding, the cells were maintained in a controlled environment at 37°C, 5% CO_2 concentration, and 95% relative humidity[18].

For the treatment, the ME3-A and ME3+A were tested at different oil concentrations (8.81 mg/mL, 5.87 mg/mL and 3.52 mg/mL), and at different timepoints (0.5, 1, 2 and 3h).

_____

6.2.4.4   Cytotoxicity evaluation

The cytotoxicity of the triphasic W/O/W microemulsions was assessed by MTT[19] in HFF1 and Calu-3 human cell lines. The cells were seeded in a 96-well plate (1×10^4 cells/well) and incubated for 24h to allow adherence. Both the formulations were diluted in media, filtered using 0.22 μm Millipore Express PES membrane and added to cells as described in the previous paragraph. After the treatments, the culture media was discarded and the cells were rinsed with 1X PBS, added with fresh MTT solution (500 μg/mL in culture media) and re-incubated for 2h. Then, MTT solution was replaced with DMSO for allowing the dissolution of formazan crystals. The optical density (OD) was measured at 550 nm using a microplate reader (Synergy HT multi-mode microplate reader, BioTek, Milano, Italy). Cell viability (%) was expressed as a percentage relative to the untreated control cells (negative control, cells treated with media alone), whose value was equal to 100%.

6.2.5 Statistics

For the characterization of blank and loaded formulations reported in Table 2, two-way ANOVA with Bonferroni's multiple test was performed, comparing the two blanks and also each loaded sample with the respective blank. For accelerated stability studies, mucoadhesion turbidimetric assay and cytocompatibility studies, two-way ANOVA with Dunnett's multiple comparisons tests were performed. Two-way ANOVA with Tukey's multiple comparisons test was used for mucoadhesion ZP analysis. Significance was calculated applying $p < 0.05$ as the minimum level. All the analysis were performed using Prism 9.5.0 (GraphPad Software, Inc., La Jolla, CA, USA).

6.3 Results and discussion

6.3.1 Preformulative studies on biphasic ME2 and characterization

6.3.1.1   Materials screening for ME2 composition

Labrafil® and Tween® 80 were selected as surfactants, while Kolliphor® and Span® 80 were chosen as co-surfactants for the preliminary studies on the preparation of the biphasic W/O ME2. IPM and Tegosoft CT were investigated as the oily phase. Labrafil® is a biocompatible and biodegradable non-ionic amphiphilic PEG derivative (HLB=9), which demonstrated to be safe when used in the formulation of microemulsions for intranasal administration[20]. Span® 80 (HLB=4.3) and Tween® 80 (HLB=15) are widely used in nanoformulations for their GRAS (generally recognized as safe) status. In particular, Tween® 80 was reported to be safe on nasal tissue[21] and to promote steric stabilization of

MEs[22]. Kolliphor®, a non-ionic surfactant (HLB=14-16), was demonstrated to stabilize hydrophilic compounds in emulsive systems[23]. Tegosoft CT (HLB=11) was considered in this screening because of its produce small and stable MEs[24]. IPM (HLB=11.5) was employed because of its ability to enhance nasal absorption of active molecules loaded into MEs[25], even if its concentration has to be maintained lower than 5% v/v to obtain a cell viability higher than 70%, due to its activity as penetration enhancer[26].

In order to obtain the quantitative composition of the primary W/O microemulsion ME2, firstly the water content was set at 10% w/V, basing on previous literature studies[17]. The surfactant ratio was set at about 20% w/V, since Akram et al.[17] demonstrated it was able to provide the formation of homogeneous droplets with low PDI values. Basing on the consideration that a mixture of hydrophilic and lipophilic surfactants provides a better stabilization of the MEs compared to a single surfactant[27], we chose to add both surfactant (Labrafil® or Span® 80) and co-surfactant (Kolliphor® or Tween® 80), in different combinations. As a consequence, 8 primary W/O MEs (from ME2-A to ME2-H) were produced, combining differently surfactants and oils, and analyzed through PCS. The obtained results are reported in Table 1. Among the prepared ME2, only ME2-A (produced with Labrafil® and Kolliphor® as surfactant mixture, and IPM as oil) showed small droplets size and great homogeneity, thus it was selected for further studies.

Table 1. PCS measurements of mean droplets size (Z-ave) and polydispersity index (PDI) of primary W/O microemulsions ME2 (from A to H). Values are reported as mean of at least 3 measurements ± SD. (nd: data not reported since the instrument was not able to measure the sample).

Sample	Z-ave (nm) ± SD	PDI ± SD
ME2-A	89.24 ± 6.37	0.188 ± 0.074
ME2-B	180.40 ± 43.97	0.588 ± 0.368
ME2-C	nd	nd
ME2-D	425.10 ± 49.14	0.874 ± 0.128
ME2-E	299.60 ± 28.36	0.390 ± 0.468
ME2-F	998.20 ± 452.30	0.609 ± 0.208
ME2-G	nd	nd
ME2-H	nd	nd

6.3.1.2 ME2-A stirring time optimization

Stirring rate was reported to have a great influence on the mean size of the obtained droplets, as deepened by Akram et al.[17], whose studies demonstrated that 500 rpm was the optimal stirring rate value: lower stirring values were not able to provide sufficient energy to the emulsive system, causing instability; on the other hand, even if high stirring rates could reduce the time needed for the obtainment of the emulsion, it could induce coalescence of the droplets limiting the stabilization due to the surfactant[17]. Moreover, it

was reported that also stirring time has a great influence on droplet size and homogeneity, and – in the situation of a multiple emulsions – on the inner phase droplets[28]. In particular, considering 500 rpm stirring, it was demonstrated that an increase in stirring time from 15 min to 45 min causes an increment in the droplets mean diameter[28]. For this reason, in our studies 500 rpm was set at the stirring rate, while different stirring times were screened on ME2-A; the obtained droplet sizes and PDI values are reported in Supplementary Figure 1. Based on the obtained results, combining both lower droplets size with good homogeneity values, 30 min was selected as the optimal stirring time.

6.3.2 Preformulative studies and characterization of the triphasic MEs

6.3.2.1 ME3 optimization and characterization

In order to obtain secondary triphasic W/O/W microemulsion (ME3), the selected primary W/O biphasic ME2-A was diluted in TRIS. Since it is well known that phase ratio and amounts of surfactants are crucial parameters in the determination of droplet size because of aggregation phenomena[29], three ME2-A to TRIS ratios (1:3, 1:6 and 1:9) were screened, adding different percentages of Tween® 80 (from 0% to 10% w/V). Tween® 80 was selected for its proper HLB value and because it was found to help obtaining O/W microemulsions with small droplet diameter (<85 nm)[30]. All the produced formulations were analyzed using PCS in order to measure mean droplet size and PDI values. The obtained results, reported in Figure 1, highlighted an initial increase in ME3-A droplet size after the addition of a minimal amount of surfactant (1% or 2% w/V), compared to the sample without Tween® 80.
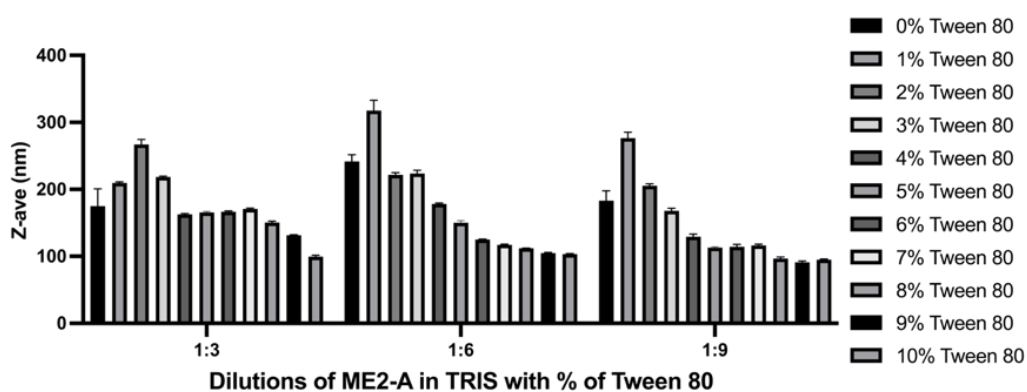

Figure 1. Mean droplet size ME3-A, with different dilutions of ME2-A in TRIS and different amounts of Tween® 80. Values are reported as mean of at least 3 measurements ± SD.

These results could be related to the insufficient amount of surfactant at the droplet interface, which enhanced coalescence. Increasing amounts of Tween® 80 led to the

formation of smaller droplets, as expected, with lower sizes at higher Tween® 80 concentrations. Basing on these considerations, ME3-A diluted in TRIS buffer at 1:3 with 4% w/V of Tween® 80 was selected as the optimal formulation and subjected to further studies, having droplets size adequate for the nasal administration and slightly negative (c.a. -8 mV) ZP values (Table 2).

6.3.2.2 *Surface modification and fluorescein loading*

As reported in literature, a neutral or negative ZP value could be suitable for both nose-to-brain and local nasal administration, while the surface modification with a cationic agent could enhance interactions with mucin[31]. Thus, aiming to increase the residence time on the nasal mucosa, the cationic surfactant DDAB was added to the primary W/O biphasic ME2-A, at a concentration of 0.15% w/V, thus obtaining ME2+A, which was subsequently converted in the secondary triphasic W/O/W microemulsion (ME3+A) by adding 4% of Tween® 80 and diluting 1:3 in TRIS. The addition of DDAB slightly decreased the mean droplet size of ME3+A compared to ME3-A; this phenomenon was already reported for another microemulsion system, where the addition of different amount of the cationic surfactant cetyltrimethylammonium bromide (CTAB) caused a variation of ME droplet size[32]. Moreover, pH and osmolality of nasal formulations have to be adequate in order to avoid mucosal toxicity. A wide pH range is well-tolerated by nasal mucosa[33], even if values close to physiological ones (4.5–6.5) are optimal; on the other hand, pH values lower than 3 or higher than 10 can promote the occurrence of irritation phenomena[34]. Osmolality also represents a crucial parameter in nasal administration, which should be isotonic, thus inhibiting ciliary activity[34], or hypotonic, increasing permeation through nasal mucosa[35]. Basing on these considerations, the results obtained from the technological characterization describe all the obtained formulations as suitable and promising for a potential nasal administration.

Table 2. Characterization of unloaded ME3-A and ME3+A, and fluorescein-loaded F-ME3-A and F-ME3+A. Mean droplet size (Z-ave), PDI, zeta potential (ZP), pH and osmolality are reported, and each value is the mean of at least three measurements ± SD. Statistics were calculated comparing the two blanks and each loaded with the respective blank. Significance was set at ***p≤0.001; ****p≤0.0001.

Sample	Z-ave (nm) ± SD	PDI ± SD	ZP (mv) ± SD	pH ± SD	Osm (mOsm/kg) ± SD
ME3-A	172.50 ± 13.15	0.301 ± 0.018	-8.00 ± 0.39	6.28 ± 0.01	0.215 ± 0.001
F-ME3-A	197.40 ± 36.35	0.321 ± 0.062	-7.99 ± 0.46	6.34 ± 0.01	0.238 ± 0.006
ME3+A	118.30 ± 16.40****	0.452 ± 0.062	+19.10 ± 0.07***	6.21 ± 0.01	0.231 ± 0.005
F-ME3+A	142.40 ± 4.95***	0.477 ± 0.045	+20.50 ± 1.98	6.23 ± 0.01	0.218 ± 0.001

6.3.2.3 Accelerated stability studies

In order to assess MEs long-term stability following ICH guidelines Q1A (R2)[16], the blank ME3s were stored in a constant climate chamber at $40\pm2°C$ and $75\pm5\%$ RH for 6 months, performing PCS analyses every month (Figure 2). Both blank ME3-A and ME3+A showed a good stability during 6 months-storage time in accelerated conditions, which is representative of 1 year stability at $25\pm2°C$ and $75\pm5\%$ RH[16]. Cationic ME3+A demonstrated higher stability, with a minimal variation in droplets size, which was expectable since net positive or negative ZP values are able to guarantee a sufficient droplets repulsion, which prevents the occurrence of instability phenomena[36]. However, even if the almost neutral superficial charge of the ME3-A system induced some variation in droplets size during storage, the droplets diameters remained into the microemulsion size range (<200 nm)[6].
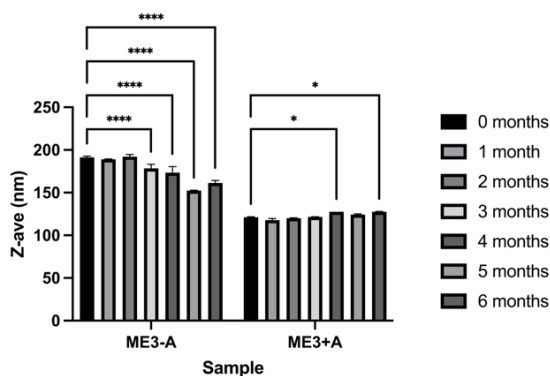
Figure 2. Z-ave (nm) of unloaded ME3-A and ME3+A stored in accelerated conditions at $40\pm2°C$ and $75\pm5\%$ RH, for 6 months. Values are reported as mean of at least 3 measurements $\pm$ SD. Significance was set at $^*p\leq0.05$; $^{****}p\leq0.0001$.

6.3.3 In vitro studies

6.3.3.1 Mucoadhesion studies

The key event in the delivery and absorption of a drug after nasal administration is its passage through the mucus. Mucin, which is formed from mucus, is a protein that has the potential to bind solutes and thus plays a critical role in the drug diffusion process[37]. Factors related to the physical-chemical properties of the formulation and to the nasal cavity may affect the nasal absorption of the drug. One of the main issues hampering drug absorption after nasal administration is the rapid mucociliar clearance that reduces the capacity of drug absorption and its bioavailability[38]. Thus, during the design of a formulation intended for the nasal route, it is of great importance to evaluate its mucoadhesive strength and its potential interaction with the main glycoprotein of the nasal mucosa. In light of these

considerations, mucoadhesive properties of ME3-A and ME3+A were evaluated after interaction with mucin at different time points (0, 0.5, 1, 2 and 3h), by assessing the variation in the ZP values (Figure 3a) and measuring the turbidity at 650 nm (Figure 3b).
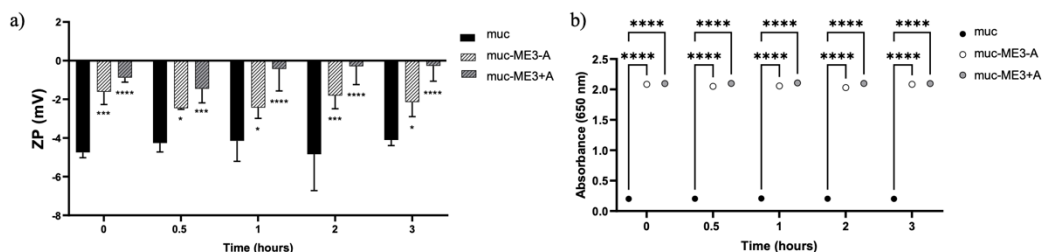

Figure 3. (**a**) Zeta potential values (ZP) of mucin (muc) before 0 and after 0.5, 1, 2 and 3h of incubation with ME3-A and ME3+A (muc-ME3-A; muc-ME3+A) at 37°C. Significance was set at [****]$p \leq 0.0001$; [***]$p \leq 0.001$; [*]$p \leq 0.05$. (**b**) *In vitro* assessment of ME3-A and ME3+A /mucin interactions by turbidimetric assay at 650 nm. Significance was set as [****]$p \leq 0.0001$ for all samples vs muc.

ZP measurements is a common method to investigate the mucoadhesive properties of several matrix and to evaluate the interactions of nanocarriers with mucin[39]. Significant variations in ZP values were reported for both MEs at all considered time points. In particular, upon addition of ME3-A and ME3+A to mucin, the negative ZP of mucin (~ -5 mV) was shifted to more neutral values (Figure 3a), and this effect was more significant for mucin mixture with ME3+A probably due to the occurrence of stronger interaction between the deprotonated carboxylate groups (sialic acid) and ester sulfates at the terminus of some sugar units on mucin glycoproteins and the DDAB tertiary amino group present on the surface of positively charged droplets. Anyway, the significant variation in ZP values, reported for ME3-A since the first analyzed timepoint, suggests its interaction with mucin, thus it also possesses interesting mucoadhesive properties.

Furthermore, absorbance measurement analysis was performed to confirm sample-mucin interaction. The mucoadhesive interaction between MEs and mucin results in the adsorption of the mucin around the surface of the droplets with a consequent slight aggregation that can be detected as an increase in UV absorbance[40]. The turbidity of ME3-A and ME3+A /mucin dispersions (Figure 3b) was significantly higher than the turbidity of the mucin dispersion itself at all the time points considered for both formulations, thus suggesting that interaction phenomena occurred for both ME3-A and ME3+A.

The reported interactions of ME3-A and ME3+A with mucin could promote the residence time of the formulations at the site of administration, offering an easily accessible route to the immune system inducing both mucosal and systemic immunity.

6.3.3.2   Fluorescein loading and release

In order to analyze the behavior of a potential encapsulated drug, fluorescein was selected as hydrophilic model drug and loaded into the inner water phase of ME2-A and ME2+A, which were subsequently added of 4% of Tween® 80 and diluted 1:3 in TRIS, thus obtaining the loaded secondary triphasic W/O/W microemulsions F-ME3-A and F-ME3+A. The physical-chemical and technological features of both the loaded ME3s resulted to be unaltered compared to the respective blank samples (Table 2). A slight not significant increment of Z-ave and PDI after encapsulation was reported and could be related to the steric hindrance of the probe, which could enlarge the inner aqueous core space[41]. pH and osmolality values were not affected by the addition of the fluorescein.

In vitro release of the probe from the two loaded ME3s was performed using dialysis bag method comparing to the free fluorescein solution (Figure 4). The obtained release profiles highlighted a different behavior for F-ME3-A and F-ME3+A. In particular, F-ME3-A performed a sustained release, with the 50% of drug released in the first 2h, reaching the 100% at 24h. F-ME3+A, on the other hand, showed a slower release, with 50% of fluorescein released after 8h from the beginning of the experiment, up to 60% after 24h. It is worth to note that the higher sustained drug release provided by F-ME3-A could be an advantage due to its reduced retention time on the nasal mucosa, compared to the positively charged system, thus both formulations show physical-chemical and technological properties that could be exploited to the advantage to the potential vaccine therapy thought nasal administration.
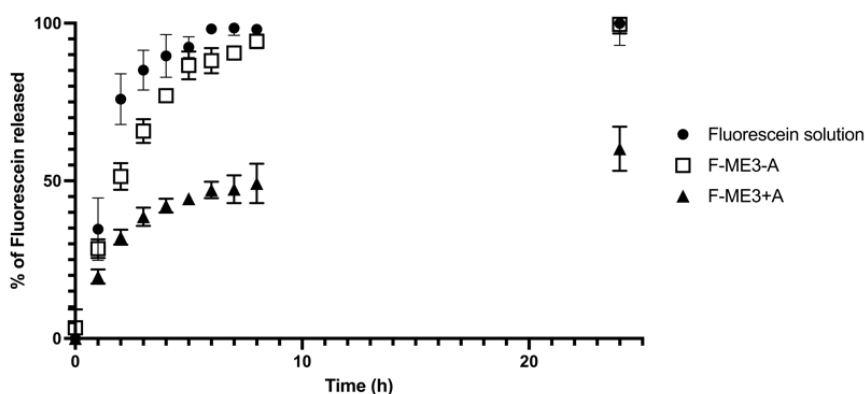

Figure 4. Fluorescein release from F-ME3-A and F-ME3+A, compared to free fluorescein solution. Values are reported as mean of at least 3 measurements ± SD.

_____

6.3.3.3   *Cytotoxicity evaluation*

Formulations biocompatibility represents an important prerequisite for their pharmaceutical application. Considering the features of the nasal administration route, the nasal tissue is the first body's barrier and its integrity must be preserved in order to perform its function properly[19]. The MTT assay, an easy and common test for cytotoxicity studies, was chosen to assess the biocompatibility of the secondary triphasic W/O/W microemulsions (ME3-A and ME3+A). The cytocompatibility of the secondary triphasic microemulsions was assessed by MTT on human airway epithelial (Calu-3) and human fibroblast (HFF1) cells lines, selected as a suitable *in vitro* model of the nasal milieu for the development of nasal products[18].The results of the cell viability after 0.5, 1, 2 and 3h exposure to both ME3-A and ME3+A treatments at different concentrations, compared with the untreated control, are reported in Figure 5.
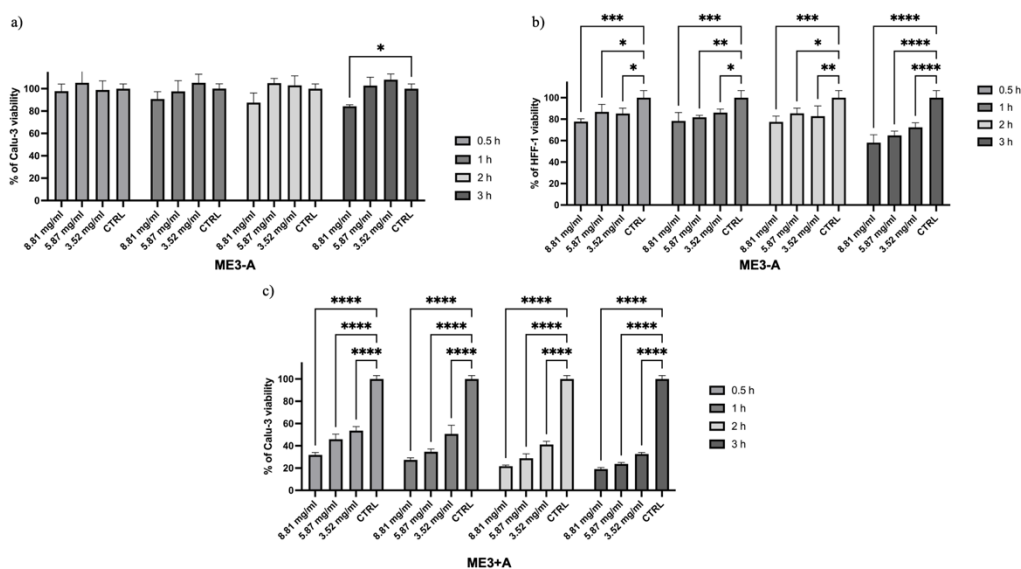
Figure 5. Cell viability of Calu-3 and HFF1 cell lines treated with different concentrations of microemulsion's at different time points (0.5, 1, 2 and 3h): neutral unloaded ME3-A treatment with Calu-3 (**a**); neutral unloaded ME3-A treatment with HFF1 cell lines (**b**); cationic unloaded ME3+A treatment with Calu-3 (**c**). Graphs display cells viability expressed as a percentage in comparison to untreated cells. Values are reported as mean ± SD of at least 3 experiments conducted in quadruplicates. Significance *p≤0.05; **p≤0.01; ***p≤0.001; ****p≤0.0001 versus untreated control.

ME3-A formulation showed to be safe on Calu-3 after 0.5, 1 and 2h of treatment for all the tested concentrations. At the highest tested concentration (8.81 mg/ml), ME3-A resulted in a small reduction in the cellular viability of approximately 16% after 3h of treatment, compared to the untreated cells (Figure 5a). This is an interesting result, since it has been

_____

reported that many intranasal formulations show a clearance half-life of about 15 min[42]. Therefore, this observed biocompatibility up to 3h, along with a good mucoadhesion, may ensure efficient drug penetration. The cytotoxicity studies on the HFF1 human fibroblasts at 0.5, 1, and 2h showed the occurrence of a slight decrease in cell viability in the treatment with the neutral ME3-A, with percentages of viability very similar to each other, thus independent of both concentration and time. However, after 3h of treatment, ME3-A reduced the cell viability in a concentration-dependent manner, with around 58% of cells viable at the highest concentration tested (Figure 5b). In the case of positively charged ME3+A, a marked reduction of cell viability was observed, in a concentration- and time-dependent manner, in Calu-3 cells (Figure 5c) and in a greater extent in HFF1 cells (data not shown). The cytotoxic effect of ME3+A agrees with previous studies reporting a higher toxicity of positively charged surfactants on cells and tissues[43–46].

As regard the effect on fibroblasts, it should be noted that this *in vitro* monolayer model does not reflect *in vivo* conditions, as the fibroblasts are located below the nasal epithelium layer[47]. Therefore, they would not be in direct contact with the formulation, but – depending on the mode of absorption through the nasal epithelium – they would be exposed to more dilute formulations or individual components. In addition, the nasal stromal tissue is highly vascularized[48], therefore the residence time of the formulation would be much shorter than the tested time points.

6.4 Conclusions

The initial screening on raw materials resulted in the selection of Kolliphor® and Labrafil® as surfactants for the preparation of the primary biphasic W/O ME, which resulted optimal with the use of IPM as oily phase. Both neutral and cationic secondary triphasic W/O/W ME3-A and ME3+A, obtained by dilution 1:3 with TRIS and the addition of a proper amount of Tween 80, demonstrated to have adequate physical-chemical and technological features for the nasal administration, with a good long-term stability. Considering its higher cytocompatibility, ME3-A represents the optimal candidate for the nasal mucosal administration of hydrophilic drugs, due to its ability to adequately interact with the site of administration providing a sustained drug release. Therefore, ME3-A should be further investigated as a potential platform for vaccine therapy through nasal mucosa.

_____

Declarations of interest: none

Conflicts of Interest: The authors declare no conflict of interest.

Supplementary Materials:

Supplementary Table 1. Quali-quantitative composition (% w/w) of ME2 (A to H).

Sample	Surfactant		Co-surfactant		Oil		Water
	Labrafil	Span 80	Kolliphor	Tween 80	Isopropyl myristate	Tegosoft CT	
ME2-A	12.8	/	6.8	/	70.4	/	10.0
ME2-B	/	12.8	6.8	/	70.4	/	10.0
ME2-C	12.8	/	/	6.8	70.4	/	10.0
ME2-D	/	12.8	/	6.8	70.4	/	10.0
ME2-E	12.8	/	6.8	/	/	70.4	10.0
ME2-F	/	12.8	6.8	/	/	70.4	10.0
ME2-G	12.8	/	/	6.8	/	70.4	10.0
ME2-H	/	12.8	/	6.8	/	70.4	10.0
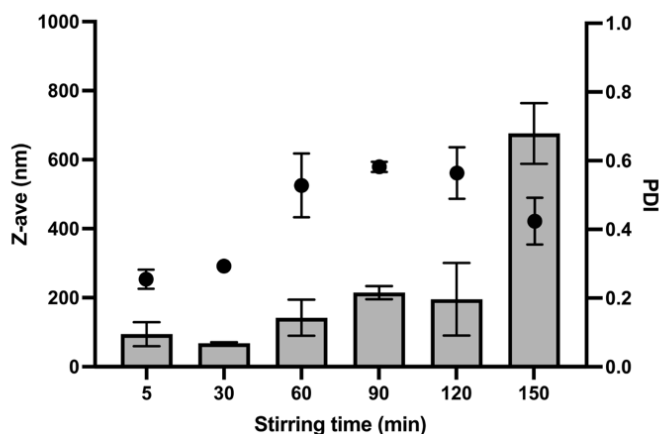
Supplementary Figure 1. Mean droplets size (Z-ave) and polydispersity index (PDI) primary W/O biphasic microemulsion ME2-A subjected to different stirring time.

References:

1. Mirchandani Y, Patravale VB, S. B. Solid lipid nanoparticles for hydrophilic drugs. *J Controlled Release*. 2021;335:457-464. doi:10.1016/j.jconrel.2021.05.032
2. Li Q, Li X, Zhao C. Strategies to Obtain Encapsulation and Controlled Release of Small Hydrophilic Molecules. *Front Bioeng Biotechnol*. 2020;8:437. doi:10.3389/fbioe.2020.00437
3. Singh Y, Meher JG, Raval K, et al. Nanoemulsion: Concepts, development and applications in drug delivery. *J Controlled Release*. 2017;252:28-49. doi:10.1016/j.jconrel.2017.03.008
4. Pan Y, Xu Y, Zhu L, et al. Stability and rheological properties of water-in-oil (W/O) emulsions prepared with a soyasaponin-PGPR system. *Future Foods*. 2021;4:100096. doi:10.1016/j.fufo.2021.100096
5. Sigward E, Mignet N, Rat P, et al. Formulation and cytotoxicity evaluation of new self-emulsifying multiple W/O/W nanoemulsions. *Int J Nanomedicine*. 2013;8:611-625. doi:10.2147/IJN.S35661
6. Dhaval M, Vaghela P, Patel K, et al. Lipid-based emulsion drug delivery systems — a comprehensive review. *Drug Deliv Transl Res*. 2022;12(7):1616-1639. doi:10.1007/s13346-021-01071-9
7. Anton N, Vandamme TF. Nano-emulsions and Micro-emulsions: Clarifications of the Critical Differences. *Pharm Res*. 2011;28(5):978-985. doi:10.1007/s11095-010-0309-1
8. Riese P, Sakthivel P, Trittel S, Guzmán CA. Intranasal formulations: promising strategy to deliver vaccines. *Expert Opin Drug Deliv*. 2014;11(10):1619-1634. doi:10.1517/17425247.2014.931936
9. Agu RU. Challenges in nasal drug absorption: how far have we come? *Ther Deliv*. 2016;7(7):495-510. doi:10.4155/tde-2016-0022
10. Sastre J, Mosges R. Local and systemic safety of intranasal corticosteroids. *J Investig Allergol Clin Immunol*. 2012;22(1):1-12.
11. Ozsoy Y, Gungor S, Cevher E. Nasal Delivery of High Molecular Weight Drugs. *Molecules*. 2009;14(9):3754-3779. doi:10.3390/molecules14093754
12. Heida R, Hinrichs WL, Frijlink HW. Inhaled vaccine delivery in the combat against respiratory viruses: a 2021 overview of recent developments and implications for COVID-19. *Expert Rev Vaccines*. 2022;21(7):957-974. doi:10.1080/14760584.2021.1903878
13. Lee D, Minko T. Nanotherapeutics for Nose-to-Brain Drug Delivery: An Approach to Bypass the Blood Brain Barrier. *Pharmaceutics*. 2021;13(12):2049. doi:10.3390/pharmaceutics13122049
14. Wu H, Hu K, Jiang X. From nose to brain: understanding transport capacity and transport rate of drugs. *Expert Opin Drug Deliv*. 2008;5(10):1159-1168. doi:10.1517/17425247.5.10.1159
15. Ramvikas M, Arumugam M, Chakrabarti SR, Jaganathan KS. Nasal Vaccine Delivery. In: *Micro and Nanotechnology in Vaccine Development*. Elsevier; 2017:279-301. doi:10.1016/B978-0-323-39981-4.00015-4
16. Agrawal M, Saraf S, Pradhan M, et al. Design and optimization of curcumin loaded nano lipid carrier system using Box-Behnken design. *Biomed Pharmacother*. 2021;141:111919. doi:10.1016/j.biopha.2021.111919
17. Akram S, Anton N, Omran Z, Vandamme T. Water-in-Oil Nano-Emulsions Prepared by Spontaneous Emulsification: New Insights on the Formulation Process. *Pharmaceutics*. 2021;13(7):1030. doi:10.3390/pharmaceutics13071030
18. Bonaccorso A, Carbone C, Tomasello B, et al. Optimization of dextran sulfate/poly-l-lysine based nanogels polyelectrolyte complex for intranasal ovalbumin delivery. *J Drug Deliv Sci Technol*. 2021;65:102678. doi:10.1016/j.jddst.2021.102678
19. Vaz G, Clementino A, Mitsou E, et al. In Vitro Evaluation of Curcumin- and Quercetin-Loaded Nanoemulsions for Intranasal Administration: Effect of Surface Charge and Viscosity. *Pharmaceutics*. 2022;14(1):194. doi:10.3390/pharmaceutics14010194
20. Patel RB, Patel MR, Bhatt KK, Patel BG. Formulation consideration and characterization of microemulsion drug delivery system for transnasal administration of carbamazepine. *Bull Fac Pharm Cairo Univ*. 2013;51(2):243-253. doi:10.1016/j.bfopcu.2013.07.002
21. Boche M, Pokharkar V. Quetiapine Nanoemulsion for Intranasal Drug Delivery: Evaluation of Brain-Targeting Efficiency. *AAPS PharmSciTech*. 2017;18(3):686-696. doi:10.1208/s12249-016-0552-9
22. Ahmed S, Gull A, Alam M, Aqil Mohd, Sultana Y. Ultrasonically tailored, chemically engineered and "QbD" enabled fabrication of agomelatine nanoemulsion; optimization, characterization, ex-vivo permeation and stability study. *Ultrason Sonochem*. 2018;41:213-226. doi:10.1016/j.ultsonch.2017.09.042
23. Kalantari A, Kósa D, Nemes D, et al. Self-Nanoemulsifying Drug Delivery Systems Containing Plantago lanceolata—An Assessment of Their Antioxidant and Antiinflammatory Effects. *Molecules*. 2017;22(10):1773. doi:10.3390/molecules22101773
24. Carriço C, Pinto P, Graça A, Gonçalves L, Ribeiro H, Marto J. Design and Characterization of a New Quercus Suber-Based Pickering Emulsion for Topical Application. *Pharmaceutics*. 2019;11(3):131. doi:10.3390/pharmaceutics11030131
25. Jiang Y, Liu C, Zhai W, Zhuang N, Han T, Ding Z. The Optimization Design Of Lactoferrin Loaded HupA Nanoemulsion For Targeted Drug Transport Via Intranasal Route. *Int J Nanomedicine*. 2019;Volume 14:9217-9234. doi:10.2147/IJN.S214657
26. Saffari M, Hoseini Shirazi F, Moghimi HR. Terpene-loaded Liposomes and Isopropyl Myristate as Chemical Permeation Enhancers Toward Liposomal Gene Delivery in Lung Cancer cells; A Comparative Study. *Iran J Pharm Res IJPR*. 2016;15(3):261-267.
27. Shahavi MH, Hosseini M, Jahanshahi M, Meyer RL, Darzi GN. Clove oil nanoemulsion as an effective antibacterial agent: Taguchi optimization method. *Desalination Water Treat*. 2016;57(39):18379-18390. doi:10.1080/19443994.2015.1092893
28. Major-Godlewska M. The influence of stirring time and frequency of impeller rotation on evaluation of drops dimensions and rheological properties of the multiple emulsion. *Chem Pap*. 2020;74(9):3135-3143. doi:10.1007/s11696-020-01146-w
29. Marto J, Gouveia L, Jorge IM, et al. Starch-based Pickering emulsions for topical drug delivery: A QbD approach. *Colloids Surf B Biointerfaces*. 2015;135:183-192. doi:10.1016/j.colsurfb.2015.07.024

---

30. Abdulla NA, Balata GF, El-ghamry HA, Gomaa E. Intranasal delivery of Clozapine using nanoemulsion-based in-situ gels: An approach for bioavailability enhancement. *Saudi Pharm J*. 2021;29(12):1466-1485. doi:10.1016/j.jsps.2021.11.006

31. Wong PT, Wang SH, Ciotti S, et al. Formulation and Characterization of Nanoemulsion Intranasal Adjuvants: Effects of Surfactant Composition on Mucoadhesion and Immunogenicity. *Mol Pharm*. 2014;11(2):531-544. doi:10.1021/mp4005029

32. Mirgorodskaya AB, Koroleva MY, Kushnazarova RA, et al. Microemulsions and nanoemulsions modified with cationic surfactants for improving the solubility and therapeutic efficacy of loaded drug indomethacin. *Nanotechnology*. 2022;33(15):155103. doi:10.1088/1361-6528/ac467d

33. Pires PC, Rodrigues M, Alves G, Santos AO. Strategies to Improve Drug Strength in Nasal Preparations for Brain Delivery of Low Aqueous Solubility Drugs. *Pharmaceutics*. 2022;14(3):588. doi:10.3390/pharmaceutics14030588

34. Javia A, Kore G, Misra A. Polymers in Nasal Drug Delivery: An Overview. In: *Applications of Polymers in Drug Delivery*. Elsevier; 2021:305-332. doi:10.1016/B978-0-12-819659-5.00011-2

35. Marx D, Williams G, Birkhoff M. Intranasal Drug Administration — An Attractive Delivery Route for Some Drugs. In: Vallisuta O, Olimat S, eds. *Drug Discovery and Development - From Molecules to Medicine*. InTech; 2015. doi:10.5772/59468

36. Da Costa S, Basri M, Shamsudin N, Basri H. Stability of Positively Charged Nanoemulsion Formulation Containing Steroidal Drug for Effective Transdermal Application. *J Chem*. 2014;2014:1-8. doi:10.1155/2014/748680

37. Lock JY, Carlson TL, Carrier RL. Mucus models to evaluate the diffusion of drugs and particles. *Adv Drug Deliv Rev*. 2018;124:34-49. doi:10.1016/j.addr.2017.11.001

38. Xu J, Tao J, Wang J. Design and Application in Delivery System of Intranasal Antidepressants. *Front Bioeng Biotechnol*. 2020;8:626882. doi:10.3389/fbioe.2020.626882

39. Corsaro R, Lombardo R, Ghelardini C, et al. Development of Eudragit® Nanoparticles for Intranasal Drug Delivery: Preliminary Technological and Toxicological Evaluation. *Appl Sci*. 2022;12(5):2373. doi:10.3390/app12052373

40. Bonaccorso A, Cimino C, Manno DE, et al. Essential Oil-Loaded NLC for Potential Intranasal Administration. *Pharmaceutics*. 2021;13(8):1166. doi:10.3390/pharmaceutics13081166

41. Sakeena MHF, Elrashid SM, Munavvar AS, Azmin MN. Effects of Oil and Drug Concentrations on Droplets Size of Palm Oil Esters (POEs) Nanoemulsion. *J Oleo Sci*. 2011;60(4):155-158. doi:10.5650/jos.60.155

42. Pathak K. Mucoadhesion; A prerequisite or a constraint in nasal drug delivery? *Int J Pharm Investig*. 2011;1(2):62. doi:10.4103/2230-973X.82383

43. Carbone C, Martins-Gomes C, Caddeo C, et al. Mediterranean essential oils as precious matrix components and active ingredients of lipid nanoparticles. *Int J Pharm*. 2018;548(1):217-226. doi:10.1016/j.ijpharm.2018.06.064

44. Ekelund K, Östh K, Påhlstorp C, Björk E, Ulvenlund S, Johansson F. Correlation Between Epithelial Toxicity and Surfactant Structure as Derived From the Effects of Polyethyleneoxide Surfactants on Caco-2 Cell Monolayers and Pig Nasal Mucosa. *J Pharm Sci*. 2005;94(4):730-744. doi:10.1002/jps.20283

45. Kusumoto K ichi, Ishikawa T. Didodecyldimethylammonium bromide (DDAB) induces caspase-mediated apoptosis in human leukemia HL-60 cells. *J Controlled Release*. 2010;147(2):246-252. doi:10.1016/j.jconrel.2010.07.114

46. Shelar SB, Dey A, Gawali SL, et al. Spontaneous Formation of Cationic Vesicles in Aqueous DDAB-Lecithin Mixtures for Efficient Plasmid DNA Complexation and Gene Transfection. *ACS Appl Bio Mater*. 2021;4(8):6005-6015. doi:10.1021/acsabm.1c00165

47. Lafci Fahrioglu S, VanKampen N, Andaloro C. Anatomy, Head and Neck, Sinus Function and Development. In: *StatPearls*. StatPearls Publishing; 2023. Accessed May 16, 2023. http://www.ncbi.nlm.nih.gov/books/NBK532926/

48. Nease C, Sturm L. Nasal Anatomy. In: *Rhinoplasty*. Elsevier; 2023:7-15. doi:10.1016/B978-0-323-69775-0.00002-0

7 SORAFENIB REPURPOSING FOR OPHTHALMIC DELIVERY BY LIPID NANOPARTICLES: A PRELIMINARY STUDY

Angela Bonaccorso[1,†], Veronica Pepe[2,†], Cristina Zappulla[2], Cinzia Cimino[1], Angelo Pricoco[2], Giovanni Puglisi[1], Francesco Giuliano[2], Rosario Pignatello[1,3] and Claudia Carbone[1,3,*]

[1] Laboratory of Drug Delivery Technology, Department of Drug and Health Sciences, University of Catania, Viale A. Doria 6, 95125 Catania, Italy.

[2] Research, Preclinical Development and Patents, SIFI S.p.A., Lavinaio-Aci S. Antonio, 95025 Catania, Italy.

[3] NANO-i, Research Centre for Ocular Nanotechnology, University of Catania, Viale A. Doria 6, 95125 Catania, Italy.

[*] Corresponding author

[†] These authors contributed equally to this work.

Abstract: Uveal melanoma is the second most common melanoma and the most common intraocular malignant tumour of the eye. Among various treatments currently studied, Sorafenib was also proposed as a promising drug, often administered with other compounds in order to avoid resistance mechanisms. Despite its promising cellular activities, the use of Sorafenib by oral administration is limited by its severe side effects and the difficulty to reach the target. The encapsulation into drug delivery systems represents an interesting strategy to overcome these limits. In this study, different lipid nanoparticulate formulations were prepared and compared in order to select the most suitable for the encapsulation of Sorafenib. In particular, two solid lipids (Softisan or Suppocire) at different concentrations were used to produce solid lipid nanoparticles, demonstrating that higher amounts were able to achieve smaller particle sizes, higher homogeneity, and longer physical stability.

The selected formulations, which demonstrated to be biocompatible on Statens Seruminstitut Rabbit Cornea cells, were modified to improve their mucoadhesion, evaluating the effect of two monovalent cationic lipids with two lipophilic chains. Sorafenib encapsulation allowed obtaining a sustained and prolonged drug release, thus confirming the potential use of the developed strategy to topically administer Sorafenib in the treatment of uveal melanoma.

Keywords: nanomedicine; drug repurposing; Softisan 100; uveal melanoma; mucoadhesion; eye irritation test; ocular delivery

7.1 Introduction

Among the intraocular malignant tumours affecting the inner eye, the most common in adults is uveal melanoma (UM) [1]. UM represents the second most common melanoma after the cutaneous one – with a lifetime risk of 1 in 2500 and an incidence of 6 per million per year – but the incidence and biological implications are different [2]. An important risk factor is the presence of ocular lesions, while sunlight seems not to be involved in the occurring of this condition, as it is prevalent in people living in northern Europe than in the ones living in the South. Moreover, the pigmentation could have a protective function since a risk factor is having a lightly coloured iris [3].

Characteristic of this melanoma is the great ability to metastasise (since the occurrence of the primary tumour, metastasis appear in 5 years for 25% of patients and in 10 years for 34%), and the most affected organ is the liver (90%), with lungs and soft tissues following [4]. Mortality in the metastatic UM is about 50% in one year and it is greatly influenced by the progression of liver involvement [5].

Based on the experience with cutaneous melanomas, various systemic treatments have been investigated also for uveal one and clinical trials demonstrated a modest efficacy [6]. Combinations of new drugs are currently studied to verify their suitability in the treatment of UM; it is worth mentioning bortezomib in combination with celecoxib, prednisone, temozolomide, dacarbazine, anti-angiogenic agents such as bevacizumab, sunitinib, cetuximab, panitumumab, erlotinib, transtuzumab, or temsirolimus, MEK inhibitors or ipilimumab [3].

In addition to the mentioned drugs analysed for UM, also Sorafenib (SRF) was proposed, generally in combined treatment with paclitaxel, doxorubicin, and siRNA, in order to overcome resistance mechanisms [1–3,7,8]. SRF is a small hydrophobic molecular

inhibitor of several tyrosine protein kinases, which rapidly accelerates fibrosarcoma (RAF) kinases. SRF was already approved for advanced renal cell carcinoma (RCC), hepatocellular carcinoma (HCC), and advanced thyroid carcinoma [9]. SRF possesses the ability to inhibit Raf kinases within the mitogen-activated protein kinase (MAPK) pathway, which mediates cellular growth signals and is constitutively active in most UM tumours [7]. Additionally, it acts on vascular endothelial growth factor receptor (VEGFR) and platelet-derived growth factor receptor (PDGFR), causing the inhibition of tumour angiogenesis [10]. *In vitro*, these phenomena occur in a dose-dependent manner, showing good anti-tumoral properties: tests on a xenograft model (with UM cell line 92.1) also demonstrated SRF capability of inhibiting tumour growth and reducing metastases (33% without treatment vs. 60% with Sorafenib) [3]. Recently, Santonocito et al. demonstrated that a new nanostructured microemulsions system carrying 0.3% Sorafenib, administered as an ophthalmic formulation, is able to deliver effective amounts of Sorafenib to the retina, reducing proinflammatory and proangiogenic mediators in reliable models of proliferative retinopathies [11].

Despite all the promising results, including phase II clinical trial with SRF monotherapy in metastatic UM [8], its clinical use is limited due to its severe side effects (diarrhoea, hand-foot skin reaction, alopecia, anorexia, weight loss, and abdominal pain [10]) consequent to oral administration [12].

Furthermore, the potential application of SRF in the treatment of UM needs to face the intrinsic difficulty of the target site, which is not easy to achieve in the case of poorly water-soluble drugs [13]. In fact, reaching the eye, especially the inner part, is a challenge both through topical and systemic administration. Topical administration is limited by eye physiological barriers, such as the cornea, which limit the access of xenobiotics [14], but also by some protection mechanisms, like blinking, tearing, and drainage, which promote a quick clearance of the drug [15]. On the other hand, it is equally difficult to make a drug reach the eye from the inside, due to the blood-aqueous barrier, which works similarly to the blood-brain barrier, preventing drug diffusion from blood to retina, through the intervention of uveal capillary endothelia and ciliary epithelia. Because of all these mechanisms, the bioavailability of drugs in the eye is poor, with an absorbed dose less than 3-5% of that administered [15].

The drawbacks related to ocular treatments could be overcome through the encapsulation of drugs into nano-sized carriers, which provide a prolonged and controlled release, the possibility to reach the target site and a longer residence time enhancing corneal permeation [16].

In order to exploit SRF potentiality, different nanoencapsulation strategies have been investigated, including liquid crystalline, lipid, and polymeric nanoparticles [10], demonstrating the possibility to protect SRF from inactivation with a considerable increase of its water solubility. Among the different nanoparticles, lipid ones have been demonstrated to be suitable for ocular delivery since they are highly biocompatible [14] and their lipid components are able to interact with the outside lipid layer of the tear, promoting longer retention thus acting as a depot [15]. Particularly, solid lipid nanoparticles (SLN), but also nanostructured lipid carriers (NLC), represent promising strategies in ocular delivery since they are able to incorporate a great amount of drug (up to 90%), sustain a prolonged residence in the precorneal area and successfully encapsulate lipophilic molecules [13–15].

The aim of this work was the development of SRF-SLN for the potential treatment of UM. As a quali-quantitative preliminary study, two solid lipids – Softisan or Suppocire – were analysed at different concentrations and the obtained systems were characterised through Photon Correlation Spectroscopy (PCS) to determine their mean size (Zave), polydispersity (PDI) and zeta potential (ZP); also, stability over time was exploited by Turbiscan® AG Station. *In vitro* SLN cytocompatibility was assessed on Statens Seruminstitut Rabbit Cornea (SIRC) cells using the Short Time Repeated Exposure (S.T.R.E.) protocol. In order to assess the suitability of the system for topical delivery of SRF to the posterior segment of the eye, mucoadhesive properties were evaluated on the selected SLN, optimised by the addition of two different positively charged coating layers: the cationic lipids didodecyldimethylammonium bromide (DDAB) or dioleoyl-trimethylammonium-propane (DOTAP) chloride. The optimised formulation was selected for the delivery of SRF, whose release profile was investigated.

7.2 Materials and Methods

7.2.1 Materials

Suppocire NB (C10-C18 Triglycerides) was obtained from Gattefossè and Softisan 100 (Hydrogenated Coco-Glycerides) was kindly provided by IOI Oleo (Hamburg, Germany GmbH). Tegin O (Gliceryl Monooleate) was purchased from ACEF (Piacenza, Italy). Didecyldimethylammonium bromide (DDAB), Tween® 80 (Polysorbate 80), N-[1-(2,3-Dioleoyloxy)propyl]-N,N,N-trimethylammonium chloride (DOTAP), Potassium phosphate monobasic and Phosphate buffered saline were purchased from Sigma Aldrich Co (St. Louis, MO, USA). Sorafenib tosylate (SRF) was supplied from Hetero Labs

Limited (Talengana, India). Sodium bicarbonate, all LC grade solvents used for high-performance liquid chromatography (HPLC) and Millex® syringe filters (PP, PES, and PVDF pore size 0.22 μm, 33 mm) were purchased from Merck (Darmstadt, Germany). Regenerated cellulose membranes (Spectra/Por CE; Mol. Wet. Cutoff 3000) were supplied by Spectrum (Los Angeles, CA, USA).

Statens Seruminstitut Rabbit Cornea (SIRC) cells were obtained from LGC Standards S.r.l. (Milan, Italy). Basal Medium Eagle (BME), gentamicin, penicillin-streptomycin, L-glutamine (L-glu), Trypsin–EDTA, and Fetal Bovine Serum (FBS) were from Lonza (Euroclone S.p.A., Milan, Italy). Reagent for MTT assay (3-(4,5-dimethilthiazol-2-yl)-2,5-dipheniltetrazolium bromide), Mucin (mucin from porcine stomach type II), and sodium chloride were purchased from Sigma-Aldrich S.r.l. (Milan, Italy). Dimethyl sulfoxide (DMSO), calcium chloride dihydrate, and potassium chloride (of analytical grade) were purchased from VWR Chemicals (Milan, Italy). Benzalkonium chloride (BAK) 50% was obtained from Novo Nordisk Pharmatech A/S (Køge, Denmark).

7.2.2 Nanoparticles Preparation

A low-energy organic solvent-free phase inversion process (PIT method) was used for the preparation of the unloaded and drug-loaded SLN [17]. Based on previous studies, Tween 80 (6%, w/v) and Tegin O (3% w/v) were selected as surfactants in combination with different amounts (5, 7, 8 or 9%, w/v) of Softisan (SLN A5, A7, A8, A9) or Suppocire NB (SLN B5, B7, B8, B9), selected as solid lipids. SRF was added at different concentrations (0.8 or 1.0%, w/v) to the melted oily phase to prepare a drug-loaded SLN. The aqueous and the oil phases were separately heated until ~80 °C. The aqueous phase was added drop by drop to the lipid phase, at constant temperature and stirring speed (~650 rpm). The mixture was slowly cooled to room temperature under continuous stirring for 2 h. The selected formulation was modified adding to the melted oily phase two different positively charged lipids DOTAP or DDAB (0.15%, w/v), thus obtaining SLN A8-DP and A8-DB, respectively. In order to purify the colloidal suspensions from the excess of surfactants and non-encapsulated drug, SLN were centrifuged at 12,000 rpm for 1 h at 4 °C, using an ultracentrifuge (SL16R Centrifuge, Thermo Scientific, Rodano, Italy) and the pellet was redispersed in PBS.

7.2.3 Photon Correlation Spectroscopy (PCS)

The mean particles diameter (Zave), polydispersity index (PDI), and zeta potential (ZP) values of all prepared SLN were determined by Photon Correlation Spectroscopy (PCS) using a Zetasizer Nano ZS90 (Malvern Instruments Ltd., Malvern, England), as previously

reported [17]. Samples (50 μL) were diluted in 1 mL of ultra-purified water before measurements. Each formulation was prepared six times, and each measure is the mean value of at least three measurements ± standard deviation (SD).

7.2.4 Sterilisation by Filtration

All samples were sterilised by filtration using three different types of hydrophilic membranes of 0.22 μm pore diameter: polypropylene (PP), polyethersulfone (PES) and polyvinylidene fluoride (PVDF) (Whatman, VWR Chemicals, Milan, Italy). SLN were filtered and, when possible, the obtained sterile formulations were analysed by PCS to verify particles diameter.

7.2.5 Osmolality and pH

Osmolality values of the prepared SLN were determined by an osmometer (Osmomat 3000, Gonotec, Berlin, Germany), previously calibrated with ultra-purified water and physiological solution. A pH meter (Mettler Toledo, Milan, Italy) was used to measure the pH values of the SLN.

7.2.6 Turbiscan® AG Station

A Turbiscan® Ageing Station (TAGS, Formulaction, L'Union, France) optical analyser was used to investigate the physical stability of unloaded-SLN suspensions. The equipment was composed of the ageing station, which allows the storage of samples in three thermo-regulated blocks [18]. The detection was operated using a pulsed near-infrared light source (λ = 880 nm), which sends information to two synchronous transmissions (T) and backscattering (BS) detectors: in particular, T detector receives the light crossing the sample at 180° from the incident beam, while the BS detector receives the light scattered backwards by the sample at 45° from the incident beam. This detection system produces 1625 acquisitions for each measurement, since it scans the entire height of the sample cell (65 mm longitude), acquiring T and BS each 40 μm. Using this instrument, it is possible to evaluate the occurrence of instability phenomena, such as particles migration or aggregation, in colloidal suspensions (liposomes, lipids, polymeric nanoparticles [18–20]. In this experiment, the cylindrical glass cell contained 20 mL of each unloaded formulation, and the storage temperatures of the three blocks were 25, 40, and 60 °C. The stability of the samples was measured through the analysis of the variation of transmission (ΔT).

7.2.7 Cell Viability Studies

Cytocompatibility of SLN was evaluated in Statens Seruminstitut Rabbit Cornea (SIRC) cells. SIRC cells were grown in a humidified 5% CO_2 atmosphere at 37 °C in a complete culture medium (CCM), made of BME containing 10% FBS, 100 U/mL of penicillin-streptomycin, 10 mg/mL gentamicin, and 2 mM L-glutamine. Each well of a 96-well tissue culture plate was seeded with 40,000 cells in 100 μL of CCM. Cells were allowed to grow at 37 °C, 5% CO_2 until subconfluence (70–90%), and then repeatedly exposed (6×) for 10 min to 100 μL of 5 mg/mL test item solutions prepared using sterile culture medium consisting of FBS-free BME. In detail, test items SLN A8, SLN B8, and SLN B9 were prepared by ultracentrifugation and resuspended in a neutral isotonic PBS (300 mOsm/kg, pH 7.2). A concentrated suspension of each nanostructured system was obtained and diluted in FBS-free BME to be successively tested on cells at a final concentration of 5 mg/mL.

Cells were also exposed to the negative control (sterile culture medium consisting of FBS-free BME, CTRL−) and positive control (0.01% BAK, CTRL+) for cytotoxicity evaluation. All samples were tested in triplicates and on two different experiment days. Treatments were removed after 10 min of exposure and all cells were re-fed with CCM.

Before re-feeding, only wells included in the "wash" protocol were washed once with BME (free of FBS, antibiotics, and L-glu). The same procedure was repeated six times at intervals of 1.5 h [Short Time Repeated Exposure (S.T.R.E.)]. At the end of the repeated exposures, cells were incubated in standard conditions, and 24 h later, the medium was removed and replaced with 100 μL of MTT solution (0.2 mg MTT/mL of CCM). Following a 30 min incubation, MTT formazan was extracted with 100 μL of 100% DMSO. The optical density of the samples obtained (O.D.) was read at 570 nm in a microplate spectrophotometer (SPECTRAFluor Plus, Tecan, Männedorf, Switzerland). Cell viability was calculated as a percentage of the negative control.

7.2.8 Encapsulation Efficiency and In Vitro Drug Release

The amount of SRF encapsulated in the lipid matrix of SLN A8 was determined after centrifugation of the sample. The pellet was diluted in tetrahydrofuran (THF) and vortexed (Heidolph Reax 2000, VWR, Milan, Italy). The amount of SRF was directly determined by using HPLC (see Section 2.9) without interference from the other formulation components. The encapsulation efficiency (EE%) was calculated from the ratio between the amount entrapped inside the nanoparticles and the total amount of drug used for their preparation (Equation (1)).

$$EE\% = \frac{\text{amount of entrapped drug}}{\text{total amount of drug used}} \times 100$$

Franz-type diffusion cells were used to analyse SRF *in vitro* release from SLN. Firstly, the moistening of the 0.75 cm^2 regenerated cellulose membranes (Spectra/Por CE; Mol. Weight Cut-off 3.5 kDa) was operated through the immersion in physiological solution for 1 h at room temperature. Then, the receptor compartment of cells was filled with 4.5 mL of a mixture of the physiological solution and ethanol (50:50 v/v), thermostated at 35 ± 2 °C, and constantly stirred at 600 rpm. Despite the lack of bio relevance, 50% ethanol was mandatory to achieve SRF sink conditions in release studies, enabling its solubility, detection, and quantification. In the donor compartment, 500 μL of SRF-SLN was applied. Withdrawn extracted by receptor compartments (200 μL) were performed at scheduled time intervals (0, 1, 2, 3, 4, 5, 6, 24, 48, 72 h) and replaced with an equal volume of fresh receiving fluid equilibrated to 35 °C. This procedure was carried out at least three times for each sample. Finally, SRF contents were measured using HPLC (as described in Section 2.9).

7.2.9 High-Performance Liquid Chromatography (HPLC) Analyses

An Agilent model 1100 liquid chromatograph (Agilent, Santa Clara, CA, USA), equipped with an autosampler Agilent model 1100 and Chemstation Agilent software for data elaboration, and a reversed-phase C18 column (Luna 100, 5 μm, 150 × 4.6 mm Phenomenex, Santa Clara, CA, USA) was used to perform high-performance liquid chromatography-UV (HPLC-UV) analysis, to measure SRF contents. As a mobile phase, a mixture of 20 mM of potassium dihydrogen-phosphate aqueous solution and acetonitrile (35:65 v/v) was used, and the column flow rate was set at 1 mL/min. The detection of the effluent was conducted at $\lambda = 260$ nm, showing a retention time of 8 min. This method was verified according to International Conference on Harmonisation (ICH) guidelines (ICH Q2 (R1) Validation of analytical procedures: text and methodology). A calibration curve was produced analysing the absorption of known concentration of SRF in THF, and the obtained linear regression value was: R2 = 0.99987. Known amounts of SRF were spiked on SLN formulation and dissolved in THF, the absorption was determined for all solutions. No interference of the other formulation components was observed.

7.2.10 Stability and Interaction of Nanoparticles in the Presence of Ocular Mucus Component

7.2.10.1 Physico-Chemical Evaluation

Optimisation of SLN A8 in terms of mucoadhesive properties was operated adding 0.15% w/v of DDAB (A8-DB) or DOTAP (A8-DP) to the lipid phase during nanoparticles preparation. The obtained formulations were incubated with mucin dispersion (1:1 v/v) in simulated tear fluid (STF: NaCl 0.68 g, NaHCO3 0.22 g, CaCl2·2H2O 0.008 g, KCl 0.14 g, and distilled deionised water to 100 mL) at 35 °C, in order to analyse the stability and interaction of nanoparticles with mucin. Mean size, PDI, and zeta potential (ZP) of the nanoparticles/mucin dispersions were measured by Zetasizer NanoZS90 at scheduled time intervals (0, 1, and 24 h).

7.2.10.2 Mucoadhesive Strength

Positively charged nanoparticles (A8-DB and A8-DP) were evaluated regarding their mucoadhesive strength based on the interaction with the negatively charged mucin. Briefly, equal volumes of mucin (0.1 w/v in STF) and nanoparticles were stirred for 15 min at room temperature and incubated for 1 and 24 h at 35 °C, and then centrifuged at 13,000 rpm (ThermoScientificTM SL16R, ThermoFisher Scientific, Waltham, MA, USA), for 1 h at 6 °C. A UV-VIS spectrophotometer (UH5300 UV-Visible Double-Beam Spectrophotometer, Hitachi Europe, Milan, Italy) was used to quantify the amount of free mucin in the supernatant at 228 nm. The calibration curve for the quantitative evaluation of mucin was linear in the following range: 1-0.06 mg/mL ($R^2 = 0.9891$). The mucin-binding efficiency (%), expressing the mucoadhesive strength of the nanoparticles, was calculated according to Equation (2):

$$\text{Mucin binding efficiency } \% = \frac{\text{total amount of mucin} - \text{free amount of mucin}}{\text{total amount of mucin}} \times 100$$

7.2.11 Statistical Analysis

All data from PCS are reported as mean values ± SD. Differences, analysed by two- sample hypothesis testing (t-test), using Origin Software (version 8.5.1), were considered statistically significant for $p < 0.05$. Cell viability data were analysed in Prism 6 (Graph-Pad Inc., La Jolla, CA, USA) by one-sample t-test (treatment vs. cut-off) assuming a cut-off value for cytotoxicity of 50% as per ECVAM protocol DB-ALM n° 17: MTT Assay (EURL ECVAM Database on Alternative Methods to Animal Experimentation. Available online: http://cidportal.jrc.ec.europa.eu/ftp/jrc-opendata/EURL-ECVAM/datasets/ DBALM/LATEST/online/DBALM_docs/17_P_MTT%20Assay.pdf, accessed on 5

___

October 2021). For the statistical analysis of nanoparticles during stability study in mucin dispersion (STF), two-way ANOVA was performed. Multiple comparisons were performed according to Sidak's multiple comparisons test. Analyses were performed using Prism 8 (GraphPad Software, Inc., La Jolla, CA, USA, version 8.0.2, last accession date 19 October 2021), applying $p < 0.05$ as the minimum level of significance.

7.3 Results and Discussion

7.3.1 Physicochemical Characterisation

As reported in the literature, nanoparticle size strongly affects drug distribution and residence time in the eye's structure, with nanoparticles smaller than 200 nm usually showing a burst release followed by a gradual release profile in vitro and a longer half-life, compared to smaller nanoparticles characterised by a longer half-life and a sustained drug release [21,22]. In order to obtain homogeneous small-sized SLN for potential ophthalmic application, a preliminary quali-quantitative screening was developed on two different solid lipids, Softisan (A) and Suppocire (B), at different concentrations (5, 7, 8, 9 % w/v). The eco-friendly PIT method, reported in the literature as an easy method with a low impact on the environment [17], was used as a lab-scale preparation procedure. The obtained results showed that the amount of the selected lipids strongly affected nanoparticles size. Notably, none of the lipids used at 5 or 7% w/v produced well-structured SLN, since the lowest concentration (5% w/v) produced particles with a high degree of heterogeneity in size (PDI >> 0.2), probably due to an excess of surfactants, compared to the amount of the solid lipid (Figure 1). The use of 7% w/v of lipid, in both cases, led to the formation of heterogeneous particles, characterised by the presence of different peaks of size distribution, as revealed by the multiple peaks of intensity (Supplementary Figure S1).
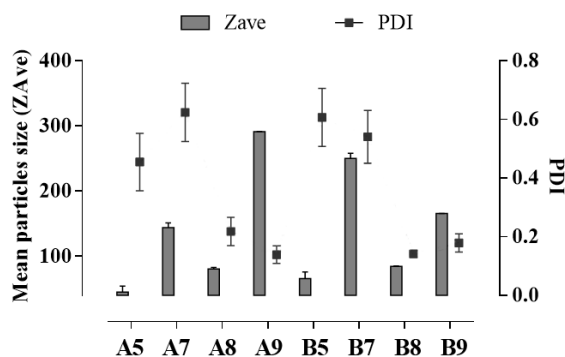

Figure 1. Mean particle size (Z-Ave, (nm)) and polydispersity index (PDI, (a.u.)) of SLN prepared with different amounts of Softisan (A5, A7, A8, and A9) or Suppocire (B5, B7, B8, and B9). Each measurement represents the mean value ± standard deviation (SD), n = 6.

___

Conversely, using higher amounts of Suppocire in SLN B8 and B9 (8 or 9% w/v) induced a better organisation of the raw materials at the interface, with the formation of smaller and more homogeneous particles, with a mean diameter below 200 nm (Figure 1). A different behaviour was observed when using 9% w/v Softisan (SLN A9), whose very bulky chemical structure led to the formation of larger nanoparticles with sizes greater than 300 nm, which is not suitable for the ophthalmic application [21–23]. Contrarily, SLN A8 showed homogeneous particles (PDI < 0.3) in the nanometer range (<100 nm), therefore appropriate for the topical treatment of UM. Therefore, according to the acquired data, SLN A5, A7, A9, B5, and B7 were excluded from further analysis while SLN A8, B8, and B9 were deeper characterised.

The obtained SLN showed pH values of around 6.5 ± 0.2 with an osmolality of 298 ± 0.10 mOsm/kg, without significant differences due to the type and amount of the used lipid. Since the ocular tissue can tolerate a pH value ranging from 4 to 9, and the osmolality of human tears is in the range of 280-300 mOsm/kg (although an osmolality between 200 and 450 mOsm/kg can be tolerated); therefore, the produced SLN were compatible with the tears film.

Since sterilisation is a mandatory prerequisite for all ophthalmic formulations, a preliminary study was performed by filtration [24]. In order to select the most suitable material for the lipid nanocarriers used in this study, the sterilisation was carried out using syringe filters with three different types of membranes: polypropylene (PP), polyethylene sulfone (PES), and polyvinylidene fluoride (PVDF), with average pore diameter equal to 0.22 μm. The experimental results showed that PP and PES filters are not suitable for the filtration of the SLN, as they retain the nanoparticles (data not shown) without the possibility to obtain a filtrated suspension. The use of PVDF filters, on the other hand, allowed the filtration of all SLN, regardless of the quali-quantitative composition of the lipid matrix. From the results of PCS analysis before and after filtration, it is possible to state that all systems maintain their initial characteristics unaltered (Table 1). Therefore, the produced SLN can be easily sterilised using PVDF membrane filters, characterised by great mechanical strength and dimensional stability (no deformation under weight), with better chemical stability, almost 10 times higher compared to PP and PES filters [25–27].

***Table 1**. Mean particles size (Z-Ave, (nm)) and polydispersity index (PDI, (a.u.)) ± standard deviation (SD) of SLN before and after filtration by PVDF membrane filters of 0.22 µm. Data reported are the mean of six different experiments. * Significance for p > 0.05.*

FILTRATION	SLN	Z-Ave ± S.D. (nm)	PDI ± S.D.
Not filtered	A8	96.63 ± 2.05	0.177 ± 0.020
	B8	70.67 ± 2.08	0.126 ± 0.003
	B9	123.5 ± 1.36	0.139 ± 0.012
Filtered (PVDF)	A8	95.53 ± 0.63	0.197 ± 0.080
	B8	72.03 ± 0.46	0.178 ± 0.008*
	B9	117.18 ± 0.82	0.165 ± 0.020

The physical stability of SLN A8, B8, and B9, a mandatory requirement for their potential industrial application [28], was investigated by Turbiscan® AGS storing samples at room temperature (25 ± 2 °C) for 30 days (Figure 2). As shown in the graph of transmission variations (ΔT) reported in Figure 2a, SLN B8 showed important instability phenomena related to particles aggregation, highlighted by ΔT variation in the middle of the graph greater than 20%. Conversely, SLN A8 and SLN B9 showed a potential long-term physical stability, as confirmed by the absence of transmission variation in sample A8, or by the presence of insignificant transmission variation (ΔT < 20%) in SLN B9. TSI values confirmed the stability decreased in the following scale: A8 ≥ B9 >> B8 (Figure 2b).
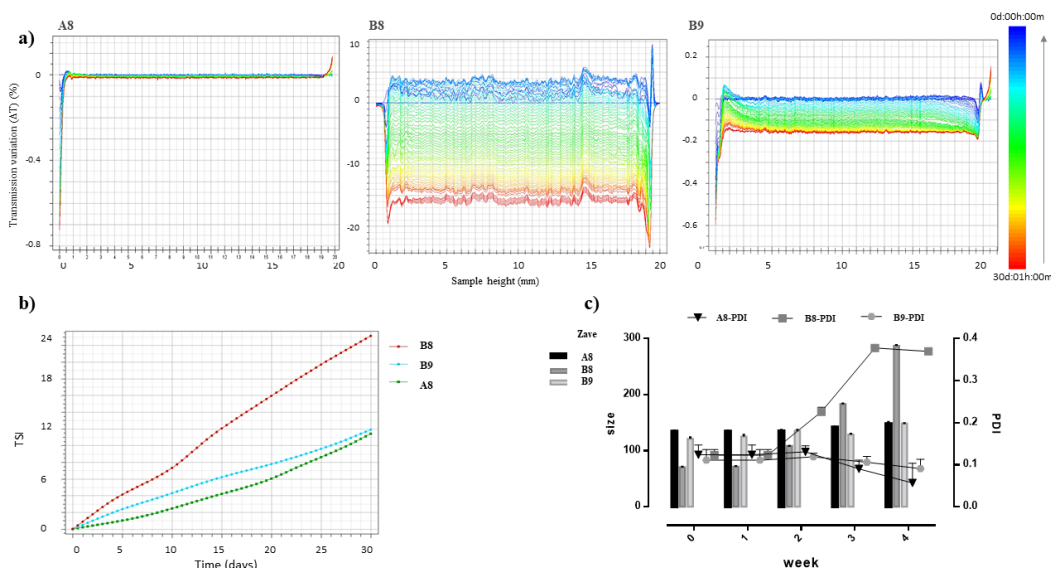
***Figure 2**. (a) Transmission profiles (ΔT) of SLN A8, B8 and B9 stored in Turbiscan® for 30 days at 25.0 ± 1.0 °C. Data are reported as a function of time in the range 0-30 days of sample height (0 to 20 mm); (b) Destabilisation kinetics in terms of evolution of Turbiscan® Stability Index (TSI) of samples stored in the instrument at 25.0 ± 1.0 °C for 30 days; (c) Mean particle size (Z-Ave, [nm]) and polydispersity index (PDI, [a.u.]) of SLN A8, B8 and B9 stored in Turbiscan® and measured by PCS after 1, 2, 3 and 4 weeks. Each measurement represents the mean value ± standard deviation (SD), n = 6.*

It is worth noting that the obtained stability results were in perfect agreement with PCS measurements of samples stored in Turbiscan® and analysed at different time intervals (1, 2, 3, or 4 weeks). The obtained data confirmed that SLN B8 underwent significant instability phenomena ($p < 0.05$) due to particle aggregation, whose size and PDI values increased already after 2 weeks of storage (Figure 2c, Supplementary Table S1). PCS analysis of stored samples also confirmed that SLN A8 represents the ideal formulation, among those prepared, since after 4 weeks of storage, at the 0.05 level of significance, the difference between population means was not significantly different for mean size and PDI values (Supplementary Table S1). The different behaviours of Suppocire and Softisan could be attributed to their different chemical structure and properties. Suppocire NB is a mixture of mono-, di-, and triglyceride esters of fatty acids (C10 to C18), with an intermediate melting point (35-39 °C). It rapidly recrystallises in the cooling phase of SLN production, thus determining the formation of smaller particles with harder solid core compared to the hydrogenated coco-glycerides (Softisan 100), whose lower melting range (33.5-35.5 °C) is probably responsible for the greater values of mean size at the highest concentration.

7.3.2 *In Vitro Characterization*

In order to evaluate the potential ophthalmic application of the developed formulations, the cytocompatibility profile of SLN A8, B8 and B9 was evaluated on the SIRC cell line using the method described above (see Section 2.7). Experimental results showed that BAK 0.01%, used as a positive control (CTRL+), induced significant cell mortality by 80-90%, causing the permanent loss of cell viability regardless of the "wash" or "no wash" condition (Figure 3). BAK was selected as CTRL+, considering that it is the major preservative component currently used in eye drops at concentrations even higher than 0.01% (i.e., 0.02%) [29,30]. SLN B8 produced statistically significant cytotoxic effects both in "wash" and "no wash" conditions, inducing cell mortality by 56 ± 1.09% and 78 ± 0.98%, respectively (Figure 3). Conversely, SLN A8 and SLN B9 were found to cause no significant effect in the "no wash" condition (Figure 3). Noteworthy, SLN B9, with particles of about 150 nm, showed a better cytocompatibility profile compared to smaller nanoparticles, as reported in Figure 3.

Consistently, the same systems (i.e., SLN A8 and SLN B9) were found to be endowed with particularly favourable profiles when tested in the "wash" protocol (Figure 3). Indeed, SLN A8 prepared using Softisan showed a more favourable profile compared to Suppocire NB, probably due to the lowest melting temperature of Softisan, which could provide a softer and more flexible structure, that is more favourable in cell interactions [27]. It is worth

_____

noting that the "wash" protocol should be considered the most predictive condition of potential corneal cytotoxic effects arising from administration to the surface of the eye. Indeed, concentrations of formulations/drug delivery systems on the corneal surface are strongly affected by several factors, including dilution, blinking, and drainage, ultimately affecting their overall pre-corneal retention time [31]. More importantly, SLN A8 and B9 showed a promising cytocompatibility profile even when tested with the "no wash" protocol, which is a very extreme testing condition that may prove to be inappropriate for extrapolations to the ocular environment posing issues of potential false positives for cytotoxic effects.

Indeed, standard cytotoxicity protocols, DB-ALM Protocol n° 17, prescribe 24 h of cell exposure to test items [32] and this exposure time is rather extreme if compared to eye drops residence time on the human ocular surface of only a few minutes [31]. Certainly, this approach is most likely overestimating true cytotoxic effects. Therefore, we developed the Short Time Repeated Exposure (S.T.R.E.) test using SIRC cells as an alternative method for assessing eye irritation merging notion from both the DB-ALM Protocol n° 17 and the short-time exposure test by Takahashi et al. to better mimic the real situation after administration of drugs to the ocular surface [33]. Thus, the protocol entails exposing the target cells to test items for 5 min for a total of six repetitions, summing up to 30 min of total exposure in a 12 h interval. Hence, we have simulated both realistic corneal residence times and repeated administration courses typically associated with ophthalmic eye drops treatments.
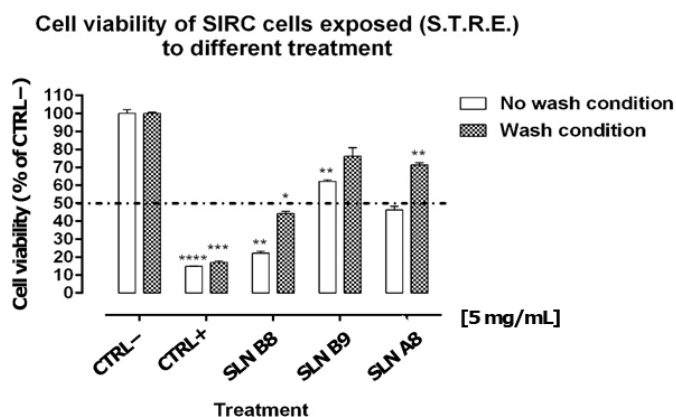

Figure 3. Cell viability of SIRC cells repeatedly exposed (6×) for 10 min with or without wash and with a step of 1.5 h between the repeated exposures (Short Time Repeated Exposure (S.T.R.E.)) to control formulations or delivery systems SLN B8, SLN B9, and SLN A8 diluted at 5 mg/mL. Dotted line is placed at 50% representing the cut-off value to determine cytotoxicity potential according to ECVAM protocol DB-ALM n° 17. Data represent the mean ± s.e.m. of three replicates for each condition. $^{*}p \leq 0.05$; $^{**}p \leq 0.01$; $^{***}p \leq 0.001$; $^{****}p \leq 0.0001$. One sample t-test vs. cut-off 50%.

_____

In order to improve the retention time after topical administration, SLN A8 was optimized with the addition of a positively charged lipid, and the effect of two monovalent cationic lipids with two lipophilic chains was investigated by mucoadhesive studies. In particular, DOTAP was selected as an FDA-approved material and, in order to reduce the cost of the final product, its effect was compared to that of DDAB, selected for its lowest cost and ability to provide a coating layer on lipid nanoparticles [34,35].

The addition of DDAB (A8-DB) or DOTAP (A8-DP) as coating layer did not significantly modify mean particles size and PDI values of the SLN A8 while, as expected, ZP values turned from negative to highly positive values (+20 mV). The stability of colloidal particles in biological fluids containing relevant levels of proteins is a crucial issue. Currently, it is broadly accepted that the size of the particles plays an important role in their ability to interact with cells and in their transport through the mucus layer, such as that of the ocular mucosa [36]. Surprisingly, despite the importance of the size, there are very few articles on the stability of colloidal particles in biological fluids. For example, Tobìo et al. showed that poly (lactic acid) nanoparticles aggregated significantly upon contact with simulated gastric fluids [37]. Similarly, it was observed that poly-ε-caprolactone nanocapsules suffered an immediate aggregation process upon their incubation with lysomes [38].

In order to investigate nanoparticles behaviour after ophthalmic administration, experiments were performed in presence of mucin, which is one of the main components of the ocular mucus layer, dispersed in STF, thus investigating the effect of proteins and ions on the stability and the mucoadhesive strength of nanoparticles intended for ocular delivery. Experiments were performed comparing the effects of the two different coating lipids (DDAB and DOTAP) to the uncoated negatively charged SLN A8.

As reported in Figure 4, statistically significant variations in particle mean size can be observed for nanoparticles/mucin dispersions over time compared to the A8, A8- DB, and A8-DP controls, with the following trend A8-DB > A8-DP > A8. This result suggested that the main interaction was established between A8-DB and mucin at all time points investigated, followed by A8-DP and as expected, the negatively charged SLN A8. Looking carefully at these results, we can observe that the increase in particle mean size for nanoparticles incubated in mucin dispersion is associated with PDI values ≤ 0.275 indicating the absence of aggregation and/or precipitation phenomena, thus revealing good stability in a simulated biological fluid (STF with mucin).
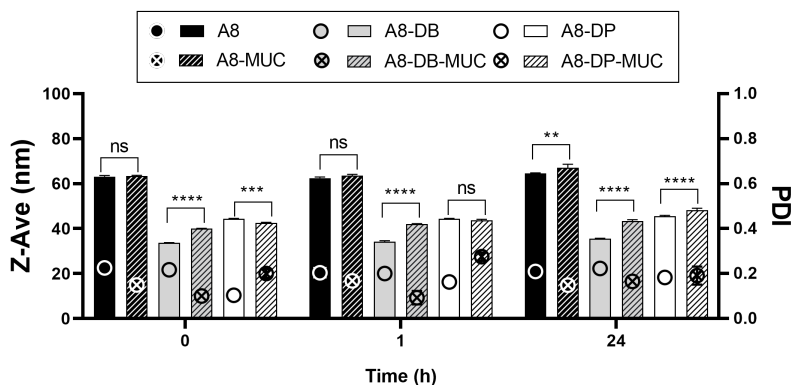
Figure 4. Nanoparticles mean size (Z-Ave, bars) and PDI (symbols) before (A8, A8-DB, A8-DP) and after (A8-MUC; A8-DB-MUC; A8-DP-MUC) 1 and 24 h of incubation with mucin at 35 °C. Significance was set as $p > 0.05$; $^{**}p \leq 0.01$; $^{***}p \leq 0.001$; $^{****}p \leq 0.0001$; ns – not significant.

ZP measurement is a common method to investigate the mucoadhesive properties of several biopolymers [39] and can be also used to evaluate the biophysical interactions of lipid nanoparticles with mucin [40], which has a negative charge. For this reason, the superficial charge of nanoparticles is an important parameter since repulsion between nanoparticles and mucin occurs with negatively charged systems while there will be an attraction to the negatively charged mucin and the positive particles [40]. Mucin has a negative charge (approximately -7 mV), thus the positive surface charges of A8-DB and A8-DP formulations are expected to strongly interact [41]. Accordingly, positive ZP values of A8-DB and A8-DP were inverted to negative values after incubation with mucin (Figure 5), suggesting that strong interactions between mucin and nanoparticles occurred, thus confirming our previous results (Figure 4).
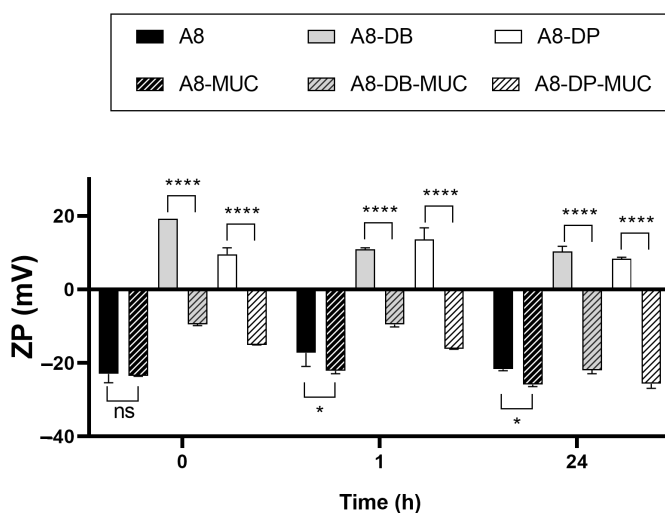
Figure 5. Nanoparticles zeta potential (ZP) before (A8, A8-DB, A8-DP) and after (A8-MUC; A8-DB- MUC; A8-DP-MUC) 1 and 24 h of incubation with mucin at 35 °C. Significance was set as $p > 0.05$; $^{*}p \leq 0.05$; $^{****}p \leq 0.0001$; ns – not significant.

The electrostatic interaction is the most expectable mucoadhesive mechanism. The decrease in ZP for both nanoparticles before and after incubation with mucin supports this observation. The occurrence of ionic interactions caused a decrease in the ZP value because mucin interacted with the positively charged surface layer of nanoparticles, neutralizing the positive charges [42]. Contrarily, the ZP of SLN A8 remained almost unchanged in the presence of mucin, or decreased furtherly and reached a relatively large negative value as a result of weaker interactions [19] and the absence of bridging effect [16], since no or low change ([**]$p \leq 0.01$) in particle size was observed (Figure 5). Based on these findings, the mucoadhesive strength of positively charged nanoparticles was furtherly investigated. Both samples (A8-DB and A8-DP) exhibited relevant mucin-binding efficiency concomitant with the conversion in the ZP values, as presented in Figure 5. The sample A8-DB possessed the maximum mucin-binding efficiency (%) (99.2 ± 1.08%), compared to A8-DP (61.5 ± 2.34%). These results highlighted a different ability of the two cationic lipids to interact with mucin, with DDAB having greater mucoadhesive properties compared to DOTAP. This effect could be related to their different chemical structure, also affecting their physical state at room temperature (DDAB exists as gel while DOTAP as liquid crystalline): both aliphatic chains of DDAB are saturated, unlike DOTAP, whose chains present a double bond in the C9 position [43]. The mucoadhesive properties are correlated with the ionic interaction between the monovalent cationic lipid and the negatively charged sialic acid groups of eye mucin, with subsequent formation of non-covalent bonds [42]. Such interaction promotes the ocular residence time and cellular uptake of nanoparticles, which is essential for effective mucosal delivery of therapeutics, enhancing drug bioavailability, through the increased rate of absorption, and drug targeting.

Based on the obtained results, considering the overall behaviour, SLN A8-DB was selected for the encapsulation of SRF, a drug approved for the treatment of kidney cancer and advanced liver cancer [44–50] that has been recently investigated for the potential treatment of uveal melanoma and retinal neovascular diseases [2,3,7,8,11,51–53].

As shown in Table 2, the addition of 0.8 or 1.0 % w/v of SRF to A8 did not modify the main properties of the SLN in terms of mean particle size and homogeneity.

Table 2. Mean particles size (Z-Ave, [nm]) and polydispersity index (PDI, (a.u.)), pH, osmolality (mOsm/Kg) and encapsulation efficiency (EE%) ± standard deviation (SD) of SLN A8 loaded with 0.8 or 1.0% w/v of Sorafenib (SRF). Each value is the average of six different replicates ± standard deviation (SD).

SLN	Z-Ave ± S.D. (nm)	PDI ± S.D.	pH ± S.D.	Osmolality (mOsm/Kg) ± S.D.	EE% ± S.D.
A8-SRF 0.8%	127.85 ± 1.50	0.215 ± 0.014	6.33 ± 0.85	308 ± 2	75.0 ± 2.1
A8-SRF 1%	150.12 ± 1.85	0.180 ± 0.013	6.25 ± 0.72	302 ± 3	74.5 ± 2.8

Both SRF-loaded nanosuspensions showed pH and osmolality values compatible with the eye and high value of EE%, corresponding to 74.5 and 75% for A8-SRF 1% and A8-SRF 0.8%, respectively. This result is consistent with literature findings investigating SRF encapsulation into lipid nanoparticles for the treatment of liver cancer, with lower EE% values found in our study probably related to the smallest size of SLN A8 nanoparticles [13,54–56].

The cumulative release rate was calculated according to the released SRF amount compared to the total SRF amount. Figure 6 shows the release profile of SRF from SLN A8 loaded with 0.8 or 1.0 % w/v and SRF-suspension *in vitro*. Interestingly, SLN A8 at both concentrations provided a controlled prolonged release of the encapsulated drug, with less than 25% of SRF released after 72 h (Figure 6). The slow release may be attributed to the good encapsulation and surface coating by the lipid layer [54,57]. These results are encouraging for the potential ophthalmic application and in accordance with previous findings not only related to lipid nanoparticles [58–60] but also reported for polymeric nanoparticles, which have been demonstrated to provide sustained release for up to 50 days when injected intravitreally in rabbits [61].
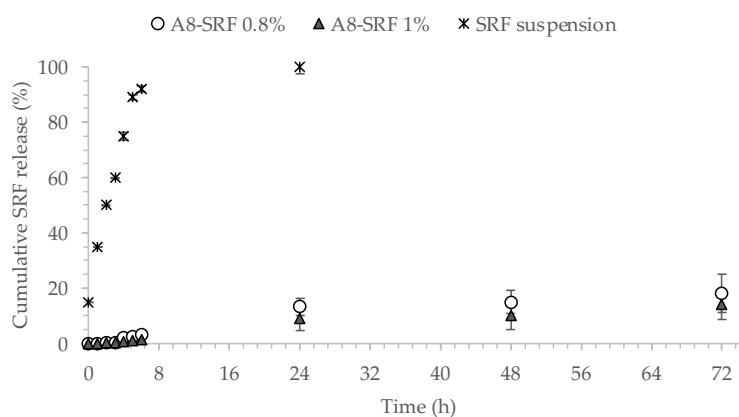
Figure 6. *In vitro* release profiles of Sorafenib (SRF) from SLN A8 loaded with 0.8% or 1.0% w/v, compared to free drug suspension 1%, w/v (mean ± SD, n = 3).

7.4 Conclusions

The results obtained in our study demonstrated that SLN prepared using Softisan as solid lipid represents a promising strategy for the topical delivery of Sorafenib in the potential treatment of uveal melanoma due to the presence of small-sized nanoparticles, characterised by stability over time, good cytocompatibility, and high mucoadhesive properties. The developed strategy opens the perspective of the potential ophthalmic

treatment of a disease that, to date, is mainly treated with systemic therapies or specific treatments directed to the liver, with a consequently positive impact on patient compliance. However, further studies need to be developed to deepen the potentiality of SRF-loaded SLN A8-DB, with particular attention on the possibility of obtaining a final freeze-dried product to be investigated in terms of stability, *in vitro* release, *in vitro* biocompatibility on SIRC, and effectiveness on a model of uveal melanoma.
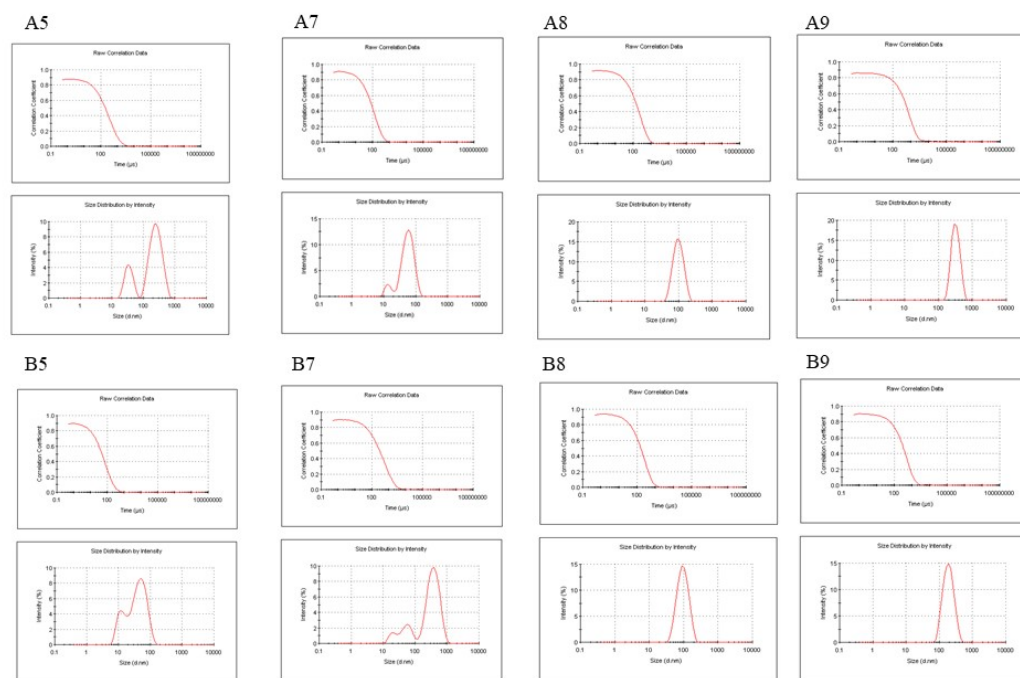
Figure S1: Intensity correlation functions of light scattered at 90° and hydrodynamic radius distribution by intensity of SLN prepared with different amount of Softisan (A5, A7, A8 and A9) or Suppocire (B5, B7, B8 and B9).

Table S1: Mean particles size (Z-Ave, [nm]) and polydispersity index (PDI, [a.u.]) ± standard deviation (SD) of unloaded SLN A8, B8 and B9 stored in Turbiscan® at 25.0 ± 1.0 °C and analysed at different time intervals. Each value is the average of six different replicates ± standard deviation (SD). * Significance for $p <$ 0.05, compared to the initial value.

	Sample	A8	B8	B9
Zave ± S.D. (nm)	1 week	135.1 ± 1.15	71.60 ± 1.12	125.5 ± 3.11
	2 weeks	135.8 ± 1.7	108.4 ± 0.4	145.6 ± 1.8
	3 weeks	138.7 ± 0.4	183.1 ± 1.4*	129.1 ± 1.4
	4 weeks	136.5 ± 2.9	287.4 ± 1.3*	156.1 ± 0.8
PDI ± S.D.	1 week	0.124 ± 0.023	0.123 ± 0.013	0.111 ± 0.025
	2 weeks	0.131 ± 0.014	0.226 ± 0.011	0.119 ± 0.009
	3 weeks	0.090 ± 0.021	0.378 ± 0.003*	0.106 ± 0.014
	4 weeks	0.057 ± 0.047	0.370 ± 0.004*	0.091 ± 0.022

References:

1. Buzzacco, D.M.; Abdel-Rahman, M.H.; Park, S.; Davidorf, F.; Olencki, T.; Cebulla, C.M. Long-Term Survivors with Metastatic Uveal Melanoma. Open. Ophthalmol. J. 2012, 6, 49–53. [CrossRef] [PubMed]
2. Niederkorn, A.; Wackernagel, W.; Artl, M.; Schwantzer, G.; Aigner, B.; Richtig, E. Response of Patients with Metastatic Uveal Melanoma to Combined Treatment with Fotemustine and Sorafenib. Acta Ophthalmol. 2014, 92, e696–e697. [CrossRef] [PubMed]
3. Velho, T.R.; Kapiteijn, E.; Jager, M.J. New Therapeutic Agents in Uveal Melanoma. Anticancer Res. 2012, 32, 2591–2598. [PubMed]
4. Collaborative Ocular Melanoma Study Group. Assessment of Metastatic Disease Status at Death in 435 Patients with Large Choroidal Melanoma in the Collaborative Ocular Melanoma Study (Coms): Coms Report No. 15. Arch. Ophthalmol. 2001, 119, 670–676. [CrossRef]
5. Kujala, E.; Makitie, T.; Kivela, T. Very Long-Term Prognosis of Patients with Malignant Uveal Melanoma. Investig. Ophthalmol. Vis. Sci. 2003, 44, 4651–4659. [CrossRef]
6. Augsburger, J.J.; Correa, Z.M.; Shaikh, A.H. Effectiveness of Treatments for Metastatic Uveal Melanoma. Am. J. Ophthalmol. 2009, 148, 119–127. [CrossRef]

7. Bhatia, S.; Moon, J.; Margolin, K.A.; Weber, J.S.; Lao, C.D.; Othus, M.; Aparicio, A.M.; Ribas, A.; Sondak, V.K. Phase II Trial of Sorafenib in Combination with Carboplatin and Paclitaxel in Patients with Metastatic Uveal Melanoma: Swog S0512. PLoS ONE 2012, 7, e48787. [CrossRef]

8. Mouriaux, F.; Servois, V.; Parienti, J.J.; Lesimple, T.; Thyss, A.; Dutriaux, C.; Neidhart-Berard, E.M.; Penel, N.; Delcambre, C.; Peyro Saint Paul, L.; et al. Sorafenib in Metastatic Uveal Melanoma: Efficacy, Toxicity and Health-Related Quality of Life in a Multicentre Phase II Study. Br. J. Cancer 2016, 115, 20–24. [CrossRef]

9. Benizri, S.; Ferey, L.; Alies, B.; Mebarek, N.; Vacher, G.; Appavoo, A.; Staedel, C.; Gaudin, K.; Barthelemy, P. Nucleoside-Lipid-Based Nanocarriers for Sorafenib Delivery. Nanoscale Res. Lett. 2018, 13, 17. [CrossRef]

10. Bondi, M.L.; Botto, C.; Amore, E.; Emma, M.R.; Augello, G.; Craparo, E.F.; Cervello, M. Lipid Nanocarriers Containing Sorafenib Inhibit Colonies Formation in Human Hepatocarcinoma Cells. Int. J. Pharm. 2015, 493, 75–85. [CrossRef]

11. Santonocito, M.; Zappulla, C.; Viola, S.; La Rosa, L.R.; Solfato, E.; Abbate, I.; Tarallo, V.; Apicella, I.; Platania, C.B.M.; Maugeri, G.; et al. Assessment of a New Nanostructured Microemulsion System for Ocular Delivery of Sorafenib to Posterior Segment of the Eye. Int. J. Mol. Sci. 2021, 22, 4404. [CrossRef]

12. Mangana, J.; Levesque, M.P.; Karpova, M.B.; Dummer, R. Sorafenib in Melanoma. Expert Opin. Investig. Drugs 2012, 21, 557–568. [CrossRef]

13. Grillone, A.; Riva, E.R.; Mondini, A.; Forte, C.; Calucci, L.; Innocenti, C.; de Julian Fernandez, C.; Cappello, V.; Gemmi, M.; Moscato, S.; et al. Active Targeting of Sorafenib: Preparation, Characterization, and in Vitro Testing of Drug-Loaded Magnetic Solid Lipid Nanoparticles. Adv. Healthc. Mater. 2015, 4, 1681–1690. [CrossRef]

14. Gonzalez-Fernandez, F.M.; Bianchera, A.; Gasco, P.; Nicoli, S.; Pescina, S. Lipid-Based Nanocarriers for Ophthalmic Administration: Towards Experimental Design Implementation. Pharmaceutics 2021, 13, 447. [CrossRef]

15. Sanchez-Lopez, E.; Espina, M.; Doktorovova, S.; Souto, E.B.; Garcia, M.L. Lipid Nanoparticles (SLN, NLC): Overcoming the Anatomical and Physiological Barriers of the Eye—Part I—Barriers and Determining Factors in Ocular Delivery. Eur. J. Pharm. Biopharm. 2017, 110, 70–75. [CrossRef]

16. Szilágyi, B.Á.; Mammadova, A.; Gyarmati, B.; Szilágyi, A. Mucoadhesive Interactions between Synthetic Polyaspartamides and Porcine Gastric Mucin on the Colloid Size Scale. Colloids Surf. B Biointerfaces 2020, 194, 111219. [CrossRef]

17. Carbone, C.; Fuochi, V.; Zielinska, A.; Musumeci, T.; Souto, E.B.; Bonaccorso, A.; Puglia, C.; Petronio Petronio, G.; Furneri, P.M. Dual-Drugs Delivery in Solid Lipid Nanoparticles for the Treatment of Candida Albicans Mycosis. Colloids Surf. B Biointerfaces 2020, 186, 110705. [CrossRef]

18. Carbone, C.; Caddeo, C.; Grimaudo, M.A.; Manno, D.E.; Serra, A.; Musumeci, T. Ferulic Acid-Nlc with Lavandula Essential Oil: A Possible Strategy for Wound-Healing? Nanomaterials 2020, 10, 898. [CrossRef]

19. Bonaccorso, A.; Musumeci, T.; Carbone, C.; Vicari, L.; Lauro, M.R.; Puglisi, G. Revisiting the Role of Sucrose in PLGA-PEG Nanocarrier for Potential Intranasal Delivery. Pharm. Dev. Technol. 2018, 23, 265–274. [CrossRef]

20. Caddeo, C.; Pucci, L.; Gabriele, M.; Carbone, C.; Fernandez-Busquets, X.; Valenti, D.; Pons, R.; Vassallo, A.; Fadda, A.M.; Manconi, M. Stability, Biocompatibility and Antioxidant Activity of Peg-Modified Liposomes Containing Resveratrol. Int. J. Pharm. 2018, 538, 40–47. [CrossRef]

21. Weng, Y.; Liu, J.; Jin, S.; Guo, W.; Liang, X.; Hu, Z. Nanotechnology-Based Strategies for Treatment of Ocular Disease. Acta Pharm. Sin. B 2017, 7, 281–291. [CrossRef] [PubMed]

22. Sakurai, E.; Ozeki, H.; Kunou, N.; Ogura, Y. Effect of Particle Size of Polymeric Nanospheres on Intravitreal Kinetics. Ophthalmic. Res. 2001, 33, 31–36. [CrossRef] [PubMed]

23. Puglia, C.; Offerta, A.; Carbone, C.; Bonina, F.; Pignatello, R.; Puglisi, G. Lipid Nanocarriers (Lnc) and Their Applications in Ocular Drug Delivery. Curr. Med. Chem. 2015, 22, 1589–1602. [CrossRef] [PubMed]

24. Souto, E.B.; Doktorovova, S.; Gonzalez-Mira, E.; Egea, M.A.; Garcia, M.L. Feasibility of Lipid Nanoparticles for Ocular Delivery of Anti-Inflammatory Drugs. Curr. Eye Res. 2010, 35, 537–552. [CrossRef]

25. Lee, Y.J.; Kwon, J.; Shin, S.; Eun, Y.G.; Shin, J.H.; Lee, G.J. Optimization of Saliva Collection and Immunochromatographic Detection of Salivary Pepsin for Point-of-Care Testing of Laryngopharyngeal Reflux. Sensors 2020, 20, 325. [CrossRef]

26. Kotsilkova, R.; Borovanska, I.; Todorov, P.; Ivanov, E.; Menseidov, D.; Chakraborty, S.; Bhattacharjee, C. Tensile and Surface Mechanical Properties of Polyethersulphone (Pes) and Polyvinylidene Fluoride (PVDF) Membranes. J. Theor. Appl. Mech. Bulg. 2018, 48, 85–99. [CrossRef]

27. Jeong, S.H.; Jang, J.H.; Cho, H.Y.; Lee, Y.B. Soft- and Hard-Lipid Nanoparticles: A Novel Approach to Lymphatic Drug Delivery. Arch. Pharm. Res. 2018, 41, 797–814. [CrossRef]

28. Paliwal, R.; Babu, R.J.; Palakurthi, S. Nanomedicine Scale-up Technologies: Feasibilities and Challenges. AAPS PharmSciTech 2014, 15, 1527–1534. [CrossRef]

29. Iwasawa, A.; Ayaki, M.; Niwano, Y. Cell viability score (CVS) as a good indicator of critical concentration of benzalkonium chloride for toxicity in cultured ocular surface cell lines. Regul. Toxicol. Pharmacol. 2013, 66, 177–183. [CrossRef]

30. Freeman, P.D.; Kahook, M.Y. Preservatives in Topical Ophthalmic Medications: Historical and Clinical Perspectives. Exp. Rev. Ophthalmol. 2009, 4, 59–64. [CrossRef]

31. Mikkelson, T.J.; Chrai, S.S.; Robinson, J.R. Altered Bioavailability of Drugs in the Eye Due to Drug-Protein Interaction. J. Pharm. Sci. 1973, 62, 1648–1653. [CrossRef]

32. EURL ECVAM Database on Alternative Methods to Animal Experimentation. Available online: http://cidportal.jrc.ec.europa. eu/ftp/jrc-opendata/EURL-ECVAM/datasets/DBALM/LATEST/online/DBALM_docs/17_P_MTT%20Assay.pdf (accessed on 5 October 2021).

33. Takahashi, Y.; Hayashi, K.; Abo, T.; Koike, M.; Sakaguchi, H.; Nishiyama, N. The Short Time Exposure (STE) test for predicting eye irritation potential: Intra-laboratory reproducibility and correspondence to globally harmonized system (GHS) and EU eye irritation classification for 109 chemicals. Toxicol. Vitr. 2011, 25, 1425–1434. [CrossRef]

34. Carbone, C.; Campisi, A.; Manno, D.; Serra, A.; Spatuzza, M.; Musumeci, T.; Bonfanti, R.; Puglisi, G. The Critical Role of Didodecyldimethylammonium Bromide on Physico-Chemical, Technological and Biological Properties of NLC. Colloids Surf. B Biointerfaces 2014, 121, 1–10. [CrossRef]

35. Carbone, C.; Tomasello, B.; Ruozi, B.; Renis, M.; Puglisi, G. Preparation and Optimization of Pit Solid Lipid Nanoparticles Via Statistical Factorial Design. Eur. J. Med. Chem. 2012, 49, 110–117. [CrossRef]

36. De Campos, A.M.; Diebold, Y.; Carvalho, E.L.; Sanchez, A.; Alonso, M.J. Chitosan Nanoparticles as New Ocular Drug Delivery Systems: In Vitro Stability, In Vivo Fate, and Cellular Toxicity. Pharm. Res. 2004, 21, 803–810. [CrossRef]

37. Tobio, M.; Sanchez, A.; Vila, A.; Soriano, I.I.; Evora, C.; Vila-Jato, J.L.; Alonso, M.J. The Role of Peg on the Stability in Digestive Fluids and in Vivo Fate of PEG-PLA Nanoparticles Following Oral Administration. Colloids Surf. B Biointerfaces 2000, 18, 315–323. [CrossRef]

38. Calvo, P.; Vila-Jato, J.L.; Alonso, M.J. Effect of Lysozyme on the Stability of Polyester Nanocapsules and Nanoparticles: Stabilization Approaches. Biomaterials 1997, 18, 1305–1310. [CrossRef]

39. Mendes, A.C.; Sevilla Moreno, J.; Hanif, M.; Douglas, T.E.L.; Chen, M.; Chronakis, I.S. Morphological, Mechanical and Mucoadhesive Properties of Electrospun Chitosan/Phospholipid Hybrid Nanofibers. Int. J. Mol. Sci. 2018, 19, 2266. [CrossRef]

40. Alp, G.; Aydogan, N. Lipid-Based Mucus Penetrating Nanoparticles and Their Biophysical Interactions with Pulmonary Mucus Layer. Eur. J. Pharm. Biopharm. 2020, 149, 45–57. [CrossRef]

41. Bonaccorso, A.; Cimino, C.; Manno, D.E.; Tomasello, B.; Serra, A.; Musumeci, T.; Puglisi, G.; Pignatello, R.; Carbone, C. Essential oils loaded NLC for potential intranasal administration. Pharmaceutics 2021, 13, 1166. [CrossRef]

42. Cordeiro, S.S.B.; Martins, A.M.; Ribeiro, H.M.; Gonçalves, L.; Marto, J. Antioxidant-Loaded Mucoadhesive Nanoparticles for Eye Drug Delivery: A New Strategy to Reduce Oxidative Stress. Processes 2021, 9, 379. [CrossRef]

43. Kubackova, J.; Holas, O.; Zbytovska, J.; Vranikova, B.; Zeng, G.; Pavek, P.; Mullertz, A. Oligonucleotide Delivery across the Caco-2 Monolayer: The Design and Evaluation of Self-Emulsifying Drug Delivery Systems (Sedds). Pharmaceutics 2021, 13, 459. [CrossRef] [PubMed]

44. Zhao, Z.B.; Long, J.; Zhao, Y.Y.; Yang, J.B.; Jiang, W.; Liu, Q.Z.; Yan, K.; Li, L.; Wang, Y.C.; Lian, Z.X. Adaptive Immune Cells Are Necessary for the Enhanced Therapeutic Effect of Sorafenib-Loaded Nanoparticles. Biomater. Sci. 2018, 6, 893–900. [CrossRef] [PubMed]

45. Vishwakarma, S.K.; Sharmila, P.; Bardia, A.; Chandrakala, L.; Raju, N.; Sravani, G.; Sastry, B.V.S.; Habeeb, M.A.; Khan, A.A.; Dhayal, M. Use of Biocompatible Sorafenib-Gold Nanoconjugates for Reversal of Drug Resistance in Human Hepatoblatoma Cells. Sci. Rep. 2017, 7, 8539. [CrossRef]

46. Tatsugami, K.; Oya, M.; Kabu, K.; Akaza, H. Evaluation of Efficacy and Safety of Sorafenib in Kidney Cancer Patients Aged 75 Years and Older: A Propensity Score-Matched Analysis. Br. J. Cancer 2018, 119, 241–247. [CrossRef]

47. Wu, L.; Zhou, J.; Zhou, W.; Huang, X.F.; Chen, Q.; Wang, W.; Zhai, L.; Li, S.; Tang, Z. Sorafenib Blocks the Activation of the Hif-2alpha/Vegfa/Epha2 Pathway, and Inhibits the Rapid Growth of Residual Liver Cancer Following High-Intensity Focused Ultrasound Therapy In Vivo. Pathol. Res. Pract. 2021, 220, 153270. [CrossRef]

48. Ye, H.; Zhou, L.; Jin, H.; Chen, Y.; Cheng, D.; Jiang, Y. Sorafenib-Loaded Long-Circulating Nanoliposomes for Liver Cancer Therapy. Biomed. Res. Int. 2020, 2020, 1351046. [CrossRef]

49. Rodriguez-Hernandez, M.A.; de la Cruz-Ojeda, P.; Gallego, P.; Navarro-Villaran, E.; Stankova, P.; Del Campo, J.A.; Kucera, O.; Elkalaf, M.; Maseko, T.E.; Cervinkova, Z.; et al. Dose-Dependent Regulation of Mitochondrial Function and Cell Death Pathway by Sorafenib in Liver Cancer Cells. Biochem. Pharmacol. 2020, 176, 113902. [CrossRef]

50. Ebadi, M.; Bullo, S.; Buskara, K.; Hussein, M.Z.; Fakurazi, S.; Pastorin, G. Release of a Liver Anticancer Drug, Sorafenib from Its Pva/Ldh- and Peg/Ldh-Coated Iron Oxide Nanoparticles for Drug Delivery Applications. Sci. Rep. 2020, 10, 21521. [CrossRef]

51. Kernt, M.; Neubauer, A.S.; Liegl, R.G.; Hirneiss, C.; Alge, C.S.; Wolf, A.; Ulbig, M.W.; Kampik, A. Sorafenib Prevents Human Retinal Pigment Epithelium Cells from Light-Induced Overexpression of Vegf, Pdgf and Plgf. Br. J. Ophthalmol. 2010, 94, 1533–1539. [CrossRef]

52. Kernt, M.; Liegl, R.G.; Rueping, J.; Neubauer, A.S.; Haritoglou, C.; Lackerbauer, C.A.; Eibl, K.H.; Ulbig, M.W.; Kampik, A. Sorafenib Protects Human Optic Nerve Head Astrocytes from Light-Induced Overexpression of Vascular Endothelial Growth Factor, Platelet-Derived Growth Factor, and Placenta Growth Factor. Growth Factors 2010, 28, 211–220. [CrossRef]

53. Kernt, M.; Staehler, M.; Stief, C.; Kampik, A.; Neubauer, A.S. Resolution of Macular Oedema in Occult Choroidal Neovascularization under Oral Sorafenib Treatment. Acta. Ophthalmol. 2008, 86, 456–458. [CrossRef]

54. Tahir, N.; Madni, A.; Li, W.; Correia, A.; Khan, M.M.; Rahim, M.A.; Santos, H.A. Microfluidic Fabrication and Characterization of Sorafenib-Loaded Lipid-Polymer Hybrid Nanoparticles for Controlled Drug Delivery. Int. J. Pharm. 2020, 581, 119275. [CrossRef]

55. Wang, Z.; Duan, X.; Lv, Y.; Zhao, Y. Low Density Lipoprotein Receptor (Ldlr)-Targeted Lipid Nanoparticles for the Delivery of Sorafenib and Dihydroartemisinin in Liver Cancers. Life Sci. 2019, 239, 117013. [CrossRef]

56. Wang, H.; Wang, H.; Yang, W.; Yu, M.; Sun, S.; Xie, B. Improved Oral Bioavailability and Liver Targeting of Sorafenib Solid Lipid Nanoparticles in Rats. AAPS Pharm. Sci. Tech. 2018, 19, 761–768. [CrossRef]

57. Herranz-Blanco, B.; Arriaga, L.R.; Makila, E.; Correia, A.; Shrestha, N.; Mirza, S.; Weitz, D.A.; Salonen, J.; Hirvonen, J.; Santos, H.A. Microfluidic Assembly of Multistage Porous Silicon-Lipid Vesicles for Controlled Drug Release. Lab Chip 2014, 14, 1083–1086. [CrossRef]

58. Li, H.; Liu, W.; Sorenson, C.M.; Sheibani, N.; Albert, D.M.; Senanayake, T.; Vinogradov, S.; Henkin, J.; Zhang, H.F. Sustaining Intravitreal Residence with L-Arginine Peptide-Conjugated Nanocarriers. Investig. Ophthalmol. Vis. Sci. 2017, 58, 5142–5150. [CrossRef]

59. Fu, T.; Yi, J.; Lv, S.; Zhang, B. Ocular Amphotericin B Delivery by Chitosan-Modified Nanostructured Lipid Carriers for Fungal Keratitis-Targeted Therapy. J. Liposome Res. 2017, 27, 228–233. [CrossRef]

60. Kumar, R.; Sinha, V.R. Lipid Nanocarrier: An Efficient Approach Towards Ocular Delivery of Hydrophilic Drug (Valacyclovir). AAPS Pharm. Sci. Tech. 2017, 18, 884–894. [CrossRef]

61. Zhang, L.; Li, Y.; Zhang, C.; Wang, Y.; Song, C. Pharmacokinetics and Tolerance Study of Intravitreal Injection of Dexamethasone-Loaded Nanoparticles in Rabbits. Int. J. Nanomed. 2009, 4, 175–183. [CrossRef]

8 NANOSTRUCTURED LIPID CARRIER FOR THE OPHTHALMIC DELIVERY OF HALOPERIDOL METABOLITE II VALPROATE ESTER (±)-MRJF22: A POTENTIAL STRATEGY IN THE TREATMENT OF UVEAL MELANOMA

Cinzia Cimino[a,b,c], Claudia Giovanna Leotta[d], Agostino Marrazzo[c,e], Teresa Musumeci[b,c], Giovanni Mario Pitari[d], Rosario Pignatello[b, c], Angela Bonaccorso[b, c], Emanuele Amata[e], Carla Barbaraci[e,1], Claudia Carbone[b,c,*]

[a] PhD in Biotechnology, Department of Biomedical and Biotechnological Sciences, University of Catania, Via Santa Sofia 97, 95123, Catania, Italy

[b] Laboratory of Drug Delivery Technology, Department of Drug and Health Sciences, University of Catania, Viale A. Doria 6, 95124, Catania, Italy

[c] NANOMED, Research Centre for Nanomedicine and Pharmaceutical Nanotechnology, University of Catania, Italy

[d] Vera Salus Ricerca S.r.l., Via Sigmund Freud 62/B, 96100, Siracusa, Italy

[e] Medicinal Chemistry Laboratory, Department of Drug and Health Sciences, University of Catania, Viale A. Doria 6, 95124, Catania, Italy

[*] Corresponding author

[1] Present address: Laboratory of Medicinal Chemistry (CSIC Associated Unit), Faculty of Pharmacy and Food Sciences, and Institute of Biomedicine (IBUB), University of Barcelona, Av. Joan XXIII, 27-31, 08028 Barcelona, Spain.

Abstract: Among the eye tumors, uveal melanoma is one of the most diffuse and aggressive, affecting mainly the choroid, but also the ciliary body and the iris. Promising pharmaceutical therapies involve histone deacetylase inhibitors and sigma-ligands: these

targets were combined in a new-synthetized prodrug, namely (±)-MRJF22, which demonstrated to perform antiangiogenic activity, as well as its (*R*)- and (*S*)-enantiomers. Since this cancer mainly occurs in the posterior segment of the eye, the therapeutical use of this prodrug is limited by the presence of ocular barriers. Herein, lipid nanoparticles were selected for their potential ophthalmic application to encapsulate (±)-MRJF22 prodrug and its (*R*)- and (*S*)-enantiomers. The prepared nanoparticles demonstrated to be suitable for the intended ophthalmic administration in terms of size, homogeneity, zeta potential, pH and osmolality. DSC and FTIR analyses were performed on the formulations, and their long-term stability was confirmed by accelerated stability studies. Mucoadhesive studies suggested a potential good interaction with ocular surface epithelia, thus enhancing the ocular residence time of the formulations. *In vitro* release studies demonstrated a sustained and prolonged release of the prodrugs loaded in the colloidal suspensions. Cytocompatibility and proliferation assays were performed on uveal melanoma 92-1 cell line, confirming the suitability of the formulations and their potential application in the treatment of uveal melanoma.

Keywords: NLC; Ophthalmic delivery; DSC; Stability; Mucoadhesion; Cell proliferation

8.1 Introduction

Uveal melanoma (UM) is one the most aggressive malignant tumor of the eye, and the most diffused primary intraocular cancer among adults [1]; the annual incidence is 0.24 per million among Blacks, 0.9 among Hispanics and 6.3 among Whites, with a prevalence for men, who develop bigger tumors. UM occurs in choroid for about 90%, in the ciliary body for 7% and in the iris for 3% [2]. One of the earliest symptoms is blurred vision, but it could be diagnosed also in asymptomatic patients through routine controls. Predisposing factors resulted to be ability to tan, hair color and skin color, BRCA1-associated protein 1 mutation, oculodermal or ocular melanocytosis, choroidal or cutaneous or iris nevus [1,3,4]. The main criticism associated with this tumor is the great tendency to metastasize: the involved organs are liver (90% of cases), lungs and soft tissues, where metastases generally occur in 5 years for 25% of patients and in 10 years for 34%, since the first tumoral occurrence [5]. The mortality rate is also quite high (80% in one year and 92% in two years [6]) and is related to liver compromission.

Nowadays, the most successful approaches involve surgery, radiotherapy and also enucleation for larger melanomas. As pharmaceutical treatments to contrast UM, inhibitors

of histone deacetylase (HDACi) could be used, since this enzyme is responsible of the increase of the transcription gene involved in cell growth, resulting in cell cycle advancement and DNA duplication: the inhibition of histone deacetylase (HDAC), using HDACi as valproic acid, induces the death of cancer cells thus reducing tumor development both *in vivo* and *in vitro* [7]. Moreover, sigma receptors are also targeted in the treatment of UM for their role in cell proliferation and survival: in particular, σ_1 increases the secretion of vascular endothelial growth factor (VEGF) and encourages motility [8, 9], while σ_2 promotes autophagy and apoptosis [10]. Recently, a new synthetized drug was developed combining valproic acid histone deacetylase inhibition and haloperidol metabolite II (HP-mII) antagonism for σ_1 and agonism for σ_2, resulting in a prodrug, ($\pm$)-MRJF22 and its enantiomers, with a great potential in the treatment of UM, as emerged from *in vitro* studies which ascertained its antiangiogenic activity on Human Retinal Endothelial Cells (HREC) [9].

Pharmacological treatments find well-known impediments related to the location of the tumor in the posterior chamber of the eye: the presence of numerous physiological barriers strongly limits the bioavailability of the drug to the active site (lower than 3–5% of the administered dose). In order to overcome these limits, drug delivery systems represent a promising strategy to reach the inner tissues of the eye, guaranteeing prolonged and sustained release, capability to achieve the target site and longer permanence which enhance corneal permeation [11].

Among the various platforms that have been proposed to achieve the inner eye, nanostructured lipid carrier (NLC) resulted to be very advantageous due to their ability to encapsulate great amount of encapsulated lipophilic drug, their high stability, the ability to perform controlled release, their efficiency in ocular delivery [12,13].

Basing on these considerations, this work aimed to the encapsulation of ($\pm$)-MRJF22 enantiomers into NLC, intended for ophthalmic application in the treatment of UM. Racemic mixture and both (*R*)- and (*S*)- enantiomers, preliminarily characterized by Differential Scanning Calorimetry (DSC), were successfully encapsulated into nanoparticulate systems using phase inversion temperature technique (PIT method), thus obtaining (*M*)-NLC, (*R*)-NLC and (*S*)-NLC, respectively. NLC were prepared using surfactant and lipids previously demonstrated to be safe on Statens Seruminstitut Rabbit Cornea (SIRC) cell line for the ophthalmic drug delivery [14]. Nanosuspensions were characterized from physico-chemical and technological points of view, measuring pH, osmolality, but also mean particles size (Z-ave), polydispersity index (PDI) and zeta potential (ZP) through Photon Correlation Spectroscopy (PCS) analysis. Accelerated

stability studies in constant climate chamber were also performed following ICH guidelines Q1A (R2), storing the samples for 6 months at 40 ± 2 °C and $75 \pm 5\%$ RH. The produced NLC were characterized through DSC analysis and Fourier-transform infrared (FTIR) spectroscopy. Preliminary mucoadhesive evaluation of NLC in simulated tear fluid (STF) was performed up to 4 h to assess their potential interaction with mucin, one of the main glycoproteins present in the mucus layer adjacent to ocular surface epithelia. Encapsulation efficiency (EE%) of the prodrug into NLC was measured and *in vitro* release studies were performed using Franz-type diffusion cells. Biological studies were performed *in vitro* on human uveal melanoma (UM) 92-1 cells to evaluate NLC safety and antiproliferative activity of enantiomer-loaded NLC.

8.2 Materials and methods

8.2.1 Materials

Kolliphor RH40 was provided by BASF Italia S.p.a. (Cesano Modena, Italy); Oleoyl Macrogol-6 Glycerides (Labrafil) was a gift from Gattefosse Italia s.r.l. (Milano, Italy); Hydrogenated Coco-Glycerides (Softisan 100) was bought from IOI Oleo GmbH (Oleochemicals, IOI group); Isopropyl myristate (IPM) was purchased from Farmalabor (Canosa di Puglia, Italy); Tris (hydroxymethyl)aminomethane buffer was bought from Merck (Darmstadt, Germany). ($\pm$)-MRJF22, (*R*)-(+)-MRJF22 and (*S*)-(−)-MRJF22 were synthetized by the research group of Prof. Marrazzo, in the Medicinal Chemistry Laboratory of the Department of Drug and Health Sciences (University of Catania) [9]. Mucin (mucin from porcine stomach type II), NaCl, NaHCO$_3$, CaCl$_2$·2H$_2$O and KCl were purchased from Sigma-Aldrich S.r.l. (Milan, Italy). Regenerated cellulose membranes (Spectra/Por CE; Mol. Wet. Cutoff 3500) were supplied by Spectrum (Los Angeles, CA, USA). Human UM 92-1 cell line was purchased from the Cell Factory-IST (Genova, Italy). Media and reagents RPMI-1640 medium, fetal bovine serum (FBS), L-glutamine, penicillin and streptomycin used for cell studies were from Euroclone S.p.A. (Pero, Milan, Italy). All solvents (LC grade) were from VWR International (Milan, Italy).

8.2.2 Preliminary studies on free prodrugs

8.2.2.1 Differential Scanning Calorimetry on free prodrugs

On a Mettler DSC 12E equipped with a Haake thermocryostat type D8-G, DSC scans of the three compounds were executed. Data were collected using a Mettler TA89E and FP89 system software and the instrument was calibrated using indium. The control pan was left

empty. Each sample was scanned at a rate of 5 °C/min for heating and 10 °C/ min for cooling in the temperature range of 10–200 °C.

8.2.2.2   Stability at PIT method's temperature

Prodrugs were diluted in a methanol-0.5% diethylamine mixture and put on a heating plate (68 ± 2 °C) for 5 min, corresponding to the time-exposure to heating of the lipid phase of NLC where the drugs had been solubilized, thus undergoing the heat treatment required by PIT technique. The prodrugs' solutions were then examined through UV–vis spectrophotometer (UH5300 UV–Visible Double-Beam Spectrophotometer, Hitachi Europe, Milan, Italy) and compared to the respective reference spectra.

8.2.3   Nanoparticle production

NLC were prepared using the PIT technique [15]. The lipid mixture (Softisan:IPM at a 2:5 wt ratio) was added with the surfactant mixture (7% w/V) [16]. The prodrugs (0.02% w/v) were added to the lipid phase. The aqueous phase consisted of TRIS buffer (pH 7.4). Both phases were heated at 68 ± 2 °C. Then, the aqueous phase was dropped into the lipid phase, leading to the formation of blank NLC or loaded formulations (*M*)-NLC, (*R*)-NLC and (*S*)-NLC, encapsulating (±)-MRJF22, (*R*)-(+)-MRJF22 and (*S*)-(−)-MRJF22, respectively. After mixing on a magnetic plate at room temperature, the samples were vortexed (Heidolph Rea×2000, VWR, Milan, Italy), then kept in the freezer for 15 min and stored at 4 °C.

Each formulation was centrifuged at 13.000 rpm for 90 min at 4 °C using an ultracentrifuge (SL16R Centrifuge, Thermo Scientific, Rodano, Italy) fitted with a fixed body rotator, in order to remove the excess of surfactants and the amount of prodrugs that remained non-encapsulated in the colloidal suspensions.

8.2.4   Physical-chemical and technological characterization of NLC

8.2.4.1   Osmolality and pH

An osmometer (Osmomat 3000, Gonotec, Berlin, Germany) was used to assess the osmolality of the samples, which was previously calibrated using ultra-purified water and physiological solution. The pH values of the samples were determined using a pH meter (Mettler Toledo, Milano, Italy), calibrated using solution with defined pH 4.0, 7.0 and 10.0.

8.2.4.2   Photon Correlation Spectroscopy (PCS)

The produced NLC were characterized by Photon Correlation Spectroscopy (PCS) using a Zetasizer Nano S90 (Malvern Instruments, Malvern, UK), to evaluate mean particle size

(Z-ave), polydispersity index (PDI) and zeta potential (ZP). Samples analyses were performed in triplicate after 1:20 dilution with ultra-purified water.

8.2.4.3 Encapsulation efficiency

The effective amount of the encapsulated prodrug in the lipid matrix of NLC was indirectly evaluated measuring the amount of prodrug not encapsulated. Each formulation was centrifuged at 13.000 rpm for 90 min at 4 °C. The obtained supernatants, separated from the resulting pellet, were diluted in methanol-0.5% diethylamine mixture (1:5 v/v) and centrifuged at 13.000 rpm for 30 min at 4 °C. The supernatants were analyzed using a UV–vis spectrophotometer. The encapsulation efficiency (EE %) was calculated using the following equation:

$$EE\% = \text{amount of prodrug entrapped/total amount of prodrug used} \times 100.$$

8.2.4.4 Accelerated stability studies

Accelerated stability studies of blank and loaded formulations were conducted as described in ICH guidelines Q1A (R2) by incubating the prepared formulations at accelerated conditions (40 ± 2 °C temperature and 75 ± 5% RH) for 6 months in constant climatic chamber (BINDER GmbH, KBF-S 115 E6, Tuttlingen, Germany). The stability was measured in terms of mean particle size and PDI. The effect of temperature and humidity was observed at specific time-points: 0, 1, 2, 3, 4, 5, and 6 months.

8.2.4.5 Dynamic scanning calorimetry

In order to investigate the influence of the preparation method on the selected prodrug-loaded NLC, DSC was performed on NLC, (*M*)-NLC, (*R*)-NLC, (*S*)-NLC and on raw materials – such as Kolliphor and Softisan – with the equipment described in Paragraph 9.2.2.1. The control pan was left empty. Each sample was scanned at a rate of 5 °C/min for heating and 10 °C/min for cooling in the temperature range of 10–130 °C.

8.2.4.6 Fourier-transform infrared (FTIR) spectroscopy

The IR spectra of nanoparticles raw materials, prodrugs and NLC formulations were recorded in KBr disks, after solubilization in dichloromethane, on a FTIR spectrometer (PerkinElmer Spectrum RX I, Waltham, MA, USA) equipped with a diamond window and a zinc selenide crystal (diamond/ZnSe) and an attenuated total reflectance (ATR) accessory.

8.2.4.7 Mucoadhesive studies

Two different *in vitro* methods were performed in order to assess the mucoadhesive properties of NLC after incubation with mucin in simulated tear fluid (STF). Briefly, mucin

(0.1% w/v) was suspended in STF (NaCl 0.68 g, NaHCO$_3$ 0.22 g, CaCl$_2$·2H$_2$O 0.008 g, KCl 0.14 g, and distilled deionized water to 100 mL) and stirred overnight to allow its complete dispersion. The interaction between each NLC and mucin was determined by mixing mucin dispersion and NLC (1:1 v/v) for 15 min at 25 °C and after incubation at 37 °C up to 4 h by turbidimetric assay and mucin particle method. In particular, turbidimetric measurements were evaluated comparing the absorbances at 650 nm by UV–vis spectrophotometer of the native mucin and each NLC-mucin dispersion after 0, 1, 2, 3 and 4 h of incubation. Mucin particle method was performed by measuring the change in NLC particles size and zeta potential after incubation with mucin at the same time points, to estimate the extent of their mucoadhesive property.

8.2.4.8   In vitro drug release

Franz-type diffusion cells (LGA, Berkeley, CA, USA) were used to assess molecules' release profiles from free prodrugs solutions and from prodrug-loaded NLC formulations. Before being installed in Franz cells, 0.75 cm^2 of regenerated cellulose membranes (Spectra/Por CE; Mol. Weight Cut-off 3.5 kDa) were moistened for 24 h in the same medium used in the receptor compartment (4.5 mL), which was a 50:50 v/v combination of tris(hydroxymethyl)aminomethane buffer (TRIS pH 7.4) and methanol-0.5% diethylamine, thermoset at 35 °C and stirred at 600 rpm. The donor compartments were then filled with 500 μL of each sample's pellet. At planned time intervals (from T = 0–24 h), 500 μL of receptor medium was withdrawn and replaced with an equivalent volume of medium equilibrated to 35 °C to guarantee pseudo-sink conditions. To evaluate the drug content, each sample was twofold diluted with medium and examined using a UV–vis spectrophotometer. Racemic mixture released from (*M*)-NLC was analyzed at both the absorption wavelengths typical of the enantiomers (λ 222.0 nm for the (*S*)-enantiomer and λ 224.0 nm for the (*R*)-enantiomer), and the mean release value was calculated.

8.2.5   In vitro cell studies

8.2.5.1   Cell cultures

Human UM 92-1 cells were maintained at 37 °C (5% CO$_2$) in RPMI-1640 medium, containing 10% fetal bovine serum (FBS), 2 mM L-glutamine, 100 units/mL penicillin and 100 μg/mL streptomycin. Cells were split when subconfluent (70–80% confluence) and investigated within passages 2-15.

8.2.5.2 Cytotoxicity and cell proliferation

Cytotoxicity was assessed in confluent UM 92-1 cell monolayers treated for 24 h with the indicated chemicals. For cell proliferation, 92-1 cells (2.6×10^3) were seeded in 96-well plates and grown at optimum culture conditions for 72 h (at a confluence of ~60%). Then, cells were treated with the indicated compounds for additional 48 h. For both assays, at the end of treatments cells were fixed (in 4% paraformaldehyde) and stained with crystal violet solution (1% aqueous solution). Crystal violet staining was evaluated by measuring the absorbance at 590 nm, after crystal violet extraction with 10% acetic acid (at room temperature for 10 min), with a microplate reader (Synergy HT, Agilent BioTek, Santa Clara, CA).

8.2.6 Statistics

Statistical analysis for physical-chemical and technological characterization was performed by Student's t-test. For mucoadhesive studies, two-way ANOVA was performed; multiple comparisons were performed according to Tukey's multiple comparisons test for the turbidimetric assay, and for particle mean size and ZP data. For biological studies, results are shown as mean ± SD of three independent experiments performed in quadruplicate; statistical comparisons were performed by unpaired Student's t-test; all analyses were done with GraphPad Prism 8 or 9.3.1 (GraphPad Software, Inc., San Diego, CA, USA). P values were considered significant at $\alpha \leq 0.05$.

8.3 Results and discussion

8.3.1 Preliminary studies on free prodrugs

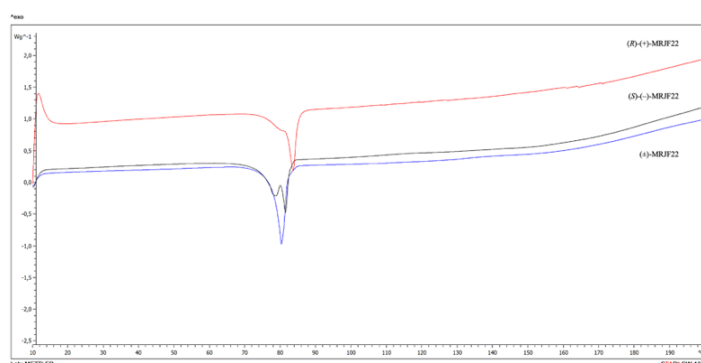In order to assess the thermal behaviour of racemic mixture and enantiomers, DSC analysis was performed.

Figure 1. DSC thermograms of (R)-(+)-MRJF22 (red line), (S)-(−)-MRJF22 (black line) and (±)-MRJF22 (blue line). (For interpretation of the references to color in this figure legend, the reader is referred to the Web version of this article.)

As it is possible to observe in Figure 1, the racemic mixture (±)-MRJF22 (blue line) showed the presence of a single well-defined peak, with a melting point of about 80 °C. This behaviour is characteristic of a species which forms racemic solid solutions. The (*S*)-(−)-MRJF22 thermogram resulted to be composed of an asymmetric peak with the main transition at 82 °C while the curve obtained for (*R*)-(+)-MRJF22 showed the presence of main transition at 84 °C with a little enlargement of the curve. The second peak highlighted in (*S*)-(−)-MRJF22 profile at 78 °C, could be related to the presence of a residuum from the synthetic process. Moreover, the presence of the melting point could relate to the possibility that molecules exist in amorphous state. The difference in melting point values for the tested molecules is not relevant and could be correlated to same thermotropic stability [17].

DSC results also suggested the suitability of the PIT method for loading the prodrugs into NLC, since the operation temperature – which is lower than the melting points of the compounds – avoids the occurrence of molecule degradation.

To further confirm the suitability of the PIT method, thermal stability studies were performed by heating the compounds solutions at 68 ± 2 °C and analyzing by UV–vis spectrophotometry. This method was already used by Rizzo and coworkers [18], who found that the formation of degradation compounds or intermediates could affect the UV value obtained at the selected wavelength. Thus, the spectra obtained after heating were compared with the ones of reference compounds' solutions (data not reported). For both enantiomers it emerged no difference in absorbance at respective characteristic peaks' wavelengths, thus confirming the stability of the prodrugs at the operative temperatures; on the other hand, a slight decrease in racemic mixture absorbance was highlighted, suggesting a possible lower stability of the compound at the operating temperature of PIT technique. The assessment of the suitability of the operative temperatures allowed to proceed with the encapsulation of prodrug into NLC using the selected organic solvent free and eco-friendly lab-scale technique [19], that has been previously reported to produce stable colloidal systems [20].

8.3.2 *Physico-chemical and technological characterization of NLC*

Raw materials for nanoparticle preparation were chosen properly to be biocompatible for ocular administration, thus allowing the interactions with cell membranes and avoiding side effects [21]. Kolliphor and Labrafil were selected as components of the surfactant mixture basing on previous studies [22], since they demonstrated to produce particles with adequate mean diameter and homogeneity, able to guarantee optimal *in vitro* release profiles. Furthermore, their biocompatibility at the ocular site was already demonstrated by our

research group [14]. Surfactants and lipids amounts were evaluated considering previous findings [16] aiming to reduce surfactant percentage – for tolerability reasons – while assuring adequate characteristics in terms of particle size.

Considering the intended ocular administration route, pH and osmolality values have to be modulated in order to fall within the ocular tolerated ranges. In particular, pH values lower than 4 or higher than 10 induce chemical damage to the eye [23], while values close to the physiological pH (7.11 ± 1.5) are well-tolerated [24]. European Pharmacopoeia and FDA both require a pH between 6.8 and 7.4 for liquid preparations used for the ocular site [25] (https://www.fda.gov/media/111063/download accessed on 25th July 2023). Regarding osmolality, this parameter has to be carefully modulated in order to provide a safe passage of particles through biological membranes; specifically, the optimal range is the tears one, between 280 and 300 mOsm/Kg [14], even though the eye is able to tolerate values from 200 to 500 mOsm/Kg (https://www.fda.gov/media/111063/download accessed on 25th July 2023). Aiming to obtain a good tolerability, TRIS buffer was selected as the aqueous phase of the colloidal system. Consequently, the prepared samples showed similar pH and osmolality values (Table 1), falling within the range required for ophthalmic administration route, thus suggesting a good cellular tolerability, which was further investigated.

As extensively reported in literature, nanoparticle size has an important influence on many parameters, such as target tolerability, formulation stability, drug distribution, residence time at the administration site. Considering ophthalmic administration, generally particles with diameter of 100 nm are actively complement receptor-mediated phagocytized in the pathway between cornea and conjunctiva, while particles in the 200–300 nm range are transported into the corneal structure through intracellular routes [26,27]. Apart for the absorption mechanism, particles smaller than 250 nm are required in order to be suitable for ophthalmic delivery [28] and a mean particle diameter lower than 200 nm is necessary in order to guarantee an adequate ocular permeation [29].

Table 1. Physical-chemical and technological characterization of NLC, (*M*)-NLC, (*S*)-NLC and (*R*)-NLC. pH, osmolality, mean particle size (Z-ave), PDI, zeta potential (ZP), and encapsulation efficiency are reported, and each value is the mean of three measurements $\pm$ SD. *p < 0.025.

Sample	pH ± SD	Osm (mOsm/kg) ± SD	Z-ave (nm) ± S.D.	PDI ± SD	ZP (mV) ± SD	EE% ± SD
NLC	7.43 ± 0.12	0.257 ± 0.019	139.1 ± 9.693	0.229 ± 0.022	-5.63 ± 0.731	/
(*M*)-NLC	7.28 ± 0.02	0.228 ± 0.005	146.6 ± 10.38	0.264 ± 0.055	-4.13 ± 0.128*	87.55 ± 11.61
(*S*)-NLC	7.36 ± 0.06	0.255 ± 0.015	142.7 ± 5.383	0.241 ± 0.022	-6.84 ± 2.91	57.17 ± 2.29
(*R*)-NLC	7.36 ± 0.06	0.254 ± 0.017	150.8 ± 6.704	0.255 ± 0.017	-6.68 ± 2.49	68.72 ± 6.56

PCS analysis showed that the produced colloidal systems were composed of small and homogeneous particles, with a mean particle size lower than 150 nm and a polydispersity

index (PDI) lower than 0.26 for all formulation, as confirmed by the single and narrow peak obtained for size distribution, with a slight increase after drug loading. According to literature, a slight increase in particle size after drug encapsulation was expected because of the accommodation space required by the active molecule into the nanoparticle [30] and due to changes in the interfacial tension or viscosity induced by the presence of the active molecule causing inefficient particle size reduction [31]. The addition of the prodrug did not significantly modify NLC Z-ave ($p < 0.025$). The optimal values of correlation coefficient (Supplementary Figure 1), obtained for all measurements, confirmed the results of the analyses. We also evaluated the ZP, a parameter that describes the particles' surface charge, which is responsible of the physical stability of the colloidal system. The almost neutral ZP values which were obtained for all formulations suggest the possible occurrence of physical instability, since ZP values between −25 mV and 25 mV are not able to guarantee long term stability due to insufficient nanoparticles repulsion, causing potential aggregational phenomena [16]. On the other hand, mean particle dimensions obtained for all the samples suggest a possible prevention of thermodynamical instability caused by Ostwald ripening [32]. Considering these hypotheses, it resulted necessary to perform further evaluations of samples' physical stability. Accelerated stability studies were performed following the ICH guidelines Q1A (R2), by storing the samples for 6 months under the effect of high temperature and humidity, thus allowing the prediction of formulations' behavior at room temperature for 1 year [33]. At each time point (0, 1, 2, 3, 4, 5 and 6 months), Z-ave and PDI were measured and compared (Figure 2). Data obtained from T0 analysis were considered the referring values for the *t*-test statistical analysis.
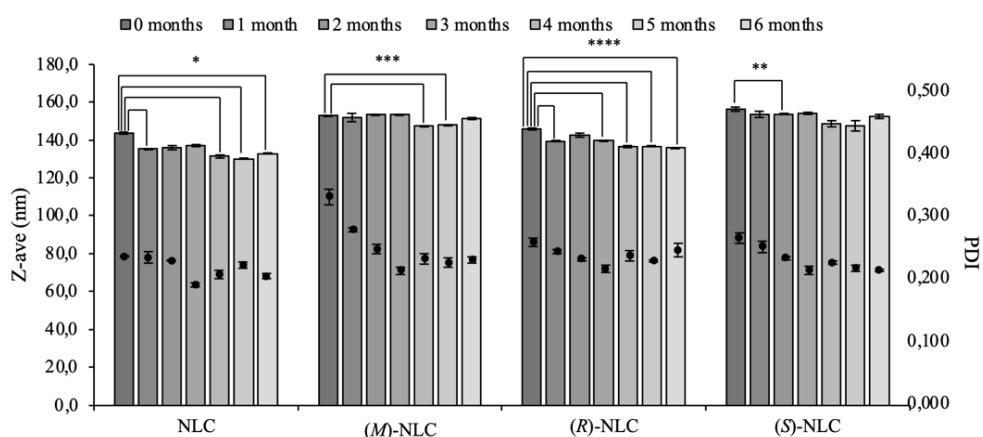

Figure 2. Effect of accelerated (40 ± 2 ◦C and 75 ± 5% RH) storage conditions on mean particle size and PDI of NLC, (*M*)-NLC, (*R*)-NLC and (*S*)-NLC. Each value is the mean of three analysis ±SD. *p<0.001; **p<0.0025; ***p<0.005; ****p<0.01.

As highlighted in Figure 2, all NLC showed a good physical long-term stability. This result could be attributable to the presence of the mixture of surfactant and co-surfactant, which provides a high stabilization of particles' surface [34]. In particular, (*S*)-NLC was the most stable sample, with particle size remaining almost unchanged during the whole storage time and showing only one significant variation in particle size after 2 months, with the lower tabulated t-value (p < 0.0025). Similarly, (*M*)-NLC was stable with significant variation (p < 0.005) in particle size after 4 and 5 months of storage at accelerated conditions, while (*R*)-NLC showed a significant variation (p < 0.01) in particle size at all analyzed time points. Even if a certain significant decrease in particle size was observed, all NLC maintained features adequate for the ophthalmic application, therefore these samples could be proposed for a storage at room temperature during industrial production and distribution. In Table 1 it is also possible to observe encapsulation efficiency values (EE%), which resulted to be higher for the racemic mixture in (*M*)-NLC compared to enantiomers, with (*R*)-enantiomer having a 10% higher EE% compared to (*S*)-enantiomer, which could be attributed to a different arrangement of each prodrug with the other NLC components.

In Figure 3 are reported the thermograms of unloaded and prodrug-loaded NLC. The lower melting temperatures and broader endothermic peaks presented by all NLC formulations indicated a less ordered crystalline structure compared to the single raw materials, as well described by values reported in Table 2. The absence of the peak related to prodrug in the loaded NLC demonstrated the successful incorporation of the molecules into the core of the nanoparticles [15,35].
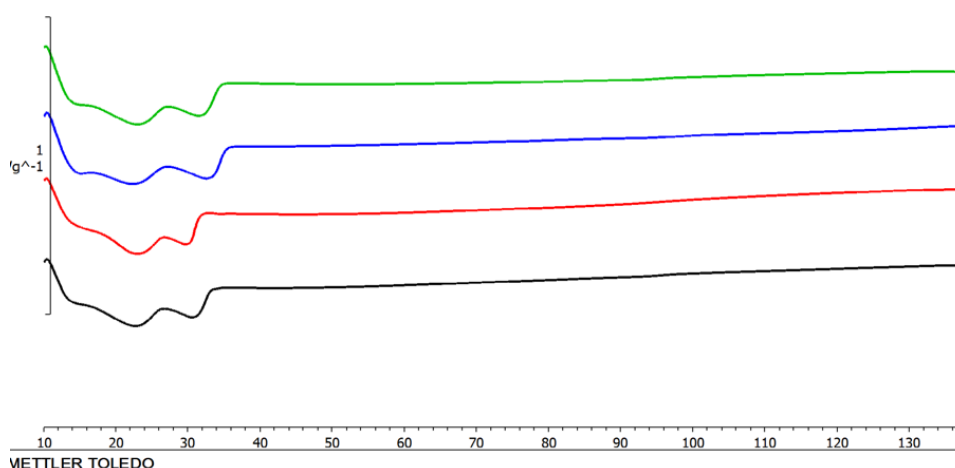

Fig 3. Thermograms of NLC (black line), (*M*)-NLC (red line), (*R*)- NLC (blue line) and (*S*)-NLC (green line). (For interpretation of the references to color in this figure legend, the reader is referred to the Web version of this article.)

Table 2. Thermal properties of raw materials and of NLC, (*M*)-NLC, (*R*)-NLC and (*S*)-NLC.

	$T_{melting}$/°C (first peak)	$T_{melting}$/°C (second peak)	$T_{melting}$/°C (third peak)
Kolliphor RH40	31.07	34.4	
Softisan 100	32.34	38.72	
NLC	22.62	30.63	145.56
(*M*)-NLC	23.03	29.70	145.14
(*S*)-NLC	22.29	32.55	145.48
(*R*)-NLC	22.86	31.45	145.95

FT-IR analysis was performed aiming to qualitatively identify the main functional groups of the materials (Supplementary Figure 2) and NLC formulations, in order to highlight the occurrence of potential chemical interactions during nanoparticles' preparation, but also to assess the encapsulation of prodrugs into NLC [36].

Comparing the spectra of the loaded-NLC to the respective free prodrugs (Figure 4-A,B,C), it is possible to highlight their successful encapsulation into the nanocarrier since some of the characteristic peaks of free molecules were not visible in loaded-NLC spectra, as the one at about 1650 cm^{-1} (C=C typical of conjugated alkene).
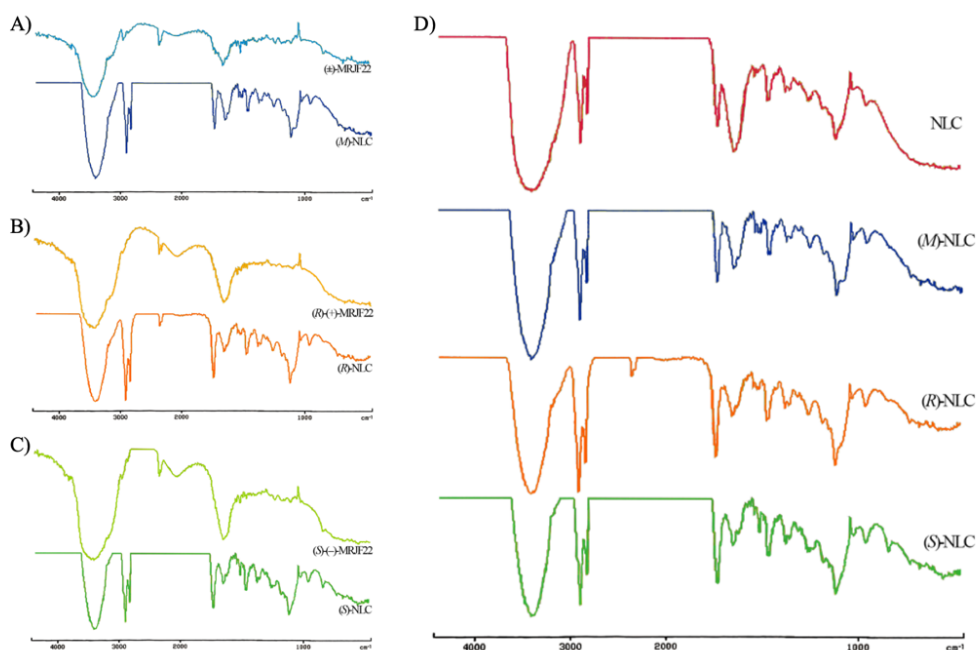

Figure 4. FT-IR curves of (±)-MRJF22 and (*M*)-NLC (**A**); (*R*)-(+)-MRJF22 and (*R*)-NLC (**B**); (*S*)-(−)-MRJF22 and (*S*)-NLC (**C**); and comparison between all the produced nanosystems (**D**).

The spectra of blank NLC and loaded-NLC (Figure 4-D) were very similar with the presence of characteristic peaks in all the obtained analysis. The peak at about 3440 cm^{-1} could be referrable at N–H stretching of I or II amines, that were present in the surfactant Kolliphor, or to O–H stretching of alcohols, typical of the co-surfactant Labrafil. The peak at about 2920 cm^{-1} is shown in all NLC formulations but also in the spectra of raw materials (Supplementary Figure 2), being relatable to C–H stretching of alkanes (largely present in

Labrafil, in the solid lipid Softisan and in the liquid lipid IPM) and to O–H stretching of intramolecular alcohols or of carboxylic acids (present in Labrafil). Peaks at about 1730 cm^{-1} were referrable to C=O stretching of esters, as in IPM structure. At lower wavelengths, in all the spectra was detected some noise, even if it is possible to identify peaks at about 1450 cm^{-1} attributable to C–H bending of alkane methyl groups (largely present in almost all the used materials) and at about 1100 cm^{-1} referrable to C–O stretching of aliphatic esters (of Labrafil and Kolliphor, as confirmed by their individual spectra in Supplementary Figure 2), but also referrable to C–F stretching (Kolliphor).

This qualitative FT-IR analysis confirmed the successful prodrugs encapsulation into nanoparticles; moreover, the absence of new peaks suggests that the interaction between prodrugs and excipients didn't produce new bonds, thus the active molecules were physically entrapped into the nanoparticles without modification of their main structure and potential activity [37].

In vitro release of (±)-MRJF22, (*R*)-(+)-MRJF22 and (*S*)-(−)-MRJF22 respectively from (*M*)-NLC, (*R*)-NLC and (*S*)-NLC was assessed using Franz-type diffusion cells (Figure 5) and compared with free prodrug release.

As expected, all prodrugs' solutions (Figure 5-A) showed an immediate release, with both enantiomers achieving 100% of drug released in 3 h, while racemic mixture was completely released in 5 h from the beginning of the experiment. As aimed, release profiles of loaded-NLC (Figure 5-B) were very different compared to prodrugs' solutions, showing a slow and prolonged release for 24 h. In particular, (*M*)-NLC showed an initial 5% of drug released, which remained basically unchanged throughout the experiment, despite racemic mixture showed the highest EE% (87.55%) among the loaded-NLC. On the other hand, (*S*)-NLC showed an initial 10% of active molecule immediately released, reaching less than 30% at 24 h. Similarly, (*R*)-NLC showed a 13% of prodrug released at T0, followed by a sustained release which reached almost 65% after 24 h from the beginning of the experiment. It is interesting to note that the release behaviours of the two enantiomers are analogue, but with a higher amplitude of (*R*)-enantiomer compared to (*S*)-enantiomer. The different release at 24 h could be referred to the different EE% values measured for (*R*)-NLC and (*S*)-NLC, which were respectively 68.72% and 57.17% and to a different accommodation of the prodrugs into the lipid matrix.

According to literature finding [38,39], NLC provided a 10% of drug release at T0 suggesting the presence of a drug-rich region on the surfactants layer [40]. All formulations were able to provide a slow and prolonged release for 24 h.
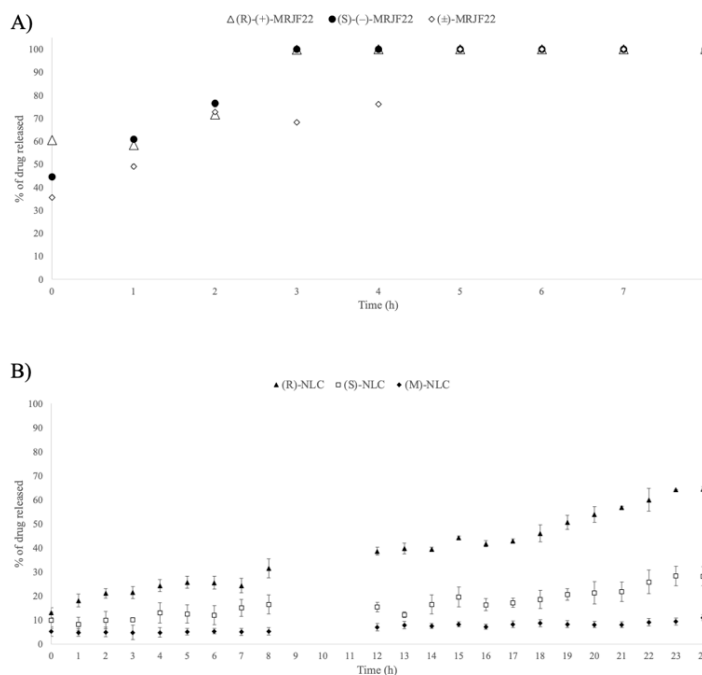
Figure 5. *In vitro* release profiles of free prodrugs solutions (**A**) and prodrug-loaded NLC (**B**) in 50:50 mixture of tris(hydroxymethyl)aminomethane buffer (TRIS) and methanol-0.5% diethylamine at 35 °C. Each point represents the mean value of three different experiments ± S.D.

The obtained release profiles resulted in agreements with previous findings on similar NLC systems developed by our research group [19], which provided a sustained and prolonged release of ferulic acid until 48 h from the beginning of the experiment. This behaviour also reflects other literature findings demonstrating that nanoparticles with diameters lower than 200 nm generally provide a burst release followed by a gradual release, while smaller ones usually provide a sustained release [38,39]. Furthermore, it was also reported that the release of the drug from the matrix is related to surfactant/lipid ratio, since increasing surfactant amounts caused a higher encapsulation of drug but also a decrease in its release rate [41]. The relation between higher encapsulation efficiency and lower release could justify (*M*)-NLC behaviour. Because of its low release, (*M*)-NLC was not further investigated.

In order to assess the potential application of NLC for ocular delivery, mucoadhesive evaluation was considered, since one of the main limitations of ophthalmic formulations is the low drug residence time on ocular surface that impairs its bioavailability. After topical instillation, the first and outermost barrier of the eye is the tear film on the ocular surface, which contains mucin, high-molecular weight glycoproteins with a protein backbone and a high carbohydrate content that contribute to the ocular mucus layer [42]. The mucus component of the tear film is currently explored as a target for drug delivery systems to deliver drugs topically to the anterior and posterior eye segments. Taking into account these

considerations, we evaluated the potential interaction of NLC suspensions with mucin in STF after incubation at physiological temperature.

As showed in Figure 6, turbidimetric assay revealed the adsorption of mucin on NLC particles surface (NLC-muc, (*R*)-NLC-muc and (*S*)-NLC-muc), which was detected as an increase of UV absorbance compared to that of the native glycoprotein at all time point considered. The significant increase of UV absorbance is the result of aggregation processes [43] that suggests the occurrence of interactions phenomena between each particles suspension and the glycoprotein in STF.
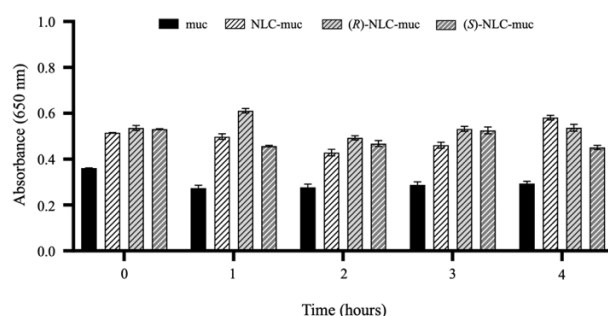
Figure 6. *In vitro* assessment of samples/mucin interactions at different time points (0, 1, 2, 3 and 4 h) by turbidimetric assay at 650 nm. Significance was set as ****$p \leq 0.0001$ for all samples vs mucin.

These findings were furtherly confirmed by mucin particle method assay. As showed in Figure 7, all samples suffered a significant variation in particles size and zeta potential after incubation with mucin confirming the occurrence of interactions [14]. The entity of interaction seems to be more evident starting from 2 h of incubation (Figure 7-A) and no difference can be detected among NLC samples (Figure 7), suggesting that the mucoadhesion has to be attributed to the carrier itself and does not depends on the encapsulated drug; this result suggests that the presence of the drug being conveyed into the particles did not affect the interaction of the system with mucin. All samples maintained their homogeneity even in the presence of mucin, as revealed by PDI values ≤ 0.3 at all time points (data not reported).
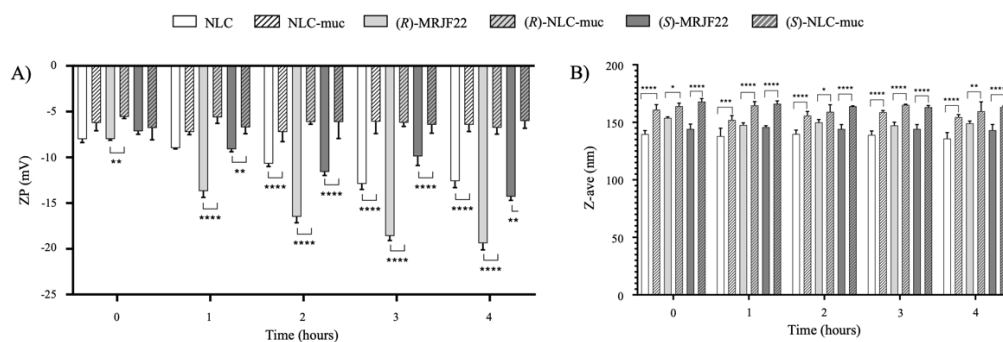

Figure 7. Zeta potential (ZP) values (**A**) and mean particle size (Z-ave) values (**B**) of samples (NLC, (*R*)-NLC and (*S*)-NLC) before 0 and after 1, 2, 3 and 4h of incubation with mucin (NLC-muc, (*R*)-NLC-muc and (S)-NLC-muc) at 37 °C. Significance was set as **$p \leq 0.01$; ****$p \leq 0.0001$ for ZP; and as *$p \leq 0.05$; **$p \leq 0.01$; ***$p \leq 0.001$; ****$p \leq 0.0001$ for Z-ave.

Interaction occurring at mucin/formulation interface is a complex process that involves different mechanisms, such as that proposed by the wetting; electronic; adsorption; fracture; mechanical; and diffusion interlocking theories [44]. Here, the interaction was probably the result of hydrogen bonds and van der Waals interaction due to the adsorption mechanism or due to the diffusion mechanism which is governed by time and concentration gradient. Following diffusion, sufficient interpenetration depth and chain entanglements induce semi-permanent mucoadhesive bond formation [45]. However, mucoadhesion is based on the contact between the instilled formulation at the mucous surface, and the interpenetration into the mucosal layer that consolidate the formed interfacial interactions. This second phase known as "consolidation stage" is crucial for formulations undergoing higher physical stresses, such as ocular administration, since it assures the entity of their binding [46].

8.3.3 *In vitro cell studies*

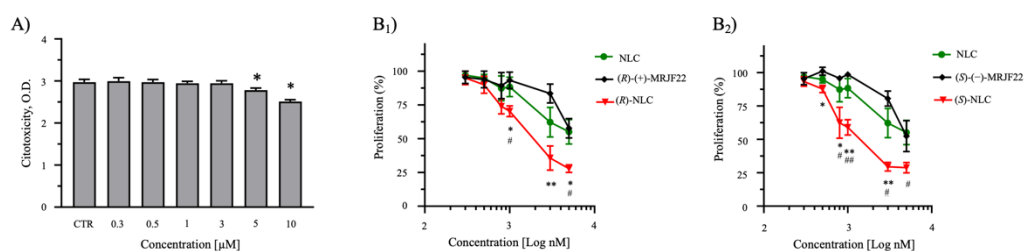Pharmacological effects of (*R*)-NLC and (*S*)-NLC were examined in human UM 92-1 cells by crystal violet staining.

Figure 8. Effects of anticancer prodrug-loaded NLC on UM cells. (**A**) Cytotoxicity in human 92-1 UM cells after 24 h treatment with unloaded NLC. *p<0.05 vs CTR by unpaired Student's t-test. (**B-C**) Dose-response curves of inhibition of proliferation by the indicated compounds. Data represent % of proliferation compared to the vehicle control (DMSO). *p<0.05; **p<0.01 vs (*R*)-(+)-MRJF22 or (*S*)-(−)-MRJF22; #p<0.5; ##p<0.01 vs NLC by unpaired Student's t-test. CTR, vehicle control DMSO.

First, non-specific cytotoxicity by NLC was checked, demonstrating that unloaded NLC does not cause overt toxicity to UM cells below 5 μM concentrations (Figure 8-A). Then, dose-response curves were carried out to investigate antiproliferative actions by loaded or unloaded NLC and free bioactive compounds (Figure 8-B,C). Compared to the respective blank NLC or free compound, both (*R*)-NLC (Figure 8-B) and (*S*)-NLC (Figure 8-C) induced a shift to the left of antiproliferative curves in UM 92-1 cells, indicating potentiation of (*R*)-(+)-MRJF22 and (*S*)-(−)-MRJF22 anticancer effects by NLC with significant extents starting at submicromolar concentrations.

Table 3. Statistical analysis of effects on UM cell proliferation by the indicate compounds. *p<0.05; **p<0.01; ***p<0.001 vs the vehicle control DMSO by unpaired Student's t-test; ns, not significant.

Dose (µM)	NLC	(R)-(+)-MRJF22	(R)-NLC	(S)-(−)-MRJF22	(S)-NLC
0.1	ns	ns	ns	ns	ns
0.3	ns	ns	ns	ns	**
0.8	ns	ns	**	ns	**
1	ns	ns	***	ns	***
3	*	*	***	**	***
5	**	**	***	**	***

Accordingly, prodrug-loaded NLC significantly inhibited UM cell proliferation at concentrations as low as 0.3 µM for (S)-NLC or 0.8 µM for (R)-NLC, compared to the vehicle control (Table 3). In contrast, blank NLC or each bioactive compound alone exerted significant antiproliferation only at ≥3 µM ranges (Table 3).

Moreover, estimations of inhibitory concentrations inducing 50% anticancer effects (IC50) confirmed that compounds delivered to cells with NLC exhibited significantly superior antiproliferative potencies than corresponding free drugs or unloaded nanocarriers, with a ~3- or 4-fold increased anticancer activity for (R)-NLC and (S)-NLC, respectively (Table 4).

Finally, compared to (R)-NLC, the nanoformulation (S)-NLC exhibited higher antiproliferative potency (Figure 8 and Table 4), despite less favorable drug encapsulation efficiency (Table 1) and release dynamics (Figure 5-B). In contrast, the free prodrugs were almost identical in inhibiting UM cell proliferation (Table 4), confirming previous findings [9]. Since (S)-NLC particles exhibit smaller diameter sizes than (R)-NLC (Table 1), it could be possible that (S)-NLC nanocarrier dimensions provide superior cell permeation capabilities [29], associated with enhanced drug concentrations at pharmacological sites of action.

Table 4. IC_{50} of NLC, (R)-NLC, (S)-NLC, (R)-(+)-MRJF22 and (S)-(−)-MRJF22 on UM 92-1 cell proliferation. Data are expressed as mean ± SD. *p<0.01 vs (R)-(+)-MRJF22; $p<0.5 vs NLC, and #p<0.001 vs (S)-(−)-MRJF22 by one-tailed, unpaired Student's t-test.

Sample	IC_{50} (µM)
NLC	6.96 ± 2.96
(R)-NLC	2.29 ± 0.69[*, $]
(S)-NLC	1.57 ± 0.22[#, $]
(R)-(+)-MRJF22	6.45 ± 2.77
(S)-(−)-MRJF22	6.72 ± 0.53

Collectively, the presented data indicate that the proposed nanostructured lipid carrier systems represent molecular facilitator tools for (R)-(+)-MRJF22 and (S)-(−)-MRJF22 anticancer pharmacology in UM 92-1 cells, probably reflecting an enhanced compound passage across cell plasma membranes and drug delivery to intracellular targets. It was already demonstrated the higher potency of (S)-(−)-MRJF22 – compared to racemic mixture and (R)-enantiomer – in reducing cell proliferation on UM 92-1 cells [9], probably

related to the inhibition of HDAC, and this activity could be additive to the intrinsic antiproliferative property of the NLC itself, resulting in a potential dual function-dual target platform as a novel therapeutic strategy for UM patients [9]. In particular, dual function, dual target (*S*)-(−)-MRJF22 loaded into NLC might provide a novel therapeutic strategy for UM patients with optimal antitumor activity.

8.4 Conclusions

The new synthetized prodrugs – both in form of racemic mixture and single enantiomers – were successfully encapsulated into lipid nanoparticles with adequate features for the intended ocular administration. Moreover, (*S*)-enantiomer loaded-NLC showed a higher *in vitro* antiproliferative activity, thus representing a safe and potentially efficient platform to be used as adjuvant in the treatment of uveal melanoma. Further studies are still ongoing to assess the NLC behavior after *in vivo* ocular administration.

Author contributions: **Cinzia Cimino**: conceptualization, data curation, formal analysis, investigation, methodology, writing – original draft, writing – review and editing. **Claudia Giovanna Leotta**: investigation, formal analysis, data curation, writing – original draft. **Agostino Marrazzo**: data curation, writing – review and editing, project administration. **Teresa Musumeci**: investigation, data curation, writing – original draft. **Giovanni Mario Pitari**: investigation, data curation, writing – original draft. **Rosario Pignatello**: data curation, writing – original draft, writing – review and editing. **Angela Bonaccorso**: investigation, formal analysis, data curation, writing – original draft. **Carla Barbaraci**: data curation, writing – review and editing. **Claudia Carbone**: conceptualization, funding acquisition, methodology, supervision, writing – original draft, writing – review and editing. All authors have read and agreed to the published version of the manuscript.

Institutional review board statement: Not applicable.

Informed consent statement: Not applicable.

Declaration of competing interest: The authors declare that they have no known competing financial interests or personal relationships that could have appeared to influence the work reported in this paper.
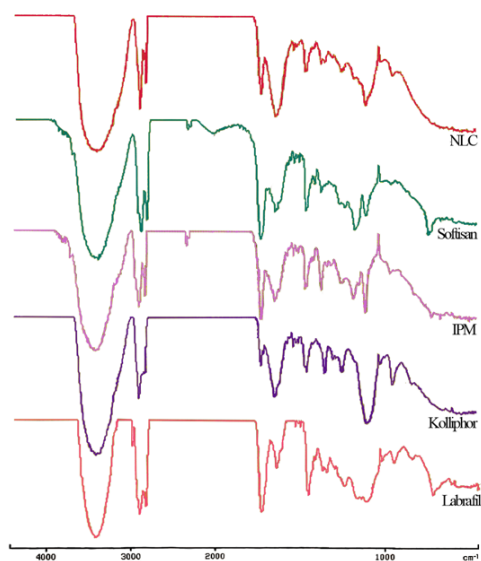
Data availability: The data that has been used is confidential.

Appendix A. Supplementary data: Supplementary data to this article can be found online at https://doi. org/10.1016/j.jddst.2023.104811.
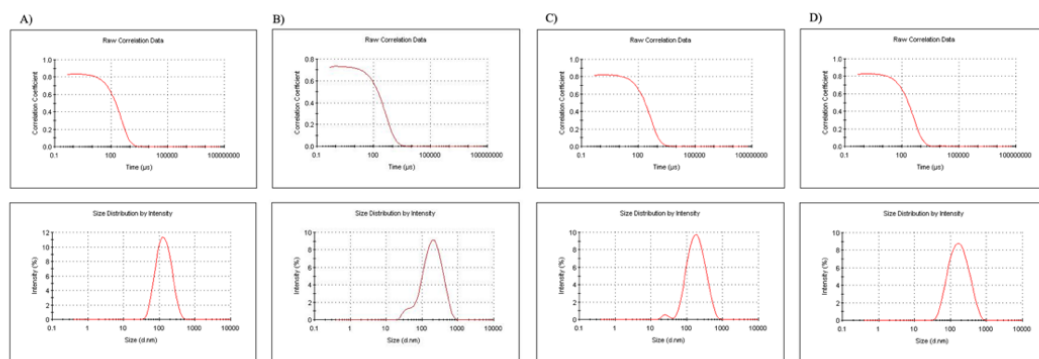
Supplementary Figure 1. Mean size distribution measured as percentage of scattered light of NLC (**A**), (*M*)-NLC (**B**), (*R*)-NLC (**C**) and (*S*)-NLC (**D**).

Supplementary Figure 2. FT-IR curves of NLC and of all raw material used for their preparation.

References:

[1] S. Kaliki, C.L. Shields, A. Mashayekhi, A. Ganesh, M. Furuta, J.A. Shields, Influence of age on prognosis of young patients with uveal melanoma: a matched retrospective cohort study, Eur. J. Ophthalmol. 23 (2) (Mar. 2013) 208–216, https://doi.org/10.5301/ejo.5000200.

[2] F. Spagnolo, G. Caltabiano, P. Queirolo, Uvealmelanoma, Cancer Treat Rev. 38(5) (Aug. 2012) 549–553, https://doi.org/10.1016/j.ctrv.2012.01.002.

[3] A. Schmidt-Pokrzywniak, K.-H. Jöckel, N. Bornfeld, W. Sauerwein, A. Stang, Positive interaction between light Iris color and ultraviolet radiation in relation to the risk of uveal melanoma, Ophthalmology 116 (2) (Feb. 2009) 340–348, https://doi.org/10.1016/j.ophtha.2008.09.040.

[4] C.L. Shields, et al., Association of ocular and oculodermal melanocytosis with the rate of uveal melanoma metastasis: analysis of 7872 consecutive eyes, JAMA Ophthalmol 131 (8) (Aug. 2013) 993, https://doi.org/10.1001/jamaophthalmol.2013.129.

[5] Assessment of metastatic disease status at death in 435 patients with large choroidal melanoma in the collaborative ocular melanoma study (COMS), Arch. Ophthalmol. 119 (2001) 670–676.

[6] M.M. Moschos, et al., The role of histone deacetylase inhibitors in uveal melanoma: current evidence, Anticancer Res. 38 (7) (Jul. 2018) 3817–3824, https://doi.org/ 10.21873/anticanres.12665.

[7] S. Landreville, et al., Histone deacetylase inhibitors induce growth arrest and differentiation in uveal melanoma, Clin. Cancer Res. 18 (2) (Jan. 2012) 408–416, https://doi.org/10.1158/1078-0432.CCR-11-0946.

[8] M. Olivieri, et al., Antiangiogenic effect of (±)-Haloperidol metabolite II valproate ester [(±)-MRJF22] in human microvascular retinal endothelial cells, J. Med. Chem. 59 (21) (Nov. 2016) 9960–9966, https://doi.org/10.1021/acs.jmedchem.6b01039.

[9] C. Barbaraci, et al., Haloperidol metabolite II valproate ester (S)-(−)-MRJF22: preliminary studies as a potential multifunctional agent against uveal melanoma, J. Med. Chem. 64 (18) (Sep. 2021) 13622–13632, https://doi.org/10.1021/acs. jmedchem.1c00995.

[10] X.-Y. Xie, et al., Synthesis, binding, and functional properties of tetrahydroisoquinolino-2-alkyl phenones as selective σ2R/TMEM97 ligands, Eur. J. Med. Chem. 209 (Jan. 2021), 112906, https://doi.org/10.1016/j. ejmech.2020.112906.

[11] E.B. Souto, et al., Advanced formulation approaches for ocular drug delivery: state-of-the-art and recent patents, Pharmaceutics 11 (9) (Sep. 2019) 460, https://doi. org/10.3390/pharmaceutics11090460.

[12] R. Liu, Z. Liu, C. Zhang, B. Zhang, Nanostructured lipid carriers as novel ophthalmic delivery system for mangiferin: improving in vivo ocular bioavailability, J. Pharmaceut. Sci. 101 (10) (Oct. 2012) 3833–3844, https://doi.org/10.1002/jps.23251.

[13] E. Sánchez-López, M. Espina, S. Doktorovova, E.B. Souto, M.L. García, Lipid nanoparticles (SLN, NLC): overcoming the anatomical and physiological barriers of the eye – Part I – barriers and determining factors in ocular delivery, Eur. J. Pharm. Biopharm. 110 (Jan. 2017) 70–75, https://doi.org/10.1016/j.ejpb.2016.10.009.

[14] A. Bonaccorso, et al., Sorafenib repurposing for ophthalmic delivery by lipid nanoparticles: a preliminary study, Pharmaceutics 13 (11) (Nov. 2021) 1956, https://doi.org/10.3390/pharmaceutics13111956.

[15] C. Carbone, A. Campisi, T. Musumeci, G. Raciti, R. Bonfanti, G. Puglisi, FA-loaded lipid drug delivery systems: preparation, characterization and biological studies, Eur. J. Pharmaceut. Sci. 52 (Feb. 2014) 12–20, https://doi.org/10.1016/j. ejps.2013.10.003.

[16] C. Carbone, C. Caddeo, M.A. Grimaudo, D.E. Manno, A. Serra, T. Musumeci, Ferulic acid-NLC with lavandula essential oil: a possible strategy for wound-healing? Nanomaterials 10 (5) (May 2020) 898, https://doi.org/10.3390/nano10050898.

[17] D.F. Bánhegyi, D. Szolcsányi, J. Madarász, E. Pálovics, Enantiomeric separation of racemic amlodipine by sequential fractional crystallization through formation of diastereomeric salt solvates and co-crystals of solvate-like compounds with specific structure — a tandem resolution, Chirality 34 (2) (Feb. 2022) 374–395, https:// doi.org/10.1002/chir.23373.

[18] L. Rizzo, S. Meric, D. Kassinos, M. Guida, F. Russo, V. Belgiorno, Degradation of diclofenac by TiO2 photocatalysis: UV absorbance kinetics and process evaluation through a set of toxicity bioassays, Water Res. 43 (4) (Mar. 2009) 979–988, https://doi.org/10.1016/j.watres.2008.11.040.

[19] C. Carbone, et al., Dual-drugs delivery in solid lipid nanoparticles for the treatment of Candida albicans mycosis, Colloids Surf. B Biointerfaces 186 (Feb. 2020), 110705, https://doi.org/10.1016/j.colsurfb.2019.110705.

[20] I. Chauhan, M. Yasir, M. Verma, A.P. Singh, Nanostructured lipid carriers: a groundbreaking approach for transdermal drug delivery, Adv. Pharm. Bull. 10 (2) (Feb. 2020) 150–165, https://doi.org/10.34172/apb.2020.021.

[21] J.-Y. Lai, Biocompatibility of chemically cross-linked gelatin hydrogels for ophthalmic use, J. Mater. Sci. Mater. Med. 21 (6) (Jun. 2010) 1899–1911, https:// doi.org/10.1007/s10856-010-4035-3.

[22] C. Carbone, et al., Mediterranean essential oils as precious matrix components and active ingredients of lipid nanoparticles, Int. J. Pharm. 548 (1) (Sep. 2018) 217–226, https://doi.org/10.1016/j.ijpharm.2018.06.064.

[23] L.T. Lim, E.Y. Ah-Kee, C.E. Collins, Common eye drops and their implications for pH measurements in the management of chemical eye injuries, Int. J. Ophthalmol. 7 (6) (2014) 1067–1068, https://doi.org/10.3980/j.issn.2222-3959.2014.06.29.

[24] W.H. Coles, P.A. Jaros, Dynamics of ocular surface pH, Br. J. Ophthalmol. 68 (8) (Aug. 1984) 549–552, https://doi.org/10.1136/bjo.68.8.549.

[25] R. Pignatello, Optimization and validation of a new method for the production of lipid nanoparticles for ophthalmic application, Int. J. Med. Nano Res. 1 (1) (Dec. 2014), https://doi.org/10.23937/2378-3664/1410006.

[26] A. Tatke, et al., In situ gel of triamcinolone acetonide-loaded solid lipid nanoparticles for improved topical ocular delivery: tear kinetics and ocular disposition studies, Nanomaterials 9 (1) (Dec. 2018) 33, https://doi.org/10.3390/nano9010033.

[27] M. Yadav, et al., Atorvastatin-loaded solid lipid nanoparticles as eye drops: proposed treatment option for age-related macular degeneration (AMD), Drug Deliv. Transl. Res. 10 (4) (Aug. 2020) 919–944, https://doi.org/10.1007/s13346-020-00733-4.

[28] A.L. Onugwu, A.A. Attama, P.O. Nnamani, S.O. Onugwu, E.B. Onuigbo, V.V. Khutoryanskiy, Development and optimization of solid lipid nanoparticles coated with chitosan and poly(2-ethyl-2-oxazoline) for ocular drug delivery of ciprofloxacin, J. Drug Deliv. Sci. Technol. 74 (Aug. 2022), 103527, https://doi. org/10.1016/j.jddst.2022.103527.

[29] L. Bonilla, et al., Lipid nanoparticles for the posterior eye segment, Pharmaceutics 14 (1) (Dec. 2021) 90, https://doi.org/10.3390/pharmaceutics14010090.

[30] H. Rouco, et al., Rifabutin-loaded nanostructured lipid carriers as a tool in oral anti-mycobacterial treatment of crohn's disease, Nanomaterials 10 (11) (Oct. 2020) 2138, https://doi.org/10.3390/nano10112138.

[31] G.I. Sakellari, I. Zafeiri, H. Batchelor, F. Spyropoulos, Formulation design, production and characterisation of solid lipid nanoparticles (SLN) and nanostructured lipid carriers (NLC) for the encapsulation of a model hydrophobic active, Food Hydrocoll. Health 1 (2021), 100024, https://doi.org/10.1016/j. fhfh.2021.100024.

[32] W. Mehnert, Solid lipid nanoparticles Production, characterization and applications, Adv. Drug Deliv. Rev. 47 (2–3) (Apr. 2001) 165–196, https://doi.org/10.1016/S0169-409X(01)00105-3.

[33] M. Agrawal, et al., Design and optimization of curcumin loaded nano lipid carrier system using Box-Behnken design, Biomed. Pharmacother. 141 (Sep. 2021), 111919, https://doi.org/10.1016/j.biopha.2021.111919.

[34] U. Ilyas, et al., Nanostructured lipid carrier-based delivery of pioglitazone for treatment of type 2 diabetes, Front. Pharmacol. 13 (Jul. 2022), 934156, https:// doi.org/10.3389/fphar.2022.934156.

[35] E. Zingale, et al., Optimization of lipid nanoparticles by response surface methodology to improve the ocular delivery of diosmin: characterization and in- vitro anti-inflammatory assessment, Pharmaceutics 14 (9) (Sep. 2022) 1961, https://doi.org/10.3390/pharmaceutics14091961.

[36] V. Teeranachaideekul, B. Morakul, P. Boonme, W. Pornputtapitak, V. Junyaprasert, Effect of lipid and oil compositions on physicochemical properties and photoprotection of octyl methoxycinnamate-loaded nanostructured lipid carriers (NLC), J. Oleo Sci. 69 (12) (2020) 1627–1639, https://doi.org/10.5650/jos. ess20093.

[37] P. Chand, et al., Design and evaluation of cabazitaxel loaded NLCs against breast cancer cell lines, Colloids Surf. B Biointerfaces 199 (Mar. 2021), 111535, https:// doi.org/10.1016/j.colsurfb.2020.111535.

[38] E. Sakurai, H. Ozeki, N. Kunou, Y. Ogura, Effect of particle size of polymeric nanospheres on intravitreal kinetics, Ophthalmic Res. 33 (1) (2001) 31–36, https://doi.org/10.1159/000055638.

[39] Y. Weng, J. Liu, S. Jin, W. Guo, X. Liang, Z. Hu, Nanotechnology-based strategies for treatment of ocular disease, Acta Pharm. Sin. B 7 (3) (May 2017) 281–291, https://doi.org/10.1016/j.apsb.2016.09.001.

[40] P.A. Makoni, K. Wa Kasongo, R.B. Walker, Short term stability testing of efavirenz- loaded solid lipid nanoparticle (SLN) and nanostructured lipid carrier (NLC) dispersions, Pharmaceutics 11 (8) (Aug. 2019) 397, https://doi.org/10.3390/ pharmaceutics11080397.

[41] B. Sharif Makhmal Zadeh, H. Niro, F. Rahim, G. Esfahani, Ocular delivery system for propranolol hydrochloride based on nanostructured lipid carrier, Sci. Pharm. 86 (2) (Apr. 2018) 16, https://doi.org/10.3390/scipharm86020016.

[42] G. As Georgiev, P. Eftimov, N. Yokoi, Contribution of mucins towards the physical properties of the tear film: a modern update, Int. J. Mol. Sci. 20 (24) (Dec. 2019) 6132, https://doi.org/10.3390/ijms20246132.

[43] P.N. Hanieh, et al., Almond oil O/W nanoemulsions: potential application for ocular delivery, J. Drug Deliv. Sci. Technol. 72 (Jun. 2022), 103424, https://doi. org/10.1016/j.jddst.2022.103424.

[44] S. Duggan, W. Cummins, O. O' Donovan, H. Hughes, E. Owens, Thiolated polymers as mucoadhesive drug delivery systems, Eur. J. Pharmaceut. Sci. 100 (Mar. 2017) 64–78, https://doi.org/10.1016/j.ejps.2017.01.008.

[45] A.M. Burhan, et al., Posterior segment ophthalmic drug delivery: role of muco- adhesion with a special focus on chitosan, Pharmaceutics 13 (10) (Oct. 2021) 1685, https://doi.org/10.3390/pharmaceutics13101685.

[46] J. Smart, The basics and underlying mechanisms of mucoadhesion, Adv. Drug Deliv. Rev. 57 (11) (Nov. 2005) 1556–1568, https://doi.org/10.1016/j. addr.2005.07.001.

9 FLUORESCENT NANOSYSTEMS FOR DRUG TRACKING AND THERANOSTICS: RECENT APPLICATIONS IN THE OCULAR FIELD

Elide Zingale[1,†], Alessia Romeo[1,†], Salvatore Rizzo[1], Cinzia Cimino[1], Angela Bonaccorso[1,2], Claudia Carbone[1,2], Teresa Musumeci[1,2] and Rosario Pignatello[1,2,*]

[1] Department of Pharmaceutical and Health Sciences, University of Catania, 95124 Catania, Italy.

[2] NANO-i—Research Center for Ocular Nanotechnology, University of Catania, 95124 Catania, Italy.

[*] Corresponding author

[†] These authors contributed equally to this work.

Abstract: The greatest challenge associated with topical drug delivery for the treatment of diseases affecting the posterior segment of the eye is to overcome the poor bioavailability of the carried molecules. Nanomedicine offers the possibility to overcome obstacles related to physiological mechanisms and ocular barriers by exploiting different ocular routes. Functionalization of nanosystems by fluorescent probes could be a useful strategy to understand the pathway taken by nanocarriers into the ocular globe and to improve the desired targeting accuracy. The application of fluorescence to decorate nanocarrier surfaces or the encapsulation of fluorophore molecules makes the nanosystems a light probe useful in the landscape of diagnostics and theranostics. In this review, a state of the art on ocular routes of administration is reported, with a focus on pathways undertaken after topical application. Numerous studies are reported in the first section, confirming that the use of fluorescent within nanoparticles is already spread for tracking and biodistribution studies. The first section presents fluorescent molecules used for tracking nanosystems' cellular internalization and permeation of ocular tissues; discussions on the classification of

nanosystems according to their nature (lipid-based, polymer-based, metallic-based and protein-based) follows. The following sections are dedicated to diagnostic and theranostic uses, respectively, which represent an innovation in the ocular field obtained by combining dual goals in a single administration system. For its great potential, this application of fluorescent nanoparticles would experience a great development in the near future. Finally, a brief overview is dedicated to the use of fluorescent markers in clinical trials and the market in the ocular field.

Keywords: nanotechnology; fluorescence; ocular delivery; probes; diagnostics; PKs

9.1   Introduction

In recent years, vision-related problems have acquired a greater relevance due to the ageing of the world's population, which leads to an increase in visual problems, such as cataracts, glaucoma, age-related macular degeneration and diabetic retinopathy, occurring more frequently among over-60s [1,2]. Many visual diseases are associated with neurodegenerative disorders [3,4]. Young people over the age of 18 also suffer from visual problems, which increase especially with the growing use of electronic devices [5]. The rising number of people with vision impairment leads to a greater interest in dedicated care and treatments. This situation increases the costs in the global economy destined for the care of these disorders [6]. In addition, ocular therapy is a serious challenge because of the difficulty in targeting a drug to the appropriate ocular tissues.

In this landscape, technological research is actively involved, with the aim of developing innovative systems for targeted drug delivery [7]. The eye is a very complex structure, both anatomically and physiologically, and the treatment of pathologies affecting this organ is therefore not simple [8–10]. This is related to the various aspects that limit the transportation of drugs to the target site: anatomical barriers, physiological processes, mechanisms and metabolic aspects [11,12]. Reaching the target becomes more complicated if therapy is addressed to the posterior segment of the eye [13–16]. For this purpose, the major administration route remains intravitreal injection, which is invasive and produces undesirable effects such as pain and discomfort, inducing patient noncompliance [17,18]. The preferred route of administration would undoubtedly be the topical one, but conventionally it is used to treat diseases of the anterior eye. In fact, it is estimated that only a very small percentage of the drug instilled in the eye surface reaches the anterior chamber (around 5%) and even less in the posterior segment [19–21].

Nanotechnology represents a field of recent interest to overcome these issues. One potential strategy for improving drug delivery to the different eye tissues uses nanocarriers with specific size and surface properties, designed to ensure successful achievement of the drug to the target tissue, as well as the potential for a controlled release of the loaded drug, reducing the frequency of treatment and improving the retention time on the corneal surface [22–24]. Currently, the most widely studied nanosystems are used in the treatment of anterior eye diseases such as cataracts [25], glaucoma [26], dry eye syndrome [27], keratitis [28], conjunctivitis [29] and uveitis [30], but also posterior eye diseases such as retinitis [31], macular degeneration [32], endophthalmitis [33] and ocular tumors [34]. Suitable drug nanocarriers possess a mean size in the nanometric range (around 200 nm) and are classified according to their structural composition and the materials used, which must be biodegradable and biocompatible [35,36]. Many reviews focus on the development of nanosystems designed for ocular delivery, but none on the ophthalmic use of fluorescent nanocarriers. It is not certain that after their administration, the drug effectively reaches the target site; therefore, during its design, tracking studies are necessary to demonstrate its distribution and positioning.

One possible strategy is to follow the nanosystem movements using a fluorescent probe. Fluorescence is a simple and non-invasive way to track the drug through the eye tissues, and it is also widely used in diagnostics to visualize diseased tissues, lesions and pathological markers. The development of personalized medicine and the need for early intervention in the diagnosis and treatment of specific diseases have promoted the birth and development of a new discipline: theranostics [37]. It can be defined as the combination of diagnostics with a specific therapeutic treatment. *In vitro* diagnostics and prognostics, *in vivo* molecular imaging, molecular therapeutics, image-guided therapy, biosensors, nanobiosensors and bioelectronics, system biology and translational medicine and point-of-care are some recent application examples.

This review deals with the use of fluorescent probes in the last 5 years applied to nanomedicine in the ophthalmic field. The aim is to illustrate state-of-the-art fluorescent nanosystems divided according to their application: fluorescent nanosystems for biodistribution studies to clarify the best performing nanoparticle design and delivery strategies able to address specific ocular diseases, for diagnostics and finally, for the emerging field of theranostics. PubMed database was used to perform an advanced search. The time frame included the range from January 2017 to February 2022. The keywords used were "fluorescence", "nanoparticles", "ocular" and "delivery", "theranostics", "diagnostics". Articles were limited to "Free full text" and "Full text" articles in the English

language published in journals with an impactor factor not less than 4. The same process was repeated on ScienceDirect database. Reference lists of articles were also reviewed for additional citations.

9.1.1 General Aspect of the Human Eye

The eyeball consists of three chambers: anterior, posterior (containing the aqueous humor) and the vitreous chamber (containing the vitreous body). The wall is composed of three tunics [8,38]. The first, called external, is composed anteriorly of the cornea and for the remaining part of the sclera. The middle tunic (uvea) is richly vascularized and pigmented and includes the iris, the ciliary body and the choroid. Finally, the internal or nervous tunic is represented by the retina [39]. The sclera is anteriorly lined by the conjunctiva. Its function is to maintain the shape of the bulb and to provide attachment to the tendons of the striated muscles of the eye [40]. The cornea is a transparent lamina without vessels (necessary conditions for the passage of light). A cross-section of the corneal tissues is shown in Figure 1. Under the cornea, there is the iris, a sphincter of pigmented smooth muscle that regulates pupillary caliber. Trophism in this district is provided by the aqueous humor [41]. The ciliary body is an ocular anatomical structure responsible for both the production of aqueous humor and the control of accommodation. The ciliary body is located immediately posterior to the iris and anterior to the choroid. Posterior to the iris and in front of the vitreous body is where the crystalline is situated, which transmits and focuses light onto the retina. It consists of a single layer of epithelial cells that, during fetal development, migrate laterally toward the equator of the lens where it inverts, elongates, synthesizes large amounts of specific proteins and finally, degrades organelles so as to increase transparency [20]. From a physiological perspective, there are two reflexes involved in vision: lens accommodation (regulates convexity) and pupillary reflex (regulates pupil caliber). The accommodation allows the focal point to fall always at the level of the retina, allowing both short- and long-distance vision. Furthermore, the pupillary reflex regulates the intensity of incoming light. Finally, the transduction of light impulses at the retinal level into visual images is mediated by photoreceptors which generate nerve stimuli that reach the contralateral posterior cortex through the optic nerve [42–44]. The delivery of a drug into the eye tissues is related to two different routes of administration, which are divided into invasive and non-invasive routes. A list of these routes is shown in Table 1.

_____

Table 1. Conventional route of ocular delivery: benefits and limits.

| ADMINI-STRATION ROUTE	BENEFITS	LIMITS	OCULAR ANTERIOR / POSTERIOR TARGET	References
Oral	• Non-invasive. • Increased compliance.	• Difficult achievement of the anterior and posterior tracts of the eye. • Possible degradation by digestive fluids. • Possible low absorption and bioavailability. • Hepatic first-pass metabolism. • Presence of anatomical barriers (blood-aqueous barrier and the blood-retinal barrier).	Potentially both	[45-48]
Systemic (Intravenous and intramuscular)	• Avoided first-pass metabolism.	• Difficult achievement of the anterior or posterior segment of the eye. • Lower compliance. • Presence of anatomical barriers (blood-aqueous barrier and the blood-retinal barrier). • Sterility of the final form	Potentially both	[48,49]
Parenteral (Intravitreal, subretinal, suprachoroidal, subconjunctival, intracameral, intrascleral, and intrastromal)	• Deposit of the therapeutic agent in the eye, in some cases directly at the site of action. • Increased local concentration of the drug. • Reduced required dose and avoided off-target actions. • Bypassing of ocular epithelium and other barriers, resulting in increased bioavailability.	• Administration performed by specialized personnel. • Invasive technique. • Short-term complications, including retinal damage, endophthalmitis, haemorrhage, intraocular inflammation, and increased Intraocular Pressure (IOP). • Sterility of the final form	Posterior	[50-55]
Topical	• Over 90% of the ophthalmic product on the market.	• Rapid precorneal elimination of the drug due to eyelid reflex, tear drainage, dilution by tears, and systemic absorption from the conjunctival sac. • Misapplication of the product to the ocular surface. • Presence of corneal epithelial barrier. • Narrow barriers at the front and back of the eye (limit and regulate fluid and solute uptake). • Complex kinetic processes of absorption, distribution and elimination, influenced by physiology, the physicochemical properties of the drug (lipophilicity, charge, size and shape of the molecule) and the formulation (pH, buffer, tonicity, viscosity, possible presence of preservatives and stabilizers). • Allowed permeation of small lipophilic molecules through the cornea and of larger or hydrophilic compounds through the conjunctiva and the sclera. • Achievement of the anterior segment for only 1% of the administered dose segment, and an even smaller percentage to the posterior segment. • Sterility of the final form	Both	[56-64]
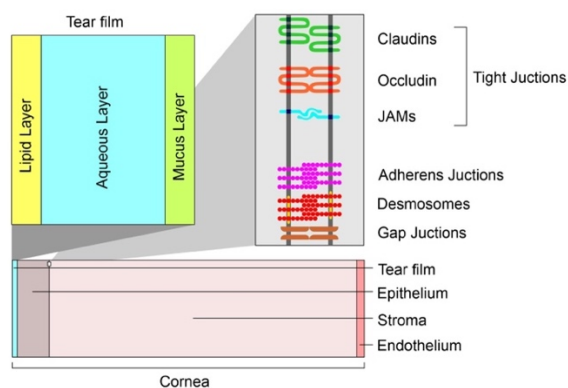
Figure 1. Cross-section of corneal tissues: barriers to drug penetration after topical instillation.

The corneal epithelium and endothelium (lipophilic in nature) consist of cells connected by tight junctions that limit the passage of large molecules (Figure 1). The hydrophilic stroma consists of tightly packed collagen. The epithelium, however, provides the greatest resistance to diffusion. The paracellular pathway through the intercellular pores is allowed for small ionic and hydrophilic molecules of size <350 Da, whereas the transcellular pathway allows the passage of larger lipophilic molecules. The variations in lipophilicity of the corneal layers allowed the realization of a parabolic relationship between corneal permeability and diffusion coefficient. pH is another important factor in corneal permeability [38]. Many studies that have examined permeability across conjunctiva, tenon and sclera have shown that the conjunctiva is more permeable to hydrophilic molecules than the cornea. The greater surface area (in humans, about 17 times bigger than the cornea) and the presence of larger pore sizes promote increased permeability compared to the cornea. However, mucus and the presence of lymphatics and vasculature increases systemic leakage [24,38]. In ocular topical administration, reaching the posterior portion is size-dependent [65]. Nanocarriers with a diameter of 20–200 nm are suitable for retinal-targeted delivery. Small nanoparticles (20 nm) are able to cross the sclera and are rapidly eliminated due to periocular circulation. The larger ones (200 nm) do not cross the sclera or the sclera-choroid-retinal pigment epithelium (RPE) and remain in the periocular site releasing their contents even for long periods. Even in the case of intravitreal administration, the kinetics are size-dependent. Nanocarriers with a diameter of 2 μm remain in the vitreous cavity or migrate into the trabeculae. Those with a diameter of less than 200 nm reach the retina [66]. In order to discuss the application of nanosystems in the ocular field, an emergent role is represented by fluorescent nanosystems. The tailor ability of design, architecture and photophysical properties has attracted the attention of many research groups, resulting in numerous reports related to novel nanosensors to analyze a great variety of biological analytes.

9.2 Fluorescent Probes in Ocular Applications

Before focusing on the published experimental studies, in this section, a brief discussion on fluorescence and on the molecules applied in the ocular field is given.

Absorption of a photon from a fluorescent chemical species causes a transition to an excited state of the same multiplicity (spin) as the fundamental state (S0). In solution, Sn states (with n > 1) rapidly relax to S1 through nonradiative processes. Ultimately, relaxation from S1 to S0 causes the emission of a photon with an energy lower than the absorbed photon. The fluorescence quantum yield (φ), one of the most important parameters, provides the efficiency of the fluorescence process; it is defined as the ratio between the number of photons emitted to those absorbed.

$$\varphi = \frac{Number\ of\ photons\ emitted}{Number\ of\ photons\ absorbed}$$

In Figure 2, we reproduce a brief history of the discovery of the fluorescence phenomenon. This discovery enabled the development of fluorescent probes that achieve single-molecule sensitivity. The figure shows that the first observation of a fluorescence phenomenon was described in 1560 by Bernardino de Sahagun; the same experiment was repeated by Nicolas Monardes in 1565. The fluorescence of the infusion known as lignum nephriticum was observed. This phenomenon was caused by the fluorescence of the oxidation product of one of the flavonoids present in those woods: matlaline. In the middle of the nineteenth century, George Gabriel Stokes coined the term fluorescence, derived from fluorite. The knowledge of atomic structure needed to understand and describe the nature of the phenomenon was not acquired until the beginning of the 20th century. By providing detailed information, this technique has enormous advantages over classical microscopy techniques [67]. In fact, literature is plentiful of studies dealing with the design of new fluorescent probes such as (bio)sensors to detect (even with the naked eye) enzymes, metals, biomaterials and others. Since 1945, the ability of analytes to promote the opening of rhodamine spirolactams has been exploited to design probes that detect metal ions and biological targets [68,69]. The pH sensitivity of fluorescein can be used to detect changes in a specific environment. By controlling the balance of ring-opening and ring-closing, following the interaction with specific targets, it can be used to detect metal ions from industrial and commercial specimens [70]. Curcumin is also widely used as a fluorescent probe for different applications, from producing drug carriers to the realization of specific sensors for ions and biomolecules [71,72].
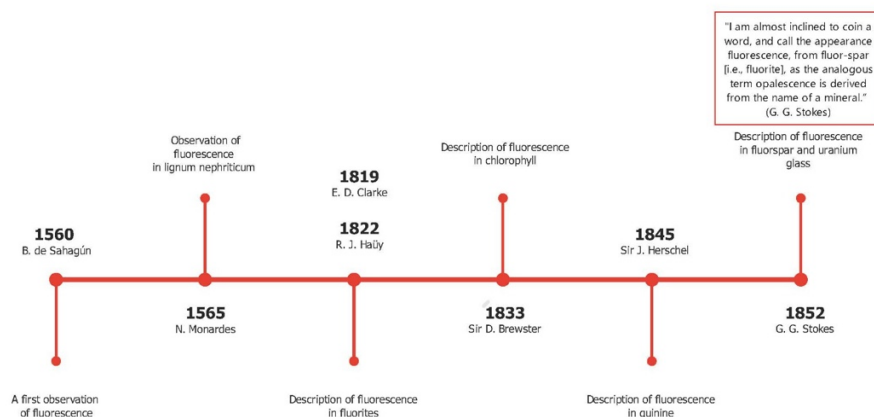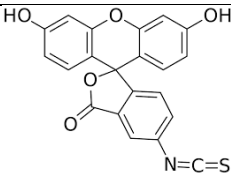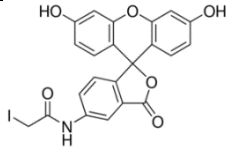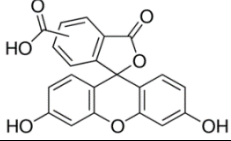
___
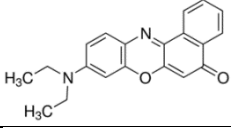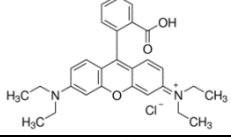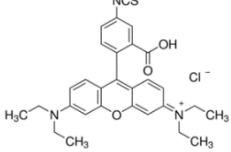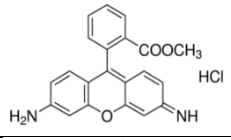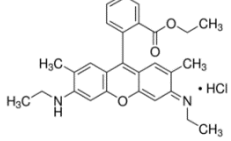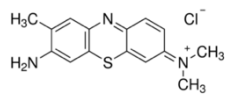
Figure 2. Timeline of the fluorescence discovery.

The following section delineates the family of fluorescent probes reported in reviewed studies, while Table 2 gathers the probes that are used in the experimental papers cited in this review.

Table 2. Physico-chemical properties of the main fluorescent probes used in bioimaging.

Probe	Chemical Structure	Molar Mass (g mol⁻¹)	Solubility in Water	Excitation (nm)	Fluorescence (nm)
Coumarin-6		350.43	Insoluble	488-666	502-649
Curcumin		368.38	Insoluble	300-470	571
Cyanine 5-phosphoramidite		944.21	Insoluble	649	666
1,1′-dioctadecyl-3,3,3′,3′-tetramethylindo-carbocyanine perchlorate		933.87	Low	550	565-588
Fluorescein		332.31	Insoluble	465-490	494
Fluorescein sodium salt		376.27	Soluble	460	512
5-aminofluorescein		347.32	Soluble	450-490	500-550

___

Probe	Chemical Structure	Molar Mass (g mol⁻¹)	Solubility in Water	Excitation (nm)	Fluorescence (nm)
Fluorescein-5-isothiocyanate		389.38	Insoluble	495	519
5-(iodoacetamido) fluorescein		515.25	Insoluble	492	518
5(6)-carboxyfluorescein		376.32	Low	495	520
Nile Red		318.37	Insoluble	543-633	550-700
Rhodamine B		479.01	Soluble	488-530	600-633
Rhodamine B isothiocyanate		536.08	Insoluble	553	563-650
Rhodamine 123		380.82	Low	488	515-575
Rhodamine 6G		479.01	Soluble	480	530
Toluidine Blue O		305.83	Soluble	595	626

9.2.1 The Coumarins Family

Coumarins have a conjugated double ring system. In the industry, coumarins find application as cosmetic ingredients, perfumers, food additives and in synthetic pharmaceuticals. In nature, coumarins are found in a wide variety of plants: tonka bean (Dipteryx odorata), sweet wood (Galium odoratum), vanilla grass (Anthoxanthum odoratum) and sweet grass (Hierochloe odorata) [73]. Among the different synthetic

derivatives, Coumarin-6 (C6) exhibits acid-base properties. In the study of Duong et al., a membrane with C6 demonstrated to exhibit colorimetric and ratiometric fluorescence properties with a dynamic pH range between 4.5 and 7.5 (the study uses blue nile in parallel) [74].

9.2.2 Fluorescein Family

Fluorescein is a xanthene dye with yellowish-green fluorescence. It was firstly synthesized in 1871 by von Bayer via Friedel's acylation/cyclodegradation reaction using resorcinol and phthalic anhydride [75]. It has a rigid tricyclic-coplanar structure with two aryl groups fused to a pyran ring. It has two distinct structures, an open fluorescent ring in the carboxylic acid form and a closed non-fluorescent ring in the spirocyclic lactone form. The open-closed equilibrium in the structure of fluorescein makes it sensitive to the pH of the medium [76]. Among the amine derivatives of fluorescein, those with one or two NH_2 groups in the phthalic residue are of particular interest. The corresponding (di)anions do not show intense fluorescence unless the amine groups are involved in new covalent bonds. In alcohols, the quantum yield, φ, is quite low. In dimethylsulfoxide (DMSO), acetone and other hydrogen bond donor solvents, φ values approach dianionic values [77]. Its sodium salt form finds wide use in angiography [78,79] and glioma studies [80]. Fluorescein 5(6)-isothiocyanate has been used for fluorescence labeling of bacteria, exosomes, proteins (immunofluorescence) and H Protein for gel chromatography. The 5-(iodoacetamido)-fluorescein is used for the synthesis of fluorescently labeled organelles, proteins, peptides and enzymes. Finally, the 5(6)-carboxyfluorescein, a fluorescent polyanionic probe, was used to measure changes in intracellular pH and to highlight processes such as dendrimer aggregation and absorption [81].

9.2.3 Rhodamine Family

These compounds were discovered in 1887. In the 4–10 pH range, their fluorescence spectra are unaffected by changes. The typical chemical structure of rhodamines involves three benzene rings, whose spirocyclic/open-ring conversion results in their off/on fluorescence [82]. In nonpolar solvents, they exist as spironolactone forms with very low φ due to disruption of p-conjugation of the xanthene core. In polar solutions, the lactone form undergoes charge separation to form a zwitterion [68]. In open-loop forms, rhodamine dyes exist as ammonium cations that can be driven into mitochondria via MMP (Matrix MetalloProteinase). A famous example is rhodamine 123, which forms the basis of the Mito-Tracker dye [83]. Lastly, the rhodamine 6G is a rhodamine analog useful in Pgp (P-glycoprotein) efflux assays, and it has been used to characterize the kinetics of MRP1

(multidrug resistance protein 1)- mediated efflux. An *in vivo* study of rhodamine B-labeled polymeric nanoparticles was conducted by Bonaccorso et al. to evaluate the distribution in brain areas after intranasal administration of the formulation [84].

9.2.4 Cyanine Family

Cyanine dyes are among the most widely used families of fluorophores. Cyanine 5 (Cy5) has five carbon atoms in the bridge. It becomes reversibly photocommutable between a bright and dark state in the presence of a primary thiol [85]. Cy5 excited by visible light undergoes thiolation with a thiol anion and transforms into a non-fluorescent thiolated Cy5. The thiolated Cy5 returns to the light-emitting dethiolated form simply by UV irradiation [86]. The photophysical properties of organic dyes with rotatable bonds are strongly governed by their internal rotation in the excited state since rotation can greatly affect molecular conformation and bond conjugation [87]. In the biological field, it finds use in comparative genomic hybridization, transcriptomics in proteomics, and RNA localization [88]. Moreover, DiI is a cyanine-derived dialkyl carbon sensitive to the polarity of the environment. It is weakly fluorescent in water but highly fluorescent in nonpolar solvents. It is commonly used as a lipophilic marker for fluorescence microscopy in the biological field. DiI molecules penetrate in cell membranes with the 2 long alkyl chains (12 carbons) immersed in the bilayer and the rings parallel to the bilayer surface. The dye emits characteristic bright red fluorescence when its alkyl chains are incorporated into membranes making it particularly useful for tracking in the biological membrane [89]. In the study by Musumeci et al. the 1-1′-dioctadecyl-3,3,3′,3′-tetramethylindotricarbocyanine iodide dye was used to label polymeric nanoparticles and study their cerebral delivery after intranasal administration [90].

9.2.5 Nile Red

Nile red is a hydrophobic dye of recent interest in the identification of microplastics [91]. It is widely used in biophysical studies focusing on proteins, lipids and live-cell analysis. Depending on the environment, Nile Red shows different absorption and fluorescence spectra. In particular, in organic solvents or nonpolar environments, it shows strong fluorescence that changes depending on the environment, presenting shifts toward blue emission in nonpolar environments [92].

9.2.6 Curcumin

Curcumin is the main natural polyphenol found in the rhizome of *Curcuma longa* (turmeric) and in others Curcuma spp. Its countless benefits in the treatment of

inflammatory states, metabolic syndrome, pain and inflammatory-degenerative conditions of the eyes are related to its antioxidant and anti-inflammatory effects [93]. Theoretical studies have predicted that its wide absorption band (410 and 430 nm) is due to the π-π^* transition, while the maximum absorption between 389 and 419 nm is related to the keto and enol form, respectively [67].

9.2.7 Toluidine Blue O

Toluidine blue (TB) is a thiazine-based metachromatic dye. It has a high affinity for acidic tissue components. This characteristic allows colorimetric identification of DNA- and RNA-rich tissues [94]. In the ocular field, Navahi et al. performed a study on the use of TB in the diagnosis of ocular surface squamous neoplasm (OSSN) [95]. In the Su et al. study, *in vivo* antibacterial efficacy of TB-mediated photodynamic therapy on bacterial keratitis by *Staphylococcus aureus* in a rabbit was demonstrated. This provides a new option for the clinical treatment of bacterial keratitis [96].

9.3 Fluorescent Nanosystems in Ocular Application

The following section is focused on recently investigated fluorescent nanomaterials and nanosystems for ocular applications. The reviewed works have been divided according to the use of such fluorescent nanosystems. Most studies concern the use of probes to assess nanosystems distribution within the ocular tissues. Among the most investigated fluorescent nanosystems, there are lipid-based nanocarriers—such as nanostructured lipid carriers (NLCs) and solid lipid nanoparticles (SLNs), polymeric nanoparticles and nanocapsules, hybrid nanoparticles, cubosomes, emulsomes, nanoemulsions, niosomes, liposomes, films, nanomicelles and hydrogels. Fluorescence is introduced through the methods commonly used to prepare nanosystems [97,98]. The fluorescent nanosystems are essentially divided into (i) probe-loaded, in which the dye or probe is encapsulated into the system mostly during the formulation processes, and (ii) labeled/grafted, in which the probe is covalently bound to the surface of the nanosystem (often linked to some matrix component, such as polymers or lipids), always forming an adduct (Figure 3).
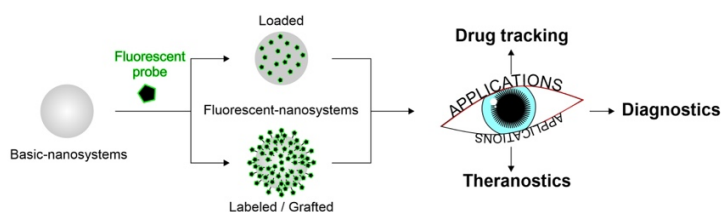

Figure 3. Schematic structure of fluorescent nanosystems for ocular applications.

9.3.1 Biodistribution

As above cited, the tissues that compose the eye are many and with different properties. The difficulty for a nanosystem to reach the target tissue is high, thus the profile of drug delivery is not always predictable. When the system target is located in deeper ocular tissues, it is even more difficult to predict the ideal pathways followed by the carriers *in vivo* and through the ocular barriers. Tracking the drug after topical administration is important for several factors. Firstly, it allows for the assessment of the effective achievement of the target site in order to accomplish the desired therapeutic action. Another factor to consider is the non-productive distribution of the drug in non-desired tissues, which could lead to the possible occurrence of side effects in addition to reducing the effective drug concentration. Furthermore, studying the pathways followed by the nanosystems is necessary to avoid issues related to barriers, tight junctions and physiological phenomenon (tear flow and blinking) which could impair the routes. Size, surface charge and morphology of the nanocarriers have a great influence on their biodistribution, clearance and cellular uptake [99-102]. Before performing biodistribution studies, it is important to characterize the system and to proceed with *in vitro* and *in vivo* assays. For instance, mean size measurement, zeta potential, mucoadhesion studies, morphological analyses are, of course, also required to make the system as conformable as possible to a correct drug release. Tracking of nanosystems can be carried out in two ways, invasive and non-invasive; bioimaging using fluorescent molecules is a non-invasive method [103,104]. Among the most important characteristics that the nanosystem should have there are small size, necessary to enter cells for allowing bioimaging, high sensitivity for effective detection, fast response, compatibility, absence of toxicity, good dispersibility in the biological environment, highly selective detection in the tissues. In Figure 4, a summary is gathered of the fluorescent probes used in the studied nanosystems discussed in Sections 3.1-3.3.
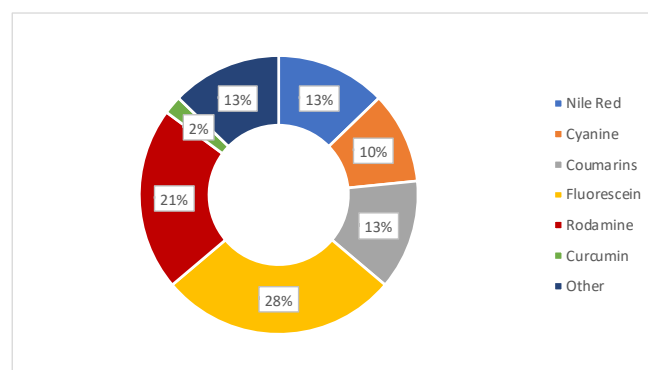

Figure 4. Graphical analysis of the fluorescent probes discussed in this review.

9.3.1.1   Fluorescent Lipid-Based Nanosystems

Lipid systems are of great interest for drug delivery in ocular tissues; their biocompatible and biodegradable composition makes them technologically safe, while their lipidic nature and structural characteristics allow them to pass through the corneal layers and achieve an efficient drug dosage even in the deepest tissues of the eye. The distribution of these systems occurs mainly in lipophilic layers, with minimal involvement of the stroma, since it has hydrophilic nature, and the lipid systems are difficult to distribute there. This was confirmed in the work of Namprem et al., in which confocal scanning microfluorometer (CSMF) analysis confirmed poor penetration of NLC labeled with Nile Red in hydrophilic compartments such as the stroma compared to corneal layers [105]. Due to eye barriers and obstacles to ocular administration, understanding the path taken by the designed nanosystem is necessary, especially if it is targeted to the back of the eye. The main route through which lipid systems reach the deeper tissues is the transcorneal one. There is growing evidence that successful drug delivery by functionalized nanocarriers depends largely on their efficient intra/paracellular transport, a process that is not fully understood yet. Therefore, the development of new imaging and diagnostic techniques is very important, particularly in a complex biological system such as the eye. Due to its lipophilic nature, one of the most used dyes for the preparation of fluorescent-lipid nanosystems is Nile Red (NR) Cubosomes labeled with Nile Red were prepared in the work of El Gendy et al. to assess the role of nine different lipids as penetration enhancers. The type of lipid used in the preparation plays an important role in tissue distribution. Among the prepared lipid systems, fluorescence analysis showed that the combination of oleic acid, Captex[®] 8000 and Capmul[®] MCM improved the penetration of the systems into the mucosa by increasing diffusivity due to both surfactant properties and the ability to disrupt the organization of the lipid bilayer [106]. Once again, Nile Red was used in the work of Kapadia et al. in order to visualize drug-loaded emulsomes. For the physico-chemical characterization and subsequent analyses, the nanosystems were loaded with triamcinolone acetonide, while for the studies of precorneal retention and ocular distribution, the fluorescent dye was loaded instead of the drug. The study revealed that after topical administration, the pathways taken to reach the back of the eye were basically three: corneal (via the iris and aqueous humor), conjunctival and systemic. The drug may diffuse through the sclera by lateral diffusion, followed by penetration of Bruch's membrane and retinal pigment epithelium (RPE). To a lesser extent, the drug may be absorbed into the systemic circulation either through the conjunctival vessels and the nasolacrimal duct, and gain systemic access to the retinal vessel [107]. Another lipophilic DiI dye (1,1-dioctadecyl-

3,3,3 tetramethyl indocarbocyanine perchlorate) was used to label lipid nanocapsules (LNCs) fluorescently. An important finding was made in the study by Eldesouky et al., where, despite the lipophilic nature of the dye, better penetration was achieved by encapsulation in lipid systems compared to simple dispersion. Fluorescence analysis showed that, without the use of lipid nanocarriers, the dye is unable to cross the hydrophobic corneal layer [108]. Mucoadhesion plays a key role in the enhancement of bioavailability. Efforts are made to design systems that have the ability to improve retention on the ocular surface. In this respect, the use of chitosan to improve the delivery of drugs into the eye tissues for its properties as a mucoadhesive agent, controlled drug release and permeation enhancer is interesting [24]. It is used in conjugation with a drug, such as in the study of Dubashynskaya et al., to improve the intravitreal delivery of dexamethasone [109]. In the major cases, it was used as a coating of nanocarriers to promote intraocular penetration, as reported by which designed modified NLCs with three different types of chitosan: chitosan acetyl-L-cysteine (CS-NAC), chitosan oligosaccharides (COS) and carboxymethyl chitosan (CMCS). The distribution profile was evaluated by loading the hydrophobic dye C6 into the NLCs. It was revealed through CLSM analysis that only NLCs modified with COS and CS-NAC were able to pass the cornea through the opening of tight junctions between epithelial cells [110]. Rhodamine-labeled NLCs were used to assess the corneal retention of such lipid nanocarriers, modified with a complex containing boronic acid, which is able to bind with high affinity the sialic acids of mucin. The NLCs were loaded with dexamethasone and designed for the treatment of dry eye syndrome. Fluorescence marking revealed the increased retention time due to the mucoadhesive property of the nanosystem, which also proved to be a potential not irritant treatment for dry eye syndrome [111]. Another key factor that improves retention time on the ocular surface is the positive charge of nanosystems interacting with the negative charges of mucin. The addition of octa-arginine (R8) to the nanoemulsions prepared by Liu et al. imparted a positive charge to the system with the aim of increasing eye retention. Once again, C6 was used to label lipid emulsions of disulfiram. In particular, the permeation of these systems under the influence of particle size and the presence of R8 was investigated and revealed that the addition of R8 and a size of ~50 nm improved the ocular delivery performance of nanosystems. In addition, the study showed that C6 passed through the corneal epithelium mainly by paracellular pathways, but there was also a fluorescent signal in the cytoplasm, indicating a transport also by transcellular pathways [112]. The internalization of lipid nanoparticles occurs mainly through an endocytosis mechanism. This is in fact the route taken by the mRNA-based solid lipid nanoparticles prepared by

Gómez-Aguado et al. The SLN were developed in order to produce IL-10 to treat corneal inflammation and was loaded with Nile Red to assess cellular uptake in corneal epithelial cells (HCE-2 cells). This platform could also be used as a theranostic model as GFP (green fluorescent protein) is produced inside the cells, so the intensity of the fluorescence is indicative of the amount of protein produced. Since GFP, once produced, remains at the intracellular level, instillation on the ocular surface of mice of the samples permitted the identification of the corneal layers where transfection occurred. All the prepared mRNA-based SLN formulations showed higher fluorescence intensity than naked mRNA, demonstrating the enhancement of their targeting ability [113]. Fluorescein is one of the most widely used fluorescent dyes for drug tracking and visualization of ocular damage following treatment. In Section 4, some clinical trials using fluorescein as a fluorescent in the study will be proposed. Fluorescein was used by Jounaki et al. for tracking vancomycin loaded NLCs. The aim of the work is the idea that NLCs for topical use could be a valid substitute of intravitreal injection in the treatment of bacterial endophthalmitis caused especially by *Staphylococcus*. Both drug-loaded and fluorescein-loaded NLCs (0.2 mg/mL) were prepared by cold homogenization technique and were used to evaluate precorneal retention with an inverted fluorescent microscope. The increased fluorescence found in the corneal epithelium demonstrated that dye-loaded, stearylamine-coated NLCs were retained more in the ocular surface. Indeed, the cationic lipid stearylamine is trapped in the mucin layer and retained due to the interaction between the fillers, facilitating the penetration and delivery of the drug to the intraocular tissues [101]. In the work of Kakkar et al., fluorescein was also used in concentrations almost like the previous work (0.25 mg/mL) to track hybrid nanoparticles. Solid lipid nanoparticles were prepared and then coated with PEG in order to encapsulate the antimycotic fluconazole. Analysis to assess the penetration into the ocular internal layers revealed that fluorescence was observed in the vitreous humor, retina, sclera and choroid after instillation of a single drop of Fluconazole-SLNs into the rat eye. In addition, the *ex vivo* study showed that the system exhibited a 164.64% higher flux through the porcine cornea when compared to the commercial drops ZoconVR [114]. In addition to coating the nanosystems, fluorescein was used to label them binding it covalently to the material of the nanosystem. In the work of Puglia et al. [66] an adduct is prepared between fluorescein and stearic acid named ODAF (N-(30,60-dihydroxy-3-oxospiro[isobenzofuran-1(3H),90- [9H]xanthen]-5-yl]-octadecanamide). In this case, the dye was grafted (and not loaded) and the conjugation of the lipid with the dye leads to a fluorescent probe. Solvent-diffusion technique was used to prepare SLNs of about 120 nm. The *in vivo* distribution from 1 h to 16 h was evaluated in rabbits and the results showed

that, after ocular instillation, ODAF SLNs were mostly located in the cornea (up to 2 h), whereas over a longer time (from the second hour to the eighth hour) the fluorescent signal gradually extended toward the back of the eye, confirming the ability of controlled delivery by the lipid nanosystems [66]. Considering that the influence of blinking and tearing on ocular drug absorption was rarely evaluated in studies, Pretor et al. evaluated absorption of two lipid-based formulations, a liposome and a SLN, in presence of these two physiological conditions. The SLNs were also labeled with a fluorescent phospholipid, thus constituting another example of a grafted nanosystem. From the study, using C6 as the fluorescent compound, it is evaluated that liposomes are shown to provide a greater absorption, despite the influence of blinking (shear stress of 0.1 Pa.) and tear flow. This interesting study was carried out by coupling the use of microfluidics with channels and cultured HCE-T cells as well as the use of a fluorescent dye to simulate the physiological mechanisms; it could be useful to add this kind of assay to the basic characterization of the nanosystem addressed to ocular targets [115]. In the rhodamine family, Rhodamine B is widely available and low-cost. The following two studies promote the use of this molecule for tracking nanosystems. The first is focused on the preparation of lipid systems (niosomes vesicles) and Eudragit nanoparticles for the treatment of eye fungal infections. Encapsulation of fluconazole within these systems resulted in being a good way to increase the bioavailability of the drug compared to free drugs. The systems obtained were innovative in terms of formulation as there is a triple step: the drug was first complexed using β-cyclodextrin, then encapsulated into niosomes, and the niosomes were finally incorporated into an in-situ gelling system made by Poloxamer, HPMC and chitosan. Niosomes were labeled with Rhodamine B and then were compared to labeled polymeric nanoparticles. The fluorescent signal of CLSM analysis increased in intensity when the NPs were incorporated into the hydrogel, whereas the signal of the pure dye was limited to the superficial epithelial layers, suggesting effective permeation of the nanosystems into the inner tissues [116]. Rhodamine B was also used to study the transport of curcumin as a model drug in multilamellar liposomes. These were coated with sodium alginate grafted acrylic acid conjugated with riboflavin. These multi-dye vesicles (rhodamine and curcumin), prepared using the lipid film hydration technique, have proven to be excellent carriers for drug delivery to the retina. The study evaluated both the encapsulation efficiency of the two dyes and their *in vitro* release. The release test in pH 7.4 medium demonstrated time-depended release, which was faster for rhodamine than for curcumin. An extended-release profile was obtained using fluorescence, red for rhodamine and green for curcumin, showing greater entrance into the cell at 12 h than at 3 h, and greater endocytosis for smaller, more spherical particles [117].

9.3.1.2   Polymer-Based Nanocarriers

Topical delivery of polymeric nanosystems is useful to improve corneal penetration and prolong the therapeutic response of several drugs. Nanocarriers need to be evaluated to find clinical application; specifically, their distribution in biological environment should be examined in order to understand the most appropriate strategy to address specific ocular pathologies. Plausible routes of topically instilled drug delivery for the treatment of ocular diseases involving the posterior segment include several pathways, including corneal, non-corneal and uveal routes. Successful nanocarrier development, therefore, involves fluorescent labeling useful for investigating mechanisms and biodistribution profiles of the designed systems. Polymeric nanostructures to be used as imaging diagnostic agents include various kinds of systems, such as nanoparticles, niosomes, film and nanomicelles and in-situ gel. The review of Swetledge et al. offers a detailed discussion on the biodistribution of polymer nanoparticles in major ocular tissues [118]. To improve retention time on the ocular surface, release profile and mucoadhesion performance, nanocarriers are often coated with polymers. Poly-lactide (PLA), polyglycolide (PGA), poly-lactide-co-glycolide (PLGA) and chitosan, Eudragit®, but also different copolymers such as PLGA-PEG, poly- (3-hydroxybutyrate-co-3-hydroxyvalerate) (PHBV) constituted by hydroxybutyrate (HB) and hydroxyvalerate (HV) and chitosan modified copolymer are some of these. Among them, many polysaccharides are used as a useful coating for nanocarriers. Some of these, including chitosan, alginate sodium, hyaluronate sodium and cellulose derivatives, are approved for ophthalmic use by the FDA and are already present in the composition of ophthalmic products on the market [119]. Depending on the type of polymer, the most suitable fluorescent probe should be chosen. A study conducted by Zhukova et al. focused on understanding the interactions between probes, polymeric nanoparticles and the biological environment. Four dyes with different degrees of hydrophobicity were encapsulated (C6, rhodamine 123, DiI) or covalently bound to the polymer (amine Cyanin 5.5, Cy5.5) in order to label PLGA nanoparticles. To increase the accuracy of the interpretation of *in vivo* biodistribution data, dual-labeled nanoparticles were administered, using C6 as the encapsulated label and Cy5.5 as the grafted label. Neuroimaging results showed that the signal of the nanoparticles bounded with Cy5.5 was detected in retinal vessels, whereas the signal of the encapsulated C6 was found outside of blood vessels and in tissue background. The extra vasal distribution of C6 could falsify the data interpretation, leading to erroneous assumptions that the nanoparticles could efficiently cross the blood-retinal barrier. Assessing the affinity of the dye to the polymer and the lipophilic structures could be useful in scaling up these issues. Although C6 has not

proved to be an ideal label, it aided in explaining the phenomenon whereby drugs are delivered to tissues through encapsulation in nanocarriers without involving any nanoparticle penetration [120]. Similar results were obtained by Zhang et al. tracking *in vivo* the distribution of PLGA-NPs in the retinal blood circulation after intravenous injection. NPs were labeled with lipophilic perchlorate carbocyanins (DiI) or hydrophilic rhodamine 123 (Rho123). DiI fluorescent signal was detected for a long time (>90 min) in retinal vessels, in contrast with Rho123 whose fluorescence was short (>15 min), due to diffusion from particles and elimination from the blood circulation. To avoid artefacts, dual-labeled nanoparticles were also injected intravenously in rats. Colocalization of fluorescent markers was performed by conjugating the polymer with Cy5.5 and loading the systems with probes (DiI/Rho 123). Cy5.5 signal was detected for both cargoes in retinal vessels for more than 90 min; however, colocalization was observed only for lipophilic DiI dye, which was more closely related to the hydrophobic polymer matrix. These findings further confirm that the affinity of the dye for the polymer and cell membranes played a key role in biodistribution kinetics [121]. The hydrophilic properties of rhodamine B make it a suitable fluorescent candidate for polymers of a hydrophilic nature such as chitosan, whose mucoadhesive qualities have been exploited by X et al. for the design of topical films for the treatment of glaucoma. Corneal permeation studies demonstrated the mucoadhesive efficacy of polymeric films in transporting rhodamine B molecules through the cornea with a high permeation rate [122]. A water-insoluble derivative of the rhodamine family is rhodamine B isothiocyanate, which has affinity for hydrophobic polymers. This dye was used as a label for nanoparticles consisting of hydrophobic PHBV polymer to obtain information regarding the depth and rate of penetration after topical administration. Confocal analysis showed improved penetration deepness of encapsulated marker compared to the free one, used as a control [123]. Recently, hydrophobic C6 was doubly used as a model drug and a fluorescent marker to track surface-modified PLGA-NPs with chitosan, glycol chitosan and polysorbate 80 in retinal tissues. Tracking of NPs after topical instillation was performed by fluorescence microscopy, revealing intense staining throughout the whole eyeball, anterior segment including cornea and conjunctiva, lens, iris/ciliary body and retina, with a peak at 30 min after administration and the disappearance of the signal after 60 min. Ocular tissue autofluorescence was distinct around the outer segments of the photoreceptor. Based on the average size of the NPs (<200 nm), the specific pathway of the NPs to the retina did not exclude any of the plausible routes of delivery to the posterior segment (corneal, noncorneal or uveal pathways) [124]. C6 was also used to label polymeric nanomicelles designed for the topical treatment of fungal keratitis. The

nanomicelles consisted of a chitosan oligosaccharide-vitamin E copolymer conjugated to phenylboronic acid (PBA-CS-VE) to enhance corneal retention. C6 delivery through a monolayer of HCE-T cells and 3D cell spheroids demonstrated strong corneal penetration ability. Several characteristics of the polymer were able to influence nanomicelle uptake, but the key role in the process of cellular endocytosis was attributed to the high-affinity interaction between the PBA portion and sialic acid on the surface of the cell membrane [125]. Another study using C6 as a fluorescent probe was reported by Sai et al., aiming to evaluate the corneal transportation of an in-situ gelling system based on mixed micelles. This formulation designed for curcumin was composed of micelles, consisting of 1,2-distearoyl-	sn-glycero-3-phosphoethanolamine-N-[methoxy(polyethyleneglycol)-2000] (PEG-DSPE) and poly(oxyethylene) esters of 12-hydroxystearic acid (Solutol HS 15), incorporated in a gellan gum gel. Incubation of human corneal epithelial cells (HCEC) with the fluorescently labeled systems showed time-dependent and improved absorption for the encapsulated dye, compared to free C6. Transcorneal penetration was investigated *in vivo* by CLSM and results suggested that curcumin was able to penetrate more effectively when incorporated into the gelled systems, probably due to the increased retention time conferred by the gellan gum, which was five-fold higher than the mixed micelles alone [126]. A pilot study with C6 was performed to evaluate the feasibility of the approach in assessing the biodistribution of PLGA-PEG nanoparticles suspended in hydrogels. The preliminary study showed an important limitation due to the high green autofluorescence of the examined ocular tissues. To deal with the drawbacks highlighted by the pilot study, PLGA nanoparticles in the full study were labeled with Cy-5, a far-red fluorophore that did not overlap with the natural autofluorescence of the ocular tissues. Results from the full study showed that topical application allowed the nanoparticles to be distributed into the outer ocular tissues (cornea, episcleral tissue and sclera) and the choroid was the only internal tissue to show a slight increased fluorescence, probably attributed to the permeation of [118]. Another dye recently used as a model drug to label mucoadhesive films with a hydrophilic nature based on chitosan and poly(2-ethyl-2-oxazoline) is fluorescein sodium. To avoid precipitation of complexes between the negatively charged dye and the positively charged chitosan backbones, concentrations less than 0.1 mg/mL were used. Films tested by *ex vivo* (bovine cornea) and *in vivo* (chinchilla rabbits) studies showed excellent corneal adhesion (up to 50 min) [127]. From this review of recently published papers, it emerged that, to ascertain the applicability of nanosystems to biodistribution studies, it was necessary to (i) take in account the degree of affinity and interference between probe, polymeric carriers and cell membranes, and (ii) accurately interpret the data by selecting

an effective labeling method upstream. The most reliable way to track the pathways of the systems remains the conjugation of the fluorescent dye to the polymeric core. Therefore, colocalization by double labeling may be the most appropriate technique to minimize errors in the interpretation of fluorescence signals. Currently, there is no unique approach to fluorescent polymer nanosystems that can be used for all types of labeling systems and probes.

9.3.1.3 *Metallic-Based and Inorganic-Based Nanosystems*

Inorganic nanodevices became of great interest in ocular delivery due to their unique properties such as low cost, easy preparation methods, small size, tuneable porosity, high surface-volume and robust stability. Fluorescent labeling has been applied to these delivery systems to assess their ability to cross ocular barriers and provide therapeutic efficacy [128]. Corneal barrier functions were investigated by Mun et al. using two types of silica nanoparticles (thiolate and PEGylated) fluorescently labeled with 5-(iodoacetamido)-fluorescein (5-IAF). Permeation studies were performed *in vitro* on intact or β-cyclodextrin pretreated bovine corneas. To provide experimental parameters close to *in vivo* conditions and to avoid artifacts such as the potential risk of corneal swelling when using Franz diffusion cells, the "whole-eye" method was used. 5-IAF-loaded thiolate silica nanoparticles, PEG-grafted silica nanoparticles (5-IAF-PEG), sodium fluorescein and fluorescein isothiocyanate dextran solutions were tested. It resulted that fluorescein salt (376 Da) did not uniformly penetrate the cornea; however, the dye was detected in the stroma. Larger molecules such as FITC-dextran (400 Da) and 5-IAF-PEG formed a layer on the corneal surface with no permeation of the epithelial membrane. B-cyclodextrin pre-treatment disrupted the integrity of the cornea by providing homogeneous permeation of the low-molecular-weight dye, although it did not improve the penetration of larger molecules. Concerning NPs, no permeation was reported regardless of surface modification, particle size and pre-treatment with β-cyclodextrin, thus suggesting that the tight junctions of the corneal epithelium acted as the main barrier to permeation. The absence of penetration and confinement on the corneal surface was observed for thiolated NPs because of the formation of disulfide bonds between the NPs thiol groups and the cysteine domains of the mucus glycoprotein layer. The interaction between mucin and -SH thiol groups remained a limiting permeation factor even after the removal of the epithelial layer. NPs PEGylation was able to mask thiol groups, allowing passage into the stroma [129]. Baran-Rachwalska et al. designed a novel platform consisting of hybrid silicon-lipid nanoparticles, aiming to deliver siRNA to the cornea by topical administration. A fluorescent oligonucleotide duplex, siRNA transfection indicator (siGLO), was employed

as a tracking probe to assess *in vitro* cellular uptake on a human corneal epithelial cell line (HCE-S) and *in vivo* corneal penetration on wild-type mice. Red fluorescence of the oligonucleotide marker allowed detection of nanoparticles in all layers of the cornea 3 h after instillation, in contrast to the control siGLO. The tracking of biodegradable nanosystems in corneal tissues was confirmed by the reduction of protein expression in the corneal epithelium, making them ideal candidates for therapeutic oligonucleotide delivery [130]. Biodegradable mesoporous silica nanoparticles (MSNs) loaded with carboplatin were designed by Qu et al. for the treatment of retinoblastoma. Carboplatin, being an anticancer drug, causes severe side effects; therefore, it is necessary to focus the action strictly on the target site. For this purpose, MSNs were surface modified by conjugation with an ideal target, epithelial cell adhesion molecule (EpCAM), in order to increase specificity as well as therapeutic efficacy. To assess the targeting efficacy of the designed systems, the authors evaluated the cellular uptake of untargeted and targeted MSNs in retinoblastoma Y79 tumor cells. Rhodamine B and Lysotracker Green were used as fluorescent probes to track cellular and subcellular uptake of the vectors. Increased cellular uptake for targeted MSNs was attributed to EpCAM-specific receptor-mediated cellular internalization. Lysosomal localization of MSNs confirmed that the nanosystems followed the endocytosis pathway for drug delivery [131]. A hexa-histidine with metal ions nanosystem was designed to deliver Avastin in the treatment of corneal neovascularization (CNV). Pre-corneal retention time and ability to cross ocular barriers were studied on a rat CNV model induced by alkaline burns by FITC labeling the systems. Avastin encapsulated in the vectors showed a longer precorneal adhesion time compared to the free drug. These innovative systems have emerged as a promising platform for ocular topical delivery of protein drugs [132]. An interesting zirconium-porphyrin metal-organic framework (NPMOF) has been designed for drug tracking and delivery. The bright fluorescence self-emitted by the metal-organic framework qualifies the carriers to be applied for imaging. NPMOF was used as a skeleton for the delivery of methylprednisolone, a very efficacious corticosteroid in the treatment of retinal degenerative diseases. Adult zebrafish with photoreceptor degeneration induced by high-intensity light exposure were used to test *in vivo* distribution and therapeutic efficacy. Red fluorescence signals were detected in choroid, retina, photoreceptors and retinal pigment epithelium for up to 7 days. Recovery of visual function by rapid regeneration of photoreceptors and proliferation of Müller's glia and retinal regeneration were reached after a single intravitreal injection. NPMOF vectors represent a novel delivery system for the treatment of diseases affecting the posterior eye segment [133].

9.3.1.4 Protein-Based Nanosystems

Protein-based nanosystems have attracted considerable interest in recent years and are designed for drug delivery, diagnostics and bioimaging. These highly bio-compatible systems, which have been extensively studied in the biomedical field, owe their properties to the protein they are composed of. Among the proteins used in their preparation, there are antibodies, enzymes, animal and plant proteins, collagen, plasma proteins, gelatin and proteins derived from virus capsids [134]. Fluorescent proteins are usually used to monitor protein-protein interactions, protein localization and gene expression. However, without any carrier, the fluorescent efficiency of a single protein is relatively low. The use of fluorescent protein-labeled nanomaterials improves loading due to increased surface area and allows the development of fluorescent nanosystems useful in bioimaging and biosensing. In the study carried out by Yang et al., nanoparticles were prepared from regenerated silk fibroin. This protein, which is the most abundant in silk, is considered to have high biocompatibility and degradability properties. In the biomedical field, it has been used for drug delivery in small nanosystems, biological drug delivery, gene therapy, wound healing and bone regeneration. The formulation is targeted for intravitreal injection with the aim of increasing the bioavailability of the drug in the retina. Fluorescein isothiocyanate labeled bovine serum albumin (FITC-BSA) has been encapsulated as a model drug. *In vitro* cytotoxicity studies were conducted on ARPE-19 cells, showing that these nanosystems were very compatible. In addition, *in vivo* comparison of the biodistribution in posterior ocular tissues in rabbits revealed increased retention in the retina due to encapsulation in the nanosystem rather than with a solution of model drug [135,136]. Albumin is widely used in the preparation of ocular nanosystems [137]. In a recent study, bovine serum albumin nanoparticles loaded with apatinib were prepared for the treatment of diabetic retinopathy. In contrast to the previous study, in this disease, invasive administration has to be avoided, so topical administration is the ultimate goal. The nanoparticles were coated with hyaluronic acid (HA) to increase mucoadhesion. The biodistribution study in retinal tissue was carried out by preparing fluorescent nanosystems with 1,1′-dioctadecyl-3,3,3′,3′-tetramethylindodicarbocyanine, 4-chlorobenzenesulfonate salt (DiD) solution in ethanol (0.5 mg/mL), which was added during the formulation phase. Through the comparative *in vivo* biodistribution study, it was shown that HA-coated nanoparticles demonstrate higher fluorescence in retinal tissue compared to uncoated nanoparticles, thus representing a viable alternative to intravitreal injection, maintaining comparable perfusion and bioavailability [138]. Another study involved the preparation of nanoparticles using pseudo-proteins for the potential treatment of ophthalmic diseases. Ten types of

nanoparticles obtained by precipitation of pseudo-proteins were prepared, then they were loaded, and some of them were also pegylated; finally, they were labeled with a fluorescent probe, fluorescein diacetate (FDA) or rhodamine 6G (Rh6G), to assess ocular penetration. Corneal fluorescence was obtained as expected, while surprising results were the reaching of tissues such as the sclera and retina. Thus, they proved to be a promising delivery system for topical use in chronic eye diseases [139].

9.3.2 Diagnostics

Labeling nanoparticles with fluorescent probes was demonstrated to be a useful approach to improve the effectiveness of some diagnostic tests aimed to detect ocular pathologies. In fact, some eye diseases require a prompt diagnosis in order to contain possible damages related to the ongoing pathways involved. Age-related macular degeneration (AMD) is the main cause of vision loss for over-65-year-olds [37]; this pathology has often been analyzed to improve diagnostic techniques since it has several predisposing factors, and early detection is crucial to avoid degeneration toward blindness [140]. AMD has an unclear etiology, although oxidative stress is considered one of the main risk factors [141]; as a matter of fact, clinical studies demonstrated the importance of supplementation with antioxidants in order to slow down the progression of AMD [142,143]. Physiological antioxidant patterns involve metallothioneins (MT), low molecular mass proteins characterized by the presence of cysteine sulfur ligands, which are able to scavenge free radicals, thus protecting cells and tissues. The retina is particularly subject to oxidative stress due to visible and UV light exposure; moreover, age progression involves a reduction of MT expression, predisposing to AMD [144]. For this reason, bioimaging these proteins in ocular tissues could be an important tool useful to highlight the tendency to develop AMD. For this purpose, fluorescent gold nanoclusters involving Cu and Zn and bioconjugated with specific primary antibodies were developed by Cruz-Alonso and coworkers [145]. Laser ablation (LA)-inductively coupled plasma (ICP)-mass spectrometry (MS) technique was used to identify $^{63}Cu^+$ and $^{64}Zn^+$ in the retina of post-mortem donors since MT bind both Cu and Zn [146]. This method showed results comparable with conventional immunohistochemistry for MT proteins, with amplification of signals related to the presence of nanoclusters, which allowed the obtainment of higher resolution bioimages. An *in vivo* model of human "wet" AMD is laser-induced choroidal neovascularization (mouse LCNV) mouse, in which the inflammatory biomarker vascular cell adhesion molecule-1 (VCAM-1) is highly expressed. Gold nanoparticles functionalized with anti-sense DNA complementary to VCAM-1 mRNA were developed by Uddin et al., who aimed to detect this molecule, thus assessing the occurrence of

oxidative stress [147]. The fluorescence in-situ hybridization (FISH) technique was used to perform photothermal-optical coherence tomography (PT-OCT) involving a fluorescent probe (Alexafluor-647) bonded to 3′ end of anti-sense DNA in order to highlight its interaction with the target mRNA. The conjugation of anti-sense DNA to gold nanoparticles proved to protect from the degradation performed by DNase while enhancing the uptake, probably through endocytosis, as suggested by transmission electron microscopic (TEM) images of retinal cells; moreover, it was verified that no inference in the fluorescence was produced due to low pH, which is characteristic of inflamed tissues. Compared to the control group, *in vivo* systemic injection in mice confirmed the enhancement in the fluorescent signal for anti-sense DNA coupled with nanoparticles, which mostly depended on VCAM-1 mRNA hybridization, thus demonstrating the potentiality of the developed platform as a tool to obtain direct images of endogenous mRNA in a tissue. In some cases, this pathology requires transplantation of photoreceptor precursors (PRPs) in the subretinal space, which was successfully performed, guaranteeing a certain vision restoration [148]. For a certain period, monitoring of the efficiency of the transplantations needs to be performed. As confirmed by Chemla and coworkers [149], gold nanoparticles could be transplanted together with photoreceptor precursors cells labeled with a fluorescent probe (Alexa 594) in order to ameliorate the efficiency of computed tomography (CT) and optical coherence tomography (OCT) in assessing the success of the transplant. The nanoparticles were firstly characterized in order to assess their safety, thus demonstrating no toxicity toward the transplanted cells and no occurrence of inflammation in the retina and vitreous. Furthermore, this platform demonstrated to enhance X-ray signal detected by CT and related to cell survival without interference from the particles secreted from the cells [150]; moreover, they were also able to increase optical signal for OCT by up to 1.4-fold and track cells migration toward layers deeper than the injection site. These results confirm the efficiency of such a platform in the monitoring of transplantation but also suggest a potential use for ameliorating existent molecular imaging in cell therapy and diagnostic. Another important diagnostic test is fundus fluorescein angiography (FFA), which allows highlighting vascular leakages in retinal and choroidal pathologies [151]. This clinical tool is useful to diagnose several ocular diseases: age-related macular degeneration, which is characterized by hemorrhaging and exudation in the retina [140]; diabetic retinopathy, which involves retinal damages related to microvascular modification which are clinically not revealable in the early stages [152]; diabetic macular edema, whose pathophysiology implicates modifications of choroidal and retinal vasculature due to BRB impairment [153]. Furthermore, the aforementioned diseases are

characterized by alterations of ocular vessels, and share the consequent compromission of visual activity, if not quickly detected and treated. Fluorescein sodium (FS) is injected intravenously to perform this analysis, diffusing in the blood vessels, thus allowing us to observe them through a confocal scanning laser ophthalmoscopy system. Despite it being considered relatively safe, nausea and vomiting frequently occur, while severe effects such as anaphylaxis are rare. The main drawbacks are the diffusion of FS into normal tissues and cellular absorption, with long retention, which were overcome using nanoparticles. Cai et al. coworkers developed a high molecular weight polyethyleneimine (PEI) nanoparticles which demonstrated to successfully couple fluorescein [151]; moreover, *in vitro* studies showed good cytocompatibility, no significant difference in apoptosis rates considering various concentration tested, no genotoxicity, and no morphological changes or significant difference in endothelial tube formation. Cellular uptake assays, carried on with different concentrations of free FS and FS-NP, confirmed similar rapid uptake by cells, with a concentration-dependent and time-dependent fluorescence of main retinal vessels and microvessels. Furthermore, free FS was longer retained in cells when compared to FS-NP, as highlighted by *in vivo* fluorescence studies, suggesting a potential decrease in FS toxicity. These results confirm the potentiality of this platform as a diagnostic tool to detect retinal vessels; moreover, PEI enhances fluorescein metabolism, thus reducing its toxicity. Other polymeric nanoparticles developed as a potential diagnostic tool are composed of copolymerized glycerol mono methacrylate (GMMA), glycidyl methacrylate (GME) and ethylene glycol dimethacrylate (EGDMA), which were functionalized with Vancomycin, Polymyxin B or Amphotericin B, in order to detect the presence of Gram-positive bacteria, Gram-negative bacteria and fungi through a specific bond with the respective antibiotic or antimycotic [154]. The occurrence of such bonds was differently highlighted using fluorescent Vancomycin, and probes such as fluorescein isothiocyanate (FITC) and Calcofluor White. Tests conducted on various microbiological strains showed a proportional increase in the fluorescence signal with the increase in the number of organisms involved; moreover, the presence of functionalized polymers favored the microorganism bonding. Besides the biocompatibility of this platform, another advantage of this platform is the possibility to be shaped as a contact lens requiring only a 30-min exposure to efficiently detect the occurrence of infection, thus demonstrating to be a promising approach for an easy diagnosis of corneal infections.

9.3.3 Nanotheranostics

The recent development of systems that integrate the treatment of diseases with their diagnostics is referred to as theranostics. When the system is in a nanoscale range, it is

called nanotheranostics. Figure 5 shows prototypes of nanosystems suitable for theranostic purposes.
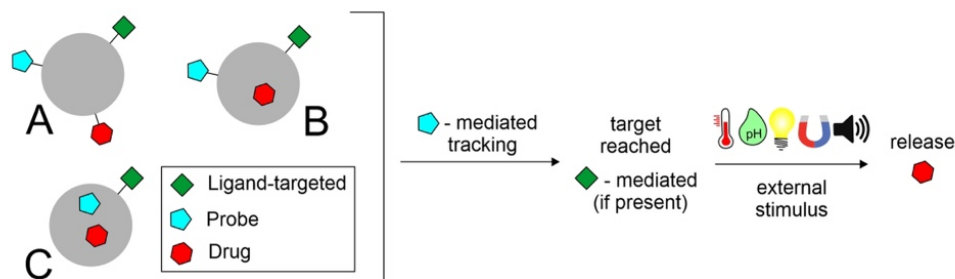

Figure 5. Prototypes of theranostic nanosystems and their mechanism of action. In figure: (A) labeling of both probe and drug; (B) loading of drug and labeling of probe; (C) co-loading of drug and probe.

The development of these applications has given researchers a new way of diagnosing and treating diseases such as cancer, diabetic retinopathy and age-related macular degeneration [37,155]. Among the major chronic eye diseases, diabetic retinopathy is the most prevalent. Angiogenesis in the posterior eye segment is the main cause of retinal impairment. Clinical management consists of pathological diagnosis and intravitreal injections of vascular endothelial growth factor (VEGF) inhibitors to suppress neovascularisation. The development of innovative nanotheranostic systems is emerging to overcome these critical problems with less invasive methods to diagnose and treat ocular angiogenesis synergistically. Silicon nanoparticles conjugated to the peptide Cyclo-(Arg-Gly-Asp-d-Tyr-Cys) (c-(RGDyC)) (SiNP-RGD) were designed by Tang et al. with the dual action of imaging and treating ocular neovascularization. The effective anti-angiogenic capability of these biocompatible theranostic nanoprobes was based on the combination of a specific detection by labelling endothelial cells and angiogenic blood vessels and a selective inhibition of neovascularization [156]. Metal NPs are receiving a lot of attention as carriers for the delivery of biomolecules, among which silver NPs (AgNPs) have found numerous applications. Stati et al. designed curcumin stabilized AgNPs using a green and cost-effective method to exploit the promising characteristics of this polyphenol in the *in vivo* treatment of human pterygo. Curcumin is a molecule suitable for theranostic application, as widely reported in the work of Shabbir et al. [157]. Pterygo is a progressive eye disease that could culminate in an irreversible impairment of visual function. Available treatments require invasive surgical procedures, such as excision, which often leads to a worsening of the clinical picture. Spectroscopic techniques revealed a strong plasmonic resonance between the silver nuclei and the curcumin molecule, demonstrating the presence of the polyphenol on the surface of AgNPs. The biological efficacy of the formulation was tested

in vitro on human keratinocytes derived from pterygium explants, showing decreased cell viability in treated samples compared to controls. Although no studies have been conducted to track the fate of NPs, the fluorescent emission of the samples could be exploited for bioimaging applications [158]. Fluorescent silicon nanoparticles modified with Vancomycin were designed by Zhang et al. for the simultaneous non-invasive diagnosis and treatment of keratitis induced by Gram-positive bacteria. These nanotheranostic agents have demonstrated, in combination with strong antimicrobial activity against *Staphylococcus aureus*, a rapid (<10 min) imaging capability both *in vitro* and *in vivo*. The rapidity with which bacterial keratitis was diagnosed at an early stage suggests that these devices may be useful in preventing the progress of the disease, which could impair visual function if not treated [159]. Oliveira et al. designed hybrid theranostic systems consisting of a lipid matrix of 1,2-dipalmitoyl-sn-glycero-3-phosphatidylcholine (DPPC), coated with Pluronic® F127, covalently bound with the fluorescent probe 5(6)-carboxyfluorescein and loaded with the photosensitizing agent verteporfin. Preliminary studies on a glioblastoma cell line (T98G) were conducted to evaluate the potential application as theranostic nanodevices. The fluorescence of the systems revealed on the cancer cell membrane and the 98% reduction in cell viability of T98G cells encouraged further investigation of such multifunctional platforms for the treatment and diagnosis of ophthalmic diseases [160]. Photothermal therapy has been making inroads into the eye sector for a couple of years now. Heat therapy refers to the use of heat as a therapeutic tool to treat diseases such as tumors. In the recent work of Li et al., an approach to treat choroidal melanoma using nanocomposites was designed. Nanosystems were synthesized based on hydrogel, which is itself based on rare-earth nanoparticles. These platforms emit fluorescence in an NIR-II region. Characterized by their tiny size of less than 5 nm, they are targeted for the treatment and simultaneous bioimaging of choroidal melanoma. They have been incorporated into biodegradable hydrogels based on PNIPAM dual response, which could release the drug in a controlled manner by responding to heat and glutathione in the tumor microenvironment. The nanocomposites were then further decorated with indocyanine green (ICS) and folic acid (FA) to enhance therapeutically and to target specificity and the possibility of achieving photothermal therapy [161]. A lot of studies showed the potential of therapeutic contact lenses in the management of eye disease [162]. Infectious endophthalmitis is a growing concern that causes irreversible damage to intraocular tissue and the optic nerve. The work of Huang et al. focuses on the design of contact lenses consisting of hybrid hydrogels based on quaternized chitosan composite (HTCC), silver nanoparticles and graphene oxide (GO). Fungal keratitis infection often leads to the formation of a biofilm,

which is particularly difficult to be penetrated by antifungal agents, especially through eye drops. In addition, the bioavailability of a drug such as Voriconazole is very limited. The function of these nanoparticles is not only to deliver Voriconazole in the treatment of fungal keratitis, but also to act as an antimicrobial agent due to its properties. In fact, the materials used, such as quaternized chitosan, have inherent antimicrobial capabilities. The dual functionality makes this system a useful theranostic approach for the treatment of eye infections [163]. The study by Jin et al. reports a therapeutic nanoplatform based on UiO-66-NH2 to combine photodynamic therapy (PDT) and targeting lipopolysaccharides (LPS) through polypeptide modification (YVLWKRKFCFI-NH2). The fluorescent used was Toluidine blue (TB), which acted as a photosensitiser (PS) and was loaded into UiO-66-NH2 nanoparticles (NPs). The dye acts both as a tracer and as a therapeutic agent through photodynamics. The release of the fluorescent is pH-dependent. The study proved beneficial against *Pseudomonas aeruginosa* and *Staphylococcus epidermidis*, and the *in vivo* model showed positive results in the treatment of endophthalmitis [164].

9.4 Fluorescent Status for Ocular Therapies in Clinical Trials and Market

Scientific progress in the field of ocular nanomedicine is constantly advancing, many nanoformulations for the treatment of ophthalmic diseases have been clinically investigated, and some have already been introduced to the market. A list of nanomedicines for eye diseases in clinical trials and approved by the Food and Drug Administration (FDA) is discussed in the review provided by Khiev et al. [165].

Novel nanosystems on the market included NorFLO, a dietary supplement based on a patented curcuma-phospholipid formula (iphytoone®). Phospholipids enhanced the targeted distribution of curcumin in the eye, and the efficacy of the formulation has been demonstrated in over 40 studies in processes triggered or sustained by chronic inflammation, found to be the cause of many eye diseases. Prolidofta is another supplement marketed as an ocular spray to counteract inflammatory processes affecting the palpebral component and restore any functional and structural changes. This spray consists of small vesicles (50–500 nm) made up of a double layer of phospholipids surrounding an aqueous core for the delivery of vitamins A and E. OMK1-LF is an ophthalmic liposomal solution based on citicolin, an endogenous molecule that restores the damage caused by glaucoma in the cell membranes and hyaluronic acid, which acts to hydrate, protect and lubricate the

tear film. TriMix is an eye drop with cross-linked Hyaluronic Acid, Trehalose and Stearylamine Liposome indicated to counteract dryness and eye irritation.

Regarding imaging in surgery, near-infrared fluorescence (NIRF) with the dye indocyanine green has been widely used. Indocyanine green (ICG) is a clinically approved NIRF dye in ophthalmology for imaging retinal blood vessels; an overview of surgical applications using indocyanine green fluorescence imaging has been proposed by Alander et al. [166]. Based on clinicaltrials.gov, a website database of clinical trials conducted around the world (as accessed on 1 April 2022), since 2010 fluorescence imaging has been used in clinical trials to assess the integrity or damage of ocular surfaces after administration of novel nanosystems. Green dye fluorescein was used in 13 clinical trials for the evaluation of nanosystems with different ocular indications, from dry eye to autoimmune Sjögren's syndrome. The role of the dye and details of the studies are given in Table 3.

Table 3. Use of Fluorescein dye in clinical trials of drug delivery systems for eye diseases.

Role of molecule in the study	Name and type of formulation tested	Name of the study	Pathologies	Status	Identified number of the study
Evaluate corneal and conjunctival damage	LAMELLEYE Liposomal suspension	Lamelleye vs Comparator for the Treatment of Dry Eye Disease	Dry Eye Syndromes	Completed	NCT03052140
Evaluate tear breack up time and corneal damage	AQUORAL LIPO (liposomal solution) in contact lens	Efficacy of "Aquoral Lipo" Artificial Tears in Contact Lens Wearers With Discomfort	Contact Lens Complication	New study (March, 2022) not yet recruiting	NCT05290727
Evaluate corneal and conjunctival damage	LAMELLEYE Liposomal suspension	LAMELLEYE for the Treatment of Dry Eye Symptoms in pSS Patients	Primary Sjögren Syndrome	Unknown	NCT03140111
Evaluate corneal damage	LIPOSIC AND TEARS NATURALE FORTE (liposomal suspension)	Comparison of the Effects of Two Tear Substitutes in Patients with Dry Eye Syndrome	Dry eye	Completed	NCT03211351
Evaluate ocular surface damage	TEARS AGAIN (liposomal spray)	Dry Eye Treatment with Artificial Tears	Dry eye	Completed	NCT02420834
Evaluate the absence of anterior chamber cells	OCS-01 (Dexamethasone Cyclodextrin Nanoparticle Ophthalmic Suspension 1.5%)	OCS-01 in Treating Inflammation and Pain in Post-cataract Patients (SKYGGN)	inflammation and pain following cataract surgery	Completed	NCT04130802
Evaluate corneal damage	Intravenous Administration of Secukinumab (AIN457) or Canakinumab (ACZ885) solution	The Effects of a Single Intravenous Administration of Secukinumab (AIN457) or Canakinumab (ACZ885) in Dry Eye Patients	Dry eye	Completed	NCT01250171
Evaluate corneal and conjunctival damages	Tanfanercept (HL036) Topical Ophthalmic Solution	A Study to Assess the Efficacy and Safety of Tanfanercept (HL036) Ophthalmic Solution in Participants With Dry Eye (VELOS-3)	Dry eye	Recruiting. Phase III	NCT05109702

Role of molecule in the study	Name and type of formulation tested	Name of the study	Pathologies	Status	Identified number of the study
Evaluate conjunctival damage	HL036 0.10 percent (%) ophthalmic solution as topical ophthalmic drops	A Study to Assess Efficacy of HL036 in Subjects With Dry Eyes (VELOS-1)	Dry eye	Completed. Phase II	NCT03334539
Evaluate changes in inferior cornea	NCX 4251 (fluticasone propionate nanocrystal)	Study Evaluating the Safety and Efficacy of NCX 4251 Ophthalmic Suspension for the Treatment of Blepharitis	Blepharitis	Completed	NCT04675242
Evaluate Tear Film Break-up Time	SYSTANE ® Complete Nanoemulsion ocular lubricant (Propylene glycol-based eye drops)	Study of Efficacy and Tolerability of SYSTANE Complete in Patients with Dry Eye Disease	Dry eye	Completed	NCT03492541
Evaluate corneal damage	TJO-087 Cyclosporine ophthalmic Nanoemulsion (0.08%)	Evaluating the Efficacy and Safety of TJO-087 in Moderate to Severe Dry Eye Disease Patients	Dry eye	Recruiting	NCT05245604
Evaluate corneal damage	OCU300 Brimonidine Tartrate Nanoemulsion	Study of Brimonidine Tartrate Nanoemulsion Eye Drops in Patients With Ocular Graft-vs-Host Disease	Ocular Graft Versus Host Disease	Completed	NCT03591874

Fluorescence for the development and clinical investigation of innovative ocular nanosystems seems to be a promising strategy to increase the number of formulations able to reach market commercialization. In Table 4, few products with fluorescein approved by the FDA are reported.

Table 4. FDA-approved products with fluorescein.

Name	Active Ingredients	Company	Description	NDA
Altafluor Benox	Benoxinate Hydrochloride; Fluorescein Sodium (0.4%;0.25%)	Altaire Pharms Inc	Solution/Drops; Ophthalmic	208582
Fluorescein Sodium And Benoxinate Hydrochloride	Benoxinate Hydrochloride; Fluorescein Sodium (0.4%;0.3%)	Bausch Lomb Ireland	Solution/Drops; Ophthalmic	211039

9.5 Challenges and Future Perspectives

The growing number of people who have blindness and visual impairment indicates a continuous increase in the need for care and treatment. Given this evidence, urgent action is required to address this largely preventable global problem and provide adequate eye care services. There are still many gaps in the literature regarding optimal design and traffic pathways within the eye. In particular, further research is needed to unravel the transport mechanisms across certain barriers in the eye. Moreover, rapid clearance remains a challenge for nanosystems as they need to release their payload before being eliminated

from the eye. Many studies focus on assessing the distribution in various tissues once the formulation has been instilled into the eye [106–132,134,137–139]. Unfortunately, few studies focus on assessing how mechanisms including blinking, tear drainage and ocular metabolism may interact with nanosystems [66,115]. Among other things, a very important aspect is the evaluation of the toxicity and the actual applicability of these systems. In fact, many of them are quite complex, and the applicability, especially in the theranostic field, is not entirely easy. The evaluation has to be as precise as possible because many eye studies use rodent models; this is highly questionable, especially in the quantification of distribution and kinetic properties of nanoparticles in the eye, as there are many significant differences between the rodent and human eye. Therefore, the most impactful future studies on this topic will come from larger animal models with eyes that are physiologically and anatomically more similar to ours.

The increasing use of fluorescent probes in the realization of biosensors for colorimetric and radiometric identification of specific targets is a great step forward since the fluorescence represents a non-invasive diagnostic method. This has important benefits in early diagnosis through self-medication screening based on membranes or other platforms containing the appropriate fluorescent probe. These tools are also applicable in epidemics through the realization of specific self-tests based on ELISA or other strategies able to identify the etiological agent selectively. A large and growing field is the use of these probes as part of theranostic photo switch structures, able to change their structure after light stimulus, releasing the therapeutic agent and activating or switching off the fluorescence of the probe. Thus, fluorescence allows accurate and quantitative identification (under certain conditions even by the naked eye as also through *in vitro* tests) of the drug release process. Therefore, the use of fluorescent probes is finding increasing use in experimental and advanced ocular chemotherapy using photo-activated systems.

9.6   Conclusions

The eye has a complex anatomical structure, representing the main difficulty for drugs to achieve this target. Nanomedicine has made it possible to overcome several difficulties related to the administration of this almost isolated compartment. The study of the pathways followed by the nanosystems makes it possible to assess the effective achievement of the target site and to consider any non-productive distribution in undesirable tissues with the possible onset of side effects. The biodistribution study also allows the correlation between the chemico-physical parameters of the nanosystems (e.g., ZP, size, morphology,

mucoadhesive properties, etc.) and the paths followed by them. This investigation is also aimed at evaluating and developing strategies to bypass physiological barriers of the eye, including tight junctions, tearing and blinking, that could compromise targeting effectiveness. The development of bioimaging mediated by fluorescent probes has improved the efficiency of some diagnostic tests for eye diseases. It is known that early (or rather preventive) diagnosis is a necessity to limit the damage, especially in the long term, caused by specific diseases. The involvement of fluorescent nanoparticles as diagnostics demonstrated to be suitable for detecting the occurrence of pathological pathways, ameliorating techniques already employed in ocular diagnostic, thus providing better results through equipment of common use (OCT, CT, FFA, etc.). This is where the important contribution of fluorescent probes to nanotheranostic approaches becomes relevant since, in these systems, diagnostic and therapy coexist. Tracking the nanoparticles makes it possible to highlight the effective achievement of the target, thus following the release of the therapeutic agent through an external stimulus (e.g., ultrasounds, magnetic fields, light, etc.). In conclusion, as highlighted in this review, the potential applications of fluorescence in the ocular field have been demonstrated as a useful strategy for translating nanoformulations into marketable drug candidates. In addition, to the best of our knowledge, there are no reviews focused on this topic, so this work aims to raise awareness and summarize the use of fluorescents in the ocular field.

Institutional Review Board Statement: Not applicable.

Informed Consent Statement: Not applicable.

References:

1. Flaxman, S.R.; Bourne, R.R.A.; Resnikoff, S.; Ackland, P.; Braithwaite, T.; Cicinelli, M.V.; Das, A.; Jonas, J.B.; Keeffe, J.; Kempen, J.; et al. Global causes of blindness and distance vision impairment 1990–2020: A systematic review and meta-analysis. Lancet Glob. Health 2017, 5, e1221–e1234. [CrossRef]

2. Marques, A.P.; Ramke, J.; Cairns, J.; Butt, T.; Zhang, J.H.; Muirhead, D.; Jones, I.; Tong, B.A.M.A.; Swenor, B.K.; Faal, H.; et al. Global economic productivity losses from vision impairment and blindness. EClinicalMedicine 2021, 35, 100852. [CrossRef]

3. Nagarajan, N.; Assi, L.; Varadaraj, V.; Motaghi, M.; Sun, Y.; Couser, E.; Ehrlich, J.R.; Whitson, H.; Swenor, B.K. Vision impairment and cognitive decline among older adults: A systematic review. BMJ Open 2022, 12, e047929. [CrossRef] [PubMed]

4. Lorenzo-Veiga, B.; Alvarez-Lorenzo, C.; Loftsson, T.; Sigurdsson, H.H. Age-related ocular conditions: Current treatments and role of cyclodextrin-based nanotherapies. Int. J. Pharm. 2021, 603, 120707. [CrossRef] [PubMed]

5. Pacheco, E.; Lips, M.; Yoong, P. Transition 2.0: Digital technologies, higher education, and vision impairment. Internet High. Educ. 2018, 37, 1–10. [CrossRef]

6. Bourne, R.R.A.; Steinmetz, J.D.; Saylan, M.; Mersha, A.M.; Weldemariam, A.H.; Wondmeneh, T.G.; Sreeramareddy, C.T.; Pinheiro, M.; Yaseri, M.; Yu, C.; et al. Causes of blindness and vision impairment in 2020 and trends over 30 years, and prevalence of avoidable blindness in relation to VISION 2020: The Right to Sight: An analysis for the Global Burden of Disease Study. Lancet Glob. Health 2021, 9, e144–e160. [CrossRef]

7. Lyu, Q.; Peng, L.; Hong, X.; Fan, T.; Li, J.; Cui, Y.; Zhang, H.; Zhao, J. Smart nano-micro platforms for ophthalmological applications: The state-of-the-art and future perspectives. Biomaterials 2021, 270, 120682. [CrossRef] [PubMed]

8. Kels, B.D.; Grzybowski, A.; Grant-Kels, J.M. Human ocular anatomy. Clin. Dermatol. 2015, 33, 140–146. [CrossRef]

9. Jonas, J.B.; Ohno-Matsui, K.; Panda-Jonas, S. Myopia: Anatomic changes and consequences for its etiology. Asia-Pac. J. Ophthalmol. 2019, 8, 355–359. [CrossRef] [PubMed]

10. Lindfield, D.; Das-Bhaumik, R. Emergency department management of penetrating eye injuries. Int. Emerg. Nurs. 2009, 17, 155–160. [CrossRef] [PubMed]

11. Maulvi, F.A.; Shetty, K.H.; Desai, D.T.; Shah, D.O.; Willcox, M.D.P. Recent advances in ophthalmic preparations: Ocular barriers, dosage forms and routes of administration. Int. J. Pharm. 2021, 608, 121105. [CrossRef] [PubMed]

12. Suri, R.; Beg, S.; Kohli, K. Target strategies for drug delivery bypassing ocular barriers. J. Drug Deliv. Sci. Technol. 2020, 55, 101389. [CrossRef]

13. Varela-Fernández, R.; Díaz-Tomé, V.; Luaces-Rodríguez, A.; Conde-Penedo, A.; García-Otero, X.; Luzardo-álvarez, A.; Fernández- Ferreiro, A.; Otero-Espinar, F.J. Drug delivery to the posterior segment of the eye: Biopharmaceutic and pharmacokinetic considerations. Pharmaceutics 2020, 12, 269. [CrossRef]

14. Madni, A.; Rahem, M.A.; Tahir, N.; Sarfraz, M.; Jabar, A.; Rehman, M.; Kashif, P.M.; Badshah, S.F.; Khan, K.U.; Santos, H.A. Non-invasive strategies for targeting the posterior segment of eye. Int. J. Pharm. 2017, 530, 326–345. [CrossRef] [PubMed]

15. Bansal, P.; Garg, S.; Sharma, Y.; Venkatesh, P. Posterior Segment Drug Delivery Devices: Current and Novel Therapies in Development. J. Ocul. Pharmacol. Ther. 2016, 32, 135–144. [CrossRef] [PubMed]

16. Kamaleddin, M.A. Nano-ophthalmology: Applications and considerations. Nanomed. Nanotechnol. Biol. Med. 2017, 13, 1459–1472. [CrossRef]

17. Yorston, D. Intravitreal injection technique. Community Eye Health J. 2014, 27, 47. [CrossRef]

18. Seah, I.; Zhao, X.; Lin, Q.; Liu, Z.; Su, S.Z.Z.; Yuen, Y.S.; Hunziker, W.; Lingam, G.; Loh, X.J.; Su, X. Use of biomaterials for sustained delivery of anti-VEGF to treat retinal diseases. Eye 2020, 34, 1341–1356. [CrossRef] [PubMed]

19. Jumelle, C.; Gholizadeh, S.; Annabi, N.; Dana, R. Advances and limitations of drug delivery systems formulated as eye drops. J. Control. Release 2020, 321, 1–22. [CrossRef] [PubMed]

20. Shiels, A.; Hejtmancik, J.F. Biology of Inherited Cataracts and Opportunities for Treatment. Annu. Rev. Vis. Sci. 2019, 5, 123–149. [CrossRef]

21. Al-Ghananeem, A.M.; Crooks, P.A. Phase I and phase II ocular metabolic activities and the role of metabolism in ophthalmic prodrug and codrug design and delivery. Molecules 2007, 12, 373–388. [CrossRef]

22. Tang, Z.; Fan, X.; Chen, Y.; Gu, P. Ocular Nanomedicine. Adv. Sci. 2022, 2003699, 1–36. [CrossRef] [PubMed]

23. Leonardi, A.; Bucolo, C.; Drago, F.; Salomone, S.; Pignatello, R. Cationic solid lipid nanoparticles enhance ocular hypotensive effect of melatonin in rabbit. Int. J. Pharm. 2015, 478, 180–186. [CrossRef] [PubMed]

24. Burhan, A.M.; Klahan, B.; Cummins, W.; Andrés-Guerrero, V.; Byrne, M.E.; O'reilly, N.J.; Chauhan, A.; Fitzhenry, L.; Hughes, H. Posterior segment ophthalmic drug delivery: Role of muco-adhesion with a special focus on chitosan. Pharmaceutics 2021, 13, 1685. [CrossRef] [PubMed]

25. Gautam, D.; Pedler, M.G.; Nair, D.P.; Petrash, J.M. Nanogel-facilitated in-situ delivery of a cataract inhibitor. Biomolecules 2021, 11, 1150. [CrossRef]

26. Gagandeep, G.T.; Malik, B.; Rath, G.; Goyal, A.K. Development and characterization of nano-fiber patch for the treatment of glaucoma. Eur. J. Pharm. Sci. 2014, 53, 10–16. [CrossRef] [PubMed]

27. Ghosh, A.K.; Thapa, R.; Hariani, H.N.; Volyanyuk, M.; Ogle, S.D.; Orloff, K.A.; Ankireddy, S.; Lai, K.; Žiniauskaitè, A.; Stubbs, E.B.; et al. Poly(Lactic-co-glycolic acid) nanoparticles encapsulating the prenylated flavonoid, xanthohumol, protect corneal epithelial cells from dry eye disease-associated oxidative stress. Pharmaceutics 2021, 13, 1362. [CrossRef] [PubMed]

28. Shi, L.; Li, Z.; Liang, Z.; Zhang, J.; Liu, R.; Chu, D.; Han, L.; Zhu, L.; Shen, J.; Li, J. A dual-functional chitosan derivative platform for fungal keratitis. Carbohydr. Polym. 2022, 275, 118762. [CrossRef]

29. Liu, Y.C.; Lin, M.T.Y.; Ng, A.H.C.; Wong, T.T.; Mehta, J.S. Nanotechnology for the treatment of allergic conjunctival diseases. Pharmaceuticals 2020, 13, 351. [CrossRef]

30. Nirbhavane, P.; Sharma, G.; Singh, B.; Begum, G.; Jones, M.C.; Rauz, S.; Vincent, R.; Denniston, A.K.; Hill, L.J.; Katare, O.P. Triamcinolone acetonide loaded-cationic nano-lipoidal formulation for uveitis: Evidences of improved biopharmaceutical performance and anti-inflammatory activity. Colloids Surfaces B Biointerfaces 2020, 190, 110902. [CrossRef]

31. Du, S.; Wang, H.; Jiang, F.; Wang, Y. Diabetic Retinopathy Analysis—Effects of Nanoparticle-Based Triamcinolone. J. Nanosci. Nanotechnol. 2020, 20, 6111–6115. [CrossRef] [PubMed]

32. Suri, R.; Neupane, Y.R.; Mehra, N.; Nematullah, M.; Khan, F.; Alam, O.; Iqubal, A.; Jain, G.K.; Kohli, K. Sirolimus loaded chitosan functionalized poly (lactic-co-glycolic acid) (PLGA) nanoparticles for potential treatment of age-related macular degeneration. Int. J. Biol. Macromol. 2021, 191, 548–559. [CrossRef] [PubMed]

33. Youssef, A.; Dudhipala, N.; Majumdar, S. Ciprofloxacin Loaded Nanostructured Lipid Carriers Incorporated into In-Situ Gels to Improve Management of Bacterial Endophthalmitis. Pharmaceutics 2020, 12, 572. [CrossRef] [PubMed]

34. Tabatabaei, S.N.; Derbali, R.M.; Yang, C.; Superstein, R.; Hamel, P.; Chain, J.L.; Hardy, P. Co-delivery of miR-181a and melphalan by lipid nanoparticles for treatment of seeded retinoblastoma. J. Control. Release 2019, 298, 177–185. [CrossRef] [PubMed]

35. Allyn, M.M.; Luo, R.H.; Hellwarth, E.B.; Swindle-Reilly, K.E. Considerations for Polymers Used in Ocular Drug Delivery. Front. Med. 2022, 8, 1–25. [CrossRef]

36. Toropainen, E.; Fraser-Miller, S.J.; Novakovic, D.; Del Amo, E.M.; Vellonen, K.S.; Ruponen, M.; Viitala, T.; Korhonen, O.; Auriola, S.; Hellinen, L.; et al. Biopharmaceutics of topical ophthalmic suspensions: Importance of viscosity and particle size in ocular absorption of indomethacin. Pharmaceutics 2021, 13, 452. [CrossRef]

37. Divya, K.; Yashwant, V.P.; Kevin, B.S. Theranostic Applications of Nanomaterials for Ophthalmic Applications. Int. J. Sci. Adv. 2021, 2, 354–364. [CrossRef]

38. Awwad, S.; Mohamed Ahmed, A.H.A.; Sharma, G.; Heng, J.S.; Khaw, P.T.; Brocchini, S.; Lockwood, A. Principles of pharmacology in the eye. Br. J. Pharmacol. 2017, 174, 4205–4223. [CrossRef]

39. Dosmar, E.; Walsh, J.; Doyel, M.; Bussett, K.; Oladipupo, A.; Amer, S.; Goebel, K. Targeting Ocular Drug Delivery: An Examination of Local Anatomy and Current Approaches. Bioengineering 2022, 9, 41. [CrossRef]

40. Atta, G.; Tempfer, H.; Kaser-Eichberger, A.; Traweger, A.; Heindl, L.M.; Schroedl, F. Is the human sclera a tendon-like tissue? A structural and functional comparison. Ann. Anat. 2022, 240, 151858. [CrossRef]

41. Lopes, B.T.; Bao, F.; Wang, J.; Liu, X.; Wang, L.; Abass, A.; Eliasy, A.; Elsheikh, A. Review of in-vivo characterisation of corneal biomechanics. Med. Nov. Technol. Devices 2021, 11, 100073. [CrossRef]

42. Zénon, A. Eye pupil signals information gain. Proc. R. Soc. B Biol. Sci. 2019, 286, 20191593. [CrossRef] [PubMed]

43. Domkin, D.; Forsman, M.; Richter, H.O. Effect of ciliary-muscle contraction force on trapezius muscle activity during computer mouse work. Eur. J. Appl. Physiol. 2019, 119, 389–397. [CrossRef] [PubMed]

44. Chow, L.S.; Paley, M.N.J. Recent advances on optic nerve magnetic resonance imaging and post-processing. Magn. Reson. Imaging 2021, 79, 76–84. [CrossRef]

45. Kaur, I.P.; Smitha, R.; Aggarwal, D.; Kapil, M. Acetazolamide: Future perspective in topical glaucoma therapeutics. Int. J. Pharm. 2002, 248, 1–14. [CrossRef]

46. Nielsen, L.H.; Keller, S.S.; Boisen, A. Microfabricated devices for oral drug delivery. Lab Chip 2018, 18, 2348–2358. [CrossRef]

47. Underhill, G.H.; Khetani, S.R. Advances in engineered human liver platforms for drug metabolism studies. Drug Metab. Dispos. 2018, 46, 1626–1637. [CrossRef]

48. Pitkänen, L.; Ranta, V.P.; Moilanen, H.; Urtti, A. Permeability of retinal pigment epithelium: Effects of permeant molecular weight and lipophilicity. Investig. Ophthalmol. Vis. Sci. 2005, 46, 641–646. [CrossRef]

49. Reinholz, J.; Landfester, K.; Mailänder, V. The challenges of oral drug delivery via nanocarriers. Drug Deliv. 2018, 25, 1694–1705. [CrossRef]

50. Kim, Y.C.; Chiang, B.; Wu, X.; Prausnitz, M.R. Ocular delivery of macromolecules. J. Control. Release 2014, 190, 172–181. [CrossRef]

_____

51. Urtti, A. Challenges and obstacles of ocular pharmacokinetics and drug delivery. Adv. Drug Deliv. Rev. 2006, 58, 1131–1135. [CrossRef] [PubMed]

52. Falavarjani, K.G.; Nguyen, Q.D. Adverse events and complications associated with intravitreal injection of anti-VEGF agents: A review of literature. Eye 2013, 27, 787–794. [CrossRef] [PubMed]

53. Ibrahim, S.S. The Role of Surface Active Agents in Ophthalmic Drug Delivery: A Comprehensive Review. J. Pharm. Sci. 2019, 108, 1923–1933. [CrossRef]

54. Liebmann, J.M.; Barton, K.; Weinreb, R.N.; Eichenbaum, D.A.; Gupta, P.K.; McCabe, C.M.; Wolfe, J.D.; Ahmed, I.; Sheybani, A.; Craven, E.R. Evolving Guidelines for Intracameral Injection. J. Glaucoma 2020, 29, 1–7. [CrossRef] [PubMed]

55. Takahashi, K.; Morizane, Y.; Hisatomi, T.; Tachibana, T.; Kimura, S.; Hosokawa, M.M.; Shiode, Y.; Hirano, M.; Doi, S.; Toshima, S.; et al. The influence of subretinal injection pressure on the microstructure of the monkey retina. PLoS ONE 2018, 13, e0209996. [CrossRef] [PubMed]

56. Sebbag, L.; Moody, L.M.; Mochel, J.P. Albumin levels in tear film modulate the bioavailability of medically-relevant topical drugs. Front. Pharmacol. 2020, 10, 1–9. [CrossRef] [PubMed]

57. Järvinen, K.; Järvinen, T.; Urtti, A. Ocular absorption following topical delivery. Adv. Drug Deliv. Rev. 1995, 16, 3–19. [CrossRef]

58. Patere, S.; Newman, B.; Wang, Y.; Choi, S.; Vora, S.; Ma, A.W.K.; Jay, M.; Lu, X. Influence of Manufacturing Process Variables on the Properties of Ophthalmic Ointments of Tobramycin. Pharm. Res. 2018, 35, 1–6. [CrossRef]

59. Lazcano-Gomez, G.; Castillejos, A.; Kahook, M.; Jimenez-Roman, J.; Gonzalez-Salinas, R. Videographic assessment of glaucoma drop instillation. J. Curr. Glaucoma Pract. 2015, 9, 47–50. [CrossRef]

60. Taneja, M.; Chappidi, K.; Harsha Ch, S.N.S.; Richhariya, A.; Mohamed, A.; Rathi, V.M. Innovative bulls eye drop applicator for self-instillation of eye drops. Contact Lens Anterior Eye 2020, 43, 256–260. [CrossRef]

61. Davies, I.; Williams, A.M.; Muir, K.W. Aids for eye drop administration. Surv. Ophthalmol. 2017, 62, 332–345. [CrossRef]

62. Hornof, M.; Toropainen, E.; Urtti, A. Cell culture models of the ocular barriers. Eur. J. Pharm. Biopharm. 2005, 60, 207–225. [CrossRef] [PubMed]

63. Juretić, M.; Cetina-Čižmek, B.; Filipović-Grčić, J.; Hafner, A.; Lovrić, J.; Pepić, I. Biopharmaceutical evaluation of surface active ophthalmic excipients using in vitro and ex vivo corneal models. Eur. J. Pharm. Sci. 2018, 120, 133–141, doi:10.1016/j.ejps.2018.04.032

64. Li, Q.; Weng, J.; Wong, S.N.; Thomas Lee, W.Y.; Chow, S.F. Nanoparticulate Drug Delivery to the Retina. Mol. Pharm. 2021, 18, 506–521. [CrossRef] [PubMed]

65. Karki, R.; Meena, M.; Prakash, T.; Rajeswari, T.; Goli, D.; Kumar, S. Reduction in drop size of ophthalmic topical drop preparations and the impact of treatment. J. Adv. Pharm. Technol. Res. 2011, 2, 192. [CrossRef]

66. Puglia, C.; Santonocito, D.; Romeo, G.; Intagliata, S.; Romano, G.L.; Strettoi, E.; Novelli, E.; Ostacolo, C.; Campiglia, P.; Sommella, E.M.; et al. Lipid nanoparticles traverse non-corneal path to reach the posterior eye segment: In vivo evidence. Molecules 2021, 26, 4673. [CrossRef]

67. Bechnak, L.; El Kurdi, R.; Patra, D. Fluorescence Sensing of Nucleic Acid by Curcumin Encapsulated Poly(Ethylene Oxide)-Block- Poly(Propylene Oxide)-Block-Poly(Ethylene Oxide) Based Nanocapsules. J. Fluoresc. 2020, 30, 547–556. [CrossRef] [PubMed]

68. Beija, M.; Afonso, C.A.M.; Martinho, J.M.G. Synthesis and applications of rhodamine derivatives as fluorescent probes. Chem. Soc. Rev. 2009, 38, 2410–2433. [CrossRef] [PubMed]

69. Han, Z.X.; Zhang, X.B.; Li, Z.; Gong, Y.J.; Wu, X.Y.; Jin, Z.; He, C.M.; Jian, L.X.; Zhang, J.; Shen, G.L.; et al. Efficient fluorescence resonance energy transfer-based ratiometric fluorescent cellular imaging probe for Zn2+ using a rhodamine spirolactam as a trigger. Anal. Chem. 2010, 82, 3108–3113. [CrossRef] [PubMed]

70. Keerthana, S.; Sam, B.; George, L.; Sudhakar, Y.N.; Varghese, A. Fluorescein Based Fluorescence Sensors for the Selective Sensing of Various Analytes. J. Fluoresc. 2021, 31, 1251–1276. [CrossRef]

71. El Khoury, E.; Patra, D. Length of hydrocarbon chain influences location of curcumin in liposomes: Curcumin as a molecular probe to study ethanol induced interdigitation of liposomes. J. Photochem. Photobiol. B Biol. 2016, 158, 49–54. [CrossRef] [PubMed]

72. Khorasani, M.Y.; Langari, H.; Sany, S.B.T.; Rezayi, M.; Sahebkar, A. The role of curcumin and its derivatives in sensory applications. Mater. Sci. Eng. C 2019, 103, 109792. [CrossRef] [PubMed]

73. Carneiro, A.; Matos, M.J.; Uriarte, E.; Santana, L. Trending topics on coumarin and its derivatives in 2020. Molecules 2021, 26, 501. [CrossRef] [PubMed]

74. Duong, H.D.; Shin, Y.; Rhee, J. Il Development of novel optical pH sensors based on coumarin 6 and nile blue A encapsulated in resin particles and specific support materials. Mater. Sci. Eng. C 2020, 107, 110323. [CrossRef] [PubMed]

75. Grimm, J.B.; Lavis, L.D. Synthesis of rhodamines from fluoresceins using pd-catalyzed c-n cross-coupling. Org. Lett. 2011, 13, 6354–6357. [CrossRef] [PubMed]

76. Rajasekar, M. Recent development in fluorescein derivatives. J. Mol. Struct. 2021, 1224, 129085. [CrossRef]

77. McHedlov-Petrossyan, N.O.; Cheipesh, T.A.; Roshal, A.D.; Shekhovtsov, S.V.; Moskaeva, E.G.; Omelchenko, I.V. Aminofluoresceins Versus Fluorescein: Peculiarity of Fluorescence. J. Phys. Chem. A 2019, 123, 8860–8870. [CrossRef]

78. Zhao, X.; Belykh, E.; Cavallo, C.; Valli, D.; Gandhi, S.; Preul, M.C.; Vajkoczy, P.; Lawton, M.T.; Nakaji, P. Application of Fluorescein Fluorescence in Vascular Neurosurgery. Front. Surg. 2019, 6, 52. [CrossRef]

79. Küçükyürük, B.; Korkmaz, T.S.; Nemayire, K.; Özlen, F.; Kafadar, A.M.; Akar, Z.; Kaynar, M.Y.; Sanus, G.Z. Intraoperative Fluorescein Sodium Videoangiography in Intracranial Aneurysm Surgery. World Neurosurg. 2021, 147, e444–e452. [CrossRef]

80. Bömers, J.P.; Danielsen, M.E.; Schulz, M.K.; Halle, B.; Kristensen, B.W.; Sørensen, M.D.; Poulsen, F.R.; Pedersen, C.B. Sodium fluorescein shows high surgeon-reported usability in glioblastoma surgery. Surgeon 2020, 18, 344–348. [CrossRef]

81. Voronin, D.V.; Kozlova, A.A.; Verkhovskii, R.A.; Ermakov, A.V.; Makarkin, M.A.; Inozemtseva, O.A.; Bratashov, D.N. Detection of rare objects by flow cytometry: Imaging, cell sorting, and deep learning approaches. Int. J. Mol. Sci. 2020, 21, 2323. [CrossRef] [PubMed]

_____

82. Wang, L.; Du, W.; Hu, Z.; Uvdal, K.; Li, L.; Huang, W. Hybrid Rhodamine Fluorophores in the Visible/NIR Region for Biological Imaging. Angew. Chem.-Int. Ed. 2019, 58, 14026–14043. [CrossRef] [PubMed]

83. Marnett, L.J. Synthesis of 5- and 6-Carboxy-X-rhodamines. Org. Lett. 2008, 10, 4799–4801.

84. Bonaccorso, A.; Musumeci, T.; Serapide, M.F.; Pellitteri, R.; Uchegbu, I.F.; Puglisi, G. Nose to brain delivery in rats: Effect of surface charge of rhodamine B labeled nanocarriers on brain subregion localization. Colloids Surf. B Biointerfaces 2017, 154, 297–306. [CrossRef] [PubMed]

85. Dempsey, G.T.; Bates, M.; Kowtoniuk, W.E.; Liu, D.R.; Tsien, R.Y.; Zhuang, X. Photoswitching mechanism of cyanine dyes. J. Am. Chem. Soc. 2009, 131, 18192–18193. [CrossRef]

86. Lim, E.; Kwon, J.; Park, J.; Heo, J.; Kim, S.K. Selective thiolation and photoswitching mechanism of Cy5 studied by time-dependent density functional theory. Phys. Chem. Chem. Phys. 2020, 22, 14125–14129. [CrossRef]

87. Bae, S.; Lim, E.; Hwang, D.; Huh, H.; Kim, S.K. Torsion-dependent fluorescence switching of amyloid-binding dye NIAD-4. Chem. Phys. Lett. 2015, 633, 109–113. [CrossRef]

88. Blower, M.D.; Feric, E.; Weis, K.; Heald, R. Genome-wide analysis demonstrates conserved localization of messenger RNAs to mitotic microtubules. J. Cell Biol. 2007, 179, 1365–1373. [CrossRef]

89. Martos, A.; Berger, M.; Kranz, W.; Spanopoulou, A.; Menzen, T.; Friess, W.; Wuchner, K.; Hawe, A. Novel High-Throughput Assay for Polysorbate Quantification in Biopharmaceutical Products by Using the Fluorescent Dye DiI. J. Pharm. Sci. 2020, 109, 646–655. [CrossRef] [PubMed]

90. Musumeci, T.; Serapide, M.F.; Pellitteri, R.; Dalpiaz, A.; Ferraro, L.; Dal Magro, R.; Bonaccorso, A.; Carbone, C.; Veiga, F.; Sancini, G.; et al. Oxcarbazepine free or loaded PLGA nanoparticles as effective intranasal approach to control epileptic seizures in rodents. Eur. J. Pharm. Biopharm. 2018, 133, 309–320. [CrossRef]

91. Capolungo, C.; Genovese, D.; Montalti, M.; Rampazzo, E.; Zaccheroni, N.; Prodi, L. Photoluminescence-Based Techniques for the Detection of Micro- and Nanoplastics. Chem.-A Eur. J. 2021, 27, 17529–17541. [CrossRef]

92. Sancataldo, G.; Avellone, G.; Vetri, V. Nile Red lifetime reveals microplastic identity. Environ. Sci. Process. Impacts 2020, 22, 2266–2275. [CrossRef]

93. Hewlings, S.J.; Kalman, D.S. Curcumin: A review of its effects on human health. Foods 2017, 6, 92. [CrossRef] [PubMed]

94. Sridharan, G.; Shankar, A.A. Toluidine blue: A review of its chemistry and clinical utility. J. Oral Maxillofac. Pathol. 2012, 16, 251–255. [CrossRef] [PubMed]

95. Aliakbar Navahi, R.; Hosseini, S.B.; Kanavi, M.R.; Rakhshani, N.; Aghaei, H.; Kheiri, B. Comparison of toluidine blue 1% staining patterns in cytopathologically confirmed ocular surface squamous neoplasias and in non-neoplastic lesions. Ocul. Surf. 2019, 17, 578–583. [CrossRef]

96. Su, G.; Wei, Z.; Wang, L.; Shen, J.; Baudouin, C.; Labbé, A.; Liang, Q. Evaluation of toluidine blue-mediated photodynamic therapy for experimental bacterial keratitis in rabbits. Transl. Vis. Sci. Technol. 2020, 9, 1–10. [CrossRef] [PubMed]

97. Craparo, E.F.; Musumeci, T.; Bonaccorso, A.; Pellitteri, R.; Romeo, A.; Naletova, I.; Cucci, L.M.; Cavallaro, G.; Satriano, C. Mpeg-plga nanoparticles labeled with loaded or conjugated rhodamine-b for potential nose-to-brain delivery. Pharmaceutics 2021, 13, 1508. [CrossRef]

98. Turcsányi, Á.; Ungor, D.; Csapó, E. Fluorescent labeling of hyaluronic acid-chitosan nanocarriers by protein-stabilized gold nanoclusters. Crystals 2020, 10, 1113. [CrossRef]

99. Romero, G.B.; Keck, C.M.; Müller, R.H.; Bou-Chacra, N.A. Development of cationic nanocrystals for ocular delivery. Eur. J. Pharm. Biopharm. 2016, 107, 215–222. [CrossRef]

100. Pignatello, R.; Corsaro, R.; Santonocito, D. Chapter A Method for Efficient Loading of Ciprofloxacin Hydrochloride in Cationic Solid Lipid Nanoparticles. Nanomaterials 2018, 8, 304. [CrossRef]

101. Jounaki, K.; Makhmalzadeh, B.S.; Feghhi, M.; Heidarian, A. Topical ocular delivery of vancomycin loaded cationic lipid nanocarriers as a promising and non-invasive alternative approach to intravitreal injection for enhanced bacterial endophthalmitis management. Eur. J. Pharm. Sci. 2021, 167, 105991. [CrossRef] [PubMed]

102. Vaishya, R.D.; Khurana, V.; Patel, S.; Mitra, A.K. Controlled ocular drug delivery with nanomicelles. Wiley Interdiscip. Rev. Nanomed. Nanobiotechnology 2014, 6, 422–437. [CrossRef] [PubMed]

103. Zhang, W.H.; Hu, X.X.; Zhang, X.B. Dye-doped fluorescent silica nanoparticles for live cell and in vivo bioimaging. Nanomaterials 2016, 6, 81. [CrossRef]

104. Siddique, S.; Chow, J.C.L. Application of nanomaterials in biomedical imaging and cancer therapy. Nanomaterials 2020, 10, 1700. [CrossRef] [PubMed]

105. Niamprem, P.; Srinivas, S.P.; Tiyaboonchai, W. Penetration of Nile red-loaded nanostructured lipid carriers (NLCs) across the porcine cornea. Colloids Surf. B Biointerfaces 2019, 176, 371–378. [CrossRef] [PubMed]

106. El-Gendy, M.A.; Mansour, M.; El-Assal, M.I.A.; Ishak, R.A.H.; Mortada, N.D. Delineating penetration enhancer-enriched liquid crystalline nanostructures as novel platforms for improved ophthalmic delivery. Int. J. Pharm. 2020, 582, 119313. [CrossRef]

107. Kapadia, R.; Parikh, K.; Jain, M.; Sawant, K. Topical instillation of triamcinolone acetonide-loaded emulsomes for posterior ocular delivery: Statistical optimization and in vitro-in vivo studies. Drug Deliv. Transl. Res. 2021, 11, 984–999. [CrossRef] [PubMed]

108. Eldesouky, L.M.; El-Moslemany, R.M.; Ramadan, A.A.; Morsi, M.H.; Khalafallah, N.M. Cyclosporine lipid nanocapsules as thermoresponsive gel for dry eye management: Promising corneal mucoadhesion, biodistribution and preclinical efficacy in rabbits. Pharmaceutics 2021, 13, 360. [CrossRef] [PubMed]

109. Dubashynskaya, N.V.; Bokatyi, A.N.; Golovkin, A.S.; Kudryavtsev, I.V.; Serebryakova, M.K.; Trulioff, A.S.; Dubrovskii, Y.A.; Skorik, Y.A. Synthesis and characterization of novel succinyl chitosan-dexamethasone conjugates for potential intravitreal dexamethasone delivery. Int. J. Mol. Sci. 2021, 22, 10960. [CrossRef] [PubMed]

110. Li, J.; Tan, G.; Cheng, B.; Liu, D.; Pan, W. Transport mechanism of chitosan-N-acetylcysteine, chitosan oligosaccharides or carboxymethyl chitosan decorated coumarin-6 loaded nanostructured lipid carriers across the rabbit ocular. Eur. J. Pharm. Biopharm. 2017, 120, 89–97. [CrossRef] [PubMed]

111. Tan, G.; Li, J.; Song, Y.; Yu, Y.; Liu, D.; Pan, W. Phenyl boronic acid-tetheredchondroitinsulfate-based mucoadhesive nanostructured lipid carriers for the treatment of dry eye syndrome. Acta Biomater. 2019, 99, 350–362. [CrossRef] [PubMed]

112. Liu, C.; Lan, Q.; He, W.; Nie, C.; Zhang, C.; Xu, T.; Jiang, T.; Wang, S. Octa-arginine modified lipid emulsions as a potential ocular delivery system for disulfiram: A study of the corneal permeation, transcorneal mechanism and anti-cataract effect. Colloids Surf. B Biointerfaces 2017, 160, 305–314. [CrossRef] [PubMed]

113. Gómez-Aguado, I.; Rodríguez-Castejón, J.; Beraza-Millor, M.; Vicente-Pascual, M.; Rodríguez-Gascón, A.; Garelli, S.; Battaglia, L.; Del Pozo-Rodríguez, A.; Solinís, M.Á. Mrna-based nanomedicinal products to address corneal inflammation by interleukin-10 supplementation. Pharmaceutics 2021, 13, 1472. [CrossRef] [PubMed]

114. Kakkar, S.; Singh, M.; Mohan Karuppayil, S.; Raut, J.S.; Giansanti, F.; Papucci, L.; Schiavone, N.; Nag, T.C.; Gao, N.; Yu, F.S.X.; et al. Lipo-PEG nano-ocular formulation successfully encapsulates hydrophilic fluconazole and traverses corneal and non-corneal path to reach posterior eye segment. J. Drug Target. 2021, 29, 631–650. [CrossRef]

115. Pretor, S.; Bartels, J.; Lorenz, T.; Dahl, K.; Finke, J.H.; Peterat, G.; Krull, R.; Dietzel, A.; Bu, S.; Behrends, S.; et al. Cellular Uptake of Coumarin-6 under Micro fluidic Conditions into HCE-T Cells from Nanoscale Formulations. Mol. Pharm. 2015, 12, 34–45. [CrossRef] [PubMed]

116. Elmotasem, H.; Awad, G.E.A. A stepwise optimization strategy to formulate in situ gelling formulations comprising fluconazole-hydroxypropyl-beta-cyclodextrin complex loaded niosomal vesicles and Eudragit nanoparticles for enhanced antifungal activity and prolonged ocular delivery. Asian J. Pharm. Sci. 2020, 15, 617–636. [CrossRef] [PubMed]

117. Anishiyachelladaisy, E.R.; Rajendran, N.K.; Jeyaraj, M.; Ramu, A.; Rajan, M. Retinal photoreceptors targeting SA-g-AA coated multilamellar liposomes carrier system for cytotoxicity and cellular uptake evaluation. J. Liposome Res. 2021, 31, 203–216. [CrossRef]

118. Swetledge, S.; Carter, R.; Stout, R.; Astete, C.E.; Jung, J.P.; Sabliov, C.M. Stability and ocular biodistribution of topically administered PLGA nanoparticles. Sci. Rep. 2021, 11, 1–11. [CrossRef]

119. Dubashynskaya, N.; Poshina, D.; Raik, S.; Urtti, A.; Skorik, Y.A. Polysaccharides in ocular drug delivery. Pharmaceutics 2020, 12, 22. [CrossRef]

120. Zhukova, V.; Osipova, N.; Semyonkin, A.; Malinovskaya, J.; Melnikov, P.; Valikhov, M.; Porozov, Y.; Solovev, Y.; Kuliaev, P.; Zhang, E.; et al. Fluorescently labeled plga nanoparticles for visualization in vitro and in vivo: The importance of dye properties. Pharmaceutics 2021, 13, 1145. [CrossRef]

121. Zhang, E.; Zhukova, V.; Semyonkin, A.; Osipova, N.; Malinovskaya, Y.; Maksimenko, O.; Chernikov, V.; Sokolov, M.; Grigartzik, L.; Sabel, B.A.; et al. Release kinetics of fluorescent dyes from PLGA nanoparticles in retinal blood vessels: In vivo monitoring and ex vivo localization. Eur. J. Pharm. Biopharm. 2020, 150, 131–142. [CrossRef] [PubMed]

122. Li, B.; Wang, J.; Gui, Q.; Yang, H. Drug-loaded chitosan film prepared via facile solution casting and air-drying of plain water-based chitosan solution for ocular drug delivery. Bioact. Mater. 2020, 5, 577–583. [CrossRef] [PubMed]

123. Álvarez-Álvarez, L.; Barral, L.; Bouza, R.; Farrag, Y.; Otero-Espinar, F.; Feijóo-Bandín, S.; Lago, F. Hydrocortisone loaded poly-(3- hydroxybutyrate-co-3-hydroxyvalerate) nanoparticles for topical ophthalmic administration: Preparation, characterization and evaluation of ophthalmic toxicity. Int. J. Pharm. 2019, 568, 118519. [CrossRef] [PubMed]

124. Tahara, K.; Karasawa, K.; Onodera, R.; Takeuchi, H. Feasibility of drug delivery to the eye's posterior segment by topical instillation of PLGA nanoparticles. Asian J. Pharm. Sci. 2017, 12, 394–399. [CrossRef] [PubMed]

125. Sun, X.; Sheng, Y.; Li, K.; Sai, S.; Feng, J.; Li, Y.; Zhang, J.; Han, J.; Tian, B. Mucoadhesive phenylboronic acid conjugated chitosan oligosaccharide-vitamin E copolymer for topical ocular delivery of voriconazole: Synthesis, in vitro/vivo evaluation, and mechanism. Acta Biomater. 2022, 138, 193–207. [CrossRef]

126. Sai, N.; Dong, X.; Huang, P.; You, L.; Yang, C.; Liu, Y.; Wang, W.; Wu, H.; Yu, Y.; Du, Y.; et al. A novel gel-forming solution based on PEG-DSPE/Solutol HS 15 mixed micelles and gellan gum for ophthalmic delivery of curcumin. Molecules 2020, 25, 81. [CrossRef]

127. Abilova, G.K.; Kaldybekov, D.B.; Ozhmukhametova, E.K.; Saimova, A.Z.; Kazybayeva, D.S.; Irmukhametova, G.S.; Khutoryanskiy, V.V. Chitosan/poly(2-ethyl-2-oxazoline) films for ocular drug delivery: Formulation, miscibility, in vitro and in vivo studies. Eur. Polym. J. 2019, 116, 311–320. [CrossRef]

128. Chi, H.; Gu, Y.; Xu, T.; Cao, F. Multifunctional organic–inorganic hybrid nanoparticles and nanosheets based on chitosan derivative and layered double hydroxide: Cellular uptake mechanism and application for topical ocular drug delivery. Int. J. Nanomedicine 2017, 12, 1607–1620. [CrossRef]

129. Mun, E.A.; Morrison, P.W.J.; Williams, A.C.; Khutoryanskiy, V.V. On the barrier properties of the cornea: A microscopy study of the penetration of fluorescently labeled nanoparticles, polymers, and sodium fluorescein. Mol. Pharm. 2014, 11, 3556–3564. [CrossRef]

130. Baran-Rachwalska, P.; Torabi-Pour, N.; Sutera, F.M.; Ahmed, M.; Thomas, K.; Nesbit, M.A.; Welsh, M.; Moore, C.B.T.; Saffie-Siebert, S.R. Topical siRNA delivery to the cornea and anterior eye by hybrid silicon-lipid nanoparticles. J. Control. Release 2020, 326, 192–202. [CrossRef]

131. Qu, W.; Meng, B.; Yu, Y.; Wang, S. EpCAM antibody-conjugated mesoporous silica nanoparticles to enhance the anticancer efficacy of carboplatin in retinoblastoma. Mater. Sci. Eng. C 2017, 76, 646–651. [CrossRef] [PubMed]

132. Xu, H.; Tang, B.; Huang, W.; Luo, S.; Zhang, T.; Yuan, J.; Zheng, Q.; Zan, X. Deliver protein across bio-barriers via hexa-histidine metal assemblies for therapy: A case in corneal neovascularization model. Mater. Today Bio 2021, 12, 100143. [CrossRef] [PubMed]

133. Wang, Y.; Liu, W.; Yuan, B.; Yin, X.; Li, Y.; Li, Z.; Cui, J.; Yuan, X.; Li, Y. The application of methylprednisolone nanoscale zirconium-porphyrin metal-organic framework (MPS-NPMOF) in the treatment of photoreceptor degeneration. Int. J. Nanomedicine 2019, 14, 9763–9776. [CrossRef] [PubMed]

134. Ding, S.; Zhang, N.; Lyu, Z.; Zhu, W.; Chang, Y.C.; Hu, X.; Du, D.; Lin, Y. Protein-based nanomaterials and nanosystems for biomedical applications: A review. Mater. Today 2021, 43, 166–184. [CrossRef]

135. Nguyen, T.P.; Nguyen, Q.V.; Nguyen, V.H.; Le, T.H.; Huynh, V.Q.N.; Vo, D.V.N.; Trinh, Q.T.; Kim, S.Y.; VanLe, Q. Silk fibroin-based biomaterials for biomedical applications: A review. Polymers 2019, 11, 1933. [CrossRef]

136. Yang, P.; Dong, Y.; Huang, D.; Zhu, C.; Liu, H.; Pan, X.; Wu, C. Silk fibroin nanoparticles for enhanced bio-macromolecule delivery to the retina. Pharm. Dev. Technol. 2019, 24, 575–583. [CrossRef]

137. Tiwari, R.; Sethiya, N.K.; Gulbake, A.S.; Mehra, N.K.; Murty, U.S.N.; Gulbake, A. A review on albumin as a biomaterial for ocular drug delivery. Int. J. Biol. Macromol. 2021, 191, 591–599. [CrossRef]

138. Radwan, S.E.S.; El-Kamel, A.; Zaki, E.I.; Burgalassi, S.; Zucchetti, E.; El-Moslemany, R.M. Hyaluronic-coated albumin nanoparticles for the non-invasive delivery of apatinib in diabetic retinopathy. Int. J. Nanomed. 2021, 16, 4481–4494. [CrossRef]

139. Zhang, W.; Kantaria, T.; Zhang, Y.; Kantaria, T.; Kobauri, S.; Tugushi, D.; Brücher, V.; Katsarava, R.; Eter, N.; Heiduschka, P. Biodegradable Nanoparticles Based on Pseudo-Proteins Show Promise as Carriers for Ophthalmic Drug Delivery. J. Ocul. Pharmacol. Ther. 2020, 36, 421–432. [CrossRef]

140. Thomas, C.J.; Mirza, R.G.; Gill, M.K. Age-Related Macular Degeneration. Med. Clin. North Am. 2021,105,473–491.[CrossRef]

141. Hanus ,J.; Anderson, C.; Wang, S. RPE necroptosis in response to oxidative stress and in AMD. Ageing Res. Rev. 2015, 24, 286–298. [CrossRef] [PubMed]

142. Hammond, B.R.; Johnson, M.A. The age-related eye disease study (AREDS). Nutr. Rev. 2002, 60, 283–288. [CrossRef] [PubMed]

143. Gregori, N.Z.; Goldhardt, R. Nutritional Supplements for Age-Related Macular Degeneration. Curr. Ophthalmol. Rep. 2015, 3, 34–39. [CrossRef] [PubMed]

144. Álvarez-Barrios, A.; Álvarez, L.; García, M.; Artime, E.; Pereiro, R.; González-Iglesias, H. Antioxidant defenses in the human eye: A focus on metallothioneins. Antioxidants 2021, 10, 89. [CrossRef] [PubMed]

145. Cruz-Alonso, M.; Fernandez, B.; Álvarez, L.; González-Iglesias, H.; Traub, H.; Jakubowski, N.; Pereiro, R. Bioimaging of metallothioneins in ocular tissue sections by laser ablation-ICP-MS using bioconjugated gold nanoclusters as specific tags. Microchim. Acta 2018, 185, 1–9. [CrossRef]

146. Osredkar, J. Copper and Zinc, Biological Role and Significance of Copper/Zinc Imbalance. J. Clin. Toxicol. 2011, 3, 1–18. [CrossRef]

147. Uddin, M.I.; Kilburn, T.C.; Yang, R.; McCollum, G.W.; Wright, D.W.; Penn, J.S. Targeted imaging of VCAM-1 mRNA in a mouse model of laser-induced choroidal neovascularization using antisense hairpin-DNA-functionalized gold-nanoparticles. Mol. Pharm. 2018, 15, 5514–5520. [CrossRef]

148. Pearson, R.A.; Barber, A.C.; Rizzi, M. Restoration of vision after transplantation of photoreceptors. Nature 2012, 485, 99–103. [CrossRef]

149. Chemla, Y.; Betzer, O.; Markus, A.; Farah, N.; Motiei, M.; Popovtzer, R.; Mandel, Y. Gold nanoparticles for multimodal high-resolution imaging of transplanted cells for retinal replacement therapy. Nanomedicine 2019, 14, 1857–1871. [CrossRef]

150. Meir, R.; Shamalov, K.; Betzer, O.; Motiei, M.; Horovitz-Fried, M.; Yehuda, R.; Popovtzer, A.; Popovtzer, R.; Cohen, C.J. Nanomedicine for Cancer Immunotherapy: Tracking Cancer-Specific T-Cells in Vivo with Gold Nanoparticles and CT Imaging. ACS Nano 2015, 9, 6363–6372. [CrossRef] [PubMed]

151. Cai, W.; Chen, M.; Fan, J.; Jin, H.; Yu, D.; Qiang, S.; Peng, C.; Yu, J. Fluorescein sodium loaded by polyethyleneimine for fundus fluorescein angiography improves adhesion. Nanomedicine 2019, 14, 2595–2611. [CrossRef] [PubMed]

152. Safi, H.; Safi, S.; Hafezi-Moghadam, A.; Ahmadieh, H. Early detection of diabetic retinopathy. Surv. Ophthalmol. 2018, 63, 601–608. [CrossRef]

153. Wang, X.; Li, S.; Li, W.; Hua, Y.; Wu, Q. Choroidal Variations in Diabetic Macular Edema: Fluorescein Angiography and Optical Coherence Tomography. Curr. Eye Res. 2018, 43, 102–108. [CrossRef] [PubMed]

154. Shivshetty, N.; Swift, T.; Pinnock, A.; Pownall, D.; Neil, S.M.; Douglas, I.; Garg, P.; Rimmer, S. Evaluation of ligand modified poly (N-Isopropyl acrylamide) hydrogel for etiological diagnosis of corneal infection. Exp. Eye Res. 2022, 214, 108881. [CrossRef] [PubMed]

155. Ladju, R.B.; Ulhaq, Z.S.; Soraya, G.V. Nanotheranostics: A powerful next-generation solution to tackle hepatocellular carcinoma. World J. Gastroenterol. 2022, 28, 176–187. [CrossRef] [PubMed]

156. Tang, M.; Ji, X.; Xu, H.; Zhang, L.; Jiang, A.; Song, B.; Su, Y.; He, Y. Photostable and Biocompatible Fluorescent Silicon Nanoparticles-Based Theranostic Probes for Simultaneous Imaging and Treatment of Ocular Neovascularization. Anal. Chem. 2018, 90, 8188–8195. [CrossRef] [PubMed]

157. Shabbir, U.; Rubab, M.; Tyagi, A.; Oh, D.H. Curcumin and its derivatives as theranostic agents in alzheimer's disease: The implication of nanotechnology. Int. J. Mol. Sci. 2021, 22, 196. [CrossRef] [PubMed]

158. Stati, G.; Rossi, F.; Trakoolwilaiwan, T.; Tung, L.D.; Mourdikoudis, S.; Thanh, N.T.K.; Di Pietro, R. Development and Characterization of Curcumin-Silver Nanoparticles as a Promising Formulation to Test on Human Pterygium-Derived Keratinocytes. Molecules 2022, 27, 282. [CrossRef] [PubMed]

159. Zhang, L.; Ji, X.; Su, Y.; Zhai, X.; Xu, H.; Song, B.; Jiang, A.; Guo, D.; He, Y. Fluorescent silicon nanoparticles-based nanotheranostic agents for rapid diagnosis and treatment of bacteria-induced keratitis. Nano Res. 2021, 14, 52–58. [CrossRef]

160. de Oliveira, D.C.S.; de Freitas, C.F.; Calori, I.R.; Goncalves, R.S.; Cardinali, C.A.E.F.; Malacarne, L.C.; Ravanelli, M.I.; de Oliveira, H.P.M.; Tedesco, A.C.; Caetano, W.; et al. Theranostic verteporfin- loaded lipid-polymer liposome for photodynamic applications. J. Photochem. Photobiol. B Biol. 2020, 212, 112039. [CrossRef]

161. Li, L.; Zeng, Z.; Chen, Z.; Gao, R.; Pan, L.; Deng, J.; Ye, X.; Zhang, J.; Zhang, S.; Mei, C.; et al. Microenvironment-triggered degradable hydrogel for imaging diagnosis and combined treatment of intraocular choroidal melanoma. ACS Nano 2020, 14, 15403–15416. [CrossRef] [PubMed]

162. Maulvi, F.A.; Desai, D.T.; Shetty, K.H.; Shah, D.O.; Willcox, M.D.P. Advances and challenges in the nanoparticles-laden contact lenses for ocular drug delivery. Int. J. Pharm. 2021, 608, 121090. [CrossRef] [PubMed]

163. Huang, J.F.; Zhong, J.; Chen, G.P.; Lin, Z.T.; Deng, Y.; Liu, Y.L.; Cao, P.Y.; Wang, B.; Wei, Y.; Wu, T.; et al. A Hydrogel-Based Hybrid Theranostic Contact Lens for Fungal Keratitis. ACS Nano 2016, 10, 6464–6473. [CrossRef] [PubMed]

164. Jin, Y.; Wang, Y.; Yang, J.; Zhang, H.; Yang, Y.W.; Chen, W.; Jiang, W.; Qu, J.; Guo, Y.; Wang, B. An Integrated Theranostic Nanomaterial for Targeted Photodynamic Therapy of Infectious Endophthalmitis. Cell Reports Phys. Sci. 2020, 1, 100173. [CrossRef]

165. Khiev, D.; Mohamed, Z.A.; Vichare, R.; Paulson, R.; Bhatia, S.; Mohapatra, S.; Lobo, G.P.; Valapala, M.; Kerur, N.; Passaglia, C.L.; et al. Emerging nano-formulations and nanomedicines applications for ocular drug delivery. Nanomateri- als 2021, 11, 173. [CrossRef]

166. Alander, J.T.; Kaartinen, I.; Laakso, A.; Tommi, P.; Spillmann, T.; Tuchin, V.V.; Venermo, M.; Petri, V. A Review of Indocyanine Green Fluorescent Imaging in Surgery. Int. J. Biomed. Imaging 2012, 2012, 7. [CrossRef] [PubMed]

10 *IN VITRO* AND *IN VIVO* STUDIES OF TOPICALLY ADMINISTERED NLC FOR THE TREATMENT OF UVEAL MELANOMA

Cinzia Cimino[1,2,3,4], Elena Sánchez López [3,5,6], Angela Bonaccorso[2,4], Lorena Bonilla[3,5], Teresa Musumeci[2,4], Josefa Badia[7,8,9], Laura Baldomà[7,8,9], Rosario Pignatello[2,4], Agostino Marrazzo[4,10], María Luisa García[3,5], Claudia Carbone[2,4*]

[1] PhD in Biotechnology, Department of Biomedical and Biotechnological Sciences, University of Catania, Via Santa Sofia 97, 95123 Catania, Italy.

[2] Laboratory of Drug Delivery Technology, Department of Drug and Health Sciences, University of Catania, Viale A. Doria 6, 95124 Catania, Italy.

[3] Department of Pharmacy, Pharmaceutical Technology and Physical Chemistry, Faculty of Pharmacy and Food Sciences, University of Barcelona, 08028, Barcelona, Spain.

[4] NANOMED, Research Centre for Ocular Nanotechnology, University of Catania.

[5] Institute of Nanoscience and Nanotechnology (IN2UB), University of Barcelona, 08028, Barcelona, Spain.

[6] Unit of Synthesis and Biomedical Applications of Peptides, IQAC-CSIC, 08034, Barcelona, Spain.

[7] Department of Biochemistry and Physiology, Biochemistry and Biomolecular Science, University of Barcelona, 08028 Barcelona, Spain.

[8] Institute of Biomedicine of the University of Barcelona (IBUB), 08028 Barcelona, Spain.

[9] Research Institute Sant Joan De Déu (IR-SJD), 08950 Barcelona, Spain.

[10] Medicinal Chemistry Laboratory, Department of Drug and Health Sciences, University of Catania, Viale A. Doria 6, 95124 Catania, Italy.

Abstract: Uveal melanoma is one of the most aggressive tumors, and, for its great capability of metastasize, results to be the most incident intraocular tumor in adult age. However, to date there is no effective treatment since achieving the inner ocular tissues still constitutes one of the greatest challenges in actual medicine, because of the complex structure and barriers characteristics of this organ. Aiming to properly vehiculate (*S*)-(–)-

MRJF22, a new custom-synthetized prodrug for the potential treatment of uveal melanoma, a novel nanotechnological approach based on nanostructured lipid carriers (NLC) has been developed. Therefore, NLC were prepared and functionalized with a cationic coating as well as polyethylene glycol (PEG). Non-coated and PEGylated NLC loading (*S*)-(–)-MRJF22 were compared. The prepared platforms were characterized in terms of particle size, homogeneity, zeta potential, pH and osmolality, being suitable for ophthalmic administration. Stability test was carried on at different temperatures using Turbiscan® Ageing Station, demonstrating good physical stability. Moreover, morphology analysis by TEM and mucoadhesive studies were performed. *In vitro* release studies were performed using Franz diffusion cells, demonstrating that the NLC were able to provide a slow and prolonged prodrug release. *In vitro* MTT test on HCE-2 and 92-1 cell lines, as well as HET-CAM assay and Draize test, confirmed the cytocompatibility of the formulations. *In vivo* antiangiogenic capability and *in vivo* preventive anti-inflammatory properties were assessed. Furthermore, *in vivo* biodistribution studies of the nanoparticles after topical instillation in rabbits' eyes, demonstrated the potential use of the developed NLC for the treatment of inner eye pathologies.

10.1 Introduction

Uveal melanoma (UM) is the most common malignant tumor of the inner eye, affecting 6 per million per year and resulting in 50% of mortality in one year relating to liver metastasis [1], [2]. Occasionally, UM could affect ciliary body (7%) and iris (3%), but its main localization is in the choroid (90%) [3]. The achievement of the ocular tissues, and its posterior segment in particular, has always been a great challenge in the clinical field. In fact, for its complex structure and for the presence of several barriers and protection mechanisms, drug targeting to the inner eye results very difficult, both through systemic route and topical instillation. Systemic administration is usually inefficient because of the presence of the blood aqueous barrier, which protects the anterior region of the eye, and the blood-retinal barrier that protects the retina. On the other hand, the success of the topical instillation is limited by the presence of the tears and by blinking and drainage mechanisms, which are responsible of the short permanence time of the drug on ocular surface (1-2 minutes) [4], [5]; when the drug succeeds to reach the cornea, its permeation is strictly controlled by the lipophilicity of the drug [6]. For the aforementioned reasons, only 2% of the administered drug is able to reach the inner eye through systemic route [7], while for topical ophthalmic administration the percentage raises to 3-5% [8]. Aiming to directly

target the inner eye, invasive methods are currently used in therapy, such as transscleral and intravitreal administrations. However, they possess low patient compliance and require highly qualified personnel [9]. To reach the inner eye through topical administration, the encapsulation of drugs into delivery systems has demonstrated to be a successful strategy, which could be exploited using several carriers and modulating their properties in order to target specific areas of the eye. For instance, particle size influences nanoparticle permeation ability, while their superficial charge could favor interaction with mucin, improving the retention time on the ocular surface [10]. Among the various carriers that could be employed for ophthalmic delivery, lipid nanoparticles – and nanostructured lipid carriers (NLC) in particular – demonstrated to be suitable for their biocompatibility and ability to act as a depot [11], as well as for their numerous advantages such as high encapsulation efficiency, reduced drug loss and high stability during storage [12]. Several NLC systems demonstrated to be potentially useful in the treatment of eye posterior segment pathologies [13], [14], and the employment of fluorescent probes allowed to follow nanoparticles distribution after *in vivo* administration [15].

Considering that the current therapy for this cancer only consists in surgery, radiation and enucleation [16], the development of novel drugs is the key for its actual cure. From the analysis of the biomolecular targets of this cancer, a new prodrug (*S*)-(–)-MRJF22 was synthetized esterifying haloperidol metabolite II (HP-mII) and valproic acid (VPA): the inhibition of histone deacetylase (HDACi) related to the VPA, and the σ1-antagonism and σ2-agonism attributable to HP-mII, resulted in a combined dual action, which was demonstrated to be promising as an adjuvant treatment for UM [17]. Aiming to provide a specific targeting to the inner eye, the encapsulation of this prodrug represents a potential strategy.

For these reasons, a NLC platform was developed (namely NLC) and successively modified PEGylating the nanoparticles surface (P-NLC) or adding a cationic DDAB coating (D-NLC). Indeed, cationic coating could favor interactions with the negatively charged mucin residues on the ocular surface [18], while PEG is able to interpenetrate the mucin chains [19], providing, in both the situations, a prolonged residence of the carrier on the ocular surface.

The three carriers were characterized in terms of particle size, homogeneity, zeta potential, pH and osmolality, and their stability was assessed using Turbiscan® Ageing Station. Moreover, NLCs morphology was analyzed through TEM studies and their mucoadhesive properties were verified. (*S*)-(–)-MRJF22 was then successfully encapsulated and its release from the carriers was evaluated using Franz diffusion cells. NLC cytocompatibility

was conformed both by *in vitro* and *in vivo* tests. *In vivo* antiangiogenic capability and *in vivo* preventive anti-inflammatory properties were also investigated. Finally, the achievement of the posterior segment of the eye was verified through *in vivo* biodistribution studies.

10.2 Materials and Methods

10.2.1 Materials

Kolliphor RH40 was provided by BASF Italia S.p.a. (Cesano Modena, Italy); Oleoyl Macrogol-6 Glycerides (Labrafil) was a gift from Gattefossé Italia s.r.l. (Milano, Italy); Hydrogenated Coco-Glycerides (Softisan 100) was bought from IOI Oleo GmbH (Oleochemicals, IOI group); Isopropyl myristate (IPM) was purchased from Farmalabor (Canosa di Puglia, Italy). Tris (hydroxymethyl)aminomethane buffer, methanol (MeOH) and ethanol (EtOH) were bought from Merck (Darmstadt, Germany). Didodecyldimethylammonium bromide (DDAB), Polyethylene Glycol 1500 (PEG 1500), Fluorescein isothiocyanate (FITC), phosphate buffer saline (PBS) components (NaCl, KCl, Na_2HPO_4, KH_2PO_4), artificial tear fluid (ATF) components ($CaCl_2 \cdot 2H_2O$, $NaHCO_3$, NaCl), mucin (mucin from porcine stomach type II), simulated tear fluid (STF) components (NaCl, $NaHCO_3$, $CaCl_2 \cdot 2H_2O$ and KCl), benzalkonium chloride, trypsin-EDTA (1X), tetrazolium bromide (MTT), DMSO, DAPI (4',6-diamidino-2-phenylindole), arachidonic acid, Hank's solution components ($CaCl_2 \cdot 2H_2O$, $MgSO_4$, KCl, K_2HPO_4, $NaHCO_3$, NaCl, Na_2PO_4, glucose), paraformaldehyde, glucose, Triton X-100, Mowiol components (Mowiol, glycerol) were purchased from Sigma Aldrich (MO, USA). OCT compound (Sakura Finetek, Torrance, CA, USA). Regenerated cellulose membranes (Spectra/Por CE; Mol. Wet. Cutoff 3500) were supplied by Spectrum (Los Angeles, CA, USA). (*S*)-(–)-MRJF22 was synthetized by the research group of Prof. Agostino Marrazzo, in the Medicinal Chemistry Laboratory of the Department of Drug and Health Sciences (Università degli Studi di Catania) [17]. All solvents (LC grade) were from VWR International (Milan, Italy). Human corneal epithelial cell line immortalized with adenovirus 12SV40 hybrid virus (HCE-2, ATCC® CRL-11135) was purchased from LGC Standards (Barcelona, Spain), while the medium used (Keratinocyte serum-free medium added with human recombinant epidermal growth factor, bovine pituitary extract, penicillin, streptomycin, insulin) was from Thermo Fisher Scientific (Life Technologies, CA, USA).

Human uveal melanoma (UM 92-1) cell line was purchased from the Cell Factory-IST (Genova, Italy), while the medium used (RPMI-1640 medium added with fetal bovine

serum (FBS), l-glutamine, penicillin and streptomycin) was from Euroclone S.p.A. (Pero, Milan, Italy).

10.2.2 Nanoparticles production

To produce the NLCs, the phase inversion temperature (PIT) method was chosen, following the previously described protocol [20]. Briefly, the lipid phase was composed of a mixture of surfactants (<7% w/v), the solid lipid and the liquid lipid (1:2.5 ratio). PEG 1% w/v or DDAB 0.15% w/v, were added to the lipid phase to prepare Pegylated NLCs (P-NLC) and cationic NLCs (D-NLC), respectively. To prepare the loaded formulations, (*S*)-(–)-MRJF22 was added at 0.02% w/v, obtaining (*S*)-NLC and (*S*)-P-NLC. The fluorescent samples were prepared using FITC at 0.01% w/v, obtaining F-NLC and F-P-NLC. The water and the lipid phases were heated separately and then the water phase was added dropwise in the melted oily phase under continuous stirring. The formulation was mixed at room temperature, vortexed (Heidolph Reax 2000, VWR, Milan, Italy), cooled, and then vortexed again. After 24h, the samples were purified to remove the excess of surfactants (see section 2.3.5).

10.2.3 Physical-chemical and technological characterization

10.2.3.1 Photon Correlation Spectroscopy (PCS)

Particle size (Z-ave), polydispersity index (PDI) and zeta potential (ZP) of the samples (1:20 diluted in ultra-purified water) were measured through Photon Correlation Spectroscopy (PCS) using a ZetaSizer NanoZS (Malvern Instruments, Worcestershire, United Kingdom). Each analysis was performed at least by triplicate.

10.2.3.2 Osmolality and pH

An osmometer (3320 Osmometer, Advanced Instruments, Norwood, MA, USA) was used to assess the osmolality of the samples, which was previously calibrated using ultra-purified water and physiological solution. The pH values of the samples were determined using a pH meter (Mettler Toledo, Milano, Italy), calibrated using solution with defined pH 4.0, 7.0 and 10.0.

10.2.3.3 TEM morphology studies

Morphologies of the purified blank formulations were studied using transmission electron microscopy (TEM) using a 1:5 water dilution on a JEOL 1010 microscope (Akishima, Japan). To visualize the samples, Carbon-coated grids (carbon support film of 200 mesh from Electron Microscopy Sciences, Hatfield, United Kingdom) were used. The grids were

activated using UV light and negative staining of the samples placed on the grid was carried out using uranyl acetate (2%) [21].

10.2.3.4 Stability studies

To assess the physical stability of the samples, 15 ml of each unloaded sample was stored into Turbiscan® Ageing Station (TAGS, Formulaction, L'Union, France) at three different temperatures (room temperature 25.0±1.0°C, physiological temperature 36.5±1.0°C and extreme temperature 50.0±1.0°C). This technique, previously described in [22], was selected for its well-known reliability in detecting the occurrence of aggregation and/or migration instability phenomena in colloidal suspensions [23]–[26]. The results were obtained as variation of transmission profiles (ΔT), which were compared between the samples, and numerically as Turbiscan® Stability Index (TSI).

10.2.3.5 Encapsulation efficiency and drug loading capacity

The percentage of non-entrapped drug was measured after ultracentrifugation (SL16R Centrifuge, Thermo Scientific, Rodano, Italy) at 13.000 rpm (90 min at 4°C). The collected supernatant was diluted in methanol-0.5% diethylamine mixture (ratio 1:5) and ultracentrifuged again for 30 min. The supernatant obtained was analyzed using UV-vis spectrophotometer (UH5300 UV-Visible Double-Beam Spectrophotometer, Hitachi Europe, Milan, Italy).

The following equation was used to calculate the encapsulation efficiency (EE%):

$$EE\% = \frac{weighted\ drug - amount\ of\ not\ entrapped\ drug}{total\ amount\ of\ drug\ used} \cdot 100$$

and the drug loading capacity (DLC%) was calculated with the equation:

$$DLC\% = \frac{amount\ of\ drug\ entrapped}{weight\ of\ lipidic\ phase} \cdot 100$$

10.2.4 In vitro studies

10.2.4.1 Mucoadhesion studies

Mucin suspension 0.1% w/v in simulated tear fluid, STF (NaCl 0.68 g, NaHCO$_3$ 0.22 g, CaCl$_2$·2H$_2$O 0.008 g, KCl 0.14 g, and distilled deionized water to 100 mL) was prepared the day before the assay and was stirred overnight. Mucoadhesive properties were analyzed by mixing mucin dispersion and nanoparticles in 1:1 v/v ratio for 15 min at 25°C, and subsequently incubating at 37°C up to 4h. Two *in vitro* methods were performed of the mixture sample-mucin at the selected time points (0, 1, 2, 3, 4h): turbidimetric measurement comparing the absorbances at 650 nm using UV-vis spectrophotometer, and

mucin particle method measuring variations in sizes and zeta potentials using Zetasizer Nano S90 (Malvern Instruments, Malvern, UK).

10.2.4.2 In vitro release studies

In vitro release of (*S*)-(–)-MRJF22 or FITC from nanoparticles was assessed using Franz-type diffusion cells (LGA, Berkeley, CA, USA), with 0.75 cm^2 of regenerated cellulose membranes (Spectra/Por CE; Mol. Weight Cut-off 3.5 kDa) moistened for 24h in the release medium. As reference, (*S*)-(–)-MRJF22 was solubilized in methanol-0.5% diethylamine solution (MeOH-0.5% DEA) while FITC was dissolved in ethanol (EtOH), in a concentration comparable to the encapsulated molecules into the nanosystems. Artificial tear fluid (ATF) was prepared by dissolving the salts in ultrapure water (for 1L: 0.08g $CaCl_2 \cdot 2H_2O$, 2g $NaHCO_3$, 6.7g NaCl) and adjusting the pH to 7.4 using HCl 1M, as reported in literature [27]. In the receptor, maintained at 35±1°C and stirred at 600 rpm, a 50:50 v/v mixture of tris(hydroxymethyl)aminomethane buffer (TRIS) and MeOH-0.5% DEA was used as release medium for prodrug-loaded NLC, while a 50:50 v/v mixture of ATF and EtOH supplemented with 2% Tween® 80 was used to assess FITC release. The donor compartment was filled with500 μL of each purified sample. At planned time interval (every hour from 0 to 8h, and then at 24h), 500 μL were withdrawn from the receptor and replaced with medium to guarantee pseudosink conditions. Each withdrawn was diluted 1:2 with medium and analyzed using UV-vis spectrophotometer. The selected wavelengths were 222 nm for (S)-(–)-MRJF22 and 500 nm for FITC.

10.2.4.3 Cell cultures

Human Corneal Epithelium HCE-2 cells were maintained in keratinocyte serum-free medium supplemented with bovine pituitary extract (BPE) 0.05 mg/ml, epidermal growth factor (EGF) 5 ng/ml, insulin 0.005 mg/ml and streptomycin 100 mg/ml. For MTT assay, passages from 41 to 52 were used.

Human UM 92-1 cells were maintained in RPMI-1640 medium, added with 10% fetal bovine serum (FBS), 2 mM L-glutamine, 100 units/mL penicillin and 100 μg/mL streptomycin. For MTT assay, passages from 10 to 13 were used. All the cells were incubated at 37°C and 5% CO_2.

10.2.4.4 Cytotoxicity

Cell viability was assessed through MTT assay on confluent monolayers. The cells were seeded and incubated for 48h at a confluence of 80%, then the medium was removed, and the cells were treated for 5h (for HCE-2) or 24h (for UM 92-1) with different concentrations of the NLC samples pellet, corresponding to 10 μM, 5 μM, 3 μM, 1 μM, 0.5 μM and 0.3

µM concentration of the encapsulated drug. Benzalkonium chloride 0.01% was used as positive control to assess effective cell death, while medium was used as a negative 100% viability control. After the treatment, the cells were incubated with 2.5 mg/ml Bromide of 3-(4,5-dimethyl-2-thiazoyl)-2,5-diphenyltetrazole (MTT), then formazan crystals were solubilized in DMSO for 5 min and the absorbance was read at λ=560 nm using an automatic ModulusTM Microplate Photometer (Turner BioSystems, CA, USA) [28]–[30]. Cell viability was expressed as percentage comparing to untreated control cells.

10.2.4.5 In vitro ocular tolerance

HET-CAM test was used to assess *in vitro* ocular tolerance of the formulations. Chorioallantoic membrane (CAM) of 10-day embryonated eggs (provided from GALLSA farm, Tarragona, Spain) were subjected to the application of 300 µL of each sample, while NaOH 0.1N and NaCl 0.9% solutions were used as positive and negative controls, respectively [30]. For 5 min, it was observed the appearance of hemorrhage, vasoconstriction, or coagulation. Since the application of lipid formulations creates a white layer, after 30 sec NaCl solution was added in order to be able to see the vessels and the eventual occurrence of damage. The formulations were classified as previously reported [31] through the calculation of the ocular irritation index (OII) [32]:

$$OII = \frac{5(301 - H)}{300} + \frac{7(301 - V)}{300} + \frac{9(301 - C)}{300}$$

Where H, V and C are the time of appearance of hemorrhage, vasoconstriction and coagulation, respectively, expressed in seconds. Results were classified as: not-irritant (0<OII<0.9), slightly irritant (1<OII<4.0), moderately irritant (5<OII<8.9), severely irritant (9<OII<21).

Moreover, a quantitative irritation measurement was carried on through the HET-CAM TBS assay. 1000 µL of 0.1% trypan blue staining (TBS) in phosphate buffered saline (pH 7.4) solution were added to the previously treated CAM for 1 min and then washed with distilled water to remove the excess of TBS. The CAM was then excised and weighted, then was put into 5 ml of formamide to extract the absorbed TBS, which was quantified through NanoDrop™ (One/OneC Microvolume UV-Vis Spectrophotometer, Thermo Fisher Scientific, Waltham, Massachusetts, USA) at 595 nm. The quantification of the absorbed dye (AD) was calculated using the following equation:

$$AD = \frac{absorbance}{membrane\ weight\ (mg)} \cdot \frac{5}{1000} \cdot 10^9\ nmol$$

Considering the obtained values, the samples were classified using the following scale: ≤ 0.19 nmol/mg not irritant; 0.10-0.15 nmol/mg moderately irritant; ≥ 0.15 nmol/mg severely irritant [31].

10.2.5 In vivo studies

10.2.5.1 Draize irritation test

Draize irritation test [33] was performed on 2 kg New Zealand albino rabbits purchased from Granja Riera and housed in individual cages. Animals were maintained in controlled temperature (17-23°C) and relative humidity (60-80%) conditions, with food and water supplemented ad libitum. This test was carried out in accordance with the Ethical Committee for Animal Experimentation of the University of Barcelona and current legislation (Decree 214/97, Gencat).

In order to perform the assessment, 50 μL of the loaded NLC and of (*S*)-(–)-MRJF22 solution were administered topically in the conjunctival sac, performing a light massage to distribute the sample on the entire surface of the eye. After 30 min, cornea, conjunctiva and iris were observed to highlight eventual damages, following the guidelines reported in Supplementary Table 1 and using the equation below to calculate the ocular irritation index (OII).

$$OII = Corneal(A \cdot B \cdot 5) + Iris(A \cdot 5) + Conjunctiva(A + B + C) \cdot 2$$

The obtained scores were classified as follow: 0 non-irritant, 0-15 slightly irritant, ≥15-30 moderately irritant, ≥30-50 irritant, ≥50 severely irritant [31].

10.2.5.2 Antiangiogenic capability

Antiangiogenic capacity of the samples was assessed using the CAM assay [31]. To perform the analysis, a window in the shell was opened on the side of 3 days fertilized eggs, and, after 24h of incubation at 37°C and 85% humidity, the CAM was treated with 40 μL of each sample. After 48h of treatment, the CAM was fixed with 4% paraformaldehyde at 4°C. After 24h, membranes were removed and observed through binocular loupe. The density of the vessels was measured automatically using ImageJ vessel analysis plugin [21].

10.2.5.3 Ocular anti-inflammatory capacity

In vivo preventive anti-inflammatory activity was analyzed on New Zealand albino rabbits administering the samples for 30 min. After this time, an inflammatory stimulus was applied by adding arachidonic acid. The occurrence of ocular damage was assessed after 30 min and then at 1, 1.5, 2, 2.5h [34]. Ocular irritation index was evaluated based on the criteria described in Supplementary Table 1 [31] and using the equation reported in section 2.5.1.

10.2.5.4 In vivo biodistribution

In vivo biodistribution was assessed by applying two 50 μL-administrations separated by 5 min of clearance of either fluorescent-NLC or FITC solution into the conjunctival sac of

New Zealand albino rabbits, massaging the eye after each administration to. After 3h, the animals were sacrificed and the eyes were enucleated and transferred into paraformaldehyde 4% in PBS, and then freeze at -80°C.

Afterwards, the freeze eyes were cut using a cryostat (Leica CM 3050 S, Leica Microsystems GmbH, Wetzlar, Germany) and the cellular nucleus were stained with DAPI. Fluorescence was assessed using a Leica Thunder Imager DMI8 (Leica Microsystems GmbH, Wetzlar, Germany) and quantified using ImageJ software [35].

10.2.6 Statistics

For the characterization of blank, loaded and fluorescent formulations, ordinary one-way ANOVA with Turkey's multiple comparison test was used, compared the blank P-NLC and D-NLC with NLC, while the loaded and the fluorescent samples were compared to their respective blanks. For mucoadhesive studies, two-way ANOVA was performed, using Tukey's multiple comparisons test for mucin particle method. For cytocompatibility, two-way ANOVA with Dunnett's multiple comparisons test was performed compared to CTRL, as well as for HET-CAM, HET-CAM TBS, *in vitro* antiangiogenic capability assay and *in vivo* anti-inflammatory activity test. All analyses were done with GraphPad Prism 9.5.0 (GraphPad Software, Inc., San Diego, CA) and p values were considered significant at p≤0.05.

10.3 Results and discussion

10.3.1 Physico-chemical characterization of unloaded NLCs

10.3.1.1 PCS analysis

As already described in a previous work [20], the PIT method – which is a green and organic solvent-free preparation technique – and the raw materials were selected for their capability to allow the formation of NLC with small and homogeneous mean diameters. Moreover, all the materials demonstrated to be tolerable for ocular topical administration, as already discussed elsewhere [23]. A blank nanosystem was prepared (NLC) and compared to surface-modified P-NLC and D-NLC, respectively obtained with the addition of PEG or the cationic lipid DDAB. In fact, in literature it was extensively demonstrated that enhanced nanoparticle permeation [18] could be obtained through cationic surface modification of the nanoparticles because of the higher mucoadhesiveness on ocular surface [23], [36] through ionic interaction with mucin [23], [37]. On the other hand,

PEGylation mainly increases the retention time on cornea surface due to the ability of interpenetrate the mucin chains [19] thus allowing a prolonged release [18], [36].

As reported in Figure 1, Zetasizer analysis showed PDI values lower than 0.25, demonstrating that all the samples were homogeneous, with a mean particles size lower than 160 nm for all the samples, without significant variations among them. The slight not significant increase in Z-ave reported for P-NLC is related to the presence of the PEG coating, as already demonstrated by Jokerst [38], while the slight not significant decrease in the mean diameter of D-NLC is caused by the addition of DDAB which was previously demonstrated to reduce particle size when compared to uncoated formulation [39]. It is well-known that Z-ave is a crucial parameter for the ophthalmic administration, since particle diameters higher than 10 μm are not well-tolerated, and in particular a mean particle size between 50 and 400 nm is preferred to avoid ocular irritations [40]. Furthermore, particle size strongly influences the distribution and the residence time of the carriers in the various ocular structures [23], where diameters lower than 200 nm are mandatory to allow ocular permeation [41] and to enhance mucoadhesion and endocytosis [36].
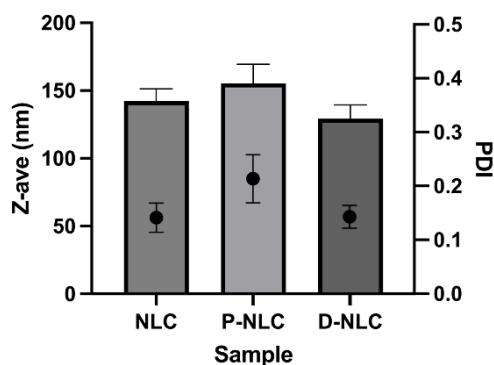

Figure 1. Z-ave (nm) and PDI values of NLC, P-NLC, and D-NLC. Not significant for p≤0.05.

10.3.1.2 pH and osmolality measurements

The prepared formulations also demonstrated to satisfy other important parameters required by both European Pharmacopoeia and FDA for liquid preparations used for the ocular site, namely pH and osmolality [Supplementary Table 2], which should fall between the range tolerated by the eye. In particular, pH should be between 6.8 and 7.4 [42] to avoid ocular chemical damages [43], while osmolality should be in the tears range (280 and 300 mOsm/Kg) to allow a safe passage of particles through the biological membranes [23].

Moreover, the ZP of the samples was measured [Supplementary Table 2], since it allows to predict the long-term stability of the samples, basing on the idea that markedly positive

or negative values could guarantee particle repulsion thus avoiding physical instability phenomena [44]. The obtained results showed neutral ZP values for NLC and P-NLC, while D-NLC resulted positively charged (+24.9 ± 0.67 mV), as expected.

10.3.1.3 TEM analysis

TEM images reported in Figure 2 confirmed, that all the formulations, showed mean particle diameter lower than 200 nm, with NLC and D-NLC showing a greater homogeneity compared to P-NLC, in accordance with PDI values (Figure 1). The shape of the particles resulted to be spherical for all the sample, and no morphological changes were highlighted after the addition of the DDAB or PEG coatings, as reported for similar NLC systems coated with DDAB [45]. These results are consistent with literature findings, where it was highlighted that the addition of PEG coating on NLC caused not significant changes in morphology, as revealed by TEM analysis [46].
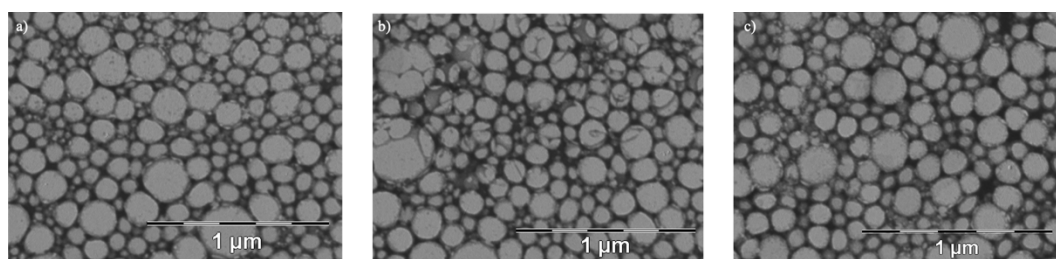

Figure 2. TEM images of NLC (a); D-NLC (b); P-NLC (c).

10.3.1.4 Physical stability

The stability of the samples was verified using the Turbiscan® Technology equipped with an Ageing Station. The samples NLC, P-NLC and D-NLC were stored for 30 days at three different temperatures: 25°C, 36.5°C and 50°C. The variation of transmission profiles (ΔT) is a parameter which describes physical instability in the sample, discerning if it is occurring a particle size increment, identified as higher ΔT values in the middle of the graph, or a particle migration phenomenon, when ΔT increasing are located in the lateral parts of the graph, depending on the type of instability phenomenon occurring (clarification, sedimentation or creaming) [45]. As reported in Figure 3, a not significant variation of transmission (ΔT<<20%) was observed at the bottom of the cuvette in all the samples stored at 25°C, related to the formation of a slight sediment which was easily redispersed by gentle shaking of the colloidal suspension. The same behavior was observed at 36.5°C and 50°C (data not showed). The destabilization kinetics showed in Supplementary Figure 1 in terms of evolution of Turbiscan® Stability Index (TSI), all the

_____

samples demonstrated a high stability at all the analyzed temperatures. The higher stability of D-NLC reflects its higher ZP value, which guarantee particle repulsion thus stability, as already discussed, and confirms previous literature findings [45].
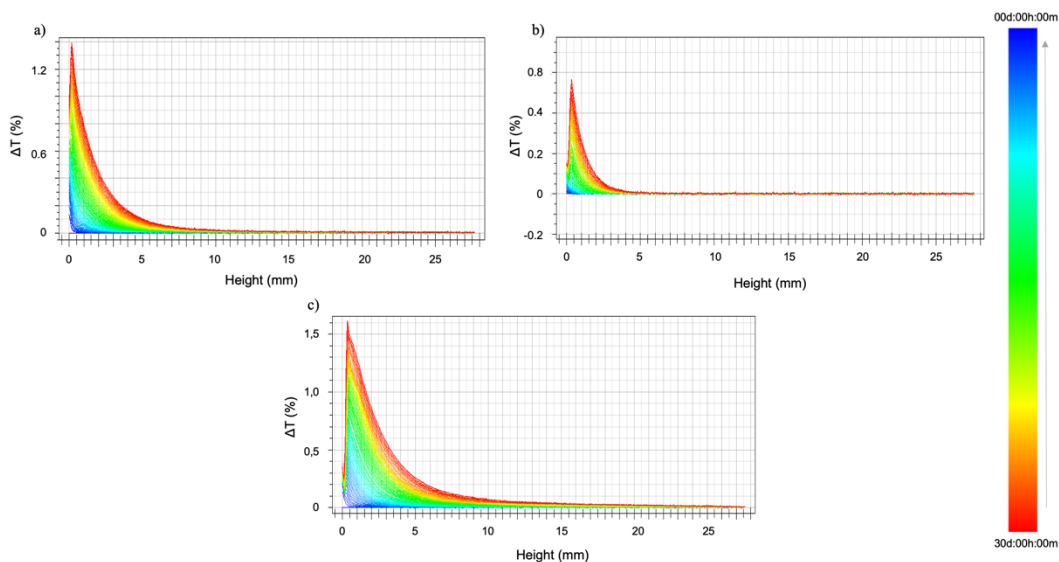

Figure 3. Variations of transmission (ΔT) profiles of samples NLC (**a**), D-NLC (**b**) and P-NLC (**c**) after 30 days of storage in Turbiscan® at 25.0±1.0°C, data are represented as a function of time (0-30 days) of sample height (0-25 mm) – the sense of analysis time is indicated by the arrow.

10.3.2 *In vitro studies on unloaded NLCs*

10.3.2.1 *Cytotoxicity*

The cytocompatibility of the blank samples was assessed using two cell lines, HCE-2 (human corneal cells) and UM 92-1 (tumoral melanoma cells). The HCE-2 cell line was selected to analyze the compatibility of the formulation on corneal cells after topical administration; for this reason, the samples were tested for 5h, since the physiological clearance mechanisms of the eye usually do not allow a longer residence time [47]. Considering that the NLCs were developed for the delivery of (*S*)-(–)-MRJF22 for the potential treatment of UM, cytocompatibility studies were also performed on 92-1 cancer cell lines. Therefore, several concentrations of NLCs were tested, from 0.3 μM to 10 μM, as previously reported [20].

As a positive cytotoxic control, BAK 0.01% was also applied [23], showing 6.64% viability on HCE cells and 4.21% on UM cells. Blank NLC (Figure 4 a,d) and P-NLC (Figure 4 b,e) showed a dose-depended viability in both cell lines, with NLC being safe (viability > 80%) up to 1 μM, and P-NLC until 3 μM. A high cytotoxicity of D-NLC on both cell lines (Figure 4 c,f), with a drastic decrease in the viability even with the more diluted concentrations.

_____

This behavior is probably related to the presence of the cationic DDAB, whose ability to electrostatically interact with the anionic ocular surface could affect the cells viability [18]. For its low cytocompatibility, D-NLC was not subjected to further studies.
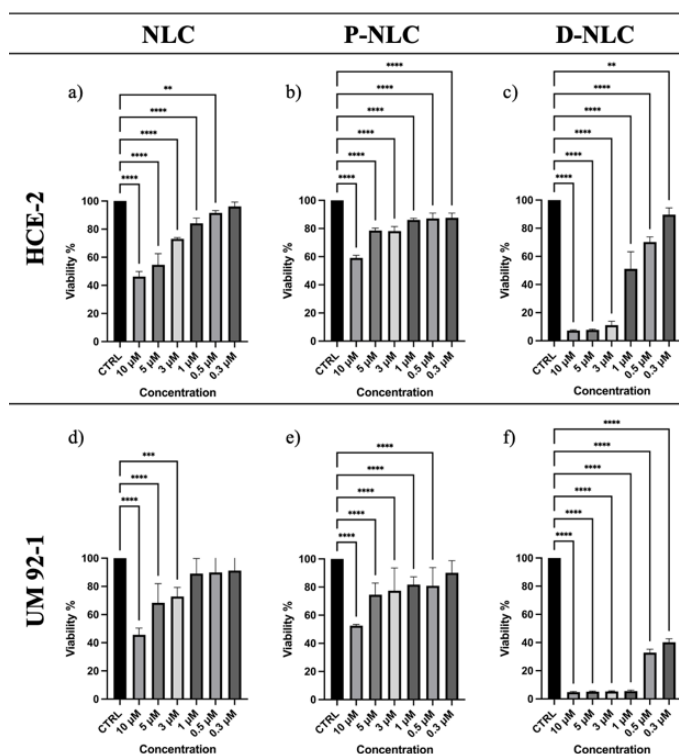

Figure 4. Cytocompatibility on HCE-2 cells (**a-c**) and on UM 92-1 cells (**d-f**) of: NLC (**a,d**); P-NLC (**b,e**); D-NLC (**c,f**). Significance was set at $^{**}p \leq 0.01$; $^{***}p \leq 0.001$; $^{****}p \leq 0.0001$.

10.3.2.2 *In vitro mucoadhesion properties*

To further assess the interaction of the nanoparticles with the ocular surface, *in vitro* mucoadhesion studies were performed on uncoated NLC and PEGylated P-NLC, incubating the samples with mucin suspension in STF up to 4h. In fact, after ophthalmic administration, the nanoparticles need to interact with ocular surface – which contains mucin, a high-molecular weight glycoprotein characterized by a negative ZP – in order to avoid the elimination with the tears.

Mucoadhesive properties of the nanoparticles could be assessed by mucin particle method, in which interaction with mucin is assessed measuring the changes in Z-ave and ZP values. As reported in Figure 5a, both the samples demonstrated to slightly interact with mucin, as highlighted by the significant increase ($^{****}p \leq 0.0001$) in particle size of muc-NLC and muc-P-NLC compared to NLC and P-NLC at all analyzed timepoints. ZP measurements confirmed these interactions, as a significant reduction ($^{***}p \leq 0.001$, $^{****}p \leq 0.0001$) in ZP

_____

values of the samples after incubation with mucin was reported at all timepoints (Figure 5b). The occurrence of mild interaction was also highlighted by the slight increase of PDI values for both samples, from 0.18 to 0.38 for NLC, and from 0.23 to 0.35 for P-NLC (however results were not significant). These results were confirmed also by the turbidimetric assay (Figure 5c), which estimates the mucoadhesiveness basing on the assumption that the interaction of the nanoparticle with mucin causes an aggregation that could be detected by UV-vis analysis. As previously reported, PEG did not increase mucoadhesiveness compared to the uncoated NLC [48]. The interaction with mucin suggests that both systems could be retained on the ocular surface, avoiding the loss related to the tears flow. However, it resulted necessary to assess their capability to migrate to the posterior chamber and to not remain indefinitely adhered on the ocular surface, as successively studied through *in vivo* biodistribution experiments.
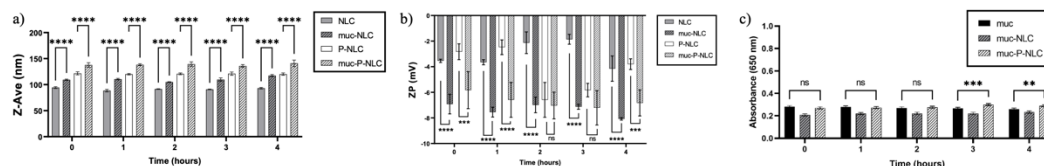

Figure 5. Z-ave values (**a**) and ZP values (**b**) of samples (NLC and P-NLC) before 0 and after 1, 2, 3 and 4h of incubation with mucin (muc-NLC, muc-P-NLC) at 37°C. Significance was set as [***]p≤0.001; [****]p≤0.0001. (**c**) *In vitro* assessment of samples/mucin interactions at different time points (0, 1, 2, 3 and 4h) by turbidimetric assay at 650 nm. Significance was set as [***]p≤0.001; [**]p ≤ 0.01.

10.3.3 Physico-chemical and technological characterization of loaded NLCs

10.3.3.1 PCS analysis, EE% and DLC% measurements of loaded NLCs

Since NLC and P-NLC demonstrated to possess interesting features for potential ophthalmic administration, both the colloidal systems were employed to encapsulate (*S*)-(−)-MRJF22, a new prodrug synthetized combining valproic acid (VPA) and haloperidol metabolite II (HP-II) [17]. (*S*)-(−)-MRJF22 was added to the nanoparticle's composition at 0.02% w/w, obtaining (*S*)-NLC and (*S*)-P-NLC, with an encapsulation efficiency of 57.73±1.91% and of 52.89±2.90% respectively, thus in line with previous results obtained for the same prodrug delivered into a similar NLC platform [20]. Drug loading capacity was also measured, resulting to be 0.083±0.001% and 0.073±0.002% for (*S*)-NLC and (*S*)-P-NLC, respectively. The Zetasizer characterization of both the loaded samples confirmed

_____

that the Z-ave, PDI and ZP values were not significantly altered by the encapsulation of the prodrug, as well as the physiological pH and osmolality values (Supplementary Table 2).

10.3.3.2   In vitro prodrug release

Release profiles of (*S*)-(–)-MRJF22 from uncoated NLC and pegylated P-NLC were analyzed using Franz type diffusion cells (Figure 6): a similar behavior characterized by a slow and prolonged release was observed for both the formulations. This behavior, which is extensively reported in literature for NLC [49], [50], is usually attributable to the diffusion of the drug from the lipid matrix [50]. The initial 9% release at the beginning of the experiment, which was reported for both the formulations, suggests that there is a drug-rich region localized on the surfactant layer of the nanoparticles [51]. After 8h, (*S*)-NLC and (*S*)-P-NLC released 14.00% and 16.47% of the encapsulated (*S*)-(–)-MRJF22 respectively, to reach then 28.20% and 19.78% of prodrug released (from (*S*)-NLC and (*S*)-P-NLC respectively) after 24h of treatment, resulting in line with previous finding [20]. The difference between the two samples at 24h is probably related to the presence of PEG coating, which is known to provide a sustained and slow release [52]. As a comparison, (*S*)-(–)-MRJF22 solution showed an initial release of 44.48% at the very beginning of the experiment, to reach a complete release after 3h. This confirms the importance of the encapsulation into drug delivery systems to provide a prolonged and sustained release of the active molecule, compared to the drug solution [50].
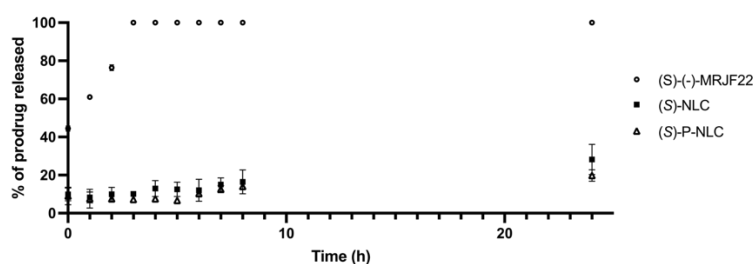

Figure 6. Release profile of (*S*)-(–)-MRJF22 from (*S*)-NLC and (*S*)-P-NLC, compared to (*S*)-(–)-MRJF22 solution.

10.3.4 In vitro studies on loaded NLCs

10.3.4.1   Cytotoxicity

The cytotoxicity produced by the loaded samples was assessed as previously reported for the blank formulations. Moreover, the toxicity of (*S*)-(–)-MRJF22 solution was evaluated (Figure 4 a,d).

_____

Prodrug encapsulation into NLCs improved its cytocompatibility on corneal HCE-2 cells up to 5 μM for (S)-NLC (viability = 78.97 %) and to 3 μM for (S)-P-NLC (viability = 77.83%), compared to the prodrug solution which was safe until 1 μM (viability = 80.54%). In tumoral UM cells, the viability results of the two loaded formulations were found to be slightly lower compared to the prodrug solution, with a viability >80% at 1 μM for (S)-NLC and 0.5 μM for (S)-P-NLC. Considering that (S)-(–)-MRJF22 resulted effective as antiproliferative agent for UM treatment at concentrations ≥5 μM [17], the encapsulation of the prodrug into both NLC and P-NLC can be exploited to protect the HCE cell from the corneal toxicity of the prodrug, while maintaining unaltered its effect on the target UM cells, highlighting the potentiality of nanocarriers in limiting the side effects of the loaded active compound.
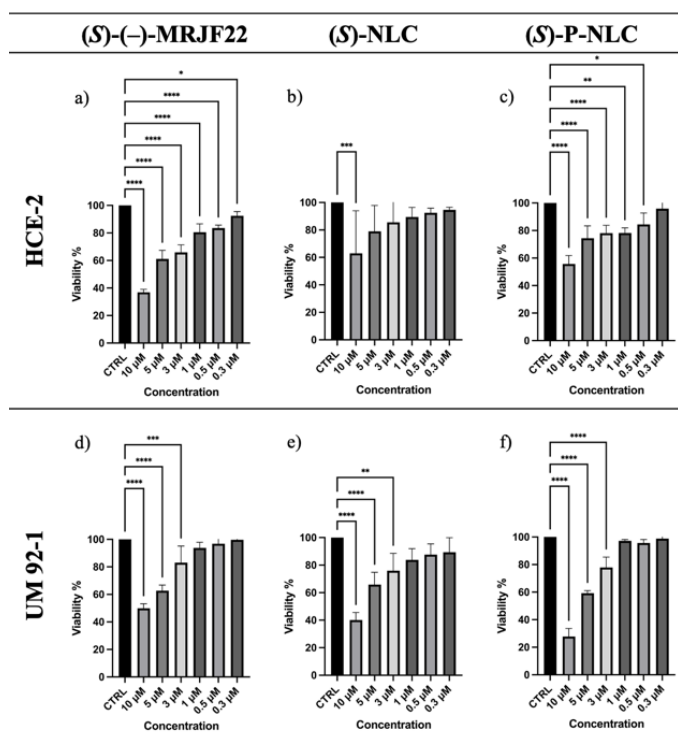

Figure 7. Cytocompatibility on HCE-2 cells (**a-c**) and on UM 92-1 cells (**d-f**) of: (S)-(–)-MRJF22 (**a,d**); (S)-NLC (**b,e**); (S)-P-NLC (**c,f**). Significance was set at $^*p{\le}0.05$; $^{**}p{\le}0.01$; $^{***}p{\le}0.001$; $^{****}p{\le}0.0001$.

10.3.4.2 *In vitro ocular tolerance*

In order to verify the *in vitro* ocular tolerance, the HET-CAM test was performed on (S)-NLC and (S)-P-NLC and on the (S)-(–)-MRJF22 solution, compared to NaOH 0.1N as a positive control and NaCl 0.9% as a negative control. This *in vitro* test is based on the analysis of the vascular damage on the blood vessels of the CAM [53], which are

_____

comparable to the ones of the rabbit conjunctiva. Subsequently, also the HET-CAM TBS was developed as a quantitative assay [54]. From the HET-CAM results (Figure 8 a-b) it clearly emerged that both (*S*)-NLC and (*S*)-P-NLC were safe and did not show any irritant effect, while for (*S*)-(–)-MRJF22 solution all the three reported events (vasoconstriction, hemorrhage, and coagulation) were recorded, with values causing moderate irritation values. An additional assessment was carried out by means of the HET-CAM TBS test (Figure 8c), which actually confirmed the non-irritant properties of both the nanosystems (OII ≤ 0.9, AD ≤ 0.10 nmol/mg) [31] and the moderately irritant behavior of (*S*)-(–)-MRJF22 (OII=5-8.9; AD=0.10-0.15 nmol/mg). These results are in agreement with the cytocompatibility on HCE-2 cells, which highlighted an increase of (*S*)-(–)-MRJF22 biocompatibility when encapsulated into the nanosystems, compared to the free prodrug, and with previous literature findings on the safety of NLC systems [55], [56].
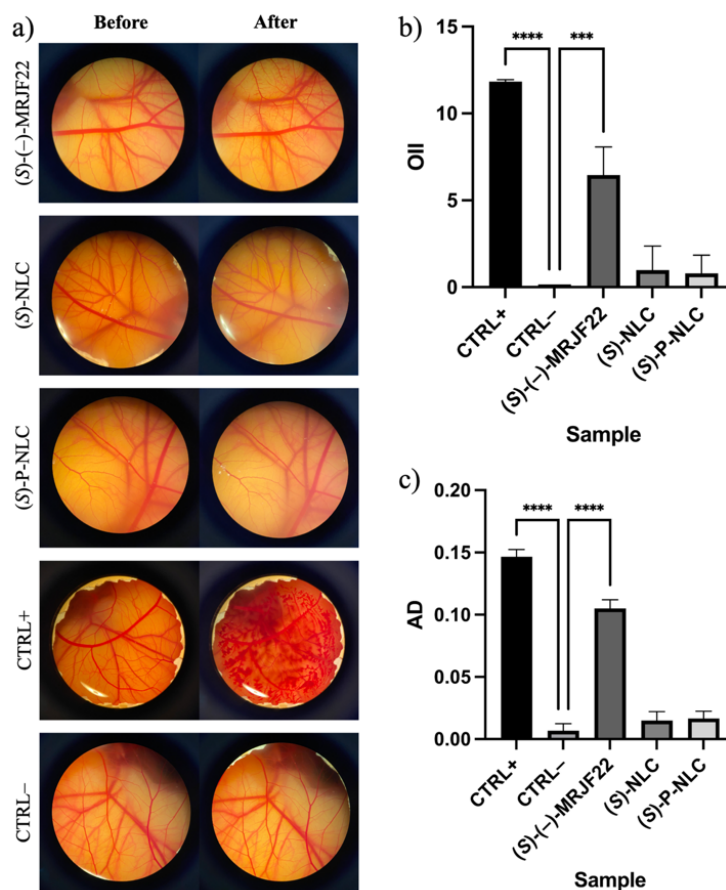

Figure 8. (**a**) HET-CAM images, before and after, of (*S*)-(–)-MRJF22 solution, (*S*)-NLC, (*S*)-P-NLC, CTRL+ NaOH and CTRL– NaCl. (**b**) Ocular irritation index (OII) results from HET-CAM test. (**c**) Absorbed dye (AD) values (nmols/mg) from HET-CAM TBS assay. Significance was set at ***p≤0.001; ****p≤0.0001 compared to CTRL–.

10.3.5 In vivo studies on loaded NLCs

10.3.5.1 Draize irritation test

As a further confirmation of the ocular tolerance of the samples, Draize test was performed on New Zealand albino rabbits. Both (*S*)-NLC and (*S*)-P-NLC and the (*S*)-(–)-MRJF22 solution were topically administered, and after 30 min cornea, iris and conjunctiva were analyzed [57] following the parameters reported in Supplementary Table 1. As can be observed in Figure 9a-b, the free (*S*)-(–)-MRJF22 solution caused a certain irritation, while both the loaded formulations produced a slight irritation which is significantly lower compared to the arachidonic acid positive control (**p≤0.01; ***p≤0.001). These results are in agreement with the cytocompatibility on HCE-2 cells and the HET-CAM results discussed above, suggesting the important role of the carrier in reducing the side effect of the loaded prodrug, thus protecting the corneal cells after the topical administration of the formulation.
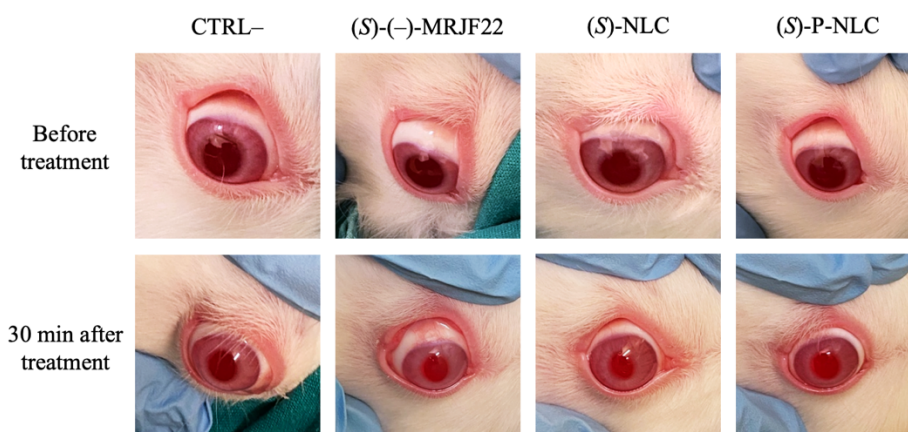

Figure 9. *In vivo* ocular tolerance Draize test after 30 min of (*S*)-(–)-MRJF22 solution, (*S*)-NLC and (*S*)-P-NLC on New Zealand albino rabbits.

10.3.5.2 Antiangiogenic capability

The antiangiogenic activity of (*S*)-NLC, (*S*)-P-NLC and (*S*)-(–)-MRJF22 solution was analyzed *in vivo* measuring the vessel density % on CAM membranes after 48h of treatment, and comparing it to NaCl, used as negative control, and bFGF growth factor, as a positive control [21]. As it is possible to see from the graph in Figure 10, all the tested samples produced an important antiangiogenic effect, with a significant decrease (****p≤0.0001) in vessel density % compared to both NaCl negative control and bFGF positive control (bFGF significance not showed in Figure 10). No significant difference

was observed between the uncoated and the pegylated NLC in respect to the free sample. This result confirms that prodrug loaded in NLC and P-NLC did not affect its effectiveness with the advantage of limiting its irritant effects. Previous studies carried on (*S*)-(–)-MRJF22 [17], demonstrated the capability of this prodrug to counteract the pro-angiogenic action of VEGF-A. In detail, the σ2 binding affinity of (*S*)-(–)-MRJF22 is able to inhibit VEGF-A, which mediates cell proliferation, tube formation and, most important, cell motility, that is responsible of the high metastatic progression of UM [58].
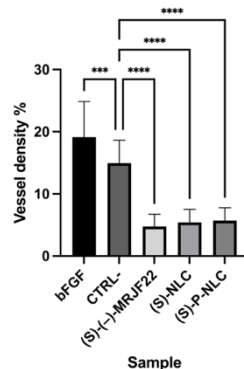

Figure 10. Antiangiogenic activity of (*S*)-(–)-MRJF22 solution, (*S*)-NLC and (*S*)-P-NLC on 3 days fertilized eggs, after 48h of treatment, compared to bFGF (CTRL+) and NaCl (CTRL–). Significance was set as ***p≤0.001; ****p≤0.0001 compared to CTRL–.

10.3.5.3 Ocular anti-inflammatory capacity

Since UM is characterized by an inflammatory phenotype [59] which involves immune cells as T lymphocytes [60], the capability of the samples to prevent ocular inflammation was assessed *in vivo* on New Zealand albino rabbits. After 30 min of treatment with (*S*)-NLC, (*S*)-P-NLC and (*S*)-(–)-MRJF22 solution, arachidonic acid was administered as an inflammatory stimulus. Subsequently, every 30 min various parameters were evaluated, aiming to assess the grade of inflammation of cornea, iris and conjunctiva [31], [34]. As highlighted in Figure 11, (*S*)-(–)-MRJF22 solution caused an initial slight decrease of the inflammation compared to control, followed by a progressive improvement of this activity, demonstrating that the prodrug possesses a protective capability against inflammation. This protective activity was enhanced by the encapsulation of (*S*)-(–)-MRJF22 into nanoparticles, since, after 30 min from the inflammatory stimulus, (*S*)-NLC and (*S*)-P-NLC were able to provide a 1.5-fold and 2.5-fold reduction (significance: ****p≤0.0001) compared to the free prodrug solution, respectively. At the end of the experiment all the formulations demonstrated to be able to provide a significant anti-inflammatory activity. The improvement of (*S*)-(–)-MRJF22 anti-inflammatory activity when encapsulated could

be related to the protection of the cornea from the irritant action of the free prodrug, as demonstrated by Draize test, and also to the slight mucoadhesive properties of the nanoparticles, which guarantee an adequate residence time on ocular surface allowing a prolonged release of the drug. Furthermore, the higher anti-inflammatory activity of (*S*)-P-NLC compared to (*S*)-NLC could be attributable to the presence of PEG 1500, which already demonstrated to have anti-inflammatory properties [61].
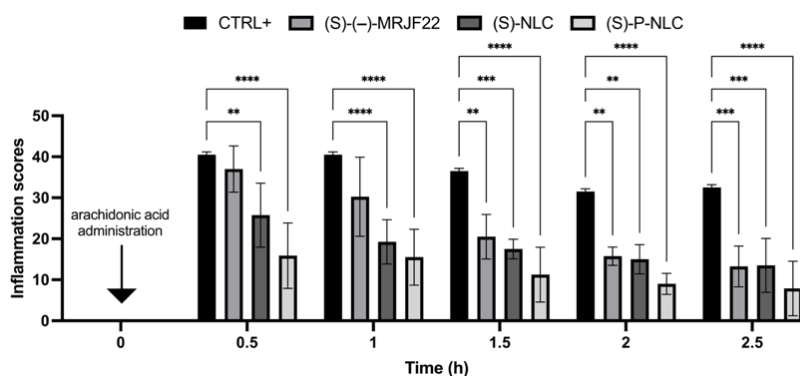

Figure 11. *In vivo* prevention of inflammation test performed on New Zealand albino rabbits treated 30 min with NaCl (CTRL+), (*S*)-(–)-MRJF22 solution, (*S*)-NLC and (*S*)-P-NLC, inflamed with arachidonic acid for 30 min and then analyzed every 30 min. Significance was set at *p≤0.05; **p≤0.01; ***p≤0.001; ****p≤0.0001 compared to CTRL+.

10.3.5.4 Characterization of fluorescent NLCs

Aiming to assess the biodistribution of the NLCs after topical ophthalmic administration, FITC was selected as lipophilic probe, since the use of fluorescein in biodistribution studies is reported in literature [62]–[64], as well as for its established use in ophthalmic diagnostic practice. FITC was encapsulated into NLC and P-NLC at a concentration of 0.01% w/V, thus obtaining F-NLC and F-P-NLC, respectively. The addition of the fluorescent probe did not modified nanoparticles feature in terms of mean size, homogeneity, ZP (data not reported). Moreover, release profiles of FITC from F-NLC and F-P-NLC, compared to FITC solution, is reported in Supplementary Figure 2.

Considering the comparable results obtained during all the mucoadhesion experiment, as well as the higher anti-inflammatory activity reported in the lasts analyzed timepoints, 3h was selected as the biodistribution time. In line with literature findings [62], FITC demonstrated to be suitable for biodistribution studies since at 3h it provided a 35.43% release from the probe solution and a <10% release from both F-NLC and F-P-NLC.

10.3.5.5 In vivo biodistribution

F-NLC, F-P-NLC and FITC solution were topically administered on New Zealand albino rabbits, to visualize the *in vivo* biodistribution of the samples. After 3h from the ophthalmic administration, the animals were sacrificed, the eyes were collected and subsequently cut into slices. The fluorescence microscopy analysis (Figure 12 a-b), highlight that both F-NLC and F-P-NLC were able to reach the posterior segment of the eye, being located mainly in the retina. As already reported in literature the achievement of the posterior segment of the eye could be performed by lipid nanoparticles in a few hours [50], [65]. In this area, Puglia and coworkers [65] suggested an absorption mechanism for lipid nanoparticles which involves an initial diffusion in the cornea and then the achievement of the retina and the sclera.
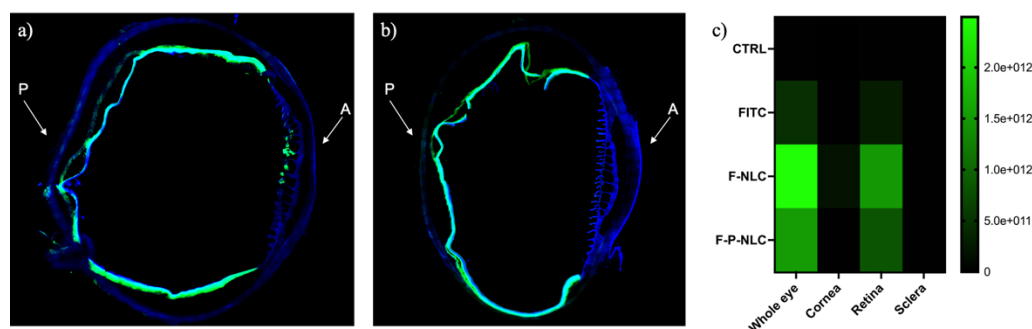

Figure 12. *In vivo* ocular biodistribution after 3h from the administration of (**a**) F-NLC and (**b**) F-P-NLC; anterior (A) and posterior (P) segments are indicated by the arrows. (**c**) Heat map of average fluorescence intensity of the main ROIs of the eye.

The heating map in Figure 12c allowed to make a quantitative comparison between the two platforms and the probe solution. It is worth to notice that the fluorescence quantification of the not-treated eye (CTRL) demonstrated no autofluorescence interference of the ocular tissues. Moreover, higher fluorescence intensity was observed in the eyes treated with the fluorescent nanoparticles, compared to the free FITC solution, and these results could be explained by the presence of the carrier which initially slightly interacts with mucin on the ocular surface – thus reducing the loss caused by tears drainage – and then favors the penetration to the posterior chamber. Therefore, PEGylation did not influence the *in vivo* fate of the nanoparticles, but it resulted advantageous for the enhancement of the anti-inflammatory activity and for the increment of cell viability. Moreover, PEG did not alter the mucoadhesion, allowing the nanoparticle to achieve the posterior chamber of the eye.

_____

10.4 Conclusion

In the present study, a novel formulation based on the second generation of lipid nanoparticles able to encapsulate a custom-synthetized drug has been developed. The produced NLC and P-NLC samples demonstrated optimal features for the intended topical ophthalmic instillation, with particle size lower than 200 nm and good homogeneity, as well as excellent ocular tolerance, assessed both *in vitro* and *in vivo*, which confirm their safety. Therefore, the new synthetized (*S*)-(–)-MRJF22 was successfully encapsulated, demonstrating that the NLC carriers were able to limit the side effects of the antitumoral prodrug, while enhancing its antiangiogenic and preventive anti-inflammatory activity. Finally, the *in vivo* biodistribution studies on the fluorescent nanosystems highlighted the ability of the carriers to achieve the inner ocular structure, thus promoting drug targeting to UM.

Supplementary materials:

**Supplementary Table 1**. Score guidelines to calculate ocular lesion on *in vivo* Draize test.

| Structure	Injury	Evaluation	Score
CORNEA	A) Degree of cloudiness or opacity		Corneal score: A·B·5 Maximum score: 80
	• Absence of ulceration	0	
	• Diffuse areas	1	
	• Translucent areas	2	
	• Opalescent areas	3	
	• Full opacity	4	
	B) Affected area		
	• None	0	
	• A quarter or less	1	
	• More than a quarter but without than half	2	
	• More than half but less than three quarters	3	
	• More than three quarters up A whole plane	4	
IRIS	A) Iris injury score		Radial score: A·5 Maximum score: 10
	• Normal	0	
	• Deep folds, congestion, swelling, moderate circumcorneal injection.	1	
	• No reaction to light, hemorrhage, great destruction	2	

_____

Structure	Injury	Evaluation	Score
CONJUNCTIVA	A) Redness		
	• Normal glasses	0	
	• Some clearly injected vessels	1	
	• Diffuse redness	2	
	• Big diffuse redness	3	
	B) Chemosis or Inflammation		Conjunctival score:
	• None	0	(A+B+C)·2
	• Some	1	
	• Marked with partial disorder of the eyelids	2	Maximum score: 20
	• Eyelid more or less closed	3	
	• Semi eyelids	4	
	C) Sweat		
	• None	0	
	• Any amount anomalous	1	
	• Wetting and eyelid hairs	2	
	• Periocular wetting	3	

Supplementary Table 2. Physical-chemical and technological characterization of unloaded NLC and P-NLC, and (*S*)-(–)-MRJF22 loaded (*S*)-NLC and (*S*)-P-NLC. Mean particle size (Z-ave), PDI, zeta potential (ZP), pH, osmolality, encapsulation efficiency and drug loading capacity are reported, and each value is the mean of at least 3 measurements ± SD. Significance was calculated comparing the loaded sample to the respective unloaded one, and it was set at: *p≤0.05; **p ≤ 0.01.

Sample	Z-ave (nm) ± SD	PDI ± SD	ZP (mV) ± SD	pH ± SD	Osm (mOsm/kg) ± SD	EE (%) ± SD	DLC (%) ± SD
NLC	142.3 ± 9.1	0.141 ± 0.027	-2.62 ± 0.19	6.75 ± 0.01	262 ± 11	/	/
(*S*)-NLC	153.3 ± 7.1	0.173 ± 0.021	-1.39 ± 0.40**	6.74 ± 0.06	256 ± 7	57.73 ± 1.91	0.083 ± 0.001
P-NLC	155.3 ± 14.1	0.213 ± 0.045	-2.81 ± 0.40	6.62 ± 0.32	274 ± 8	/	/
(*S*)-P-NLC	147.4 ± 16.8	0.225 ± 0.011	-1.40 ± 0.23*	6.73 ± 0.18	278 ± 9	52.89 ± 2.90	0.075 ± 0.002
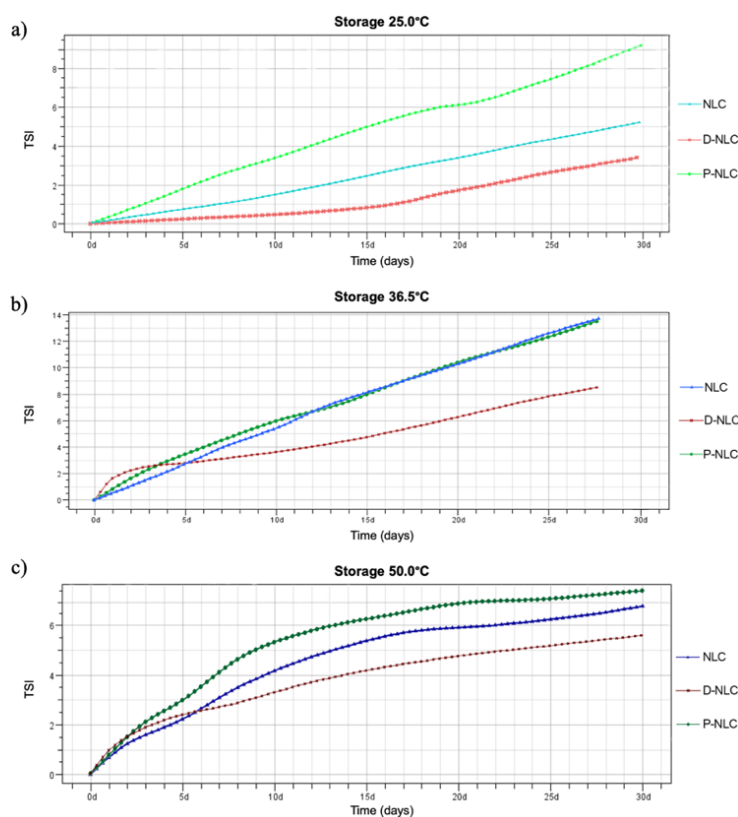
Supplementary Figure 1. Destabilization kinetics in terms of evolution of Turbiscan® Stability Index (TSI) of samples NLC, D-NLC and P-NLC stored for 30 days at 25.0±1.0°C (**a**), 36.5±1.0°C (**b**), 50.0±1.0°C (**c**).
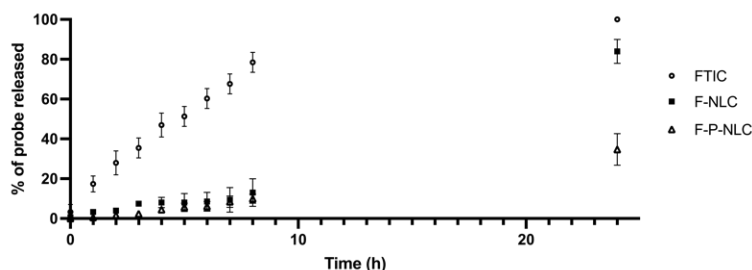
Supplementary Figure 2. Release profile of FITC from F-NLC and F-P-NLC, compared to FITC solution.

References:

[1] A. Niederkorn, W. Wackernagel, M. Artl, G. Schwantzer, B. Aigner, and E. Richtig, 'Response of patients with metastatic uveal melanoma to combined treatment with fotemustine and sorafenib', Acta Ophthalmol. (Copenh.), vol. 92, no. 8, pp. e696–e697, Dec. 2014, doi: 10.1111/aos.12432.

[2] E. Kujala, T. Ma¨kitie, and T. Kivela¨, 'Very Long-Term Prognosis of Patients with Malignant Uveal Melanoma', Investig. Opthalmology Vis. Sci., vol. 44, no. 11, p. 4651, Nov. 2003, doi: 10.1167/iovs.03-0538.

[3] F. Spagnolo, G. Caltabiano, and P. Queirolo, 'Uveal melanoma', Cancer Treat. Rev., vol. 38, no. 5, pp. 549–553, Aug. 2012, doi: 10.1016/j.ctrv.2012.01.002.

[4] Ameeduzzafar, J. Ali, M. Fazil, M. Qumbar, N. Khan, and A. Ali, 'Colloidal drug delivery system: amplify the ocular delivery', Drug Deliv., vol. 23, no. 3, pp. 700–716, Mar. 2016, doi: 10.3109/10717544.2014.923065.

[5] J. V. Natarajan et al., 'Sustained Release of an Anti-Glaucoma Drug: Demonstration of Efficacy of a Liposomal Formulation in the Rabbit Eye', PLoS ONE, vol. 6, no. 9, p. e24513, Sep. 2011, doi: 10.1371/journal.pone.0024513.

[6] E. Sánchez-López, M. Espina, S. Doktorovova, E. B. Souto, and M. L. García, 'Lipid nanoparticles (SLN, NLC): Overcoming the anatomical and physiological barriers of the eye – Part I – Barriers and determining factors in ocular delivery', Eur. J. Pharm. Biopharm., vol. 110, pp. 70–75, Jan. 2017, doi: 10.1016/j.ejpb.2016.10.009.

[7] V. Delplace, S. Payne, and M. Shoichet, 'Delivery strategies for treatment of age-related ocular diseases: From a biological understanding to biomaterial solutions', J. Controlled Release, vol. 219, pp. 652–668, Dec. 2015, doi: 10.1016/j.jconrel.2015.09.065.

[8] P. Hughes, O. Olejnik, J. Changlin, and C. Wilson, 'Topical and systemic drug delivery to the posterior segments', Adv. Drug Deliv. Rev., vol. 57, no. 14, pp. 2010–2032, Dec. 2005, doi: 10.1016/j.addr.2005.09.004.

[9] T. R. Thrimawithana, S. Young, C. R. Bunt, C. Green, and R. G. Alany, 'Drug delivery to the posterior segment of the eye', Drug Discov. Today, vol. 16, no. 5–6, pp. 270–277, Mar. 2011, doi: 10.1016/j.drudis.2010.12.004.

[10] L. Bonilla et al., 'Lipid Nanoparticles for the Posterior Eye Segment', Pharmaceutics, vol. 14, no. 1, p. 90, Dec. 2021, doi: 10.3390/pharmaceutics14010090.

[11] A. Urtti, 'Challenges and obstacles of ocular pharmacokinetics and drug delivery', Adv. Drug Deliv. Rev., vol. 58, no. 11, pp. 1131–1135, Nov. 2006, doi: 10.1016/j.addr.2006.07.027.

[12] C. Viegas, A. B. Patrício, J. M. Prata, A. Nadhman, P. K. Chintamaneni, and P. Fonte, 'Solid Lipid Nanoparticles vs. Nanostructured Lipid Carriers: A Comparative Review', Pharmaceutics, vol. 15, no. 6, p. 1593, May 2023, doi: 10.3390/pharmaceutics15061593.

[13] I. F. De Oliveira et al., 'Cutting-edge advances in therapy for the posterior segment of the eye: Solid lipid nanoparticles and nanostructured lipid carriers', Int. J. Pharm., vol. 589, p. 119831, Nov. 2020, doi: 10.1016/j.ijpharm.2020.119831.

[14] C. B. M. Platania et al., 'Novel ophthalmic formulation of myriocin: implications in retinitis pigmentosa', Drug Deliv., vol. 26, no. 1, pp. 237–243, Jan. 2019, doi: 10.1080/10717544.2019.1574936.

[15] J. Li, G. Tan, B. Cheng, D. Liu, and W. Pan, 'Transport mechanism of chitosan-N-acetylcysteine, chitosan oligosaccharides or carboxymethyl chitosan decorated coumarin-6 loaded nanostructured lipid carriers across the rabbit ocular', Eur. J. Pharm. Biopharm., vol. 120, pp. 89–97, Nov. 2017, doi: 10.1016/j.ejpb.2017.08.013.

[16] A. Rahmi et al., 'Proton beam therapy for presumed and confirmed iris melanomas: a review of 36 cases', Graefes Arch. Clin. Exp. Ophthalmol., vol. 252, no. 9, pp. 1515–1521, Sep. 2014, doi: 10.1007/s00417-014-2735-y.

[17] C. Barbaraci et al., 'Haloperidol Metabolite II Valproate Ester (S)-(−)-MRJF22: Preliminary Studies as a Potential Multifunctional Agent Against Uveal Melanoma', J. Med. Chem., vol. 64, no. 18, pp. 13622–13632, Sep. 2021, doi: 10.1021/acs.jmedchem.1c00995.

[18] M. S. Razavi, P. Ebrahimnejad, Y. Fatahi, A. D'Emanuele, and R. Dinarvand, 'Recent Developments of Nanostructures for the Ocular Delivery of Natural Compounds', Front. Chem., vol. 10, p. 850757, Apr. 2022, doi: 10.3389/fchem.2022.850757.

[19] B. Grassiri, Y. Zambito, and A. Bernkop-Schnürch, 'Strategies to prolong the residence time of drug delivery systems on ocular surface', Adv. Colloid Interface Sci., vol. 288, p. 102342, Feb. 2021, doi: 10.1016/j.cis.2020.102342.

[20] C. Cimino et al., 'Nanostructured lipid carrier for the ophthalmic delivery of haloperidol metabolite II valproate ester (±)-MRJF22: A potential strategy in the treatment of uveal melanoma', J. Drug Deliv. Sci. Technol., p. 104811, Aug. 2023, doi: 10.1016/j.jddst.2023.104811.

[21] E. Sánchez-López, M. J. Gómara, and I. Haro, 'Atorvastatin-loaded peptide amphiphiles against corneal neovascularization', Nanomed., p. nnm-2023-0133, Aug. 2023, doi: 10.2217/nnm-2023-0133.

[22] C. Carbone, C. Caddeo, M. A. Grimaudo, D. E. Manno, A. Serra, and T. Musumeci, 'Ferulic Acid-NLC with Lavandula Essential Oil: A Possible Strategy for Wound-Healing?', Nanomaterials, vol. 10, no. 5, p. 898, May 2020, doi: 10.3390/nano10050898.

[23] A. Bonaccorso et al., 'Sorafenib Repurposing for Ophthalmic Delivery by Lipid Nanoparticles: A Preliminary Study', Pharmaceutics, vol. 13, no. 11, p. 1956, Nov. 2021, doi: 10.3390/pharmaceutics13111956.

[24] C. Carbone, A. Campisi, T. Musumeci, G. Raciti, R. Bonfanti, and G. Puglisi, 'FA-loaded lipid drug delivery systems: Preparation, characterization and biological studies', Eur. J. Pharm. Sci., vol. 52, pp. 12–20, Feb. 2014, doi: 10.1016/j.ejps.2013.10.003.

[25] D. Santonocito et al., 'Curcumin Containing PEGylated Solid Lipid Nanoparticles for Systemic Administration: A Preliminary Study', Molecules, vol. 25, no. 13, p. 2991, Jun. 2020, doi: 10.3390/molecules25132991.

[26] C. Puglia et al., 'Ocular Formulation Based on Palmitoylethanolamide-Loaded Nanostructured Lipid Carriers: Technological and Pharmacological Profile', Nanomaterials, vol. 10, no. 2, p. 287, Feb. 2020, doi: 10.3390/nano10020287.

[27] S. Tambe, D. Jain, and P. Amin, 'Simultaneous determination of dorzolamide and timolol by first-order derivative UV spectroscopy in simulated biological fluid for in vitro drug release testing', Spectrochim. Acta. A. Mol. Biomol. Spectrosc., vol. 255, p. 119682, Jul. 2021, doi: 10.1016/j.saa.2021.119682.

[28] C. Folle et al., 'Surface-Modified Multifunctional Thymol-Loaded Biodegradable Nanoparticles for Topical Acne Treatment', Pharmaceutics, vol. 13, no. 9, p. 1501, Sep. 2021, doi: 10.3390/pharmaceutics13091501.

[29] C. Folle et al., 'Thymol-loaded PLGA nanoparticles: an efficient approach for acne treatment', J. Nanobiotechnology, vol. 19, no. 1, p. 359, Dec. 2021, doi: 10.1186/s12951-021-01092-z.

[30] A. López-Machado et al., 'Development of topical eye-drops of lactoferrin-loaded biodegradable nanoparticles for the treatment of anterior segment inflammatory processes', Int. J. Pharm., vol. 609, p. 121188, Nov. 2021, doi: 10.1016/j.ijpharm.2021.121188.

[31] G. Esteruelas et al., 'Development and optimization of Riluzole-loaded biodegradable nanoparticles incorporated in a mucoadhesive in situ gel for the posterior eye segment', Int. J. Pharm., vol. 612, p. 121379, Jan. 2022, doi: 10.1016/j.ijpharm.2021.121379.

[32] E. Sánchez-López et al., 'Dexibuprofen Biodegradable Nanoparticles: One Step Closer towards a Better Ocular Interaction Study', Nanomaterials, vol. 10, no. 4, p. 720, Apr. 2020, doi: 10.3390/nano10040720.

[33] E. Sánchez-López et al., 'PEGylated PLGA nanospheres optimized by design of experiments for ocular administration of dexibuprofen—in vitro, ex vivo and in vivo characterization', Colloids Surf. B Biointerfaces, vol. 145, pp. 241–250, Sep. 2016, doi: 10.1016/j.colsurfb.2016.04.054.

[34] E. Vega, M. A. Egea, O. Valls, M. Espina, and M. L. García, 'Flurbiprofen Loaded Biodegradable Nanoparticles for Ophtalmic Administration', J. Pharm. Sci., vol. 95, no. 11, pp. 2393–2405, Nov. 2006, doi: 10.1002/jps.20685.

[35] S. Swetledge, R. Carter, R. Stout, C. E. Astete, J. P. Jung, and C. M. Sabliov, 'Stability and ocular biodistribution of topically administered PLGA nanoparticles', Sci. Rep., vol. 11, no. 1, p. 12270, Jun. 2021, doi: 10.1038/s41598-021-90792-5.

[36] P. Niamprem, S. P. Srinivas, and W. Tiyaboonchai, 'Penetration of Nile red-loaded nanostructured lipid carriers (NLCs) across the porcine cornea', Colloids Surf. B Biointerfaces, vol. 176, pp. 371–378, Apr. 2019, doi: 10.1016/j.colsurfb.2019.01.018.

[37] P. Nirbhavane et al., 'Triamcinolone acetonide loaded-cationic nano-lipoidal formulation for uveitis: Evidences of improved biopharmaceutical performance and anti-inflammatory activity', Colloids Surf. B Biointerfaces, vol. 190, p. 110902, Jun. 2020, doi: 10.1016/j.colsurfb.2020.110902.

[38] J. V. Jokerst, T. Lobovkina, R. N. Zare, and S. S. Gambhir, 'Nanoparticle PEGylation for imaging and therapy', Nanomed., vol. 6, no. 4, pp. 715–728, Jun. 2011, doi: 10.2217/nnm.11.19.

[39] A. A. Date et al., 'Lecithin-based novel cationic nanocarriers (LeciPlex) I: fabrication, characterization and evaluation', Nanomed., vol. 6, no. 8, pp. 1309–1325, Oct. 2011, doi: 10.2217/nnm.11.38.

[40] B. Silva, B. São Braz, E. Delgado, and L. Gonçalves, 'Colloidal nanosystems with mucoadhesive properties designed for ocular topical delivery', Int. J. Pharm., vol. 606, p. 120873, Sep. 2021, doi: 10.1016/j.ijpharm.2021.120873.

[41] A. L. Onugwu, A. A. Attama, P. O. Nnamani, S. O. Onugwu, E. B. Onuigbo, and V. V. Khutoryanskiy, 'Development and optimization of solid lipid nanoparticles coated with chitosan and poly(2-ethyl-2-oxazoline) for ocular drug delivery of ciprofloxacin', J. Drug Deliv. Sci. Technol., vol. 74, p. 103527, Aug. 2022, doi: 10.1016/j.jddst.2022.103527.

[42] R. Pignatello, 'Optimization and Validation of a New Method for the Production of Lipid Nanoparticles for Ophthalmic Application', Int. J. Med. Nano Res., vol. 1, no. 1, Dec. 2014, doi: 10.23937/2378-3664/1410006.

[43] L. T. Lim, E. Y. Ah-Kee, and C. E. Collins, 'Common eye drops and their implications for pH measurements in the management of chemical eye injuries', Int. J. Ophthalmol., vol. 7, no. 6, pp. 1067–1068, 2014, doi: 10.3980/j.issn.2222-3959.2014.06.29.

[44] T. Musumeci, A. Bonaccorso, C. Carbone, G. Russo, F. Pappalardo, and G. Puglisi, 'Design and optimization of PEGylated nanoparticles intended for Berberine Chloride delivery', J. Drug Deliv. Sci. Technol., vol. 52, pp. 521–530, Aug. 2019, doi: 10.1016/j.jddst.2019.05.012.

[45] C. Carbone et al., 'The critical role of didodecyldimethylammonium bromide on physico-chemical, technological and biological properties of NLC', Colloids Surf. B Biointerfaces, vol. 121, pp. 1–10, Sep. 2014, doi: 10.1016/j.colsurfb.2014.05.024.

[46] G. Karmakar, P. Nahak, P. Guha, B. Roy, R. K. Nath, and A. K. Panda, 'Role of PEG 2000 in the surface modification and physicochemical characteristics of pyrazinamide loaded nanostructured lipid carriers', J. Chem. Sci., vol. 130, no. 4, p. 42, Apr. 2018, doi: 10.1007/s12039-018-1448-x.

[47] E. L. Kiss et al., 'Development and Characterization of Potential Ocular Mucoadhesive Nano Lipid Carriers Using Full Factorial Design', Pharmaceutics, vol. 12, no. 7, p. 682, Jul. 2020, doi: 10.3390/pharmaceutics12070682.

[48] A. Bonaccorso, T. Musumeci, C. Carbone, L. Vicari, M. R. Lauro, and G. Puglisi, 'Revisiting the role of sucrose in PLGA-PEG nanocarrier for potential intranasal delivery', Pharm. Dev. Technol., vol. 23, no. 3, pp. 265–274, Mar. 2018, doi: 10.1080/10837450.2017.1287731.

[49] A. C. Ortiz, O. Yañez, E. Salas-Huenuleo, and J. O. Morales, 'Development of a Nanostructured Lipid Carrier (NLC) by a Low-Energy Method, Comparison of Release Kinetics and Molecular Dynamics Simulation', Pharmaceutics, vol. 13, no. 4, p. 531, Apr. 2021, doi: 10.3390/pharmaceutics13040531.

[50] S. P. Balguri, G. R. Adelli, and S. Majumdar, 'Topical ophthalmic lipid nanoparticle formulations (SLN, NLC) of indomethacin for delivery to the posterior segment ocular tissues', Eur. J. Pharm. Biopharm., vol. 109, pp. 224–235, Dec. 2016, doi: 10.1016/j.ejpb.2016.10.015.

[51] P. A. Makoni, K. Wa Kasongo, and R. B. Walker, 'Short Term Stability Testing of Efavirenz-Loaded Solid Lipid Nanoparticle (SLN) and Nanostructured Lipid Carrier (NLC) Dispersions', Pharmaceutics, vol. 11, no. 8, p. 397, Aug. 2019, doi: 10.3390/pharmaceutics11080397.

[52] S. A. Duncan et al., 'Prolonged Release and Functionality of Interleukin-10 Encapsulated within PLA-PEG Nanoparticles', Nanomaterials, vol. 9, no. 8, p. 1074, Jul. 2019, doi: 10.3390/nano9081074.

[53] P. Anantaworasakul, W. Chaiyana, B. B. Michniak-Kohn, W. Rungseevijitprapa, and C. Ampasavate, 'Enhanced Transdermal Delivery of Concentrated Capsaicin from Chili Extract-Loaded Lipid Nanoparticles with Reduced Skin Irritation', Pharmaceutics, vol. 12, no. 5, p. 463, May 2020, doi: 10.3390/pharmaceutics12050463.

[54] A. G. L. de Oliveira, R. S. Silva, E. N. Alves, R. de F. Presgrave, O. A. F. Presgrave, and I. F. Delgado, 'Ensaios da membrana cório-alantoide (HET-CAM e CAM-TBS): alternativas para a avaliação toxicológica de produtos com baixo potencial de irritação ocular', Rev. Inst. Adolfo Lutz, vol. 71, no. 1, pp. 153–159, Feb. 2012, doi: https://doi.org/10.53393/rial.2012.v71.32405.

[55] R. Varela-Fernández et al., 'Lactoferrin-loaded nanostructured lipid carriers (NLCs) as a new formulation for optimized ocular drug delivery', Eur. J. Pharm. Biopharm., vol. 172, pp. 144–156, Mar. 2022, doi: 10.1016/j.ejpb.2022.02.010.

[56] S. Aher, R. P. Singh, and M. Kumar, 'Preparation and Characterization of Nano Structured Lipid Carriers for Ocular Bacterial Infection', J. Pharm. Res. Int., pp. 8–23, Aug. 2021, doi: 10.9734/jpri/2021/v33i40A32215.

[57] K. Adibkia et al., 'Piroxicam nanoparticles for ocular delivery: Physicochemical characterization and implementation in endotoxin-induced uveitis', J. Drug Target., vol. 15, no. 6, pp. 407–416, Jan. 2007, doi: 10.1080/10611860701453125.

[58] E. A. Seftor et al., 'Molecular determinants of human uveal melanoma invasion and metastasis', Clin. Exp. Metastasis, vol. 19, no. 3, pp. 233–246, 2002, doi: 10.1023/A:1015591624171.

[59] I. H. G. Bronkhorst and M. J. Jager, 'Inflammation in uveal melanoma', Eye, vol. 27, no. 2, pp. 217–223, Feb. 2013, doi: 10.1038/eye.2012.253.

[60] I. De Waard-Siebinga, C. G. J. M. Hilders, B. E. Hansen, J. L. Van Delft, and M. J. Jager, 'HLA expression and tumor-infiltrating immune cells in uveal melanoma', Graefes Arch. Clin. Exp. Ophthalmol., vol. 234, no. 1, pp. 34–42, Jan. 1996, doi: 10.1007/BF00186516.

[61] T. Aghaie, M. H. Jazayeri, A. Avan, A. Anissian, and A. Salari, 'Gold nanoparticles and polyethylene glycol alleviate clinical symptoms and alter cytokine secretion in a mouse model of experimental autoimmune encephalomyelitis', IUBMB Life, vol. 71, no. 9, pp. 1313–1321, Sep. 2019, doi: 10.1002/iub.2045.

[62] K. Jounaki, B. S. Makhmalzadeh, M. Feghhi, and A. Heidarian, 'Topical ocular delivery of vancomycin loaded cationic lipid nanocarriers as a promising and non-invasive alternative approach to intravitreal injection for enhanced bacterial endophthalmitis management', Eur. J. Pharm. Sci., vol. 167, p. 105991, Dec. 2021, doi: 10.1016/j.ejps.2021.105991.

[63] S. Kakkar et al., 'Lipo-PEG nano-ocular formulation successfully encapsulates hydrophilic fluconazole and traverses corneal and non-corneal path to reach posterior eye segment', J. Drug Target., vol. 29, no. 6, pp. 631–650, Jul. 2021, doi: 10.1080/1061186X.2020.1871483.

[64] J. Shen, M. Sun, Q. Ping, Z. Ying, and W. Liu, 'Incorporation of liquid lipid in lipid nanoparticles for ocular drug delivery enhancement', Nanotechnology, vol. 21, no. 2, p. 025101, Jan. 2010, doi: 10.1088/0957-4484/21/2/025101.

[65] C. Puglia et al., 'Lipid Nanoparticles Traverse Non-Corneal Path to Reach the Posterior Eye Segment: In Vivo Evidence', Molecules, vol. 26, no. 15, p. 4673, Aug. 2021, doi: 10.3390/molecules26154673.

PUBLICATIONS LIST

Cimino, C.; Maurel, O.M.; Musumeci, T.; Bonaccorso, A.; Drago, F.; Souto, E.M.B.; Pignatello, R.; Carbone, C. *Essential Oils: Pharmaceutical Applications and Encapsulation Strategies into Lipid-Based Delivery Systems*. Pharmaceutics. 2021 Mar 3; 13(3):327. doi: 10.3390/pharmaceutics13030327.

Bonaccorso, A.; Cimino, C.; Manno, D.E.; Tomasello, B.; Serra, A.; Musumeci, T.; Puglisi, G.; Pignatello, R.; Carbone, C. *Essential Oil-Loaded NLC for Potential Intranasal Administration*. Pharmaceutics. 2021 Jul 28; 13(8):1166. doi: 10.3390/pharmaceutics13081166.

Bonaccorso, A.; Pepe, V.; Zappulla, C.; Cimino, C.; Pricoco, A.; Puglisi, G.; Giuliano, F.; Pignatello, R.; Carbone, C. *Sorafenib Repurposing for Ophthalmic Delivery by Lipid Nanoparticles: A Preliminary Study*. Pharmaceutics. 2021 Nov 18; 13(11):1956. doi: 10.3390/pharmaceutics13111956.

Tortorici, S.; Cimino, C.; Ricupero, M.; Musumeci, T.; Biondi, A.; Siscaro, G.; Carbone, C.; Zappalà, L. *Nanostructured lipid carriers of essential oils as potential tools for the sustainable control of insect pests.* Industrial Crops and Products. 2022 Mar 19; 181:114766. doi: 10.1016/j.indcrop.2022.114766.

Zingale, E.; Romeo, A.; Rizzo, S.; Cimino, C.; Bonaccorso. A.; Carbone, C.; Musumeci, T.; Pignatello, R. *Fluorescent Nanosystems for Drug Tracking and Theranostics: Recent Applications in the Ocular Field.* Pharmaceutics. 2022 Apr 28; 14(5):955. doi: 10.3390/pharmaceutics14050955.

Cimino, C.; Leotta, C.G.; Marrazzo, A.; Musumeci, T.; Pitari, G.M.; Pignatello, R.; Bonaccorso, A.; Amata, E.; Barbaraci, C.; Carbone, C. *Nanostructured lipid carrier for the ophthalmic delivery of haloperidol metabolite II valproate ester (±)-MRJF22: A potential strategy in the treatment of uveal melanoma*. Journal of Drug Delivery Science and Technology. 2023 Aug 4; doi: 10.1016/j.jddst.2023.104811

Cimino, C.; Bonaccorso, A.; Tomasello, B.; Anfuso Alberghina, G.; Musumeci, T.; Puglia, C.; Pignatello, R.; Marrazzo, A.; Carbone, C. *W/O/W microemulsions for nasal delivery of hydrophilic compounds: a preliminary study*. <u>Submitted</u> to Journal of Pharmaceutical Sciences.

Cimino, C.; Sánchez López, E.; Bonaccorso, A.; Bonilla, L.; Musumeci, T.; Badia, J.; Baldomà, L.; Pignatello, R.; Marrazzo, A.; García, M.L.; Carbone, C. *In vitro and in vivo studies of topically administered NLC for the treatment of uveal melanoma*. <u>In progress</u> to be submitted to Journal of Controlled Release.

_____

CONGRESSES LIST

12th World Meeting on Pharmaceutics, Biopharmaceutics and Pharmaceutical Technology, 11-14 May 2021, Vienna, Austria (online) – <u>poster</u> – Cimino, C.; Bonaccorso, A.; Romeo, A.; Musumeci, T.; Pignatello, R.; Carbone, C. *Mediterranean EO-NLC for potential intranasal delivery.*

XXVII Congresso Nazionale della Società Chimica Italiana, 14-23 Sep 2021 (online) – <u>poster</u> – Cimino, C.; Marrazzo, A.; Pepe, V.; Zappulla, C.; Puglisi, G.; Pignatello, R.; Carbone, C. *Solid lipid nanoparticles for sorafenib ophthalmic delivery.*

Biologicals in Therapy, 20th Advanced Course in Pharmaceutical Technology, 27-29 Sep 2021 (online) – <u>poster</u> – Cimino, C.; Marrazzo, A.; Bonaccorso, A.; Manno, D.E.; Serra, A.; Pignatello, R.; Puglisi, G.; Musumeci, T.; Carbone, C. *Nanostructured lipid carriers for the potential intranasal administration of essential oils.*

MedChem2022, XI Paul Ehrlich Euro-PhD Network Meeting, 14-16 July 2022, Barcelona, Spain – <u>oral communication</u> – Cimino, C.; Leotta, C. G.; Barbaraci, C.; Musumeci, T.; Pitari, G. M.; Carbone, C.; Marrazzo, A. *Haloperidol metabolite II Valproate ester-loaded NLC as promising strategy for the treatment of Uveal Melanoma.*

Strategie terapeutiche per le patologie vascolari: il ruolo della tecnologia farmaceutica, XXI Scuola Dottorale in Tecnologia Farmaceutica, 5-7 September 2022, Roma, Italy – <u>poster</u> – Cimino, C.; Bonaccorso, A.; Tomasello, B.; Musumeci, T.; Pignatello, R.; Marrazzo, A.; Carbone, C. *W/O/W nanoemulsions as a potential platform for nasal delivery of hydrophilic compounds: a preliminary study.*

XXVII National Meeting in Medicinal Chemistry, 11-14 September 2022, Bari, Italy – <u>poster</u> – Cimino, C.; Leotta, C. G.; Barbaraci, C.; Amata, E.; Musumeci, T.; Pitari, G. M.; Carbone, C. and Marrazzo, A. *NLC as promising platform to deliver new prodrugs in the treatment of ophthalmic cancer.*

Controlled Release Society Italy Workshop 2022, 7-9 October 2022, Genova, Italy – <u>poster</u> – Cimino, C.; Leotta, C. G.; Barbaraci, C.; Musumeci, T.; Pitari, G. M.; Marrazzo, A.; Pignatello R.; Carbone, C. *NLC for the delivery of new prodrugs in the treatment of uveal melanoma.*

I Jornada de Recerca i Divulgació de Doctorat de la UB, 19 May 2023, Barcelona, Spain – <u>poster</u> – Cimino, C.; Leotta, C. G.; Barbaraci, C.; Sanchez Lopez, E.; Musumeci, T.; Pitari, G. M.; Marrazzo, A. and Carbone, C. *Lipid Nanoparticles loaded with new synthetized (±)-MRJF22 as promising platform for Uveal Melanoma treatment.*

_____

New drugs and old barriers: a challenging match, XXII Scuola Dottorale in Tecnologia Farmaceutica, 13-15 September 2023, Trieste, Italy – <u>oral communication</u> – Cimino, C.; Marrazzo, A.; Carbone, C. *Potential treatment of uveal melanoma with (S)-(–)-MRJF22 loaded-nanostructured lipid carriers: preliminary in vitro and in vivo studies*.

Controlled Release Society Italy Workshop 2023, 5-7 October 2023, Palermo, Italy – <u>poster</u> – Cimino, C.; Sanchéz Lopéz, E.; Marrazzo, A.; Musumeci, T.; Bonaccorso, A.; Pignatello, R.; Barbaraci, C.; Carbone, C. *Preliminary in vitro and in vivo studies of (S)-(–)-MRJF22 loaded-NLC for potential treatment of uveal melanoma*.

RINGRAZIAMENTI

Alla fine di questo percorso di dottorato, e di questa tesi, la parte forse più complessa è proprio questa dei ringraziamenti, perché non c'è cosa più difficile di dover racchiudere in poche righe l'esperienza più bella della mia vita.

Il primo e più importante ringraziamento è per i miei due tutor, grazie ai quali ho avuto l'opportunità e la fortuna di vivere contemporaneamente due ambiti di ricerca tanto differenti quanto interconnessi. Poter mescolare la tecnologia farmaceutica con la chimica farmaceutica è stato quel *plus* che ha reso la mia esperienza di ricerca ancor più completa e stimolante.

Grazie al professore Agostino Marrazzo per essersi imbarcato con me in questa avventura (un po' "a scatola chiusa"!), dandomi la completa libertà di portare avanti il mio progetto: è stato l'inizio di una collaborazione che ha dato ancor più valore alla mia esperienza. È proprio vero: l'unione fa la forza! Grazie per la sua disponibilità e la sua fiducia, che non mi ha mai fatto mancare.

Grazie alla professoressa Claudia Carbone, che, fin dal primo, giorno è stata una mamma, un'amica e un'ispirazione, oltre che un'eccezionale guida: grazie per avermi sempre coinvolta e valorizzata, per aver creduto in me e nelle mie capacità anche nei momenti più impegnativi, per avermi dato fiducia e avermi lasciata sempre libera di fare le mie scelte (e a volte anche di sbagliare!). Soprattutto grazie per avermi trasmesso la sua passione e per avermi fatta innamorare della ricerca.

Uno speciale ringraziamento anche alla professoressa Elena Sánchez López, che, seppur non mi conoscesse, mi ha accolta a braccia aperte nel suo laboratorio durante i meravigliosi sei mesi trascorsi a Barcellona. Grazie per avermi dato l'opportunità di realizzare gli esperimenti che avevo sempre sognato di fare (e anche molti più di quelli che speravo!) e per avermi fatto scoprire un diverso modo di vivere la ricerca, allargando i miei orizzonti e permettendomi di crescere professionalmente.

Grazie a tutti i professori e i ricercatori che mi sono stati vicini durante questo percorso: il coordinatore prof. Vito De Pinto; il mio bellissimo gruppo di ricerca con il prof. Giovanni Puglisi, il prof. Rosario Pignatello, la prof. Teresa Musumeci e la dott.ssa Angela Bonaccorso; le collaborazioni "*in vitro*" con la prof.ssa Barbara Tomasello e la Vera Salus Ricerca nelle persone della dott.ssa Claudia Giovanna Leotta e del prof. Giovanni Mario Pitari; la collega dott.ssa Carla Barbaraci, mia chimica farmaceutica di fiducia; il gruppo di ricerca di Fisicoquímica che mi ha ospitato a Barcellona nella persona della prof.ssa

María Luisa García, e il dipartimento di Bioquímica con le prof.sse Josefa Badia e Laura Baldomà.

Grazie ai miei studenti in tesi, Miriam Giardinaro, Giovanni Anfuso Alberghina e Serena Giglio, aiuto concreto e sostegno anche nei momenti più impegnativi.

Grazie ai colleghi Cristina Torrisi, Rosamaria Lombardo, Alessia Romeo, Elide Zingale, Giuliana Costanzo e Salvatore Rizzo, per tutti i momenti condivisi ai congressi e in dipartimento. Grazie anche ai miei colleghi spagnoli Lorena Bonilla Vidal, Gerard Esteruelas Navarro, Xavi Roig Soriano e Francesca Barrera per avermi trasmesso le vostre conoscenze senza gelosia e per non avermi mai fatto mancare il vostro sostegno nella quotidianità.

Grazie anche a tutti coloro con cui ho collaborato: Oriana Maurel, Filippo Drago, Eliana Maria Barbosa Souto, Daniela Erminia Manno, Antonio Serra, Veronica Pepe, Cristina Zappulla, Angelo Pricoco, Francesco Giuliano, Simona Tortorici, Michele Ricupero, Antonio Biondi, Gaetano Siscaro, Lucia Zappalà, Emanuele Amata, Carmelo Puglia.

"Quando guardate, guardate lontano,
e anche quando credete di star guardando lontano,
guardate ancor più lontano!"

Robert Baden-Powell